University of Alberta

Geotechnical Behavior of In-Line Thickened Oil Sands Tailings

by

Silawat Jeeravipoolvarn

A thesis submitted to the Faculty of Graduate Studies and Research
in partial fulfillment of the requirements for the degree of

Doctor of Philosophy

in

Geotechnical Engineering

Civil and Environmental Engineering

Spring 2010
Edmonton, Alberta

Examining Committee

Dr. Rick J. Chalaturnyk, Co-supervisor, Civil and Environmental Engineering

Dr. J. Don Scott, Co-supervisor, Civil and Environmental Engineering

Dr. Alireza Bayat, Civil and Environmental Engineering

Dr. Jozef Szymanski, Civil and Environmental Engineering

Dr. John M. Shaw, Chemical and Materials Engineering

Dr. Paul H. Simms, Civil and Environmental Engineering, Carleton University

Abstract

This research is an experimental, field and numerical study of the sedimentation and consolidation of in-line thickened oil sands fine tailings. In-line thickening is a process that adds flocculant and coagulant into a modified tailings pipeline in a multi stage fashion to improve the dewatering behaviour of oil sands fine tailings cyclone overflow.

The parent untreated cyclone overflow, in-line thickened tailings and sheared in-line thickened tailings were investigated in the laboratory. In-line thickened tailings were produced in the laboratory using the same process as in the field project and sheared in-line thickened tailings were prepared by shearing the thickened tailings with a specified shearing effort to simulate tailings transportation. A combination of hindered sedimentation tests, compressibility standpipe tests and large strain consolidation tests with vane shear tests was then used to capture a full range of sedimentation, consolidation and shear strength characteristics for these materials. Results show that the in-line thickening process significantly improves hydraulic conductivity and undrained shear strength of the fine tails. Shearing damages some of the floc structure but does not cause the material to fully return to the original state of the cyclone overflow.

The laboratory data of the in-line thickened tailings was compared with field performance at two in-line thickened tailings pilot scale ponds and with a validation standpipe test by utilizing a developed finite strain consolidation model. Good agreements were obtained between the field performance, the laboratory test results and the validation standpipe test. These good agreements confirmed the validity of the laboratory determined geotechnical parameters and of the developed numerical model

and indicated that it is possible to model large scale field performance with small scale laboratory tests.

Finally, composite tailings was made from the in-line thickened tailings and was found to have a similar segregation boundary to that of gypsum treated composite tailings made with mature fine tailings but had a much higher hydraulic conductivity and shear strength which were inherited from the flocculated fines.

Acknowledgments

I would like to express my sincere and grateful thanks to my supervisors, Dr. Don Scott and Dr. Rick Chalaturnyk, for their excellent guidance, patience, encouragement and continual technical and financial support throughout my time at the University of Alberta. It has been a great honour to work with Dr. Scott and Dr. Chalaturnyk and be part of the geotechnical group.

I would like to thank Bill Shaw of WHS Engineering who provided the opportunity to work on this interesting topic and endowed me with exceptional field supervision and industrial experience. Thank you to Nan Wang of Syncrude and Gerry Cyre of Geoforte for their field investigation support. Our laboratory experimental work could not have been performed without the great support from Syncrude's research team including Warran Zubot, Geoff Halferdahl, Ron Lewko and Simon Yuan and from our geotechnical laboratory team including Stephen Gamble and Christine Hereygers. Their swift responses and exceptional inputs during the laboratory program are greatly appreciated. Also thank you to Dr. Sean Sanders and Sorta Amarebh for recommendations on laboratory techniques. Nathan Deisman, Dr. Peter Steffler, Dr. Dave Chan and Dr. Paitoon Kongsereeparp gave me a jump start on numerical modeling and provided me with very helpful discussions. Thank you to Dr. Baki Ozum, Dr. Robert Donahue and Saidul Alam who always provided laboratory support and great recommendations on water chemistry. Thank you to Dr. David Carrier, Dr. Ed McRoberts, Dr. Gord McKenna and Dr. Dave Sego for their helpful inputs on tailings behavior and modeling.

I would like to express my sincere gratitude to Syncrude Canada Ltd. and the University of Alberta who provided financial support throughout this research program. I also would like to thank all the faculty and staff of the Geotechnical and Geoenvironmental Engineering group for providing a pleasant and friendly environment.

Special thanks to my close friends Chang Ho Lim, Chengmai Guo, Soe Moe Kyaw Win, Wonganan Sukcharoenkana, Paitoon Kongsereeparp, Arash Eshraghian, Reza Moussavi Nik and Anh Dung Nguyen for their encouragement and friendship. My thanks are extended to all my colleagues and friends in Canada and Thailand.

Finally, I would like to express my gratitude to my father, mother, brother and Mari for their love and understanding throughout my long journey in Canada.

Table of Contents

List of Tables

List of Figures

Chapter 1 Introduction

1.1 Statement of problem

The oil sands mining operations in Northern Alberta produce large volumes of tailings composed of sand, silt, clay and a small amount of bitumen. Upon deposition, the tailings segregate with the sand dropping out forming dykes and beaches and about one-half of the fines and most of the bitumen flow into the tailings pond as thin fine tailings which are only about 8% solids. In the pond, sedimentation occurs and in about two years reaches approximately 30% solid. The tailings at this point is called mature fine tailings (MFT). At this solids content the process of sedimentation ceases and the process of self-weight compression governs. Field measurements show that the tailings compress very slowly in the tailing ponds and the major reasons for this behavior are believed to be caused by a very low hydraulic conductivity and a high thixotropic strength of the material.

The very slow compression behavior of mature fine tailings causes major problems for oil sand companies to manage containment ponds and to increase the amount of the recycle water for bitumen production. This has led to considerable research on alternative solutions for tailings deposition and dewatering. Major tailings developments were the production of composite tailings and endpit ponds. In the production of composite tailings, the tailings stream is cycloned and the underflow sand is combined with MFT and a coagulant. The cyclone overflow which is mainly fines is deposited in a tailings pond and becomes more MFT.

To search for an alternative tailings technology, a new type of oil sands fine tailings called in-line thickened tailings is being investigated. The in-line thickening process is aimed to improve settling and strength behavior of thin fine tailings. To achieve these new tailings, chemical additives are used to increase hydraulic conductivity, shear strength and size of clay flocs in the cyclone overflow tailings. By binding fine particles in the low solids content of the cyclone overflow into a floc, the hydraulic conductivity is increased because the flocs are far apart, tortuosity is decreased and the mass of the falling flocs is increased. This results in tailings that can sediment

quickly to the end of sedimentation and when some compression occurs, suitable shear strength is obtained at the surface of the tailings deposit allowing a surcharge load application.

The advancement of the in-line thickening process by Syncurde was designed for the fastest rate of sedimentation, the lowest overflow solids content and the highest underflow solids content. The technology however was not developed to achieve specific engineering properties, that is, hydraulic conductivity, compressibility and shear strength of the material. In order to understand how the in-line thickening process has changed the material behavior, these specific engineering properties were studied in this thesis. Geotechnical field investigations, laboratory studies and numerical studies were carried out to understand material behavioral change in laboratory and how these properties correlate to the field behavior. The capability of a finite strain consolidation numerical model that uses laboratory determined parameters to predict a large scale field experiment was examined to determine if a small scale laboratory could possibly model a large scale field deposit. A validation standpipe experiment was also performed to model a large scale field deposit. Lastly since the in-line thickened tailings is a new source of high solids content fines, the use of the in-line thickened tailings to create composite tailings was investigated.

1.2 Objective and scope of the thesis

The objective of this research was to develop extensive geotechnical properties and understanding for the in-line thickening technology on oil sands fine tailings. In order to achieve these objectives, the research was divided into three main categories including numerical study, laboratory study and field study. These subdivisions were combined and analyzed together to establish the overall understanding of the in-line thickening process. The objectives of each component of this study can be listed as followings.

- A one dimensional finite strain consolidation model is developed, extended and examined to provide a theoretical simulation and analysis for the in-line thickened tailings in both laboratory and field scale experiments. This development is specifically aimed to explore different forms of constitutive relationships to improve a finite strain consolidation prediction.

- To use a one dimensional finite strain consolidation theory with parameters that are commonly determined in the geotechnical field to simulate slurry behavior in a continuously operating thickener. This is to support an original work on the in-line thickening technology as it was initially developed for a thickener.
- To support a field data analysis and explore implications of multidimensional flow, a quasi-multi-dimensional finite strain consolidation model is investigated.
- To study field performance of the in-line thickened tailings and extract field geotechnical parameters for the tailings.
- To use a combination of hindered sedimentation tests, compressibility standpipe tests and large strain consolidation tests with vane shear tests to capture a full range of sedimentation and consolidation characteristics of the parent cyclone overflow tailings and of the in-line thickened tailings.
- To validate a theoretical model and the laboratory determined parameters for the in-line thickened tailings, they were compared with the field behavior and with a laboratory validation standpipe test. This is performed to investigate if a small scale laboratory could possibly predict a large scale field behavior.
- To investigate the use of the in-line thickened tailings to create a composite tailings.

This study utilized Syncrude's cyclone overflow tailings produced from a hydro cyclone in the composite tailings plant to create in-line thickened tailings. The study is limited to Syncrude's best performance flocculant and coagulant used in the pilot in-line flocculation program. A numerical simulation is mainly focused on a one dimensional finite strain consolidation analysis. For an investigation of composite tailings made from in-line thickened tailings, the study is limited to a sand to fines ratio of 4:1 and without further chemical amendment.

1.3 Organization of the thesis

This thesis is organized into 10 chapters. A brief introduction to each chapter is given as followings.

Chapter 2, Literature review, begins with a brief review of the oil sands industry, origin of the oil sands and oil sands tailings followed by a detailed presentation of settling

and compression behavior of slurries. Theoretical and phenomenological aspects of sedimentation, consolidation and related phenomena were reviewed. Factors affecting settling behavior are discussed and the coagulation/flocculation process is presented. The chapter closes with a review of several experimental techniques used to study slurry behavior.

In Chapter 3, One dimensional finite strain consolidation modeling, one dimensional consolidation models were developed, investigated and discussed for both quiescent and pond filling problems. A technique of using an interaction coefficient to simulate sedimentation and consolidation phenomena was also proposed and the application of the model to a real problem was shown. Lastly, the finite strain consolidation theory was extended to capture over-consolidation and creep behavior for problematic slurry such as mature fine tailings.

Chapter 4, Thickener modeling, is part of a one dimensional model development and investigation. This chapter presents a utilization of a nonlinear finite strain consolidation theory with parameters that are commonly determined in the geotechnical field to simulate slurry behavior in a continuously operating thickener.

Chapter 5, Multi dimensional finite strain consolidation modeling, presents a development of a multi dimensional consolidation model and explores its implications on dewatering of tailings affected by containment geometry and drainage conditions.

Chapter 6, Field investigation of the in-line thickened tailings, presents results and analyses of the geotechnical field investigation which was performed at the Syncrude in-line thickened tailings pilot ponds in 2005 and 2006. Results were presented in chronological order for each pilot pond followed by a proposed settling mechanism of the material and a history matching analysis by a finite strain consolidation theory.

In Chapter 7, Laboratory investigation of the in-line thickened tailings, a full range of geotechnical sedimentation-consolidation parameters were determined by using a combination of hindered sedimentation tests, compressibility standpipe tests and large strain consolidation tests with vane shear tests. Results from the test program were combined, analyzed and compared to evaluate the impact of the in-line thickening

process on the material's geotechnical behavior. The parameters obtained in this chapter were also compared to those found in the field pilot program to determine whether the small scale laboratory tests could accurately forecast large scale field performance.

Chapter 8 presents a validation of the theoretical model and the experimentally determined parameters with a 2 m validation standpipe test performed to simulate a pond filling condition. Interface settlement, pore water pressure response, a final void ratio profile and a final undrained shear strength profile were monitored and used for the validation purposes.

Chapter 9 investigates the production of composite tailings made from the in-line thickened tailings by experiments on the consolidation and segregation behavior of the tailings and compares the results with that of composite tailings made from cyclone overflow tailings.

In Chapter 10, a summary of the observations and conclusions developed throughout the thesis is then given.

Chapter 2 Literature Review

This chapter begins with a brief review of the oil sands industry, origin of the oil sands and oil sands tailings followed by detailed presentation of settling and compression behavior of slurries. Theoretical and phenomenological of sedimentation, consolidation and related phenomena were reviewed. Factors affecting settling behavior are discussed and coagulation/flocculation process which is one of the main mechanisms to improve settling process of slurry is presented. The chapter is finalized with a review of several experimental techniques used to study slurry behavior and summary.

2.1 Oil sands tailings

2.1.1 Introduction

In northern Alberta, Canada, tar sands or oil sands have been discovered since the 1760s in Fort McMurray area. The high consumption of fossil fuel and need of more energy brought developments of oil sands industry in Alberta.

The Alberta oil sands consist of three deposits as shown in Figure 2.1 (Athabasca, Cold Lake and Peace River). These deposits contain in-place reserves of approximately 275 billion cubic meters of mineable and in-situ crude bitumen with 28 billion cubic meters as initial established reserves (ERCB, 2009). Amongst the three deposits, the Athabasca deposit is the largest deposit containing an initial volume of crude bitumen of about 223 billion cubic meters. Essentially more than half of the bitumen reserves in this deposit are contained within the Lower Cretaceous Wabiskaw-McMurray Formation. In this deposit, there is about 20.7 billion cubic meters of crude bitumen that has overburden less than 65 meters which makes it suitable for surface-mining technologies. This is unlike the rest of Alberta's crude bitumen area, where in-situ methods are required (EUB, 2004). For the surface-mining technique, 1.0 m^3 of the in-place oil sands will produce a tailings stream volume of 3.3 m^3 if the solids content of the tailings stream is 40% or a tailings stream volume of 1.9 m^3 when solids content of the tailings is 60% (Jeeravipoolvarn, 2005).

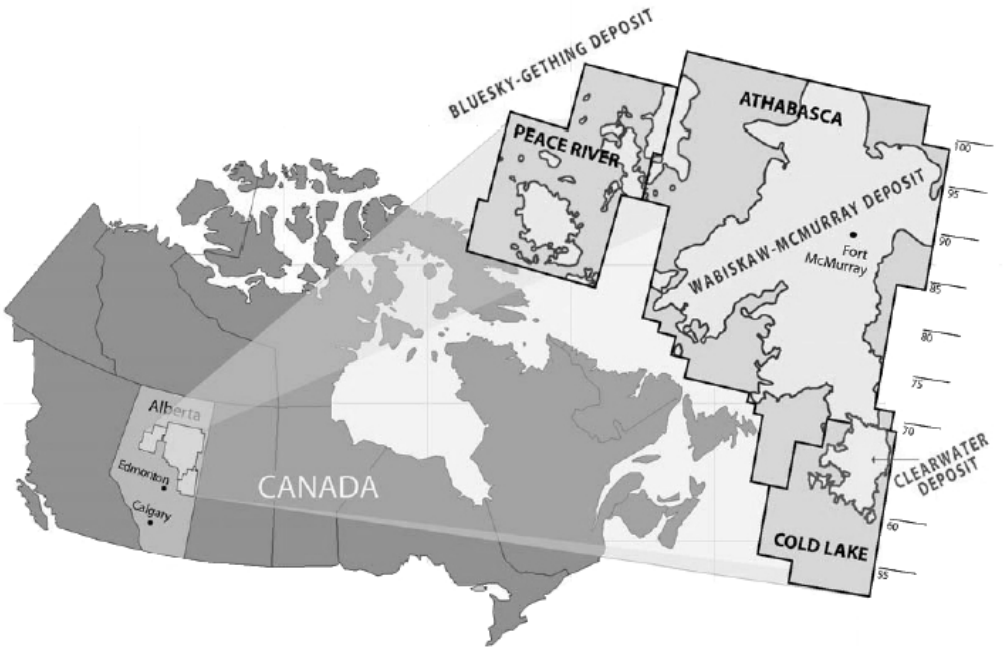

Figure 2.1 Alberta's three oil sands areas (Modified from ERCB, 2009)

The oil sands sediments generally compose of uncemented quartzose sands and associated finer grained lithologies. The sand grains, predominately quartz, are covered by a microscopic layer of water with bitumen filling the pores. The sand was deposited in these formations approximately 100 million years ago. In this period, streams flowed from the Rocky Mountains in the west and from the Precambrian Shield in the east. These streams brought sand and shale which filled in between the ridges running through Alberta and Saskatchewan. Eventually the area was the location of an ancient inland sea which spread the sand more widely. The sands then became saturated with oil which was originated at depth to the south-west and then flowed into the sand deposits. In Figure 2.2, the micro structure of the oil sands was captured by scanning electron microscope (SEM). The sand grains in the formation are locked sands with some fines accumulated at particle contacts (Figure 2.2b). These fines, however, do not have a significant contribution to the total amount of fines in the tailing streams. It is the fines from interbedded clay-shale which is broken up by the mining and extraction processes that is the major contribution (Scott et al., 2004). For the Athabasca oil sand deposit, the average bitumen content is about 9.7% by total mass. The amount of water relative to the bulk mass averages about 4.2% (EUB, 2004).

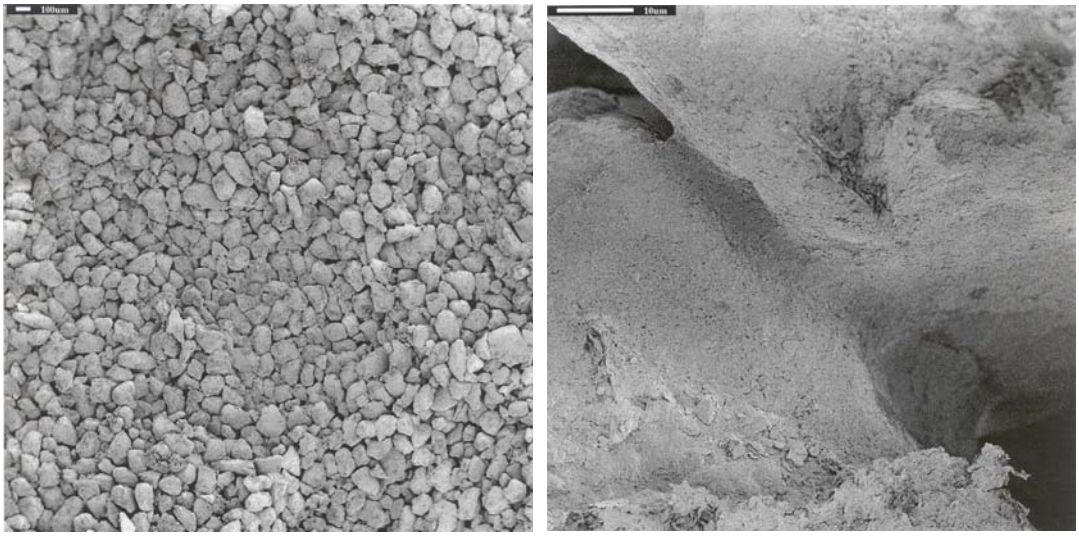

(*a*) **(*b*)**

Figure 2.2 Scanning electron micrographs of bitumen-free McMurray Formation oil sand (*a*) overview of sand structure (*b*) fines between sand particles (Modified from Touhidi, 1998)

2.1.2 Bitumen extraction process at surface-mined projects

The bitumen extraction process of the oil sands was initially based on the pioneer work of Professor Karl Clark, who used a combination of hot water, steam and sodium hydroxide (NaOH) to separate the bitumen from the oil sands and the process is called the Clark Hot Water Extraction Process (CHWE). This process adds sodium hydroxide to the oil sands slurry to aid in the extraction process. The sodium hydroxide disperses the clay-shale stringers and seams in the oil sands and the process breaks the clay-shale down to small booklets or clay flakes. The particle size distribution of resulted tailings is directly influenced by the extraction process.

A generalized scheme of the CHWE process is shown in Figure 2.3. For Syncrude, Suncor, Albian Sands and CNRL commercial productions, oil sands are mined by a truck and shovel method. From the truck discharge, the oil sands are partially conditioned in transport pipelines and at the extraction plant are digested and conditioned in large tumblers with the addition of hot water, steam and sodium hydroxide to separate the bitumen from the oil sands. This is the first stage of extraction called conditioning. During this stage sodium hydroxide is used to assist in maintaining the pH of the solution between 8.0 and 8.5 in order to separate the bitumen from the mineral solids. As a result the bitumen can be easily separated and the silt and clay particles become well dispersed.

In the second stage, called separation, hot water is added to the solution to better separate the sand particles and to float the bitumen. The bitumen is separated as a froth floating to the surface in large vessels known as primary separation vessels. The sands settle to the bottom and are removed as a tailings stream.

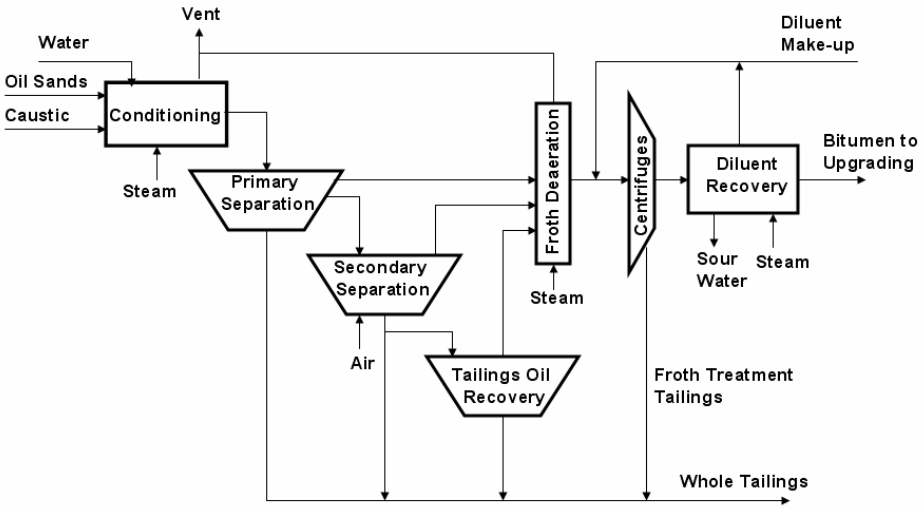

Figure 2.3 Generalized scheme of Clark Hot Water Extraction Process (Modified from Chalaturnyk et al., 2004)

After the primary separation, a central portion of the slurry, known as middlings, in the primary vessels is removed and is further processed to recover the fine oil droplets which remain unfloated in the first two stages. This stage is called scavenging. At Syncrude, the tailings and middlings streams from the primary separation vessels are combined and further processed in large deep cone vessels where additional bitumen is recovered from both tailings and middlings. The additional bitumen is then added into the primary separation vessels. The company produces bitumen froth which contains significant amounts of water and fine particles, mainly clays, which must be removed prior to the upgrading process where bitumen is converted into a light synthetic crude oil.

2.1.3 Conventional tailings disposal method

Tailings coming directly from the extraction process are called whole tailings. Whole tailings are composed of solids, water and small residual quantities of bitumen. In general, the tailings are a warm aqueous suspension of sand, silt, clay, residual bitumen

and naphtha at a pH between 8 and 9. The whole tailings generally have a solids content (by mass) varying from 40 to 60% and a fines content (by mass) varying from 10 to 30%.

Conventional tailings deposition is that the whole tailings are pumped into large tailing ponds where the coarse particles settle out to form dykes and beaches while much of the fines and residual bitumen flow into the ponds as a thin fine tailings stream at approximately 8% solids. Once the stream slows down, particulate settling and hindered settling of the fines take place leaving a supernatant water layer on the top. This water will be recycled for extraction. A schematic cross section of an oil sands tailings pond is shown in Figure 2.4.

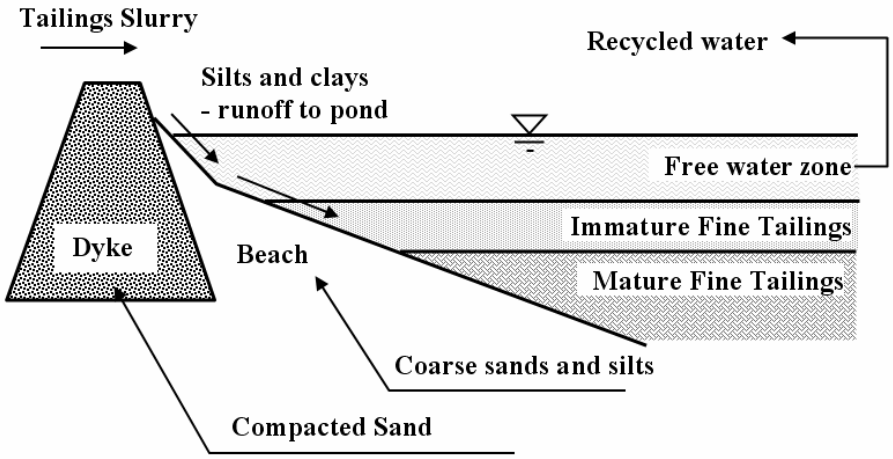

Figure 2.4 Cross section of an oil sands tailings settling basin (Modified from FTFC, 1995)

Over time, three zones have developed in the tailing ponds (Figure 2.4). The top 1 to 3 m of the pond will be a clear water zone. The release water in this zone is continuously pumped back for the extraction. Under the clear water is an immature fine tailing zone - a transition zone of water and settling particles and this zone is about 1 to 2 m thick. Below this zone is the mature fine tailings (MFT) zone, a layer of silts and clays, fine sands, bitumen, and water which increases in density with depth from sand settling through the MFT and self-weight consolidation. The sands are wind blown sands from the dykes of the tailings pond. The depths of the mature fine tailings zones vary from 15 to 20 m not including the higher sand content material at the bottom and at Syncrude, the pond can have a maximum depth of about 50 m in some areas (Guo, 2009).

2.1.4 Type of oil sands tailings

2.1.4.1.1 Mature fine tailings

In tailings ponds, after fine tailings flow into the middle of the pond, sedimentation takes place. Sedimentation of oil sands fine tailings generally takes about 2 years to reach solids content of about 20% where a matrix starts to form and after the slurry reaches this solid content, any increase in density arises from the process of self-weight consolidation (Scott and Dusseault, 1982). Mature fine tailings (MFT) is fine tailings that has fines content of about 90% and settle to solids content of 30% after which the compression of this material appears to be very slow. Above this solids content, oil sands tailings are called immature fine tailings. MFT is a major problem for the oil sands industry because 84% of the volume is water which is not released quickly via the natural process of self-weight consolidation. MFT storage therefore requires a large containment pond which posts wide environmental, engineering and economical concerns.

2.1.4.1.2 Cyclone underflow/overflow

Hydrocyclones are used in the oil sands industry to separate coarse and fine particles. The amount of sands and fines in the overflow and underflow can be adjusted by the cyclone. Generally cyclone underflow (CUF) can be categorized as sand or coarse tailings and cyclone overflow (COF) can be referred to as fine tailings. Cyclone underflow can be used as construction material and for production of composite tailings (CT). Cyclone overflow is a source of new fines and one of the contributions to new MFT. Cyclone overflow is either directly deposited into a tailings pond or further processed to improve settling behavior by a thickener or other methods.

2.1.4.1.3 Composite tailings and nonsegregating tailings

Composite tailings (CT) and nonsegregating tailings (NST) are a mix of sands and fine tailings with chemical additives to produce a nonsegregating behavior tailings that can settle and consolidate quickly.

Bromwell and Oxford (1977) discussed the success that has been obtained in experiments involving the mixing of sand with pre-thickened waste clay. In this method,

a thickener is used to increase the solids content of fine tailings and the tailings are mixed with sand. The study by Bromwell and Oxford (1977) was done on phosphatic clays and a mechanical thickening which is capable of partially dewatering the clays in a short period of time was used. They reported that pre-thickening clay slurry to 12-13% solids is required for successful sand-clay mixing and by proper mixing this clay with sand, non-segregating tailings are formed.

In the Alberta oil sands industry, an attempt to apply CT technology to MFT via geotechnical understanding was initiated by Caughill (1992) who studied the use and effects of coagulant and flocculant (mainly CaO) on the geotechnical properties of CT. It is noted that coagulants are agents that cause aggregation of colloids by changing their surface characteristics or surface charges. This is generally achieved by changing the solution electrolyte strength. Flocculants are referred to those chemical agents that cause chemical bonding of colloids.

According to Caughill (1992), settlement of the tailing mixes after flocculation occurs very quickly due to hindered settling which is dependent on the amount of the additives. Self-weight consolidation then follows at a much slower rate. A sand matrix at a void ratio of 0.75 was also found for the 17% fines content tailings and at this point the effective stress increased dramatically. Regarding the amount of the additives, there is an optimum lime concentration in terms of settling and self-weight properties of the tailings. Too low a concentration results in insufficient coagulation while too high a concentration results in a too strong floc structure resisting self-weight stress. Polymer application with lime helps prevents segregation but does not increase the self-weight consolidation.

Boratenec (2003) studied CT samples treated with 900 and 3200 g/m^3 of phosphogypsum (PG) and it was found that there was a slight difference in settling velocities and transition void ratios from sedimentation to consolidation (void ratios of 16.1 and 14.9 respectively). He also stated that the increasing PG dosage is an increase in electrolyte concentration which causes a decrease in pH, bicarbonate concentration and net interparticle repulsion. The hydraulic conductivity measurements of CT indicate a trend that more PG dosage makes the CT more permeable at low solids contents. From the SEM images, the increase in hydraulic conductivity is directly related to the average pore diameter and range of pore size. The settling and large strain consolidation test

results, however, are intriguing as the settling test does not yield a volume at steady state equilibrium required by the self-weight stresses. This raises a question on the method of compressibility determination, side friction in the tests and/or a complex compressibility behavior of the tailings at low effective stresses.

Matthews et al. (2002) summarized the development of CT technology at Syncrude Ltd. They presented a CT schematic flow showing major processes related to the production of CT (Figure 2.5). Essentially, there is no difference in their method of making CT from the conventional method which is to mix coarse and fine tailings together with chemical additives. The desired results are tailings that are non-segregated, have greater self-weight consolidation and higher permeability. Key advantages of the CT technology stated by the authors are

- The existing volume of MFT will be reduced.
- Disturbed area will be reclaimed for terrestrial use faster.
- Dry landscape at the closure will be larger which will give a positive response to public and regulations related to the long term tailings deposition.
- Tailings management and storage cost will be reduced and the increase in dry landscape promotes other cost saving activities.

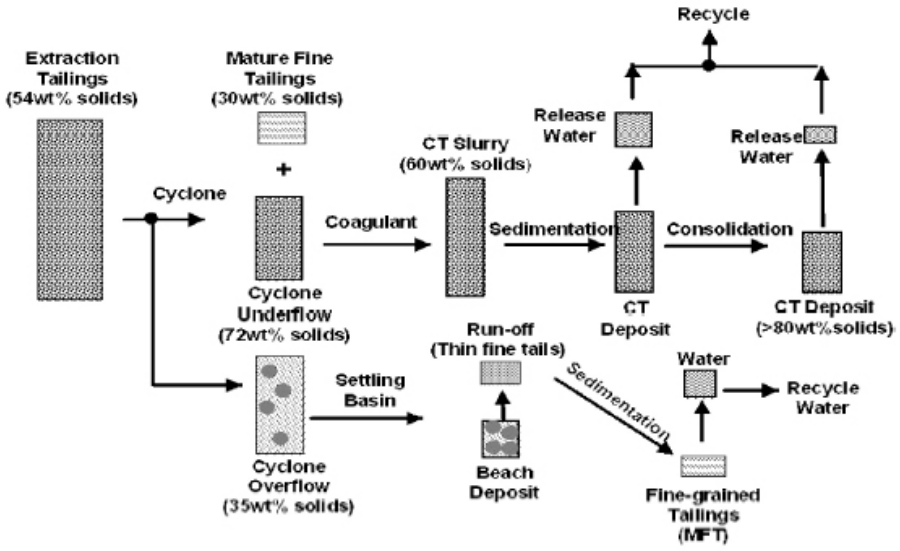

Figure 2.5 Composite tailings process (Modified from Matthews et al., 2002)

To produce a working CT, the mix must not segregate. Factors that affect segregation of CT include fines content, fines/(fines+water) ratio, particle size gradation, mineralogy of fines fraction and water chemistry. In general, coagulant is necessary in the CT process to prevent segregation. The coagulant changes the fines matrix properties so it is able to hold sand particles at low solids contents. The coagulation process can be controlled by pH adjustment, salinity, specific cation adjustment or by cation exchange (Matthews et al., 2002).

To select a proper type of coagulant, factors that need consideration are release water quality, sedimentation-consolidation rate, segregation and economics. At Syncrude, after a coagulation screening process, gypsum was selected due to its robustness and availability. Field experiments of gypsum produced CT showed that the laboratory specified gypsum amount was not able to prevent segregation in the field. Therefore the amount of gypsum in the field was increased up to two times the amount determined from laboratory. The reason for this discrepancy was given by Matthews et al. (2002) that a difference grade of gypsum was used in the field. It must be noted that the transportation and deposition techniques of the CT also affect the CT segregation behavior.

Even though CT gained credibility from experimental results, CT has been found to be difficult to produce and several relating concerns are gypsum supply, sand availability, MFT supply, feed density and deposition performance (Strueby, 2004). Major CT problems are mainly sand segregation and unreliable shear strength.

2.1.4.1.4 Thickened tailings (TT)

Thickened tailings (TT) refer to tailings which are composed of silt and clay sized particles and have been processed in a thickener with chemical additives to have a suitable deposition behavior. In the oil sands industry, this type of tailings is generally created from cyclone overflow tailings. Compared to CT, TT is generally preferred because TT occupies less volume and the coarse fraction of the whole tailings is not required thus is available as a construction material.

TT is generally prepared by mixing fine tailings in a thickener to create a discharge with solids contents ranging from 6% to 40%. This is succeeded with the aid of

various coagulant and flocculant additions at different dosages to promote dewatering (Xu and Cymerman, 1999). A thickener has a rake mechanism that transports bed material to the underflow, assists dewatering of the bed material and scrapes away deposits from the base (Rudman et al., 2008). Water is rapidly released from the tailings in the thickener. The water generally contains very small solids contents (< 1 %) which make it suitable for recycling as make up water for extraction purposes. The thickened tailings at the bottom of the thickener are then pumped to tailings disposal areas.

2.1.4.1.5 In-line thickened tailings

Bromwell and Oxford (1977) discussed that the simplest procedure to enhance settling behavior is a common-line disposal in which tailings and waste clay streams are mixed in-line and discharged simultaneously. A result is an improvement in dewatering of the waste clay but it is not significant. A more effective method is to incorporate chemical additives into the process. When a suitable reagent is injected into the tailings stream prior to sand-clay mixing, the retention of tailings in promoted. Dewatering is significantly improved. This process, however, is dependent on availability and properties of the clay and sand tailings. Because these parameters can vary significantly in practice, the implementation of this process would be technically useful only with a proper coordination with beneficiation plant operations (Bromwell and Oxford, 1977).

A similar method of common-line disposal was adopted in experimental studies at Syncrude in 2004 by in-line mixing of cyclone overflow tailings with chemical additives. According to Shaw and Wang (2005), the goal of the in-line thickened tailings program was to rapidly densify the fine tailings which would reduce short term and eliminate long term fluid shortage. In order to reach the goal, several objectives were drawn and they were to obtain solids contents over 35% and 0.2 kPa yield strength. The slope angle was to be ~1% and the deposit had to be able to sustain a hydraulically placed sand cap for reclamation. It is noted that the process at Syncrude takes advantage of a known property of cyclone overflow tailings prior to an in-line thickening process unlike the conventional common-line disposal. This has a greater advantage by having a better control over the material behavior.

A schematic flow of the ILTT process is shown in Figure 2.6. The process is to first dilute the high fines low solids cyclone overflow tailing stream followed by a three

stage chemical amendment –flocculation, coagulation and aggregation. This three stage chemical amendment was introduced by Yuan and Shaw (2007) for Syncrude oil sands tailings with sand fine ratios (SFR) from 0 to 0.4. They showed that the conventional process of using a single flocculant, a single coagulant or floculant-coagulant combination was ineffective for Syncrude marine ore tailings. They then experimented to find a new technique and found that a sequence of flocculant, coagulant and flocculant (FCF) provide the best flocculated tailings settling performance. This FCF sequence was found to produce large aggregates from Syncrude tailings with a clear supernatant water with less than 0.13% solids. Shaw and Wang (2005) then utilized this technique in an in-line thickening pilot scale program. The detailed procedure of in-line thickening used by Shaw and Wang (2005) is as following.

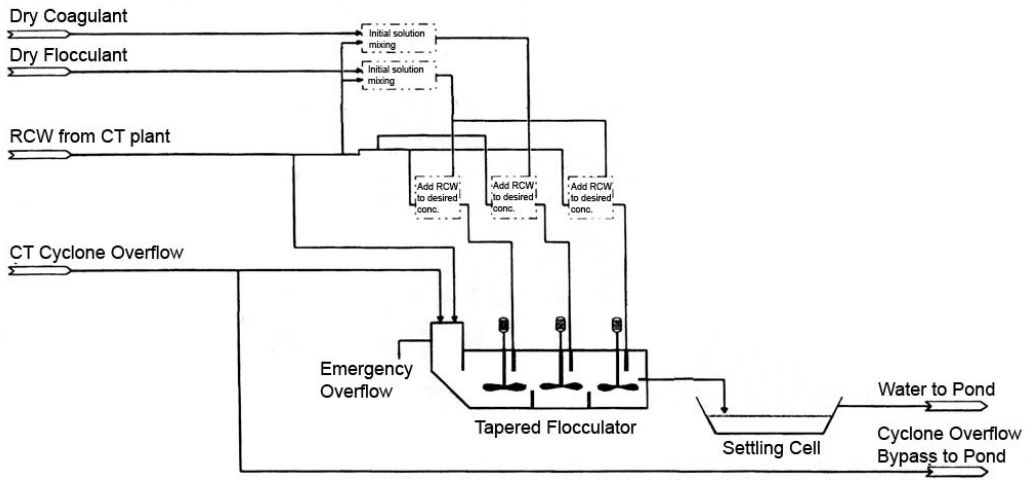

Figure 2.6 Schematic indicating significant components in In-line Thickened System (Modified from Shaw and Wang, 2005)

The feed stream was CT cyclone overflow at an average solids content of 10%. This stream was diluted to achieve 5% solids content that allowed efficient chemical mixing.

The first stage of the flocculation occurs in the first cell. The feed stream is mixed with flocculant CIBA MF 6260 at an average dosage of 250 grams (dry weight) per ton of dry solids with an impeller tip speed of 1 m/s. The mixing is done by pumping a diluted flocculant solution into the feed cyclone overflow stream. The chemical pump is

required to pump the chemical at a specific rate so that the above recipe is obtained. The solution of the flocculant is prepared with recycle water to obtain a concentration of 2 g/L. This solution is mixed with recycle water by 100:1 before mixing. Therefore the concentration is about 0.02 g/L. This is to ensure that the amount of chemical can be controlled effectively in the field. During the first stage, clay particles are attached together forming a larger clay lump. According to Yuan and Shaw (2007), very fine grained particles are not efficiently aggregated during this stage (Figure 2.7a).

The second stage of mixing is coagulation. The tailings stream from the first stage flows into the second mixing cell where coagulant MF 368 at a dosage up to 800 grams per dry ton of solids is added and mixed with an impeller tip speed of 2.3 m/s. During this stage the remaining fine grained particles from the first stage are attached together forming groups of fines (Figure 2.7b).

The last stage of the mixing process is agglomeration. The stream from the second stage proceeds to the last cell where the same flocculant is added at a dosage of 60 grams per ton of dry solids. During this stage the groups of fines particles from the first and the second stages are combined to form the largest aggregate possible (Figure 2.7c). The impeller tip speed is lower than 1 m/s to prevent aggregate rupture.

The Syncrude ILTT pilot project was composed of two pilot ponds. Two distinct discharging methods were used for each pond. The first one was discharging through a half-pipe chute (Figure 2.8(*a*)) into the west pond (located at the west side of the ILTT mixing plant). This type of discharge results in high energy which causes shearing of the ILTT aggregates. The relationship between shearing effort and aggregate size is postulated in Figure 2.9. This shearing of the aggregates results in a smaller aggregate size which is believed to have detrimental effects on the ILTT settling and compression behavior. To avoid aggregate breakage as much as possible, another type of ILTT deposition, a sub-TT discharge was used for the east pond (Figure 2.8(*b*)). This discharging method utilized an inverted spill box which was located lower than the mixing plant. The third ILTT stage (Figure 2.7(*c*)) was also moved to this box. This type of discharge provides a lower energy deposition technique. After deposition, the ILTT flowed outward forming a fan. Large aggregates were visible rolling along the bed within the flow channels.

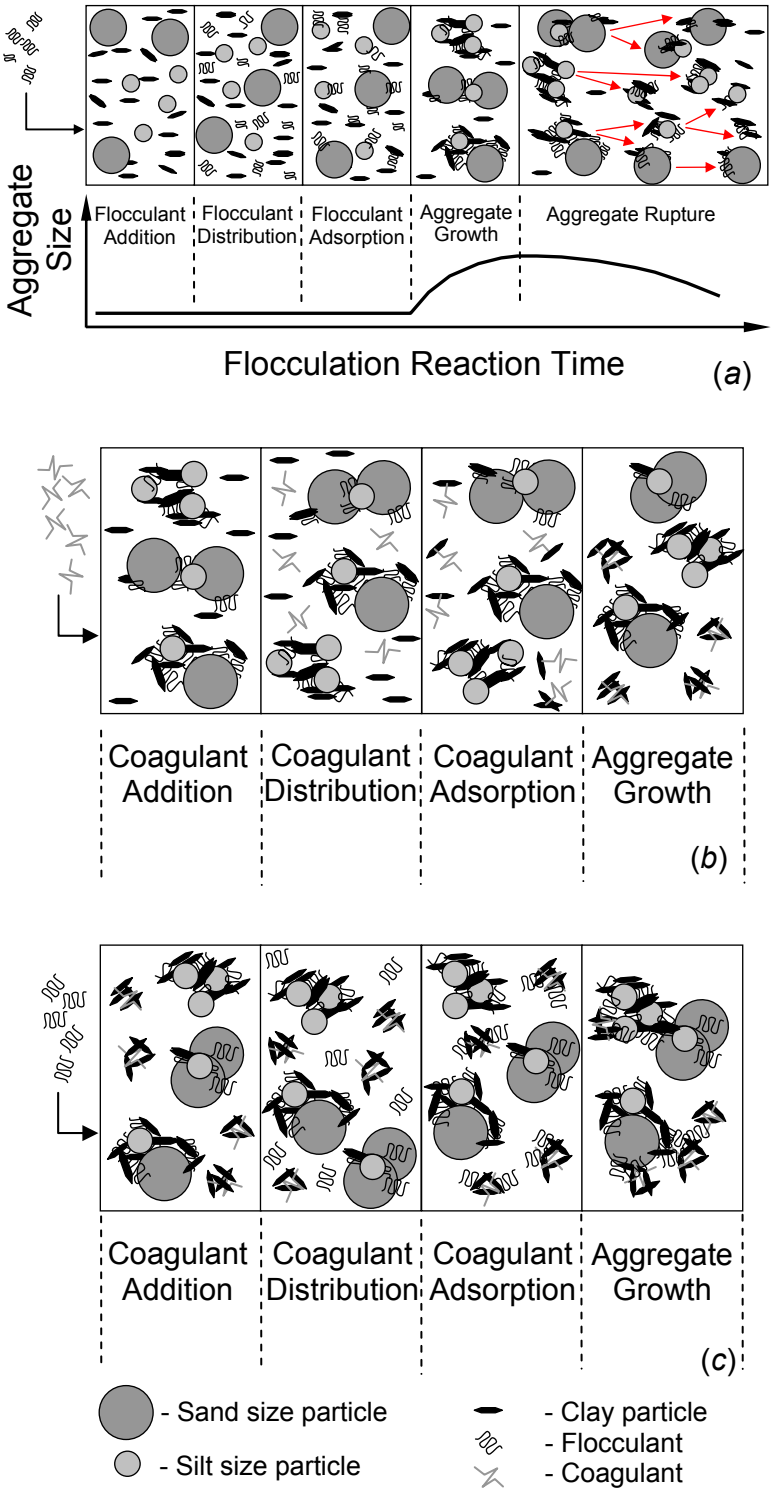

Figure 2.7 Tapered flocculation (*a*) stage 1 -first addition of flocculant, (*b*) stage 2- addition of coagulant and (*c*) stage 3-second addition of flocculant (Modified from Yuan and Shaw, 2007)

According to Shaw and Wang (2005), the west pond contained a total of 37,241 m^3 of diluted slurry at an initial 4.89% solids content. Fines contents varied between 60% and 90% with an average of 77%. The west cell slurry conductivity was 3800 μs/cm and the pH was 8.8. The actual dosage of additives used was 280, 900 and 100 g/dry ton of tailings for stages 1, 2 and 3 respectively.

The east pond contained a total of 58,728 m^3 of ILTT with an initial solids content of 3.7%. The fines content ranged from 60 to 90% with an average of 74%. The slurry conductivity was 3700 μs/cm and the pH was 8.0. The actual dosage of additives used was 280, 685 and 115 g/dry ton of tailings for stages 1, 2 and 3 respectively.

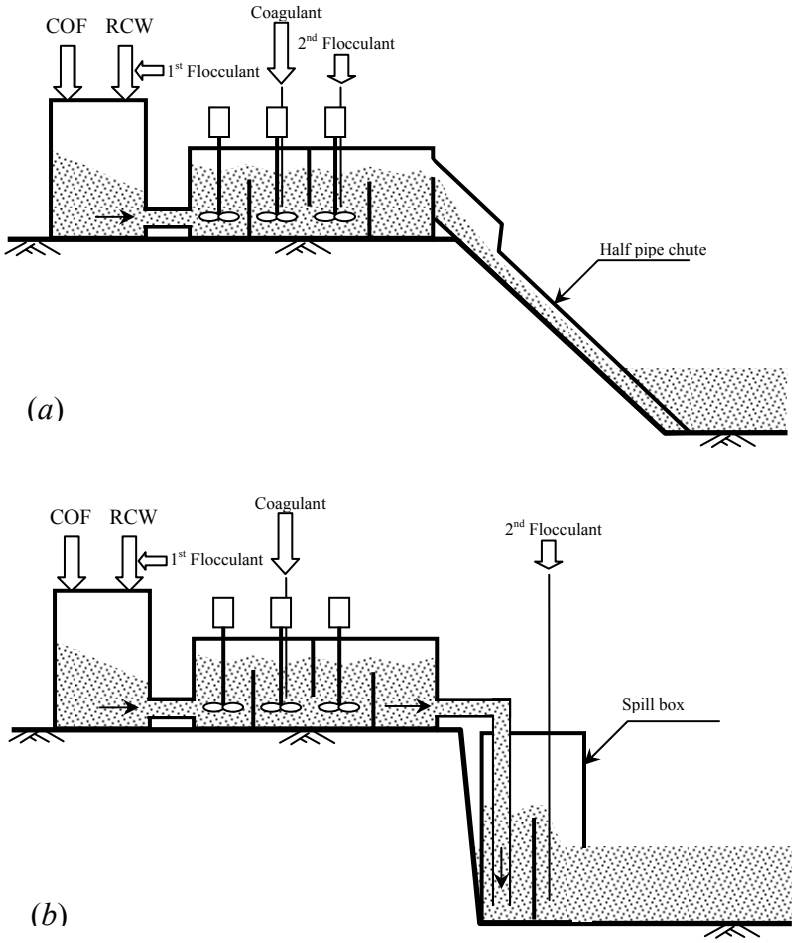

Figure 2.8 Discharge methods (*a*) a half-pipe chute discharge (*b*) sub-TT discharge

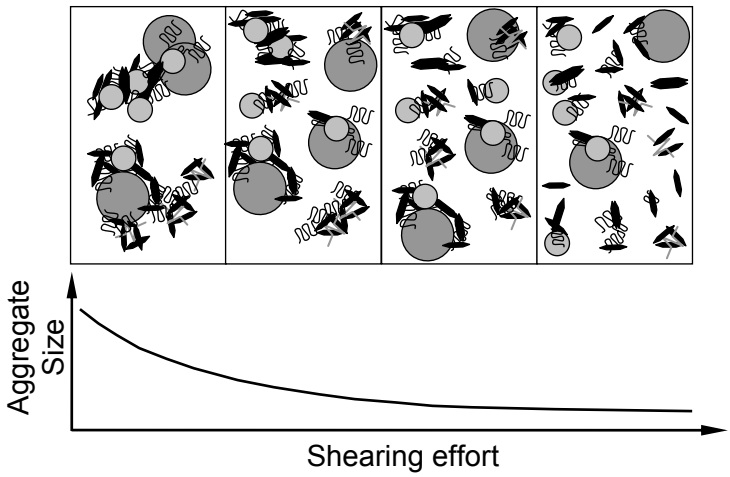

Figure 2.9 Aggregate rupture (Modified from Shaw and Wang, 2005)

According to Shaw and Wang (2005), the pilot deposits rapidly dewatered from solids contents of 4% to 20% within hours and reached 30% within a few months. The runoff water had a very low solids content of less than 0.5% during this process. They also stated that the ILTT can reach 50% solids content in a few months (modeled by FSconsol) instead of stopping at 30% solids content as with MFT. This FSconsol projection was performed with parameters obtained for Aurora tailings which are not the same as the ILTT in the pilot pond which was produced from cyclone overflow tailings at the base mine. The compression performance of the ILTT is strongly dependent on many factors (e.g. mineralogy, slurry water chemistry, types of chemical additive, mixing method and etc.) therefore soil parameters required for a finite strain consolidation analysis must be obtained directly.

The in-line thickening technology needs to be integrated with other important plant processes to make the in-line process operate reliably and consistency. The key to success of this process is to be able to define the properties of the original material prior to the process and assign a specific recipe to obtain the desired deposition behavior.

2.2 Settling processes and related phenomena

Settling processes of soil can be very complex. The word settling alone combines many processes including particulate settling, sedimentation, channeling, consolidation, flocculation and segregation. All these phenomena are either inter-related or occurring

simultaneously. In general the main processes considered in tailings deposition are sedimentation and consolidation.

The process of sedimentation to consolidation has been described by Imai (1981) as consisting of three stages which are shown in Figure 2.10(a). It is explained that "*at the first stage no settling takes place but the flocculation yields flocs. In a second stage, the flocs gradually settle and form a layer of sediment, which undergoes consolidation and reduction in water content. The boundary between the upper settling zone and the sediment is the birth place of new sediment. While the sediment grows, the settling zone becomes thinner and finally vanishes. In the last stage, all of the sediment thus formed undergoes self-weight consolidation and finally approaches an equilibrium state*".

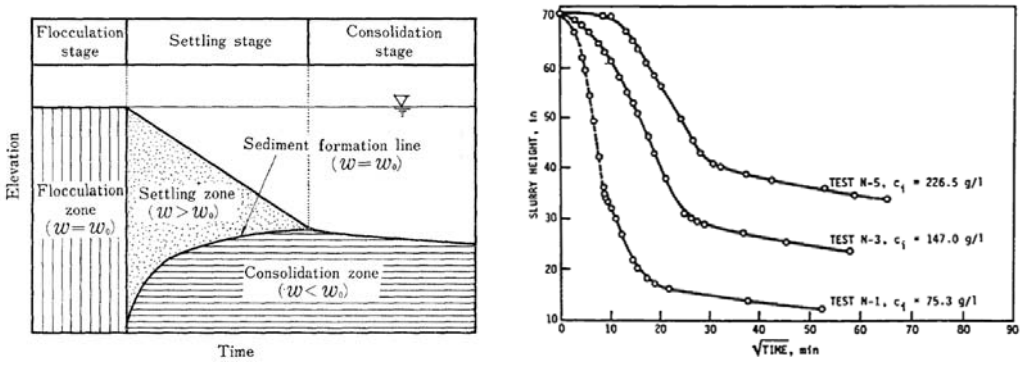

(*a*) (*b*)

Figure 2.10 The characteristics of sedimentation of clay-water mixture (*a*) The general characteristics of sedimentation (Modified from Imai, 1981), (*b*) Settling behavior of a slurry (Modified from Lin and Lohnes, 1984)

This generalized sedimentation-consolidation diagram by Imai (1981) covers the concept of these phenomena adequately while there are also other important phenomena that should be considered in the context of sedimentation and consolidation of tailings. In this section, some of these phenomena are presented.

2.2.1 Particulate settling

Particulate settling (also known as a clarification region) is defined as a condition when soil particles settle freely and do not hinder each other. This condition generally

occurs when a solids content of a mixture is very low (i.e. soil particles are very far apart). During this stage, heavier particles such as sand settle much more quickly to the bottom of a settling volume than lighter particles such as clay and silt which are left suspended in the water and settle much slower. As a result, particle segregation or particle sorting occurs during this stage. A theoretical formula for this mode of settling was presented by Stokes as Equation [2.1].

$$V_s = \frac{2}{9}\frac{r^2 g\left(\rho_p - \rho_f\right)}{\eta} \qquad [2.1]$$

Where V_s is particle settling velocity, r is a Stokes radius of particle, g is gravitational acceleration, ρ_p is particle density, ρ_f is fluid density and η is fluid viscosity.

2.2.2 Sedimentation

2.2.2.1 Phenomenon

Sedimentation or hindered sedimentation refers to a mode when soil particles settle together *en-masse*. Settling of this type leaves a typically clear interface between the top of the settling volume and the supernatant fluid. During hindered sedimentation, this interface typically moves down linearly with time. This constant rate of settling has led to a believe that the settling velocity is a unique function of solid concentration (Holdich and Butt, 1997). In this zone at low solids contents, there is no effective stress (Been and Sills, 1981).

As the soil settles and the solids content increases, there is a zone in which the mixture changes from a suspension to a soil. The settling behavior in this zone is not well defined and it can be either sedimentation or consolidation (Tan et al., 1990). Studies suggest that there may be a transition zone where effective stresses are partially developed (Tan et al., 1990; Been, 1980; Been and Sills, 1981). The end of the hindered sedimentation is considered a birth place of soil when grain to grain interaction is obtained and the effective stress significantly develops.

2.2.2.2 Theory

A sedimentation theory was given by Kynch (1952). The theory assumes that the speed of falling particles dispersed in a fluid is determined by the local particle density only. Kynch (1952) stated that the settling process is determined entirely from a continuity equation, without knowing the details of the forces on the particles. He started deriving the governing equation by introducing particle flux.

$$S = \rho v \qquad [2.2]$$

S is particle flux which is defined by the number of particles crossing a horizontal section per unit area per unit of time. ρ is density and v is fall velocity. It also assumes that the concentration is the same across any horizontal layer.

By defining x as height of any level above the bottom of the column of dispersed particles, if S varies with x, the concentration will vary. Consider layers at x and $x + \mathrm{d}x$.

$$\frac{\partial \rho}{\partial t} = \frac{\partial S}{\partial x} \qquad [2.3]$$

$$\frac{\partial \rho}{\partial t} + V(\rho)\frac{\partial \rho}{\partial x} = 0 \qquad [2.4]$$

Where $V(\rho) = -\dfrac{dS}{d\rho}$

Equation [2.4] is a governing equation of hindered sedimentation and the solution of the equation can be obtained by using the method of characteristics for hyperbolic partial differential equations or other numerical methods.

2.2.3 Segregation

Segregation refers to soil particle sorting or a tendency for certain sizes to preferentially collect in one or another physical zone (Mihiretu et al., 2008). Segregation occurs because of a low shear strength in the soil matrix which is caused by low initial density and low attractive forces between particles. A result of segregation is that

coarser/heavier particles fall to the bottom of a settling volume and leave smaller/lighter particles suspended in higher elevations. The smaller particles will settle with time but slowly. In tailing deposition, a major problem related to segregation phenomenon is that the segregated tailings contain a large amount of fines which have a low hydraulic conductivity and low self-weight stress. As a result, the retention time of the tailings in a pond is exceedingly long. Whether segregation occurs or not depends on the grain size distribution of the solids, the void ratio and the rheological properties of the fines-water matrix.

Sridharan and Prakash (1999) studied consolidation behavior of segregated and non-segregated clay slurry. They found that a general mechanism of segregation causes coarser particle and less compressible materials to deposit at the bottom while finer and more compressible materials are left at the top. This segregation causes the overall compressibility of the whole material to be less compared to a homogeneous soil because the bottom part is subjected to a higher pressure but this part is less compressible compared to the top where there is little self-weight stress. For kaolinite soil, the compressibility reduces as the effective stress increases for the segregated condition and this was explained to be caused by an increase in shear strength in the top part which was subjected to a small effective stress. For the homogeneous condition, the compressibility increases as a result of the contribution from the compression of an entire soil layer then decreases as the strength of soil develops at higher effective stress. For montmorillonite clay, the behavior of the homogeneous and segregated soils was similar excepting that the segregated one compressed less than kaolinite soils. A reason was given that in montmorillonite soils at higher water contents, the electrical forces, particularly repulsive forces, dominate. The compressibility behavior of montmorillonite soils is governed by the diffuse double layer repulsion (Sridharan and Venkatappa Rao, 1973) and the repulsion is responsible for the “overconsolidation-like” behavior in compressibility. They explained that with an increase in the effective stress, the repulsive pressure is overcome by the applied consolidation pressure therefore more compression results. But this reduction in the interparticle spacing causes, again, an increase in the double layer repulsion thus the compressibility once again decreases. Sridharan and Prakash showed that montmorillonite clays behave as an over-consolidated soil while the kaolinite does not in the low effective stress range of 0.25 to 0.8 kPa.

Mihiretu et al. (2006) showed the importance of yield strength of fine particles in his study on segregation of sands in kaolinite clay-water mixtures where the yield strength of the fine matrix contributes to sand capture. The kaolinite's rheological behavior was found to agree well with a Herschel-Bulkley model but a theoretical prediction of sand size captured by the fines matrix yield strength was inaccurate and a multiplying factor was therefore required.

The rheology, a physical property, of a slurry is one factor controlling segregation and this property is affected by type of pore fluid, a chemical property, as shown by Mihiretu et al. (2008). Islam (2008) showed that segregation behavior of clay-sand slurry is a function of the distribution of the monovalent and divalent cations on clay mineral surfaces. He showed that at constant solids and fines contents, segregation behavior can be manipulated by changing the distribution of Ca^{2+} and Na^{+} ions adsorbed to the clay mineral surfaces. Donahue et al. (2008) later performed a detailed geochemical investigation on NaOH treated kaolinite sand slurries and found that the slurries could be changed from segregating to non-segregating by increasing the exchangeable Ca^{2+} to 50% of the total cation exchange capacity (CEC) and increases in exchangeable Ca^{2+} beyond 50% did not improve segregation behavior. Donahue et al. (2008) indicated that segregation behavior is a function of the Ca^{2+}/Na^{+} ratio or divalent to monovalent cation ratio on the clay surfaces.

An attempt to model segregation was performed by Yang and Chalaturnyk (2004) who used computational fluid dynamics (CFD) to simulate segregation behavior in a one meter thickener (Figure 2.11). Results indicate that there were some differences between measurements and predictions. They pointed out that there are several factors contributing to the discrepancy. The major effect was from the flocculant used in the experiment which was not incorporated into the model. The solids content profile would be higher at the top rather than just release water if flocculant were not used in the experiment. Regardless of this the discrepancy, it was concluded that CFD can be used to optimize the design of thickener (Yang and Chalaturnyk, 2004).

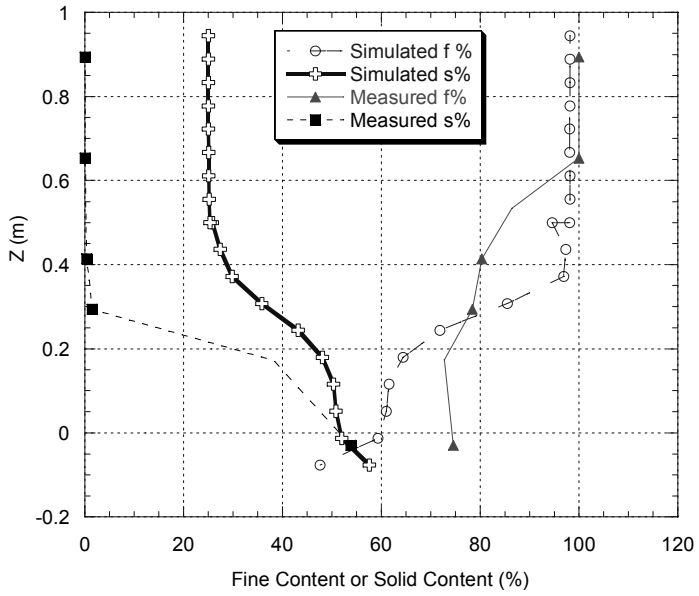

Figure 2.11 Comparison of simulated and measured solids and fines content profiles (Modified from Yang and Chalaturnyk, 2004)

To overcome the segregation problem, a segregation boundary, defined as the boundary between segregated and non-segregated mixes, is used for tailings mix design (Figure 2.12). This segregation boundary is constructed base on segregation tests and a segregation criterion. It is noted that in the oil sands industry, 95% fines capture is generally adopted as the criterion. It can be seen from Figure 2.12 that segregation can be prevented by producing higher solids content mixes, increasing fine contents or by using chemical additives to change the segregation boundary.

Most of the testing performed to define the segregation boundary is static. For dynamic segregation, a mimic of the shearing mechanism in a real practical situation is usually applied. An example of this dynamic segregation is an experiment of a 1 rpm rake shearing in a 2 L cylinder to simulate the production of NST presented by Apex Engineering and NEGRF (2005). It was found that a much higher solids content was required to prevent segregation in the shearing tests compared to the static tests and the difference can be decreased by increasing the dosage of the chemical additive. The effect of shearing can also be different depending on how the test is performed. For example, Apex Engineering and NEGRF (2005) reported that the pumping and shearing simulated by using a Philadelphia Mixer shearing 0.8 L tailings samples at 1080 rpm for 24 minutes makes the segregation boundary of sheared samples located at a slightly lower solids

content compared to non sheared static segregation tests. Small amount of air entrained in this experiment was reported to strongly affect the location of the segregation boundary.

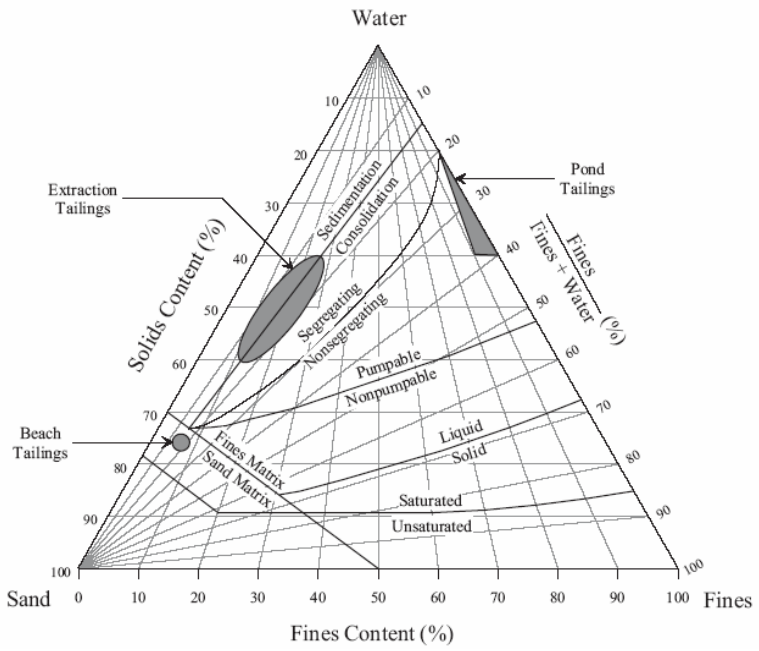

Figure 2.12 Tailings properties diagram of oil sands tailings (Modified from Azam and Scott, 2005)

2.2.4 Consolidation

Consolidation phenomenon is a process by which soils decrease in volume due to applied stresses. During this process soils gain effective stress through a dissipation of excess pore pressure. Unlike sedimentation, effective stresses exist and control the deformation of soil structure during consolidation. The boundary between sedimentation and consolidation is generally not understood and it was shown by Imai (1981) that the void ratio where the effective stresses start to exist is not uniquely defined and is dependent on the initial void ratio. This also led to his suggestion that countless compression curves exist under very low effective stresses. Similar findings were also published by Been (1980), Sills (1998) and Bartholomeeusen (2003). Although the starting void ratio for consolidation is unclear and there are countless compressibility relationships at low effective stresses, Carrier et al. (1983) made a suggestion that the initial void ratio does not significantly affect the calculation of tailings storage capacity in a pond in practice. This is logical as in a practical situation, the depth of a pond is quite

large therefore it would have much higher effective stresses than those discussed by other authors. For instance, tailings with an initial density of 1.2 g/cm^3 and a pond with a depth of 20 m, a typical depth of mine tailings deposition ponds, will have a difference of about 0.5 m or 2.5% of total height under the condition that the effective stresses are not unique (effective stresses ≤ 1 kPa). Carrier also suggested that in most practical applications, the value of an initial void ratio is approximately equal to the void ratio corresponding to the liquid limit multiplied by seven (Equation [2.5]).

$$e_i = 0.07 G_s \times w_L \qquad [2.5]$$

Where e_i is the void ratio at the start of consolidation, G_s is the specific gravity of the solids particles and w_L is the liquid limit in percent.

A selection of the end of sedimentation and the starting of consolidation is generally arbitrarily chosen due to the fact that it is difficult to distinguish.

In this section, classical theory and the finite strain consolidation theory are presented. The modeling of consolidation phenomenon by a finite strain consolidation theory is also discussed.

2.2.4.1 Classical theory

In geotechnical engineering, the settlement calculation of clays is performed by the use of a classical one dimensional consolidation theory derived by Karl Terzaghi in 1923. The theory was derived by combining a fluid flow relationship, a continuity equation and the principle of effective stress. The Terzaghi one dimensional consolidation theory is mathematically expressed as Equation [2.6].

$$c_v \frac{\partial^2 u}{\partial z^2} = \frac{\partial u}{\partial t} \qquad [2.6]$$

Where c_v is coefficient of consolidation, u is excess pore pressure, t is time and z is a one dimensional vertical coordinate.

For soft material such as oil sands tailings, the main disadvantages of this theory for consolidation prediction are the assumptions of constant material properties and small strain. Even though the classical theory is successfully used for normal geotechnical work it is not sufficient for a consolidation problem in very soft soils whose compressibility and hydraulic conductivity are highly non-linear and the large settlements occurring in soft soil can not be considered as a small strain problem. These differences have led to a development of the finite strain consolidation theory.

2.2.4.2 Finite strain theory

The one dimensional finite strain consolidation theory introduced by Gibson, England and Hussey (1967) is used to model consolidation phenomenon of soft fine grained soil or slurry. The theory was developed to unlock the restrictions of the conventional model from small strain and linearity therefore allowing more complex problems to be analyzed. The theory is often used in the slurry world of geotechnical engineering where most of its applications relate to a self-weight consolidation problem which gives answers to tailings pond containment size, strength implications and pore pressure dissipation in the slurry.

There are three formulations in the theory which are void ratio, excess pore pressure and porosity formulations. The theory assumes that Darcy's law is valid and the soil skeleton has no time dependent effect. The governing equation in terms of void ratio was given by Gibson, England and Hussey (1967) as following

$$\pm\left(\frac{\rho_s}{\rho_f}-1\right)\frac{d}{de}\left[\frac{k(e)}{(1+e)}\right]\frac{\partial e}{\partial z}+\frac{\partial}{\partial z}\left[\frac{k(e)}{\rho_f(1+e)}\frac{d\sigma'}{de}\frac{\partial e}{\partial z}\right]+\frac{\partial e}{\partial t}=0 \qquad [2.7]$$

Where ρ_s is solids density, ρ_f is fluid density, e is void ratio, k is hydraulic conductivity, σ' is effective stress, t is time and z is a reduced or material coordinate

Somogyi (1980) utilized Koppula's (1970) rearrangement of continuity and fluid flow relationships and the governing equation [2.7] becomes

$$\frac{\partial}{\partial z}\left[\frac{k(e)}{\gamma_w(1+e)}\right]\frac{\partial u}{\partial z}+\frac{k(e)}{\gamma_w(1+e)}\frac{\partial^2 u}{\partial z^2}+\frac{de}{d\sigma'}\frac{\partial u}{\partial t}-\frac{de}{d\sigma'}\left[(G_s-1).\gamma_w\frac{d(\Delta Z)}{dt}\right]=0 \quad [2.8]$$

This equation is a finite strain consolidation governing equation in terms of excess pore pressure, *u*. Another formulation is a porosity formulation by Lee (1979). The porosity formulation was cast in a convective coordinate therefore it is more difficult to program due to changes in settlement during consolidation. The porosity formulation is expressed as

$$-\frac{\partial}{\partial x}\left[\frac{k(1+e)}{\rho_f}\frac{d\sigma'}{de}\frac{\partial n}{\partial x}\right]-\left\{(G_s-1)\frac{d\left[k(1-n)^2\right]}{dn}-\frac{\partial q}{\partial n}\frac{d}{dn}\left[\frac{k}{\rho_f}(1-n)\right]\right\}\frac{\partial n}{\partial x}$$
$$+\frac{k}{\rho_f}\frac{\partial^2 q}{\partial x^2}(1-n)=\frac{\partial n}{\partial t} \quad [2.9]$$

Where *n* is porosity, *q* is applied stress and *x* is convective vertical coordinate.

It can be seen that the finite strain consolidation theory is either cast in convective or Largrangian coordinates. Euler's approach is to fix attention on an element of space through which the medium moves and to consider the sequence of events in this element. While Lagrange's approach is to consider an element of mass which always encloses the same material particles and the event taking place is described in the moving and distorting of the element as time progresses. Since in the finite strain consolidation problem, the thickness of the soil sample is continuously changing, the boundary is always moving. Thus the top boundary is time dependent and this is inconvenient to follow for each soil element. The use of Lagrangian coordinates overcomes this problem because the material spatial coordinate is fixed thus already in its exact location. In Euler's approach, the spatial coordinate is fixed on an element which is assumed not to distort. This is the case for small strain theory where distinction between the two is negligible.

All the formulations stated above are theoretically identical however different formulations will result in different initial and boundary conditions to solve the governing

equations. Therefore different formulations are utilized only for convenience for different cases.

2.2.4.2.1 Forms of compressibility and permeability constitutive relationships

In finite strain consolidation modeling, two important relationships are used: a void ratio-effective stress relationship and a hydraulic conductivity-void ratio relationship. These two constitutive relationships are used to solve the finite strain consolidation governing equation as shown in Equation [2.8] where the derivatives of effective stress and hydraulic conductivity require constitutive relationships to reduce the unknowns and solve for void ratios.

Conventional and current approaches are to determine continuous functions from an experimental data and use the functions and numerical methods to obtain the finite strain solution (e.g. Somogyi, 1980; Cargill, 1982; Carrier et al., 1983). An interpolation of experimental data points is also used to obtain the relationships (Bartholomeeusen et al., 2002). Mathematical formulas that are often used for compressibility and hydraulic conductivity include Equations [2.10] and [2.11] by Somogyi, Equations [2.12] and [2.13] by Carrier et al. (1983) and Equations [2.14] and [2.15] by Bartholomeeusen et al (2002). In Equations [2.10] to [2.15], parameters *A*, *B*, *C*, *D, E* and *F* are laboratory determined parameters.

$$e = A\sigma'^{B} \quad [2.10]$$

$$k = Ce^{D} \quad [2.11]$$

$$e = A(\sigma' + B)^{C} \quad [2.12]$$

$$k = \frac{Ee^{F}}{(1+e)} \quad [2.13]$$

$$e = A\ln\sigma' + B \quad [2.14]$$

$$e = C\ln k + D \quad [2.15]$$

The use of different functions dictates the finite strain model behavior. A reason to use different mathematical formulas is to construct constitutive relationships as close to the real soil behavior as much as possible and to provide mathematical convenience to

the solution. However, consolidation experimental data are not always used to obtain the constitutive relationships, Carrier et al. (1983) proposed empirical correlations to obtain compressibility and hydraulic conductivity from Atterberg limits. This was done similar to Skempton's (1944) approach by correlating data between liquidity index and effective stresses. An equation obtained from the correlation is combined with the compressibility to obtain the finite strain consolidation parameters.

Equation [2.16] shows a correlation between liquidity index (I_L) with effective stress. Equation [2.16] can be combined with the compressibility function [2.10] to obtain the finite strain consolidation parameters A and B via Equations [2.17] and [2.18] respectively.

$$I_L = x\sigma'^{y} - z \qquad [2.16]$$

$$A = xGs\left(\frac{I_P}{100}\right) \qquad [2.17]$$

$$B = y \qquad [2.18]$$

Similarly, permeability can also be correlated to the liquidity index (Equation [2.19]) and the finite strain parameters E and F in Equation [2.13] can be obtained through Equations [2.20] and [2.21].

$$I_L = q[k(1+e)]^r - s \qquad [2.19]$$

$$E = \left[qG_s\frac{I_P}{100}\right]^{-\frac{1}{r}} \qquad [2.20]$$

$$F = \frac{1}{r} \qquad [2.21]$$

Where A, B, E and F are finite strain parameters and x, y, z, q, r and s are empirical parameters.

Carrier et al. (1983) mentioned that the value of the Plasticity Index (I_P) has a double effect on the consolidation properties; a higher I_P will indicate that at a given

effective stress there will be a higher void ratio and a lower hydraulic conductivity. The empirical correlations by Carrier et al. (1983) are only for the preliminary design of disposal facilities and to estimate consolidation times by the finite strain consolidation theory.

Another investigation on a form of the constitutive relations was by Merckelbach and Kranenburg (2004) who presented equations for effective stress and permeability of clay-silt-sand mixtures. The equations were derived on the basis of a scale-invariant structure of the soil to enhance physical interpretation of the empirical coefficients. The equations were verified with consolidation experiments of soft mud and the results showed good agreement for the effective stress but the permeability agreement was only fair.

A recent approach is given by Wong et al. (2008) who proposed a logical mechanistic explanation of compressibility and hydraulic conductivity of nonsegregating tailings. The compressibility was divided into three stages which are stage one-coarse sand grains suspended in a fines matrix, stage two-formation of local contacts between coarse grains and stage three-formation of coarse grain skeleton. The compressibilities of sand and fines are then used to interpret their effect on the NST compressibility based on mixture theory. Good results were obtained. For hydraulic conductivity, the effect of coarse and fine particles on NST's hydraulic conductivity is similar to the use of fines void ratio to interpret hydraulic conductivity data by Pollock (1988).

Regardless of all the mathematical formulas available and empirical parameters in the literatures, constitutive relationships for detailed consolidation analysis of soft soil should only be determined from direct measurements and the mathematical form to be used should be decided by the experimental data to cover the range of void ratio that the material would experience in the field.

2.2.4.2.2 Finite strain consolidation modeling and behavior

There are generally two methods in the literatures to perform finite strain consolidation analyses. These include incremental small strain such as developed by Olson and Ladd (1979), and Yong, Siu and Sheeran (1983) and a finite strain

consolidation method such as developed by Somogyi (1980) and Cargill (1982). Incremental small strain models maintain the simplicity of the Terzaghi formulation and constitute a logical next step to extend its applicability. These models are linear in each sub layer thus they need to continuously update material properties and the coordinates of the numerical mesh during calculations which makes the solution computationally laborious. This computational complexity is dramatically reduced by using the finite strain consolidation theory approach (Krizek and Somogyi, 1984).

Conventionally the finite strain consolidation theory is numerically solved by a finite difference method with either explicit or implicit schemes. Krizek and Somoyi (1984) stated that explicit numerical techniques have the advantage that the solution is advanced from known values of the dependent variable and corresponding material properties while the implicit method when applied to nonlinear problems requires the material properties corresponding to unknown values of the dependent variable. Therefore these material properties must be either estimated or allowed to lag one time increment behind the solution. The implicit method, however, has an advantage that it is computationally more efficient and unconditionally stable. Krizek and Somogyi (1984) also stated that stability and convergence may be equally difficult to prove for highly nonlinear problems but it can be conveniently demonstrated by trial. Bromwell (1984) showed a comparison of field interface settlement with two finite strain consolidation computer programs written by Schiffman (1983) and by Somogyi (1980). The results show that Schiffman's program which is explicit finite difference gives better prediction compared to Somogyi's program which is implicit finite difference. Bromwell (1984) stated that he scaled data from the published paper and the two computer solutions, for this case at least, gave similar results. The author of this thesis believes that the early discrepancy from the Somogyi's model came directly from the assigned implicit finite difference scheme. Somogyi (1980) also stated that the fully implicit method utilizes soil parameters at a previous time step which causes parameter lagging. However the error decays when the discretization is small enough and the scheme is unconditionally stable. It is obvious that the implementation of the implicit method requires small time steps to obtain accuracy especially at the beginning of the simulation. From the author's experience in this thesis, both schemes give similar if not identical predictions given that proper spatial and temporal variations are selected.

Bromwell (1984) also compared the conventional consolidation theory with the finite strain consolidation theory and showed that the finite strain theory predicts a smaller influence of height on consolidation times than does the conventional theory, with the consolidation times proportional to about $H_0^{1.3}$ rather than H_0^2. Schiffman et al. (1984) also discussed the behavior of finite strain consolidation by first comparing the finite strain consolidation model with a conventional model. Results show that the nonlinear finite strain consolidation theory predicts a progress of settlement substantially faster than when constant parameters are assumed. This finding agrees well with field observations that the conventional theory is an over-predictor of settlement times. It is noted that although the finite strain theory predicts faster compression times, it predicts slower dissipation of excess pore pressure. This led to a conclusion by Schiffman et al. (1984) that *"the conventional wisdom which holds that deformation and excess pore pressure dissipation are in one to one correspondence is not valid"*. This difference depends on the extent of the nonlinearity of clay being studied. The authors also discussed tailings application. They showed that good interface prediction by the finite strain theory was met and indicated serious under estimation of excess pore pressure by the conventional theory. Comparison of void ratio profiles and interface settlement from Florida phosphatic clay field investigations shows excellent results over the conventional theory. Schiffman et al. (1984) also suggested that for oil sands fine tailings, organic silt and sand-clay mixtures can be considered two distinct deformable skeletons with their own deformation characteristics. Also the assumption that the void ratio is an intrinsic function of effective stress alone is questionable. The author suggested $e = f(\sigma', t)$. Regardless of the time dependent effect, Pollock (2004) presented a consolidation model without a consideration of a creep for Syncrude oil sands CT phototype and results showed that finite strain consolidation is capable of predicting interface settlement of the CT. It was proved that the finite strain consolidation theory is able to capture CT and TT behaviors but has difficulty to predict MFT compression behavior due to gas and creep. Model and/or parameter adjustments are required (Pollock, 2004).

The recommendation of time effect on compressibility leads to series of research on creep compression. There are also other behavioral factors that affect consolidation prediction. These factors will be discussed in details in Section 2.3. Other factors that have been suggested to have a significant influence on prediction capability are overdredging factor, removal efficiency factor, transport efficiency factor and

containment system efficiency (Krizek and Somogyi, 1984). On volume of material, it was stressed that without a reasonably accurate knowledge of the quantities of dredged materials that are actually placed, one cannot hope to properly predict the contained volume at any given time or to adequately size the area. These factors, although very important, are highly influenced by other operational factors not the soil behavior and will not be further discussed in this thesis.

Krizek and Somogyi (1984) after pointing out some discrepancies between prediction and observation, stated the practical approach that there are two choices when measured and calculated values do not agree, one can either tune the model or seek improved material property relationships from a sampling program. One critical statement by the authors is that "*Even a correct prediction does not necessarily validate the model or its input, because the complexity of the many factors involved allows the right overall behavior to be obtained by using a fortuitous combination of erroneous material properties, boundary conditions, and mathematical formulation". "Throughout the trying times and seemingly endless criticisms that serve to enhance our ability to handle successfully this highly nonlinear problem frought with uncertainties, we must keep the situation in perspective; toward this end, remember that we are usually more than willing to accept a ± 20% error in most of our analyses. Can we expect better for this problem?"*

After this statement in 1984, several important aspects that were not considered in the conventional finite strain theory have been advanced. These include desiccation theory for soft cohesive soils by Abu-Hejleh and Znidarčić (1995), a finite strain consolidation theory for gassy soils by Wichman et al. (2000) and a unified model by Bartholomeeusen (2003) who incorporated a time dependent compressibility surface.

For finite strain consolidation modeling behavior of the filling condition, Watari (1984) performed experimental studies on the rate of settlement and the speed of placement by fixing the amount of total solids and initial water content. Results showed that the amount of each placement little affects the speed of placement. In other words, the rate of filling does not significantly affect the final height of the volume. This is true and was earlier shown by Carrier et al. (1983) that if a pond is filled with the same tailings at different rates and periods but aiming at the same total dry solids, generally the

same pond capacity is obtained. Essentially they pointed out that the steady state solution of finite strain consolidation is independent of the filling history. This is true because the driving mechanism in the process of consolidation is the applied stress or, in this case, a self-weight stress. Given a soil with the same properties, initial conditions and applied stresses, at the end of consolidation the amount of settlement should be same regardless the filling history. It is noted that the agreed behavior of laboratory models and mathematical model indicates that the driving mechanism of the process is largely a self-weight stress.

2.2.4.2.3 Multi dimensional finite strain consolidation models

A two dimensional finite strain consolidation theory was introduced by Bromwell Engineering Inc. in 1982 and it is called pseudo two dimensional finite strain consolidation analyses. According to Somogyi et al. (1984) the theory refers to an idealization of the actual process that the soil particles are constrained to move in the vertical direction while the pore fluid may move both vertically and horizontally. Modeling by this method does not include multi-dimensional constitutive relations and failure criteria. It also precludes the ability to model lateral particle movements. Both Somogyi et al. (1984) and Bromwell (1984) did not show the governing equation of the pseudo two-dimensional finite strain consolidation in their paper however Huerta and Rodriguez (1992) presented a pseudo bi-dimensional extension and the governing equation is expressed as Equation [2.22].

$$\frac{\partial}{\partial z}\left[-\frac{kz}{\gamma_w(1+e)}\frac{\partial u}{\partial z}\right]+(1+e)\frac{\partial}{\partial x}\left[-\frac{k_x}{\gamma_w}\frac{\partial u}{\partial x}\right]+\frac{de}{d\sigma'}\left[\gamma_b\frac{\partial \sigma_b}{\partial t}-\frac{\partial u}{\partial t}\right]=0 \qquad [2.22]$$

Where x is horizontal coordinate, k_x is horizontal hydraulic conductivity and k_z is vertical hydraulic conductivity.

Huerta and Rodriguez (1992) used Equation [2.22] to model the influence of vertical drains and showed that the drain influence is obviously more important during the first stages of consolidation because it induces large pore pressure gradients localized close to it. Bromwell (1984) suggested that the two dimensional effects only became significant when the width to height ratio was on the order to 5 or less (side drainages).

One case history was presented by Somogyi et al. (1984) who indicated that quasi-two dimensional finite strain consolidation can provide accurate estimates of full-scale behavior. In their analysis, one dimensional finite strain consolidation was also used and the authors stated that the 1-*D* solution greatly underestimates the actual performance. The 2-*D* solution also underestimated the performance initially before inclusion of seepage stress.

Recently, a two-dimensional analysis of sedimentation and consolidation in various shapes of a thickener was presented by Bürger et al. (2004). An important assumption that the volumetric solids concentration is constant across each horizontal cross section was drawn. As a result, model thus gives a flat interface meaning that self-leveling was implemented through the above assumption. The simulation of a cone shape containment vessel indicated that settling velocity is decreased, different final settlements are yielded and a faster rate of sediment growth is obtained when compared to a cylinder shape containment. This approach does not explicitly consider horizontal pore water flow such as the models proposed by Somogyi et al. (1984) and Huerta and Rodriguez (1992).

2.2.4.3 Sedimentation-consolidation models

Sedimentation and consolidation phenomena of slurries should be simulated together rather than as separate phenomena. This is because the phenomena are inter-related and in practical purposes it is often required to calculate both simultaneously. Following the finite strain consolidation theory by Gibson et al. (1967) and sedimentation theory by Kynch (1952), Been (1980) considered that the only differences between the two processes, equation wise, were the presence of the effective stress principal and the coordinate used in the derivation. Been (1980) then demonstrated that consolidation and hindered sedimentation could be derived from the same basic principles and showed that hindered sedimentation can be deduced from consolidation theory by setting the effective stress to zero.

Following Been (1980), Pane and Schiffman (1985) presented a note about a method to link sedimentation and consolidation together. They proposed that for a value of void ratio greater than a certain void ratio, where the mixture behaves as a suspension,

the effective stress becomes absent and the finite strain consolidation equation reduces to Kynch's equation. They introduced an interaction coefficient, β, which connects the processes of sedimentation and consolidation via the effective stress equation as

$$\sigma = \beta(e)\sigma' + u_w \qquad [2.23]$$

Where $\beta(e)$ is an interaction coefficient which is a function of void ratio and u_w is pore water pressure.

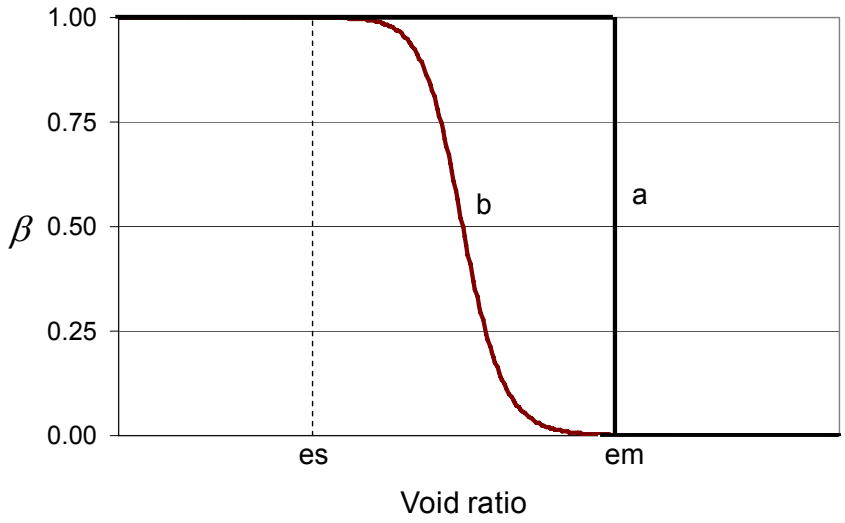

Figure 2.13 Forms of the interaction constitutive relationship (Modified from Pane and Schiffman, 1985)

The interaction coefficient is a monotonic function of the void ratio. Two reasonable forms of the coefficient are shown in Figure 2.13. One form is a step function changing the coefficient from 0 in a suspension stage to 1 in a soil stage (a in Figure 2.13) and another form is a gradual change of the interaction coefficient (b in Figure 2.13). They partly showed how to implement the proposed model in a practical situation using the method of characteristics in the sedimentation region while the integration of the consolidation region was not shown. A fully detailed implementation of the method was thus not presented. The implementation of the method has a difficulty in numerically solving the governing equation because of the discontinuity in the diffusion coefficient by the proposed interaction coefficient β. The application of the idea of an interaction

coefficient however creates confusion in the way the effective stress and the coefficient are evaluated (Tan, 1995).

Following Philip and Smiles (1982), Shodja and Feldkamp (1993) argued that the effective stress equation should be left unchanged because of the fact that in the dispersion region there is really no effective stress and the effective stress should be set to zero. They instead proposed that the distinction between the two processes should be done through constitutive models constructed to describe a material behavior. Shodja and Feldkamp (1993) stated that the constitutive model should be one that changed compressibility abruptly from a finite value to infinity. They proposed a threshold function to control the rapidity with which the compressibility changes from compressible to infinitely compressible. This idea is similar to the interaction coefficient of Pane and Schiffman (1985) in that it essentially controls the presence of effective stress. This method again leads to a difficulty in solving the governing equation as the equation will behave like a hyperbolic partial differential equation during sedimentation and change to a hyperbolic-parabolic differential equation when the threshold void ratio is reached. Similar to Pane and Schiffman (1985), they presented the numerical prediction by a finite element method without any application to a real problem.

Masala (1998) proposed a one dimensional coupled sedimentation consolidation numerical model which is derived from both conventional sedimentation and finite strain consolidation. Based on the fact that the hydraulic conductivity of slurry materials extends to both sedimentation and consolidation phases regardless of the presence of effective stresses, they used the hydraulic conductivity as a hydrodynamic interaction or a constitutive law for solid-fluid interaction in suspensions. The author derived a governing equation in terms of solids concentration for mathematical convenience and used an explicit finite difference method to solve the governing equation. Masala (1998) indicated that there is a difficulty in modeling their governing equation in Eulerian coordinates with explicit finite difference. They also tried the TVD and ENO schemes and indicated that the schemes were unable to capture discontinuity properly. They then used the Lagrangian coordinates for the governing equation and solved it by the Eulerian time forward marching scheme. It was found that this method works quite well when the time step is decreased for a uniform initial condition. The predictions in their paper indicate

good agreement with experimental results given by Toorman (1999) but step density profiles observed in many literature experiments were not shown or simulated.

The above mentioned models are referred as geotechnical formulations (Gibson et al., 1967) which are constructed mainly from the principal of effective stress, conservation laws and Darcy-Gersevanov flow relationships. There is another formulation used in the chemical engineering field and it is called a fluid dynamic formulation (Auzerais et al., 1988). Eckert et al. (1996) showed that theoretically both fluid dynamic and geotechnical formulation are identical with only a different frame of reference. In fluid dynamic formulation, the spatial coordinate is used while Lagrangian is used in geotechnical formulation. They also showed that the modified model of Kynch theory to allow the matrix to support loads (Auzerais et al., 1988) can predict sedimentation phenomenon quite adequately. They further compared their model with the Bustos and Concha (1988) model which was developed by another method based on fluid dynamics principles and qualitatively good agreement was obtained. The difference of their model and Bustos and Concha's model is that the Bustos and Concha's model was nonlinear and the solutions were discontinuous.

2.2.5 Desiccation

Desiccation is a process of drying and cracking. Desiccation affects consolidation by changing stress, degree of saturation and drainage path. A desiccation model is generally applied to an arid area where evaporation is considerably more than precipitation.

Seneviratne et al. (1996) proposed a finite strain consolidation model with evaporation. The evaporation mechanism in their model produces a similar effect to desiccation in that as the evaporative potential increases more than the water available suction is generated. This causes the top surface to be under suction pressure similar to when it dries. Earlier, Abu-Hejleh and Znidarčić (1995) proposed a finite strain consolidation model with desiccation for fine grained soils and they illustrated that their physical model gives a correct sense of what happens in practice. The process of consolidation and desiccation is modeled in four consecutive segments which correspond chronologically to the phases that a soft soil undergoes in the field after deposition. These

phases are one dimensional consolidation, one dimensional shrinkage, propagation of desiccation vertical cracks with tensile stress release and three dimensional shrinkage. Their model is in qualitative good agreement with the reported observations. The model does not include sedimentation and quantitative verification is left for future work. Another model was developed by Qui (2000). This model is capable of predicting sedimentation, consolidation, desiccation, crack initiation, crack propagation, crack dimensions (spacing, depth and width), tailings volume, and water available for recycling. He concluded that the model works well for both sandy and clayey tailings and it has the ability to predict the initiation and propagation of a primary desiccation crack within a tailings deposit. From simulation results provide by Qui and Sego (2007), sedimentation was not studied in detail and further verification of this model is needed. Desiccation modeling is beyond the scope of this thesis and will not be further discussed.

2.2.6 Gas generation

Classification of unsaturated soil can be divided into three main different soils (Figure 2.14 (*a*), (*b*) and (*c*)). Soil(*a*) is a soil with a low degree of saturation where the gas phase is continuous but the water, forming menisci at the grain contacts, is discontinuous. At intermediate saturation levels (Soil(*b*)) both water and gas are continuous with a high degree of saturation and Soil(*c*) is a soil where the water is continuous but the gas, in the form of discrete bubbles, is discontinuous.

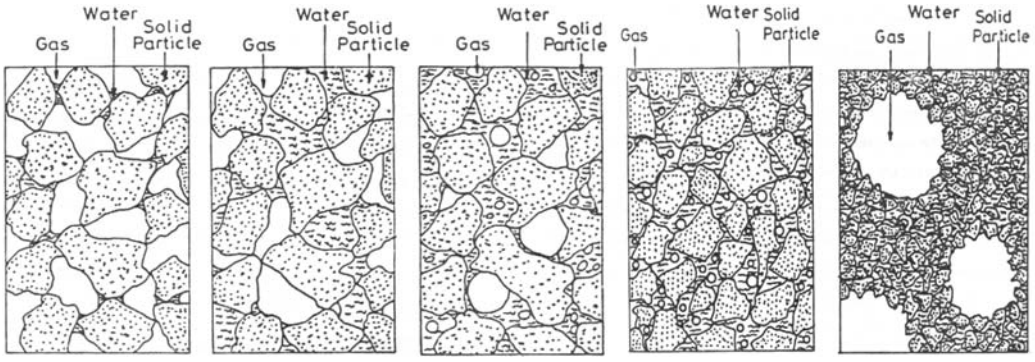

Figure 2.14 Unsaturated soils (*a*) continuous gas, discontinuous water (*b*) continuous gas, continuous water, (*c*) discontinuous gas, continuous water (*d*) gas bubble much smaller than soil particles (*e*) gas bubbles much larger than soil particles. (Modified from Wheeler, 1988)

From SEM and laboratory experiment, oil sands fine tailings can be classified as Soil(*c*) namely gassy soils (Nageswaran, 1983). Soil(*c*) can be further refined into soil with gas bubbles much smaller than soil particles (Figure 2.14(*d)*) and soil with gas bubbles much larger than soil particles (Figure 2.14(*e*)). According to SEM images of the gassy oil sand tailings, gas bubbles are much larger than soil particles (Guo, 2009).

For Syncrude oil sands tailings, biological gas generation started in the mid 1990's and it released carbon dioxide and methane. This gas generation is found to be caused by a mathanogen - a micro organism in the tailings. The gas generation occurred after depletion of sulfate from the pore water. This is because the methanogens and Sulfate Reducing Bacteria (SRB) are competing for some electron donors and the utilization of available substrates such as H_2 or acetate by SRB yields more energy than that by methanogens. Therefore SRB obtain more energy and out-compete the methanogens if sulfate is available. As sulfate is consumed and reduced, the lack of sulfate directly reflects the low amount of SRBs and the increase of the methanogens. With the low sulfate concentration, gas generation is not inhibited. For CT, gypsum ($CaSO_4$) which is used in the CT process contains sulfate thus the SRB activity is stimulated. With time, it is hypothesized that the methanogenesis will commence. Details about effects of sulfate on methanogens and SRBs can be found elsewhere (Fedorak et al., 2002; Holowenko et al., 2000).

Guo (2009) studied the gas generation behavior of Syncrude MFT and showed that in small-scale column tests microbial activity and biogas generation can accelerate water drainage from the MFT, and acetate itself has little influence on MFT densification except in its role in stimulating microbial activity. Large cracks and fractures were observed during intense microbial activity. Combined data analysis suggested that the gas generation causes changes in the MFT structure which results in increasing the MFT's hydraulic conductivity therefore increasing the rate of compression. The densified MFT has become more aggregated than that before microbial activity and some large fractures could become favorable drainage paths for water drainage and gas bubble migration.

Wichman et al. (2000) developed a self-weight consolidation computer program to simulate the consolidation of the gassy sludge from Rotterdam harbor, Netherlands. Assumptions in their theory are that gas voids are fixed in the soil skeleton, gas void ratio

is constant across the bed height, in-situ gas pressure is equal to the total vertical stress plus atmospheric pressure, the initial increase in gas content occurred instantaneously and gas void ratio at atmospheric pressure remained constant. The computer simulation and laboratory tests demonstrated that the effect of the gas is to retard the self-weight consolidation and the final settlement is less compared to the saturated case. Because of the presence of gas, the self-weight per unit volume is less effective and the drainage path lengths are increased. It is noted that their finding is opposite to the experimental study by Guo (2009) mainly because there was a gas migration and change in drainage path in the later case.

2.3 Factors affecting settling behavior of slurries

In this section, several factors affecting the settling behavior of slurries are reviewed. Some of the factors have been previously reviewed by Jeeravipoolvarn (2005) and Suthaker (1995) thus the discussion in this section is only confined to current analogy and available data of the compression behavior of oil sands tailings and similar slurry.

2.3.1 Compressibility and creep

Compressibility is the most discussed subject in slurry consolidation. This is because it constitutes the response of soil particles to the applied pressure (i.e. matrix compressibility) and having an appropriate compressibility will lead to a better estimation of settlement. The compressibility of oil sands fine tailings is showed in Figure 2.15. It can be seen that the compressibility of the oil sands fine tailings is not unique and is dependent on the initial void ratio and the compressibility indicate over-consolidation behavior. The over-consolidation behavior is believed to be caused by a thixotropy gain in strength from bonding/structural change between soil particles.

This compressibility behavior that depends on initial void ratio is similar to other findings in the literature (Scully et al., 1984; Imai, 1981; Been and Sills, 1981). It can also be observed from Figure 2.15 that unlike normal slurry, this tailings compressibility shows apparent pre-consolidation behavior at a low effective stress of around 1 kPa. At higher effective stresses, all the compressibility values start to converge around an effective stress of 10 kPa. It is noted that Scully et al. (1984) who tested a phosphatic tailings also found that the compressibility curves show apparent pre-consolidation effect

in the low effective stress range of 0.1 to 1 kPa and Sridharan and Prakash (2001) show that montmorillonite clay behaves as an over consolidated soil in an effective stress range of 0.25 to 8 kPa. Similar converging behavior was also shown by Myint Win Bo et al. (2003) who suggested that the transition between ultra soft soils to Terzaghi soils is approximately at an effective stress of 10 kPa.

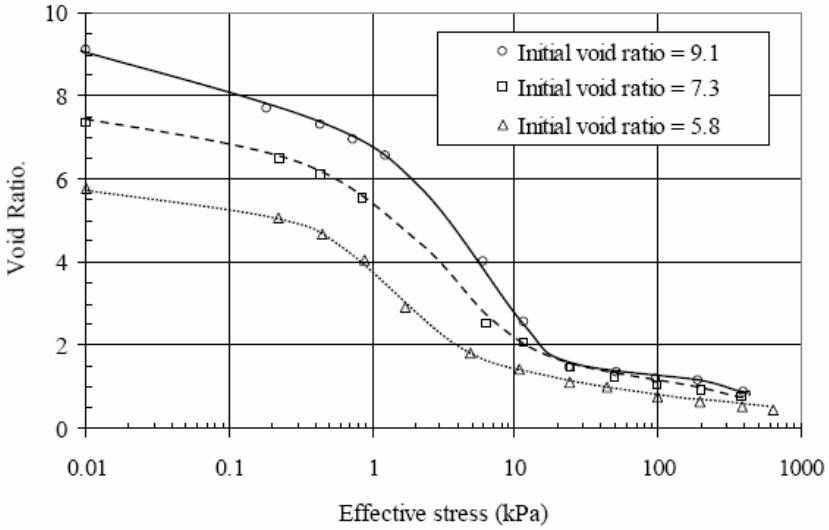

Figure 2.15 Compressibility of MFT (Modified from Suthaker, 1995)

To be able to capture this non unique compressibility behavior in a numerical model, the most appropriate way is to include time in the constitutive relation in a form of void ratio, effective stress and rate of compression (Bartholomeeusen, 2003; Kim and Leroueil, 2001; Imai and Hawlader, 1997; Leroueil et al., 1985; Bjerrum, 1967). Bartholoeeusen (2003) was the first one who utilized a compressibility surface in a form of e, σ' and $\dot{e}$ for slurry. This concept originated from Bjerrum (1967) and Leroueil (1985) and the difference is that a compressibility surface function and a fluid dynamic formulation are used by Bartholomeeusen (2003). To use this method, a compressibility standpipe test is performed with X-ray density measurements which results in void ratio and effective stress data at different times (Figure 2.16a). In order to make use of these data, void ratio at different times is plotted in material coordinates and for separate soil layers. For each layer, the change in void ratio with time can be obtained thus yielding rate of void ratio ($\dot{e}$). Void ratio and effective stress data for different rates of void ratio

change are then obtained (Figure 2.16b). Bartholomeeusen used a surface function (Equation [2.24]) for this set of curves.

$$e = A_s\left(\sigma' + Z_s\right)^{B_s} + \frac{\dot{e}}{C_s} + D_s \qquad [2.24]$$

Where A_s, B_s, C_s, D_s and Z_s are calibration parameters.

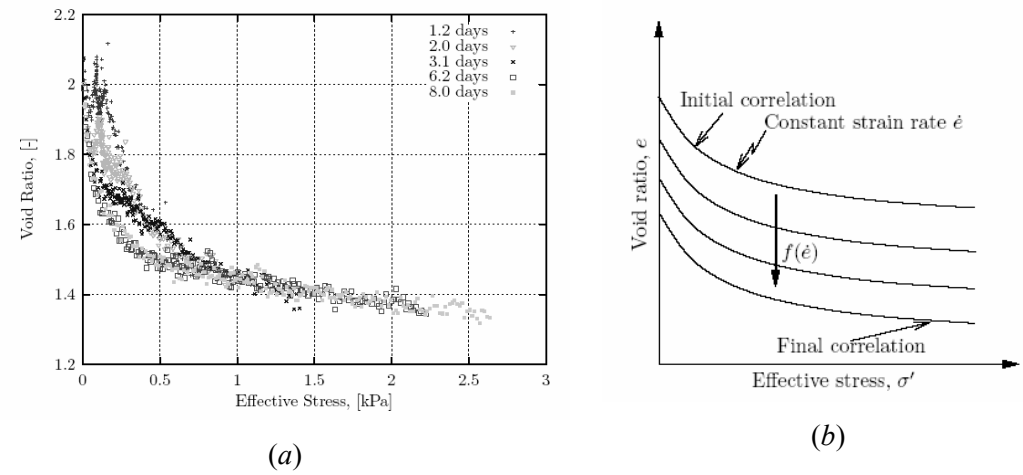

(*a*) (*b*)

Figure 2.16 Creep and Compressibility (*a*) compressibility experiment Sidc3 (*b*) Theoretical approach (Modified from Bartholomeeusen, 2003)

2.3.2 Hydraulic conductivity

Another constitutive relationship used in the finite strain consolidation model is the hydraulic conductivity-void ratio relationship. Elnaggar et al. (1973) performed a numerical demonstration of how the consolidation behavior is affected by non-Darcian flow. The hypothesis of his work is that under a low hydraulic gradient the movement of water in a soil mass is largely influenced by the force field existing between soil particles but under a high gradient this effect is relatively small. According to the authors, this was drawn from considerable published evidences. Elnagger et al. (1973) assigned a four parameter model for the velocity-gradient relationship to Terzaghi's conventional consolidation theory. It was found that the rate of consolidation for soils which exhibit non-Darcian flow behavior is less than that predicted by the conventional theory. As time passes, the modified theory indicates that the rate of pore pressure dissipation may be considerably less than the conventional theory.

Scully et al. (1984) showed that at higher void ratios by measuring permeability with a flow pump permeability test, the value of hydraulic conductivity is generally lower than that measured by constant rate of deformation (CRD) test. This lower hydraulic conductivity value, in turn, gives better agreement between theory and experiment. The difference is the CRD test uses back calculation to obtain hydraulic conductivity during compression while the flow pump test is a direct measurement at the end of each multiple step loading. The hydraulic conductivity of the flow pump test was performed at hydraulic gradient of 2 and lower while the hydraulic gradient during the CRD test was not reported by the authors. According to Scully et al. (1984), by measuring hydraulic conductivity at hydraulic gradients smaller than those used in the flow pump test, lower hydraulic conductivity values were observed which provided a much better agreement of theory with centrifugal prototype.

Bowders and Daniel (1987) investigated what concentration of organic chemical in pore water significantly changes the hydraulic conductivity of clays. Results of their investigation showed that dilute organic chemicals (less than 80% by volume in an aqueous solution) have little effect on hydraulic conductivity of compacted clays. Their results support a hypothesis that if an organic liquid does not affect sedimentation characteristics or Atterberg limits (compared to water), the liquid will not affect hydraulic conductivity. If the liquid does affect sedimentation and Atterberg limits, the liquid may or may not affect hydraulic conductivity. They concluded that hydraulic conductivity testing is required to determine whether hydraulic conductivity is affected or not.

The earlier statements by Elnagger et al. (1973) and Scully et al. (1984) imply that the lower the hydraulic gradient the lower the hydraulic conductivity. This is opposite to the hydraulic conductivity behavior found for oil sands MFT by Suthaker (1995) who showed that lower hydraulic gradients will result in higher hydraulic conductivities. Suthaker (1995) postulated that a residual bitumen in the pores flows into pore throats to block flow paths at high hydraulic gradients and suggested that the laboratory hydraulic conductivity test must be performed at the field hydraulic gradient to obtain representative values. As the field hydraulic gradient caused by self-weight of low density MFT is very small, laboratory permeability test gradients must be very small.

According to many field measurements and laboratory verification standpipes for oil sands fine tailings, a discrepancy between theory and measurement often exists. A theory which applies Darcy's law and laboratory experiments that uses a relatively high hydraulic gradient to measure hydraulic conductivity to construct a constitutive relationship generally overestimates reality. Non-Darcy flow behavior (Elnagger et al., 1973; Scully et al,. 1984) may indicate a reason for this discrepancy as the low hydraulic gradient caused by self-weight stress could result in the hydraulic conductivity of the tailings being much lower. However, this contradicts the experimental results of Suthaker (1995). It is also noted that Pollock (1988) performed hydraulic conductivity measurements on 1982 MFT. Pollock stated that there was no indication of a threshold gradient and the flow velocity was only marginally faster when approached from a smaller gradient. He explained that the large flow velocity most likely caused a migration of the fines or bitumen to decrease the permeability. His hydraulic gradient vs. flow velocity plots however do not show a clear deviation from Darcy's law. Future research is still required to understand the flow behavior of fluid in the oil sands fine tailings.

2.3.3 Thixotropy

Thixotropic phenomenon is defined as an isothermal, reversible time dependent process occurring under conditions of constant composition and volume whereby the material stiffens while at rest and is softened or liquefied by remolding (Mitchell, 1993). The mechanics of thixotropy is explained by van Olphen (1977) that shear causes breakdown of the particle links in the soil skeleton structure of the flocculated system and the restoration of the original yield strength at rest is caused by the Brownian motion bringing the particles back together. Thixotropy stiffening is essentially the same as slow coagulation in a dilute soil therefore the rate of thixotropy will depend on the size of the residual energy barrier (van Olphen, 1977).

The apparent over-consolidation behavior in oil sands fine tailings is believed to be caused by thixotropy. This over-consolidation behavior is a disadvantage to dewatering because it likely resists consolidation due to self-weight and applied stress (Somogyi and Grey, 1977). It was suggested that the dewatering has to be done concurrently with pond filling or before pond filling. Such dewatering may include

installations of sand drains or wick drains which can be completed on the extremely low bearing capacity surface (Somogyi and Gray, 1977).

Although the above discussion about the compressibility and thixotropy is of interesting a calculation of settlement including the apparent over-consolidation pressure shows that the effect is not significant (Section 3.4). An effort to empirically incorporate time dependent compressibility in the model also showed only a small effect. It is known that the thixotropic behavior in oil sands tailings causes the material to stiffen up with time, it develops gel and this jelly-like material has a significant increase in shear strength (Banas, 1991; Miller et al., 2010). As discussed by Scott et al. (2004), the true effective stress should increase following the increase of the shear strength by thixotropy. The (R-A) forces in the true effective stress equation (Mitchell, 1993) then is not equal to zero and is expected to increase with time due to thixotropy. Achari et al. (1999) indicated that the electrical double layer around clay particles affects the hydraulic flow and they proposed a cluster model to predict hydraulic conductivity of clays. Because the double layer is directly related to the (R-A) forces, it is not unreasonable to argue that thixotropy changes the hydraulic conductivity in clay soils as well. It would appear necessary to investigate this stiffened state of material for other important characteristics of the material, especially hydraulic conductivity, as it will improve material understanding, constitutive relationships and consolidation simulation. It is noted that there is evidence indicating that a change in material consistency can affect the hydraulic conductivity (Bowders and Daniel, 1987).

2.4 Clay-water electrolyte system

2.4.1 Double layer theory

Soil does not have a net electrical charge. The particle charge must be internally compensated in the soil. The balance of charges in soil is incorporated in the concept of the electrical double layer (EDL). Soil particles can obtain charges from imperfection within the interior of the crystal lattice and preferential adsorption of certain ions on the particle surfaces. Configuration of the electric double layer is shown in Figure 2.17(*a*). The double layer consists of a particle charge and an equivalent amount of ionic charges which are accumulated in the fluid near the surface of the particle.

Figure 2.17(*b*) shows potential energy distribution with particle separation distance. The double layer provides that the repulsive potential V_R reflects the electric double layer repulsion and the attractive potential V_A is from the van der Waals attraction. In detail, the total repulsive force is a combination of double layer repulsion, entropic repulsion, short range hydration repulsion and born repulsion while the total attractive force consists of van der Waals attraction, electrostatic attraction, bridging of particles by poly functional long-chain compounds and bridging by a second immiscible liquid component (van Olphen, 1977).

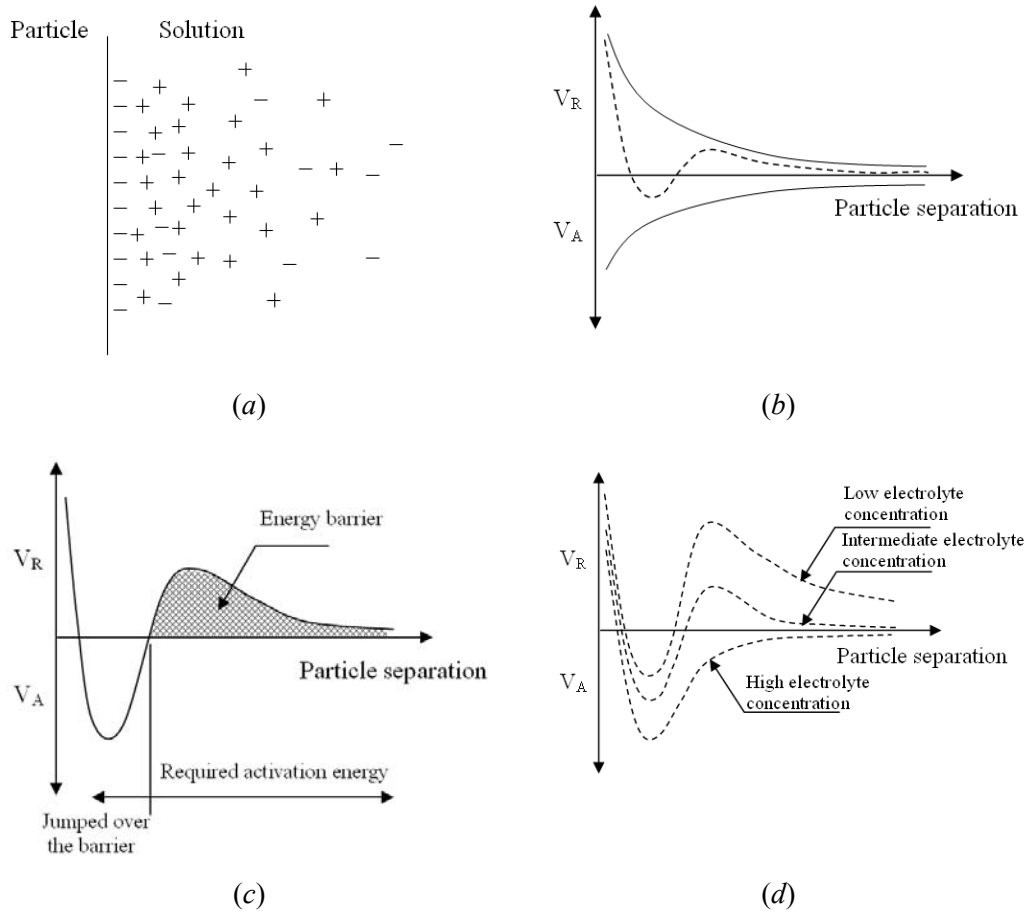

Figure 2.17 Clay-water electrolyte system (*a*) electric double layer by Gouy, (*b*) Balance of the energy on particle (*c*) Energy barrier (*d*) Repulsive and attractive energy as a function of particle separation at three electrolyte concentration (Modified from van Olphen, 1977)

In order to bring two particles into contact, energy is required which must be greater than the energy barrier (Figure 2.17(*c*)). To lower the energy barrier and ease particle agglomeration, an effective method is to change electrolyte concentration (Figure

2.17(*d*)). For high electrolyte concentration, if particles come close, they will agglomerate while for low electrolyte concentration, the agglomeration takes a long time and the soil is considered to be stable. The compression of the EDL by the electrolyte concentration can be explained through Gouy-Chapman theory expressed as Equation [2.25]. This equation indicates that the increase in electrolyte concentration results in a thinner electric double layer.

$$t = \sqrt{\frac{\varepsilon KT}{8\pi e^2 v^2}} \qquad [2.25]$$

Where t is electric double layer thickness, ε is dielectric constant, K is Boltzman constant, T is temperature, n is electrolyte concentration, e is elementary change and v is ionic valence.

The EDL concept is also used as part of an explanation of a combined pH and electrolyte influence on coagulation behavior of kaolinite clays (Tombácz and Szekeres, 2006). One layer of kaolinite clay is composed of one silica-tetrahedron sheet $(Si_4O_{11})^{6-}$ and one alumina octahedron sheet $Al_2(OH)_6$ and the sheets are connected by van der Waals force and hydrogen bonding. The silica-tetrahedron and alumina octahedron face are referred to as T-face and O-face respectively. Due to crystal lattice imperfection and isomorphous substitution, the T-face contains permanent negative charges (Figure 2.18). At O-face and edge of the clay, however, an electrical charge is highly dependent on pH. According to Tombácz and Szekeres (2006), when pH is lower than the pH of point of zero charge (PZC), both the O-face and the edge are positively charged. The charge is opposite when the pH is higher than PZC. pH at PZC is measured where the net surface proton charge is zero and for kaolinite, pH at PZC is around 6 to 6.5.

The heterogeneous surface charge of kaolinite clay particles has an implication on particle coagulation. This is explained through a concept of EDL in Figure 2.19. When the pH is higher than pH_{PZC} and a low electrolyte concentration is given, the kaolinite clay particles could form a dispersed and deflocculated structure. As pH is altered to lower than pH_{PZC} at the same low electrolyte concentration, surface charge heterogeneity is formed and the clay structure should form aggregated and deflocculated conditions. Face to face association is possible while edge to face is not because the thick surface

double layers cover the edge double layer (Figure 2.19). As an electrolyte concentration is increased in both pH cases, the electric double layers of the surfaces are compressed and this opens up the edge double layer. In Figure 2.19, the edge to face association is now possible when the pH is lower than pH_{PZC}. In this case, aggregated and flocculated structures are formed as edge to face and face to face associations. For the case of pH higher than pH_{PZC}, the compression of the double layer should not change the configuration of the kaolinite clay structure according to this theory.

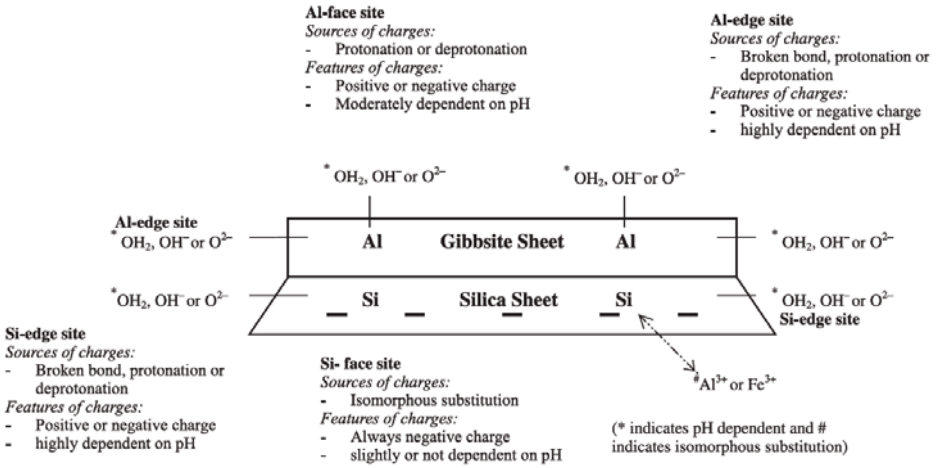

Figure 2.18 Mineral composition and surface charge characteristics of kaolinite clay (Modified from Wang and Siu, 2006)

It is noted that even though the heterogeneous coagulation at pH higher pH_{PZC} is not shown in Figure 2.19, a stability plot against pH of kaolinite clay by Tombácz and Szekeres (2006) indicates that when a very high concentration of NaCl is added to the clay, a very small stability ratio can be obtained. This indicates that the fast coagulation regime of the clay is possibly explained by Figure 2.17(*d*) that as high electrolyte concentration is used, the attraction potential dominates.

pH alterations in kaolinite provide obvious changes in average particle size due to surface charge heterogeneous coagulation while this effect is less pronounced for montmorillonite clay due to a substantial difference in particle geometry. For monmorillonite, a much higher electrolyte concentration is required compared to kaolinite clay for particle agglomeration (Tombácz and Szekeres, 2006).

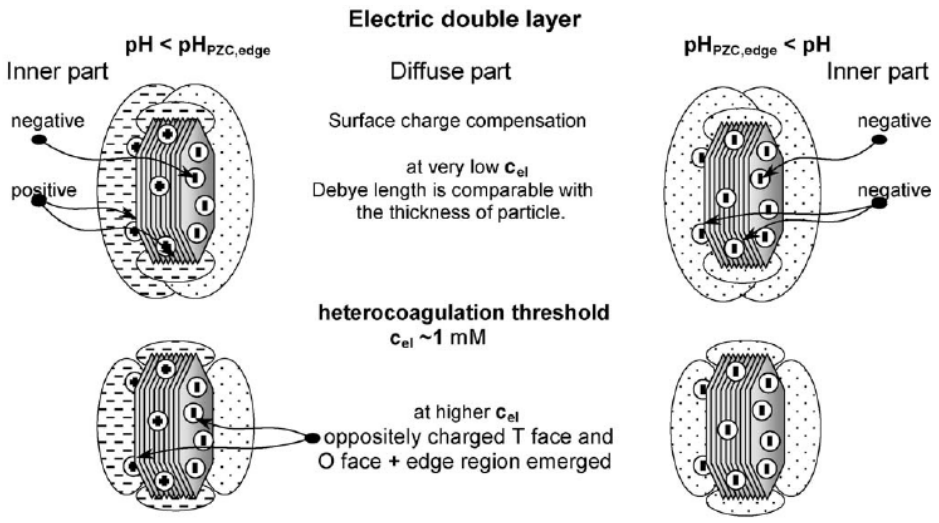

Figure 2.19 Schematic representation of electrical double layers forming around kaolinite clay particles (Modified from Tombácz and Szekeres, 2006)

2.4.2 Flocculation and coagulation

Flocculation is traditionally referred to chemical bonding of colloids with flocculant and coagulation is designated for aggregation of colloids by changing their surface characteristics or surface charge with a coagulant. Both processes can be referred to as particle destabilization. The particle destabilization can be achieved by compression of the double layer by increasing the fluid's ionic strength, by charge neutralization, and by adsorption and inter particle bridging by using a polymer.

Flocculation and coagulation are basically processes of aggregating dispersed fine particles into larger units. In general the process involves three steps (Hogg, 2000).

- Destabilization of the suspended fine particles or elimination of any interparticle repulsion due to electrical charges that oppose aggregation.
- Floc formation and growth: the development of aggregates due to particle to particle collision and adhesion.
- Floc degradation: mechanical breakage of the aggregates due to shear turbulence in the slurry.

All of these three stages occur in any practical destabilization process. While the third step is normally considered to be detrimental, it can also play a positive role in the redistribution of particles and reagents as flocs develop and grow.

Hogg (2000) explained that the fine particles in suspension often exhibit a significant degree of stability, tending to resist aggregation. Most commonly, the stability results from the electrical charge acquired by particles dispersed in aqueous media but it may be enhanced by the presence of protective adsorbed layers on particle surfaces. Destabilization can generally be accomplished by eliminating these factors. The electrical charge is generally from the interaction between the particle and the water and this can usually be controlled by pH. At some pH, the so-called iso-electric point, the particles have no net charge and the particles become unstable. pH control is therefore an effective method of destabilization but it can be impractical when the iso-electric point occurs in an inconvenient pH range and in the acidic pH range undesired heavy metal ions may present in the pore water.

An alternative is to shield the charge from one particle to another by using a high concentration of a specific ion in the water. This effectively compresses the electrical double layers surrounding the particles permitting them to approach one another closely enough to fall into the range where attractive forces dominate. Chemical additives such as lime, alum and gypsum are applied in practice. Hydrolysable cations can be highly effective in the destabilization of dispersion. In addition to causing the double-layer to compress, the hydrolyzed species are highly surface active and attain an iso-electric point. These species can also promote aggregation through surface precipitation of colloidal hydroxides.

Polymer substances are also very effective. They consist of long-chain molecules with ionizing groups which are usually located along the entire length of the chain. They function as highly charged ionics but they act primarily though a charge patch mechanism. The result of the destabilization is the formation of small flocs which can grow to larger sizes but are generally fragile (Hogg, 2000). It is recommended that a polymer be added after addition of salt in the clay water system as it this will yield stronger flocs (van Olphen, 1977).

2.4.3 Floc development, breakage and practical implication

After destabilization occurs, flocs can grow as a result of collision between particles which can be caused by Brownian motion arising from thermal energy in the suspending fluid, velocity gradients in mechanically agitated suspensions and differential settling of individual particles of flocs. For very small particles, Brownian motion is the dominant mechanism (Hogg, 2000).

Hogg et al. (1987) shows that the faster the rate of polymer addition the better the settling rate but that fast addition and prolong agitation is not recommended for a flocculation process because this leads to a large floc size but which can be destroyed more easily in the agitation process. The final product then may be worse compared to a slow addition. Rattanakawin and Hogg (2001) showed that there is a limiting floc size where the growth and breakage rates are equal. Hogg (2000) stated that while it is clear that breakage rates increase with floc size and agitation intensity and decrease with floc strength, specific relationships have yet to be established. The agitation process is necessary for adequate mixing of the flocculant with the suspension and to promote particle to polymer and particle to particle collision leading to destabilization and floc growth. Regarding the use of high molecular weight polymer flocculants, they are ineffective for destabilization but serve primarily as binding agents, enhancing floc strength and reducing breakage rates, therefore permitting growth to proceed to substantially larger sizes (Hogg, 2000).

In order to take full control of the binding effect, flocculants need to be added and mixed with the flocs at the solids content that will be used in practice (Hogg et al., 1993). This can lead to a substantial increase in limiting floc size, however, prolong mixing, as previously stated, can also have a detrimental effect. The limiting floc size typically decreases as polymer addition/mixing time is increased at a fixed total polymer dosage. Too short mixing, however, can lead to reduced floc size and increased floc fragility. The performance of a flocculation process should properly be assessed in terms of floc size distribution and floc structure (Hogg, 2000). In practice, settling rate, supernatant turbidity and compressibility are used to indirectly measure flocculant performance. It was reported that a general trend of results from laboratory studies of continuous flocculation for batch processes can be reproduced in the field but the effect tends to be less (Hogg, 2000). A general rule is that shorter mixing times lead to larger

flocs for the same polymer dosage. It is noted that the geometry of a flocculation tube can have an effect on the flocculation efficiency. Carissimi and Rubio (2005) showed that coil or curve tubes allow more flocculation than the linear one and they successfully produce large floc that can settle quickly.

After best flocculation conditions (polymer dosage, mixing time and agitation intensity) are applied, soil particles are flocculated and hindered settling takes place. Following the hindered settling, compression dominates at a certain solids content. During compression, the extent of the flocculation appears to be a minor factor since the large flocs break down easily and water must flow through smaller pores. It has been found that the flocculation conditions have a major influence on sedimentation but little to no effect on consolidation (Hogg et al., 1993). However, the compression process appears to be limited by the small or relatively dense aggregates produced in the destabilization step. These micro flocs require significant stress to overcome their yield strength and the rate of releasing water can be very low. Since the destabilization is important and the formation of micro flocs does not seem to be affected by how the destabilization was achieved, chemical approaches to enhance the compression regime have met with very little success (Hogg, 2000). In order to achieve more dewatering, a mechanical method is therefore required. Deep sediment and filtration are usually considered as mechanical methods. The deeper the depth of soils means the higher the self-weight effective stresses. This concept must be considered in thickeners and settling ponds (Weiland et al., 1994). This, however, also has an adverse effect on drainage length. A filtration process, on the other hand, uses externally applied pressure to further dewater the flocs. The floc structure is important to this process as the higher the permeability the easier for the water to flow out and better the filtration. Polymer addition generally helps to increase slurry permeability for more effective filtration.

For Syncrude fine tailings, experiments have been performed to investigate whether destabilization is important for the flocculation process of the tailings (Sworska et al., 2000). Mg^{2+} and Ca^{2+} ions and also pH were controlled in their study. Their results show that the flocculation response is dependent on pH and the presence of Mg^{2+} and Ca^{2+} dramatically improves the clarity of the supernatant water in an alkaline environment. The best flocculation response could be achieved either in an acidic pH or a basic pH with the addition of divalent cations. Sworska et al. (2000) also presented a

selection of flocculants for Syncrude fine tailings. They indicated that the choice of flocculants is determined by chemical factors but the performance for the flocculants depends more on physical variables such as agitation intensity and the addition rate of flocculants. Different flocculation conditions such as mixing speed, polymer concentration and rate of polymer addition are required for different flocculants. It was found that good flocculation can be achieved with a lower polymer dosage when using more dilute polymer solutions and continuous polymer addition during conditioning. This was also confirmed by Shaw and Wang (2005) in that the more dilute the slurry, the more efficient the flocculation and coagulation.

The effect of hydrodynamic conditions on flocculation of Syncrude tailings was also investigated by Yuan and Shaw (2007). It was indicated that the hydrodynamic conditions in flocculation have a strong effect on the flocculation performance. They also stressed that adsorption and flocculation are not separate processes but occur simultaneously with fast kinetics thus it is important to optimize the attaching opportunity by optimizing the hydrodynamic conditions in mixing of the flocculant and slurry. Yuan and Shaw tested two high molecular weight flocculants on Syncrude tailings with three different mixing methods; namely, manual inversion, manual plunger and power flocculation. Results showed that the power flocculation gave higher solids content, higher fines/(fines+water) ratio, clearer or same supernatant solids and a higher initial settling rate. In order to obtain optimum design parameters, Yuan and Shaw used three parameters including initial settling rate, supernatant solids content and sediment solids content as the targets while conditioning time and impeller speed were used as variables. Results are shown in Figure 2.20.

It was concluded that for this particular bench scale experiment, flocculate conditioning between 20 and 40 seconds, coupled with a mixing speed of 250 to 300 rpm, were the optimum conditions for the Aurora fine tailings with a SFR of 1:1. They also found that the flocculant adsorption/redistribution kinetic model gave a better interpretation of the power flocculation process.

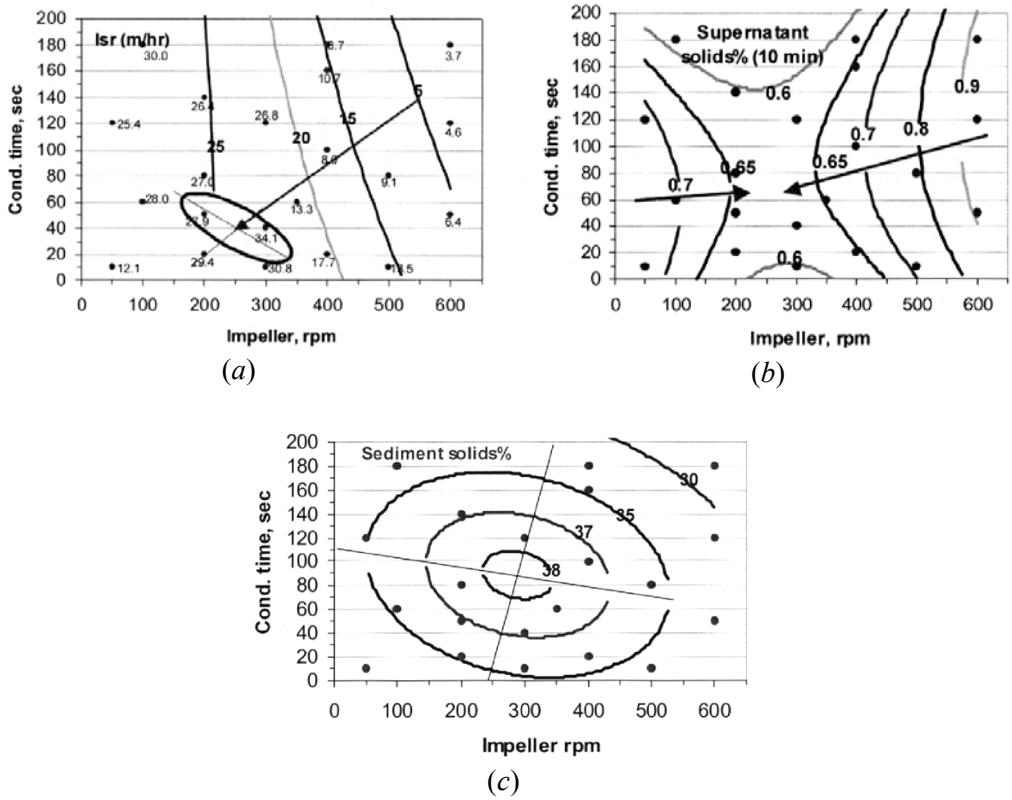

Figure 2.20 Effect of conditioning speed and time on (*a*) initial settling rate (*b*) supernatant solids (*c*) sediment solids (Modified from Yuan and Shaw, 2007)

2.5 Shear strength development in slurry

Watari (1984) presented vane shear strength measurement at different moisture contents for marine clay (Figure 2.21(*a*)). With the correlation between shear strength and void ratio obtained from the experiments, he estimated the shear strength on the top of a reclaimed land and suggested that the strength near the top is so small (1 kPa) that the bearing capacity can hardly be relied on.

Inoue et al. (1990) followed the Matsui and Ito (1977) procedure using the parameter w/w_L to normalize the yield shear stress versus water content from different clays and found that when yield shear strength is plotted against the ratio of w/w_L, a unique behavior is obtained (Figure 2.21(*b*)). It is noted that the shear strength with water content plot (Figure 2.21(*a*)) from different soils will generally not follow the same path. From Figure 2.21(*b*), the shear strength properties are divided by two limits into three distinct regions namely one with negligible shear strength, a transition zone showing appreciable shear strength and a paste region where the shear strength increases

dramatically. The higher ratio limit is considered a point where shear strength is negligible and the lower ratio limit is the boundary when a clay slurry becomes a paste. From their study the higher limit is approximately 2. Ito et al., (1975) stated that the microscopic mechanism of the water clay system will change at a value of w/w_L of 1.4 to 2 while Watari (1984) suggested that the yield shear strength of the vane type test changes dramatically at a w/w_L, of 1.6. It is likely that the yield shear strength of slurry is controlled by the clay properties of the slurry because w_L is used to normalize the water content.

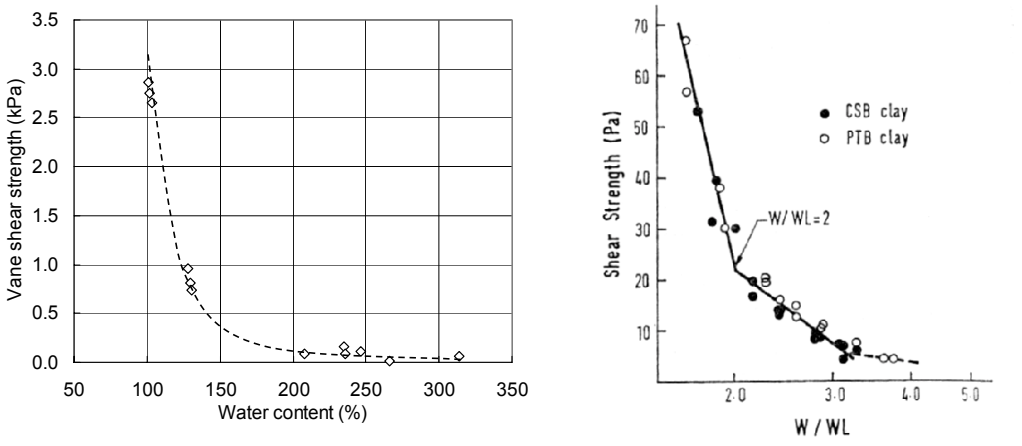

(*a*) (*b*)

Figure 2.21 Shear strength behavior of soft clays (*a*)Vane shear strength vs. water content (Modified from Watari, 1984) (*b*) shear strength vs. w/w_L (Modified from Inoue et al., 1990)

Tan et al. (1994) studied shear strength and liquid limit of clay-sand mixtures by a thin plate penetration method. They found that for the tested clay-sand mixtures, the liquid limit seems to follow the linear mixture law unless a substantial amount of sand is added (greater than 60% in most cases). The linear mixture law states that the liquid limit and clay content of the clay-sand mixture can be explained by a linear relationship. The law used in their discussion was slightly different from others (Seed et al. 1994a, 1994b) that Tan et al. used silt fraction instead of clay fraction. Tan et al.'s linear mixture law is expressed as Equation [2.26].

$$w_L^*(x) = \frac{(100-x)}{100} w_L(0) \qquad [2.26]$$

Where x is percentage of sand (> 0.063mm) of the total solids content, and $w_L(0)$ is the liquid limit of the silt-clay mixture (< 0.063mm) without any sand.

To study the effect of sand on shear strength, Tan et al. (1994) applied a similar method for shear strength analysis by assuming that the shear strength was due solely to the clay and silt fraction and the addition of sand changes the water content according to Equation 2.27. The best fit curve through the measured results was obtained for the case where no sand had been added. Then based on this curve, a new curve with a different sand content can be calculated.

$$w(x) = \frac{(100 - x)}{100} w(0) \qquad [2.27]$$

Where $w(x)$ is water content for x percent sand content and $w(0)$ is water content for no sand content slurry.

Tan et al. found that this method gives a good estimation of the shear strength of clay-sand mixtures up to about 60% sand content. They also found that the increase in shear strength due to the addition of sand is only caused by the geometric proximity of the sand particles not the interaction between clay and sand. In other words, the shear strength of the mixtures remained unchanged when the addition of sand did not lower the apparent void ratio (volume of fines+water/volume of sand) to 5 or less in this particular study. It was also found that both predicted liquid limit and shear strength agreed well with the linear mixture law until the amount of sand reached the apparent void ratio.

2.6 Experiments

2.6.1 Hindered sedimentation test and standpipe test

A hindered sedimentation test is a test to measure the settling velocity of the interface between slurry and supernatant water. In this thesis, the use of a hindered sedimentation test is mainly to obtain hydraulic conductivity values and correlate them with void ratios to define the hydraulic conductivity-void ratio relationship at large void ratios. Hydraulic conductivity is calculated via the falling interface velocity by Equation

[2.28] given by Been (1980) and Pane and Schiffman (1997). A hindered sedimentation test is generally performed at different initial solids contents to obtain sufficient data for the constitutive relationship.

$$v_s = -\left(\frac{\gamma_s}{\gamma_w} - 1\right)\frac{k}{1+e} \qquad [2.28]$$

Where v_s is initial settling velocity, γ_s is unit weight of solids, γ_w is unit weight of water, k is hydraulic conductivity and e is an initial void ratio.

Similarly to Equation [2.28], a non linear part of the settlement curve may also be used to obtain hydraulic conductivity via Kynch theory (Tan et al., 1990). In order to perform this analysis the surface solids concentration must be determined. Based on Kynch theory, Tan et al. (1990) proposed an expression to calculate solids concentration as Equation [2.29].

$$\left(x + t\frac{dx}{dt}\right)_p = \frac{M}{\eta} \qquad [2.29]$$

Where x is height, t is time, M is total mass of solids, η is concentration and subscript p indicates a point on a settlement curve. Equation [2.29] is the same as an equation proposed by Renko (1998) which is derived in terms of solids concentration. In this thesis, settling characteristics are expressed in terms of void ratio therefore Equation [2.29] was reformulated in terms of height and void ratio as shown in Equation [2.30].

$$e = \frac{(1+e_0)(h+v_{sp}t)}{H} - 1 \qquad [2.30]$$

Where e is void ratio, e_0 is initial void ratio, h is height at an interest point, v_{sp} is a tangential velocity at an interest point and H is initial height.

This test is well accepted when slurry is undergoing hindered sedimentation but it is generally believed that during consolidation this method can not be used. Pane and

Schiffman (1997) stated that this equation is valid only when there is a suspension at the initial void ratio at the sediment-water interface or as long as the settling velocity is constant. Toorman (1999) strictly indicated that the initial settling rate of self-weight consolidation can be used to estimate hydraulic conductivity where diffusive effects are negligible. This is theoretically identical to a one dimensional finite strain consolidation theory which will also give a constant initial settling velocity for high initial void ratios. Thus the use of Equation [2.28] during the consolidation phase may give an acceptable hydraulic conductivity value associated with a high initial void ratio. In a real situation, however, piping can occur (Edil and Fox, 2000) and the void ratio at the interface could be altered as well as the settling velocity. One would expect that Equation [2.28] will only hold true through a certain void ratio until the influence of compressibility becomes large. When compressibility becomes significant, hydraulic conductivity determination can easily be handled by a direct measurement of hydraulic conductivity during a large strain consolidation test.

A standpipe test is generally used for two main purposes, one is to use it for a compressibility determination and another is for a theoretical validation. To use a standpipe for compressibility determination, the consolidation is completed, the soil is sampled in layers and the measured void ratio is correlated with effective stress for the different layers (Scott et al., 2008; Scully et al., 1984). Another method to determine compressibility from the standpipe test is to continuously evaluate effective stress and void ratio via pore pressure measurements and density measurements (Bartholomeeusen, 2003; Sills, 1995; Been and Sills, 1981). For a validation standpipe test, the water-slurry interface, pore pressure, void ratio and total stress are periodically measured to evaluate the progress of sedimentation and consolidation. All hindered and standpipe tests are alike in that they are performed in a cylinder cell and all are assumed to be under one dimensional compression. Related problems in the tests are the side wall friction and accuracy in measuring solids content.

Been and Sills (1981) observed that for mud of void ratios from 4 to 10, the magnitude of side wall friction was small enough to be neglected. Elder (1985) studied the influence of column diameter on the settling process and observed that the settlement rate was not influenced by a column diameter of 100 mm and larger while Caughill (1992) found that at small void ratios the diameter to height ratio should be more than 2:1

in order to minimize the wall friction that can affect the settlement rate. The horizontal effective stress level is the cause of to the friction and it comes from the self-weight vertical stress. The deeper the column the higher the effective stresses during consolidation and the higher the wall friction. Therefore a height and diameter ratio and a percent consolidation may exist for a negligible wall friction. As tests conducted by Elder (1985) only used a height between 50 mm to 200 mm, this guideline could be problematic when a tall column is used in conjunction with a diameter of 100 mm. The Caughill (1992) statement is more generic. It is noted that for cohesive material such as MFT, at low effective stresses the influence of wall friction could also be affected by adhesion of the material to the wall.

At the University of Alberta, a sampling method is used for a large ten meter high standpipe test. The sampling apparatus is designed to be able to maintain pore pressure during sampling (Jeeravipoolvarn, 2005). Results showed that it can be used satisfactorily for clayey material but has poor performance for sandy material. To avoid sampling disturbance; an alternative is to measure the density profile by measuring transmitted rays. An X-ray method was first used at Oxford university in the 1980s by Been and Sills. This method yields high quality density measurements. A completely automated system to study sedimentation and consolidation was also proposed by Alexis et al. (2004). This system uses gamma ray instead of X-ray for cost effectiveness and it has a fully automatic controlling system. Otherwise it is similar to that of Been and Sills (1981).

2.6.2 Consolidation test

2.6.2.1 Multi-step loading large strain consolidation test

At the University of Alberta, large strain consolidation testing uses a multi-step loading test. The test follows the conventional large strain consolidation test (Sheeran and Krizek, 1971; Monte and Krizek, 1976). Briefly, the large strain consolidation test uses load increments to increase the effective stress. At the end of each loading step, void ratio and effective stress are obtained and a hydraulic conductivity test is performed.

The advantage of the large strain consolidation test is that it is a direct measurement and it does not include any complicated data interpretation, however it also

has disadvantages. The multi-step testing takes a long time to complete especially when a low hydraulic conductivity sample is tested starting at a low initial solids content. A test on a MFT sample from a void ratio of 5 to 1 could take 6 to 12 months to complete depending on drainage conditions, initial height and initial void ratio of a sample. The inconvenience of a long test period led to the development of the constant rate of deformation test (Znidarčić et al., 1986)

2.6.2.2 Seepage consolidation test

A seepage consolidation test was proposed by Imai (1979) and was used to study consolidation of very soft clay soils (Imai et al., 1984). The principal of this method is to apply pressure on a soil sample through water flow. Effective consolidation stress increases with depth and is caused by a combination of seepage force and by the buoyant weight of a soil. Imai incorporated this in to his experiment and therefore at the end of each applied hydraulic pressure, water content and pore pressure with depth have to be determined. With the knowledge of pore pressure and water content, compressibility can be calculated. The flow rate measurement which is the same throughout the depth of the sample is used with the pore pressure measurements to calculate the hydraulic conductivity.

Fox and Baxter (1997) developed a modified hydraulic consolidation test for soft soil. They proposed a closed form equation for data interpretation of this test by using three assumptions: (i) compression and flow are one dimensional, (ii) a one to one linear relationship exists between the logarithm of vertical effective stress and the logarithm of vertical hydraulic conductivity and (iii) the contribution of side friction and self weight are negligible when compared to the applied stress. To perform the hydraulic consolidation test, a two-stage flow procedure was proposed. The first step is to apply a small surcharge on the top of the sample. Specimen height and flow velocity are measured at the steady state. The second stage is that a doubled pressure is applied and at the steady state sample height and flow velocity are again measured. At the end of the second stage, a sample is cut into layers to obtain a void ratio profile. With the closed form equations available, the data obtained from the two-stage flow test is used in the equations to obtain the hydraulic conductivity and effective stress relationship. With the measured void ratio profiles, the void ratio-effective stress and hydraulic conductivity-

void ratio relationships are obtained. The advantage of their method is that the test is relatively easy to perform; the mathematical forms of hydraulic conductivity-void ratio and effective stress-void ratio relationship are not fixed and the data analysis is easy with closed form formulas. The limitation of the method is that it can not be used with a sample that has an effective stress of zero at the top. They have shown that the results from this method can have good agreement with a multi-step loading test and it reduces the duration of testing by 75%. It is noted that assumption (ii) used for this test may be questionable for unusual materials.

Following Imai (1979), Sridharan and Prakash (1999) also proposed a simplified seepage consolidation test for soft sediments. The difference is the proposed test does not consider varying void ratio with depth but it uses the average void ratio at a certain applied pressure. They apply a hydraulic gradient to a small sample in their simplified seepage consolidation test. Once interface settlement becomes negligible, the average void ratio is calculated and correlated with the applied pressure. At the end of each application of pressure, a hydraulic conductivity test is performed by applying a smaller hydraulic head on the sample and measuring the amount of flow. After the hydraulic conductivity determination, a higher hydraulic gradient is applied. All applied gradients are gradually increased to the desired amount. They found that the test gave similar results as the conventional consolidation test. The simplified seepage consolidation test therefore can be used satisfactorily to study compressibility and permeability characteristics of soft sediments at the low effective stress level.

2.6.2.3 Constant rate of deformation (CRD) test

Znidarčić et al. (1986) proposed an analysis of a constant rate of deformation (CRD) test on slurry. The CRD test requires pore pressures at the top and at bottom of a sample to be measured for the effective stress evaluation. The effective stress and deformation are used in a computer program to calculate compressibility and hydraulic conductivity based on the finite strain consolidation theory. The method utilized by Znidarčić uses the theory to obtain consolidation parameters. The method proved to give similar results to the multi-step large strain consolidation test for several demonstrated tailings. The main advantage of this test is that it takes much a shorter time compared to the conventional direct measurement test.

Scully et al. (1984) conducted settling tests, multi-step consolidation tests, CRD tests and centrifugal tests to determine consolidation characteristic of phosphatic clays. Compressibility obtained from these methods indicates that the compressibility of the clays is not unique and is dependent on the initial void ratio. This was a further confirmation for the results published by Imai (1981) and Been and Sills (1981). It was also observed that the compressibility curves show apparent pre-consolidation effect. In general, measurements of hydraulic conductivity were consistent. Scully stated that more work is needed to examine if at high void ratios the hydraulic conductivity determined by the CRD test is too high.

For oil sands tailings, a CRD test was conducted by Caughill (1992). Results showed that a multi-step loading test required about two months to complete for CT. A CRD test was also used but due to a water leaking problem at the top piston, the test was abandoned. This was because the combination of low friction with an effective seal on the loading piston was not found for the setup (Caughill, 1992). A total stress cell with a better piston seal should be implemented for future work with the CRD test. In this way, neither the applied stress nor the piston friction is required to be evaluated but the stress on a sample is directly measured by the total stress cell at the base of the sample. The CRD test requires more elaborate instrumentation otherwise a conventional multi-step testing should be used. One interesting comment by Caughill was that to follow recommendations by ASTM D-4186 and by Smith and Wahls (1969) which requires the excess pore pressure to remain between 3% to 20% and less than 50% respectively of the applied stress, the CRD test would have to be performed almost as slow as a multi-step loading test. Caughill (1992) performed CRD tests with much larger excess pore pressure than the recommendation and he concluded that the interpretation of the CRD test is complex and the effect of the magnitude of excess pore pressure on the test is still uncertain. Multi-step loading tests provide more consistent compressibility relationships but require longer test times.

2.6.3 Scanning electron microscope and X-ray diffraction

Slurry microstructure is examined by scanning electron microscopy (SEM) and the current SEM test procedure on a slurry is given by Azam and Scott (2009). Since the

electron-microscopic observation technique requires a high vacuum, only dry or frozen samples can be observed. There is no guarantee, therefore, that the electron micrograph reflects the shape and size of the particles when they are in a natural condition. In most cases there is little doubt that plates remain plates and needles remain needles when suspended in water (van Olphen, 1977). However, SEM tests provide good qualitative information or comparative information for analyzing oil sand fine tailings. In general, for oil sands tailings, the SEM analysis is performed to obtain information on fine tailings structure and X-ray analysis is performed to obtain elemental information on clay mineralogy and other compositions in the tailings.

For oil sands tailings, an extensive SEM image analysis was performed to investigate the effects of bicarbonate, NaOH, organic matter, sodium naphthenate, gypsum, and processing temperature on the structure of MFT by Tang et al. (1997). Results showed that the bicarbonate and the NaOH in the tailings water are dominant agents which cause the card-house structure of kaolinite clay-water systems similar to those in the oil sands tailings. It was observed that the bitumen and organic matter in the tailings may also have an effect on the soil structure. The addition of gypsum to MFT was not found to change the structure but it made the structure finer and stronger. The addition of sodium naphthenate did not affect the structure of the kaolinite clay-water system. It appears that this surfactant is not responsible for the dispersed structure.

Tang (1997) also indicated that the exchangeable sodium ratio (ESR) of a clay-water system resulting from different bitumen extraction processes can be used to forecast and identify whether a fine tailings will have a flocculated structure or a dispersed card-house structure. Generally ESR is often used to identify possible clay structure status in salt impacted soils. ESR relates the compositions of the solution phase to the compositions of the absorbed phases. It provides a prediction of adsorbed phases based on the concentration of ions in the solution. ESR can be calculated by the Gapon equation as follows:

$$ESR = 0.015 \times SAR = \frac{0.015[Na^+]}{\sqrt{\frac{[Ca^{2+}]+[Mg^{2+}]}{2}}} \qquad [2.31]$$

Where ESR is exchangeable sodium ratio, SAR is sodium adsorption ratio and soluble cation concentrations are in meq/L (meq/L = (mg/L)/(atomic weight/change of the ion)).

According to Dawson et al. (1999), ESR value of 0.1 or more, sodium ions will occupy adsorption sites on the clay resulting in a high potential of dispersion. SAR values higher than 20 (ESR of 0.3) are likely to be in a dispersed state for oil sands fine tailings and SAR values greater than 40 (ESR of 0.6) will be in a completely dispersed state (Miller et al., 2010).

2.7 Summary

Oil sands fine tailings post serious engineering, environmental and economical problems. This is due to the very slow water releasing behavior of the tailings. Different tailings technology and deposition schemes were developed to increase the rate of compression of this material. For Syncrude, one of the approaches is to use a tapered flocculation technique referred to as in-line thickening process. This process is used with cyclone overflow tailings to increase their rate of compression. The in-line thickened tailings compression characteristics are not known and detailed study of the material is essential.

The slow compression behavior is caused by the fine grained materials and the complex clay-water interaction of the tailings. According to a finite strain consolidation prediction, the oil sands fine tailings will take many decades to be fully consolidated. The real tailing performance is even expected to be poorer as many field and laboratory analyses indicate that the theory generally overestimates the true performance. Compressibility and hydraulic conductivity constitutive relationships should be revised by the incorporation of missing physics; possibly non-Darcian flow, thixotropy and time dependent behavior.

Various methods to obtain compressibility and hydraulic conductivity relationships for soft clays are available in literatures. Most of the new test developments are focused on decreasing the test time and they often require back calculations assuming that a consolidation theory is valid. With the uncertainty observed in theoretical

predictions for oil sands tailings, the best method to study compression behavior appears to be to perform direct measurements.

Different deposition schemes for tailings are available for different tailings management plans. A selection of a deposition scheme for a specific type of tailings needs to be evaluated case by case based on factors such as availability of water, material behavior and site conditions which can vary significantly. An important aspect is the use of numerical capability to explore possible deposition schemes. The numerical model has to be constructed with the best approximated material behavior and field conditions.

Chapter 3 One Dimensional Finite Strain Consolidation Modeling

3.1 Introduction

One dimensional finite strain consolidation theory introduced by Gibson, England and Hussey in 1967 is used to model the consolidation process of soft fine grained soils or slurries. The theory unlocks the restrictions of the conventional model from small strain and linearity therefore allowing more complex problems to be analyzed. In geotechnical engineering, the theory is often used to simulate slurry consolidation behavior specifically self-weight consolidation problems which gives answers to containment size, strength implications and excess pore pressure dissipation in the slurry.

In order to explore the performance of the finite strain consolidation theory and apply the theory for simulations in later chapters, in this chapter the conventional one dimensional finite strain consolidation model was developed, investigated and discussed for both quiescent and pond filling problems. A technique of using an interaction coefficient with the finite strain consolidation theory to simulate sedimentation and consolidation phenomena was proposed and the application of the model to a real problem was shown. Lastly, the theory was extended to capture over-consolidation and creep behavior for problematic slurry such as mature fine tailings.

3.2 Non-linear finite strain consolidation theory

Non-linear finite strain consolidation is a consolidation theory that includes non-linear soil properties (compressibility and hydraulic conductivity) and allows large deformations. The non linearity behavior of soils is implemented through constitutive relationships determined from laboratory testing which will be discussed in Chapter 7. The use of material coordinates allows a large deformation theory.

The governing equation in terms of void ratio was given by Gibson et al. as

Section 3.3 has been published. Jeeravipoolvarn, S., Chalaturnyk, R.J., and Scott, J.D., 2009. "Sedimentation-consolidation modeling with an interaction coefficient", Computer and Geotechnics, Vol. 36(5), pp. 751-761.

Section 3.4 has been published. Jeeravipoolvarn S., Chalaturnyk R.J. and Scott J.D., 2008. Consolidation Modeling of Oil Sands Fine Tailings: History Matching. Proceedings of 61st Canadian Geotechnical Conference, Edmonton, Alberta, Canada, September 22-24, pp. 190-197.

$$\pm\left(\frac{\rho_s}{\rho_f}-1\right)\frac{d}{de}\left[\frac{k(e)}{(1+e)}\right]\frac{\partial e}{\partial z}+\frac{\partial}{\partial z}\left[\frac{k(e)}{\rho_f(1+e)}\frac{d\sigma'}{de}\frac{\partial e}{\partial z}\right]+\frac{\partial e}{\partial t}=0 \qquad [3.1]$$

Where ρ_s is solids density, ρ_f is fluid density, e is void ratio, $k(e)$ is hydraulic conductivity, σ' is effective stress, t is time and z is material coordinate.

Another formulation that will be used in this chapter is an excess pore pressure formulation by Somogyi (1980). The formulation is expressed as Equation [3.2].

$$\frac{\partial}{\partial z}\left[\frac{k(e)}{\gamma_w(1+e)}\right]\frac{\partial u}{\partial z}+\frac{k(e)}{\gamma_w(1+e)}\frac{\partial^2 u}{\partial z^2}+\frac{de}{d\sigma'}\frac{\partial u}{\partial t}-\frac{de}{d\sigma'}\left[(G_s-1).\gamma_w\frac{d(\Delta Z)}{dt}\right]=0 \quad [3.2]$$

Where u is excess pore pressure, G_s is specific gravity, γ_w is unit weight of water and Δz is the material coordinate difference between surface and the point in question.

The consolidation equation [3.2], which will be mostly used in this thesis, can be recognized as a second order nonlinear convection diffusion equation unlike the conventional equation which is a second order linear diffusion type equation.

3.2.1 Quiescent condition

Quiescent condition is a condition where soil is consolidating under any loading condition without losing or gaining solids material and without changing applied stresses. The quiescent condition is generally applied for soil that is filled in a containment pond quickly enough that the consolidation during filling can be neglected. In this section, a development of a quiescent finite strain consolidation model is presented.

3.2.1.1 Power functions for compressibility and permeability

In order to solve the differential equation, many researchers implement correlations of void ratio-effective stress and hydraulic conductivity-void ratio into the governing equation. The most popular relationship was first introduced by Somogyi

(1980) who used a power law to handle the nonlinearity of void ratio-effective stress and hydraulic conductivity-void ratio relationships.

$$e = A\sigma'^{B} \quad [3.3]$$

$$k = Ce^{D} \quad [3.4]$$

Parameters *A*, *B*, *C* and *D* are curve fitted constants. The compressibility can be written in a differential form as

$$\frac{de}{d\sigma'} = AB\sigma'^{(B-1)} \quad [3.5]$$

Substitute [3.5] in to the governing equation [3.2], Equation [3.6] is obtained.

$$\frac{\partial u}{\partial t} + \frac{\sigma'^{\beta}}{\alpha}\left(\frac{k}{1+e}\right)\frac{\partial^2 u}{\partial z^2} + \frac{\sigma'^{\beta}}{\alpha}\frac{\partial\left(k/1+e\right)}{\partial z}\frac{\partial u}{\partial z} = \gamma_b \frac{d(\Delta Z)}{dt} \quad [3.6]$$

Where

$\gamma_b=\gamma_s-\gamma_f$

$\alpha=AB\gamma_f$

$\beta=1-B$

A fully implicit (backward time central space) finite difference method is chosen due to its stability to solve Equation [3.6]. The disadvantage of this numerical scheme is that it needs to know material properties at the next time step in order to calculate the present time. To overcome this problem, the present time step is put to the next time step with a very small increment of time to ensure that little variation will occur. Somogyi (1980) stated that the stability of the implicit finite difference method will cause the error introduced by this approximation to decay. The governing Equation [3.6] in terms of differences becomes.

$$S_i^j\delta\left(K_i^j + D_i^j\right)u_{i+1}^{j+1} + (1-2S_i^j K_i^j\delta)u_i^{j+1} + S_i^j\delta(K_i^j - D_i^j)u_{i-1}^{j+1} = u_i^j + \gamma_b\left(\Delta Z\right) \quad [3.7]$$

Where

$$S_i^j = \frac{\sigma_i'^{j\beta}}{\alpha}$$

$$K_i^j = \frac{k_i^j}{(1+e_i^j)}$$

$$D_i^j = \frac{1}{4}\left(\frac{k_{i+1}^j}{(1+e_{i+1}^j)} - \frac{k_{i-1}^j}{(1+e_{i-1}^j)}\right)$$

$$\delta = \frac{\Delta t}{(\Delta z)^2}$$

i is the material coordinate index, j is the time index, Δt is the time increment, and Δz is the material coordinate increment.

The governing equation then can be solved by setting the initial condition and boundary condition to the problem. For both pond filling and quiescent problems, the upper drainage boundary set is $u_{i-1}^{j+1} = 0$ and the bottom undrained boundary set is $u_{i-1}^{j+1} = u_{i+1}^{j+1}$. If it is a double drainage problem, excess pore pressure is set to zero at the bottom boundary. The initial condition is defined by the initial solids content or void ratio which is related to hydraulic conductivity and effective stress through Equations [3.4] and [3.3] respectively. The initial self-weight pressure is calculated from the height of the deposit multiplied by the buoyant unit weight.

With the initial condition and boundary condition, the governing equation can be solved. The implicit method yields a system of linear equations which can be solved for excess pore pressure for the next time step by a direct method (inverse matrix) or an iterative method (Gauss-Seidel and Gauss-Seidel with SOR). In this thesis, both methods were analyzed and they gave the same result. The iterative method, however, is preferred as the computational time can be much shorter. After each time step the material parameters are updated as the void ratio changes due to consolidation and the parameters are used for the next time step. The programming scheme of the model is shown in Figure 3.1.

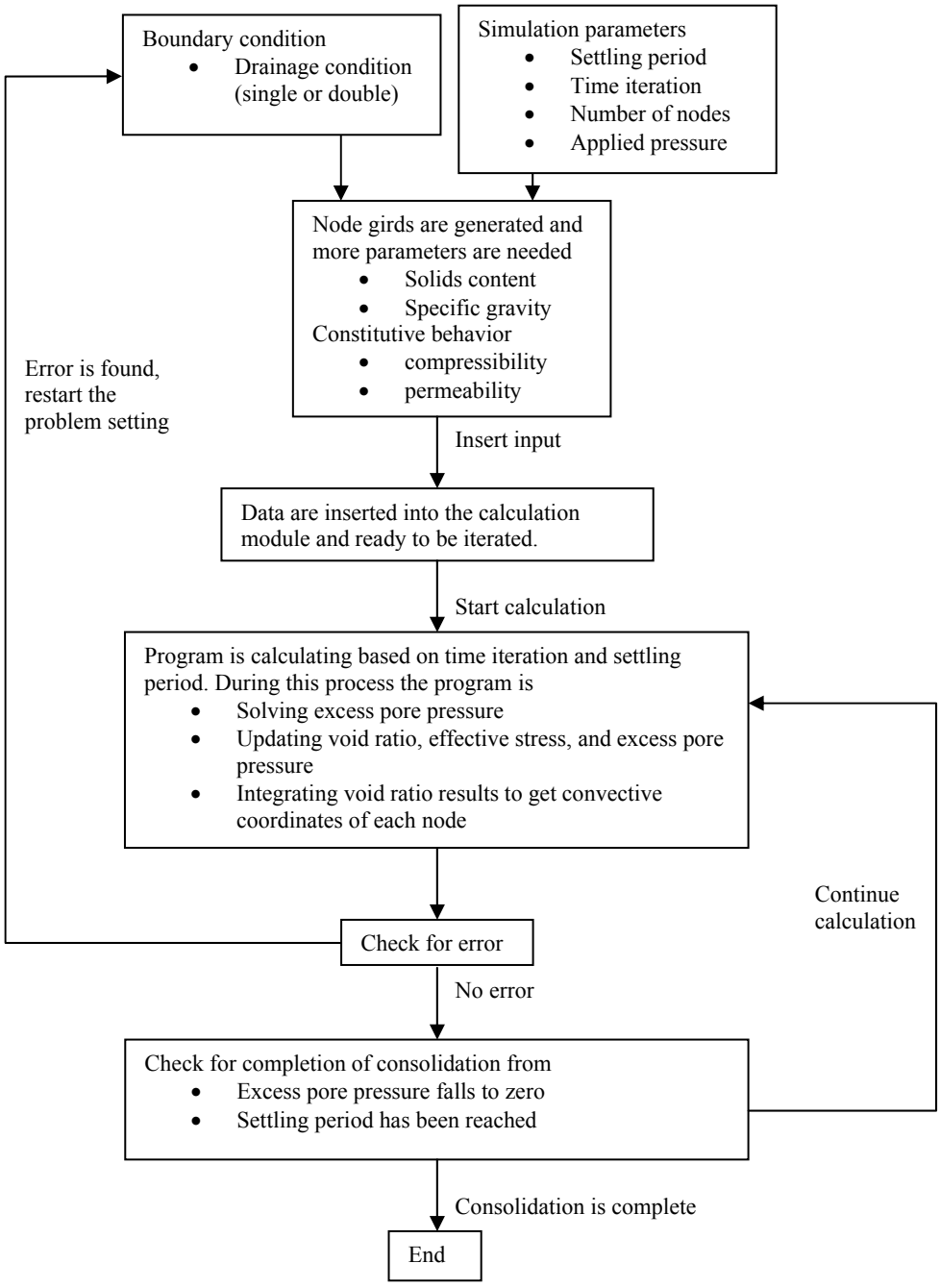

Figure 3.1 A computational scheme for quiescent model

In order to verify the developed computer program, a bench mark case published by Townsend and McVay (1990) is used for comparisons. The simulation by the developed program was performed on the scenario A: quiescent consolidation, uniform initial void ratio and the given parameters are S_i = 16% (initial solids content), H_i = 9.6 m (initial depth), G_s = 2.82 and finite strain parameters A = 7.72, B = -0.22, $C = 2.532\times10^{-7}$ and D = 4.65 (units in kPa, m/day). The simulation results are compared with the literature in Figures 3.2, 3.3 and 3.4 showing qualitatively similar solutions. The slight difference and discrepancy of other simulation results could come from the applied numerical methods, the governing equations, temporal increment and spatial increment.

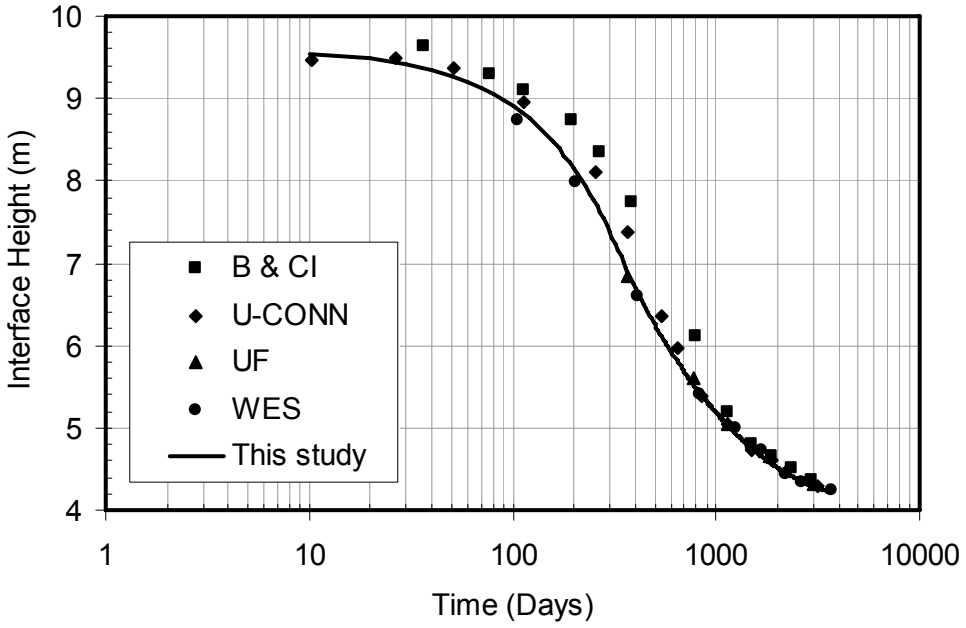

Figure 3.2 Interface settlement comparison (Modified from Townsend and McVay, 1990)

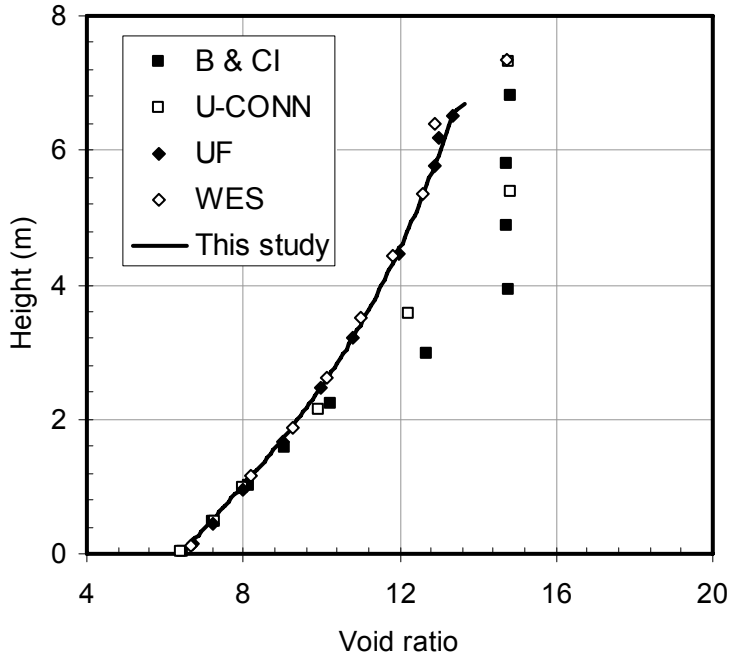

Figure 3.3 Void ratio profile (Modified from Townsend and McVay, 1990)

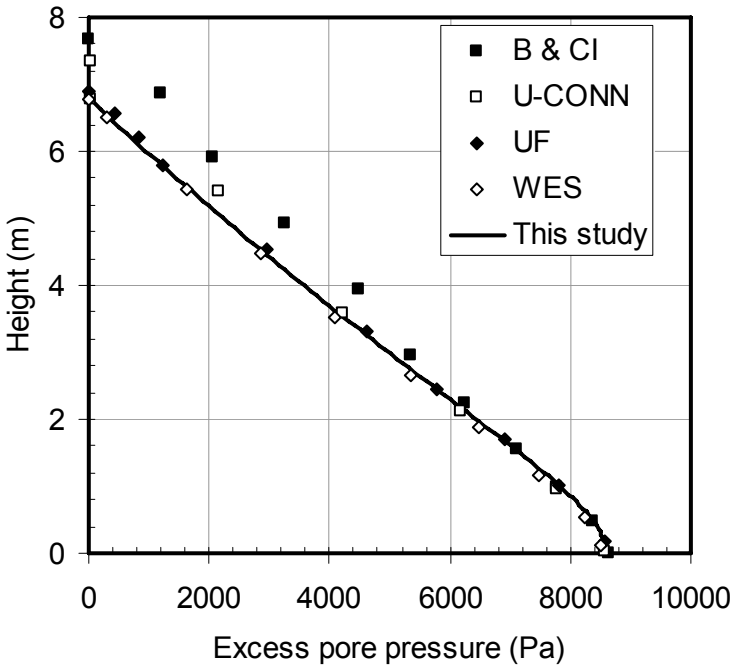

Figure 3.4 Excess pore pressure profile (Modified from Townsend and McVay, 1990)

3.2.2 Multiple filling and settling model

A multiple step filling and settling model is important for tailings pond planning and management. The model determines the rate of consolidation of tailings under an operating rate of disposal. Information from the model is used to determine the available capacity of the pond and the availability of recycle water. Moreover, it determines the generation of effective stress which may be correlated to undrained shear strength of the tailings in the pond.

In this section, the multiple step filling and settling is modeled by using a finite difference method. The upwind differencing scheme is chosen for the multiple step filling and settling model due to the fact that the method is unconditional stable. This model also utilized a multiple node technique per deposition layer (Huerta and Rodriguez, 1992) to increase accuracy of the filling simulation. The domain discretization for one and multiple nodes per time step (two nodes per time step is shown) is illustrated in Figures 3.5 and 3.6. After a filling period is over, a quiescent condition is satisfied and the model in Section 3.2.1 can be applied to predict the tailings settling behavior.

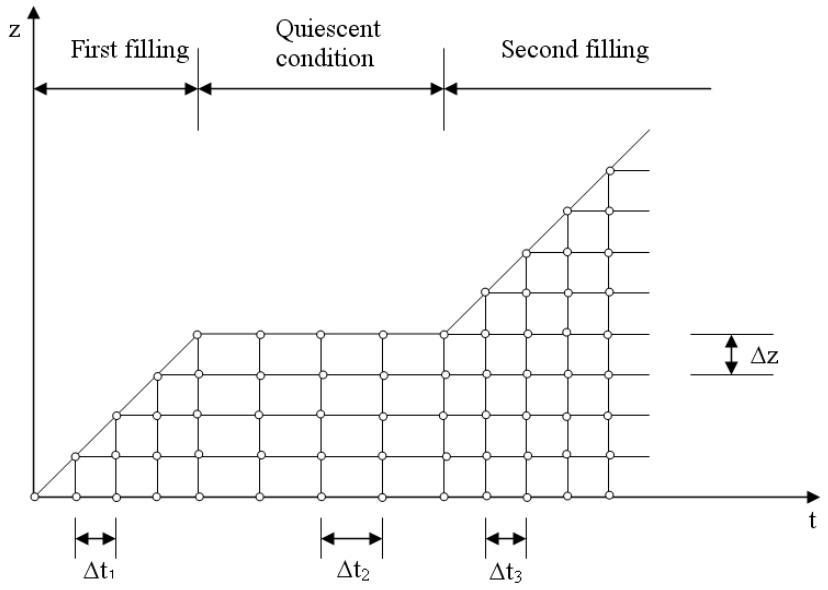

Figure 3.5 Domain discretization for filling problem (one node added per time step) (Modified from Huerta and Rodriguez, 1992)

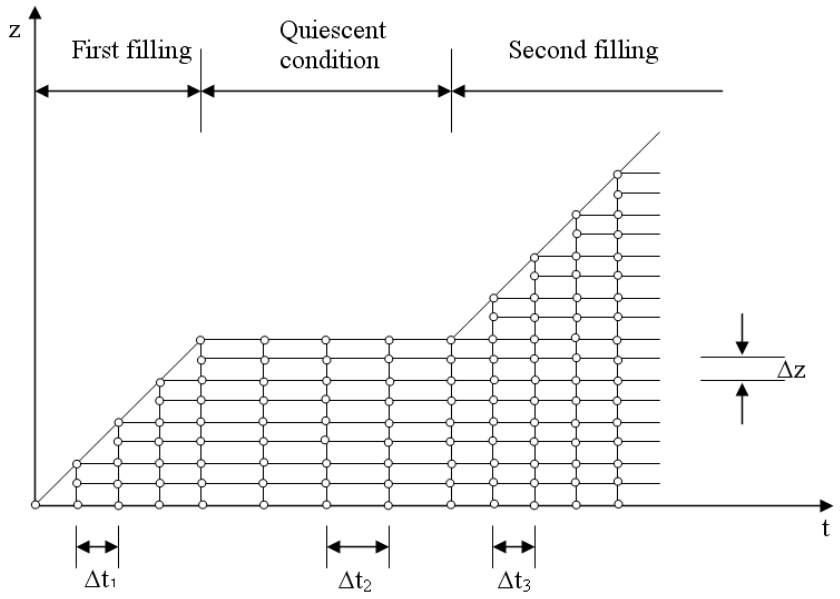

Figure 3.6 Domain discretization for filling problem
(multiple nodes added per time step, only two nodes per time step is shown)
(Modified from Huerta and Rodriguez, 1992)

3.2.2.1 Programming filling and settling

In order to model a filling period, a pond area and a rate of filling are required. In Figure 3.7, a trapezoidal shape pond area is shown. Area changing due to shape of the pond is incorporated by recalculation of the surface area at every time step based on tailings level which is numerically determined in the model. The calculation of a new area can be done by knowing tailings interface level, beach slope angle and the base length through Equation [3.8].

$$A_t = L_B + \frac{2 \times H_t}{\tan\theta} \qquad [3.8]$$

Where A_t is an area of pond at any time step per unit length, L_B is a base width, H_t is a tailing surface level at any time step and θ = beach slope angle.

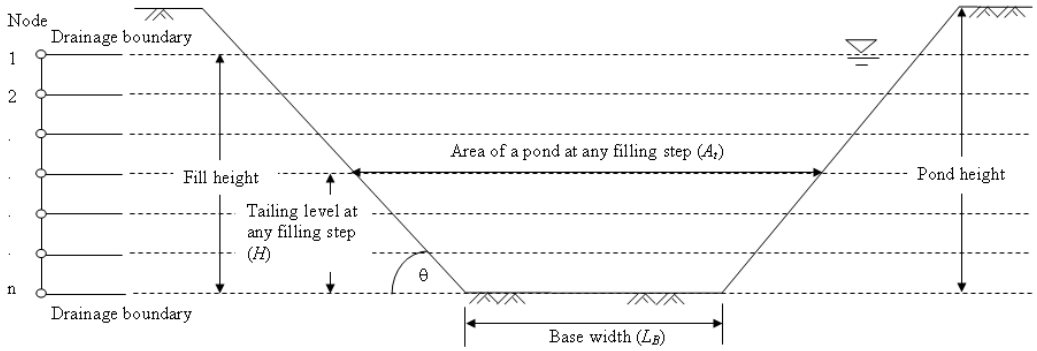

Figure 3.7 Pond area

The flow scheme of the filling model is presented in Figure 3.8. The scheme starts from defining the boundary condition, filling and settling parameters. The information feeds into the nodes and a system of linear equations are established. When calculation starts, the program solves for dissipation of excess pore pressure and inserts the calculated excess pore pressure as new information into the next time step. The excess pore pressure is also used to determine the effective stress and void ratio at the end of each time step calculation. The effective stress and void ratio information is sent to the next time step as new information. In the next time step, the material is added by stacking nodes either one node per time step or multiple nodes per time step depending on user input (Figures 3.5 and 3.6). The new height which is obtained from a new reduced coordinate is used in this calculation step to determine an amount of material fed in the nodes. The excess pore pressure is automatically calculated from the new information. The new step is now ready for a new calculation. The excess pore pressure and other parameters are then used to solve the system of equations and the process is repeated.

After any of the filling constraints (pond height, fill height and filling period) is reached, the program automatically stops and prompts for the settling calculation. The settling period is handled by the same technique presented in Section 3.2.1.

The next filling step retains all the information calculated from the quiescent period however excess pore pressure is recalculated from the new filling nodes which are stacking in the same method discussed in the first filling step. The calculation is then repeated in the same manner through the whole process.

To verify the developed program with other models in the literature, a bench mark case published by Townsend and McVay (1990) is used and results of the comparison of the multiple filling simulations are shown in Figures 3.9, 3.10 and 3.11 for tailing water interface, void ratio profiles and excess pore pressure profiles respectively.

It can be seen that the model performs quantitatively similar to other models. Slight difference from all models can be seen in all results, this study and McGill models are showing slightly higher interface settlement prediction compared to other models at the end of prediction, TAGA and U-CONN have almost identical interface and void ratio predictions but different excess pore pressure profiles. Results from WES show an unique interface settlement which is not similar to other models however it predicts very similar void ratio and excess pore pressure profiles with others at the end of the quiescent condition. This is, of course, because of the same self-weight stress. In Figure 3.10, WES, UF and TAGA models have surface void ratios higher than the initial void ratio. This indicates that at the one year mark, the models start to fill the second layer already (initial void ratios are 14.8 and 22.8 for 1^{st} and 2^{nd} layers respectively). The comparison is endless however it is important to note that almost all the models have shown quantitatively similar results in this specific example.

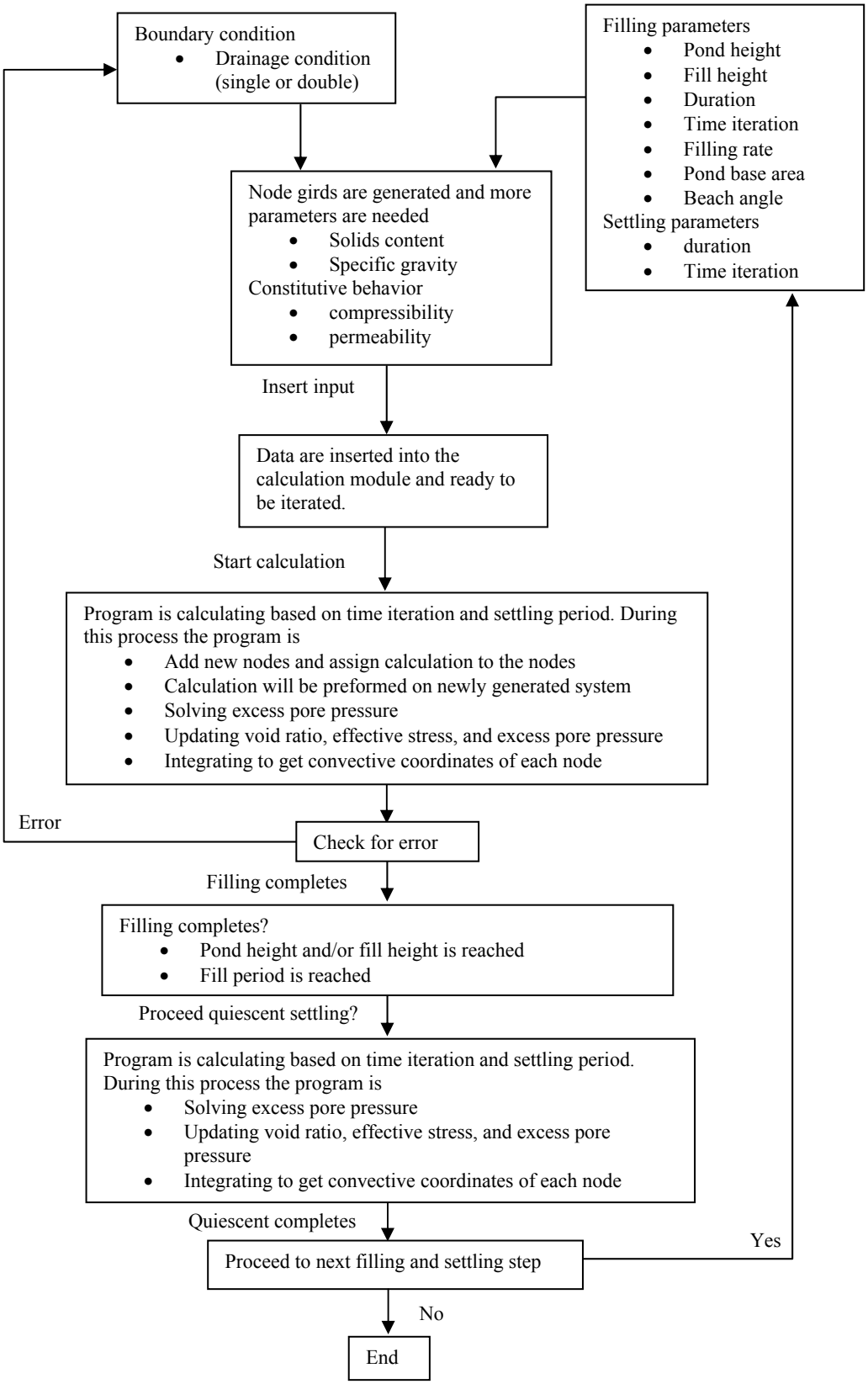

Figure 3.8 A computational scheme of multiple filling and settling model

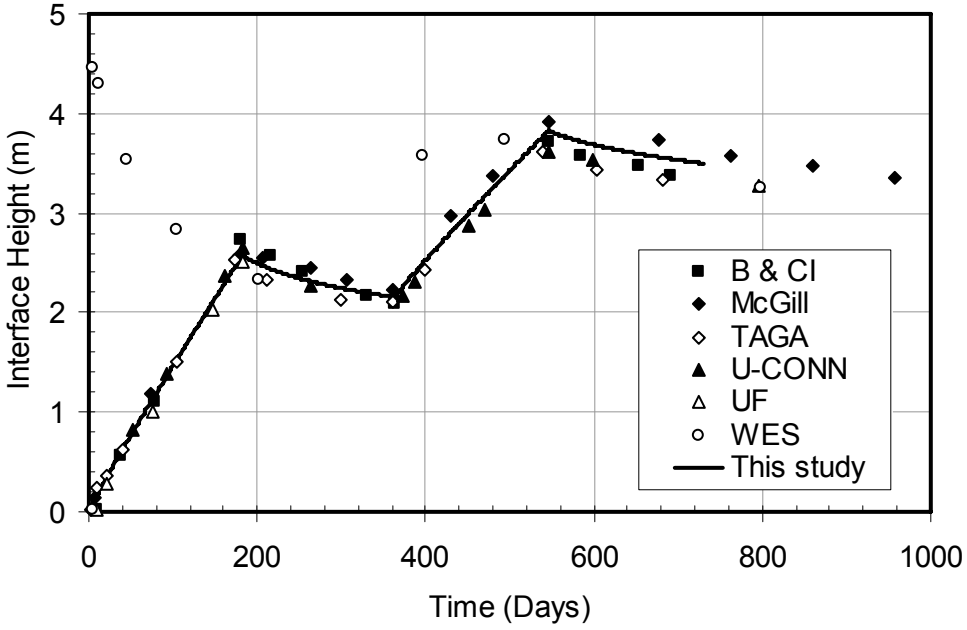

Figure 3.9 Interface settlement vs. time in multiple stage filling problem

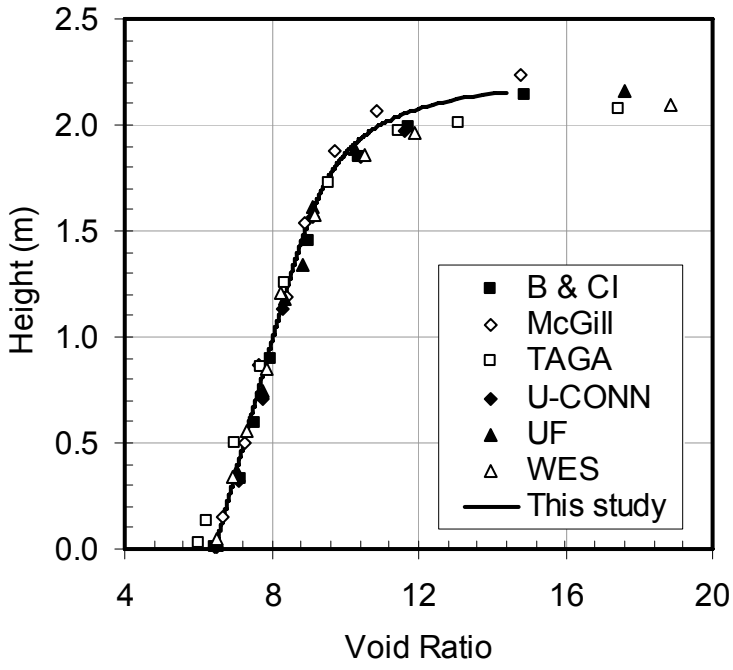

Figure 3.10 Void ratio profiles in multiple stage filling problem at 1 year

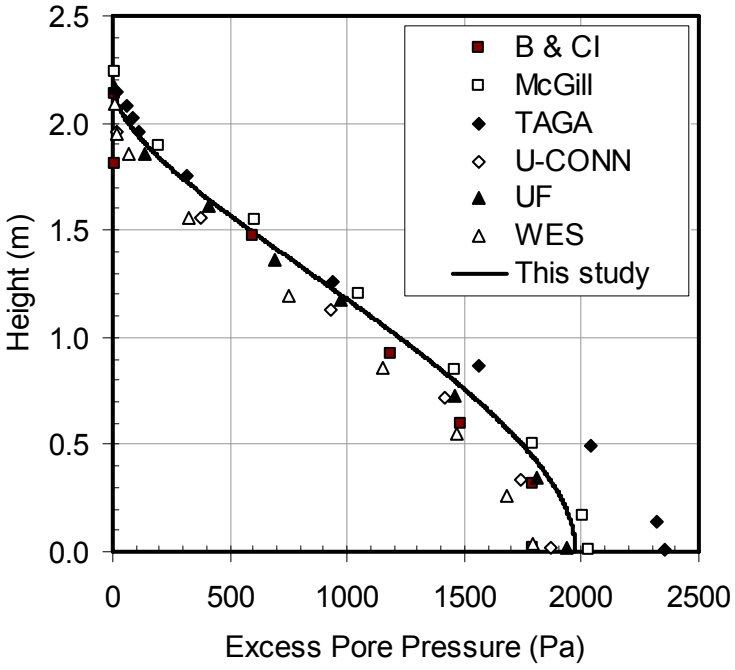

Figure 3.11 Excess pore pressure profiles in multiple stage filling problem at 1 year

3.2.2.2 Approximation of a filling condition with a quiescent condition

Carrier et al. (1984) stated that interface settlement predictions during filling by a finite strain consolidation theory is dependent on the amount of solids filled and that if a pond is filled with the same tailings at different rates and periods but aiming at the same total dry solids, generally the same pond capacity is obtained. Essentially this statement also implies that the steady state solution of finite strain consolidation is independent of the filling history. This is because the driving mechanism in the process of consolidation is the self-weight stress. The same amount of solids therefore results in the same amount of settlement. In this section, finite strain consolidation predictions for a filling condition and a quiescent condition are compared. An approximation of a filling condition with a quiescent condition is then presented.

To study model behavior, compressibility and hydraulic conductivity relationships of COF are used as the study material parameters. These parameters include an initial solids content of 20%, specific gravity of 2.52 and A, B, C and D parameters of 3.179, -0.196, 3.52×10^{-6} and 4.232 respectively (units in kPa and m/day). Pond base area

is arbitrary assigned to be 1 km^2 and the total amount of tailings is 1,460,000 tons for all cases. Ten scenarios are selected for this purpose and modeling parameters for each case are listed in Table 3.1.

Table 3.1 List of parameters for filling and quiescent parametric study

Scenario	Type	Fill height (m)	Dyke angle (°)	Filling rate (ton/day)	1st filling period (years)	1st quiescent period (years)	2nd filling period (years)	2nd quiescent period (years)
1	Quiescent	1.284	90	-	-	1.2	-	-
2	Filling	-	90	10000	0.4	1	-	-
3	Filling	-	90	20000	0.2	1	-	-
4	Filling	-	90	80000	0.05	1	-	-
5	Filling	-	45	20000	0.2	1	-	-
6	Filling	-	90	20000	0.1	0.5	0.1	0.5
7	Filling	-	90	40000	0.05	0.5	0.05	0.5
8	Filling	-	90	80000	0.025	0.5	0.025	0.5
9	Filling	-	90	40000	0.05	0.55	0.05	0.55
10	Filling	-	90	80000	0.025	0.575	0.025	0.575

To investigate a single filling and settling period, results of finite strain simulations of Scenarios 1 to 4 are shown in Figure 3.12. During the filling period, the interface heights are approximately linear showing high coefficients of correlation to a linear function. The solutions of the finite strain consolidation theory for Scenarios 2, 3 and 4 show that the interface settlement predictions after filling are similar to that of the Quiescent model (Scenario 1). It can also be seen from the comparison that as the filling rate is low (Scenario 4), a slight disagreement between the quiescent model (Scenario 1) and the slow filling rate prediction occurs. This difference may be practically insignificant and it also disappears with time due to the identical material characteristics and stress conditions.

Scenario 5 which was intended to simulate a pond that has a slope to the sides such as shown in Figure 3.7 is compared with Scenario 3 in Figure 3.13. Contrary to the previous finding, the prediction results do not agree. Moreover during the filling period the interface height is not as linear compared to other scenarios. This is because a one-dimensional condition filling does not prevail in Scenario 5 due to the side slope. As the sediment accumulates by a constant fill rate while the filling area increases, the interface height-time plot becomes nonlinear. The smaller interface height at the end of the simulation period is also caused by the same reason.

The investigation continued to two filling step scenarios to reveal if the good agreement found earlier can still be applied for more than a single step pond filling. Two types of filling which are filling at the same time and filling at different time are simulated. Figure 3.14 compares Scenarios 1, 6, 7 and 8 while Figure 3.15 compares Scenarios 6, 9 and 10.

In Figure 3.14, it is found that when the second filling step starts at different times, prediction of interface height will not provide the same result while the final interface settlements are identical. The quiescent condition provides that the ultimate settlement of many filling periods can be estimated while the transient stage can not be obtained from it. This is, of course, due to a different degree of consolidation and the same self-weight stress. Figure 3.15 confirms this by comparing Scenarios 6, 9 and 10.

It can be concluded from this modeling experiment that in a one dimensional condition, when the same amount of tailings is placed and the same amount of time is allowed for tailings to consolidate, the same amount of settlement can be expected and this is due to an identical self-weight stress and similar dissipation time. As a result, for a one dimensional single pond filling condition, a quiescent finite strain consolidation model can be used to estimate an interface settlement. For a multiple filling scenario and varying pond surface condition, a quiescent model can not be used.

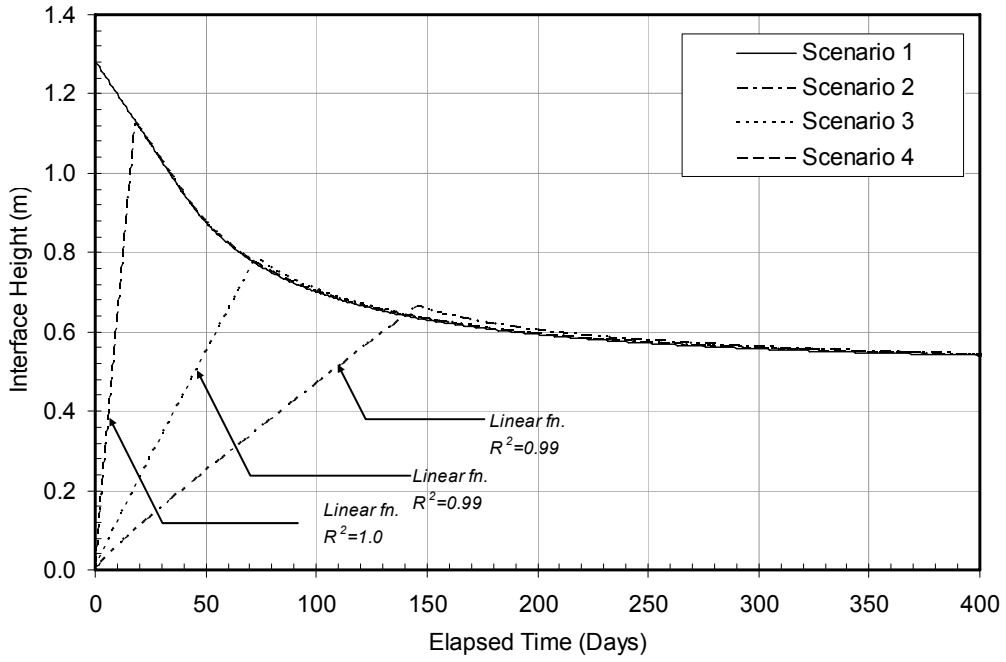

Figure 3.12 Comparison of interface height prediction for scenarios 1 to 4

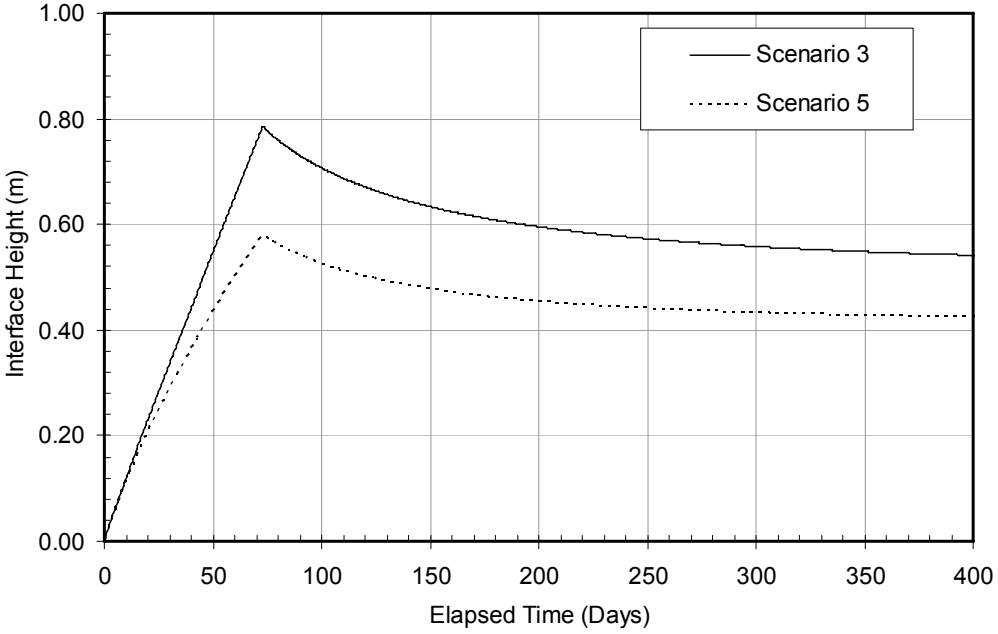

Figure 3.13 Comparison of interface height prediction for scenarios 3 and 5

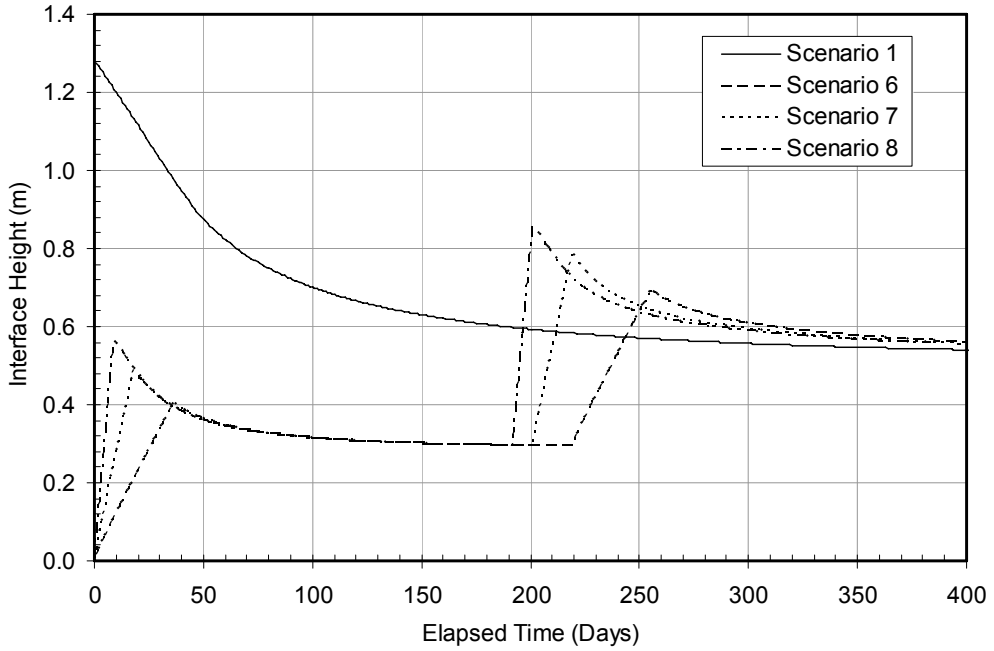

Figure 3.14 Comparison of interface height prediction for scenarios 1, 6, 7 and 8

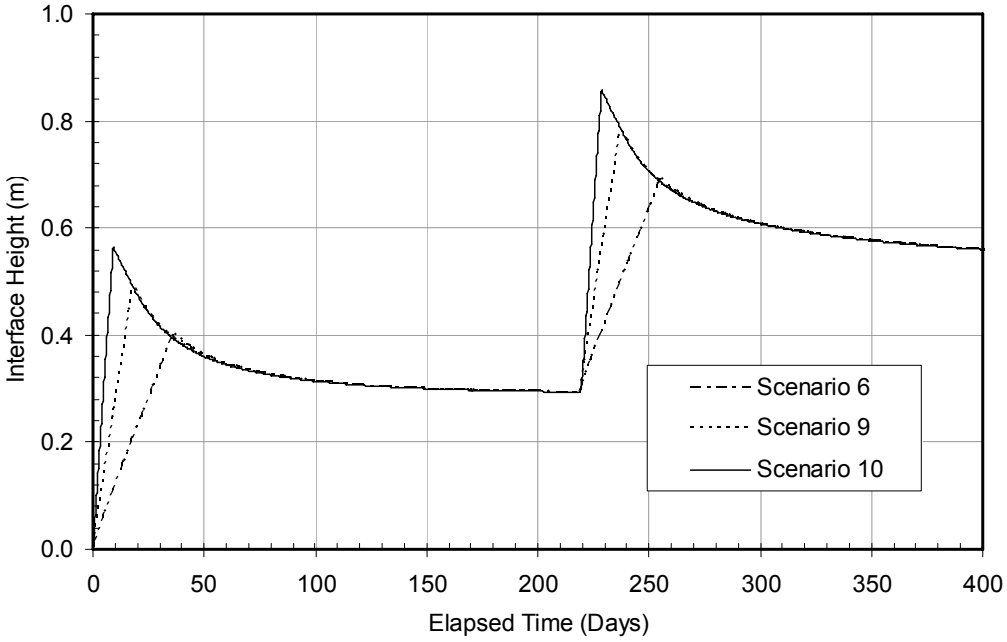

Figure 3.15 Comparison of interface height prediction for scenarios 6, 9 and 10

3.3 Sedimentation and finite strain consolidation theory

In Chapter 2, it was indicated that a sedimentation theory (Kynch, 1952) and a finite consolidation theory (Gibson et al., 1967) are closely related. The finite strain consolidation theory was derived from the conservation of mass and momentum, a flow relationship and an effective stress principal. This is similar to the hindered sedimentation theory proposed by Kynch excepting that effective stress is not considered by Kynch.

The finite strain consolidation theory is used in slurry handling processes which usually consists of two consecutive phenomena - sedimentation and consolidation. The importance of both processes has led to considerable research on combining these two processes into one analysis (e.g. Pane and Schiffman, 1982; Shodja and Feldkamp, 1993; Eckert et al., 1996; Masala, 1998; Toorman, 1999; Bartholomeeusen, 2003; Bürger and Karlsen, 2003).

Amongst different approaches in the literature, an interaction coefficient is of interest due to its direct connection to the conventional finite strain theory. In this section, a technique of using the interaction function with the finite strain consolidation theory is presented and the application to a real problem of predicting sedimentation and consolidation is shown. Based on the interaction coefficient, some characteristics of a selected coefficient function are investigated with different model parameters. The implementation was done by using the finite difference method to solve the governing equation. Investigations on the form of an interaction function, a parametric analysis of the model parameters and a discussion of the shortcomings of the technique are presented.

3.3.1 Derivation of a sedimentation and consolidation model

3.3.1.1 Volume fraction formulation

In this section, a sedimentation and consolidation model with an interaction coefficient is derived. A form of an interaction coefficient, β, is shown in Figure 3.16. A maximum suspension void ratio, e_m, *is* a state of void ratio where there is no effective stress and the interaction coefficient is zero. This void ratio is called the maximum void ratio as an initial void ratio larger than this is not stable and subjected to particle

arrangement without applied stress. A void ratio, e_s, represents a structural void ratio where effective stress is present and the interaction coefficient is equal to unity. The zone of void ratio between the maximum suspension and structural void ratios is called the transition zone. The classical principal of effective stress is

$$\sigma = \sigma' + u_w \qquad [3.9]$$

where σ is total stress, σ' is effective stress and u_w is pore water pressure. For sedimentation-consolidation modeling, the effective stress is modified by an interaction coefficient as

$$\sigma' = \beta(e)\sigma'_c(e) \qquad [3.10]$$

$\beta(e)$ is an interaction coefficient as a function of void ratio and $\sigma'_c(e)$ is an effective stress-void ratio relationship as normally obtained from a large strain consolidation test. As this effective stress-void ratio relationship is for a consolidation zone, a subscript c is assigned to identify that it is not a generalized form of a constitutive relationship throughout the range of sedimentation and consolidation. A combination of the two functions in Equation [3.10] provides a generalized effective stress-void ratio constitutive relationship for a sedimentation-consolidation model.

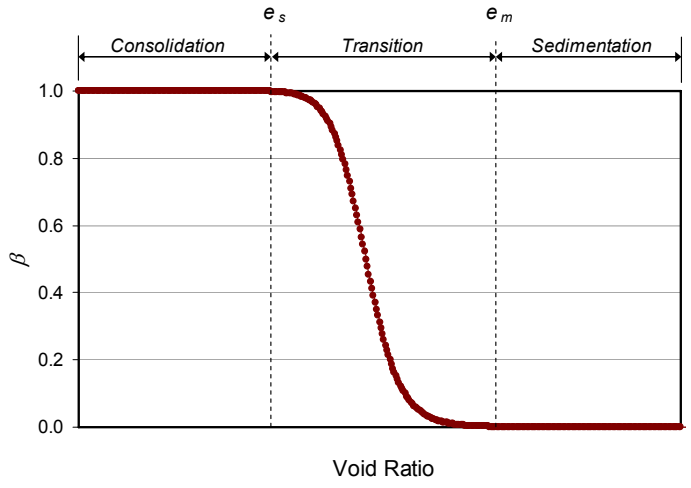

Figure 3.16 Interaction function, structural void ratio (e_s) and maximum suspension void ratio (e_m)

By combining Equations [3.1], [3.9] and [3.10], the governing equation is expressed as

$$\left(\frac{\gamma_s}{\gamma_f}-1\right)\frac{d}{de}\left[\frac{k(e)}{(1+e)}\right]\frac{\partial e}{\partial z}+\frac{\partial}{\partial z}\left[\frac{k(e)}{\gamma_f.(1+e)}\beta(e)\frac{d\sigma_c'(e)}{de}\frac{\partial e}{\partial z}\right]$$
$$+\frac{\partial}{\partial z}\left[\frac{k(e)}{\gamma_f(1+e)}\sigma_c'(e)\frac{d\beta(e)}{de}\frac{\partial e}{\partial z}\right]+\frac{\partial e}{\partial t}=0 \qquad [3.11]$$

By expanding Equation [3.11], we have

$$\left(\frac{\gamma_s-\gamma_f}{\gamma_f}\right)\frac{d}{de}\left[\frac{k(e)}{(1+e)}\right]\frac{\partial e}{\partial z}+\frac{\partial}{\partial z}\left[\frac{k(e)}{\gamma_f.(1+e)}\beta(e)\frac{d\sigma_c'(e)}{de}\right]\frac{\partial e}{\partial z}+\left[\frac{k(e)}{\gamma_f.(1+e)}\beta(e)\frac{d\sigma_c'(e)}{de}\right]\frac{\partial^2 e}{\partial z^2}$$
$$+\frac{\partial}{\partial z}\left[\frac{k(e)}{\gamma_f(1+e)}\sigma_c'(e)\frac{d\beta(e)}{de}\right]\frac{\partial e}{\partial z}+\left[\frac{k(e)}{\gamma_f(1+e)}\sigma_c'(e)\frac{d\beta(e)}{de}\right]\frac{\partial^2 e}{\partial z^2}+\frac{\partial e}{\partial t}=0 \qquad [3.12]$$

Equation [3.12] can be reduced to a simple form as

$$\frac{1}{\gamma_f}\left[\left(\gamma_s-\gamma_f\right)\psi(e)+\frac{\partial\phi(e)}{\partial z}+\frac{\partial\varphi(e)}{\partial z}\right]\frac{\partial e}{\partial z}+\frac{1}{\gamma_f}\left[\phi(e)+\varphi(e)\right]\frac{\partial^2 e}{\partial z^2}+\frac{\partial e}{\partial t}=0 \qquad [3.13]$$

where

$$\psi(e)=\frac{d}{de}\left(\frac{k(e)}{1+e}\right)$$
$$\phi(e)=\frac{k(e)}{1+e}\beta(e)\frac{d\sigma_c'(e)}{de}$$
$$\varphi(e)=\frac{k(e)}{1+e}\sigma_c'(e)\frac{d\beta(e)}{de}$$

Tan et al. (1995) stated that the settling behavior in a transition zone is not well defined and it can be either a sedimentation or a consolidation process. It was also suggested that a transition zone may exist where effective stresses are partially developed (Tan et al., 1995) and physically this phase is where flocs in suspension come into contact and start breaking up (Been and Sills, 1981). To be able to control the transition zone, a Harris model is implemented to couple sedimentation and consolidation phenomena. A Harris model is one of several yield density models used to predict population growth.

The use of a Harris model was employed in this study because it allows the thickness of the transition zone that couples the two processes to be adjustable and it is a continuous function. This technique has the advantage of being able to control the transition zone for different types of slurry. It is noted that a step function was not considered for this numerical model as a similar technique has already been investigated by other researchers (Bürger and Karlsen, 2001) and also because the governing equation of a hyperbolic – parabolic type contains a discontinuity and becomes unsuitable for the selected numerical scheme.

A Harris model is expressed as Equation [3.14]. In Equation [3.14], the power of void ratio can become infinity. Because of this reason, β_t, a threshold interaction coefficient whose value is very small approaching zero, is arbitrarily selected. For constitutive relationships, the conventional form of power law void ratio – effective stress and hydraulic conductivity – void ratio relationships are chosen and expressed as Equations [3.15] and [3.16] respectively. It is noted that other forms of the constitutive relationship functions can also be applied in a similar manner and the choice is largely dependent on the behavior of the subject slurry. The major concern about the constitutive relationship is not the form of the relationship but rather the time dependent compressibility behavior of the slurry as indicated by Sills (1998). This is not considered in this section.

$$\beta = \begin{cases} \left(\dfrac{1}{E + Fe^{G}}\right) & ,\beta > \beta_t \\ \beta_t & ,\beta \le \beta_t \end{cases} \qquad [3.14]$$

$$e = \begin{cases} A\left(\sigma_c'\right)^B = A\left(\dfrac{\sigma'}{\beta}\right)^B & ,e > e_s \\ A\left(\sigma_c'\right)^B = A\left(\sigma'\right)^B & ,e \le e_s \end{cases} \qquad [3.15]$$

$$k = Ce^{D} \qquad [3.16]$$

where A and B are compressibility parameters, C and D are hydraulic conductivity parameters and E, F and G are interaction coefficient parameters.

As it can be seen in Equation [3.15], $\sigma'_c(e)$ is modified by an interaction coefficient and therefore the effective stress–void ratio constitutive relationship for the

sedimentation-consolidation model, $\sigma'(e)$,can be viewed as shown in Figure 3.17. The figure shows that effective stress, σ', is very small to zero in the sedimentation and transition regions. During the transition from e_m to e_s, the effective stress increases significantly from almost zero to a finite number and when the void ratio is lower than e_s, the effective stress-void ratio constitutive relationship for sedimentation-consolidation becomes the constitutive relationship for a consolidation zone. It is also noted that to calculate effective stresses for parameter updating in the model, Equation [3.15] must be used.

A finite difference method with a backward time central space scheme was chosen to solve the governing equation due to its stability. An upwind difference was also applied in the advection term of the governing equation to resolve the shock like behavior of the equation.

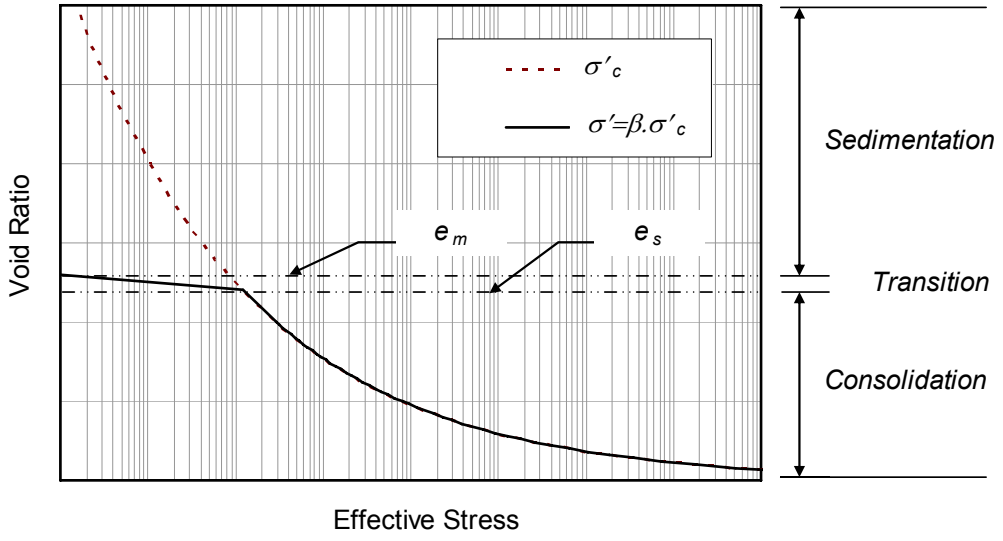

Figure 3.17 Effective stress-void ratio relationship

3.3.1.2 Excess pore pressure formulation

An excess pore pressure formulation is found to be convenient for the formulation of the boundary conditions. Following Koppula (1970), Somogyi (1980) reformulated the governing equation in terms of excess pore pressure, u, instead of void ratio as

$$\frac{\partial}{\partial z}\left[-\frac{k(e)}{\gamma_f(1+e)}\frac{\partial u}{\partial z}\right]+\frac{de}{d\sigma'}\frac{\partial \sigma'}{\partial t}=0 \qquad [3.17]$$

Based on Equations [3.9] and [3.10], Equation [3.17] can be written as

$$\frac{\partial}{\partial z}\left[\frac{k(e)}{\gamma_f(1+e)}\frac{\partial u}{\partial z}\right]+\frac{de}{d(\beta\sigma_c')}\frac{\partial u}{\partial t}=0 \qquad [3.18]$$

According to Equations [3.14] and [3.15], we define

$$\omega(e)=\frac{de}{d(\beta\sigma_c')}=\left(\sigma_c'\frac{d\beta}{de}+\beta\frac{d\sigma_c'}{de}\right)^{-1} \qquad [3.19]$$

By rearranging Equation [3.18] with [3.19], the governing equation of sedimentation-consolidation in terms of excess pore pressure becomes

$$\frac{1}{\gamma_f.\omega(e)}\frac{\partial}{\partial z}\left[\frac{k(e)}{(1+e)}\right]\frac{\partial u}{\partial z}+\frac{k(e)}{\gamma_f.\omega(e).(1+e)}\frac{\partial^2 u}{\partial z^2}+\frac{\partial u}{\partial t}=0 \qquad [3.20]$$

Constitutive relationships [3.15] and [3.16] were applied to Equation [3.20] and a finite difference method with the same discretization used in the previous section was chosen to solve the governing equation.

Both volume fraction and excess pore pressure formulations give identical predictions. To follow the original formulation by Gibson et al. the volume fraction formulation will be further used to explore the prediction capability of this method of modeling sedimentation-consolidation.

3.3.2 Sensitivity of the model parameters

In this section, the sensitivity of the parameters used in the sedimentation-consolidation model is explored. These parameters include the thickness of a transition zone, structural and maximum suspension void ratios, an initial solids content and a sample height. An initial solid content dictates the initial hydraulic conductivity and

therefore the initial settling rate of the slurry and a sample height contributes to drainage length so they are chosen in this section. For the thickness of a transition zone, a structural void ratio and a maximum suspension void ratio are the controlling parameters based on an interaction function. It is noted that for all simulations in this section, $n = z / \Delta z = 200$ and $\Delta t = 10^{-3}$ are used (n, z, t denote total node number, material coordinate length and time).

3.3.2.1 Thickness of the transition zone

Due to the fact that a mathematical form of a Harris model [3.14] does not explicitly express e_s and e_m, parameters must be chosen to satisfy the interaction $\beta \sim 1$ at the void ratio $\sim e_s$ and $\beta \sim 0$ at the void ratio $\sim e_m$. Five different sets of interaction parameters, which represent different thicknesses of the transition zone, were selected and shown in Table 3.2 and Figure 3.18. According to Shodja and Feldkamp (1993), the thickness of a transition zone is related to the particle size distribution, particle packing characteristics and the nature of interparticle forces.

Simulations were performed with the same initial void ratio which was constant with depth. The oil sands fine tailings were selected for these analyses. The soil parameters are S_i = 12.5% (initial solids content by mass), H_i = 0.36 m (initial depth), G_s = 2.28, and the finite strain parameters are A = 3.38, B = -0.31, $C = 6.51\times10^{-6}$ and D = 3.82 (units in kPa and m/day).

Table 3.2 Five interaction functions for different thicknesses of a transition zone

Modeling parameters	Parameter set 1 $e_s \sim 12.1$, $e_m \sim 17.2$	Parameter set 2 $e_s \sim 12.1$, $e_m \sim 14.8$	Parameter set 3 $e_s \sim 12.1$, $e_m \sim 13.2$	Parameter set 4 $e_s \sim 12.1$, $e_m \sim 12.7$	Parameter set 5[a] $e_s \sim 12.1$, $e_m \sim 12.5$
E	1.0	1.0	1.0	1.0	1.0
F	1.0×10^{-30}	1.0×10^{-50}	1.0×10^{-110}	1.0×10^{-200}	1.0×10^{-300}
G	25.9	44.4	99.8	183.0	275.5

[a] $\beta_t = 10^{-4}$ was assigned

The five sets of parameters illustrate the behavior of the model with the chosen interaction function. These parameters are used to initially explore the interface between the soil and slurry therefore e_s is set as a constant and e_m is varied. The interface settlements with time for all simulations are shown in Figure 3.19.

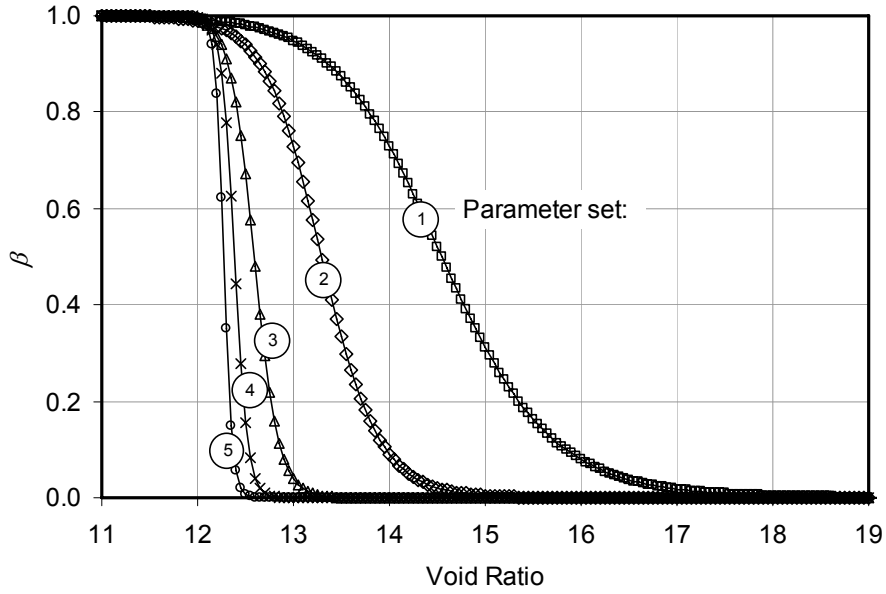

Figure 3.18 Five interaction functions for different thicknesses of a transition zone

The interface comparisons show that in general there is no difference in the initial rate of settlement. This is expected as an initial settling rate depends on sedimentation while consolidation affects the rate later on when the void ratio reaches a structural void ratio and the interaction coefficient becomes unity. It can be seen that the interface settling rate dramatically changes when the soil-suspension interface meets the slurry-water interface approximately at 6 days. The different interaction parameters indicate that the interface settlement around 6 days will be slightly different and is dependent on e_m. Obviously if e_m is obtained at a higher void ratio, consolidation can start earlier causing the interface settlement to slow down as excess pore pressure dissipation is required for further compression. Also the gradual change in parameter set 1 (Figure 3.18) clearly represents a system that does not display a distinction between the consolidation and sedimentation regimes while parameter set 5 shows a sharp distinction. The closer an interaction function is to a step function the more similar will be the values of e_s and e_m.

Void ratio profiles and effective stress profiles for parameter sets 1, 2, 4, and 5 are shown in Figures 3.20 and 3.21 respectively. The profiles for parameter set 3 falls in between those for parameter sets 2 and 4. The predicted void ratio profiles in Figure 3.20

show a process of reduction of void ratio by sedimentation and consolidation. During sedimentation a clear water-suspension interface settles and the suspension-soil interface builds from bottom up. The function of the interaction coefficient predicts sedimentation and consolidation in difference soil systems. That is, parameter set 1 can be regarded as a clayey soil that has a larger transition zone between sedimentation and consolidation while parameter set 5 can be regarded as a coarse grained soil with a sharp transition zone. Even though there is a significant difference in the shape of the void ratio profile, there is very little to no effect of the interaction coefficient on the final effective stress values; being about 0.23 kPa at the bottom and zero at the top (Figure 3.21).

It is worth mentioning that the closer e_s *is* to e_m (than those assigned in parameter set 4) there is very little further variation in the void ratio profiles. Conversely, parameter set 1 shows a void ratio profile resembling those predicted by the conventional finite strain consolidation model. These behaviors depend on e_m and on the initial void ratio.

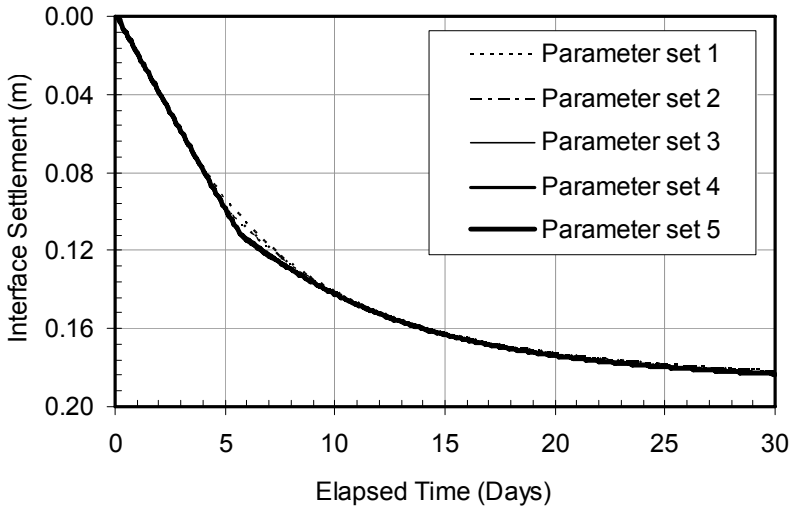

Figure 3.19 Interface vs. time for the five parameter sets

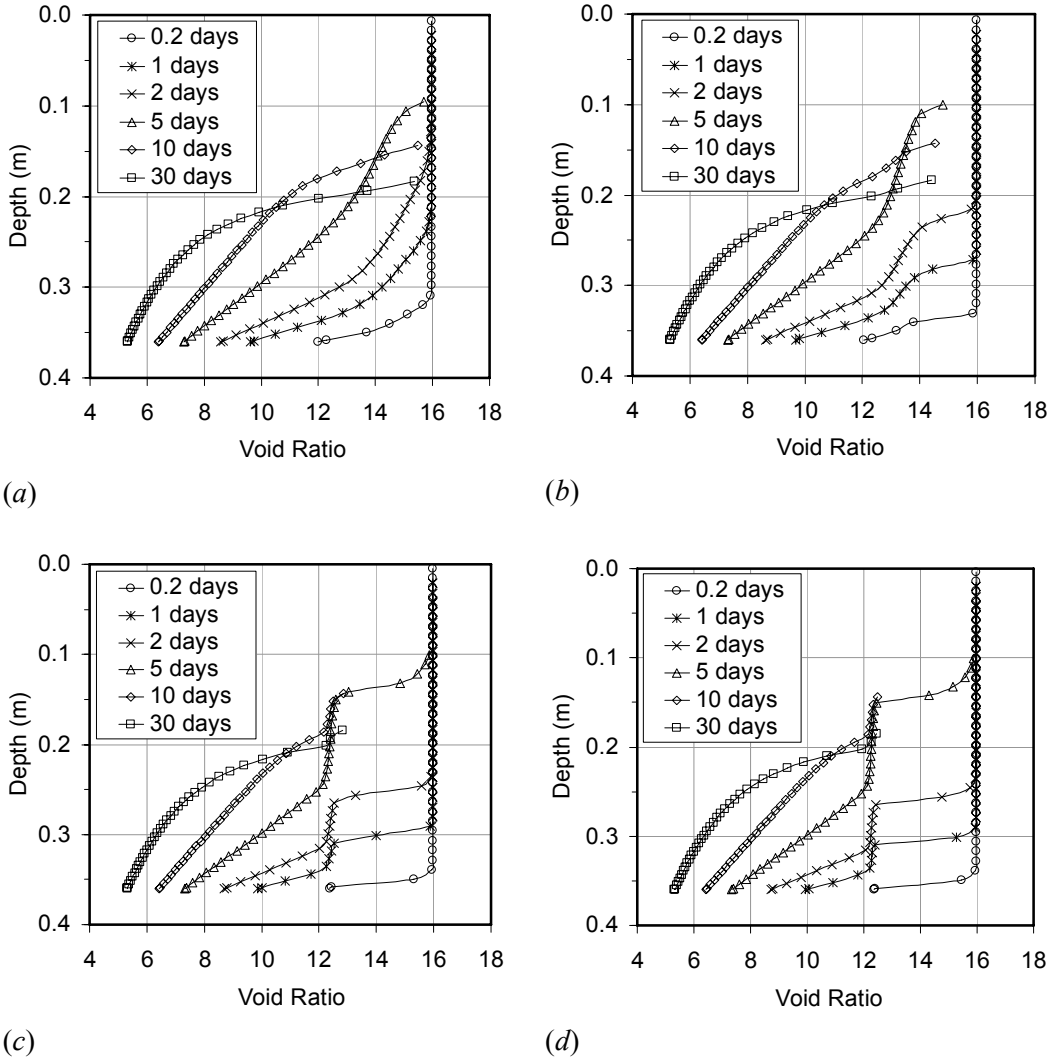

Figure 3.20 Void ratio profiles (*a*) parameter set 1, (*b*) parameter set 2, (*c*) parameter set 4, (*d*) parameter set 5

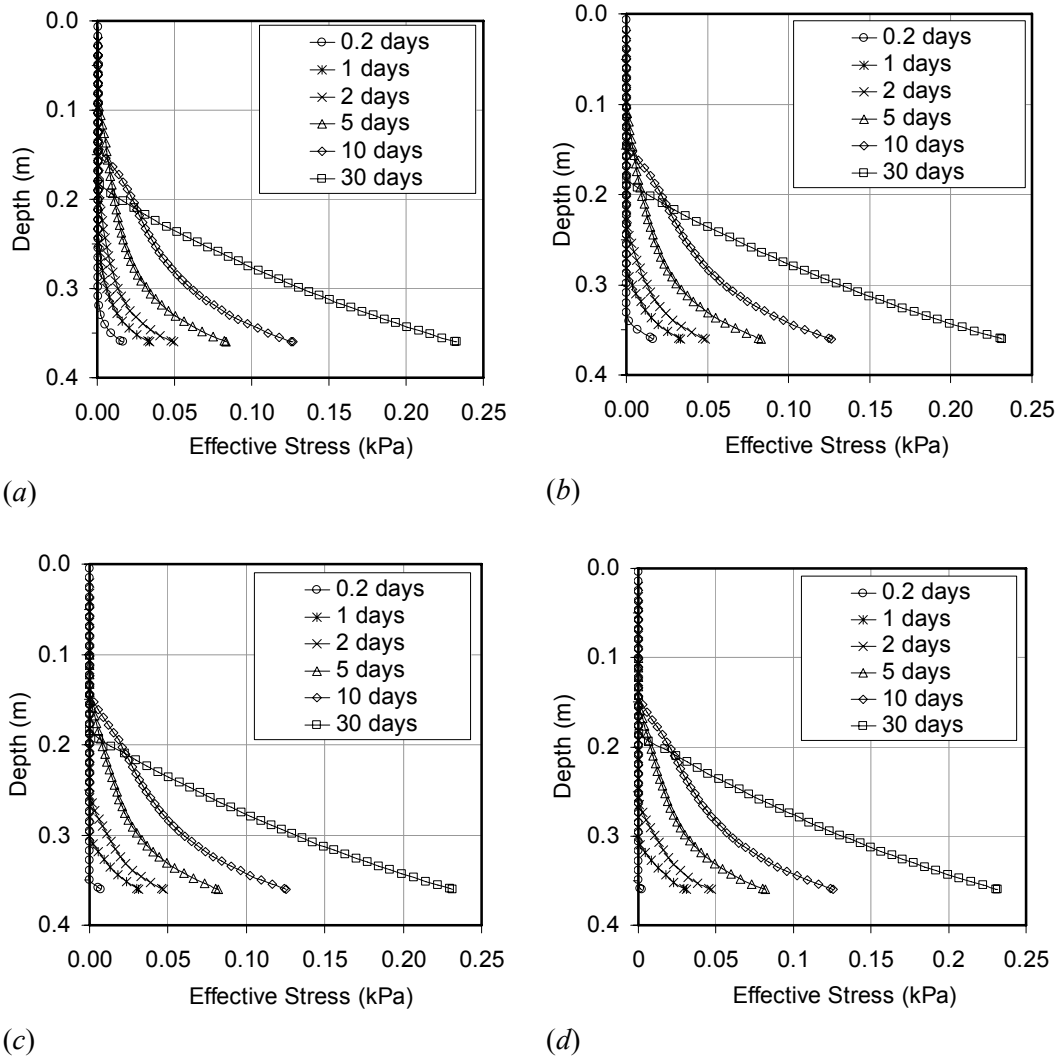

Figure 3.21 Effective stress profiles (a) parameter set 1, (b) parameter set 2, (c) parameter set 4, (d) parameter set 5

3.3.2.2 Structural void ratio and maximum suspension void ratio

Structural void ratio, e_s, and maximum suspension void ratio, e_m, are important parameters for sedimentation-consolidation behavior. They are studied for a fixed thickness of the transition zone in this section. The previous section has shown that parameters F and G have a significant contribution to a step density profile observed in many batch sedimentation tests. It was also shown that a range of parameters F and G in the parameter sets 1 to 4 does not require β_t therefore this range of F and G parameters

are used in this section. Two sets of e_s and e_m are shown in Table 3.3 and Figure 3.22 to demonstrate the influence of these parameters.

Table 3.3 Two interaction functions (different e_s and e_m)

Modeling parameters	Parameter set 1 $e_s \sim 9.7$, $e_m \sim 10.3$	Parameter set 2 $e_s \sim 12.1$, $e_m \sim 12.7$
E	1.0	1.0
F	10^{-150}	10^{-200}
G	149.8	183.0

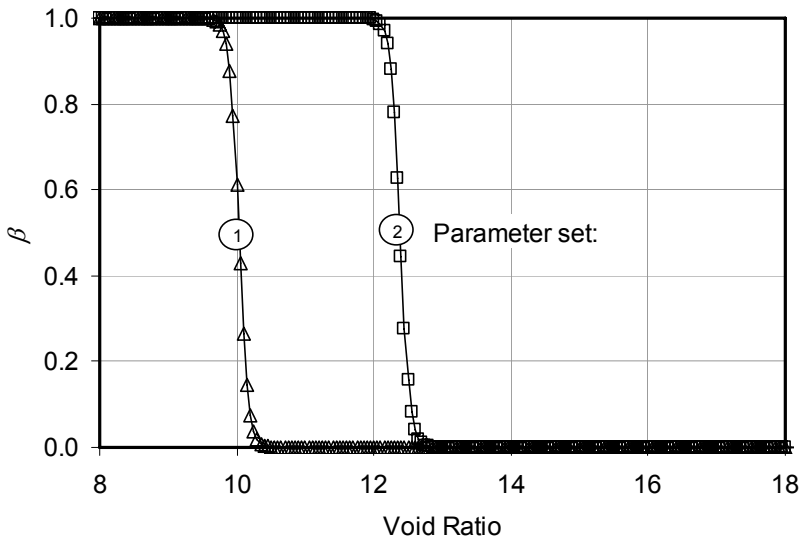

Figure 3.22 Two interaction functions (different e_s and e_m)

The modeling results for interface settlement, void ratio profiles and effective stress profiles are shown in Figures 3.23, 3.24 and 3.25 respectively. It can be seen that e_s and e_m control the thickness of the sediment at the end of sedimentation (Figure 3.24). And by changing the structural void ratio, the initial void ratio of the sediment layer shifted according to the values of e_s and e_m assigned (Figure 3.22). This model behavior, however, does not affect the initial settling rate which is dependent on an initial solid concentration as described by Kynch's hindered sedimentation theory. As time progressed the interfaces of both simulations approached a similar result (Figure 3.23) due to the same self-weight consolidation pressure. It is noted, however, that e_s and e_m are important to capture void ratio profiles correctly and should be determined from laboratory measurements.

During the transient stage, the development of effective stresses was slightly different with a higher value of effective stress at the same elevation for the higher values of e_s and e_m. The difference was, however, narrowed down as consolidation progressed (Figure 3.25). According to the model results, it can be concluded that if two soils have the same constitutive relationships, the soil exhibiting higher values of structural and maximum suspension void ratios will start consolidation sooner at higher void ratios and show higher effective stresses near the surface of the deposit during consolidation.

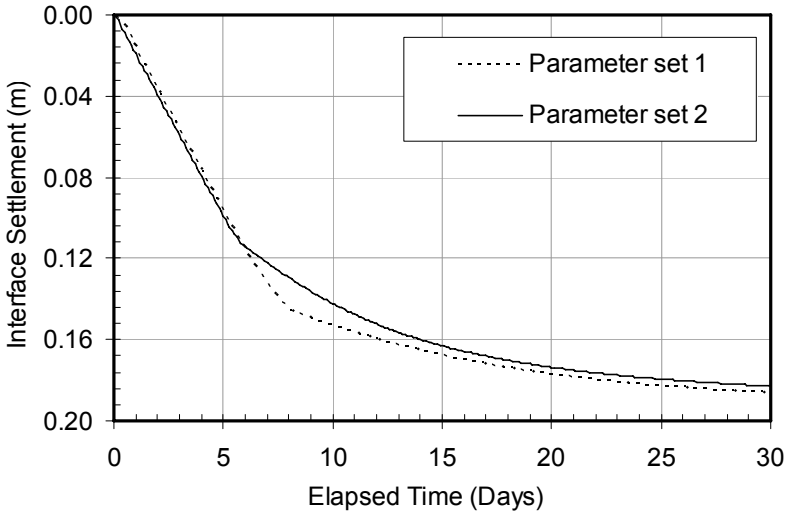

Figure 3.23 Interface settlement vs. time for different e_s and e_m

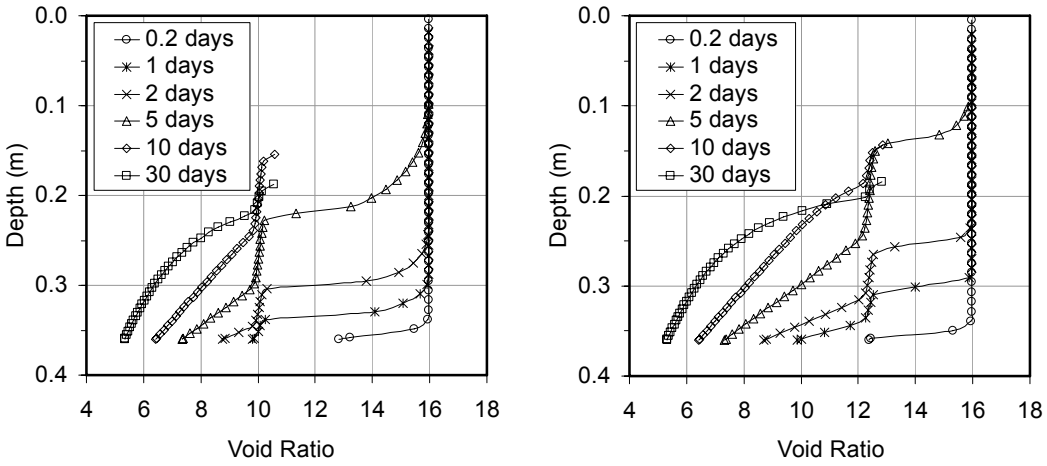

(*a*) (*b*)

Figure 3.24 Void ratio profile of (*a*) e_s =9.7 and e_m= 10.3, (*b*) e_s =12.1 and e_m= 12.7

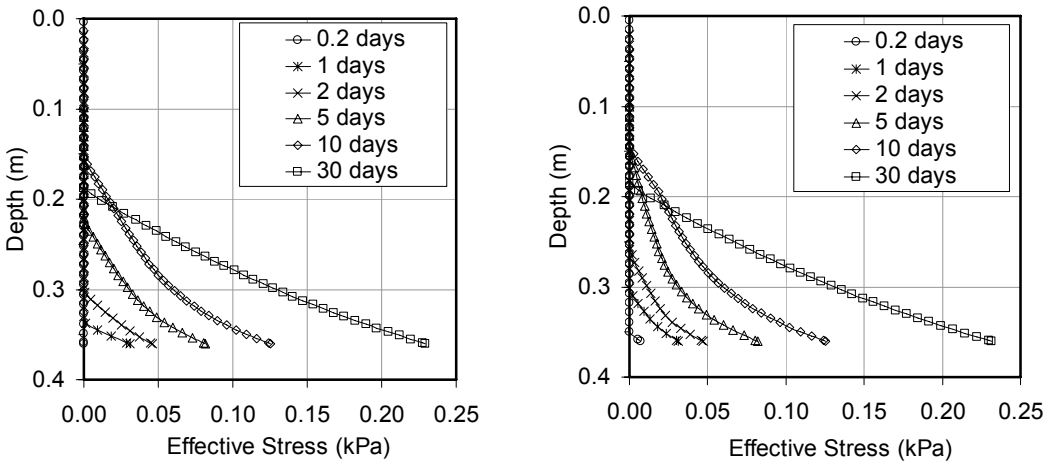

Figure 3.25 Effective stress profile of (*a*) e_s =9.7 and e_m= 10.3, (*b*) e_s =12.1 and e_m= 12.7

3.3.2.3 Initial solids content

Based on Kynch's hindered sedimentation theory, the settling velocity is dependent only on particle solids content. To test if the present model conforms to this statement, three different initial solids contents, 10.0%, 12.5% and 17.5%, are chosen. The interface settlement with time for all the simulations are shown in Figure 3.26 and void ratio profiles and effective stress profiles for initial solids contents of 10.0% and 17.5% are shown in Figure 3.27 and 3.28 respectively. For an initial solids content of 12.5% the profiles were previously shown in Figures 3.20(*c*) and 3.21(*c*).

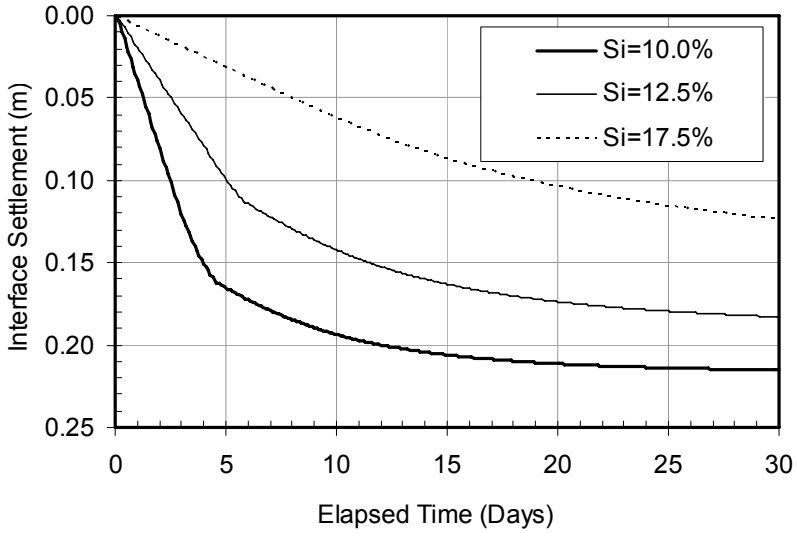

Figure 3.26 Interface settlements vs. time for different initial solids content

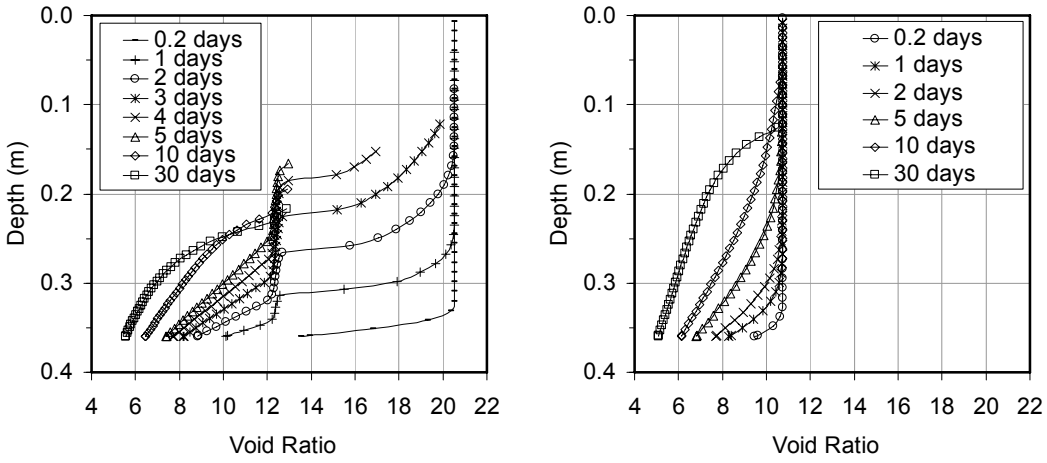

Figure 3.27 Void ratio profiles (*a*) S_i=10%, (*b*) S_i=17.5%

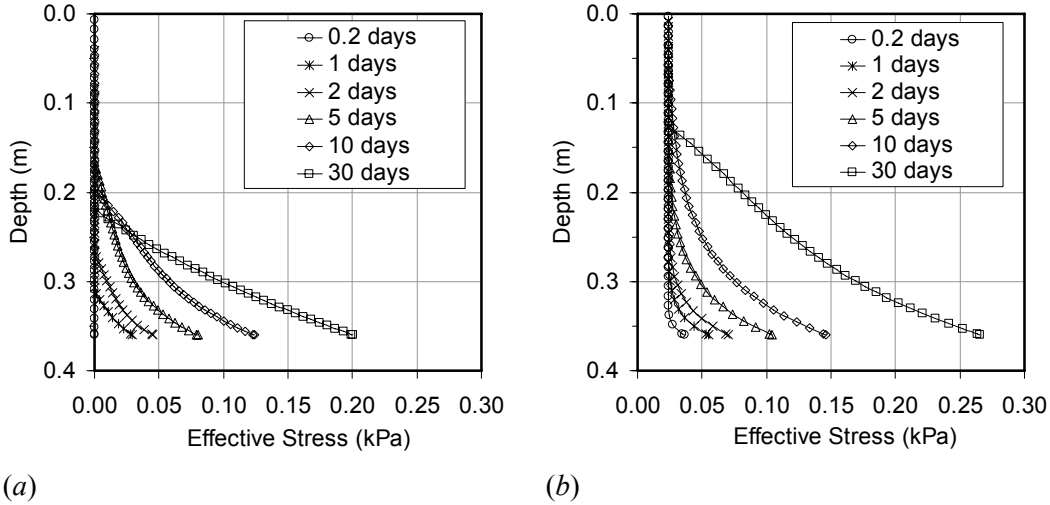

Figure 3.28 Effective stress profiles (*a*) S_i=10%, (*b*) S_i=17.5%

The higher the initial solids content the slower the settling rate as one would expect from a batch sedimentation test (Figure 3.26). For a system with an initial void ratio larger than the structural void ratio, sedimentation behavior (Figure 3.27(*a*)) is expected. With a lower initial void ratio than the structural void ratio, only a consolidation regime is exhibited (Figure 3.27(*b*)). The proposed modeling technique, at this stage, clearly can simulate the sedimentation and consolidation behavior for the different initial void ratio conditions in the examples. However, as can be seen from Figure 3.27(*a*), if a low initial solid content is used, there is a significant difference

between the maximum suspension void ratio and the initial void ratio. As a result, from the selected numerical scheme, a smeared interface is expected.

In Figure 3.26, for a case of initial linear settling velocity, the initial settling rate can be correlated to the initial hydraulic conductivity via an equation proposed by Pane and Schiffman 1997. The results (Table 3.4) show that the selected numerical and model parameters give less than a 2.2% difference in the initial settling velocity compared to those calculated from Pane and Schiffman's equation. According to the numerical model, the higher the solids content the slower the settling rate which appears to be logical as at the higher solids content consolidation governs. Nevertheless, the percent difference in Table 3.4 likely occurs from two major reasons; one is that the Pane and Schiffman's equation considers no consolidation which is not the case in this presentation. Another is that a backward time central space scheme is likely giving a small error to the initial predictions. This is due to the fact that it utilizes material parameters at a current time step for a consecutive time step. Somogyi (1980) stated that the stability of this method will cause the error introduced to decay.

Table 3.4 Difference of initial settling velocity

Initial solids content (%)	$v_{i\text{-}sc}$, initial settling velocity from a sedimentation-consolidation model[a] (m/day)	$v_{i\text{-}PS}$, initial settling velocity from Pane and Schiffman (1997) (m/day)	$(v_{i\text{-}sc} - v_{i\text{-}PS})/ v_{i\text{-}PS} \times 100$ (%)
10.0	6.380×10^{-3}	6.240×10^{-3}	2.2
12.5	1.967×10^{-2}	1.959×10^{-2}	0.4
17.5	4.005×10^{-2}	4.036×10^{-2}	-0.8

[a] calculated from 0-3 days

3.3.2.4 Initial height of slurry

Initial height controls the drainage length of the slurry settling process. In sedimentation, it is known that the drainage length has no effect on the velocity of the falling solid particles. The sedimentation-consolidation model, therefore, must be able to capture the initial interface velocity of sedimentation that is independent of the initial slurry height. In this analysis initial heights of 0.36 m, 0.72 m, and 1.50 m are chosen for this verification. An initial solid content of 12.5% is used and others parameters remain unchanged. The interface settlements with time for all the predictions are shown in Figure 3.29. Void ratio profiles and effective stress profiles for initial heights of 0.72 m

and 1.50 m are shown in Figures 3.30 and 3.31 respectively while the profiles for a height of 0.36 m were previously shown in Figure 3.20(*c*) and 3.21(*c*).

In Figure 3.29, there is little to no variation in the predicted hindered settling velocities of the three different initial heights. During hindered sedimentation, a sediment layer is forming at the bottom of the slurry and self-weight is built up. Subsequently the self-weight induces excess pore pressure and as dissipation occurs, consolidation happens. The time of consolidation is largely affected by the drainage length and the excess pore pressure gradient therefore different interface settlement rates for different sample heights are expected during the consolidation regime.

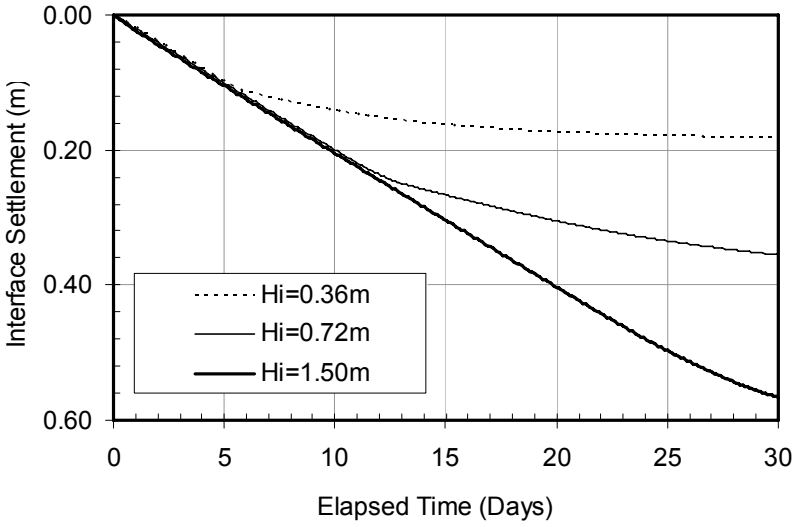

Figure 3.29 Interface settlement of different initial height

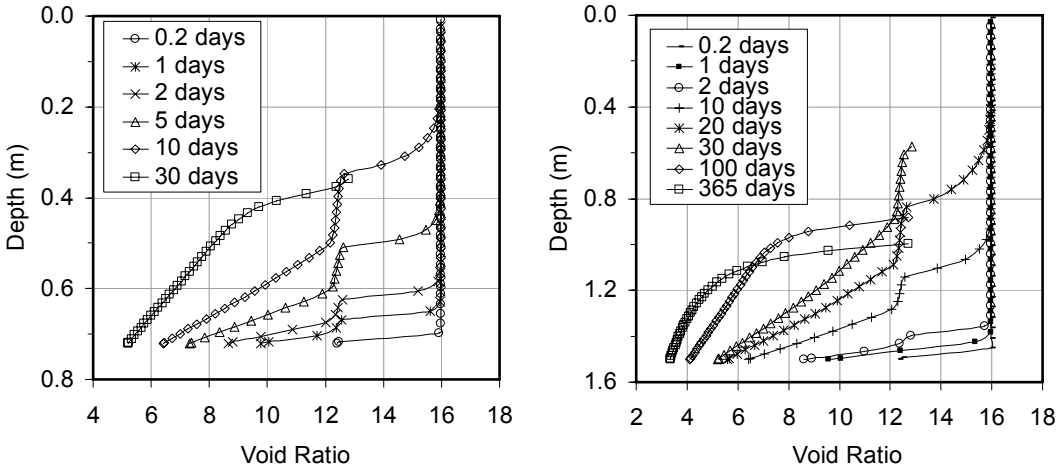

(*a*) (*b*)

Figure 3.30 Void ratio profiles (*a*) H_i=0.72m, (*b*) H_i=1.50m

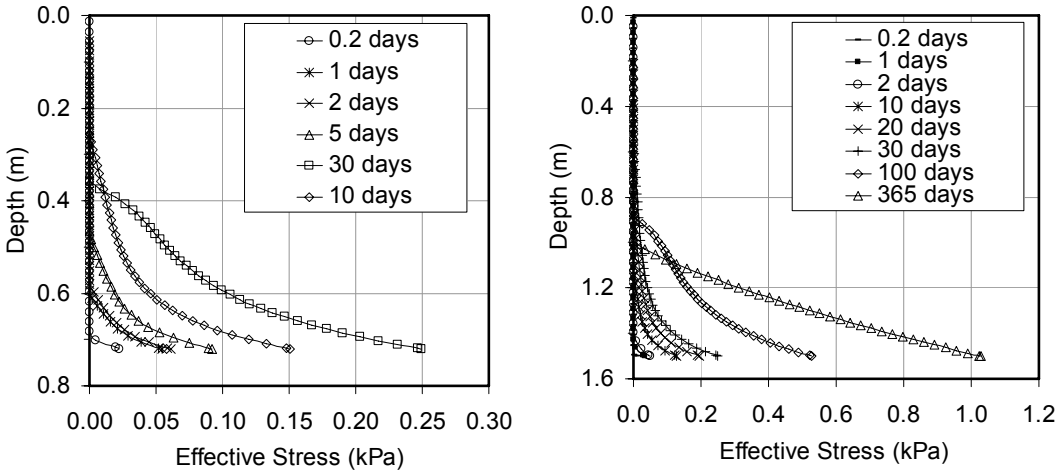

(*a*) (*b*)

Figure 3.31 Effective stress profiles (*a*) H_i=0.72m, (*b*) H_i=1.50m

Figures 3.30 and 3.31 show that the higher the deposit the larger is the bottom effective stress and thus there is a smaller bottom void ratio. However, the surface void ratio remains at e_m and the effective stress is zero at the surface. This indicates that, for this model, a slurry that has an initial void ratio higher than e_m always ends up having an effective stress of zero at the surface at the end of self-weight compression. Even if an initial void ratio of e_s is used, there will still be a very low effective stress at the surface, generally less than 5 kPa, corresponding to the e_s. The practical implication of this result is that there is no way to safely put any load, in general civil engineering work, on the top

of a slurry deposit because there is not the strength to support it. Surface/ground improvement or other densifying phenomenon (e.g. desiccation) must be incorporated.

3.3.3 Comparison of the sedimentation-consolidation model with experimental data and predictions from other models

In the previous section, it was shown that the interaction coefficient method has met expectations to capture general sedimentation and consolidation behavior. In this section, the method is further used to simulate an experimental sedimentation-consolidation problem and also to compare the model with other sedimentation-consolidation models available in the literature. For these tasks, experimental results from Been and Sills (1981), and numerical predictions from Eckert et al. (1996) and Bustos et al. (1999) were selected. Model parameters from these references are listed in Table 3.5. Explanations on how these parameters were obtained are discussed in the following subsections. It is also noted that the numerical parameters were chosen depending on the initial height of the sample and on the duration of each case.

Table 3.5 Modeling parameters of various soils (units in kPa, m/day)

Modeling parameters	Been and Sills (1981) batch experiment # 15	Copper fine tails predictions by Eckert et al. (1996) and Bustos and Concha (1988)	Bustos et al. (1999) sedimentation with compression model
H_i (m)	0.643	0.401	2.000
S_i (%)	20.40	25.96	25.96
G_s	2.66	2.50	2.50
A	3.090	2.089	2.303
B	-0.279	-0.401	-0.340
C	9.50×10^{-4}	0.260	0.190
D	2.323	2.720	2.904
E	1.0	1.0	1.0
F	1.0×10^{-200}	1.0×10^{-200}	1.0×10^{-150}
G	200.0	280.0	291.0

3.3.3.1 Batch experiment # 15 by Been and Sills

The interface settlement rate and the void ratio profiles were predicted for experiment #15 presented by Been and Sills (1981). This experiment was selected specifically because a similar prediction by Eckert et al. (1996) was available.

Constitutive relationships used in our model are shown in Table 3.5 and they were fitted by a power law function to experimental data determined by Been (1980). The structural void ratio and the maximum suspension void ratio of the slurry are approximately between 8.8 and 12.0. According to the current model, a deflection point of a void ratio profile at the bottom can represent the structural void ratio and a deflection point of a void ratio profile at the top represents the maximum suspension void ratio. A void ratio of 8.8 was directly obtained from the bottom deflection of Been's data. For the maximum suspension void ratio, the top deflection is not clearly shown in experiment #15. This may suggest that the maximum suspension void ratio is higher than the initial void ratio. Further investigation on other experiments, #7 and #8 performed on the same soil specimen, indicates that the maximum suspension void ratio should range between 10.0 and 14.0. Due to the uncertainty in selecting these parameters, an averaged void ratio of 10 from the void ratio range of experiment #15 was chosen for this simulation.

Both experimental and prediction results of interface settlement are shown in Figure 3.32 and the void ratio profiles are given in Figure 3.33. For this simulation, $n = z / \Delta z = 200$ and $\Delta t = 10^{-2}$ were used.

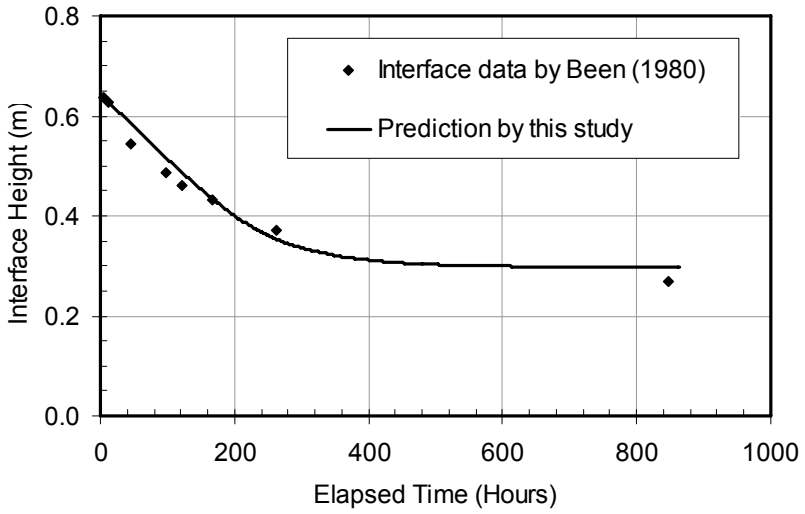

Figure 3.32 Interface settlements vs. time comparison of experiment and model

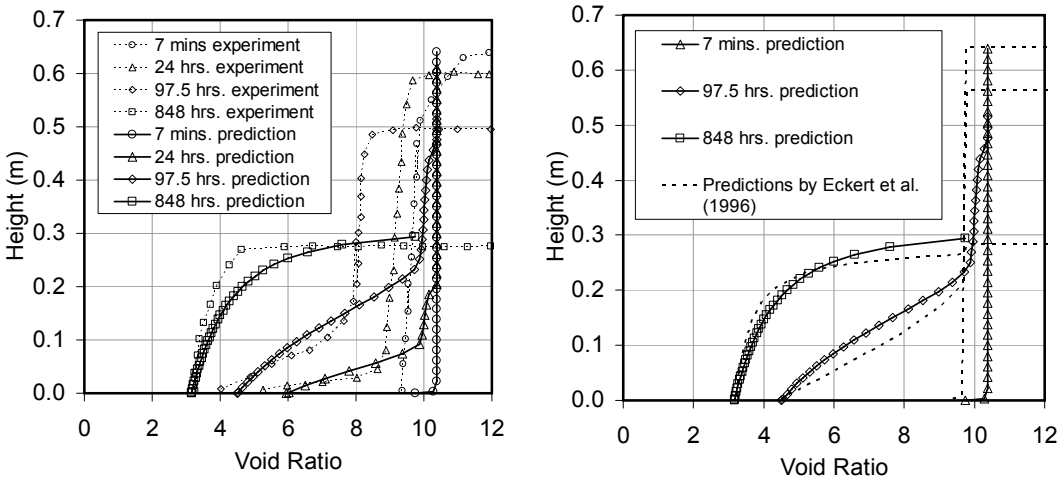

(*a*) (*b*)

Figure 3.33 Void ratio profile comparison (*a*) experiment and the model (b) this study model and Eckert et al. (1996) model.

In Figure 3.32, the model captured the slurry-water interface settlement of the experiment adequately. In general, it can be said that the model and the experimental data are quantitatively similar. This good agreement for the slurry-water interface settlement, however, can also be captured without implementation of sedimentation in the finite strain consolidation model. This is because the power law assigned for the compressibility only gives a small effective stress based on the initial void ratio. This small effective stress has negligible influence on the initial settling rate which is largely controlled by hydraulic conductivity.

The void ratio profiles are of greater interest. Figure 3.33(*a*) clearly shows that the soil used in the experimental data of Been (1980) exhibited a significant decrease in void ratio in the upper part with time. This could be a time dependent phenomenon discussed by Sills (1998) and this time dependent compressibility should be considered in the model to capture such behavior. This phenomenon happens in the transition zone above the soil-suspension interface and does not appear to affect the void ratio in the soil phase as the predicted and experimental void ratio profiles below the soil-suspension interface are quantitatively similar.

Comparison of Eckert's fluid dynamic model with our model is shown in Figure 3.33(*b*). Because in the current analysis the e_s and e_m are set to be approximately 10 which results in the soil-suspension front moving upward, the profiles are slightly different. The

simulation in this section also used the original data presented by Been (1980) so the initial profile is slightly different from the one predicted by Eckert et al. (1996) who used the initial solid content from the 7 minute void ratio profile of Been (1980). Results similar to those predicted by Eckert et al. (1996) can be obtained by the finite strain consolidation theory setting the initial void ratio lower than that specified by Been (1980) and using a smooth transition function such as the one utilized in Figure 3.18 (parameter set 1).

3.3.3.2 Fine tails from a copper concentrator by Bustos and Concha and Eckert et al.

Bustos and Concha (1988) proposed a model to simulate batch sedimentation-consolidation. Eckert et al. (1996) used the same soil parameters with their sedimentation-consolidation model to make similar predictions. The same soil parameters and conditions have been used in this paper to model sedimentation-consolidation with the proposed modified finite strain consolidation theory. The soil parameters used by Bustos and Concha (1988) and Eckert et al. (1996) were in a form of yield stress, settling velocity and solid volume fractions. In order to use these parameters in the interaction-coefficient model, conversion to effective stress, hydraulic conductivity and void ratio was needed via Equations [3.21] and [3.22]. It is noted that a, b, u_∞, and α are parameters in the fluid dynamic model by Eckert et al. and these parameters were obtained from the experimental results according to Bustos and Concha.

$$k = \frac{\gamma_f u_\infty (1-\phi)^{\alpha+1}}{(\gamma_s - \gamma_f)\phi} \qquad [3.21]$$

$$\sigma' = ae^{b\phi} \qquad [3.22]$$

After the transformation, a power law was fitted to the fluid dynamic parameters for void ratios ranging from 2.6 to 7.7 as this range represented the operating range of the problem. The resulting parameters are listed in Table 3.5. Due to this fitted function, a slight difference in the fluid dynamics parameters and the finite strain parameters was introduced. For the structural and maximum suspension void ratios, values of 5.1 and 5.3 were arbitrarily selected because they were not specified in the references. Nevertheless,

the choice of these void ratios has not significantly affected the steady state void ratio profiles presented in Sections 3.3.2.1 and 3.3.2.2. Figure 3.34 shows the predictions of the finite strain model compared to Eckert et al. (1996) and Bustos and Concha (1980) fluid dynamic models. The finite strain simulation used $n = z / \Delta z = 200$ and $\Delta t = 10^{-5}$.

The slurry-water interface in the current prediction is similar to that predicted by Eckert et al. (1996) and the final heights from both predictions are virtually identical (Figure 3.34). The selected structural and maximum suspension void ratios, however, contribute to a slight difference in the soil-suspension interface.

Notable distinctions are the predictions of the iso-concentration lines of 0.20 and 0.27 (constant void ratio lines of 4.0 and 2.7) from the three models. Strictly speaking, none of the models were quantitatively identical. In order to investigate this discrepancy, the steady state void ratio location was examined. It was found that the void ratio of 4.0 should be located 0.14 m from the bottom of the material. This location agrees well with the current prediction. In the case of the iso-concentration line of 0.27 (void ratio of 2.7), its approximated final location is at 0.05 m from the bottom. The current prediction being only 0.008 m lower than this approximate location also shows a satisfactorily agreement. This agreement gives confidence in the predicted iso-concentration lines.

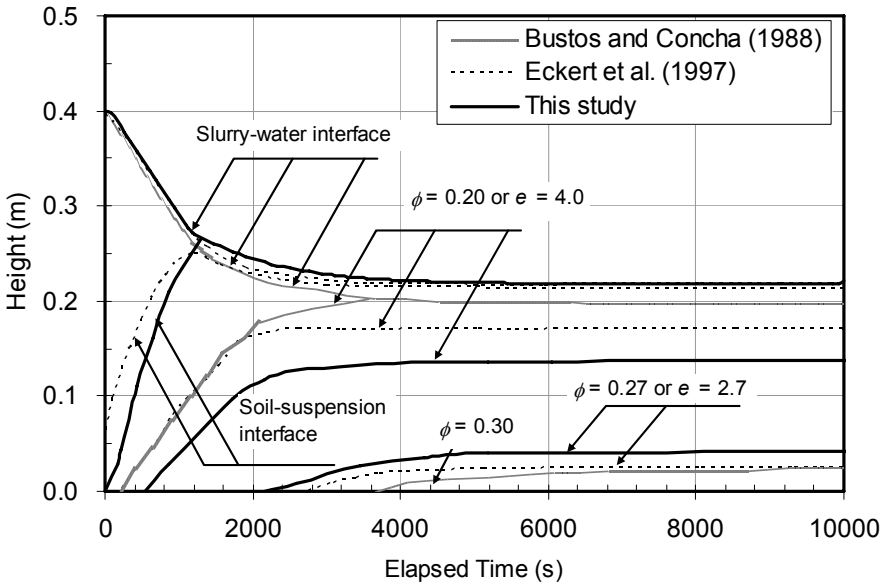

Figure 3.34 Predictions of sedimentaion consolidation of fine tails from copper concentrator

3.3.3.3 Sedimentation-consolidation model by Bustos et al.

This section compares the proposed interaction coefficient model with the widely used model of Bustos et al. (1999) to further confirm the proposed model is giving correct predictions. Based on the Kynch hindered sedimentation theory, they proposed a model of sedimentation-consolidation for batch conditions. Their model is a fluid dynamics formulation where the Kynch sedimentation flux and a constitutive relation for effective stress-solids volume fraction are used. Discontinuity is present in the diffusion coefficient of their governing equation and they applied the variable splitting method to solve this governing equation. In order to use their parameters, Kynch flux has to be converted to hydraulic conductivity by Equation [3.23] given by Bartholomeeusen (2003) while the effective stress can be readily used after a power function is fitted to it.

$$k = \frac{f_{bk}\gamma_f}{(1-n)^2\left(\gamma_s - \gamma_f\right)} \qquad [3.23]$$

where f_{bk} is Kynch batch flux density function and n is porosity.

The simulation results for the slurry-water interface and iso-concentration lines are shown in Figure 3.35. $n = z / \Delta z = 200$ and $\Delta t = 5\times10^{-5}$ were used for this simulation.

The predicted slurry water interfaces and the soil-suspension interfaces from both models are very similar. However, the constant void ratio lines of $e = 2.45$ and $e = 1.86$ from both models are not in the same location similar to the results in the previous section. At 24 hours elapsed time, the current model predicted a location of the void ratio of 2.45 approximately 12% lower, while the void ratio of 1.86 was 48% higher, compared to Bustos's model. Calculating of the steady state void ratio from the self-weight effective stress, however, results in only a 1% difference with the proposed model in the void ratio at 24 hours.

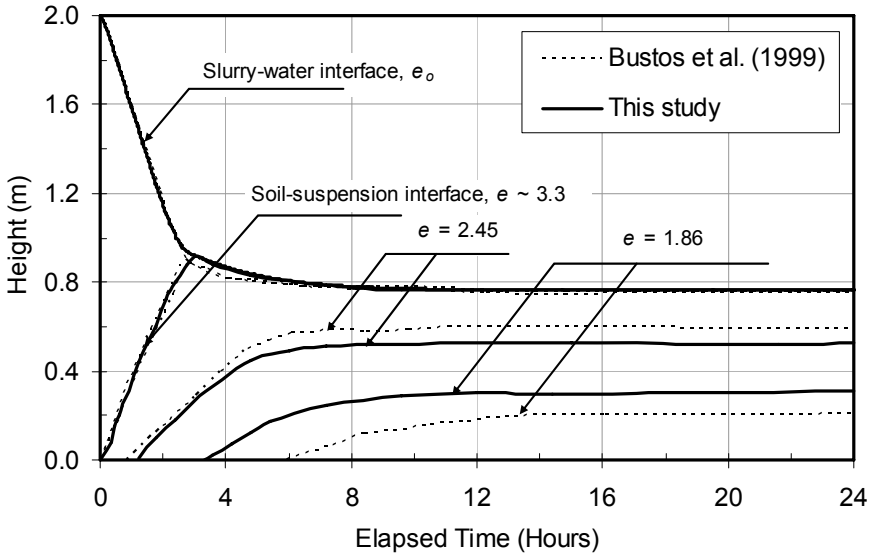

Figure 3.35 Comparison of the sedimentation with compression models between this study and by Bustos et al. (1999)

From all the numerical examples, it can be seen that the technique employed using an interaction coefficient to capture sedimentation-consolidation phenomena with the finite strain consolidation theory shows good predictions compared to other models in the literature. Slight deviations are observed which are most likely due to the power law fitting constitutive relations.

3.3.4 Conclusions for sedimentation-consolidation modeling

Full implementation of a continuous interaction function technique has shown that the sedimentation and consolidation phenomena can be modeled with the large strain consolidation theory using an interaction coefficient. From the presented numerical examples, good prediction results can be obtained. The numerical method used for the model is uncomplicated and gives satisfying results.

To model the two processes, two important void ratios (e_s and e_m) are needed in a form of an interaction function. Mixtures that have a of void ratio lower than the structural void ratio e_s are known to be soils while those who have a void ratio larger than e_m are suspensions. An interaction coefficient has to be determined directly from a

laboratory measurement to define these void ratios. The Harris model was selected in this development and it is found to be suitable to use as an interaction function.

This type of an interaction coefficient does not exactly represent the sedimentation-consolidation processes defined in conventional theories but rather an approximate solution of the processes. This is because a step function is not used and the choice of a gradual interaction function can lead to a very small effective stress during sedimentation. Nevertheless, the model study of the proposed model has shown that this small variation leads to a negligible difference in the rate of sedimentation.

Compared to experimental results in the literature, the model gives good approximations. Future development should include a time dependent behavior to better capture the void ratio profiles in the suspension and transition zones. Compared to the fluid dynamic formulations, the presented model gives qualitatively similar predictions.

Numerically, the chosen finite difference scheme can handle the analysis adequately but due to the shock like behavior of the governing equation, temporal and spatial parameters have to be small. This can cause a longer computational time in some cases. Moreover, in situations when a high initial void ratio and a narrow transition zone are used, numerical dissipation is expected. If this is of concern, other forms of an interaction function and other numerical technique such as an adaptive mesh refinement are recommended.

3.4 Modified compressibility function

As has been discussed in Chapter 2, compressibility of oil sands fine tailings exhibits both pre-consolidation and time dependent behavior. To be able to model compression behavior of this material and similar tailings, modifications of a finite strain consolidation model are performed in this section to include pre-consolidation compressibility and creep compressibility into a finite strain consolidation analysis.

3.4.1 Pre-consolidation behavior analysis

According to considerable evidence from large strain consolidation tests (Pollock, 1988; Suthaker, 1995; Jeeravipoolvarn et al., 2007), the compressibility of oil sands fine tailings and similar tailings exhibits pre-consolidation behavior. This behavior makes the use of a power law function [3.3] for compressibility questionable. In order to include pre-consolidation compressibility behavior into the analysis, it is proposed that a Weibull function [3.24] is used instead of the conventional power law function. This specific function is employed for this study because it can capture the pre-consolidation behavior and gives a better coefficient of determination compared to that of the power law function. Weibull compressibility function is expressed as

$$e = A - B.\exp[-E.\sigma'^{F}] \qquad [3.24]$$

Where parameters A, B, E and F are laboratory determined parameters. By reformulating Equation [3.2] with the use of Equation [3.24], a modified finite strain consolidation governing equation is expressed as

$$\frac{\partial}{\partial z}\left[\frac{k(e)}{\gamma_w(1+e)}\right]\frac{\partial u}{\partial z}+\frac{k(e)}{\gamma_w(1+e)}\frac{\partial^2 u}{\partial z^2}+B.E.F.\exp[-E.\sigma'^{F}].\sigma'^{(F-1)}\left[\frac{\partial u}{\partial t}-(G_s-1).\gamma_w\frac{d(\Delta Z)}{dt}\right]=0 \quad [3.25]$$

The governing equation [3.25] in terms of differences can be expressed as

$$\frac{\Delta t}{4\mathrm{B}\Delta z^2}\left[4\mathrm{E}+\Phi\right]u_{i+1}^{j+1}+\left[1-\frac{2\mathrm{E}\Delta t}{\mathrm{B}\Delta z^2}\right]u_i^{j+1}+\frac{\Delta t}{4\mathrm{B}\Delta z^2}\left[4\mathrm{E}-\Phi\right]u_{i-1}^{j+1}=u_i^{j}+\mathrm{A}\Delta Z \quad [3.26]$$

Where

$$\mathrm{A}=(G_s-1).\gamma_w$$

$$\mathrm{B}=B.E.F.\exp[-E.\sigma'^{F}].{\sigma'_i}^{j(F-1)}$$

$$\mathrm{E}=\frac{k_i^j}{\gamma_w(1+e_i^j)}$$

$$\Phi=\frac{1}{\gamma_w}\left(\frac{k_{i+1}^j}{1+e_{i+1}^j}-\frac{k_{i-1}^j}{1+e_{i-1}^j}\right)$$

The initial condition and boundary condition can be set the same way as shown in Section 3.2.1. The use of a Weibull function has an advantage in capturing the initial compressibility behavior of the oil sands tailings therefore the finite strain consolidation model with this function will be a better predictor than a power law function for special case tailings such as mature fines tailings whose compressibility is *S-shape* as recommended by Suthaker (1995). The function however has a drawback. An improper use of this function can make the governing equation non solvable, such a condition includes the setting of a higher initial void ratio than that determined from the laboratory. In order to use this function, a laboratory test should be performed on a material at the initial void ratio that is going to be used in the prediction. It is recommended to use the conventional power function for a high initial void ratio condition.

3.4.2 Creep compression analysis

Creep is assumed to have two modes which are based on two similar concepts. The first one is called creep type 1 which is creep behavior that occurs independently of consolidation. This type of creep is based on compression behavior observation of the fine tailings in both field and laboratory. Detailed philosophy of this compression mode is presented by AGRA (1997). Based on this philosophy, total deformation is therefore a combination of independent creep compression and consolidation. A creep function is postulated and it is expressed as Equation [3.27].

$$\dot{e} = M.\exp[e.N] \qquad [3.27]$$

Where M and N are experimentally determined parameters. This creep function is fitted from experimental data of creep rates versus void ratio.

A flow chart of creep type 1 analysis is illustrated in Figure 3.36. The analysis is performed by explicitly combining creep deformation (Δe_{cr}) to consolidation deformation (Δe_{con}) at the end of each time step (Δt) of the numerical solution. As this will cause an incompatibility of compressibility, it must be adjusted to follow the resulted deformation as indicated in Figure 3.36.

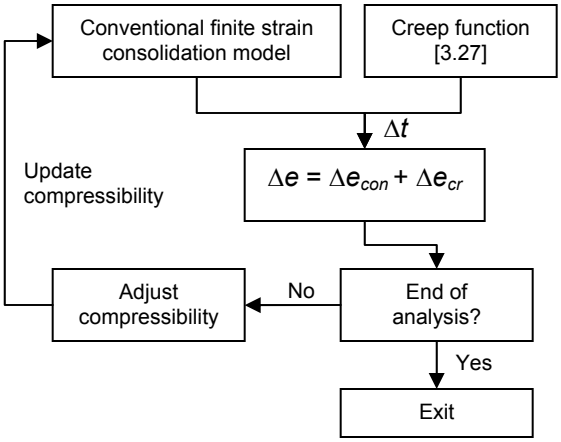

Figure 3.36 A computational scheme of creep type 1

The second mode, creep type 2, is based on a concept of strain rate presented by Leroueil (1985). Creep type 2 is performed by assuming a constitutive relationship in a form of $e = f(\sigma', \dot{e})$. A form of a function used to combine rate of compression and compressibility is selected as Equation [3.28] where G, H, I and J are experimental determined parameters and A is finite strain parameter from Equation [3.3]. This relationship is assumed to exist and available experimental data are used to obtain parameters in the relationship.

$$A = G - H.\exp[-I.\dot{e}^{J}] \qquad [3.28]$$

A flow chart of creep type 2 analysis is shown in Figure 3.37. The analysis is performed by calculating $\dot{e}$ and subsequently redefining soil compressibility based on $\dot{e}$ data. As a new compressibility is obtained based on the void ratio rate correlation, a next time step is performed until the end of a specified simulation period.

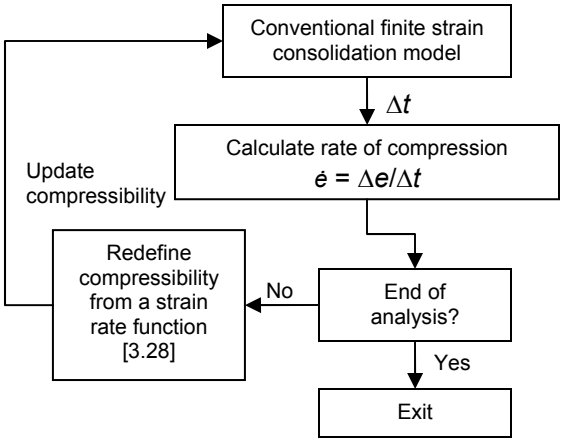

Figure 3.37 A computational scheme of creep type 2

3.4.3 Modeling parameters

In order to model compression behavior of mature fine tailings based on the newly developed models and also illustrate the model behavior, best estimated model parameters based on available data were extracted from the literature and are presented in this section. Four sets of parameters are presented for conventional analysis, pre-consolidation analysis, creep type 1 analysis and creep type 2 analysis.

The conventional modeling parameters are obtained by using a power law on compressibility and hydraulic conductivity in Figures 3.38 and 3.39. The pre-consolidation model uses a Weibull function instead of a power law for compressibility (Figure 3.38). Creep models use the same compressibility and hydraulic conductivity to the conventional model with additional creep functions. Creep type 1 parameters (M, N) are obtained by a fitted curve on experimental creep data (Figure 3.40) with Equation [3.27] and creep type 2 parameters (G, H, I, J) arbitrary chosen based on limited compressibility and strain rate relations (Figure 3.41) of the fine tailings given by Jeeravipoolvarn (2005).

Modeling parameters are listed in Table 3.6. An implicit finite difference method was chosen to solve all governing equations numerically due to its stability. Numerical parameters used for the models are $\Delta z = z/200$, $\Delta t = 0.1$ for spatial and temporal resolutions. Initial conditions and soil parameters of the fine tailings in the verification

standpipe are an initial height of 10 m, an initial solids content of 30.6% (e = 5.17, w = 227%) and a specific gravity of 2.28.

Table 3.6 Modeling parameters (units in kPa, m/day)

Parameters	Conventional	Pre-consolidation	Creep type 1	Creep type 2
A	3.391	5.504	3.391	3.391
B	-0.308	4.974	-0.308	-0.308
C	6.510×10^{-6}	6.510×10^{-6}	6.510×10^{-6}	6.510×10^{-6}
D	3.824	3.824	3.824	3.824
E	-	1.031	-	-
F	-	-0.674	-	-
G	-	-	-	2.823
H	-	-	-	1.033
I	-	-	-	1.249×10^{3}
J	-	-	-	1.218
M	-	-	9.195×10^{-11}	-
N	-	-	3.798	-

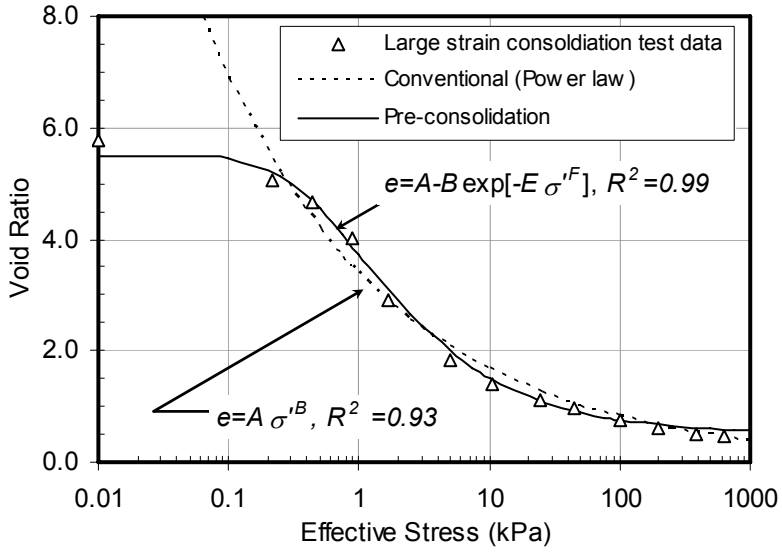

Figure 3.38 Compressibility of mature fine tailings

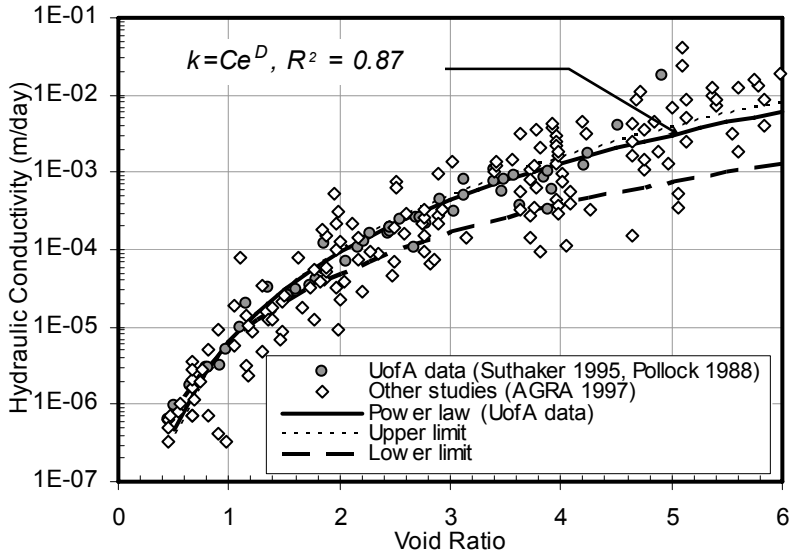

Figure 3.39 Hydraulic conductivity of mature fine tailings

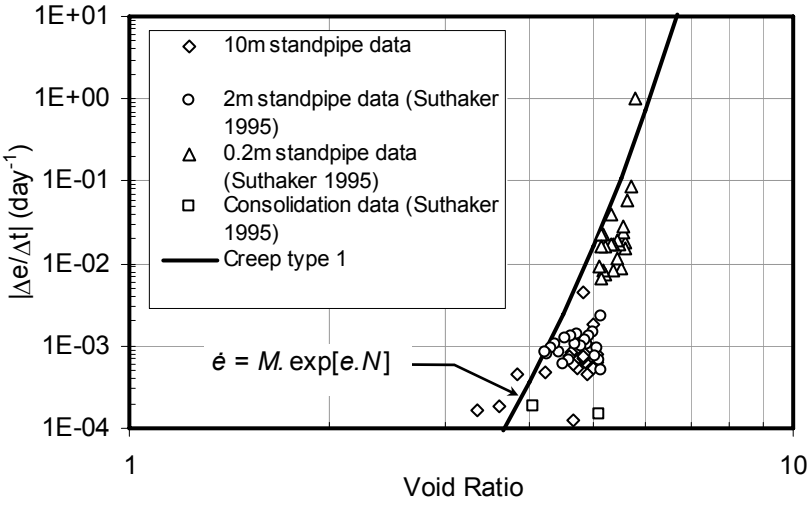

Figure 3.40 Creep rate vs. void ratio of mature fine tailings

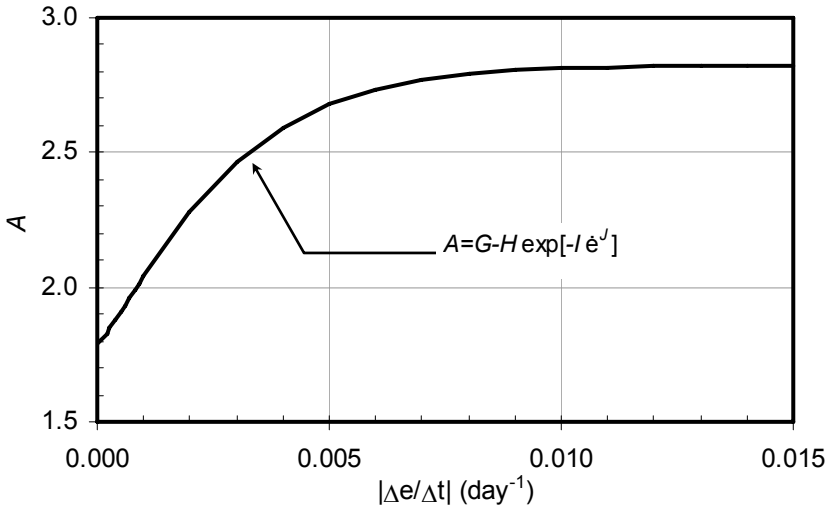

Figure 3.41 Creep rate vs. compressibility parameter *A*

3.4.4 Modeling results

The tailings-water interface measurement is shown with all simulation results in Figure 3.42. Comparisons of experimental measurement of void ratio profiles, excess pore water pressure profiles and effective stress profiles with numerical predictions are shown in Figures 3.43, 3.44 and 3.45 respectively. Elapsed times of 2 days, 10 years and 20 years are chosen for the profile comparisons while experimental data and predictions for other elapsed times fall between these numbers.

It is shown by the interface settlement comparison (Figure 3.42) that the conventional finite strain consolidation theory with the assigned power law functions to compressibility and hydraulic conductivity is able to capture the interface settlement up to about 4 years but fail to capture further interface settlement data of the fine tailings with an overestimation error of 33% at 21 years. The profile predictions of this model are shown in Figures 3.43(*a*), 3.44(*a*) and 3.45(*a*). The results indicate that none of the profiles are in good agreement. These disagreements led to extensive investigations of other possible mechanisms affecting the compression behavior of the fine tails (Banas, 1991; Suthaker, 1995; Tang et al., 1997; AGRA, 1997; Jeeravipoolvarn, 2005).

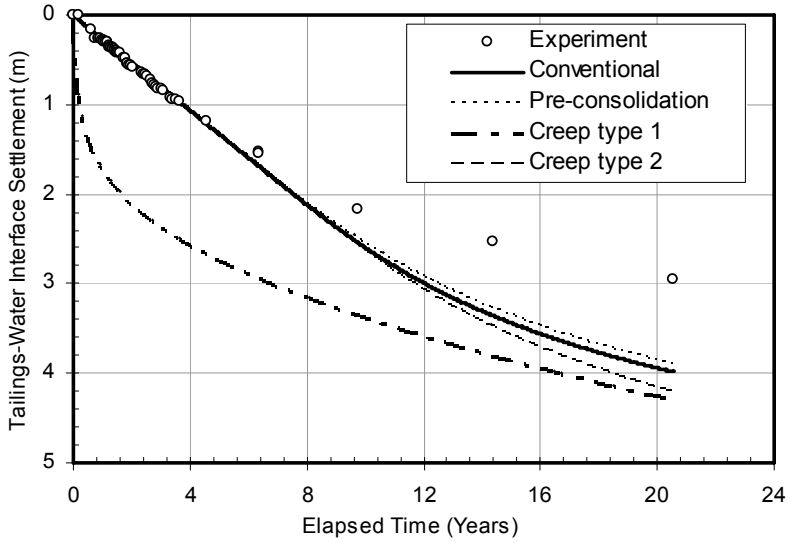

Figure 3.42 Tailings water interface settlement comparison

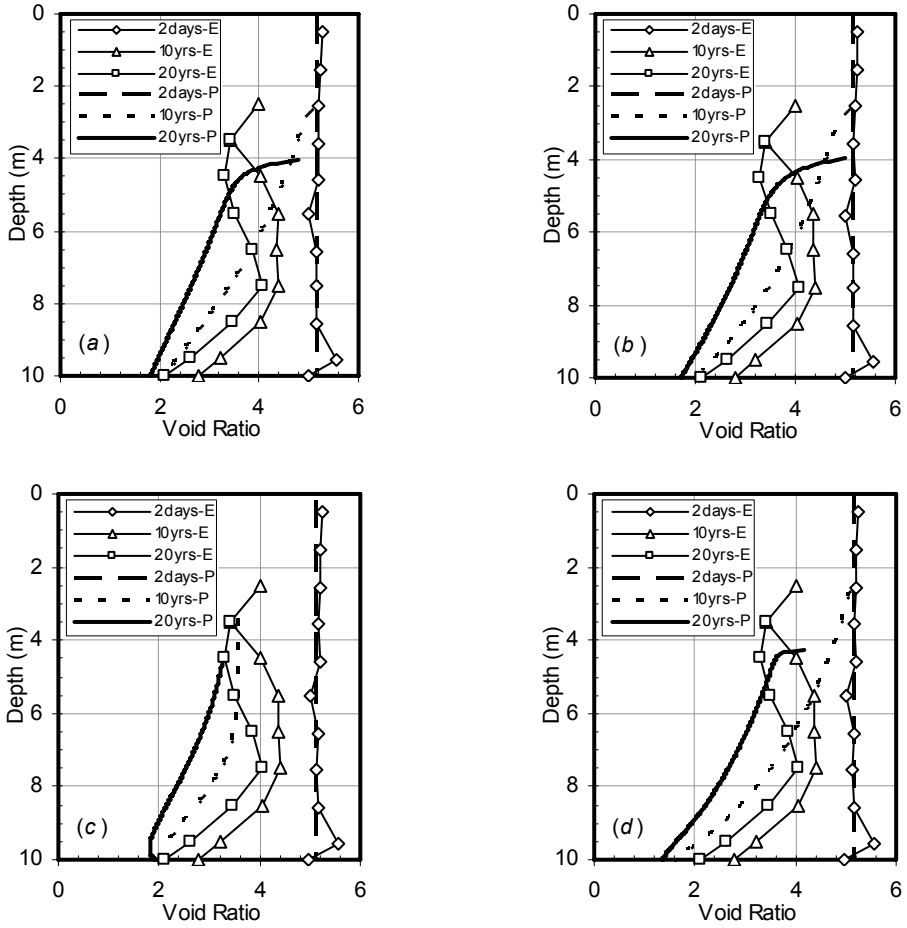

Figure 3.43 Void ratio comparison (*a*) conventional (*b*) pre-consolidation (*c*) creep type 1 (*d*) creep type2

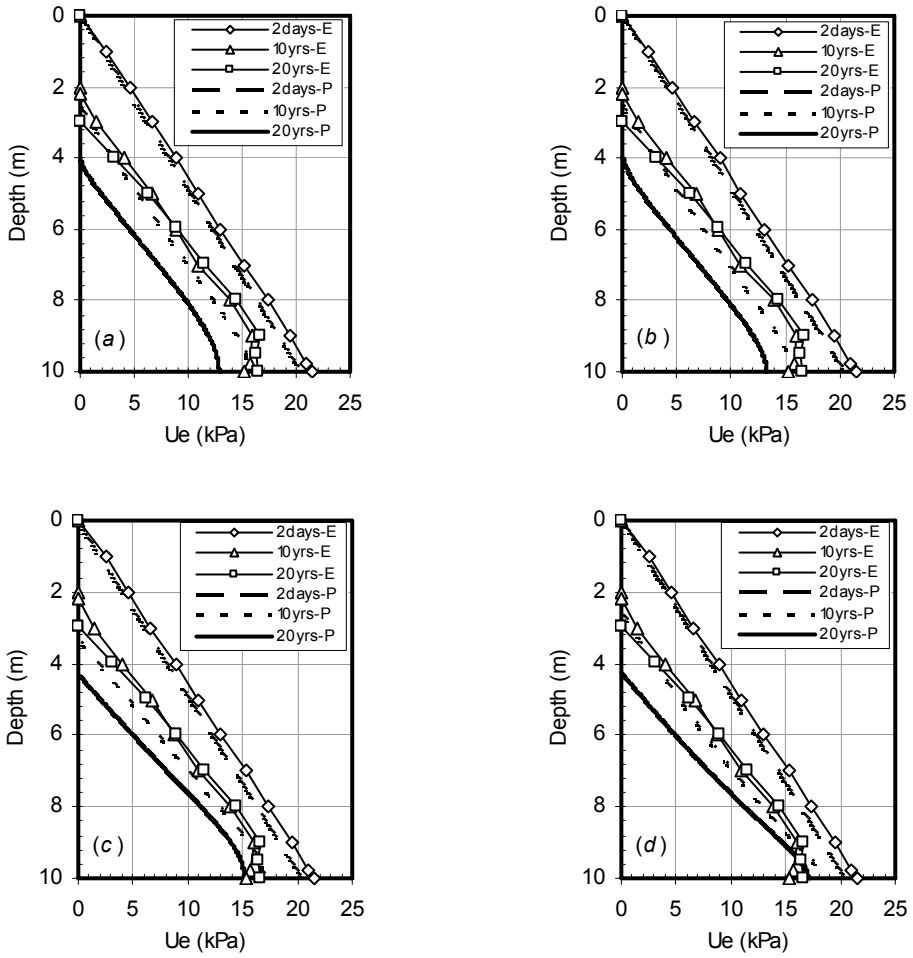

Figure 3.44 Excess pore water pressure comparison (*a*) conventional (*b*) pre-consolidation (*c*) creep type 1 (*d*) creep type2

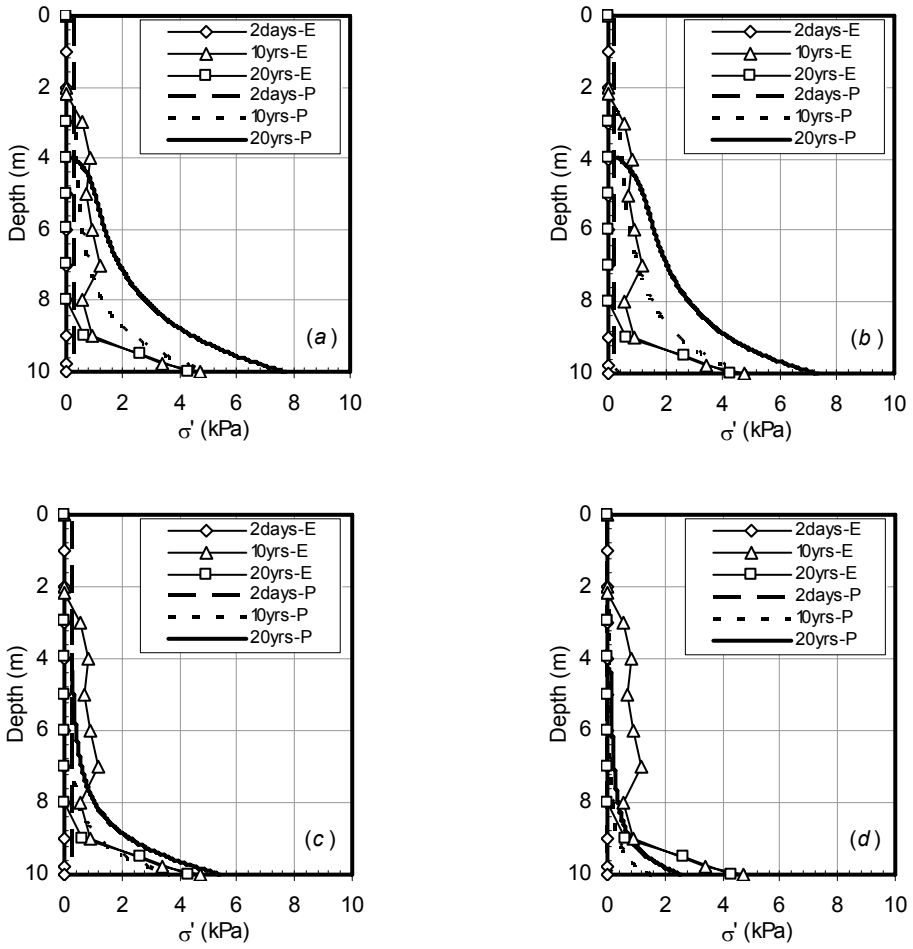

Figure 3.45 Effective stress comparison (*a*) conventional (*b*) pre-consolidation (*c*) creep type 1 (*d*) creep type2

Believed to be caused by a high thixotropy gain in strength of the fine tailings, the pre-consolidation compressibility approach even though it contains a considerably better compressibility function (higher coefficient of determination) only gives a slight improvement of the interface settlement prediction (Figure 3.42). Figures 3.43(*b*), 3.44(*b*) and 3.45(*b*) show that the pre-consolidation approach is not significantly different to the conventional approach. Given that the initial void ratio is 5.17, there certainly is a small over-consolidation pressure to overcome by self-weight stresses (Figure 3.38).

The creep type 1 interface prediction gives a large deviation from the experimental data. The void ratio profiles (Figure 3.43(*c*)) give an intriguing reduction in void ratio where there is no consolidation similar to experimental observations. These are

however not unexpected as the additional strain was introduced by creep Equation [3.27]. Nevertheless, creep type 1 is unable to capture experimental data in all aspects giving that the hydraulic conductivity is unchanged. According to AGRA (1997), an improved prediction can be obtained when a lower bound hydraulic conductivity is implemented in a similar model as creep type 1.

Rate dependent compressibility, the creep type 2, gives a good agreement of interface prediction to about 4 years similar to the conventional approach while the prediction starts to diverge greater than the conventional method after 10 years (Figure 3.42). The effective stress and excess pore pressure responses at the 20 year prediction appear to be closer to experimental data however this may be deceiving as the interface error is larger than the conventional approach.

Considering a creep mechanism, the compressibility of soils is likely greater due to the viscous response as the duration of consolidation increases. This conflicts with the philosophy of thixotropy gain in strength behavior where it is assumed that the pre-consolidation is caused by increasing undrained shear strength due to the development of gel structure with time. Sills (1998) and Barthomeeusen (2003) showed measurements of effective stress response with time for various slurries and from their experimental data it can be concluded that viscous response significantly makes slurry more compressible with time. According to Leroueil (1985), the magnitude of pre-consolidation pressure is a consequence of compression rate. This is consistent with the compressibility data of the fine tailings in Figure 2.15. As a higher initial void ratio with the same sample thickness implies a relatively higher rate of compression compared to a lower void ratio, the higher pre-consolidation pressure belongs to the higher initial void ratio. Therefore, it is concluded that for oil sands fine tailings, the cause of the apparent pre-consolidation pressure remains unknown but the magnitude of it is potentially related to the rate of compression. The influence of the pre-consolidation on compression behavior is small and by considering a creep mechanism, it is conceivably negligible.

An attempt to history match MFT compression behavior was performed by Jeeravippolvarn et al. (2008) and it was concluded that a reasonable history matching can be obtained only by considering changes in hydraulic conductivity parameters. It was suggested that possible mechanisms that affect micro and macro structures and therefore

hydraulic conductivity of the slurry should be further investigated to extend the current stage of understanding. The history matching of the MFT behavior is not part of the scope of this thesis, further information on the history matching analysis for MFT is given in Jeeravipoolvarn et al. (2008).

3.5 Summary

Finite strain consolidation theory is one of the most advanced theories in Geotechnical engineering for slurry consolidation prediction. Most of the finite strain consolidation models generally give similar predictions. There appears to be very little difference in the predictions from different methods used to handle a finite strain consolidation governing equation in both quiescent and pond filling conditions.

For a pond filling numerical experiment, when the same amount of tailings is placed and the same amount of time is allowed for tailings to consolidate, the same amount of settlement can be expected. For a one dimensional single pond filling condition, a quiescent finite strain consolidation model can be used to estimate interface settlement prediction both in filling and quiescent periods but the quiescent model can not be utilized for a multiple filling step. For a pond with a cross-section area changing with height, the filling interface curve can become nonlinear therefore this curve can not be estimated by a quiescent model.

Full implementation of a continuous interaction function technique has shown that the sedimentation and consolidation phenomena can be modeled with the large strain consolidation theory using an interaction coefficient. From the presented numerical simulations, good predictions can be obtained. The numerical method used for the model is uncomplicated and gives satisfying results. The sedimentation-consolidation model was also compared to experimental results in the literature. The results show that the model gives good approximations. When compared to fluid dynamic models, the presented model gives qualitatively similar predictions.

Modified compressibility constitutive relationships for pre-consolidation and creep analyses were developed and investigated. The pre-consolidation behavior is modeled by a Weibull compressibility function which is a better form of compressibility

for mature fine tailings compared to the conventional power law. Results from this approach give a slight improvement of interface settlement prediction. Void ratio, effective stress and excess pore pressure profile predictions however show a negligible advantage of this method. For creep analyses, both creep type 1 and type 2 increase deformations with time due to a viscous effect. As a result, the interface prediction with creep further overestimates the measured interface settlement data. As the compressibility investigations showed small success, it is recommended that possible mechanisms that affect micro and macro structures and therefore hydraulic conductivity of the slurry should be further investigated to extend the current stage of understanding.

Chapter 4 Thickener Modeling by a Finite Strain Consolidation Theory

4.1 Introduction

In mineral processing industries, a gravity thickener, a cylindrical vessel with an inverted conical base, is generally used to dewater initially diluted slurry through sedimentation and self-weight compression processes. Generally, slurry mixed with a flocculation chemical is fed into the top of a thickener. The material then undergoes hindered sedimentation and when it reaches a void ratio where sedimentation ends consolidation will begin. During these processes, slurry increases its density by releasing water. This supernatant water then flows out of the top of the thickener as a thickener overflow. Simultaneously thickened material at the bottom is withdrawn and is called a thickener underflow. A typical continuously operating thickener is shown in Figure 4.1.

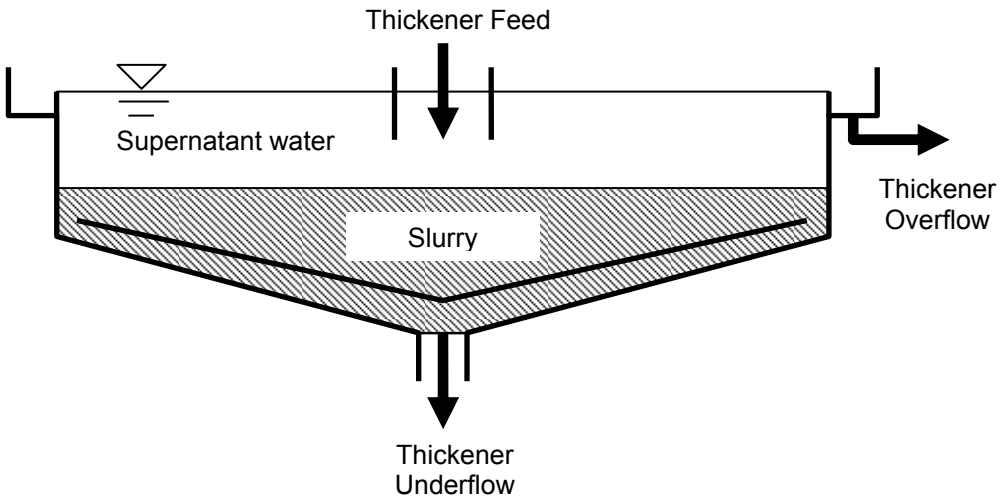

Figure 4.1 A typical continuously operating thickener

In order to design a thickener, a requirement is that a thickener should have an appropriate size and residence time to allow a certain amount of slurry to reach a designated thickener underflow solids content. The design generally aims to use the smallest thickener which has the required capacity. According to Bustos et al. (1999), there are three types of thickener designing methods and they are (i) those based on the

macroscopic balances, (ii) those based on kinematical models and (iii) those based on dynamical models.

The macroscopic balance design method (Coe and Clevenger, 1916; Mishler, 1912) is based on a steady state operation of a thickener and a knowledge of hindered settling velocities at different solids contents. This method uses the settling velocity to define the flow rate of thickener overflow (water) therefore a minimum thickener area can be determined. The kinematical model is based on the hindered sedimentation theory developed by Kynch (1952). This method of design is similar to the macroscopic approach however it only requires one properly selected sedimentation test and Kynch's hindered sedimentation theory is used to provide the information necessary (Bustos et al., 1999).

The dynamical models are based on a phenomenological model, also known as a fluid dynamic model (e.g. Bürger et al., 2008; Nasser and James, 2007; Burgos and Concha, 2005; Bustos et al., 1999; Eckert et al., 1996) and a simulation of a continuous thickener based on the fluid dynamic model is presented by Bürger and Narváez (2007). This phenomenological model is based on two main phenomena; hindered sedimentation and consolidation. As shown by Eckert et al. (1996), the theories used in this model are similar to a "nonlinear finite strain consolidation theory" developed by Gibson et al. (1967).

The "nonlinear finite strain consolidation theory", a geotechnical formulation, was derived from the conservation of mass and momentum, a flow relationship and an effective stress principal. Been (1980) indicated that Gibson's finite strain consolidation theory is similar to the hindered sedimentation theory proposed by Kynch (1952) excepting that effective stress was not considered by Kynch. This similarity is the reason that these two theories are closely related. A method of coupling these two theories was presented earlier in Chapter 3 by implementing an interaction coefficient, β, which connects the processes of hindered sedimentation and consolidation via the effective stress equation as shown in Equation [4.1].

$$\sigma = \beta\sigma_c' + u_w \qquad [4.1]$$

Where σ is total stress, σ'_c is effective stress from consolidation test data, β is interaction coefficient and u_w is total pore pressure.

With this modified effective stress equation, a sedimentation equation included a finite strain consolidation governing equation is given in Equations [4.2] and [4.3] in terms of void ratio and solids content respectively.

$$\frac{1}{\gamma_w.}\frac{\partial}{\partial z}\left[\frac{k}{(1+e)}\right]\frac{\partial u}{\partial z}+\frac{k}{\gamma_w.(1+e)}\frac{\partial^2 u}{\partial z^2}+\frac{de}{d(\beta\sigma')}\frac{\partial u}{\partial t}=0 \qquad [4.2]$$

$$\frac{1}{\gamma_w.}\frac{\partial}{\partial z}\left[\frac{k}{(1+G_s(100/s-1))}\right]\frac{\partial u}{\partial z}+\frac{k}{\gamma_w.(1+G_s(100/s-1))}\frac{\partial^2 u}{\partial z^2}+G_s\frac{d((100/s-1))}{d(\beta\sigma')}\frac{\partial u}{\partial t}=0 \qquad [4.3]$$

Where γ_w is unit weight of water, e is void ratio, k is hydraulic conductivity, z is material coordinate, σ' is effective stress, β is interaction coefficient, u is excess pore pressure, s is solids content by mass in percentage, G_s is specific gravity and t is time.

As part of model development and investigation in this thesis, an objective of this chapter is to use a nonlinear finite strain consolidation theory with parameters that are commonly determined in the geotechnical field to simulate slurry behavior in a continuously operating thickener. It also aims to use the developed thickener model to study the influence of solids volume flow rate and thickener height on steady state solids content and void ratio profiles. In order to achieve these objectives, a new thickener model based on a geotechnical formulation is developed in the following section.

4.2 Modeling of a continuously operating thickener

In this thesis, a continuously operating thickener is referred to as a thickener that is continuously fed with a new material on the top and at the same time a thickened material, a thickener underflow, is also continuously withdrawn from the bottom. A material balance in a one dimensional continuously operating thickener is shown in Figure 4.2.

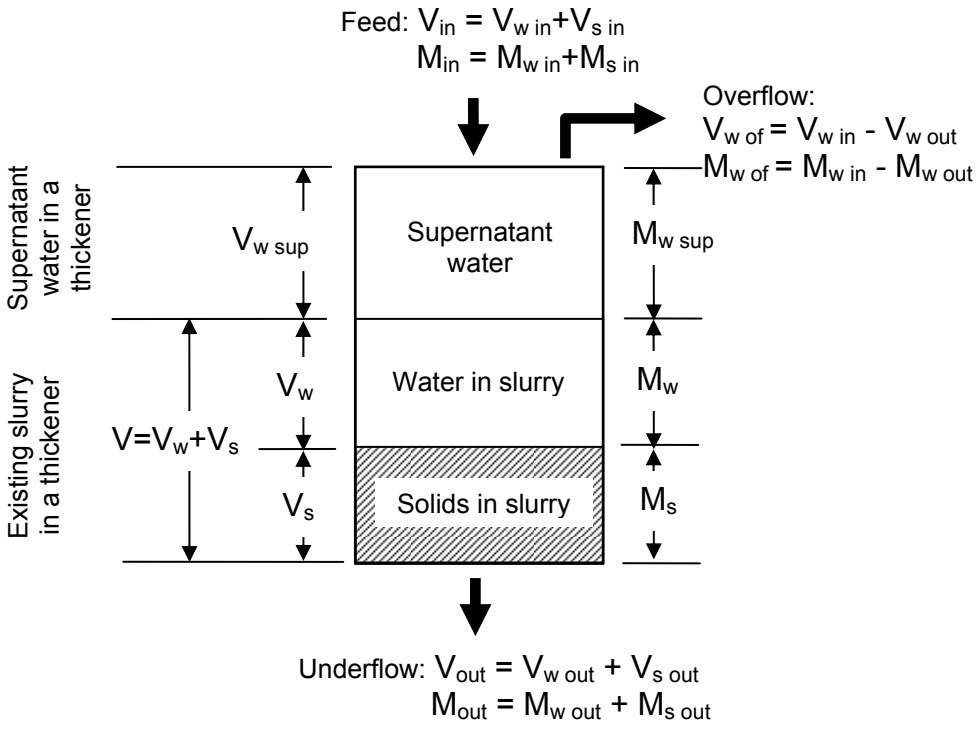

Figure 4.2 Material balances in a continuously operating thickener

In a steady state operation, a mass of solids (M_s) in slurry can be preliminary chosen as a design parameter for a thickener. This amount of solids with the amount of water (V_w) together specifies an average solids content of slurry inside a thickener. Arbitrary criteria can be used to establish the thickness of supernatant water at the top of the slurry (Bustos et al., 1999) and it is chosen to give an ample depth of clear liquid to accommodate fluctuations in the feed (Coe and Clevenger, 1916). A thickener is also designed to handle a certain feed rate at a certain solids content. A volume feed rate is generally dependent on the amount of slurry required to be processed and a solids content of the feed is directly related to the slurry settling behavior with the fastest settling rate. These quantities can be externally controlled and are given quantities (Bürger et al., 1999).

According to Mishler (1912), solids mass flow rates in the feed and the discharge must be equal. This assures that no solids are accumulating in the thickener. This is the same as indicated by Bürger et al (1999) that the discharge solids flux density must equal the feed solids flux density. Therefore conservation of solids mass can be expressed as

$$M_{s\ in} = M_{s\ out} \qquad [4.4]$$

Where $M_{s\ in}$ is feed solids mass and $M_{s\ out}$ is discharge solids mass.

Considering a finite strain consolidation theory, the use of a fixed reference system to describe behavior of consolidation is inappropriate due to the large displacement of the top boundary of a consolidating layer. To overcome this problem, Gibson et al. (1967) utilized a reduced coordinate (McNabb, 1960) which is suitable for large strain modeling because it describes the consolidating layer at any time in terms of volume of solids. The reduced or material coordinate used in Gibson's formulation is shown in Figure 4.3 with Lagrangian and convective coordinate systems which are utilized to physically describe large deformations in this theory (Gibson et al., 1981).

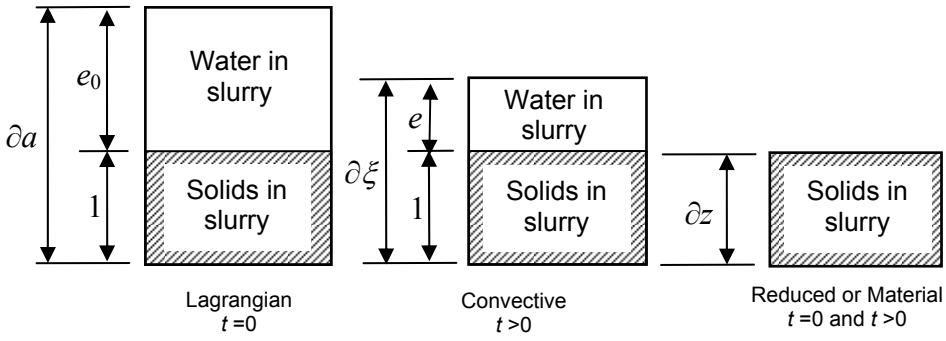

Figure 4.3 Coordinate system

According to Figure 4.3, the three coordinate transformations are related to each other by the following conversions.

$$\frac{\partial a}{\partial \xi} = \frac{1+e_0}{1+e} \qquad [4.5]$$

$$\frac{\partial z}{\partial a} = \frac{1}{1+e_0} \qquad [4.6]$$

$$\frac{\partial \xi}{\partial z} = 1+e \qquad [4.7]$$

Where a is an initial volume, ξ is a volume at time = t, z is a reduced or material coordinate, e_0 is initial void ratio and e is void ratio at time = t.

The presence of the reduced coordinate in the derivation of the finite strain consolidation theory is convenient for modeling of a continuously operating thickener by assuming that solids particles are incompressible thus the mass of feed solids ($M_{s\ in}$) and mass of discharge solids ($M_{s\ out}$) can be directly related to the volumes of solids via solids specific gravity (G_s). In a continuously operating thickener, the feed solids volume is equal to the discharge solids volume and they are expressed as Equation [4.8]. As a continuous adjustment of spatial nodes of the reduced coordinate, z, directly simulates the conservation of solids volume in a continuously operating thickener, a finite strain consolidation theory's spatial node addition and elimination are given for modeling of a thickener as Equation [4.9].

$$V_{s\ in} = V_{s\ out} \qquad [4.8]$$

$$\Delta z_{in} = \Delta z_{out} \qquad [4.9]$$

Where $V_{s\ in}$ is feed solids volume, $V_{s\ out}$ is discharge solids volume, Δz_{in} is an incremental addition of nodes and Δz_{out} is an incremental elimination of nodes.

Two finite strain consolidation theory based numerical programs are modified for thickener modeling and design: (i) a gradual filling model and (ii) an instant filling sedimentation-consolidation model. In order to model a continuous thickener, schematic node modifications corresponding to Equation [4.9] are shown in Figures 4.4 and 4.5 for the gradual filling model and the instant filling model respectively. In Figures 4.4 and 4.5, during a filling period, n_1 is a number of node additions per single temporal variation, Δt_1. During a continuous filling and withdrawing period, n_2 denotes a number of node additions/eliminations per single temporal variation, Δt_2, and for all simulations n represents a total node number.

The modified gradual filling model, referred to as Thickener Model 1, is shown in Figure 4.4. In this model, slurry is initially filled at a specified rate of $n_1.\Delta z/\Delta t_1$ to a certain specified volume, $n.\Delta z$. When the filling is complete at the end of a filling period,

instead of having a quiescent period, with a specified feed rate, a multi-node addition and elimination is used to simulate filling and discharging of material from a thickener. Temporal variation, Δt_2, can be adjusted at this time to obtain a specified feed rate of $n_2.\Delta z/\Delta t_2$. As new material is continuously fed into the top and a thickener underflow is withdrawn from the bottom, the shaded area during the continuously thickening in Figures 4.4 and 4.5 represents old material traveling through a thickener with time. Residence time for a material to travel from the top to the bottom of a thickener is calculated by dividing total volume of solids, $n.\Delta z$, by the solids volume flow rate of $n_2.\Delta z/\ \Delta t_2$.

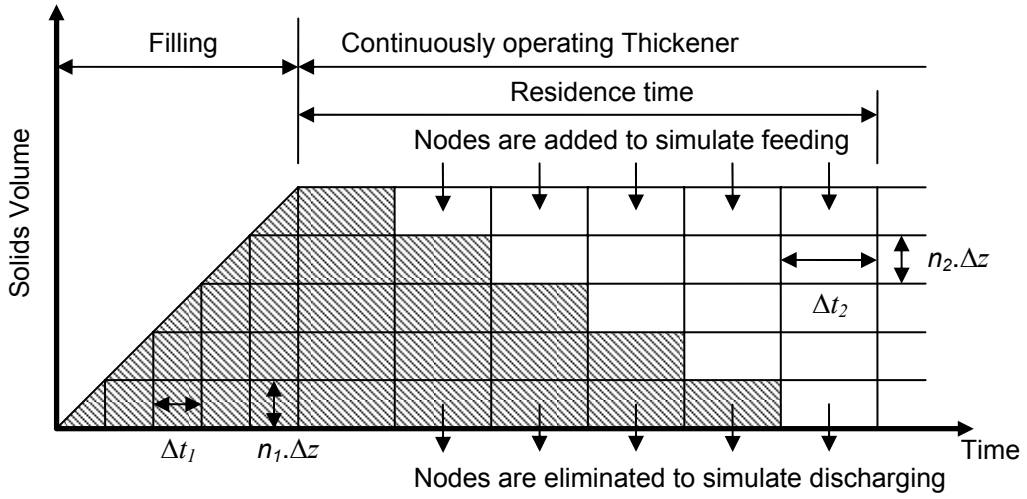

Figure 4.4 Node modifications in the filling model, Thickener Model 1

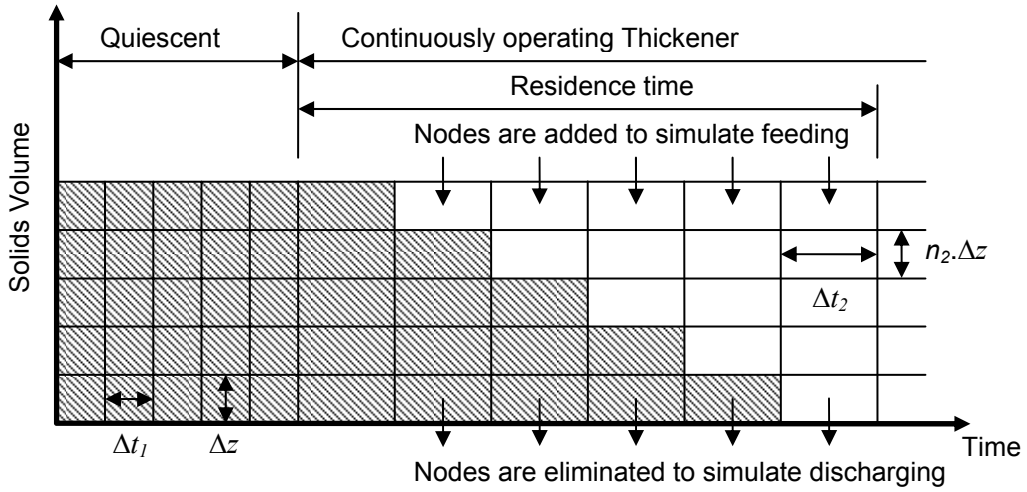

Figure 4.5 Node modifications in the quiescent model, Thickener Model 2

In Figure 4.5, the modified instant filling model, which is a model that applies a instant filling and quiescent conditions during the filling period before a thickening period, is shown. This model is referred to as Thickener Model 2. It is assumed in this model that a thickener is filled instantaneously to a specified solids volume. The bottom of the thickener is closed therefore the discharge flux is zero. After a specified quiescent period is over, a new material is fed at the top of a thickener at a rate specified by $n_2.\Delta z/\Delta t_2$. Concurrently a thickener underflow is continuously discharged at the same solids volume flow rate. For boundary conditions of both Thickener Models 1 and 2, the top boundary is a drained boundary and Dirichlet boundary condition type is applied as excess pore water pressure is equal to zero. The bottom boundary is an undrained boundary and a Neumann boundary condition, $\partial u/\partial z=0$, is used for the entire simulation.

To solve the governing equation, material constitutive relationships are also required. For this purpose, a form of bi-power law void ratio – effective stress and hydraulic conductivity – void ratio relationships (Azam et al., 2009) are chosen and expressed as Equations [4.10] and [4.11] respectively. The interaction coefficient, β, is assumed to follow those soils having a large transition zone shown in Section 3.3.2.1 and is assumed equal to unity. It is noted that other forms of the constitutive relationship functions and interaction coefficient can also be applied in a similar manner and the choice is largely dependent on the material properties of the slurry.

$$e = \begin{cases} A_1 \sigma'^{B1} & , e \geq e_s \\ A_2 \sigma'^{B2} & , e < e_s \end{cases} \qquad [4.10]$$

$$k = \begin{cases} C_1 e^{D1} & , e \geq e_s \\ C_2 e^{D2} & , e < e_s \end{cases} \qquad [4.11]$$

Where e is void ratio, σ' is effective stress, k is hydraulic conductivity, e_s is structural void ratio and parameters A, B, C and D are finite strain consolidation parameters. It is noted that structural void ratio, e_s, is a boundary void ratio at which sedimentation ends and consolidation begins.

With Equations [4.10] and [4.11] and the method of modeling indicated in Figures 4.4 and 4.5, thickener models with a finite strain consolidation theory can be simulated numerically. A finite difference method with a backward time central space scheme was chosen to solve the governing Equation [4.2] due to its stability. An upwind difference was also applied in the advection term of the governing equation to resolve the shock like behavior of the equation.

4.3 Numerical Study

In this section, the developed computer program was compared with a fluid dynamic based model in the literature and the sensitivity of the new model was investigated. It is indicated by Bustos et al. (1999) that a thickener is required to have an adequate size but be the smallest possible. It also requires a thickener underflow to have a high solids content (by mass) or a small void ratio. Therefore rates of filling and heights of slurry were used for a sensitivity study in this section to explore how these parameters affect the underflow void ratio. Both Thickener Model 1 and Thickener Model 2 were simulated and compared to investigate both model behaviors.

4.3.1 Comparison with a fluid dynamics based model (Garrido et al. 2003)

To verify the developed model, an existing model based on differences in both formulation and modeling approach presented by Garrido et al. (2003) was selected. This particular model was chosen due to the fact that the phenomenological theory used in this model is well accepted by the international scientific society (Concha and Bürger, 2002) and is implemented into an end-user based program (Burgos and Concha, 2005). For the verification purposes, ideal continuous thickener (ICT) modeling results for one volume average velocity, q, and three specified solids flux density, f, given by Garrido et al. (2003) were used. Garrido's approach is to define a solids volume fraction for the underflow and a solids fill rate. The design from their approach provides sizes of a thickener as an output. The developed finite strain consolidation model uses a different approach, the amount of solids mass in a thickener is predefined and the size of a thickener is provided by solids volume flow rate as an input. Therefore, an amount of solids volume fraction, ϕ, from Garrido's solution was digitized and integrated to obtain the initial height of a slurry inside a thickener with a given initial solids content of 35%

by mass. The solids volume fraction, ϕ, was also converted to void ratio, e, to compare with solutions from the developed model via Equation [4.12].

$$e = \frac{1-\phi}{\phi} \qquad [4.12]$$

In order to use Garrido's input parameters, it also required that the Kynch flux, f_{bk}, and solids density function, $q\phi$+$f_{bk}(\phi)$, be converted to the hydraulic conductivity, k, and rate of solids volume, $\Delta z/\Delta t$ respectively. Kynch flux is converted to hydraulic conductivity by Equation 4.13 given by Bartholomeeusen (2003). Solids volume rate is determined by assigning the specified solids volume fraction of underflow and Kynch flux function corresponding to the solids volume fraction into the solids density function directly.

$$k = \frac{f_{bk}\gamma_w}{(1-n)^2(\gamma_s - \gamma_w)} \qquad [4.13]$$

Where f_{bk} is Kynch batch flux density function, n is porosity, γ_w is unit weight of water and γ_s is unit weight of solids.

Model parameters are shown in Table 4.1. It is noted that an initial filling period is not necessary in Garrido's model so a specified quiescent period of 1 day was arbitrary chosen. For this comparison, the thickener model was assigned to operate a total of 10 days at which time the interface settlement change and changes in void ratio profiles had ceased. The simulation results for the slurry-water interface and void ratio profiles are shown in Figures 4.6 and 4.7.

The interface settlement prediction in Figure 4.6 shows that during a quiescent period, a period without material being filled or withdrawn, interface settlement increases with time and when a continuous operating thickener mode is activated, the interface settlement is adjusting itself to reach a steady state condition within 10 days where a unique void ratio profile is determined for a specific amount of material inside a thickener and specific fill/withdraw rate. The predicted void ratio profiles from the developed model for different fill rates given by Garrido et al. (2003) are shown in Figure 4.7. The

comparison between Garrido's results and the developed finite strain consolidation model results are qualitatively similar. Slight deviations are observed which are likely due to the digitization of the input and the output data from Garrido's paper and the power law fitting constitutive relation that is not in the same form as Kynch flux and compressibility given by Garrido.

The three different steady state void ratio profiles shown in Figure 4.7 are due to differences in rates of filling and amounts of material inside a thickener. It can be seen that for the same type of material filling a thickener at different fill rates leads to different underflow solids contents of stable slurry inside a thickener. It can also be observed from the interface settlement prediction (Figure 4.6) that to obtain a steady state, the volume of material can be increased, decreased or stable after a quiescent period. These influences will be further investigated in the following sections.

Table 4.1 Model parameters for three solids density functions (units in kPa and m/day)

	Unit	*f*1	*f*2	*f*3
S_0	%	35.0	35.0	35.0
e_0	-	4.64	4.64	4.64
G_s	-	2.5	2.5	2.5
H_0	m	10.52	5.62	3.75
$\Delta z/\Delta t$	m/s per 1 m^2	5.86×10^{-6}	5.64×10^{-6}	5.34×10^{-6}
A_1	-	2.22	2.22	2.22
A_2	-	2.50	2.50	2.50
B_1	-	-0.37	-0.37	-0.37
B_2	-	-0.26	-0.26	-0.26
C_1	m/day	5.19×10^{-2}	5.19×10^{-2}	5.19×10^{-2}
C_2	m/day	0.022	0.022	0.022
D_1	-	3.89	3.89	3.89
D_2	-	4.60	4.60	4.60
$S_{underflow}$	%	62.0	61.1	60.2
$e_{underflow}$	-	1.53	1.59	1.65
H_f	m	5.64	3.08	2.10
$V_{underflow}$	m/s per 1 m^2	1.49×10^{-5}	1.46×10^{-5}	1.41×10^{-5}
$V_{overflow}$	m/s per 1 m^2	1.82×10^{-5}	1.72×10^{-5}	1.60×10^{-5}
V_{feed}	m/s per 1 m^2	3.31×10^{-5}	3.18×10^{-5}	3.01×10^{-5}

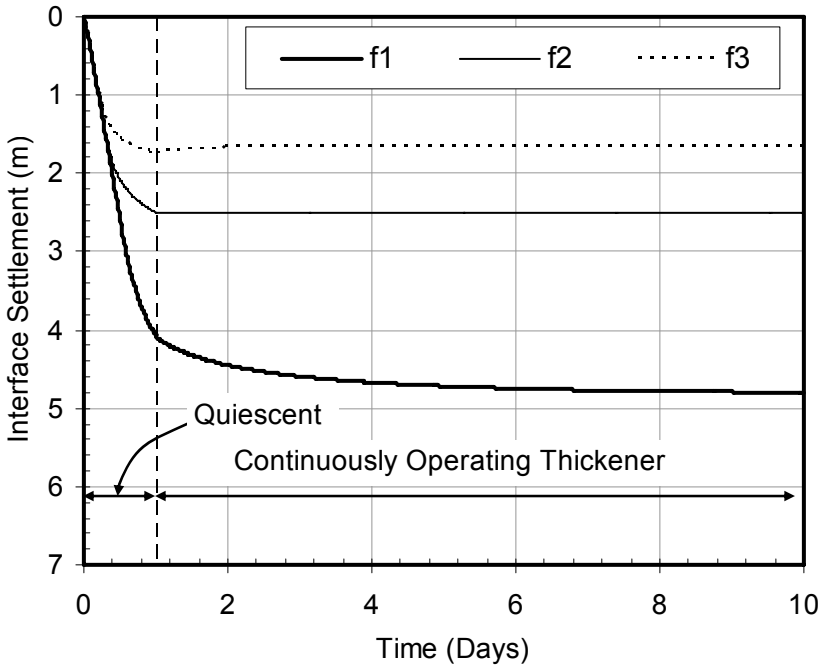

Figure 4.6 Interface settlement vs. time for three solids density functions

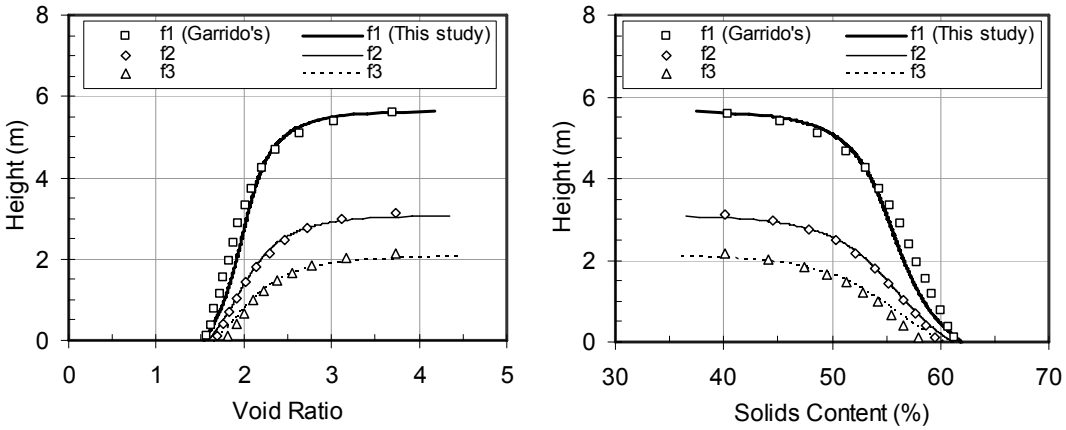

(*a*) (*b*)

Figure 4.7 Profile comparisons for three solids density functions (a) Void ratio profiles (b) Solids content profiles

4.3.2 Comparison of Thickener Models 1 and 2.

In this section the two developed models are compared. Thickener Model 1, the model that simulates initial filling of a thickener with a closed bottom and when the thickener design height is reached the bottom of the thickener is opened to allow thickened material to flow out, and Thickener Model 2 in which the initial filling stage is

assumed instantaneous. Conceptually an initial filling period should not have any influence on the steady state condition, which is dependent of the rate of filling and withdrawing, given that the amount of solids inside a thickener is controlled to be the same. This concept will be illustrated in this section by using flocculated oil sands tailings as a study material in this section. The modeling parameters for the tailings are shown in Table 4.2. The initial filling period and quiescent period for Thickener Models 1 and 2 are arbitrary defined as 1 day and the thickener operation period is 9 days.

Interface settlement comparison of both models is shown in Figure 4.8 and the development of void ratio profiles for Thickener Models 1 and 2 are shown in Figure 4.9. In Figure 4.8, it can be seen that Thickener Model 1 yields the same interface settlement as that of Thickener Model 2. This result confirms the finding by Carrier et al. (1984) that interface settlement prediction during filling by a finite strain consolidation theory is only dependent on the amount of solids filled. If a pond is filled with the same tailings at different rates and periods but filled with the same total dry solids, generally the same pond capacity is obtained. This result is due to the fact that in a one dimensional condition, when the same amount of tailings is placed and the same amount of time is allowed for the tailings to consolidate, the same amount of settlement can be expected. This is due to a similar self-weight stress distribution and dissipation time.

Table 4.2 Modeling parameters for flocculated oil sands fine tailings (units in kPa and m/day)

	Unit	Thickener Model 1	Thickener Model 2
S_0	%	15.0	15.0
e_0	-	14.17	14.17
G_s	-	2.50	2.50
$\Delta z/\Delta t$ during filling	m/day	0.185	-
$\Delta z/\Delta t$ during thickening	m/day	0.075	0.075
H_0	m	-	4.55
A_1, A_2	-	4.10	4.10
B_1, B_2	-	-0.283	-0.283
C_1, C_2	m/day	2.00×10^{-5}	2.00×10^{-5}
D_1, D_2	m/day	5.00	5.00

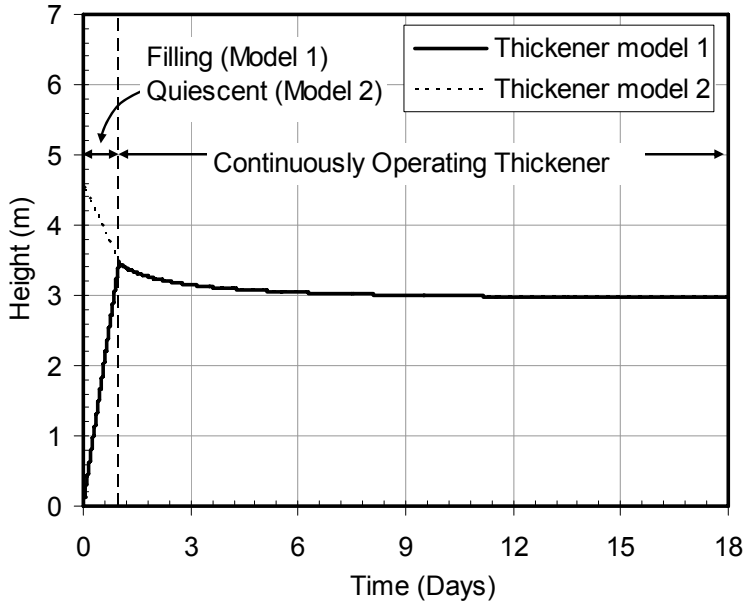

Figure 4.8 Interface settlement predictions from Thickener Models 1 and 2

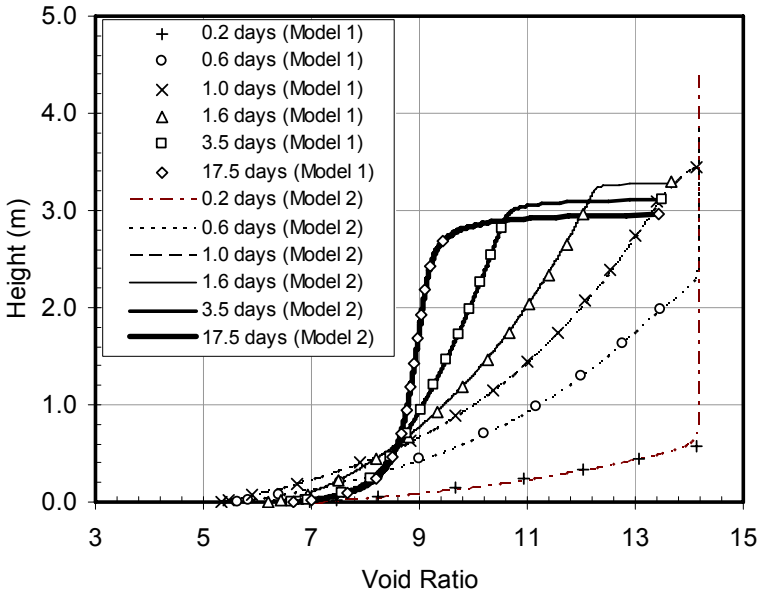

Figure 4.9 Void ratio profile predictions from Thickener Models 1 and 2

In Figures 4.9, the evolution of the material in the thickener can be observed. As material is filled into a thickener, the simulation of void ratio profiles indicates a growing of sediment layer from the bottom up. During the filling period, the thickener bottom is closed therefore the material keeps increasing in both height (Figure 4.8) and bottom solids content (decreasing of void ratio) with time (Figure 4.9). After the filling period,

the solids capacity of this thickener is defined and continuously filling and withdrawing are commenced at this point. The balance between the reduction in volume (hindered sedimentation and consolidation and underflow discharging) and the increase in volume (material filling) leads to a steady state condition in the thickener. Comparison between the void ratio prediction from this point to the steady state condition shows that both models are essentially identical. This finding confirms that the filling period has no influence on the steady state void ratio profile which is dependent on the solids volume fill rate during continuous thickening as shown in this numerical example. Thickener Model 1 is a tool to demonstrate the process of thickening in a thickener from a filling period to a steady state operation. Since the steady state operation is of more interest in thickener design, the Thickener Model 2 will only be investigated further for the rest of this chapter.

4.3.3 Parametric study of the model

In this section, parameters relating to thickener size are selected to study slurry settling behavior of the model. These parameters are flow rates of solids volume and amounts of solid volume inside a thickener.

4.3.3.1 Influence of a solid volume flow rate on a steady state void ratio profile

The feed flow rate is normally a design parameter (Christian, 1994). As the feed enters a thickener, an increase in height of material in a thickener within an infinitesimal time is dictated by the feed volume divided by the horizontal cross section area of a thickener. For a given design feed flow rate, there exists many solids volume rates depending on the size of the horizontal area. The influence of the solids volume flow rate on steady state void ratio profiles is investigated in this section. Four different solids volume flow rates are selected and shown in Table 4.3.

Simulated slurry-water interface height and void ratio profiles corresponding to the four solids volume flow rates are shown in Figures 4.10 and 4.11. In Figure 4.10, it is shown that after a thickener starts to operate, a faster flow rate yields a thicker sediment height. This behavior can be explained through Figure 4.11. In Figure 4.11(a), the void

ratio profiles show that the void ratio is increasing (solids content is decreasing) with time and finally approaches the initial feed void ratio. This is due to the fact that the thickener underflow is withdrawn too fast; faster than the newly feed can densify. The result is a build up of a thin slurry inside a thickener and a negligible change in void ratio of the thickened material withdrawn from the bottom. Considering the other extreme in the current examples, Figure 4.11(d) shows that after a thickener is started, slurry continues to decrease in void ratio (increase in solids content) resulting in a smaller sediment height inside a thickener. With a thickener operating at this solids volume rate, a thickener underflow yields a void ratio of 6.73 releasing more than 61% of its initial volume of water. For the other two solids volume rates in Figures 4.11(b) and (c), the same trend can be expected that the slower the solids volume flow rate, the lower the thickener underflow void ratio. This finding is summarized in Figure 4.12 where thickener underflow's void ratios are plotted against solids volume flow rates. The slower solids volume flow rate theoretically provides a longer residence time of a material inside a thickener, a time that allows a material to compress under its own weight before it leaves at the bottom of a thickener. This allows sedimentation and consolidation phenomena to take place resulting in a reduction of void ratio.

Table 4.3 Four solids volume rates

	Unit	Solids volume flow rate 1	Solids volume flow rate 2	Solids volume flow rate 3	Solids volume flow rate 4
S_0	%	12.5	12.5	12.5	12.5
e_0	-	17.5	17.5	17.5	17.5
Gs	-	2.50	2.50	2.50	2.50
H_o	m	7.00	7.00	7.00	7.00
$\Delta z/\Delta t$	m/day	3.78	0.189	0.126	0.0757
$S_{underflow}$	%	13.0	21.7	24.1	27.2
$e_{underflow}$	-	16.7	9.00	7.89	6.70
H_f	m	6.99	4.87	4.34	3.74

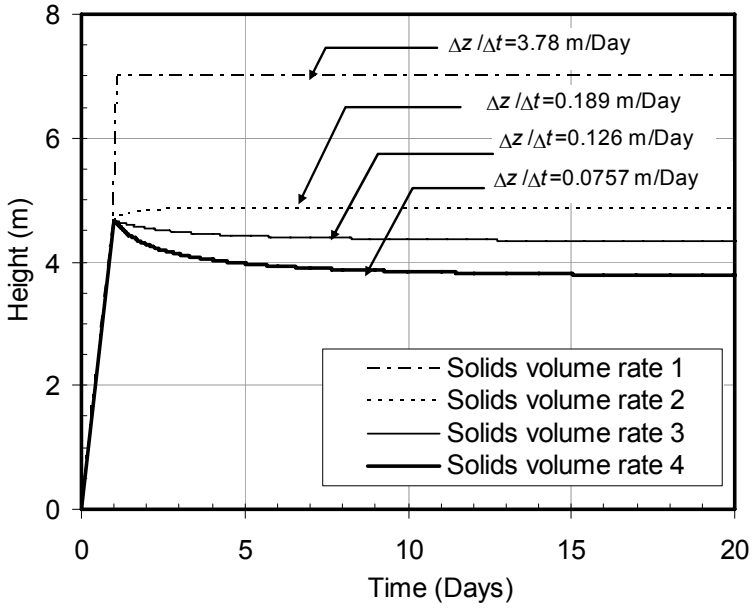

Figure 4.10 Interface settlement simulation for four different solids volume rates

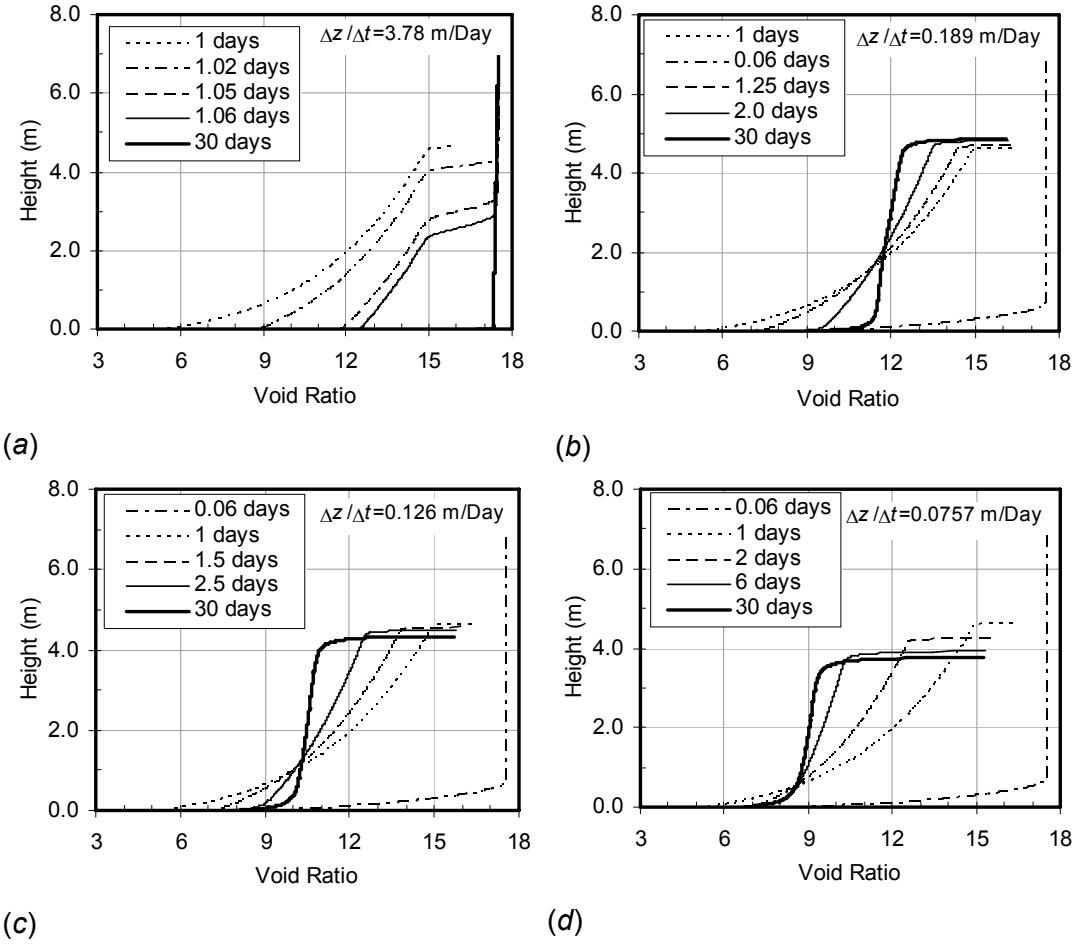

Figure 4.11 Void ratio profile predictions of different solids volume flow rates

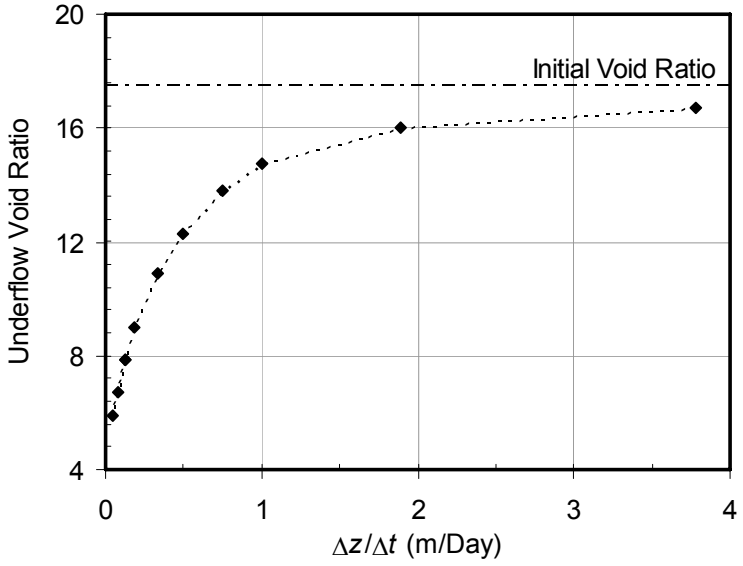

Figure 4.12 Influence of solids volume flow rate on underflow void ratio

Considering the situation when a thickener is overfilled resulting in an ineffective operation, Dixon (1979) explains that a thickener can overflow in three ways: (i) when the feed has very fine particles that cannot settle, (ii) when the feed rate exceeds the settling capacity of the settling zone, and (iii) when the feed rate is higher than the discharge rate. It is shown in Figure 4.11(a) that conditions (i) and (ii) can happen when the feed rate is too fast, faster than the densifying speed of material inside a thickener plus discharge rate. As this occurs, there is not enough residence time and the void ratio of a material flowing out is eventually the same as that of the material flowing in. For the current simulations, the feed and discharge rate are identified by the same solids volume therefore the maximum tailings volume will not exceed the initially specified volume by the initial solids content and total solids volume. For the last case (iii), if an underflow discharge rate is lowered to increase a residence time, there will be an accumulation of solids mass because of the inequality of the feed and discharge solids volume flow rates. Consequently the tailings-water interface will grow and eventually overflow. This last situation is also shown by Coe and Clevenger (1916) and Mishler (1912) that the solids volume flowing in has to be equal to the solids volume flowing out. This concept is built into the thickener models in this chapter and is illustrated by a schematic of a thickener process in Figures 4.4 and 4.5.

Providing that other parameters are identical and the solids volume flow rate is directly related to the thickener horizontal cross section area, the results of the numerical experiment in this section suggest that a large thickener diameter generally provides a higher solids thickener underflow because of a slower solids flow rate per unit area. It also demonstrates that overflowing of a thickener or ineffective use of a thickener can occur when the solids volume flow rate is too fast.

4.3.3.2 Influence of material height inside a thickener on a steady state void ratio profile

High compression thickeners are gaining wider acceptance in minerals processing (Green, 1995) and one of the reasons is that there is a high demand for higher underflow solids contents. In order to achieve a high compression thickener, one of the important modifications is that the bed depth is increased to give a deeper compression zone. Farrow et al. (2000) in their continuously operating thickener experiment on kaolinite clay also found that a thicker material inside a thickener provides a higher solids content thickener underflow. The increased height of the compression zone theoretically increases both the residence time and self-weight stress of a slurry inside a thickener. In order to illustrate this concept and explore the extent of it on a hypothetical thickener, four different initial heights of 2.0 m, 4.5 m, 7.0 m and 9.5 m were used. As a control, the solids volume flow rate of 7.57×10^{-2} day^{-1} and an initial solids content of 12.5% were used for all simulations.

Simulation results are shown in Figure 4.13, it can be seen that when a thickener is filled at the same solids volume fill rate but allowing more material inside a thickener, a thicker material will result as well as a lower underflow void ratio. To better illustrate the results; in Figure 4.14, the thickener underflow void ratio is plotted with initial heights. When the height of material is higher (from Figures 4.13(a) to (d)), the underflow void ratio is decreased rapidly from 6.73, flattens off and stabilized at a void ratio of around 6.69 as the height is increased further. In Figure 4.13(c) where the smallest void ratio is obtained in the current examples, the solids volume is 3.5 times more than the base case (Figure 4.13(a)). The underflow void ratio has decreased from 6.73 to 6.69 releasing additional water of about 0.7%. This influence of the height on underflow void ratio can be more pronounced for other slurries but it appears that the

influence is small for the flocculated oil sands tailings due to its very low hydraulic conductivity as the void ratio is decreased. In Figure 4.13, it is also suggested that there is a possibility of an optimum height where a minimum void ratio can be achieved under a specified solids volume flow rate. This is because an increase in material height increases self-weight stress, residence time as well as drainage path. A further decrease in the thickener underflow void ratio would require more time consuming consolidation to take place.

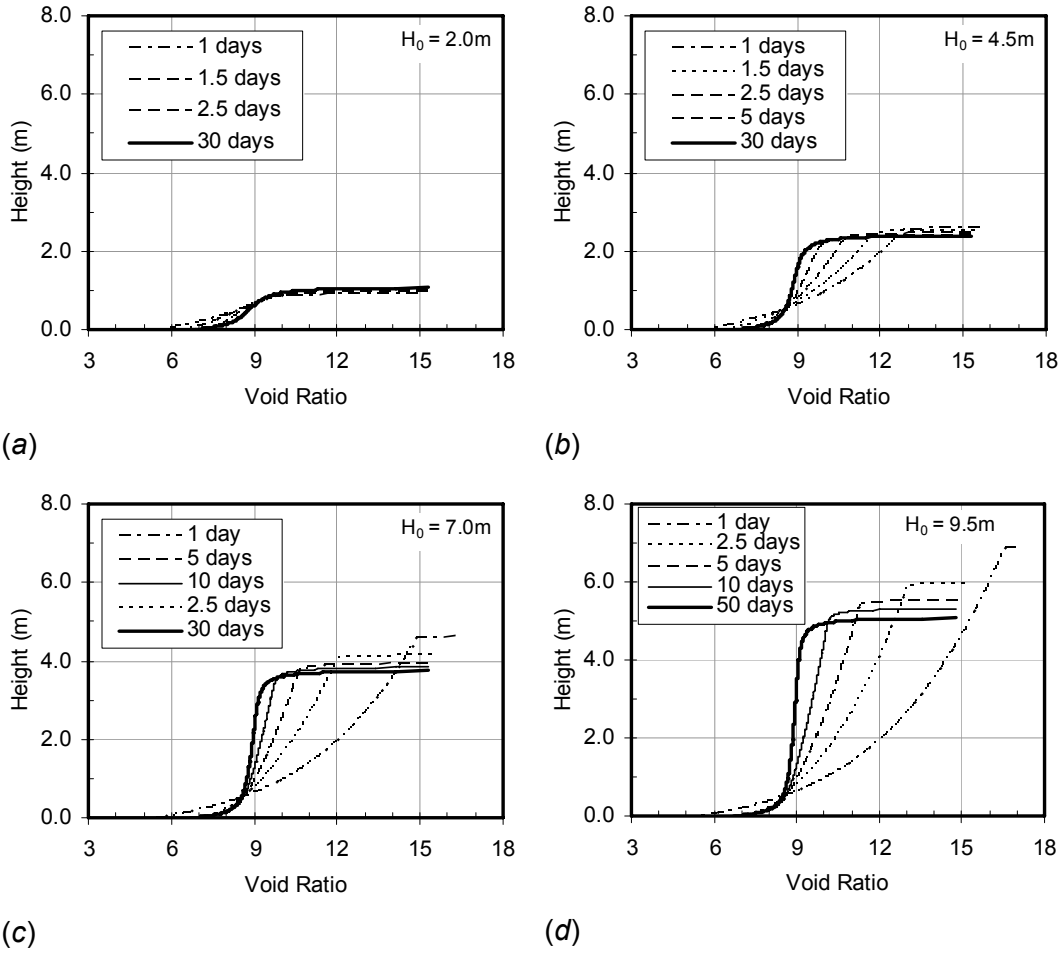

Figure 4.13 Void ratio profile simulation for four different initial heights

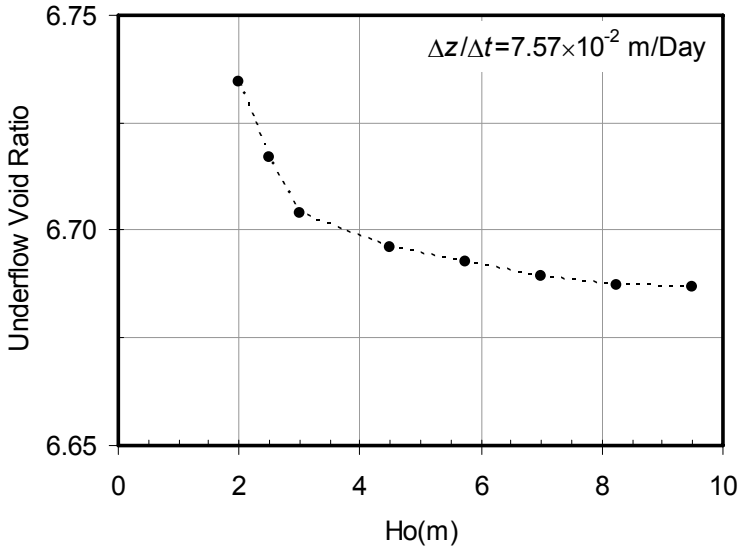

Figure 4.14 Influence of initial height on under flow void ratio

4.4 Conclusions

A finite strain consolidation theory is known in geotechnical engineering as a theory for predicting consolidation of soft soil exhibiting nonlinear soil behavior and large deformation. This theory was utilized for modeling of slurry settling behavior in a continuously operating thickener in this chapter. This modeling was performed by multi-node addition and elimination. The developed thickener model was compared with a fluid dynamic model from the literature and a quantitatively good agreement is obtained.

A total of two thickener models were developed; one with an initial filling period and another with instantaneously filling. A comparison of both models confirmed that an initial filling rate does not have any influence on the steady state void ratio profile during a continuously operating thickener. This is because the steady state operation is not dependent on the initial rate of filling but the rate of filling/withdrawing during continuous operation. Therefore it is not necessary to simulate the starting of a thickener.

A parametric study of the model was also performed to investigate the influence of solids volume flow rate and initial material height on steady state void ratio profiles. It was found that a slower solids volume flow rate generally provides a higher solids thickener underflow. This is due to a longer residence time. It was also shown that

overflowing of a thickener or ineffective use of a thickener can occur when the solids volume flow rate is too fast.

The concept of a high compression thickener by increasing the initial material thickness was investigated and it was found that an increase of the bed thickness can increase the underflow solids content. From the numerical experiment on the selected oil sands fine tailings, a small increase in the underflow solids content can be obtained with a significant increase in material thickness inside a thickener. This is because a time consuming consolidation phenomena is required for a low hydraulic conductivity material to compress to lower void ratio. Increase in height is not only increasing the self-weight stress but also increasing the residence time and the length of the drainage path.

Chapter 5 Multi Dimensional Finite Strain Consolidation Modeling

5.1 Introduction

The consolidation analysis of a slurry deposit is generally performed by the one-dimensional finite strain consolidation theory developed by Gibson, England and Hussey (1967). The one-dimensional approach is usually valid because most containment ponds have small depth compared to the width and the length of the pond. The pore fluid flow direction and the settlement are thus primarily vertical and the one-dimensional assumption is suitable. However, in special cases, deposition of slurry in a containment pond with different dimensions and drainage conditions can result in a more complex multi-dimensional flow. This has an implication on the dewatering time of the slurry therefore a multi-dimensional consolidation model becomes necessary.

To develop a multi dimensional finite strain consolidation model and explore its implications on water release behavior of tailings, a quasi-multi-dimensional finite strain consolidation equation was derived and the equations were numerically implemented in both two and three dimensional problems. The models were verified and then used in several deposition schemes to evaluate the initial rate of slurry consolidation which was affected by containment geometry and drainage conditions.

5.2 Quasi-two-dimensional finite strain consolidation theory

Two dimensional problems can arise in a containment pond that has a very long length compared to width. Two dimensional consolidation problems can be a deposition of tailings into a long trench with different cross-section shapes and drainage conditions. In this section, a quasi-two-dimensional finite strain consolidation theory is derived. The coordinate transformation used in this chapter follows those presented in Chapter 4.

A version of this chapter has been published. Jeeravipoolvarn S., Scott J.D. and Chalaturnyk R.J., 2008. Multi-Dimensional Finite Strain Consolidation Theory: Modeling Study. Proceedings of 61st Canadian Geotechnical Conference, Edmonton, Alberta, Canada, September 22-24, pp. 167-175.

In two dimensions, a small element in the soil can be illustrated in Figure 5.1 for time $t = 0$ and $t > 0$. First assumption for this model is that the mode of movement of any soil element in the domain is predominately vertical therefore horizontal movement is neglected. This assumption is illustrated in Figure 5.1.

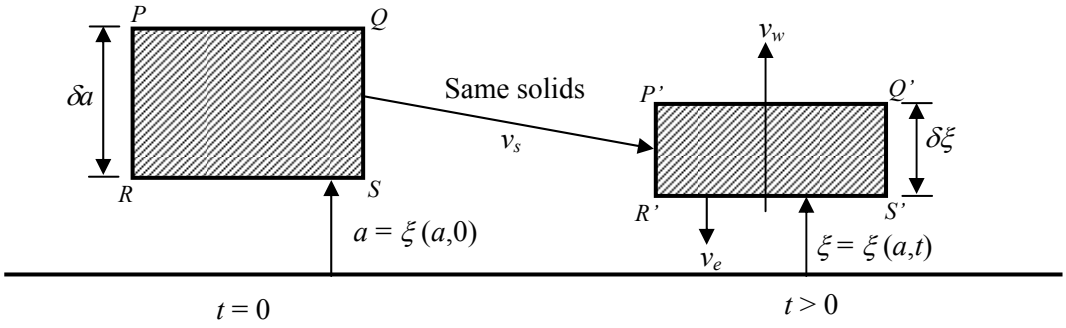

Figure 5.1 Two dimensional configuration of soil under consolidation

5.2.1 The conservation of mass of the pore water

Considering water flow in a soil element, Figure 5.2 shows two dimensional water flow into an element *P'Q'R'S'* at anytime *t*. In the vertical direction, the pore water flows into the element *P'Q'R'S'* with an influx $J_{wv}(\xi,t)$ across the face *R'S'* and flows out of the element, across *P'Q'* with an efflux $J_{wv}(\xi + \delta\xi, t)$.

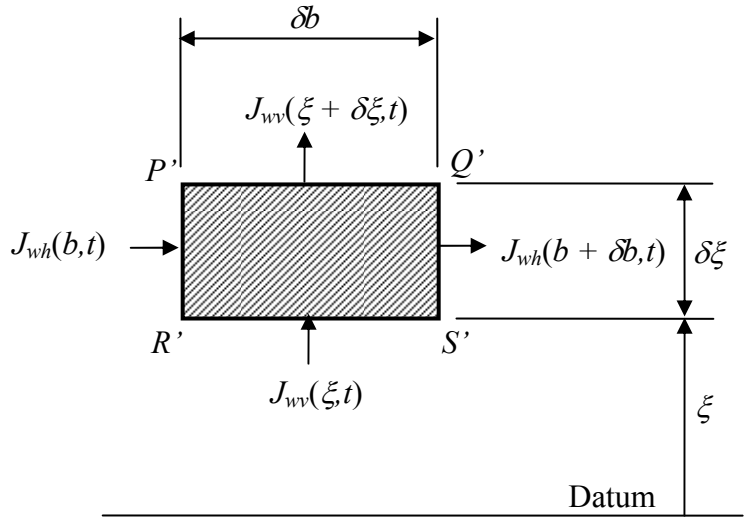

Figure 5.2 Flux of pore water through the representative elementary volume

The pore water crosses the face *R'S'* which has an area of δb with a relative velocity (v_{wv} - v_{ev}), so that the influx of pore-water is

$$J_{wv}(\xi,t) = \gamma_w n(\xi,t)[v_{wv}(\xi,t) - v_{ev}(\xi,t)]\delta b \qquad [5.1]$$

Where

$$v_{ev} = \frac{\partial \xi}{\partial t} \qquad [5.2]$$

v_{ev} is the velocity of the element in the vertical direction therefore

$$J_{wv}(\xi,t) = \gamma_w n[v_{wv} - \frac{\partial \xi}{\partial t}]\delta b \qquad [5.3]$$

The efflux is $J_{wv}(\xi+ \delta\xi,t)$. By a Taylor series expansion the efflux is expressed as

$$J_{wv}(\xi + \delta\xi,t) = J_{wv}(\xi,t) + \frac{\partial J_{wv}}{\partial \xi}\delta\xi + \ldots \qquad [5.4]$$

The net efflux is the second term on the right hand side of Equation [5.4] which is

$$\frac{\partial J_{wv}}{\partial \xi}\delta\xi = \frac{\partial}{\partial \xi}\left[\gamma_w n\left(v_{wv} - \frac{\partial \xi}{\partial t}\right)\right]\delta\xi.\delta b \qquad [5.5]$$

The net efflux in term of the Lagrangian variable *a* is

$$\frac{\partial J_{wv}}{\partial a}\delta a = \frac{\partial}{\partial a}\left[\gamma_w n\left(v_{wv} - \frac{\partial \xi}{\partial t}\right)\right]\delta a.\delta b \qquad [5.6]$$

In a horizontal direction, pore water flows into the element *P'Q'R'S'* with an influx $J_{wh}(b,t)$ across the face *P'R'* and flows out of the element, across *Q'S'* with an

efflux $J_{wh}(b+\delta b,t)$. Similarly as for the vertical direction, an influx in a horizontal direction can be expressed as

$$J_{wh}(b,t) = \gamma_w n(b,t)[v_{wh}(b,t)]\delta\xi \qquad [5.7]$$

The net efflux is

$$\frac{\partial J_{wh}}{\partial b}\delta b = \frac{\partial}{\partial b}(\gamma_w n v_{wh})\delta\xi.\delta b \qquad [5.8]$$

Using a coordinate transformation, the net efflux in a horizontal direction is expressed as

$$\frac{\partial J_{wh}}{\partial b}\delta b = \frac{\partial}{\partial b}\left[\gamma_w n v_{wh}\right]\left(\frac{1+e}{1+e_0}\right)\delta a.\delta b \qquad [5.9]$$

The volume of the pore water in the element *P'Q'R'S'* can be expressed as

$$\delta V_w = n\,\delta\xi\delta b \qquad [5.10]$$

The rate of change of the mass of pore water in the representative elementary volume is

$$\frac{\partial M_w}{\partial t} = -\frac{\partial}{\partial t}\left[\gamma_w n\,\delta\xi\delta b\right] \qquad [5.11]$$

Since *a* and *b* are dependents of time, Equation [5.11] can be rewritten as

$$\frac{\partial M_w}{\partial t} = -\frac{\partial}{\partial t}\left[\gamma_w n\frac{\partial\xi}{\partial a}\right]\delta a\delta b \qquad [5.12]$$

The law of conservation of mass requires that, in the absence of any mass transfers, the net efflux must be equal to the rate of change of the mass of pore water in the element. By equating Equations [5.6], [5.9] and [5.12], we obtain

$$\frac{\partial}{\partial a}\left[\gamma_w n\left(v_{wv}-\frac{\partial \xi}{\partial t}\right)\right]\delta a\delta b+\frac{\partial}{\partial b}\left[\gamma_w n v_{wh}\right]\left(\frac{1+e}{1+e_0}\right)\delta a\delta b=-\frac{\partial}{\partial t}\left[\gamma_w n\frac{\partial \xi}{\partial a}\right]\delta a\delta b \qquad [5.13]$$

In Lagrangian framework, the velocity of the element (v_{ev}) is the same velocity as the velocity of solid (v_{sv}).

$$v_{sv}=v_{ev}=\frac{\partial \xi}{\partial t} \qquad [5.14]$$

Therefore, Equation [5.13] becomes

$$\frac{\partial}{\partial a}\left[\gamma_w n\left(v_{wv}-v_{sv}\right)\right]+\frac{\partial}{\partial b}\left[\gamma_w n v_{wh}\right]\left(\frac{1+e}{1+e_0}\right)=-\frac{\partial}{\partial t}\left[\gamma_w n\frac{\partial \xi}{\partial a}\right] \qquad [5.15]$$

Since γ_w is constant, Equation [5.15] becomes a continuity equation for the pore water expressed as

$$\frac{\partial}{\partial a}\left[n\left(v_{wv}-v_{sv}\right)\right]+\frac{\partial}{\partial b}\left[n v_{wh}\right]\left(\frac{1+e}{1+e_0}\right)=-\frac{\partial}{\partial t}\left[n\frac{\partial \xi}{\partial a}\right] \qquad [5.16]$$

5.2.2 The conservation of mass of the solids

The continuity of the flow of solids can be developed in the same manner as for the pore water by replacing n with (1 - n) and v_w by v_s and γ_w by γ_s. Therefore Equation [5.16] becomes

$$\frac{\partial}{\partial a}\left[(1-n)\left(v_{sv}-v_{sv}\right)\right]+\frac{\partial}{\partial b}\left[(1-n)v_{sh}\right]\left(\frac{1+e}{1+e_0}\right)+\frac{\partial}{\partial t}\left[(1-n)\frac{\partial \xi}{\partial a}\right]=0 \qquad [5.17]$$

Velocity of solids in the horizontal direction is zero therefore we obtain a continuity equation for solids as

$$\frac{\partial}{\partial t}\left[(1-n)\frac{\partial \xi}{\partial a}\right]=0 \qquad [5.18]$$

5.2.3 The continuity of the mixture

To obtain the continuity of the mixture, Equations [5.16] and [5.18] are combined. The resulting equation is expressed as

$$\frac{\partial}{\partial a}\left[n\left(v_{wv}-v_{sv}\right)\right]+\frac{\partial}{\partial b}\left[nv_{wh}\right]\left(\frac{1+e}{1+e_0}\right)+\frac{\partial}{\partial t}\left[n\frac{\partial \xi}{\partial a}\right]+\frac{\partial}{\partial t}\left[(1-n)\frac{\partial \xi}{\partial a}\right]=0 \qquad [5.19]$$

$$\frac{\partial}{\partial a}\left[n\left(v_{wv}-v_{sv}\right)\right]+\frac{\partial}{\partial b}\left[nv_{wh}\right]\left(\frac{1+e}{1+e_0}\right)+\frac{\partial}{\partial t}\left[\frac{\partial \xi}{\partial a}\right]=0 \qquad [5.20]$$

Introducing the Darcy-Gersevanov relationship in the vertical direction,

$$n(v_{wv}-v_{sv})=\frac{-k_v(e)}{\gamma_w}\frac{\partial u}{\partial \xi} \qquad [5.21]$$

And in the horizontal direction, horizontal solids velocity is zero ($v_{sh} = 0$) thus

$$n(v_{wh})=\frac{-k_h(e)}{\gamma_w}\frac{\partial u}{\partial b} \qquad [5.22]$$

By substituting Equations [5.21] and [5.22] into Equation [5.20], we obtain

$$\frac{\partial}{\partial a}\left[\frac{-k_v(e)}{\gamma_w}\frac{\partial u}{\partial \xi}\right]+\frac{\partial}{\partial b}\left[\frac{-k_h(e)}{\gamma_w}\frac{\partial u}{\partial b}\right]\left(\frac{1+e}{1+e_0}\right)+\frac{\partial}{\partial t}\left[\frac{\partial \xi}{\partial a}\right]=0 \qquad [5.23]$$

It is noted that the term u is excess pore pressure. By using a coordinate transformation and changing subscripts of the horizontal components to x, Equation [5.23] becomes

$$\frac{1}{(1+e_0)}\frac{\partial}{\partial z}\left[\frac{-k_v(e)}{\gamma_w(1+e)}\frac{\partial u}{\partial z}\right]+\frac{\partial}{\partial x}\left[\frac{-k_x(e)}{\gamma_w}\frac{\partial u}{\partial x}\right]\left(\frac{1+e}{1+e_0}\right)+\frac{\partial}{\partial t}\left[\frac{1+e}{1+e_0}\right]=0 \quad [5.24]$$

By rearranging Equation [5.24], we obtain

$$\frac{\partial}{\partial z}\left[\frac{-k_v(e)}{\gamma_w(1+e)}\frac{\partial u}{\partial z}\right]+(1+e)\frac{\partial}{\partial x}\left[\frac{-k_x(e)}{\gamma_w}\frac{\partial u}{\partial x}\right]+\frac{\partial e}{\partial t}=0 \quad [5.25]$$

Compressibility of soil can be expressed as

$$\frac{\partial e}{\partial t}=-a_v(e)\frac{\partial \sigma'}{\partial t}=\frac{de}{d\sigma'}\frac{\partial \sigma'}{\partial t} \quad [5.26]$$

Substituting Equation [5.26] into Equation [5.25] gives

$$\frac{\partial}{\partial z}\left[\frac{-k_v(e)}{\gamma_w(1+e)}\frac{\partial u}{\partial z}\right]+(1+e)\frac{\partial}{\partial x}\left[\frac{-k_x(e)}{\gamma_w}\frac{\partial u}{\partial x}\right]+\frac{de}{d\sigma'}\frac{\partial \sigma'}{\partial t}=0 \quad [5.27]$$

The effective stress equation can be expressed as

$$\frac{\partial \sigma'}{\partial t}=(Gs-1).\gamma_w\frac{\partial \Delta z}{\partial t}-\frac{\partial u}{\partial t} \quad [5.28]$$

Substituting Equation [5.28] into Equation [5.27] gives

$$\frac{\partial}{\partial z}\left[\frac{-k_v(e)}{\gamma_w(1+e)}\frac{\partial u}{\partial z}\right]+(1+e)\frac{\partial}{\partial x}\left[\frac{-k_x(e)}{\gamma_w}\frac{\partial u}{\partial x}\right]+\frac{de}{d\sigma'}\left[(Gs-1).\gamma_w\frac{\partial \Delta z}{\partial t}-\frac{\partial u}{\partial t}\right]=0 \quad [5.29]$$

This equation is a governing equation for quasi-two-dimensional finite strain consolidation in term of excess pore water pressure.

5.3 Quasi-three-dimensional finite strain consolidation theory

In a three dimensional situation, a small element in the soil can be illustrated in Figure 5.3 for time = 0 and time = *t*. The assumption used in the two dimensional case is also applied here as shown in Figure 5.3.

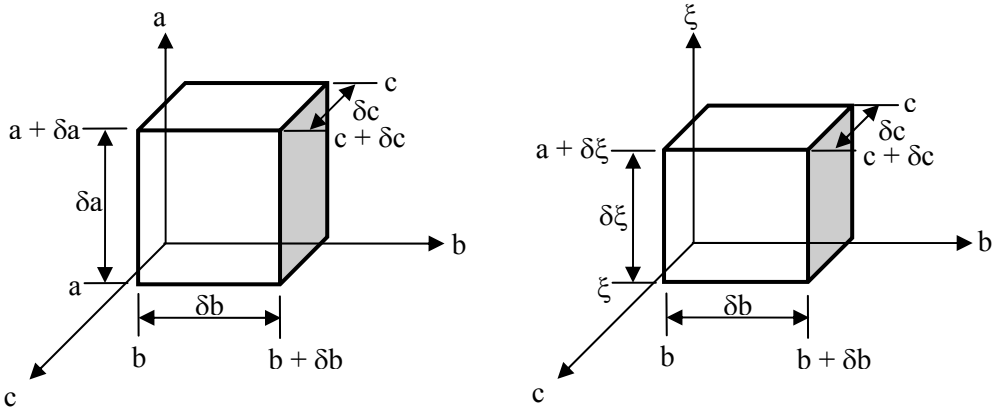

Figure 5.3 Three dimensional configuration of soil under consolidation

5.3.1 The conservation of mass of the pore water

Pore water flow in a soil element is illustrated in Figure 5.4 showing three dimensional water flow into an element *L'M'N'O'P'Q'R'S'* at anytime *t*. In the vertical direction, pore water flows into the element with an influx $J_{wv}(\xi,t)$ across the face *N'O'R'S'* and flows out of the element, across *L'M'P'Q'* with an efflux $J_{wv}(\xi+\delta\xi,t)$.

The pore water crosses the face *R'S'N'O'* which has an area of $\delta b\delta c$ with a relative velocity (v_{wv} - v_{ev}), so that the influx of pore water is

$$J_{wv}(\xi,t) = \gamma_w n(\xi,t)[v_{wv}(\xi,t) - v_{ev}(\xi,t)]\delta b\delta c \qquad [5.30]$$

v_{ev} is the velocity of the element in a vertical direction. Then

$$J_{wv}(\xi,t) = \gamma_w n[v_{wv} - \frac{\partial \xi}{\partial t}]\delta b\delta c \qquad [5.31]$$

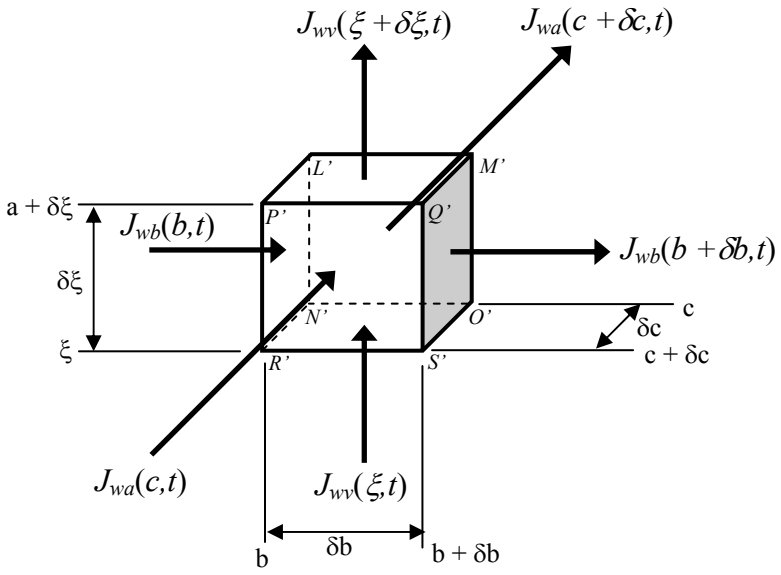

Figure 5.4 Flux of pore water through the representative elementary volume

The net efflux is the second term in a Taylor series expansion which is

$$\frac{\partial J_{wv}}{\partial \xi}\delta\xi = \frac{\partial}{\partial \xi}\left[\gamma_w n\left(v_{wv} - \frac{\partial \xi}{\partial t}\right)\right]\delta\xi.\delta b.\delta c \qquad [5.32]$$

The net efflux in term of the Lagrangian variable *a* is

$$\frac{\partial J_{wv}}{\partial a}\delta a = \frac{\partial}{\partial a}\left[\gamma_w n\left(v_{wv} - \frac{\partial \xi}{\partial t}\right)\right]\delta a.\delta b.\delta c \qquad [5.33]$$

In the horizontal (*b*) direction, the pore water flows into the element with an influx $J_{wb}(b,t)$ across the face *P'R'L'N'* and flows out of the element, across *Q'S'M'O'* with an efflux $J_{wb}(b+\delta b,t)$. Similar to the vertical direction equation, the influx in the horizontal (*b*) direction can be expressed as

$$J_{wb}(b,t) = \gamma_w n v_{wb}.\delta\xi.\delta c \qquad [5.34]$$

And the net efflux is

$$\frac{\partial J_{wb}}{\partial b}\delta b = \frac{\partial}{\partial b}\left(\gamma_w n v_{wb}\right)\delta\xi.\delta b.\delta c \qquad [5.35]$$

Using a coordinate transformation, the net efflux in the horizontal (b) direction is

$$\frac{\partial J_{wb}}{\partial b}\delta b = \frac{\partial}{\partial b}\left[\gamma_w n v_{wb}\right]\left(\frac{1+e}{1+e_0}\right)\delta a.\delta b.\delta c \qquad [5.36]$$

In the horizontal (c) direction, pore water flows into the element with an influx $J_{wc}(c,t)$ across the face *P'Q'R'S*' and flows out of the element, across *L'M'N'O'* with an efflux $J_{wc}(c+\delta c,t)$. Similar to the vertical direction equation, the influx in the horizontal (c) direction can be expressed as

$$J_{wc}(c,t) = \gamma_w n v_{wc}.\delta\xi.\delta b \qquad [5.37]$$

And the net efflux is

$$\frac{\partial J_{wc}}{\partial c}\delta c = \frac{\partial}{\partial c}\left(\gamma_w n v_{wc}\right)\delta\xi.\delta b.\delta c \qquad [5.38]$$

Using a coordinate transformation, the net efflux in the horizontal (c) direction is

$$\frac{\partial J_{wc}}{\partial c}\delta c = \frac{\partial}{\partial c}\left[\gamma_w n v_{wc}\right]\left(\frac{1+e}{1+e_0}\right)\delta a.\delta b.\delta c \qquad [5.39]$$

The volume of the pore water in the element *P'Q'R'S'L'M'N'O'P'* can be expressed as

$$\delta V_w = n\,\delta\xi\,\delta b\,\delta c \qquad [5.40]$$

The rate of change of the mass of the pore water in the representative elementary volume is

$$\frac{\partial M_w}{\partial t} = -\frac{\partial}{\partial t}\left[\gamma_w n\,\delta\xi\delta b\,\delta c\right] \qquad [5.41]$$

Since a is dependent of time, Equation [5.41] becomes

$$\frac{\partial M_w}{\partial t} = -\frac{\partial}{\partial t}\left[\gamma_w n\frac{\partial \xi}{\partial a}\right]\delta a\,\delta b\,\delta c \qquad [5.42]$$

The net efflux must be equal to the rate of change of the mass of pore water in the element. By equating Equations [5.33], [5.36], [5.39] and [5.42], we obtain

$$\frac{\partial}{\partial a}\left[\gamma_w n\left(v_{wv} - \frac{\partial \xi}{\partial t}\right)\right]\delta a\,\delta b\,\delta c + \frac{\partial}{\partial b}\left[\gamma_w n v_{wb}\right]\left(\frac{1+e}{1+e_0}\right)\delta a\,\delta b\,\delta c$$
$$+ \frac{\partial}{\partial c}\left[\gamma_w n v_{wc}\right]\left(\frac{1+e}{1+e_0}\right)\delta a\,\delta b\,\delta c = -\frac{\partial}{\partial t}\left[\gamma_w n\frac{\partial \xi}{\partial a}\right]\delta a\,\delta b\,\delta c \qquad [5.43]$$

In Lagrangian framework the velocity of the element is the same velocity as the velocity of the solid. Equation [5.43] thus becomes

$$\frac{\partial}{\partial a}\left[\gamma_w n\left(v_{wv} - v_{sv}\right)\right] + \frac{\partial}{\partial b}\left[\gamma_w n v_{wb}\right]\left(\frac{1+e}{1+e_0}\right) + \frac{\partial}{\partial c}\left[\gamma_w n v_{wc}\right]\left(\frac{1+e}{1+e_0}\right) = -\frac{\partial}{\partial t}\left[\gamma_w n\frac{\partial \xi}{\partial a}\right] \qquad [5.44]$$

Since γ_w is constant, we obtain a continuity equation of pore water as

$$\frac{\partial}{\partial a}\left[n\left(v_{wv} - v_{sv}\right)\right] + \frac{\partial}{\partial b}\left[n v_{wh}\right]\left(\frac{1+e}{1+e_0}\right) + \frac{\partial}{\partial b}\left[n v_{wh}\right]\left(\frac{1+e}{1+e_0}\right) = -\frac{\partial}{\partial t}\left[n\frac{\partial \xi}{\partial a}\right] \qquad [5.45]$$

5.3.2 The conservation of mass of the solids

The continuity of the flow of solids can be developed in the same manner as for the pore water by replacing n with (1 - n) and v_w by v_s and γ_w by γ_s. Equation [5.45] thus becomes

$$\frac{\partial}{\partial a}\left[(1-n)(v_{sv}-v_{sv})\right]+\frac{\partial}{\partial b}\left[(1-n)v_{sb}\right]\left(\frac{1+e}{1+e_0}\right)+\frac{\partial}{\partial c}\left[(1-n)v_{sc}\right]\left(\frac{1+e}{1+e_0}\right)+\frac{\partial}{\partial t}\left[(1-n)\frac{\partial \xi}{\partial a}\right]=0 \quad [5.46]$$

Velocities of solids in both horizontal directions are zero therefore the continuity equation of solids is

$$\frac{\partial}{\partial t}\left[(1-n)\frac{\partial \xi}{\partial a}\right]=0 \quad [5.47]$$

5.3.3 The continuity of the mixture

By combing Equations [5.45] and [5.47]

$$\frac{\partial}{\partial a}\left[n(v_{wv}-v_{sv})\right]+\frac{\partial}{\partial b}\left[nv_{wb}\right]\left(\frac{1+e}{1+e_0}\right)+\frac{\partial}{\partial c}\left[nv_{wc}\right]\left(\frac{1+e}{1+e_0}\right)+\frac{\partial}{\partial t}\left[n\frac{\partial \xi}{\partial a}\right]$$
$$+\frac{\partial}{\partial t}\left[(1-n)\frac{\partial \xi}{\partial a}\right]=0 \quad [5.48]$$

$$\frac{\partial}{\partial a}\left[n(v_{wv}-v_{sv})\right]+\frac{\partial}{\partial b}\left[nv_{wb}\right]\left(\frac{1+e}{1+e_0}\right)+\frac{\partial}{\partial c}\left[nv_{wc}\right]\left(\frac{1+e}{1+e_0}\right)+\frac{\partial}{\partial t}\left[\frac{\partial \xi}{\partial a}\right]=0 \quad [5.49]$$

By introducing the Darcy-Gersevanov flow relationship in the vertical direction, we have

$$n(v_{wv}-v_{sv})=\frac{-k_v(e)}{\gamma_w}\frac{\partial u}{\partial \xi} \quad [5.50]$$

It is assumed that the horizontal hydraulic conductivity in (*b*) and in (*c*) are equal and subscript *h* (horizontal) is used. In the horizontal direction (*b*),

$$n(v_{wb}) = \frac{-k_h(e)}{\gamma_w}\frac{\partial u}{\partial b} \qquad [5.51]$$

In the horizontal direction (c),

$$n(v_{wc}) = \frac{-k_h(e)}{\gamma_w}\frac{\partial u}{\partial c} \qquad [5.52]$$

By substituting Equations [5.50], [5.51] and [5.52] into Equation [5.49], we obtain

$$\frac{\partial}{\partial a}\left[\frac{-k_v(e)}{\gamma_w}\frac{\partial u}{\partial \xi}\right]+\left(\frac{1+e}{1+e_0}\right)\left\{\frac{\partial}{\partial b}\left[\frac{-k_h(e)}{\gamma_w}\frac{\partial u}{\partial b}\right]+\frac{\partial}{\partial c}\left[\frac{-k_h(e)}{\gamma_w}\frac{\partial u}{\partial c}\right]\right\}+\frac{\partial}{\partial t}\left[\frac{\partial \xi}{\partial a}\right]=0 \qquad [5.53]$$

By using coordinate transformation and change subscripts of the horizontal components from b to x and c to y, Equation [5.53] becomes

$$\frac{1}{(1+e_0)}\frac{\partial}{\partial z}\left[\frac{-k_v(e)}{\gamma_w(1+e)}\frac{\partial u}{\partial z}\right]+\left(\frac{1+e}{1+e_0}\right)\left\{\frac{\partial}{\partial x}\left[\frac{-k_h(e)}{\gamma_w}\frac{\partial u}{\partial x}\right]+\frac{\partial}{\partial y}\left[\frac{-k_h(e)}{\gamma_w}\frac{\partial u}{\partial y}\right]\right\}+\frac{\partial}{\partial t}\left[\frac{1+e}{1+e_0}\right]=0 \qquad [5.54]$$

Compressibility of soil can be expressed as

$$\frac{\partial e}{\partial t} = -a_v(e)\frac{\partial \sigma'}{\partial t} = \frac{de}{d\sigma'}\frac{\partial \sigma'}{\partial t} \qquad [5.55]$$

Substituting Equation [5.55] into Equation [5.54]

$$\frac{\partial}{\partial z}\left[\frac{-k_v(e)}{\gamma_w(1+e)}\frac{\partial u}{\partial z}\right]+(1+e)\left\{\frac{\partial}{\partial x}\left[\frac{-k_h(e)}{\gamma_w}\frac{\partial u}{\partial x}\right]+\frac{\partial}{\partial y}\left[\frac{-k_h(e)}{\gamma_w}\frac{\partial u}{\partial y}\right]\right\}+\frac{de}{d\sigma'}\frac{\partial \sigma'}{\partial t}=0 \qquad [5.56]$$

From the effective stress equation

$$\frac{\partial \sigma'}{\partial t} = (Gs-1).\gamma_w \frac{\partial \Delta z}{\partial t} - \frac{\partial u}{\partial t} \qquad [5.57]$$

Substituting Equation [5.57] into Equation [5.56] gives

$$\frac{\partial}{\partial z}\left[\frac{-k_v(e)}{\gamma_w(1+e)}\frac{\partial u}{\partial z}\right] + (1+e)\left\{\frac{\partial}{\partial x}\left[\frac{-k_h(e)}{\gamma_w}\frac{\partial u}{\partial x}\right] + \frac{\partial}{\partial y}\left[\frac{-k_h(e)}{\gamma_w}\frac{\partial u}{\partial y}\right]\right\}$$
$$+ \frac{de}{d\sigma'}\left[(Gs-1).\gamma_w \frac{\partial \Delta z}{\partial t} - \frac{\partial u}{\partial t}\right] = 0 \qquad [5.58]$$

This equation is a governing equation for quasi-three-dimensional finite strain consolidation in terms of excess pore pressure.

5.4 Conventional 2*D* and 3*D* consolidation theory

It is of interest to show that the equations derived earlier are similar to the conventional consolidation theory. In this section the assumptions of the infinitesimal strain consolidation theory are applied to the governing equation for quasi-multi-dimensional finite strain consolidation.

Equation [5.27] can be restated as

$$\frac{\partial}{\partial z}\left[\frac{-k_v(e)}{\gamma_w(1+e)}\frac{\partial u}{\partial z}\right] + (1+e)\frac{\partial}{\partial x}\left[\frac{-k_x(e)}{\gamma_w}\frac{\partial u}{\partial x}\right] + \frac{\partial e}{\partial t} = 0 \qquad [5.59]$$

Transforming material coordinates back to Lagrangian coordinates gives

$$(1+e_0)\frac{\partial}{\partial a}\left[\frac{-k_v(e)(1+e_0)}{\gamma_w(1+e)}\frac{\partial u}{\partial a}\right] + (1+e)\frac{\partial}{\partial x}\left[\frac{-k_x(e)}{\gamma_w}\frac{\partial u}{\partial x}\right] + \frac{\partial e}{\partial t} = 0 \qquad [5.60]$$

In a small strain theory, $e_0 \approx e$, coordinate a is an initial height Z, and hydraulic conductivity and γ_w are constant therefore

$$\frac{\partial^2 u}{\partial Z^2}+\frac{\partial^2 u}{\partial x^2}=\frac{\gamma_w}{k(1+e_0)}\frac{\partial e}{\partial t} \qquad [5.61]$$

$$\frac{\partial^2 u}{\partial Z^2}+\frac{\partial^2 u}{\partial x^2}=-\frac{\gamma_w a_v}{k(1+e_0)}\frac{\partial \sigma'}{\partial t} \qquad [5.62]$$

$$\frac{\partial u}{\partial t}=C_v\left(\frac{\partial^2 u}{\partial Z^2}+\frac{\partial^2 u}{\partial x^2}\right) \qquad [5.63]$$

Equation [5.63] is a general form of a quasi-two-dimension small strain consolidation theory.

The 3*D* finite consolidation equation [5.58] is restated as

$$(1+e_0)\frac{\partial}{\partial a}\left[\frac{-k_v(e)(1+e_0)}{\gamma_w(1+e)}\frac{\partial u}{\partial a}\right]+(1+e)\left\{\frac{\partial}{\partial x}\left[\frac{-k_h(e)}{\gamma_w}\frac{\partial u}{\partial x}\right]+\frac{\partial}{\partial y}\left[\frac{-k_h(e)}{\gamma_w}\frac{\partial u}{\partial y}\right]\right\}+\frac{\partial e}{\partial t}=0 \qquad [5.64]$$

Using the same assumptions stated above in 2*D*, Equation [5.64] is reduced to

$$\frac{\partial u}{\partial t}=C_v\left(\frac{\partial^2 u}{\partial x^2}+\frac{\partial^2 u}{\partial y^2}+\frac{\partial^2 u}{\partial Z^2}\right) \qquad [5.65]$$

Equation [5.65] is a general form of a quasi-three-dimension small strain consolidation theory.

5.5 Numerical analysis of the multidimensional consolidation model

In the earlier sections, quasi 2*D* and 3*D* finite strain consolidation governing equations were developed. In this section, the 2*D* and 3*D* finite strain consolidation models are coded in FlexPDE program which is a finite element partial differential equation solver. The derivation of the governing equations utilized material coordinates. This utilization provides convenience in solving the equations in the FlexPDE program as a coordinate stays unchanged during the consolidation process. In order to transform

material coordinates back to Lagrangian or convective coordinate systems, a coordinate transformation (Figure 4.3) must be used.

Due to the fact that FlexPDE performs many operations to setup a problem and solve a differential equation, a numerical experiment was performed to verify the developed model by comparing a one-dimensional finite strain consolidation model by finite difference methods (programmed in Visual Basic) and a quasi-multi-dimensional finite strain consolidation model (one-dimensional equivalent) in the FlexPDE program. Results from both models are compared and discussed.

5.5.1 1*D* equivalent model in FlexPDE results and discussion

FlexPDE is a scripted finite element model builder and numerical solver. It accepts a script written by a user to define a problem. After a problem is setup by a user, the program performs operations necessary to solve partial differential equation systems. The FlexPDE program is selected to be a solver for the 2*D* and 3*D* models in this thesis due to its flexibility and ability to solve PDEs.

Mature fine tailings (MFT) is selected to be a material used for the current comparison. Input parameters are solids content = 30.6%, specific gravity = 2.28, A = 28.71, B = -0.3097, $C = 7.538\times10^{-11}$, D = 3.824 (units in Pa and m/s), depth = 1.0 m and duration of 1 year.

Interface settlements from the two models are shown in Figure 5.5. It appears that both models provide identical interface settlement predictions. Changes in void ratio with depth from both models show decreases of void ratio from bottom up which is expected from self-weight consolidation (Figure 5.8). Increases in effective stress and dissipation of excess pore pressure due to consolidation are shown in Figures 5.6 and 5.7 respectively. Both numerical programs provide identical results.

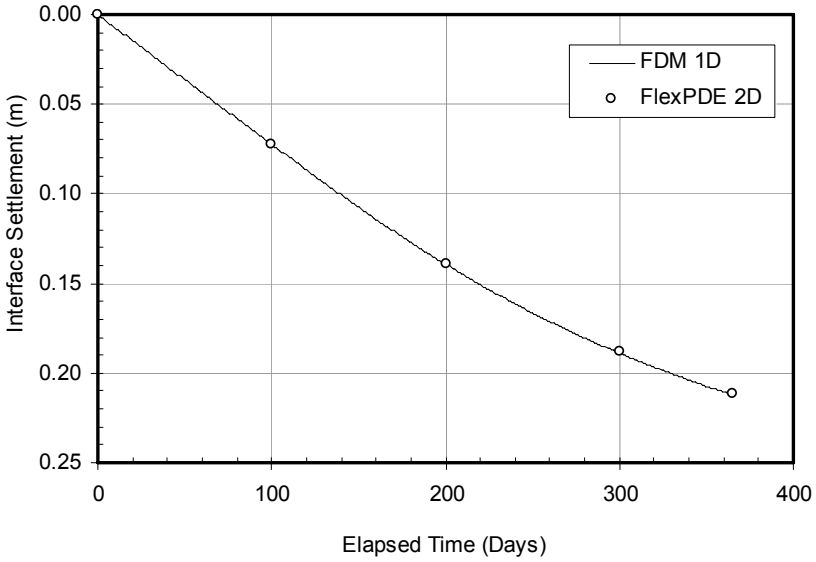

Figure 5.5 Interface settlement prediction comparison between 1*D* model (FDM) and 2*D* model (FEM in FlexPDE-1*D* equivalent)

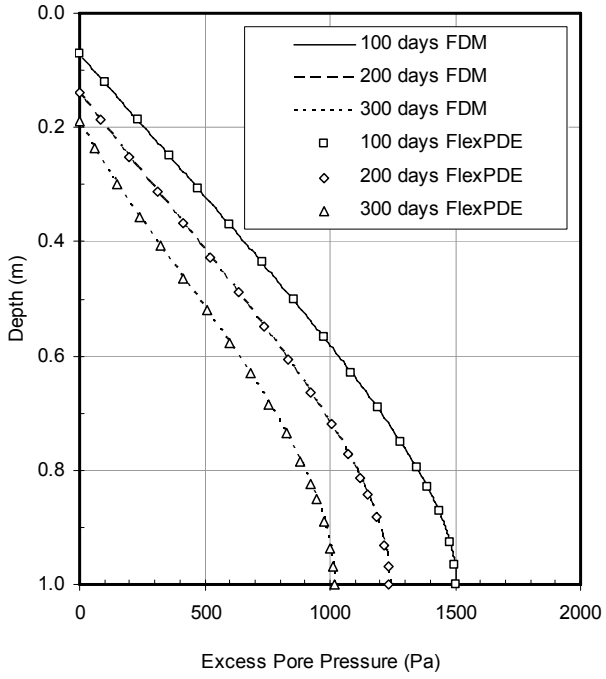

Figure 5.6 Excess pore pressure prediction comparison between 1*D* model (FDM) and 2*D* model (FEM in FlexPDE-1*D* equivalent)

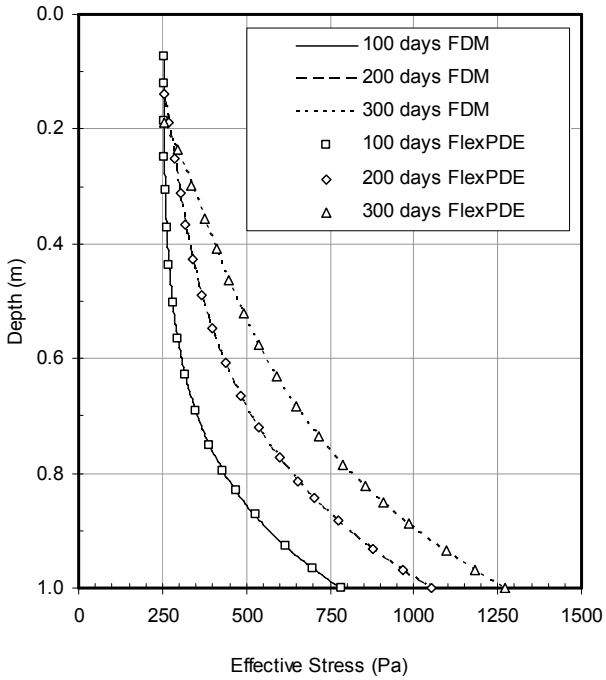

Figure 5.7 Effective stress prediction comparison between 1*D* model (FDM) and 2*D* model (FEM in FlexPDE-1*D* equivalent)

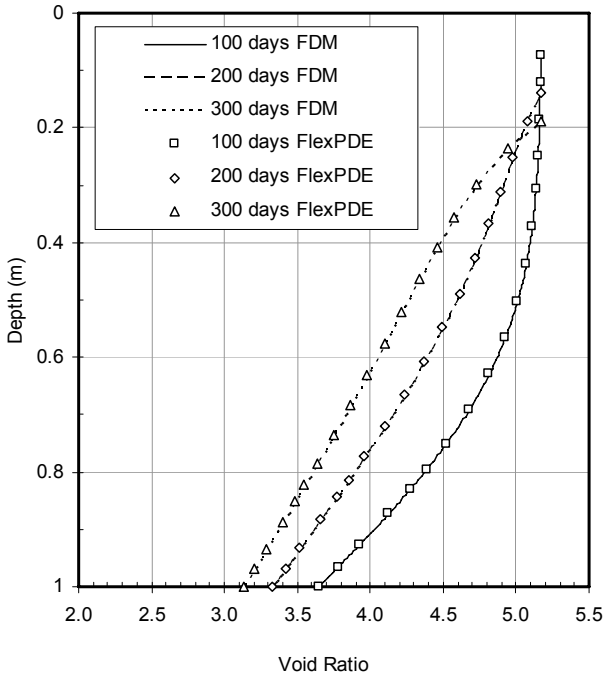

Figure 5.8 Void ratio prediction comparison between 1*D* model (FDM) and 2*D* model (FEM in FlexPDE-1*D* equivalent)

From the comparison of the results form both modeling approaches, the multidimensional model coded in FlexPDE (FEM) provides identical solutions as those predicted by a one dimensional theory numerically modeled by a finite difference method. This gives confidence that the multidimensional model coded in FlexPDE performs correctly. The implementation of the program is uncomplicated therefore allows complex problems to be solved with ease. In the next section, 2*D* and 3*D* consolidation models will be used to study geometry and drainage conditions for different types of containment.

5.6 Parametric study of the multi-dimensional consolidation models

It is a common practice in tailings deposition that tailings are pumped into a large pond with little to no concern about the shape of a pond and/or the optimum drainage condition for self-weight consolidation. It is realized that the size and shape of these containments are controlled by many factors (most of them relating to economic and mining considerations). Different considerations could be valuable, however, when rapid dewatering of the tailings is crucial and when the geometry and drainage conditions can contribute to the rate of consolidation. More importantly, in order to evaluate tailings performance in a pilot scale pond where the one-dimensional condition is questionable, engineers must know the extent of water seepage through the dykes and foundation. This consideration makes the understanding of the multidimensional consolidation of tailings more important. In this section, a parametric study of the models is performed. Simulations are only focused on containment shape, drainage and surface slope under quiescent conditions. Hydraulic conductivity in all directions is assumed to be equal and vertical self-weight stress is assumed to be the only driving mechanism in this investigation.

5.6.1 Two dimensional consolidation modeling study

The pond geometry study in this section is done by choosing oil sands tailings as the study material. The material parameters used in this section thus are identical to the previous section. Factors that will be investigated are containment shape, drainage and tailing's surface slope.

5.6.1.1 Containment shape

5.6.1.1.1 Width to depth ratio

The investigation of width to depth ratio (W:D) of a rectangular cross-sectional shape pond (Figure 5.9) is performed by varying the W:D ratio to 1:2, 1:1, 2:1, 3:1 and 4:1. A simulated pond is assumed to have a rectangular cross sectional area and has the length to width very large so a 2*D* problem can be assumed. The pond depth is set to be 1 m and the width of the pond is varied according to the specified ratio. Oil sands tailings material parameters used are solids content = 30.6%, specific gravity = 2.28, depth = 1.0 m and the finite strain parameters are A = 28.71, B = -0.3097, $C = 7.538\times10^{-11}$, and D = 3.824 (units in Pa and m/s). The consolidation period was chosen to be 5 years after which the excess pore pressure was considered negligible for this particular material.

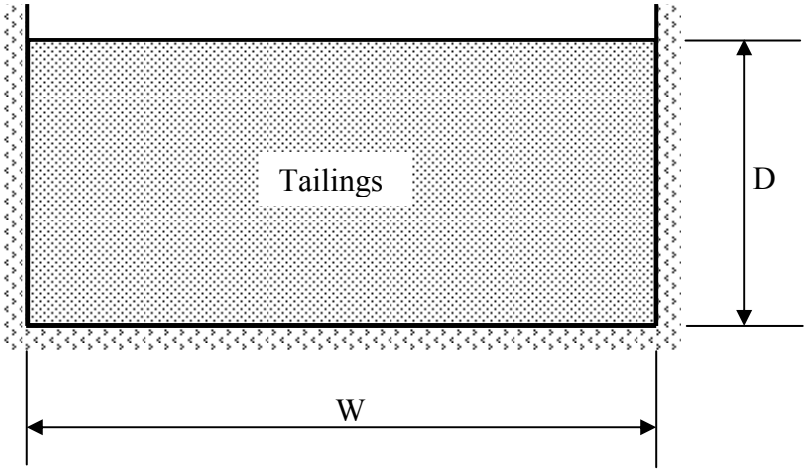

Figure 5.9 Rectangular cross section containment

Figure 5.10 shows average void ratio with time for different W:D ratios. The results indicate that the changes of the W:D ratio does not affect the rate of change in void ratio.

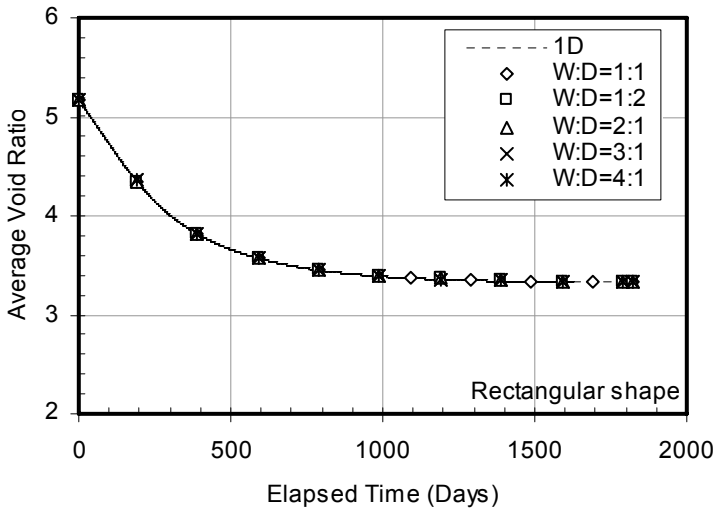

Figure 5.10 Average void ratio change vs. time at the center of a model pond

5.6.1.1.2 Dyke angle

Dyke angle, α, is defined as the angle between the dyke slope and the ground (Figure 5.11). In order to see the effect of the dyke angle on the rate of change in void ratio at the center of the pond, the depth of the pond is kept constant and the dyke angle is varied from 10° to 85°. For each of the dyke angles, the width of the base is also varied to W_1:D = 0:1, 1:2, 1:1 and 2:1 to study the influence of the base length relative to the drainage length from the center to the dyke.

Figure 5.12 shows the comparison of average void ratio changes with time for W_1:D of 1:2, 1:1 and 2:1 (dyke angle is varied from 10° to 85°). The results show that at the center of the pond, the rate of a reduction in void ratio is not affected by the slopes and the base width and show the same compression behavior found in the one dimensional case. When the base width is reduced to zero (V-shape pond), however, the average void ratio change with time is affected by the dyke angle (Figure 5.13). The V-shape pond indicates that the slope of the dyke has an influence on the rate of self-weight consolidation therefore consolidation in a trapezoidal shape pond should also be affected by the dyke slope. By plotting the average void ratio change with time at the edge of the base of the pond, the effect of the dyke slope on the rate of consolidation can be seen in Figure 5.14.

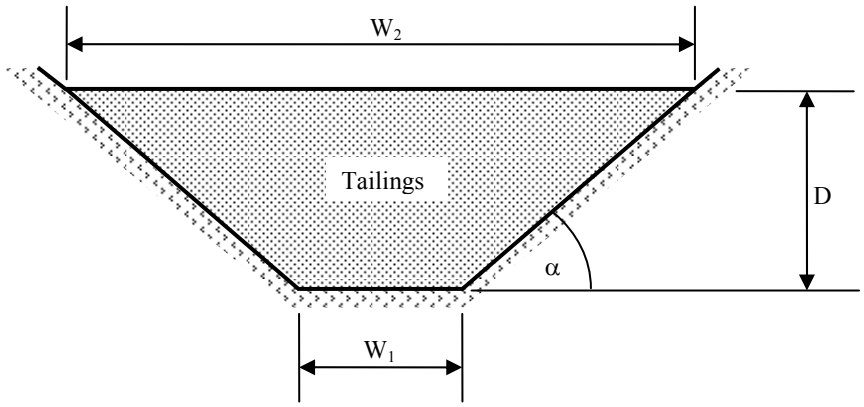

Figure 5.11 Trapezoidal cross section containment

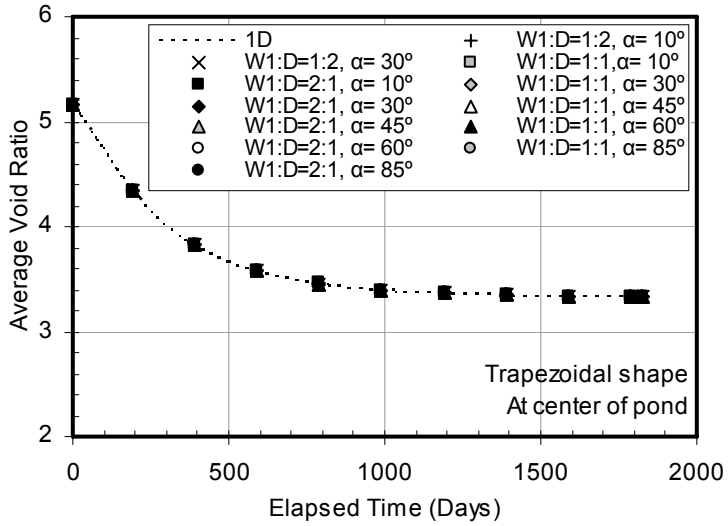

Figure 5.12 Average void ratio change vs. time for trapezoidal shape at center of pond

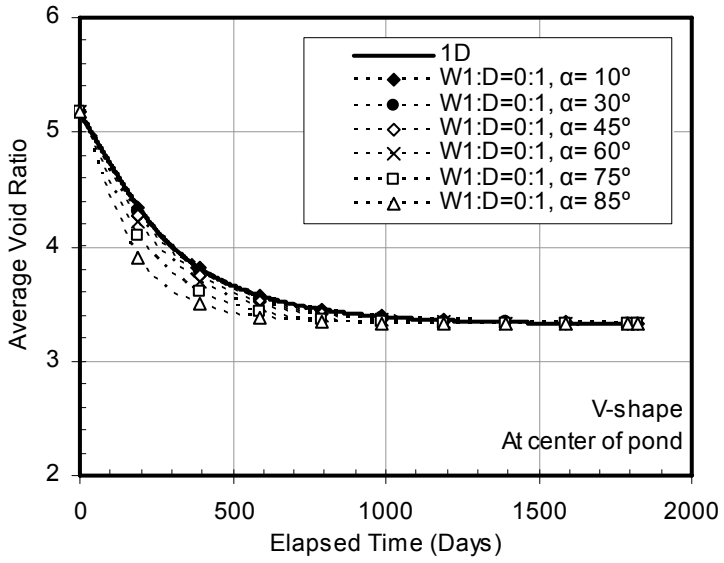

Figure 5.13 Average void ratio change vs. time for V-shape at center of pond

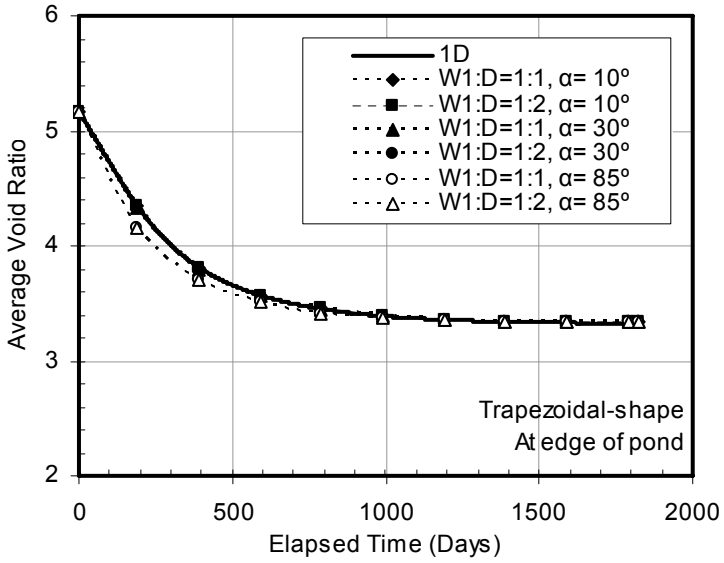

Figure 5.14 Average void ratio change vs. time for trapezoidal shape at the edge of pond

To summarize the findings, comparison between different dyke slopes is performed through plotting the percent rate of change of the initial compression (the initial linear portion of the void ratio-time plot) against the dyke slope (Figure 5.15). The base rate in the comparison is the one dimensional rate of consolidation. The results indicate that the compression rate at the center of a V-shape pond decreases as the dyke

angle decreases. The maximum rate appears to be about 55% at a dyke angle of about 85° (maximum value modeled) for this particular investigation. A further reduction in the dyke slope causes a rapid reduction in the compression rate to a value close to the one dimensional case when the angle is reduced to 10°. It was also found that the rate of consolidation at the center of a trapezoidal shape pond is independent of the W_1:D ratios used in this investigation.

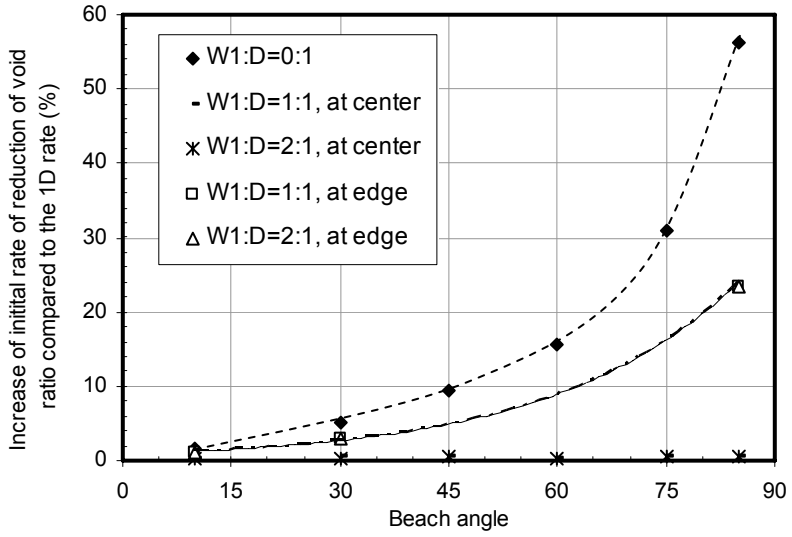

Figure 5.15 Percent increase of initial rate of void ratio reduction at the toe of dyke vs. dyke angle

It can be concluded that for a case of a zero base width (V-shape pond), the steeper the slope the better the drainage performance. This is because the shorter drainage path elements (elements on the dyke) are closer together and the consolidation of these elements are relatively faster compared to the center (the drainage path is longer) as self-weight consolidation propagates from bottom up. Due to lower excess pore pressures in these elements compared to the center, the excess pore pressure gradient occurs horizontally and induces the excess pressure in the center to dissipate sideways and causes faster consolidation at the center of a pond.

At the edge of a pond, the dyke slope also appears to affect the rate of consolidation but the base width does not. The same conclusion is made that the steeper the dyke slope the better the rate of consolidation at the edges of the pond. In addition, if

the dyke slope is a constant, the base length should be minimized as the condition is moving towards the V-shape pond. It can be concluded from the results that in order to take advantage of the pond shape, the dyke slope has to be steep. Although this conclusion is intuitive, this numerical analysis evaluates the degree to which the dyke slope is important.

To illustrate the behavior of the quasi 2*D* finite strain consolidation theory and support the analogy of the model behavior, the simulation results for a trapezoidal shaped pond is used. Void ratio and excess pore pressure distributions from the simulation are presented in Figures 5.16 and 5.17 respectively for 4 different elapsed times. The simulations shown in Figures 5.16 and 5.17 are plotted in a convective coordinate which allows the void ratio profiles to be seen in the real sense. It is noted that the pond height is 1 m, the base length is 1 m and the dyke slope is 45° on both sides.

The figures illustrate the assumption used in the derivation of the theory that only vertical deformation is allowed. Figures 5.16 (*a*) and 5.17(*a*) show the beginning of the consolidation phenomenon. Pore pressure dissipation occurs at the edges of tailings surface where the drainage part is the shortest and the effective stress is the smallest. During the consolidation process, the dissipation occurs faster in the triangular sections compared to the middle section at the same elevations (Figure 5.17 (*b*) and (*c*)). This is because self-weight consolidation always propagates from bottom up due to the triangular stress distribution in the slurry. Therefore it can be said that at the same elevation or same initial self-weight stress, the soil in the triangular area is likely to consolidate faster because the dissipation reaches the specific soil element faster. Consolidation is almost completed in Figure 5.16 (*d*). At this time, the void ratio profiles indicate a bottom void ratio of 2.5 and a surface void ratio of 5.17 (initial surface void ratio).

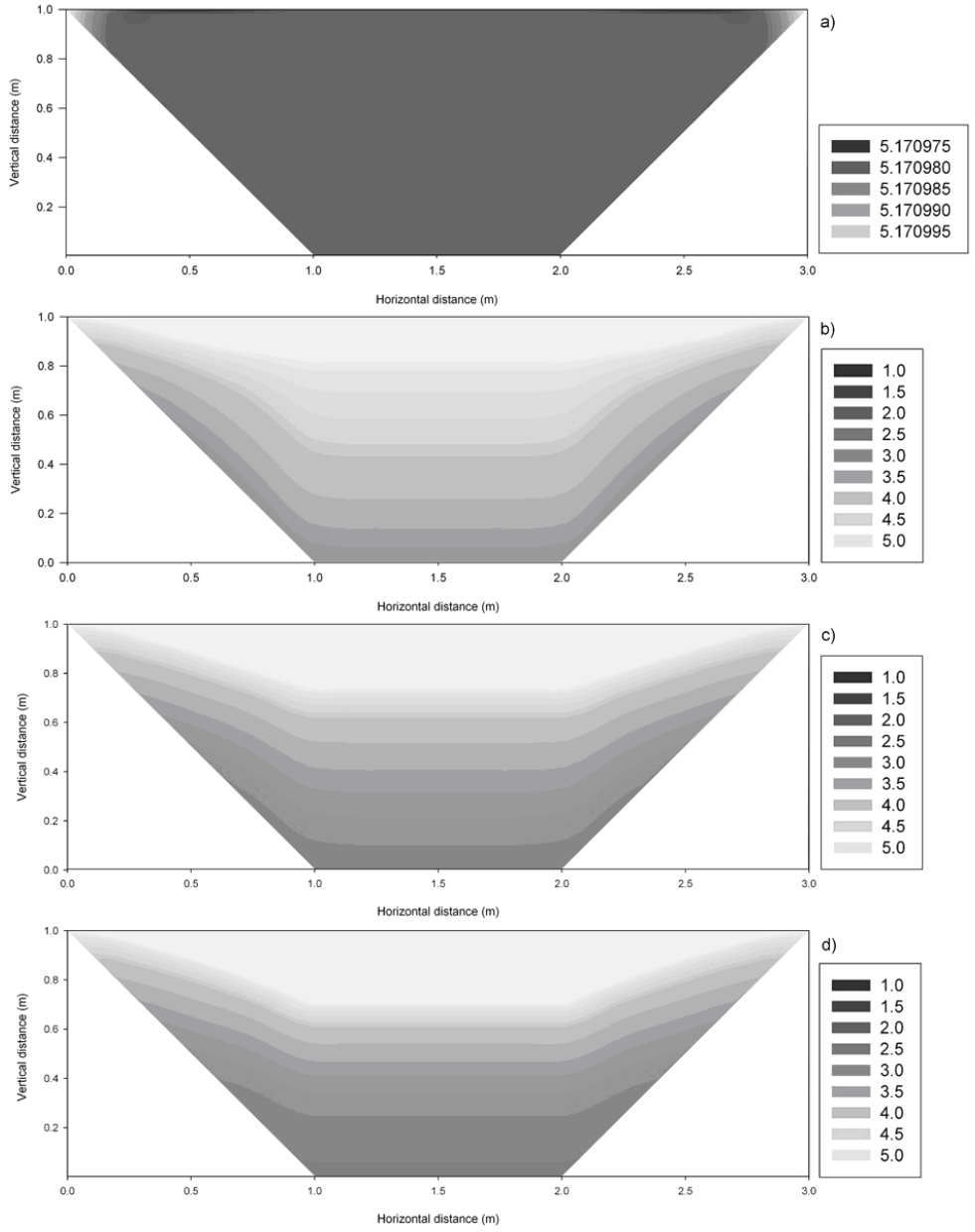

Figure 5.16 Void ratio contours with time in trapezoidal shape pond (*a*) 0.1 days, (*b*) 240days, (*c*) 590 days, and (*d*) 1825 days.

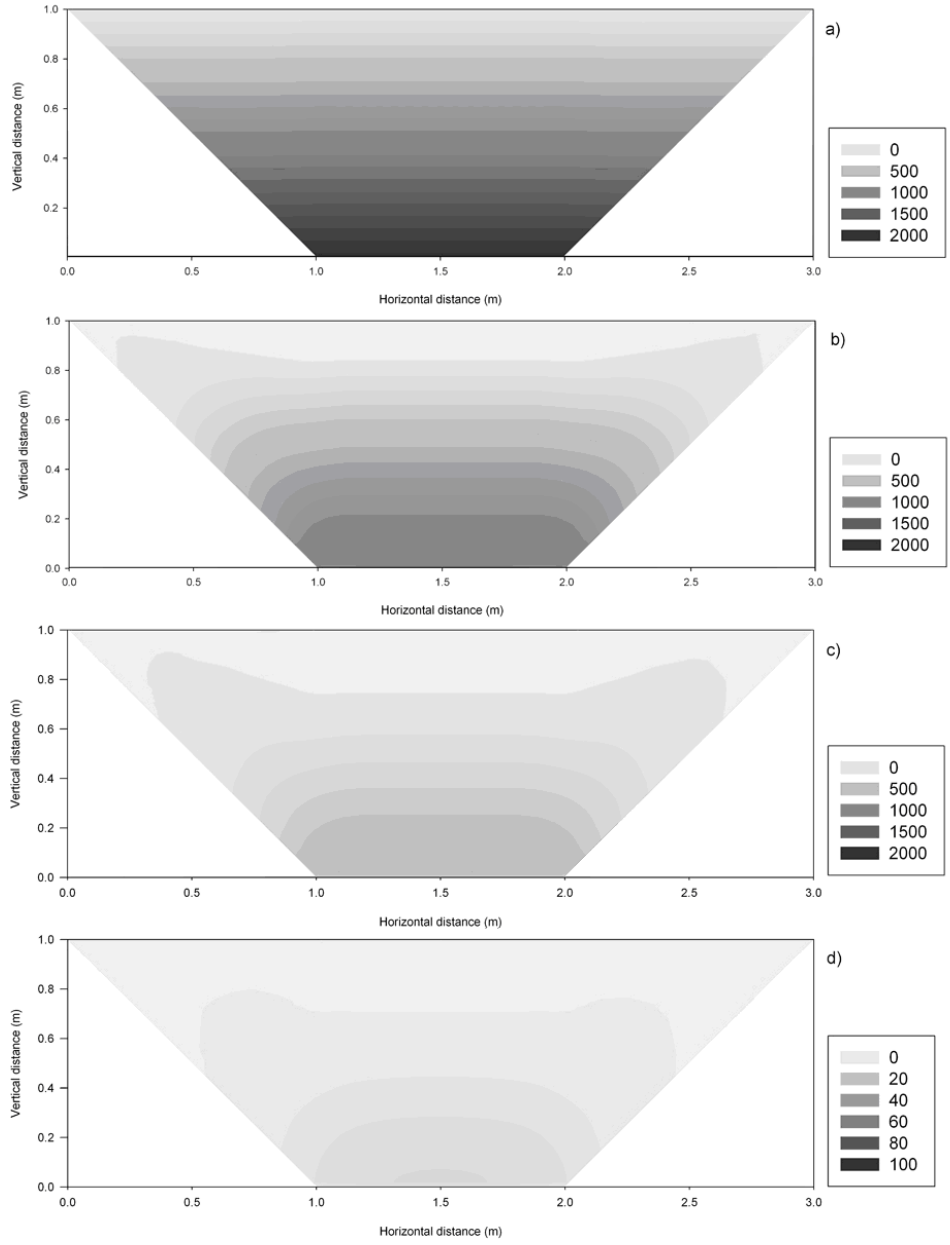

Figure 5.17 Excess pore pressure distribution in Pa with time in trapezoidal shape pond (*a*) 0.1 days, (*b*) 240days, (*c*) 590 days, and (*d*) 1825 days.

5.6.1.2 Drainage conditions

To study the effect of drainage through dykes and a foundation, different boundary conditions are used in this section. To eliminate other shape factors, a rectangular shaped pond is selected. The results are shown in Figures 5.18 and 5.19. In Figures 5.18 and 5.19, DD, FD and AD stand for dyke drainage, foundation drainage and all direction drainage conditions.

Figure 5.19 shows the percent increase of initial rate of reduction in void ratio for all three drainage conditions. The results show that the drainage from all boundaries gives the highest initial rate of consolidation and the foundation drainage is a more influential boundary condition compared to dyke drainage. This is due to the distribution of the self-weight stress. At the center of the pond, the drainage through the foundation can increase the initial rate of reduction in void ratio more than 65% for all base widths while the drainage through the dyke increases the rate slightly under 20%. The effect of the drainage through the dyke can become more pronounced as the W:D ratio decreases.

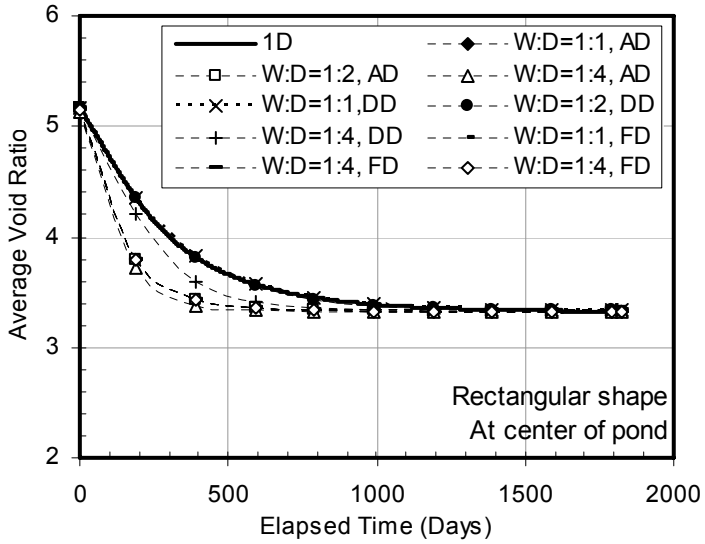

Figure 5.18 Average void ratio change vs. time for three drainage conditions at the center of a pond

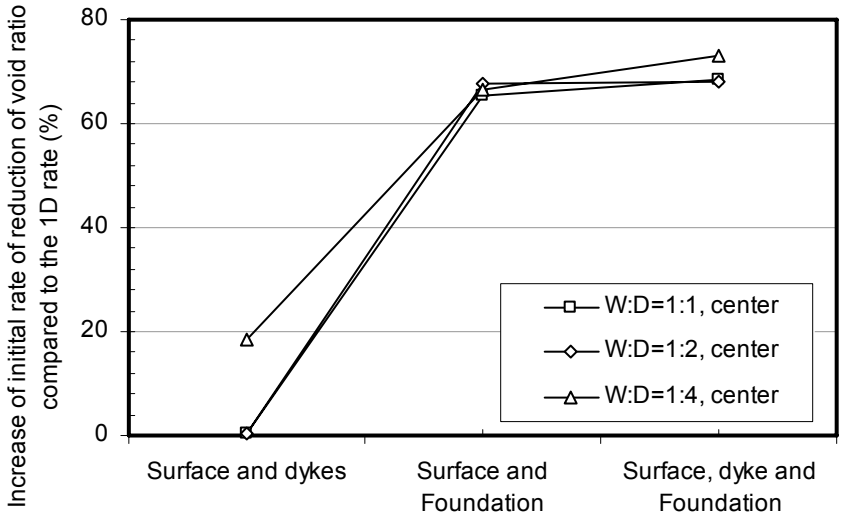

Figure 5.19 Percent increase of initial rate of reduction of void ratio at the center for different drainage conditions

It is obvious that if self-weight consolidation is the only consolidating mechanism in a pond, the drainage conditions should be included for optimum dewatering. It can be argued however that in a real practice, the bottom of the tailings can seal off a permeable foundation due to consolidation. Pond design must search for the maximum drainage condition and one of a clear choice is a mixed application of sand capping and sand columns or wick drains.

Even though it is shown in Figures 5.18 and 5.19 that the drainage through the dyke does not improve the rate of reduction in void ratio significantly, the overall improvement must also be evaluated considering the consolidation between the dyke slope and the center of the pond. Therefore simulations were performed to investigate this area by plotting the rate of change in void ratio at the middle between the dyke slope and the center of the pond. The results are shown in Figures 5.20 and 5.21. The effect of the drainage through the dyke becomes greater and it implies that the overall consolidation of the pond with drainage through the dyke will be higher. It also verifies that the narrower the pond width, the more the positive influence on consolidation from dyke drainage.

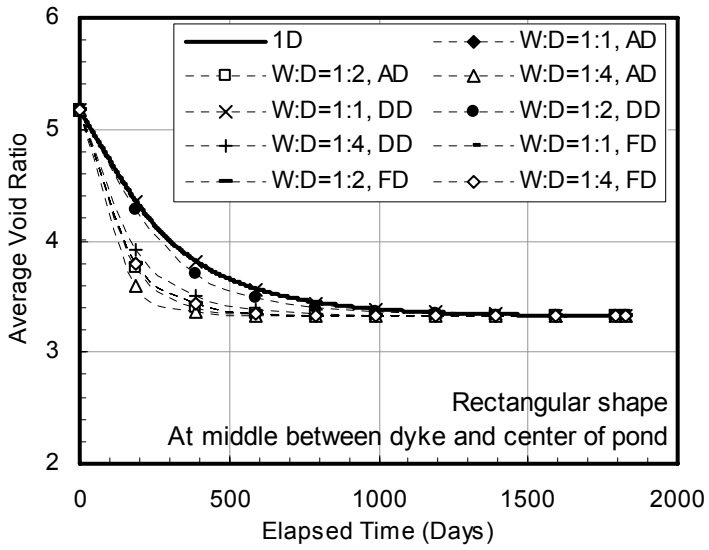

Figure 5.20 Average void ratio change vs. time for three drainage conditions at half-way between the dyke and the center of a pond

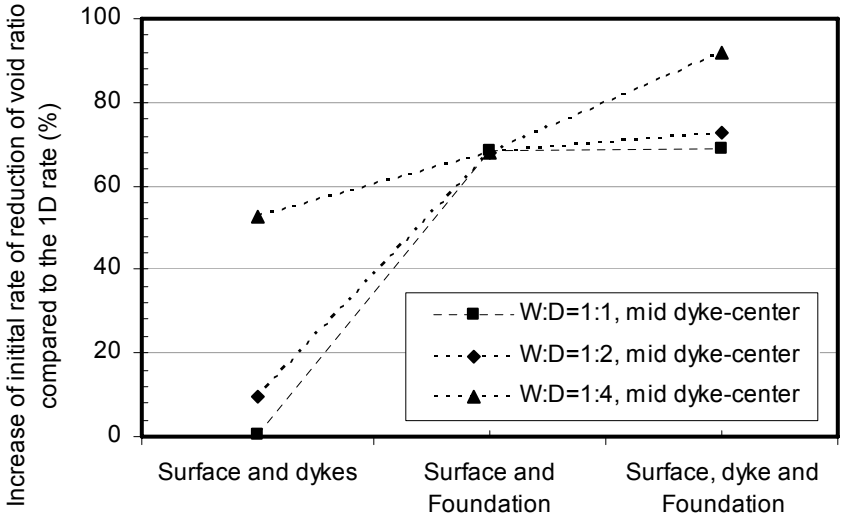

Figure 5.21 Percent increase of initial rate of reduction of void ratio at the middle between the dyke and the center of pond for different drainage conditions

It is concluded that the simulation shows that drainage through the foundation is more influential than dyke drainage and is unaffected by the W:D ratio. An increase in the rate of consolidation by dyke drainage can be obtained by decreasing the width of the pond. Again, although these conclusions are intuitive, the magnitude of these different drainage conditions has been determined in this study.

5.6.1.3 Pond surface slope

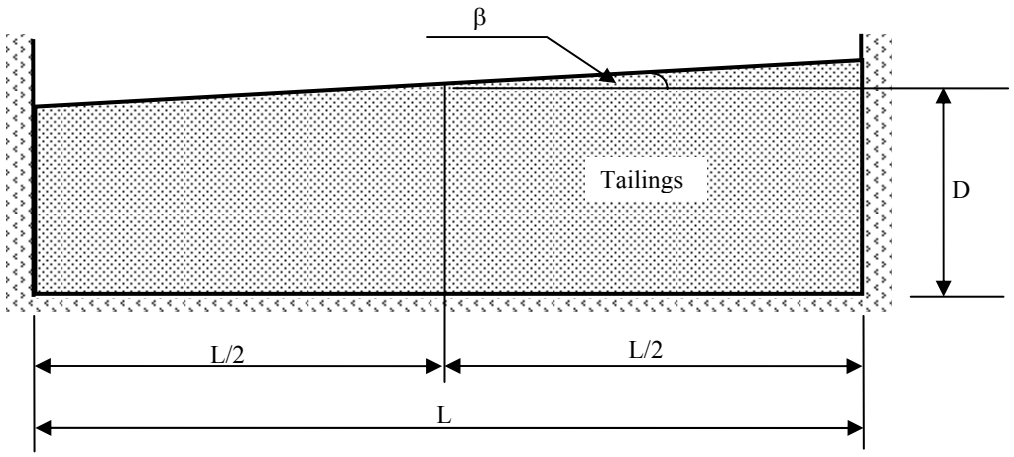

Figure 5.22 Surface sloping pond

The pond surface slope can be controlled by changing the tailings properties and is a viable method to enhance lateral drainage. In this section the pond surface slope, β, is varied between 0° to 10°. Similar to the previous section, a cross section of a pond used in this section is a rectangular shape to eliminate other shape factors (Figure 5.22).

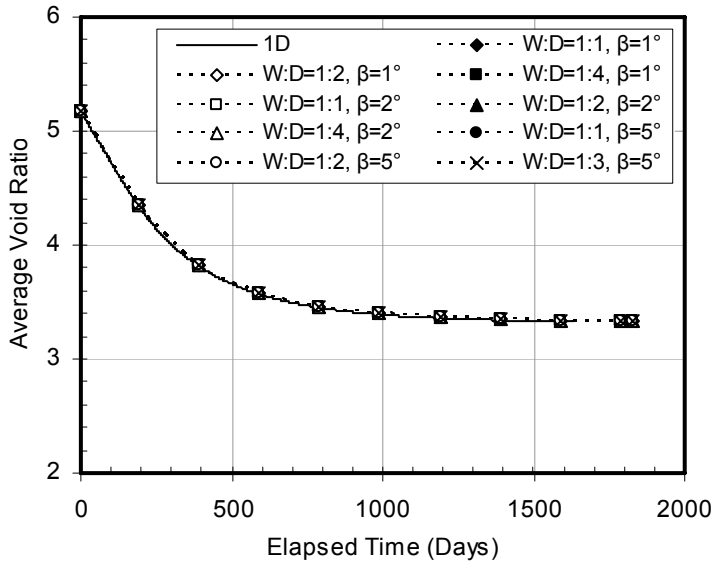

Figure 5.23 Average void ratio vs. time at the center of pond

In Figure 5.23, it was found that all simulations gave negligible changes (<0.5%) compared to the 1*D* case. This is possibly because the combination of the width and angle creates high and low pressure areas at the upstream and downstream areas of the pond.

The steeper the angle, even though it gives shorter horizontal drainage paths, also creates higher excess pore pressure in the upstream side at the center. The evaluation of the surface slope, therefore, should be evaluated at the same controlled stress. The investigation, therefore, was changed to fix the upstream depth and vary the surface angle and the length of the pond. Results are shown in Figure 5.24 and the percent increase of the rate of consolidation with the surface slope angle is shown in Figure 5.25.

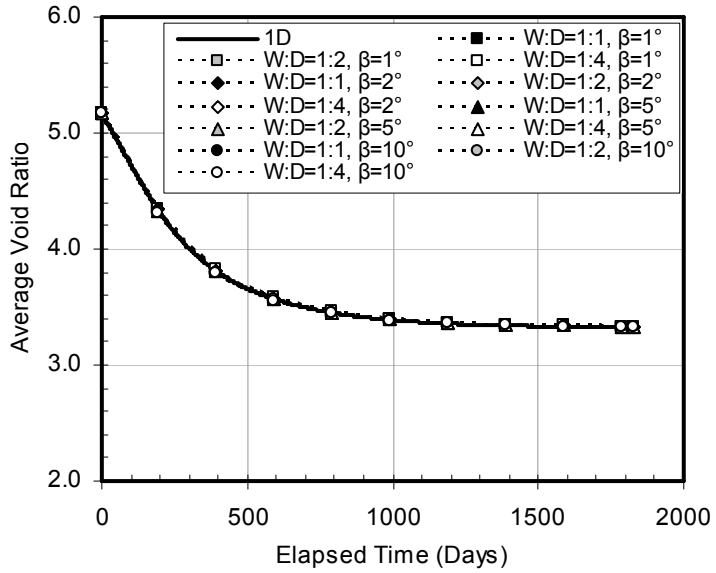

Figure 5.24 Average void ratio vs. time at the upstream dyke

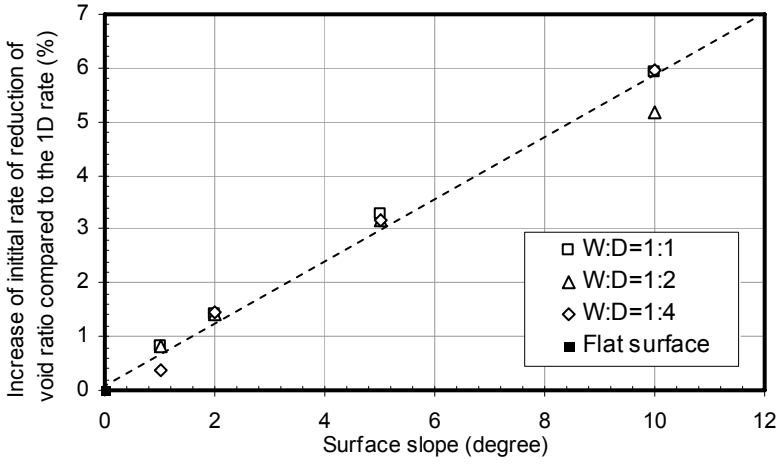

Figure 5.25 Percent increase of initial rate of reduction in void ratio vs. surface slope

Figure 5.25 indicates that the steeper the slope the faster the rate of consolidation. This result is because although the pore pressure is controlled to be the same, the pore

water can flow both vertically and horizontally along the length of the pond. With the steeper slope surface, a shorter horizontal drainage path will allow excess pore pressure to dissipate more quickly. This has a slight advantage over a flat surface geometry which shows the same rate as the 1*D* condition. It is noted that the effect of horizontal drainage is also affected by the horizontal hydraulic conductivity. Generally horizontal hydraulic conductivity is higher than vertical hydraulic conductivity but in this example, the hydraulic conductivity is assumed to be equal in both directions. The influence of the surface slope drainage would be higher in a real case when the horizontal hydraulic conductivity is specified to be higher than the vertical hydraulic conductivity. It is concluded that the rate of consolidation is slightly increased by the increase of a tailings surface slope.

It is of interest to simulate the behavior of the quasi theory therefore void ratio and excess pore pressure contours for the case of 5° surface slope were chosen for illustration (Figures 5.26 and 5.27 respectively). The void ratio initially was the same everywhere in the pond and consolidation progressed from bottom up. The excess pore pressure dissipates relatively quickly at the thinner downstream end. In the last elapsed time (Figure 5.26(d)), the void ratio profiles show that the downstream end has a higher void ratio at the bottom, caused by the lower self-weight effective stress at this location, compared to the upstream void ratio at the bottom.

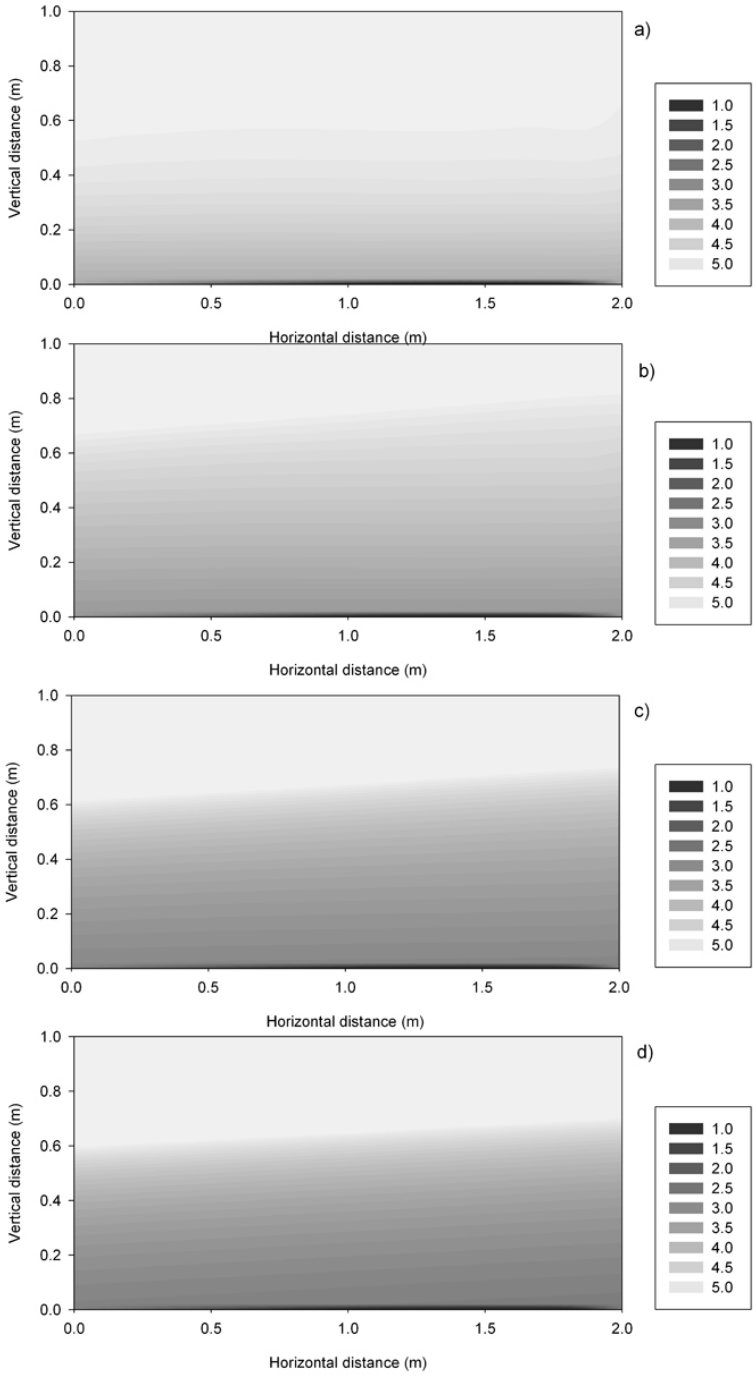

Figure 5.26 Void ratio distribution with time in 5° surface sloping pond (*a*) 90 days, (*b*) 240days, (*c*) 590 days, and (*d*) 1825 days.

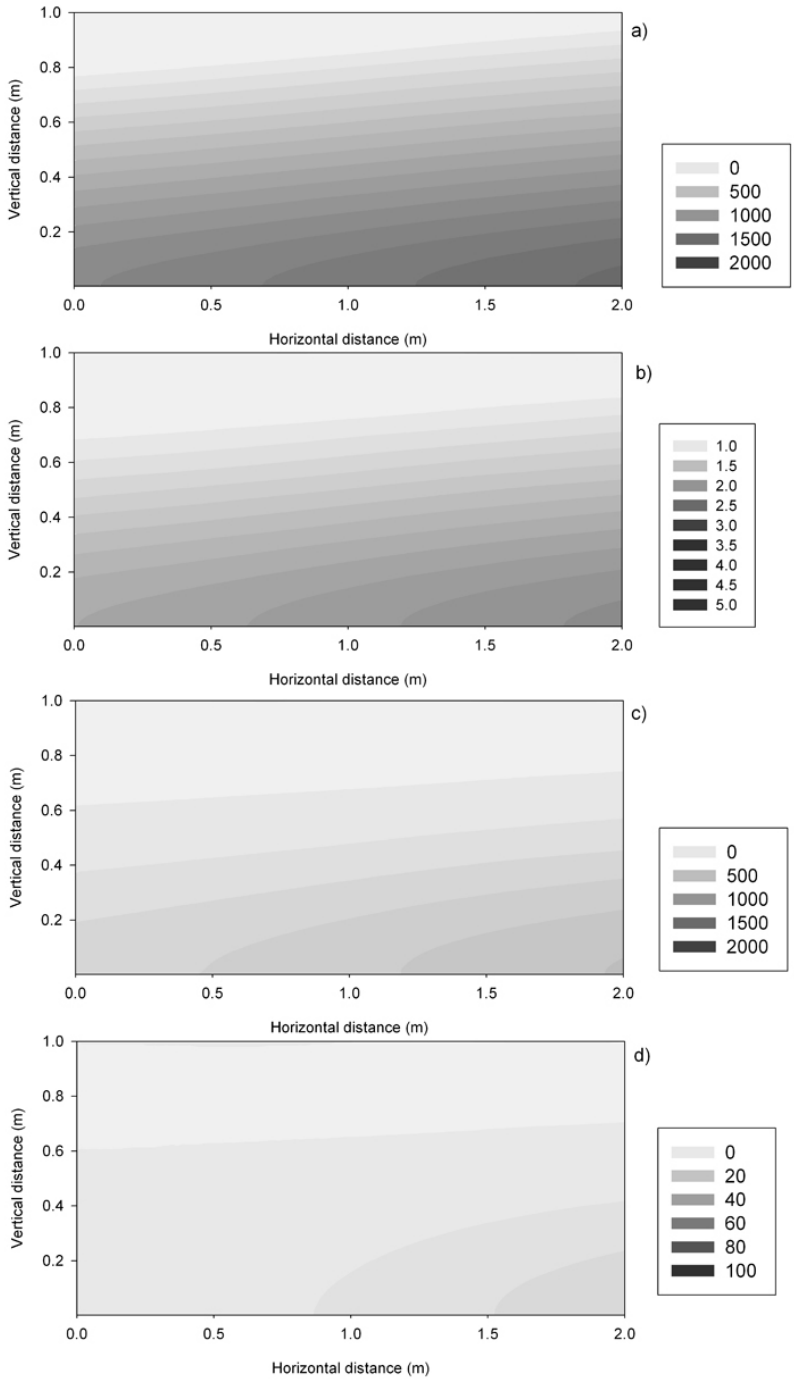

Figure 5.27 Excess pore pressure distribution in Pa with time in 5° surface sloping pond (*a*) 90 days, (*b*) 240days, (*c*) 590 days, and (*d*) 1825 days.

5.6.2 Three dimensional consolidation modeling study

This section further examines the earlier finding that the dyke angle has an influence on the consolidation rate in a three-dimensional analysis. This study is performed by comparing a cylinder-cone shape containment (Figure 5.28) with the 2*D* trapezoidal results. The cone has an angle with the vertical of 30° and is 0.8 m high and the cylinder on the top is 0.2 m high.

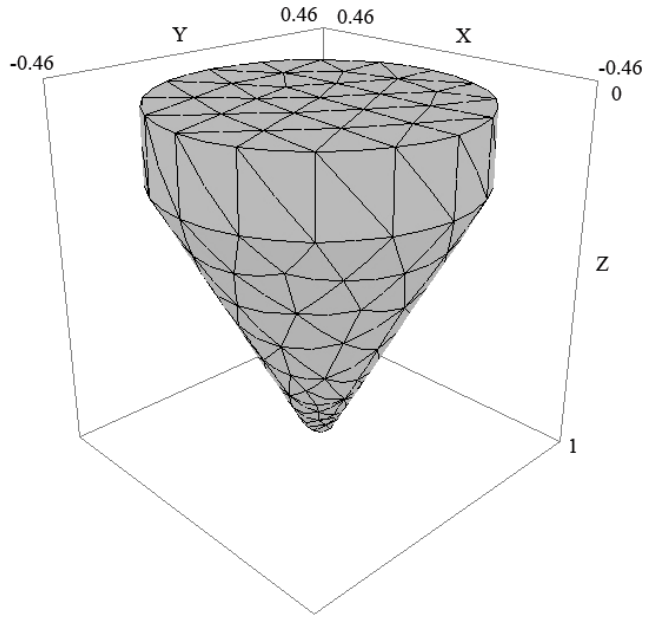

Figure 5.28 a cylinder-cone shape containment

The consolidation behavior in the containment vessel shows fast consolidation at the tip of the cone. The rate of compression at the center is compared with the 1*D* and 2*D* ponds in Figure 5.29. Simulation of the 3*D* cylinder cone shape containment gives an increase in consolidation rate of 20% compared to the 1*D* condition while the 2*D* V-shape pond with the same dyke angle gives a 15% increase. The cause of the increase in the rate of the 3*D* model is the same as indicated in the 2*D* pond in which excess pore pressure dissipated horizontally near the angled dyke. However, for a cone shape containment, the water can flow in all three-dimensional directions contributing to the further increase in the rate of reduction of void ratio. Void ratio and excess pore pressure distributions of slurry in this containment vessel are shown in Figures 5.30 to 5.37. It is noted that a reduced coordinate is used.

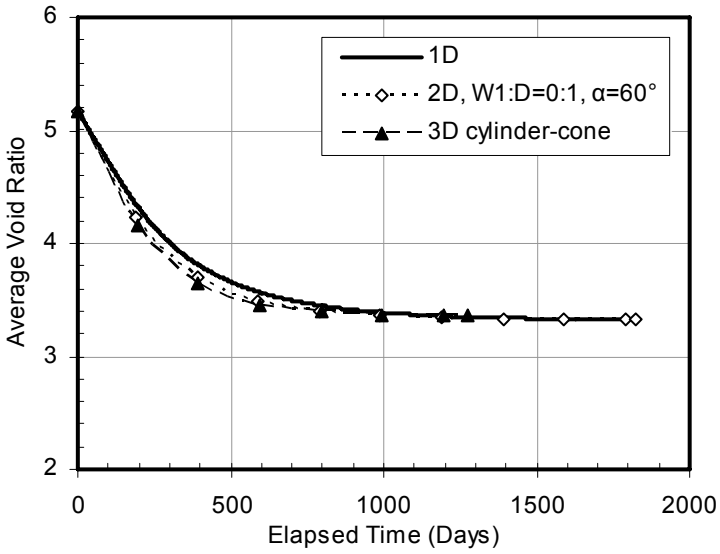

Figure 5.29 Comparison of rate of reduction in void ratio of 3*D* cylinder-cone thickener

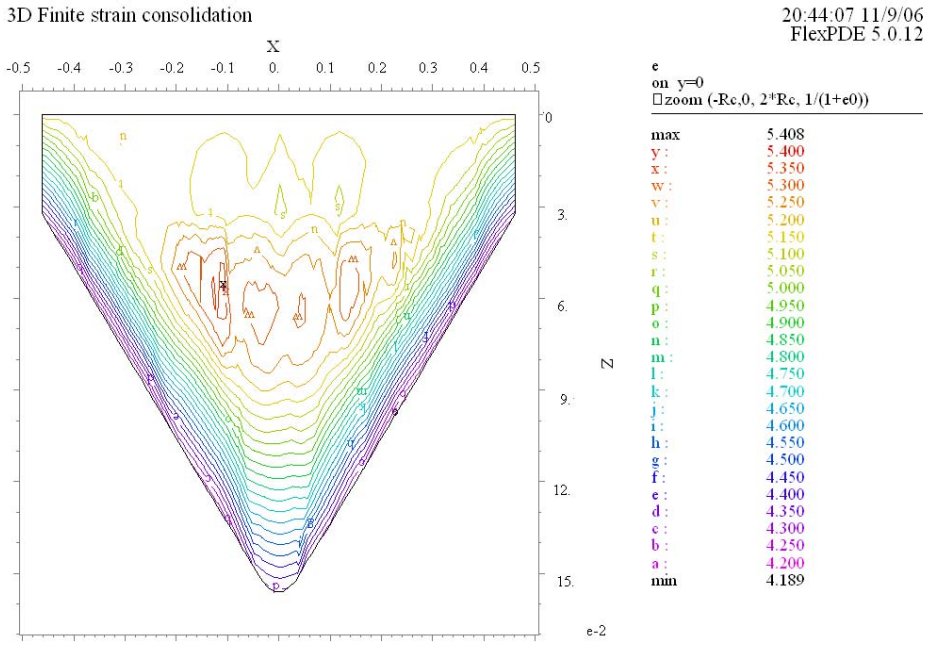

Figure 5.30 Void ratio distribution in a cylinder-cone thickener at 25 days

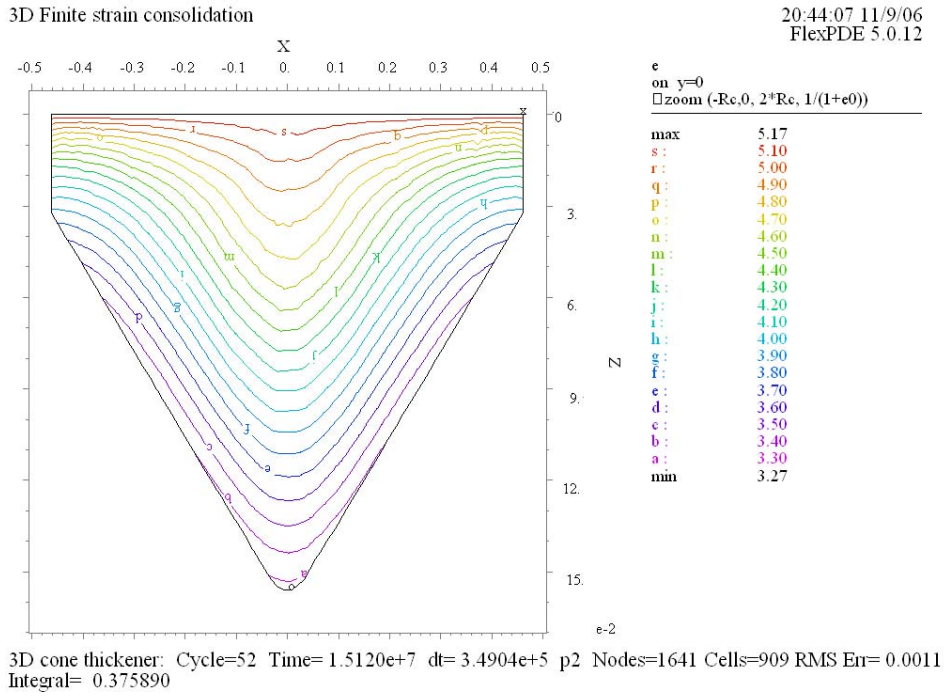

Figure 5.31 Void ratio distribution in a cylinder-cone thickener at 175 days

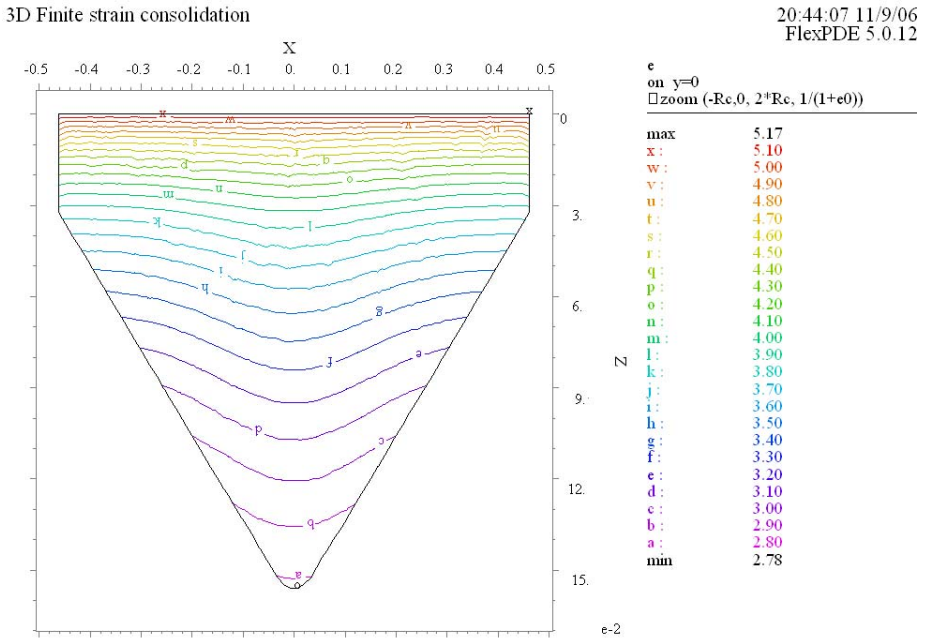

Figure 5.32 Void ratio distribution in a cylinder-cone thickener at 520 days

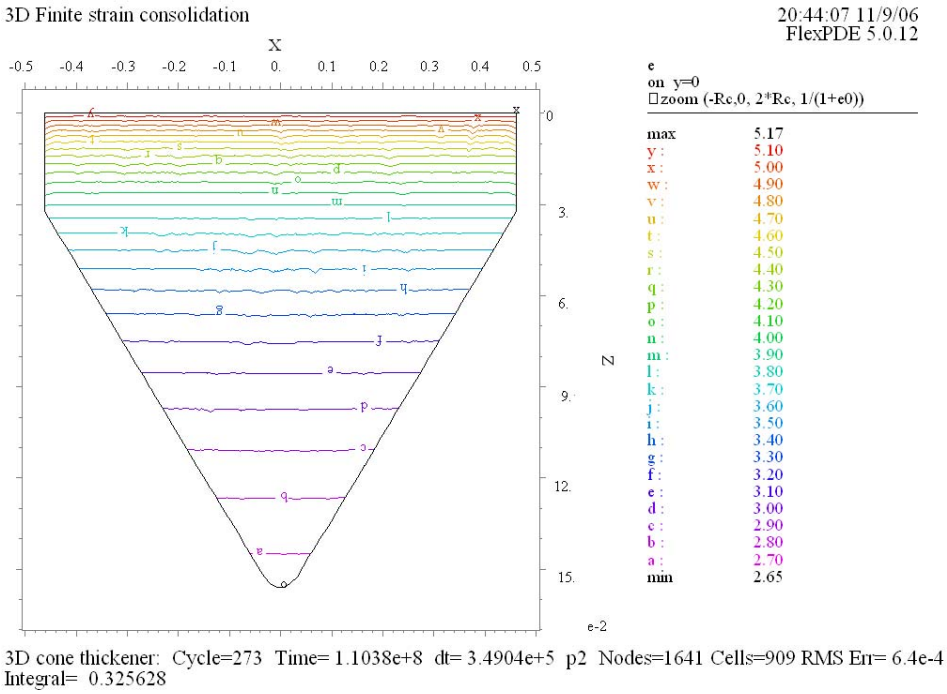

Figure 5.33 Void ratio distribution in a cylinder-cone thickener at 1277 days

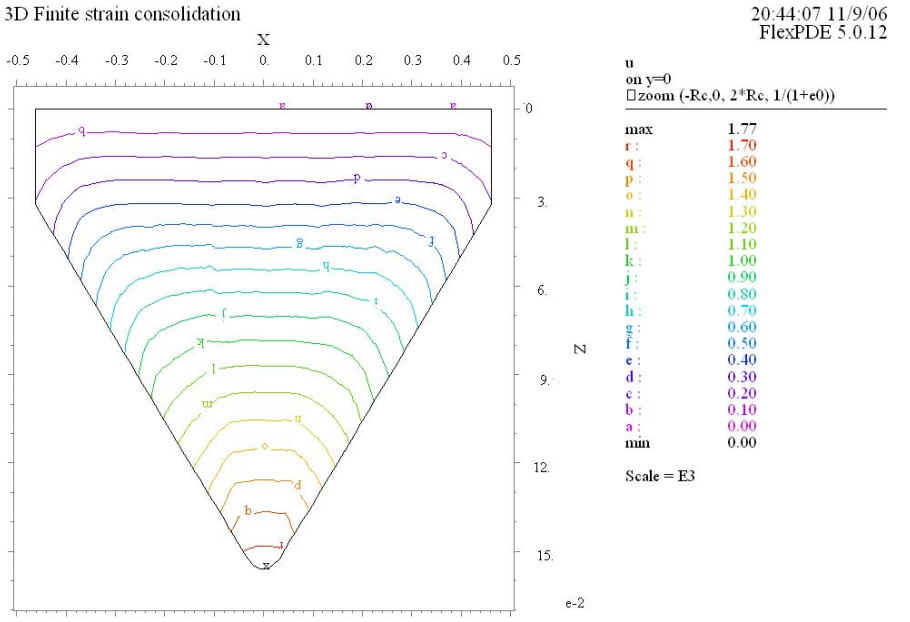

Figure 5.34 Excess pore pressure distribution in a cylinder-cone thickener at 25 days

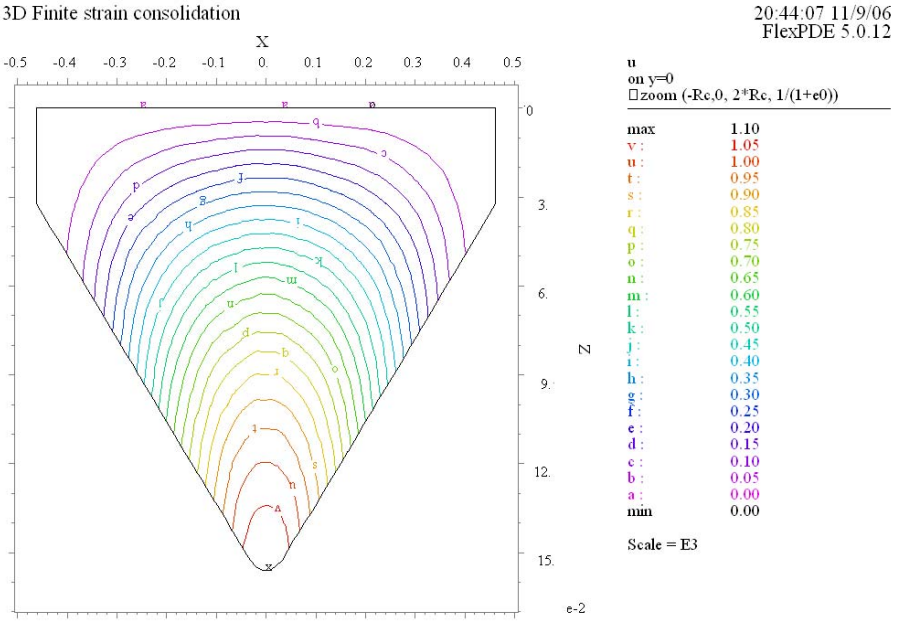

Figure 5.35 Excess pore pressure distribution in a cylinder-cone thickener at 175 days

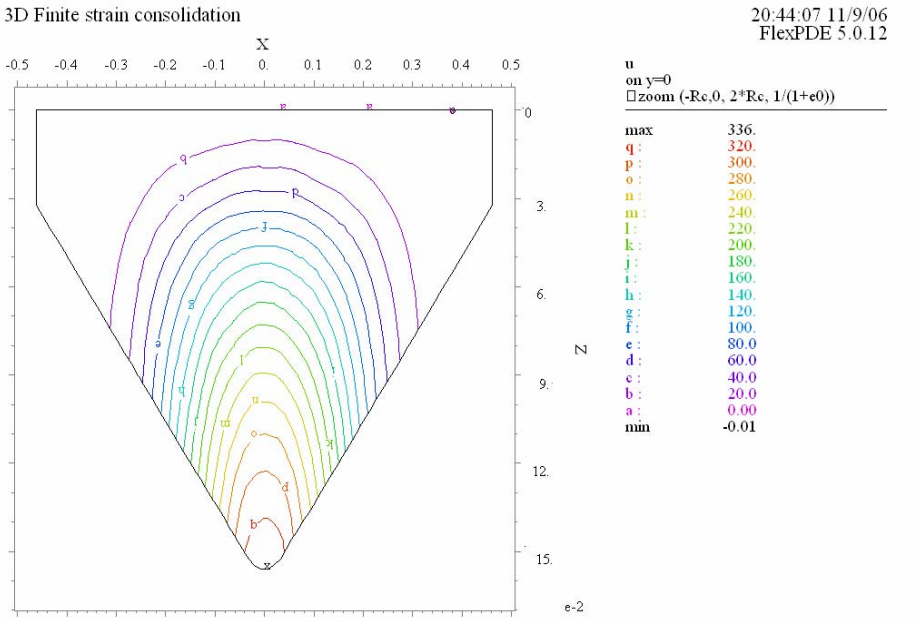

Figure 5.36 Excess pore pressure distribution in a cylinder-cone thickener at 520 days

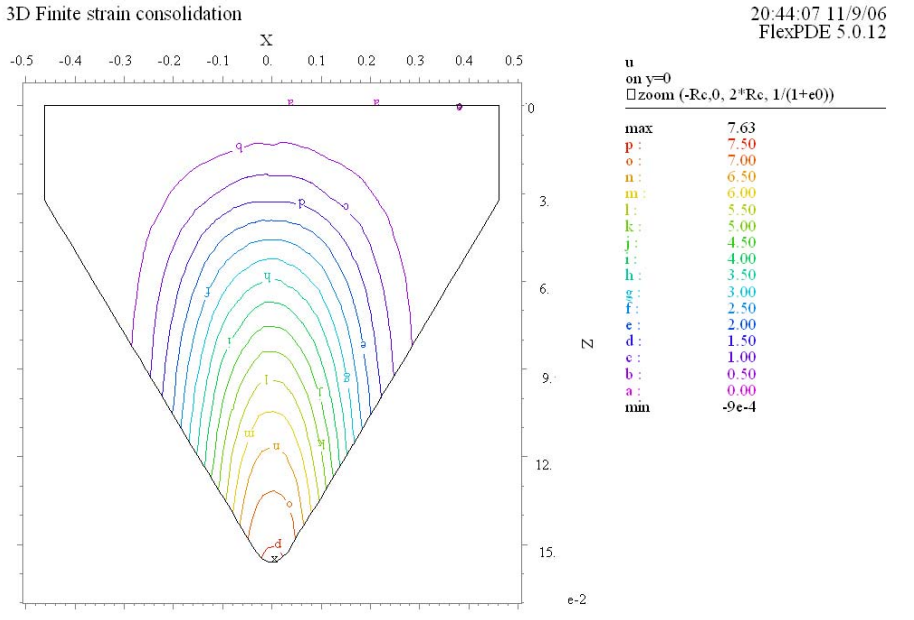

Figure 5.37 Excess pore pressure distribution in a cylinder-cone thickener at 1277 days

5.7 Conclusions

A quasi-multi-dimensional finite strain consolidation theory was derived in terms of excess pore water pressure. The major assumptions used in the theory are that the pore fluid is permitted to flow in any direction but that deformation is strictly vertical. Mixing, flowing, sliding and shearing are neglected. The equations were coded in a FlexPDE finite element program which was implemented for modeling of 2*D* and 3*D* consolidation problems.

Based on the derived theory, a comparative study was performed to investigate the consolidation model's behavior of slurry for ponds with various shapes and boundary conditions for the quiescent condition. Only one driving mechanism, a vertical self-weight stress, was examined in all simulations and horizontal and vertical hydraulic conductivity were assumed identical.

The 2*D* consolidation model studies show that there is no shape effect for a rectangular shaped containment pond and is not different than 1*D* consolidation behavior. For V-shaped cross sectional ponds, the steeper the dyke slope, the better the rate of consolidation. For trapezoidal shaped ponds, the dyke slope does not show a significant effect at the center of the pond. However at the toe of the dyke, it can be observed that the steeper the dyke the better the rate of consolidation. The surface slope of the pond is found to give a small increase in the rate of consolidation due to the shorter horizontal drainage path. The larger the angle of the surface slope of the pond, the faster the initial rate of consolidation.

Drainage from all boundaries is the ideal case for slurry dewatering. Drainage through the foundation has a pronounced influence on the initial rate of consolidation while drainage through a dyke has negligible effect at the center of a pond. In an area between the dyke and the center of a pond, the dyke drainage, however, helps to increase the rate of consolidation. The smaller the base width the more the effect of the drainage through dykes. It is noted that blinding of the foundation drainage could occur in a longer term and was not studied here.

The shape of a cylinder-cone containment vessel provides an increase in the initial rate of reduction in void ratio. The increased rate is faster than the 2*D* V-shaped pond with the same slope. This is due to the three-dimensional flow.

Several aspects of the theory were investigated and the importance of containment shapes and drainage conditions on the simulated rate of consolidation were shown. The theory precludes several aspects of slurry consolidation that can be significant in some cases. Future extension of the quasi-multi-dimensional finite strain theory should be aimed to include 3*D* self-weight stress analysis, horizontal deformation and flowing and sliding mechanisms.

Chapter 6 Field Investigation of the In-Line Thickened Tailings

6.1 Introduction

The in-line thickened tailings pilot program was operated at Syncrude's base mine to evaluate the technical feasibility and operational costs of the in-line thickening technology (Shaw and Wang 2005). The pilot plant was designed to process 500 m^3/hour of cyclone overflow tailings from the composite tailings plant. ILTT was produced and it was discharged into two pilot ponds to test field deposition behavior.

In order to study the field performance of ILTT, a geotechnical field investigation was proposed and pursued at the Syncrude in-line thickened tailings pilot pond. The field investigation included sampling, interface measurement, pore water pressure measurements and undrained shear strength measurements. This chapter presents results and analyses of the geotechnical field investigation. Results are presented in chronological order for each pilot pond followed by a proposed settling mechanism of the material. A history matching analysis by a finite strain consolidation theory is then presented and conclusions of the field investigation program are given.

6.2 In-line thickened tailing pilot ponds

Before a presentation of the field investigation program in this chapter, it is important to discuss deposition techniques in each pond, measuring stations and dimensions of the ponds as this will be directly related to the data obtained from the field investigation program. In Chapter 2, it was discussed that the Syncrude ILTT pilot project was composed of two pilot ponds; the west pond and the east pond. Although the tailings stream is produced from extraction of ore bodies from many mining locations; in the pilot operations the west pond ILTT was mainly from marine oil sands ore and the east pond ILTT was mainly from estuarine oil sands ore. Marine ore contains a higher percentage of highly active clay minerals which detrimentally affect extraction and the resulting tailings contain more active clay minerals and bitumen. Flocculation and coagulation of these

A version of this chapter has been published. Jeeravipoolvarn, S., Scott, J.D., Chalaturnyk, R.J., Shaw, W., and Wang, N., 2008. "Sedimentation and Consolidation of In-Line Thickened Fine Tailings", Proceedings of International Oil Sands Tailings Conference, December 7-10, Edmonton, AB, 209-223.

methods were used for each pond. The ILTT was discharged down a half-pipe chute (Figure 6.1(*a*)) into the west pond (located at the west side of the ILTT mixing plant). This type of discharge results in high energy deposition which causes shearing of the ILTT aggregates. This shearing of the aggregates results in a smaller aggregate size which is believed to have detrimental effects on the ILTT settling, compression and segregation behavior. To avoid aggregate breakage as much as possible, another type of ILTT deposition, a sub-TT discharge was used for the east pond (Figure 6.1(*b*)). This discharging method utilized an inverted spill box which was located lower than the mixing plant. The third flocculant addition was also moved to this box. This type of discharge provides a lower energy deposition technique.

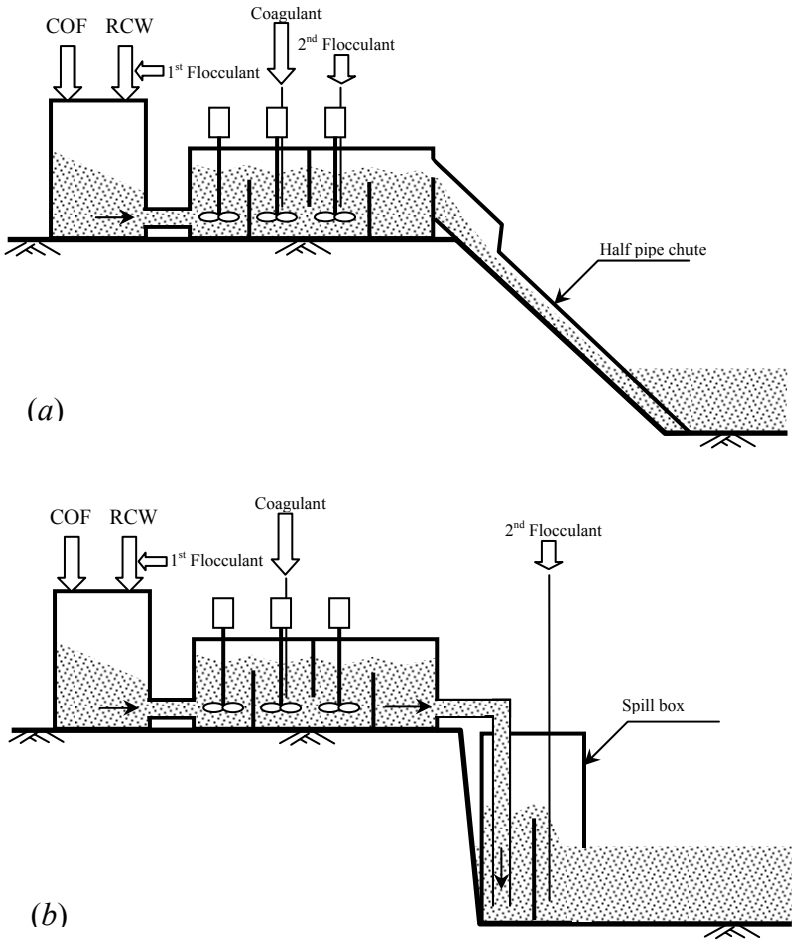

Figure 6.1 Discharge methods (*a*) a half-pipe chute discharge (*b*) sub-TT discharge (Modified from Shaw and Wang, 2005)

Both pilot ponds have identical design dimensions. It has a depth of 3 m, a width of 50 m and a length of 100 m. The plan view of both ponds is illustrated in Figure 6.2. The pond is equally divided into three sections for sampling, pore pressure monitoring and undrained shear strength measurements. Each section contains a center station for the monitoring and there are also two extra stations at the inlet and outlet of the pilot ponds. Interface measurement stations are located in the middle of each section. Both pore pressure and sampling stations are located approximately 1 m away from interface measurement stations. The slope of pond dykes was generally 45° or more.

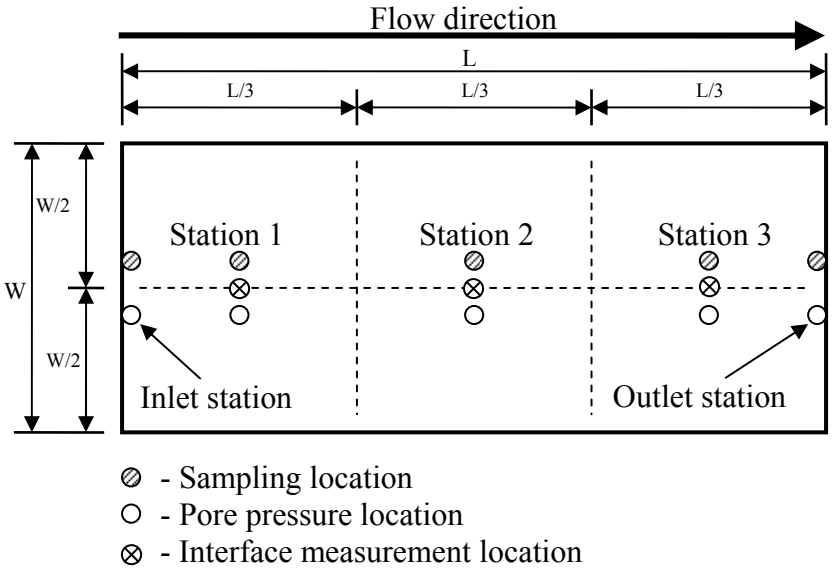

Figure 6.2 Pilot pond

The ILTT-west pond was filled between the 6th and 12th of November 2005 and the ILTT-east pond was filled from 20th to 27th of November 2005. Both ponds were under monitoring until the latest field measurement on 10th July 2006 when Syncrude decided to cap the ponds due to dyke construction constraints.

6.3 History of field investigation

In this section, the history of the ILTT filed investigation performed by a research team from the University of Alberta is presented in chronological order. Field test data

obtained from each time of investigation is presented and discussion of solids and fines contents is given separately in the next section.

6.3.1 28th November 2005 and extra samples on 24th December 2005

On 28th November 2005, the first geotechnical field investigation was performed on the east pilot pond. Due to accessibility and time constraint, pore pressure was only measured at the inlet and outlet stations. Samples of COF and ILTT from the inlet and the outlet stations of both ponds were obtained. The tailings in both ponds were quite warm at the time of the field investigation. Temperature of the deposits was measured to be about 20°C.

On 24th December 2005, a shipment of samples from the pilot ponds arrived at the University of Alberta. The samples were obtained from the middle three stations of the ponds. The materials were frozen and had to be thawed before solids and fines content determination.

Properties of the inlet and outlet ILTT samples obtained on 28th November 2005 are shown in Table 6.1. ILTT samples from Stations 1, 2 and 3 obtained on 24th December 2005 are shown in Table 6.2. The Cyclone Overflow (COF) samples are shown in Table 6.3. The pore water pressure measurements were done with a Slope Indicator vibrating wire piezometer PW model and MB-6T Roctest readout unit at the inlet and outlet stations of the east pond. The results are presented in the section of field results and discussion. Shear strength measurements were not performed at this time.

6.3.2 10th July 2006

On 10th July 2006, the second field investigation was performed. Interface measurements, sampling, pore pressure measurements and vane shear strength measurements were done at the three stations in the middle of the pilot ponds.

Both ponds showed a desiccated layer on the top. The desiccated layers were sampled and brought back to determine their densities and shear undrained strengths which are shown in Table 6.4. Desiccation is not expected as the precipitation in Fort

McMurray area is higher than evaporation however continuously decanting the supernatant water and seepage into a sandy foundation can dry the tailings surfaces on shallow ponds like these.

Sampling for the solids and fines contents were done by using a thin walled piston sampler provided by Geoforte Services Ltd. This sampler was designed to retrieve a core sample from a tailings pond. To obtain a sample, the sampler was pushed to the designated depth with the piston at the bottom of the tube. The sampler cut through tailings and the tailings were pulled into the tube under suction in the sampler as the piston was withdrawn. The core sample was extruded out of the sampler and divided into sections for solids and fines content determinations. Samples were stored in containers which were sealed when an adequate sample at each elevation was obtained. Sampling was done at 0.25 m intervals at each location. The properties of each sample are shown in Tables 6.5 and 6.6 for the east pond and the west pond respectively.

The pore pressure measurements were performed at every station at 0.25 m depth intervals. Vibrating wire piezometers used in the measurement were two Roctest PW models, two Slope Indicator PW models. A vibrating wire readout unit MB-6TL and a MB-6T unit were used. It is noted that all equipment was calibrated in a laboratory to verify the calibration parameters before the field investigation. The pore pressure measurements are shown in the section of field results and discussion for the both pilot ponds. The in-situ vane shear strength tests were also performed at all stations and the results are shown in Table 6.7 and in the section on field results and discussion.

Table 6.1 Samples from inlet and outlet of pilot ponds on 28th November 2005

Sample	Location	Depth (m)	Average solids content (%)	Fines content (%)	Bulk density (g/cm^3)	Void ratio, *e*	Gs	b (%)	Remarks
W1	West pond inlet	-	28.5	93.6	1.20	6.20	2.47	4.7	floc like material, soft
W2	West pond outlet	-	44.3	65.2	1.36	3.16	2.52	3.4	looks like typical fine tailings
E1	East pond inlet	0 to 1.5	48.6	65.0	1.42	2.68	2.54	2.8	floc like material, dense
E2	East pond outlet	0 to 1.0	52.2	73.0	1.46	2.30	2.51	3.6	floc like material, dense

Table 6.2. Samples from centers of east and west pilot ponds on 24th December 2005

Sample	Location	Depth (m)	Average solids content (%)	Fines content (%)	Bulk density (g/cm^3)	Void ratio, *e*	Volume (L)	Mineral solids (kg)	Remarks
W3	West pond station 1	0 to 1.0	30.9	93.7	1.23	5.61	1.8	0.67	
W4	West pond station 1	1.0 to 2.0	40.1	66.3	1.32	3.75	1.8	0.93	
W5	West pond station 2	0 to 1.0	29.7	95.3	1.22	5.93	1.8	0.64	
W6	West pond station 2	1.0 to 1.75	33.8	85.0	1.26	4.91	1.8	0.75	Materials were partly frozen at arrival. They were thawed at room temperature for 1 day. The materials were then mixed gently by hand to minimize aggregate rupture before sub samples were taken. All of them show floc like structure.
W7	West pond station 3	0 to 0.75	25.5	98.3	1.18	7.34	1.8	0.53	
W8	West pond station 3	0.75 to 1.75	31.3	92.4	1.23	5.51	1.8	0.68	
E3	East pond station 1	0 to 1.0	34.5	90.3	1.26	4.78	1.8	0.77	
E4	East pond station 1	1.0 to 1.75	45.7	61.2	1.38	2.98	1.8	1.11	
E5	East pond station 2	0 to 1.0	34.0	91.5	1.26	4.87	1.8	0.76	
E6	East pond station 2	1.0 to 1.75	40.5	87.1	1.32	3.69	1.8	0.94	
E7	East pond station 3	0 to 1.0	33.3	93.4	1.25	5.03	1.8	0.74	

Average G_s=2.51 is used for all calculation

Table 6.3 Cyclone overflow samples obtained on 28th November 28th 2005

Sample	Initial solids content (%)	Settled solids content (%)	Fines content (%) (sub samples)	Fines content (%) (PSD)	Settled bulk density (g/cm^3)	Settled void ratio, *e*	Settled volume (L)	Mineral solids (kg)	Remarks
C1	10.1	16.2	92.5	92.6	1.11	12.99	5.9	1.05	After arrival, material was allowed to settle and leave supernatant water on the top. The material formed thick soft sediment with a dense 1cm sediment at the bottom.
C2	10.8	15.7	93.0	-	1.10	13.44	7.2	1.26	
C3	11.0	16.6	91.5	-	1.11	12.61	6.1	1.13	
C4	22.2	30.9	93.9	94.1	1.23	5.60	8.2	3.12	After arrival, material was allowed to settle and leave supernatant water on the top. The material formed a thick sediment (quite dense compared to C1, C2 and C3).

Average G_s=2.51 is used for all calculation

Table 6.4 Crust samples on 10th July 2006

Sample	Location	Thickness (cm)	Average solids content (%)	Bulk density (g/cm^3)	Void ratio, *e*	Vane shear strength (kPa)	Remarks
EP-ST1	East pond station 1	15.4	73.4	1.79	0.91	99.0	
EP-ST2	East pond station 2	19.5	70.6	1.74	1.05	96.6	
EP-ST3	East pond station 3	17.5	70.5	1.74	1.05	93.9	The crust thickness shown here is lower than the crack depth
WP-ST1	West pond station 1	19.0	66.9	1.67	1.24	56.7	
WP-ST2	West pond station 2	17.5	66.0	1.66	1.29	53.7	
WP-ST3	West pond station 3	12.7	59.6	1.56	1.70	44.9	

Average G_s=2.51 is used for all calculation

Table 6.5 Samples from the east pilot on 10th July 2006

Sample	Depth (m)	Average solids content (%)	Average fines content (%)	Bulk density (g/cm^3)	Void ratio, *e*	Volume (L)	Remarks
EP-ST1-1	0 to 0.154	73.4	-	1.79	0.91	-	crust sample
EP-ST1-2	0.40	44.2	87.8	1.36	3.17	4.4	visually uniform, sandy bottom can be seen from a core sample
EP-ST1-3	0.70	49.5	87.2	1.42	2.56	3.5	
EP-ST1-4	1.15	51.7	96.2	1.45	2.35	1.9	
EP-ST2-1	0 to 0.195	70.6	-	1.74	1.05	-	crust sample
EP-ST2-2	0.45	44.6	87.4	1.37	3.11	3.8	visually uniform, sandy bottom can be seen from a core sample
EP-ST2-3	0.70	49.7	81.7	1.43	2.55	3.5	
EP-ST2-4	0.90	52.0	91.8	1.45	2.32	1.9	
EP-ST3-1	0 to 0.175	70.5	-	1.74	1.05	-	crust sample
EP-ST3-2	0.40	44.4	80.1	1.36	3.14	3.5	visually uniform, sandy bottom can be seen from a core sample
EP-ST3-3	0.70	50.4	90.3	1.43	2.47	3.1	
EP-ST3-4	1.00	56.7	94.5	1.52	1.92	1.9	

Average G_s=2.51 is used for all calculation

Table 6.6 Samples from the west pilot pond on 10th July 10th 2006

Sample	Depth (m)	Average solids content (%)	Average fines content (%)	Bulk density (g/cm^3)	Void ratio, *e*	Volume (L)	Remarks
WP-ST1-1	0 to 0.190	66.9	-	1.67	1.24	-	crust sample
WP-ST1-2	0.40	54.8	67.1	1.49	2.07	1.9	quite soft
WP-ST1-3	0.75	73.9	15.2	1.80	0.89	0.9	presence of sand layer, quite stiff
WP-ST1-4	1.00	66.1	19.2	1.66	1.29	0.9	sandy sample, quite soft
WP-ST2-1	0 to 0.175	66.0	-	1.66	1.29	-	crust sample
WP-ST2-2	0.40	39.6	95.9	1.31	3.84	3.8	visually uniform
WP-ST2-3	0.70	46.3	90.8	1.39	2.91	3.5	visually uniform
WP-ST2-4	1.00	70.3	50.7	1.73	1.06	1.3	quite sandy
WP-ST3-1	0 to 0.127	59.6	-	1.56	1.70	-	crust sample
WP-ST3-2	0.35	42.4	95.2	1.34	3.42	3.1	-
WP-ST3-3	0.70	41.5	88.3	1.33	3.54	3.5	-
WP-ST3-4	0.825	71.9	17.0	1.76	0.98	6.3	quite sandy

Average G_s =2.51 is used for all calculation

Table 6.7 Field vane shear strength on 10th July 2006

Station	Depth (m)	Vane shear strength (kPa)	Remarks
EP-ST1	0.25	1.90	-
	0.50	1.57	-
	0.75	2.00	-
	1.00	3.90	-
	1.25	5.20	bottom is about 1.25m
EP-ST2	0.25	2.20	-
	0.50	1.80	-
	0.75	2.70	-
	1.00	4.25	bottom is about 1.05m
EP-ST3	0.25	2.00	-
	0.50	1.60	-
	0.75	2.60	-
	1.00	3.80	bottom is about 1.05m
WP-ST1	0.25	3.40	-
	0.50	4.20	-
	0.75	10.5	sand layer (quite dense)
	1.00	2.58	-
	1.25	9.20	bottom is about 1.25m
WP-ST2	0.25	1.05	-
	0.50	0.82	-
	0.75	1.75	-
	1.00	3.20	bottom is about 1.10m
WP-ST3	0.25	0.40	-
	0.50	0.70	-
	0.75	1.80	-
	1.00	4.60	bottom is about 1.03m

6.4 Field test results and discussion

In this section, both the data obtained from the field investigation conducted by the University of Alberta research team and data collected by Syncrude are combined. The test results are presented and discussed in four sections which are tailings-water interface measurements, solids and fines contents measurements, pore water pressure measurements and vane shear strength measurements.

6.4.1 Tailings-water interface measurements

On 20th November 2005, the ILTT east pilot pond was filled continuously for over 7 days at a solids content of about 3.7% (void ratio of 65.6) and a fines content of 89% (based on measurements on 10th July 2006). The average solids content at the end of the 7 day filling period was about 32.6% (void ratio of 5.2). Then it was left to settle under its own weight for approximately 232 days. The tailings-water interface height of ILTT in the east pilot pond is shown in Figure 6.3.

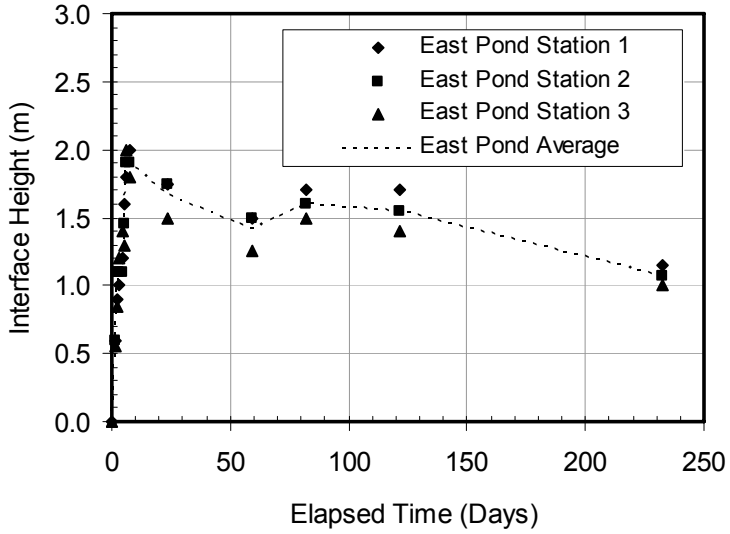

Figure 6.3 Interface height measurements for the east pilot pond

An incongruity in the interface height measurements was observed around 80 days. This was during the winter period where accurate measurement was difficult. The last measurement was performed at 233 days. At this time, the surface was desiccated by

a winter freeze-thaw process and natural drying. The average interface height was 1.08 m and an average crust thickness was about 17.5 cm.

For the west pilot pond, the tailings-water interface measurements are shown in Figure 6.4. ILTT was filled continuously for approximately 6 days at a solids content of about 4.89% (void ratio of 47.7) and fines content of about 77%. The material was left to settle under its own weight for approximately 245 days. At 245 days, the surface was desiccated by a winter freeze-thaw process and natural drying. The average final interface height was 0.94 m and an average crust thickness was about 16.4 cm.

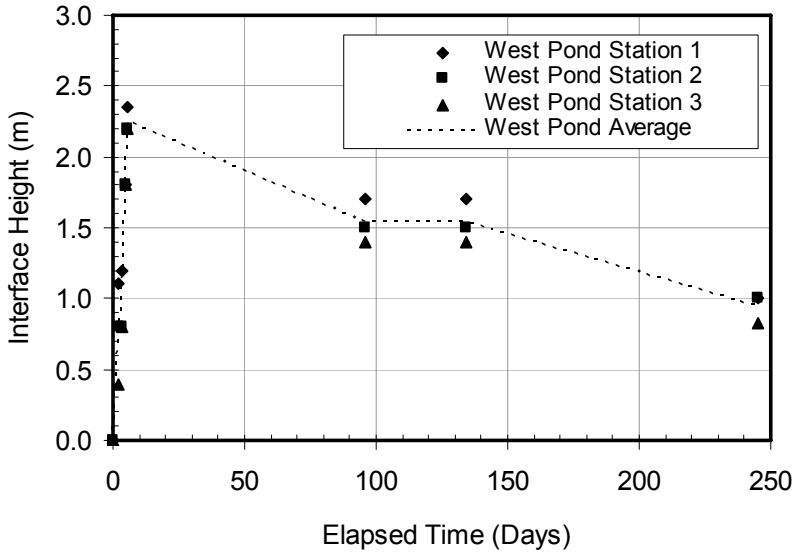

Figure 6.4 Interface height measurements for the west pilot pond

6.4.2 Solids and fines content measurements

6.4.2.1 East pond

The measurements of solids content profiles at different elapsed times at the three sampling stations from the east pilot pond are shown in Figures 6.5(*a*), (*b*) and (*c*). The fines content profiles at the three stations are given in Figures 6.5(*d*), (*e*) and (*f*).

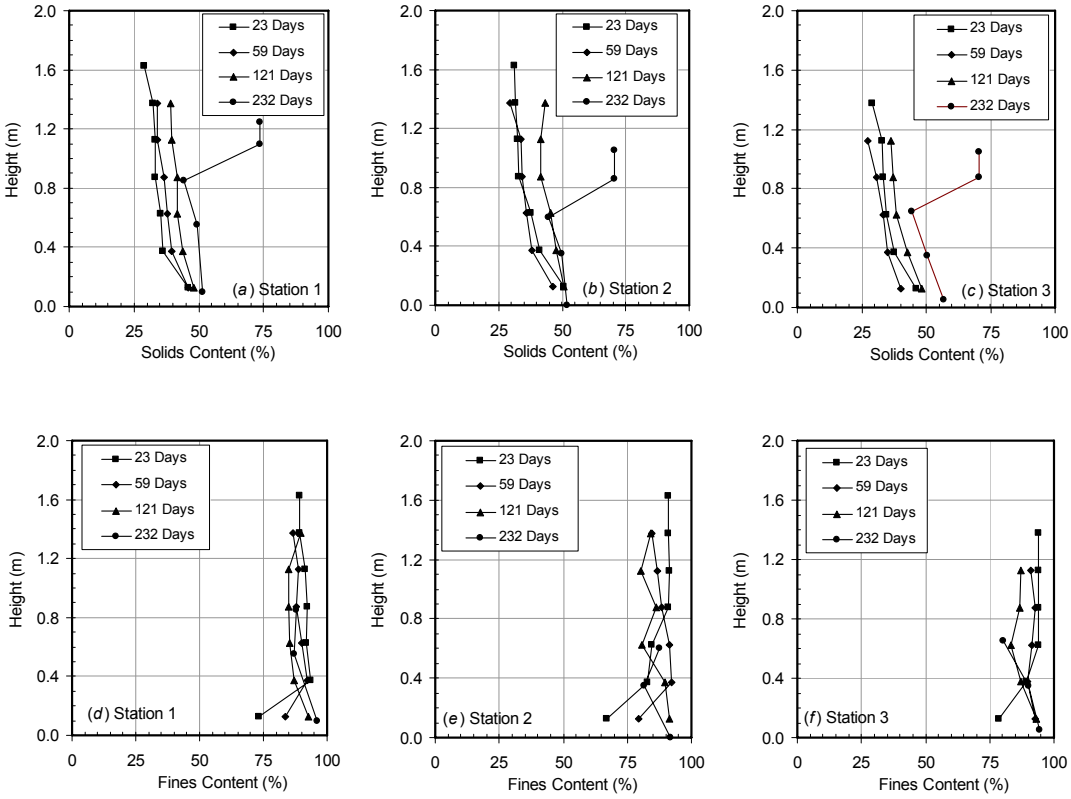

Figure 6.5 Solids and fines content profiles of the east pilot pond

The solids content profiles in Figure 6.5 indicate that there is a rapid increase in solids content from an initial solids content of 3.7% (void ratio of 65.6) to an average solids content of 35.8% (void ratio of 4.5) within 23 days. After filling, the pond was allowed to compress under self-weight stress. The surface of the pond has gone through freezing, thawing and drying during the quiescent period which developed a dry crust throughout the surface of the pond. The thickness of the crust varied throughout the pond between 15 and 19 cm at the three stations. The averaged thickness was about 17.5cm. Below the crust the average solids content was about 50% (void ratio of about 2.5).

From the fines content profiles in Figure 6.5, the average fines content of the ILTT was found to be 89% and the profiles indicate that the ILTT is a nonsegregating mix showing minimal changes in the fines content profiles during the observation period of 232 days.

6.4.2.2 West pilot pond

The measurements of solids content profiles at different elapsed times at the three sampling stations in the west pilot pond are shown in Figures 6.6(*a*), (*b*) and (*c*). The fines content profiles at the three stations are given in Figures 6.6(*d*), (*e*) and (*f*).

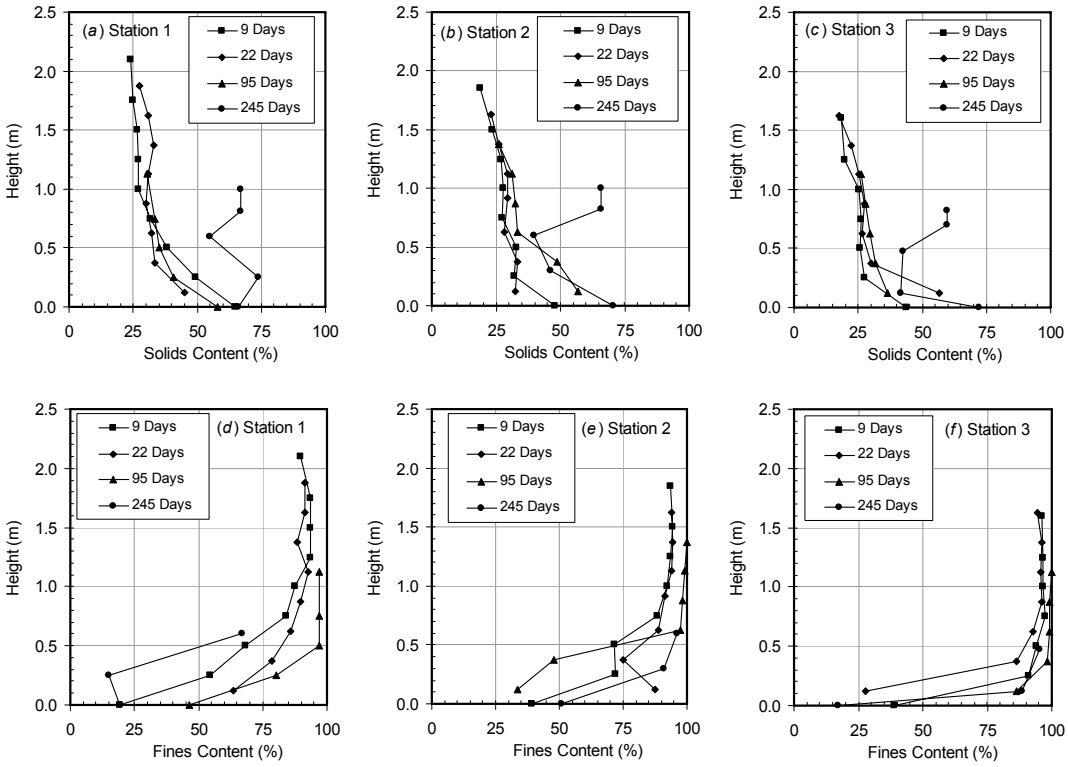

Figure 6.6 Solids and fines content profiles of the west pilot pond

In Figure 6.6, the solids content profiles of the west pilot pond show similar behavior to the east pilot pond that there is a rapid increase in solids content from an initial solids content of 4.89% (void ratio of 47.7) to an average solids content of 30.5% (void ratio of 5.6) within 22 days. After freezing and thawing during the winter and subsequent drying during the summer, a dry crust developed all over the surface of the pond. Crust thickness varied throughout the pond from about 13 to 19 cm at the three stations. The averaged thickness was about 16.4 cm. Below the crust the average solids content was about 56% (void ratio of 1.9).

From the fines content profiles in Figure 6.6, the shape of fines content profiles of the west pond ILTT shows a decreasing of fines content with depth which indicates that ILTT in the west pond has partially segregated.

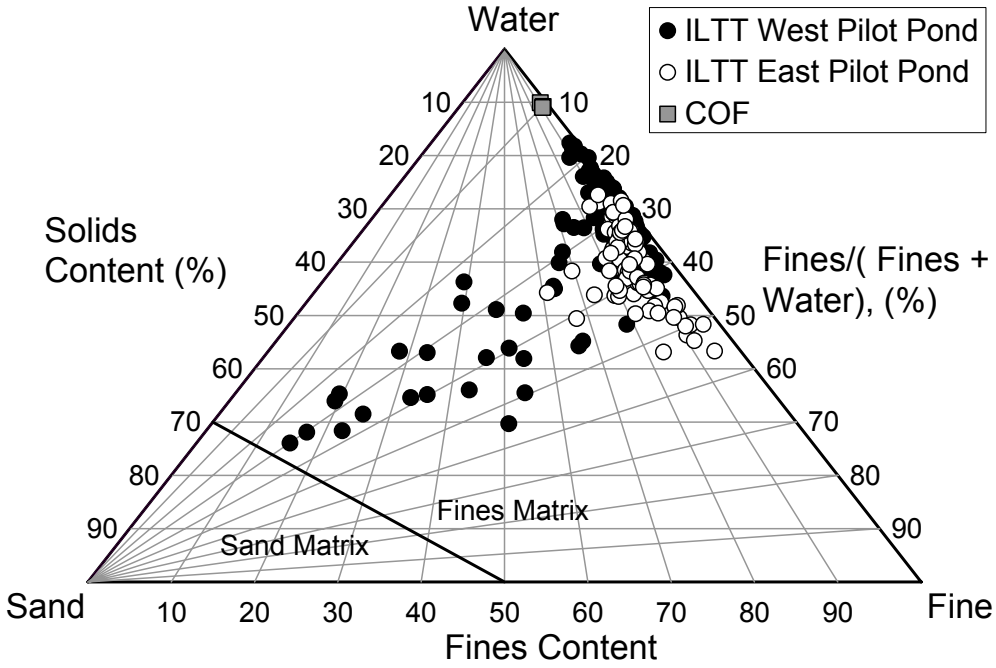

Figure 6.7 Ternary diagram of ILTT material from east and west pilot ponds

In order to confirm the finding that ILTT from the east pilot pond is nonsegregating while the ILTT from the west pilot pond is partially segregating, solids and fines content data from both pilot ponds were plotted in a tailings properties diagram in Figure 6.7. The diagram reveals that the ILTT samples obtained from the east pilot pond show a small segregation. If a fines capture of 95% is applied as a segregation boundary and if 90% original fines content for the COF is used, 76% of the collected data from the east pilot pond does not segregate and shows increasing in FWR from an initial value of 10% to about 55% in a small range of fines content between 80 to 100%. The average solids content from all stations not including the crust sample is 49% and the fines content is 89%. This yields a FWR of about 46%. For the west pond ILTT, Figure 6.7 indicates segregating behavior by showing a reduction of fines content along constant fine/(fines+water) ratios and only 42% of the collected data in this pond shows nonsegregating behavior. The difference between the two pilot ponds was the discharging method and the tailings ore type. Due to the fact that marine ore such as the one deposited in the west pilot pond can be flocculated by the in-line thickening process (Yuan and

Shaw, 2007), the higher energy deposition method in the west pond is believed to be the main reason that caused aggregate breakage and the segregation behavior of the ILTT in this pond.

Due to the occurrence of segregation and the high amount of sand in the west pilot pond material, the tailings in this pond is less representative to the in-line thickening process which is aimed to thicken a high fines tailings stream such as cyclone overflow. Therefore, further results and discussions will be focused on the east pilot pond as it better represents the ILTT tailings behavior with a lower energy deposition technique.

To summarize the processes that occurred in the east ILTT pilot project, a mechanistic diagram of the ILTT process is illustrated in Figure 6.8. First the cyclone overflow is mixed with recycle water and chemical additives via the in-line thickening process. This produces an ILTT material at a solids content of about 4% (fines void ratio of about 66). The ILTT then undergoes rapid sedimentation releasing more than 90% of its original water volume as it reaches a fines void ratio of about 5. At this point both consolidation and segregation phenomena can occur simultaneously in the material causing both a reduction in the fines void ratio and the fines content. Generally the ILTT continues to undergo consolidation to a lower void ratio while some whose structure was broken during the deposition process can show a small amount of segregation.

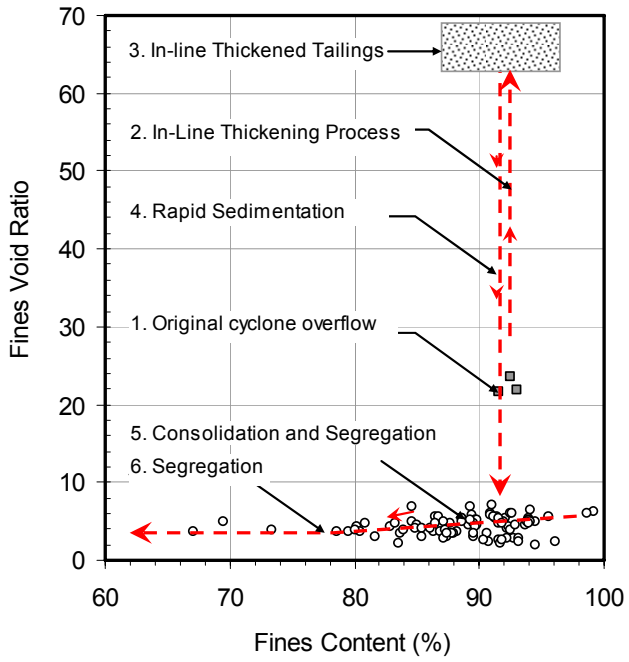

Figure 6.8 The in-line thickening process

6.4.3 Pore water pressure measurements

Pore water pressure measurements in a pond are essential to monitor dissipation of excess pore pressure which is an indication of the consolidation progress in a tailings deposit. The pore pressure measurements were performed by using push-in piezometers with a vibrating wire readout unit. In the pilot ponds, four piezometers were pushed in the pond simultaneously to different elevations. The piezometers were kept in place until the pore water pressure measurements became stable and the pressure values were taken. In this section, the pore pressure measurements in both pilot ponds are presented and discussed.

6.4.3.1 Pore water pressure measurements on 28th November 2005

On 28th November 2005, pore pressure measurements were performed at the inlet and outlet stations of the east pilot pond. At this time of investigation, samples at the inlet and outlet, where the pore pressures were measured, were not obtained with depth therefore the sample in December 2005 is used to estimate the solids content profile shape of the inlet and outlet stations for total stress calculation.

Figure 6.9 shows that the density of the ILTT increases with depth which was determined from the December 2005 samples. This density profile is then used to approximate the total stress distribution with depth at the inlet and outlet stations shown in the same figure.

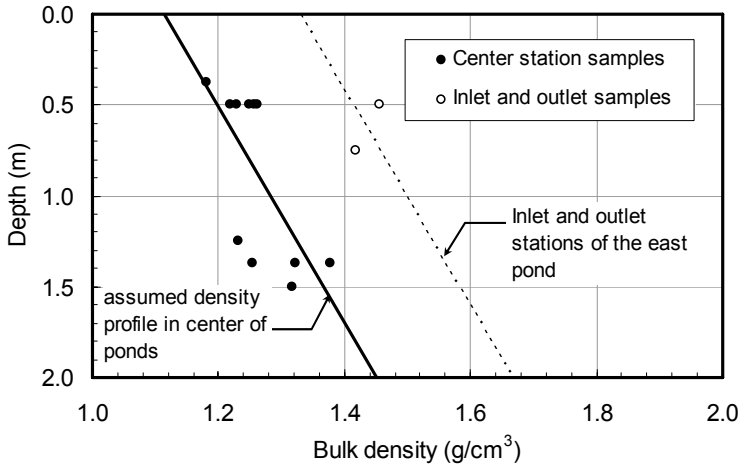

Figure 6.9 Density with depth in pilot ponds (November 28th, 2005)

With the density profiles obtained in Figure 6.9, total stress can be calculated. Figure 6.10 shows calculated total stresses, measured pore water pressures and calculated hydrostatic pressures for both stations of the east pond. The results indicate that on 28th November 2005, one day after filling, there appears to be some consolidation at the bottom of the east pond showing dissipation of excess pore pressure occurred at both the inlet and outlet stations. At the inlet station, a double drainage condition can be seen while there seems to be a slight under drainage condition with ground water lowering in the outlet station. This behavior of the pore water pressure response suggests that the underlying sand and adjacent sand dykes at the stations probably acted as pervious boundaries facilitating an early consolidation process at these locations.

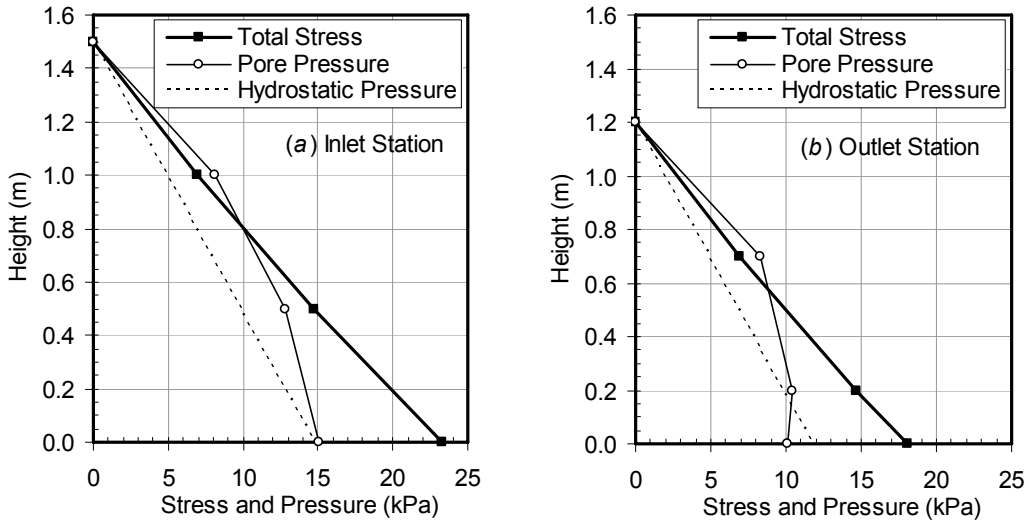

Figure 6.10. Pore water pressure measurements on November 28th, 2005 (*a*) inlet station (*b*) outlet station

6.4.3.2 Pore water pressure measurements on 10th July 2006

6.4.3.2.1 East pilot pond

The last pore pressure measurements at 232 days in the east pond are shown in Figures 6.11(*a*), (*b*) and (*c*) for Stations 1, 2 and 3 respectively. The total stresses shown were calculated from the solids content profiles from Figure 6.5. The pore pressure measurements at Stations 1 and 2 indicate that double drainage conditions prevailed in these locations as the pore pressure was equal to the hydrostatic pressure at the bottom of the stations. At Station 3 the pore pressure at the bottom was equal to zero. The pore pressure measurement that was lower than hydrostatic pressure was also found earlier in the outlet station nearby. A possible explanation for Station 3 was that the underlying sand foundation was fully drained in this particular location. This bottom pore pressure would create a draw down condition on the tailings at this location. The pore pressures being approximately equal to the total stress above the pond bottom indicate that any downward drainage must have consolidated a layer of tailings at the bottom which sealed the pond bottom and prevented further significant downward drainage.

6.4.3.2.2 West pilot pond

Pore water pressure measurements in the west pilot pond are shown in Figures 6.12(*a*), (*b*) and (*c*) for Stations 1, 2 and 3 respectively. In Station 1 the pressure response of the piezometer is quite erratic. This is suspected to be caused by a sand layer present at

this station (Figure 6.6(*d*)). The explanation for this pressure profile is that the existence of the sand layer from 0.6 m and below is likely connected to the outside water table which is well below the bottom of the pond. This could possibly lead to a zero reading from the piezometer similar to the pressure reading from Station 3 in the east pond. The excess pore pressure could have rapidly dissipated due to a shorter drainage path and the relatively high hydraulic conductivity of the sandy material resulting in the pore pressure profile shown in Figure 6.12 (*a*). In Stations 2 and 3, the process is likely to be similar to the east pond indicating some consolidation at the bottom because of a double drainage boundary condition.

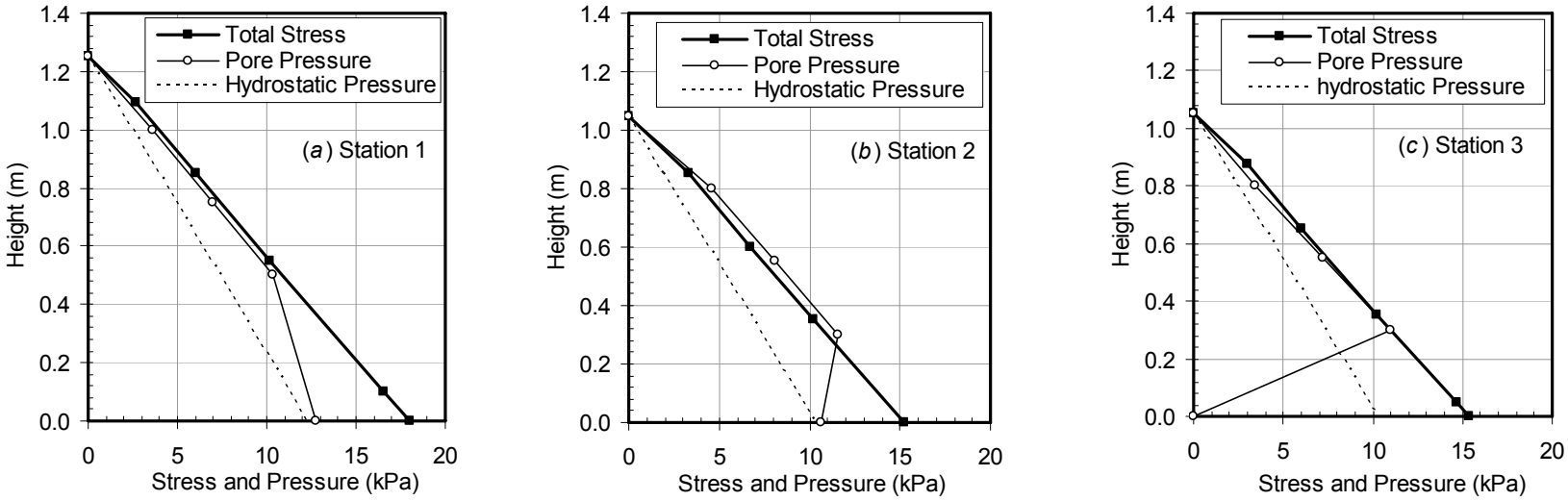

Figure 6.11 Pore water pressure measurements in the east pilot pond on 10th July 2006 (*a*) Station 1 (*b*) Station 2 and (*c*) Station 3.

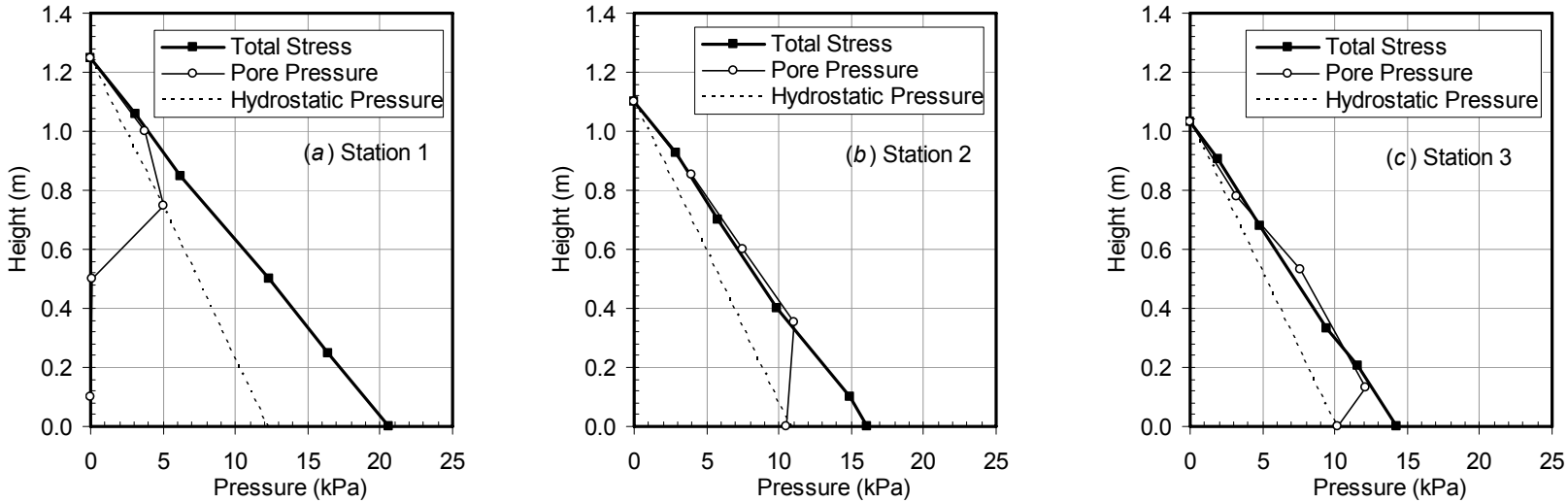

Figure 6.12 Pore water pressure measurements in the west pilot pond on 10th July, 2006 (*a*) Station 1 (*b*) Station 2 and (*c*) Station 3.

6.4.4 Undrained shear strength

The undrained shear strength of the ILTT materials was measured by pushing a field vane apparatus directly into the deposits. The vane was pushed down 25 cm at a time to obtain shear strength with depth. The measured undrained shear strength values of the east pilot pond and the west pilot pond at the last field investigation program are shown in Figures 6.13 (*a*) and (*b*) respectively.

The undrained shear strength of the east pond varied from 1.6 kPa (solids content of 46% and void ratio of 3.0) under the crust to 5.2 kPa (solids content of 52% and void ratio of 2.3) near the bottom of the pond. The dry crust of the east pond had a surface undrained shear strength of about 96 kPa at a solids content of about 72% (void ratio of 1.0). The undrained shear strength profiles of the east pond indicate good undrained shear strength consistency between all stations. This is because the settling processes are similar at all stations and the ILTT materials are quite homogeneous throughout the pond.

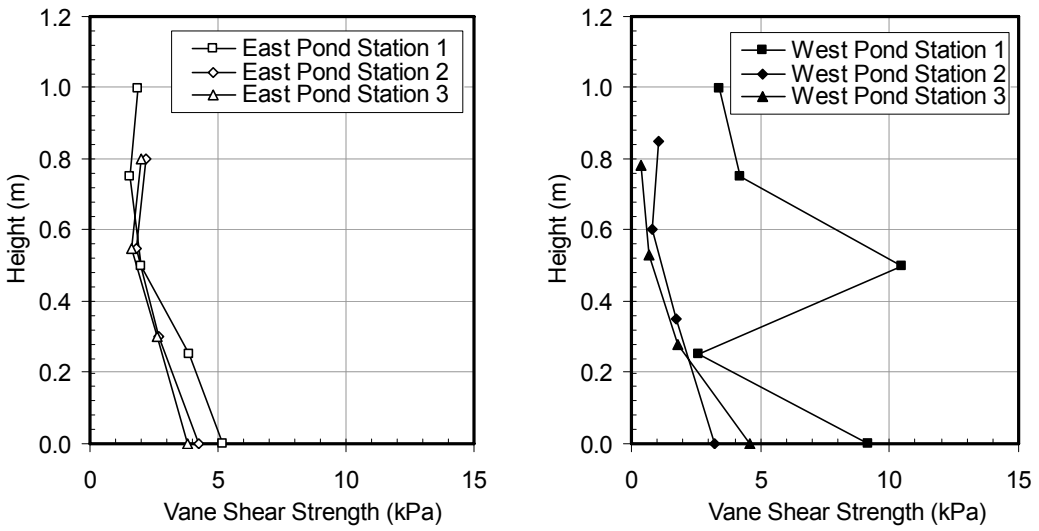

(*a*) (*b*)

Figure 6.13 Undrained shear strength measurements on July 10th 2006 (*a*) east pilot pond (*b*) west pilot pond.

For the west pond, due to the high sand content near the inlet station possibly by a more sandy feed and sand segregation due to the high energy deposition technique, it has erratic undrained shear strength response at Station 1 compared to Stations 2 and 3.

6.5 Field constitutive relationships

In the east pilot pond, it is shown in Figure 6.11 that significant consolidation occurred at the bottom at all stations. This indicates that a significant effective stress exists at the bottom of the pond. These effective stresses can be correlated with the measured void ratios at these locations to obtain a constitutive relationship between effective stress and void ratio for the field material. The results are shown in Figure 6.14 with a power law function fitted to the data points. This set of data can later be used to evaluate consolidation behavior and undrained shear strength characteristic of the ILTT material in this pond.

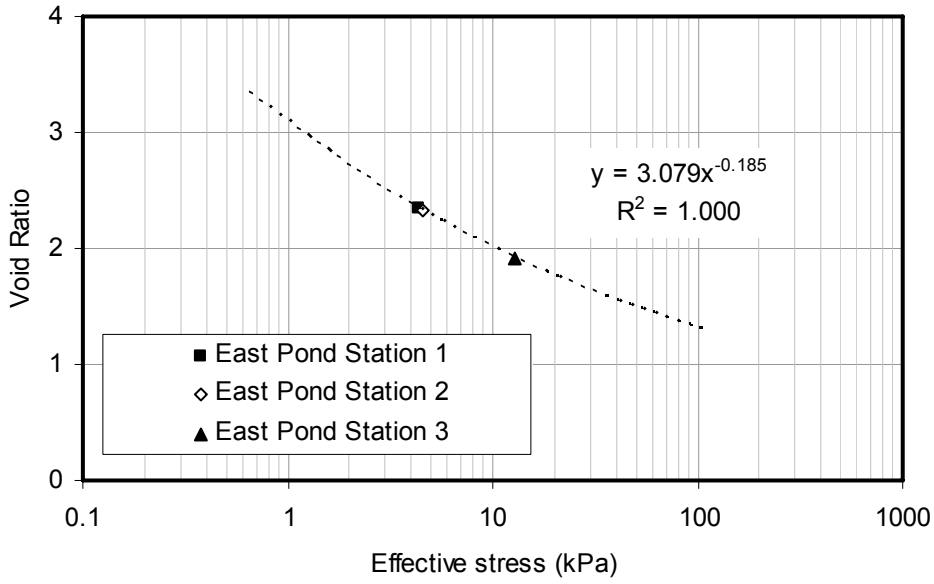

Figure 6.14 Compressibility of ILTT material in the east pilot pond

Another constitutive relationship which can be obtained from the field data is the vane shear strength and void ratio relationship. From Figures 6.5 and 6.13, void ratio and vane shear strength data of the east pond can be used to construct a vane shear strength-void ratio constitutive relationship as shown in Figure 6.15.

With the constitutive relationships from Figures 6.14 and 6.15, a τ_u/σ'_{vo} ratio can be developed and the results are shown in Figure 6.16. The field data indicates at a first glance that the τ_u/σ'_{vo} ratio of ILTT material is much larger than typically found in normally consolidated clays. The large shear strength at high void ratios is believed to be

an indicator of the strong bond in the flocs introduced by the in-line thickening process flocculant and coagulant. The τ_u/σ'_{vo} ratio and floc structure will be further discussed in Chapter 7 where this ratio is constructed from laboratory data.

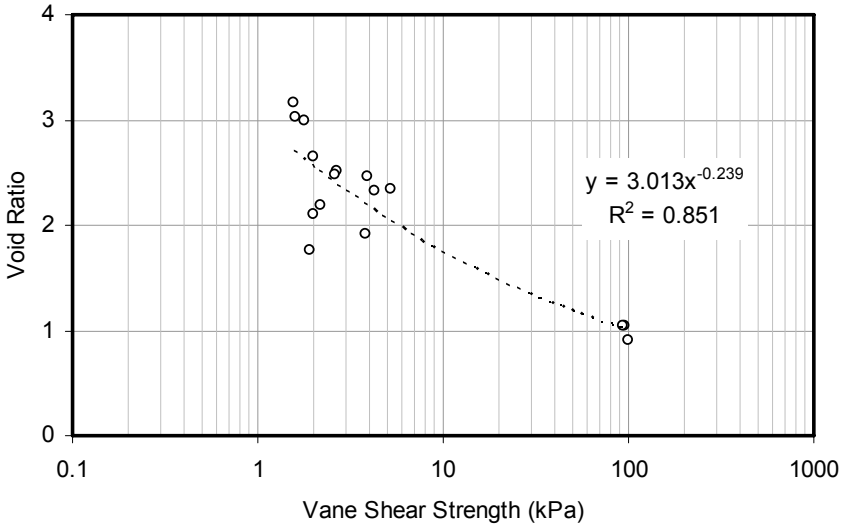

Figure 6.15 Field vane shear strength and void ratio relationship for the east pilot pond

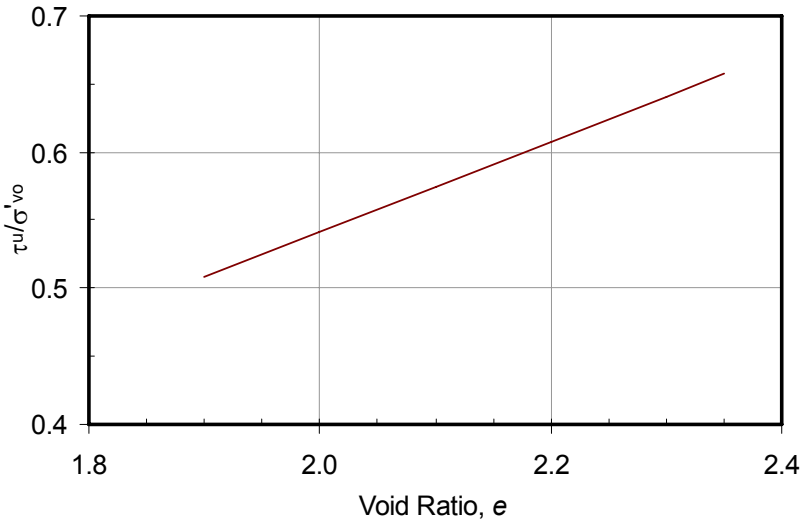

Figure 6.16 Constructed field vane shear strength-effective stress ratio vs void ratio

6.6 History matching analysis of the east pilot pond

In order to understand ILTT field performance and its compressibility and hydraulic conductivity, a finite strain consolidation theory was utilized to history match the field interface height measurements. A one dimensional condition is assumed due to the much larger width and length of the pond compared to the depth of the slurry. The study of a multidimensional model in Chapter 5 also suggests that a one dimensional condition prevails at the center of a pond where the field measurements were taken.

To demonstrate an effect of the in-line thickening process by increasing solids content with time especially during a filling period, a quiescent condition was assigned in the model. For a filling period, it has been earlier discussed in Chapter 3 that a prediction of an interface settlement is essentially independent on filling history but follows the total amount of solids filled in a pond and the interface height is also essentially linear during the filling period. This is true when the filling rate is constant and the one dimensional pond condition is satisfied. This condition was assumed to be valid for the current simulation therefore the interface during the filling period was obtained from this approach. Boundary conditions for the simulation are depicted in Figure 6.11. The pilot pond clearly shows a double drainage condition. Therefore a Dirichlet boundary condition with excess pore pressure set to zero is assigned for both top and bottom boundaries.

The history match was done by searching compressibility and hydraulic conductivity functions based on the power law relationships. The mathematical formula of the relationships remain the same, however, the compressibility function was assigned to have a bi-power form as at effective stresses lower than 10 kPa, large amounts of oil sands tailings compressibility data suggest little to no variations (Jeeravipoolvarn, 2005). Therefore the form of the compressibility is chosen as Equation 6.1 while a hydraulic conductivity-void ratio function remains a conventional power law function expressed as Equation 6.2.

$$e = \begin{cases} A_1 \sigma'^{B_1} & for \quad \sigma' < 10kPa \\ A_2 \sigma'^{B_2} & for \quad \sigma' \geq 10kPa \end{cases} \qquad [6.1]$$

$$k = Ce^D \qquad [6.2]$$

An initial height of the pond was back calculated from the final solids content profiles in Figure 6.5 and the initial solids content of 3.7%. The initial height was found to be 20.4 m. The simulation period was allowed to go up only to 70 days. This period was chosen due to the fact that the pilot pond experienced freezing, thawing and drying after this period.

A consolidation computer program developed earlier in Chapter 3 was utilized in this analysis. A fully implicit finite difference scheme with upwind in a convection term is used to solve the governing equation. The scheme was selected due to its stability and numerical parameters $n = 40$ and $\Delta t = 10^{-4}$ are used in the model (n and Δt denote a total node number and incremental time respectively).

A result of an interface height simulation with time is shown with the average east pilot pond field measurements in Figure 6.17 while Figure 6.18 shows the increase in solids content with time due to the in-line thickening process.

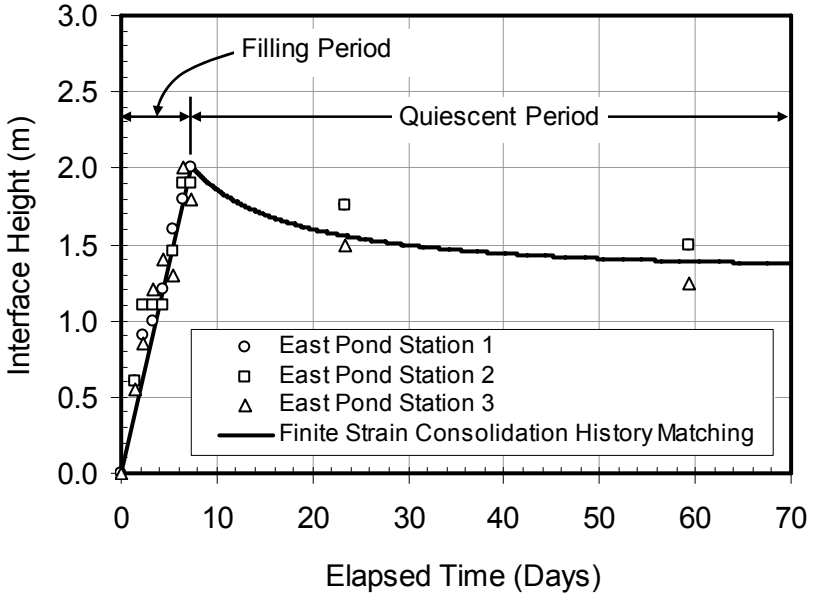

Figure 6.17 History matching of interface height vs. time

In Figure 6.17, the ILTT material was filled into a pond in a period of 7.4 days. During this period, Figure 6.18 shows that ILTT has changed its solids content from the

initial value of 3.7% to 31.2% (void ratios of 65.6 and 5.5 respectively). After it released more than 90% of its water during this period, the ILTT was allowed to undergo self-weight compression up to 70 days when the simulation period was over. Further increase in solids content slows down dramatically as the hydraulic conductivity reduces and excess pore pressures dissipate slowly.

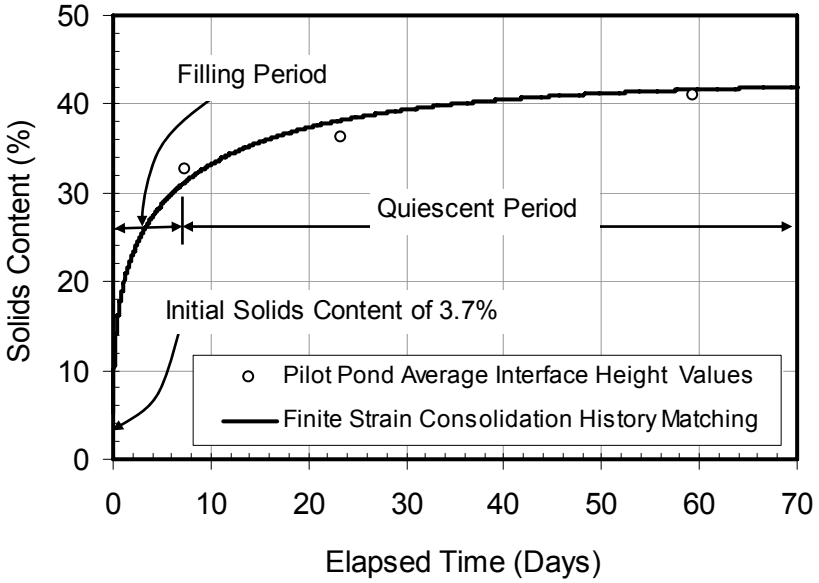

Figure 6.18 History matching of increase in solids content with time

The good agreement between the history matching simulation and the field data shown above was performed by the incorporation of the void ratio-effective stress and hydraulic conductivity-void ratio relationships shown in Figures 6.19 and 6.20 respectively. The field investigation data from Figure 6.14 and typical MFT behavior are also included for relationship comparison.

In Figure 6.19, field data appears to agree well with the history matching compressibility. Compared to typical MFT compressibility, compressibility of the field ILTT is more compressible by having a higher value of compression index. The history matching compressibility function also indicates that it would take a higher effective stress to compress the ILTT material to the same void ratios in the pond compared to the MFT at void ratios of around 2 and higher. It is postulated that the field ILTT was more difficult to compress than the MFT because of the fairly strong large flocs in the field. If

the flocs were broken by shearing action it would likely make the material easier to compress.

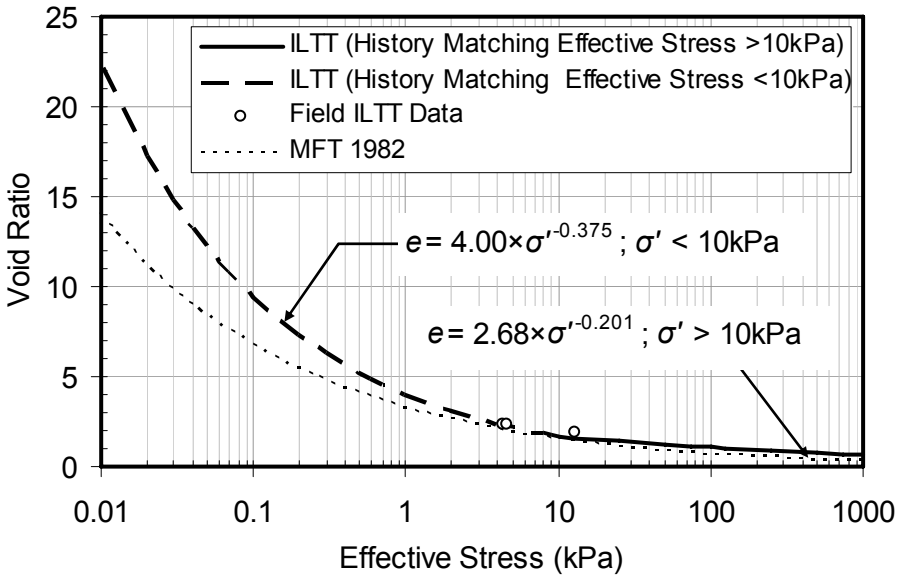

Figure 6.19 Field ILTT history matching compressibility relationship compared with field data and MFT compressibility

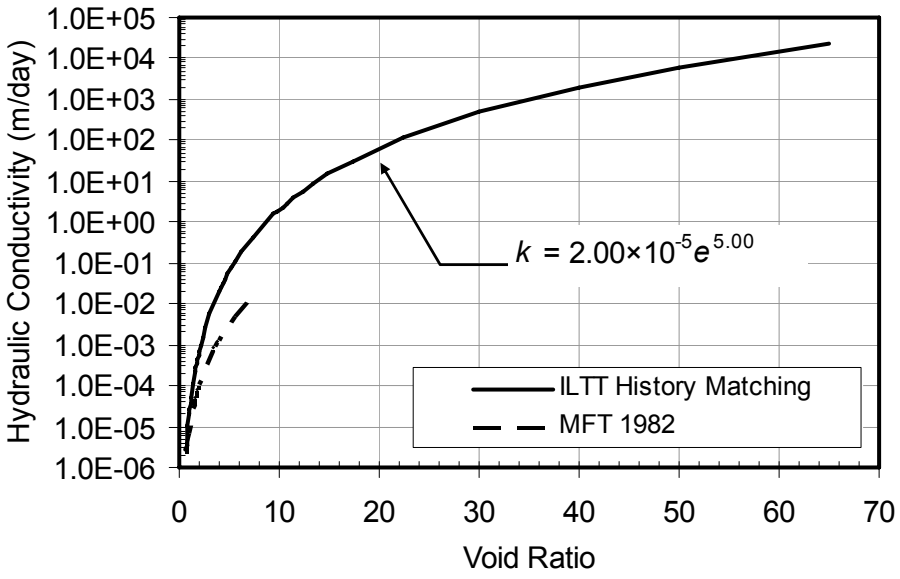

Figure 6.20 Field history matching hydraulic conductivity relationship

Considering hydraulic conductivity (Figure 6.20), at 30% solids (void ratio of about 5.9) (which is a typical MFT solids content) the field hydraulic conductivity of

ILTT is about 20 times more than that of the typical MFT. This great difference in permeability at the same solids content is caused by the difference in structure of the flocculated ILTT vs. the dispersed MFT.

The history matching compressibility and hydraulic conductivity in Figures 6.19 and 6.20 will be later used in Chapter 7 for comparison with the laboratory ILTT and with the parent cyclone overflow tailings.

6.7 Summary

An in-line thickening process was developed to provide a method that can rapidly recover water and produce thickened tailings without the aid of a thickener. Field pilot programs were conducted and were successful.

Two ILTT pilot ponds were filled. The major difference between the ponds was the discharge method. The west pond had a half-pipe chute discharge while the east pond had a sub-TT discharge (tremie technique). The latter discharging method was a lower energy deposition technique which minimized aggregate rupture in the ILTT material.

In the east pilot pond, it was found that the tailings compressed from an initial solids content of 3.7% to 31.2% (void ratios of 65.6 and 5.5 respectively) in about 7.4 days after the filling period was over and to about 50% solids content (void ratio of 2.5) at a depth of 1 m in 4 months. The fines content profiles were consistent with depth and have an average value of 89%. The pore pressure measurements in this pond showed some consolidation at the bottom at all stations as the pond had a pervious foundation. It appeared that a layer of tailings consolidated at the bottom and sealed it preventing further significant downward drainage.

Evident segregation was found in the west pilot pond. A hypothesis on the cause of segregation was that the high discharging energy in this pond broke floc structure allowing the sand to settle out. Further research is required to confirm the influence of shearing on ILTT segregation behavior.

The east pilot pond was history matched by utilizing a finite strain consolidation theory and by searching compressibility and hydraulic conductivity functions based on power law relationships. Good agreement was obtained for matching the field interface height with time and the increase in solids content with time. Field history matching compressibility and hydraulic conductivity functions were obtained.

Comparison of the field history matching constitutive relationships indicated that the field ILTT was more difficult to compress than typical MFT because of the fairly strong large flocs in the ILTT.

The field ILTT was more permeable than typical MFT. At 30% solids content the field hydraulic conductivity was about 20 times more permeable than that of MFT. This great difference in hydraulic conductivity was caused by the difference in structure of the flocculated ILTT vs. the dispersed MFT.

Chapter 7 Laboratory Investigation of the In-Line Thickened Tailings

7.1 Introduction

The in-line thickening process is a process that utilizes a specific mixing technique and certain types of chemicals to improve the engineering properties of oil sands fine tailings. It was developed to maximize an initial rate of water release and minimize the amount of solids in the released water (Yuan and Shaw, 2007). The process however was not developed to achieve specific engineering properties, that is, hydraulic conductivity, compressibility and shear strength of the material. The knowledge of these properties is important in understanding how the in-line thickening process has improved the material. Of more importance, these will allow the quantification of the extent of the behavioral improvement of the process and identify controlling parameters. Therefore a laboratory investigation of the geotechnical properties of the in-line thickened tailings was proposed and the results are discussed in this chapter.

A laboratory investigation was developed to test cyclone overflow, field in-line thickened tailings, laboratory in-line thickened tailings and laboratory sheared in-line thickened tailings for their sedimentation and consolidation geotechnical parameters. A full range of the parameters was determined by utilizing a test program to measure a wide range of compressibility and hydraulic conductivity functions (Scott et al., 2008). Sedimentation and consolidation characteristics of the laboratory in-line thickened tailings were then compared to those of cyclone overflow to evaluate this new tailings treatment process. The sedimentation and consolidation characteristics of the in-line thickened tailings determined in the laboratory were also compared to those measured in the field pilot project to determine whether the small scale laboratory tests could accurately forecast large scale field performance.

This chapter begins with material introductions and preparations followed by the materials' index properties and water chemistry. The results from the full test program,

A version of this chapter has been published. Jeeravipoolvarn S., Scott J.D. and Chalaturnyk R.J. 2009. "Geotechnical characteristics of laboratory in-line thickened oil sands tailings", Proceedings of Tailings and Mine Waste Conference 2009, November 1-4, Banff, AB, 813-828.

including hindered sedimentation tests, compressibility standpipe tests and large strain consolidation tests are then presented. All results from the test program are then combined, analyzed and compared. Conclusions on this research are then given.

7.2 Test materials

Before the presentation of the laboratory investigation, it is important to describe the tailings materials being investigated as they were specifically obtained from the field cyclones and field pilot ponds and then were prepared in a laboratory environment. The following tailings were investigated in the experimental program.

7.2.1 Cyclone overflow tailings obtained on 28th November 2005

On 28th November 2005, cyclone overflow tailings were obtained directly from the Syncrude composite tailings plant in four 20 L buckets as discussed in Section 6.3. The samples were obtained 1 day after the filling period of the pilot pond was complete. All samples were mixed thoroughly by a hand mixer inside the containers to homogenize the material before sub samples were obtained for any testing.

7.2.2 Field in-line thickened tailings obtained on 10th July 2006

The field ILTT samples investigated in this chapter are those samples obtained from the east and west pilot ponds during a field investigation on 10th July 2006 as discussed in Section 6.3. The samples were obtained by a thin wall sampler and stored in 7 L containers. The samples were transported to the University of Alberta where the samples were mixed gently by hand to prevent extensive disruption of floc structure but at the same time homogenize the sample before testing proceeded.

7.2.3 Cyclone overflow tailings obtained on 14th April 2008

Cyclone overflow tailings for the main test program were delivered from Syncrude's composite tailings plant to the University of Alberta on 14th April 2008. A total of 2 m^3 of cyclone overflow tailings were shipped in two 1000 L polyethylene tanks. Cyclone overflow was allowed to settle inside the tanks then the release water from the

tailings was pumped into five polyethylene barrels (~700 L). The top of the tank was then cut off and the settled cyclone overflow was mixed to homogenize it and pumped into two polyethylene barrels (~200 L). After the tank was emptied, the cyclone overflow tailings inside the two barrels were mixed once again with a drill mixer. Sub samples were then taken for solids and fines contents.

7.2.4 Preparation of laboratory in-line thickened tailings

In order to produce ILTT for the main laboratory experiments, the cyclone overflow shipped from the Syncrude on 14th April 2008 was characterized to obtain initial solids content, specific gravity and grain size distribution. Anionic flocculant (CIBA Magnafloc 6260) was prepared by mixing powder flocculant with demineralized water to a concentration of 0.5 g/L. Cationic coagulant (CIBA Magnafloc 368) was similarly prepared by mixing powder coagulant with demineralized water to a concentration of 1.0 g/L. It is noted that both chemicals were left for at least 2 hours before usage and the chemical solutions that were older than 2 days were all discarded.

In order to prepare ILTT to a design solids content and volume, total mass and solids mass of cyclone overflow is calculated by Equations 7.1 and 7.2. Total mass of a design mix is calculated by Equation 7.3.

$$M_{COF} = \frac{sV}{s_{COF}}\left(\frac{G_s}{G_s + s(1-G_s)}\right) \quad [7.1]$$

$$M_S = sV\left(\frac{G_s}{G_s + s(1-G_s)}\right) \quad [7.2]$$

$$M = V\left(\frac{G_s}{G_s + s(1-G_s)}\right) \quad [7.3]$$

Where M is total mass of design ILTT, M_{COF} is total mass of cyclone overflow, s is design solids content, V is design volume and G_s is specific gravity of the solids.

With a known mass of solids (M_s) from Equation 7.2, the amount of chemicals used for the three mixing steps is calculated by Equation 7.4 and the amount of water required for the mix is subsequently calculated by Equation 7.5.

$$V_i = \frac{d_i M_s}{c_i} \quad [7.4]$$

$$M_{wa} = M - M_{COF} - \sum_{i=1}^{3} \rho_i V_i \quad [7.5]$$

Where V is the volume of solution required, d is the dosage of the prepared chemical solutions, c is the concentration of the prepared chemical solutions, M_{wa} is the additional recycled water required and ρ is the density of the solution. The subscript i defines mixing steps which run from 1 to 3.

To prepare ILTT at a solids content of s and a volume of V, cyclone overflow with a total mass of M_{COF} is mixed with recycled water with a mass of M_{wa}. Flocculant for step 1, coagulant for step 2 and flocculant for step 3 are prepared at volumes of V_1, V_2 and V_3 respectively.

To start the mixing process, cyclone overflow and recycled water are mixed for 1 minute inside a mixing chamber with a controlled mixing blade tip speed of 0.8 m/s. There are two sizes of mixing chamber and mixing propeller which are shown in Figures 7.1 and 7.2. A 15 L mixing chamber (Figure 7.1) is used to prepare large amount of ILTT for a compressibility standpipe test and a large strain consolidation test while a 2 L mixing chamber (Figure 7.2) is used to mix ILTT for a hindered sedimentation test. After cyclone overflow is mixed with recycle water for 1 minute, a timer is started and the first flocculant is added continuously through a syringe into the middle of a mixing container. Within 30 seconds all of the first flocculant is mixed at a dosage of 250 g/T of dry solids. Then the second coagulant is added at 800 g/T of dry solids with the same discharging time and technique. Finally the third flocculant is discharged similarly at a dosage of 60 g/T of dry solids. After 1.5 minutes the mixing is completed, the mixer is stopped and ILTT is ready for the laboratory investigation.

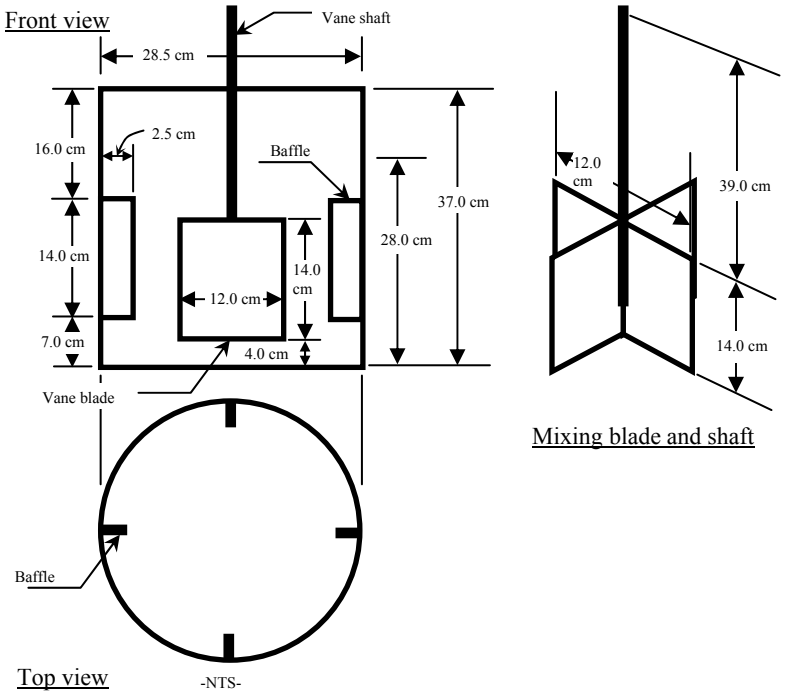

Figure 7.1 Mixing tank and mixing blade (15 L)

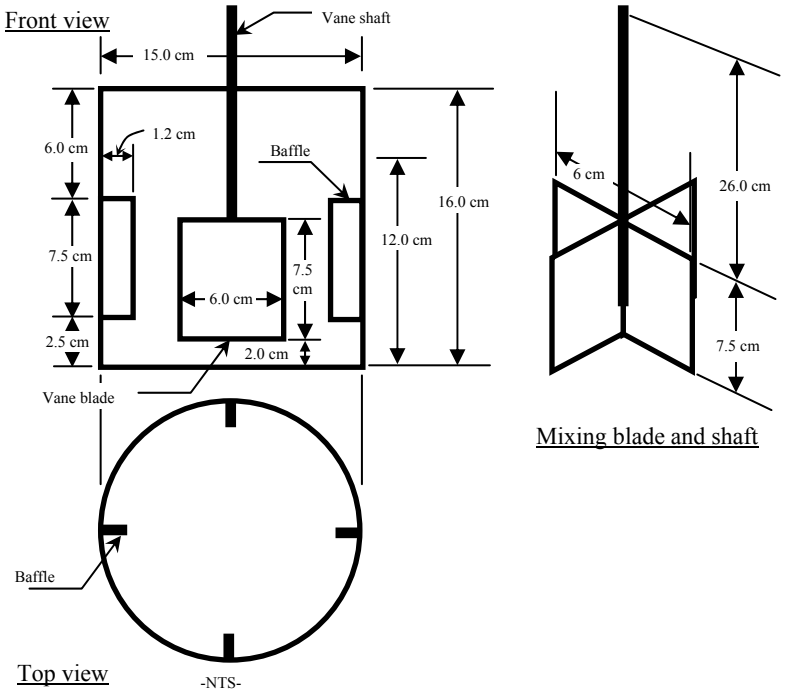

Figure 7.2 Mixing tank and mixing blade (2 L)

In order to investigate shearing effects on ILTT settling behavior, sheared ILTT is also prepared according to the above guideline then ILTT is allowed to release water to a design solids content. Supernatant water is decanted from the tailings and the tailings are subjected to shearing inside a mixing tank to create sheared ILTT. Shearing effort applied to the tailings follows a technique used in the industry to simulate pumping by using a mixer shearing samples at 1080 rpm for 24 minutes (Apex Engineering and AEGRF 2005). After shearing is complete, the sheared ILTT is immediately poured into different test cells for different tests to commence.

7.3 Index testing

Index testing including grain size distribution, specific gravity, mineralogy and morphology are presented in this section to assist in the behavioral interpretation of the tailings.

7.3.1 Grain size distribution

7.3.1.1 Tailings from field investigation

Standard particle size determination method (ASTM D 422-63) was performed on ILTT materials obtained at inlet and outlet stations of the ILTT pilot ponds on 28th November 2005. The results are shown in Figure 7.3. It appears that at both inlet and outlet stations of the east pilot pond, particle size distributions are similar. An average fines content (< 45 μm) and an average clay size content (< 2 μm) of the east pond ILTT at these locations are 67% and 30% respectively. Fines content of the east pond ILTT appears to be relatively small compared to the field data of the east pond showing an average fines content of 89%. The lower fines content at the inlet and outlet stations of the east pilot pond was unexpected and was possibly caused by an intrusion of sand from the adjacent sandy dykes.

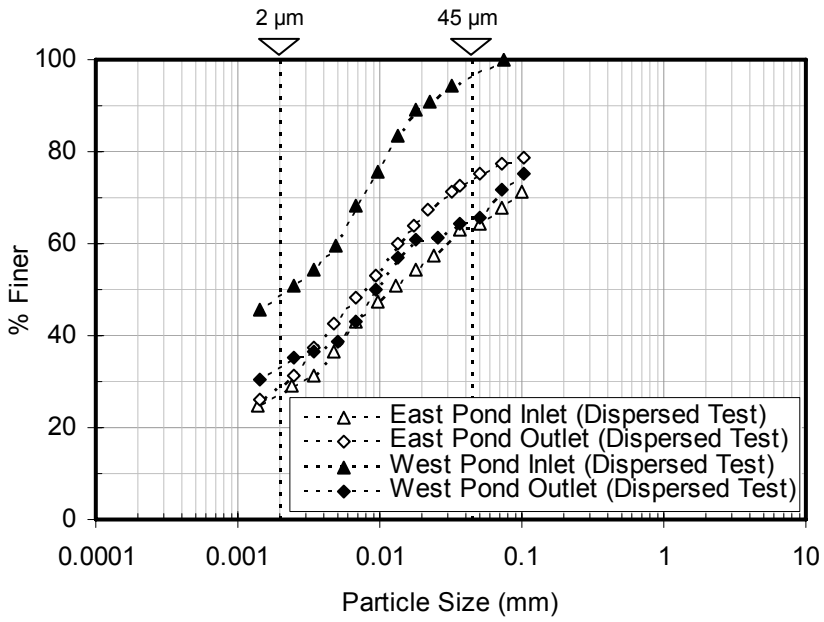

Figure 7.3 Particle size distributions of ILTT from inlet and outlet station of ILTT pilot ponds on 28th November 2005

For the west pond ILTT, results indicate that the fines contents are 96% at the inlet station while it is 65% at the outlet station. Clay size contents appear to be 48% and 33% for the inlet and out let stations respectively. All the samples have similar clay to fines ratios of about 0.5. This indicates that the clay and fines portions in the samples are qualitatively similar and the difference in the particle size distributions could possibly be caused by intrusion of sand.

Cyclone overflow obtained on 28th November 2005 and ILTT shipped from Syncrude on 24th December 2005 were also tested for their dispersed particle size distributions. ILTT samples from the middle of the ponds (Station 2) were used. Particle size distribution of cyclone overflow, east pond ILTT and west pond ILTT are shown in Figures 7.4, 7.5 and 7.6 respectively.

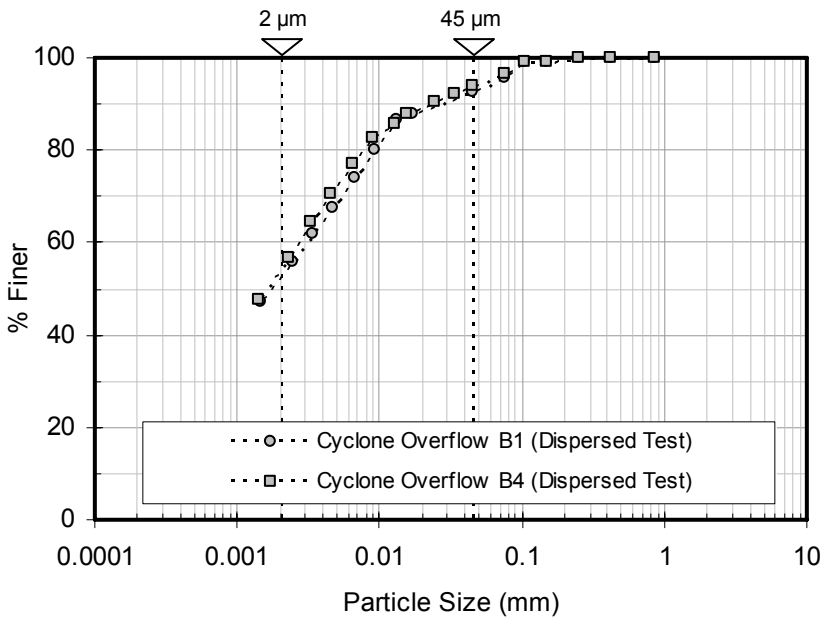

Figure 7.4 Particle size distributions of cyclone overflow tailings obtained from Syncrude on 28th November 2005

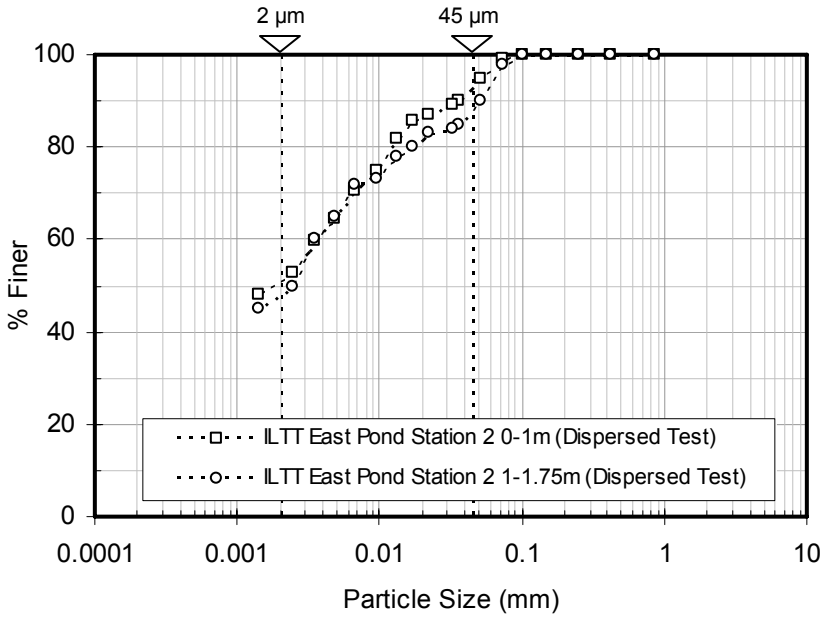

Figure 7.5 Particle size distributions of ILTT from the east pilot pond shipped from Syncrude on 24th December 2005

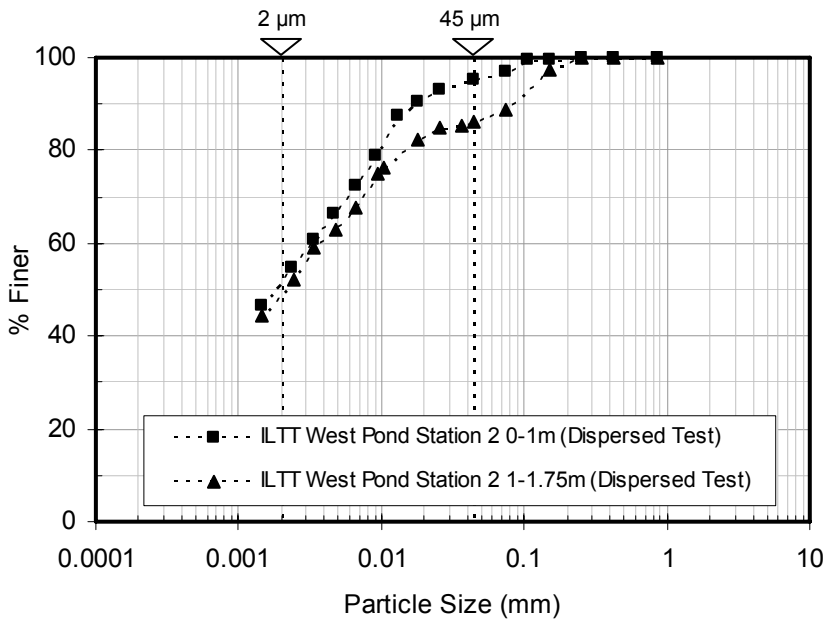

Figure 7.6 Particle size distributions of ILTT from the west pilot pond shipped from Syncrude on 24th December 2005

Figure 7.4 indicates that the cyclone overflow tailings obtained from Syncrude on 28th November 2005 consist of 93% fines and 53% clay size material. The ILTT from the middle of the east pond at depth of 0 to 1 m contains 92% fines and 51% clay size material and at depth of 1 to 1.75 m the ILTT contains 88% fines and 48% clay size material (Figure 7.5). Fines content measurements of all east pond samples obtained on 24th December 2005 were shown earlier in Table 6.2 of Chapter 6. The grain size distribution agrees well with the fines data in Table 6.2 indicating that majority of the ILTT material in the east pond has an average fines content of around 90%.

In Figure 7.6, the results indicate that the ILTT from the middle of the west pond at depth of 0 to 1 m contains 96% fines and 51% clay size material and at depth of 1 to 1.75 m the ILTT contains 86% fines and 49% clay size material. Average fines and clay-sized contents at Station 2 are 91% and 50% respectively.

7.3.1.2 Cyclone overflow shipped from Syncrude on 14th April 2008

Two dispersed and two non-dispersed particle size analyses were performed on the cyclone overflow sample and the results are shown in Figure 7.7. Non-dispersed particle size distribution of cyclone overflow indicates that the material has

approximately 94% fines and 30% clay size particles (< 2 μm) while the dispersed test indicates 94% fines and 50% clay size particles. These results contradict the conventional believe that the fine tailings are completely dispersed by the Clark hot water bitumen extraction process and there is no difference between dispersed and non-dispersed hydrometer tests for the oil sand fine tailings (Jeeravipoolvarn et al., 2008). The lower amount of clay size material in the non-dispersed test might suggest a change in water chemistry possibly an increase in electrolyte concentration in the pore water.

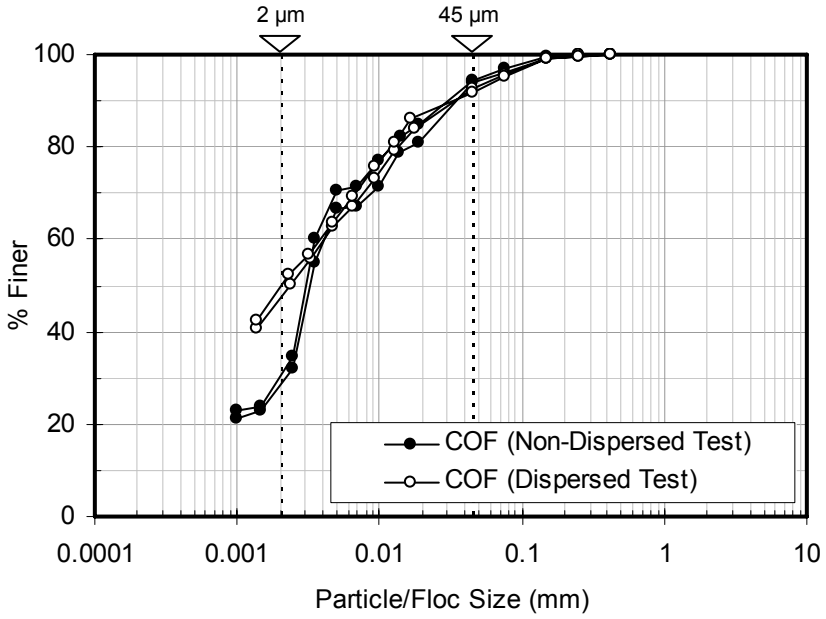

Figure 7.7 Particle size distributions of cyclone overflow tailings shipped from Syncrude on 14th April 2008

7.3.1.3 Laboratory non-sheared ILTT

Apparent particle size distribution of ILTT was measured by 5 non-dispersed hydrometer tests and wet sieve tests and the results are shown in Figure 7.8. The ILTT apparent particle size distribution indicates that the material has an individual fines content (< 45 μm) of less than 5%. All other fines are tied up in larger flocs. The large apparent particle size of the material indicates the strong influence of the in-line thickening process that brings small particles together forming large aggregates that should settle in a very rapid manner.

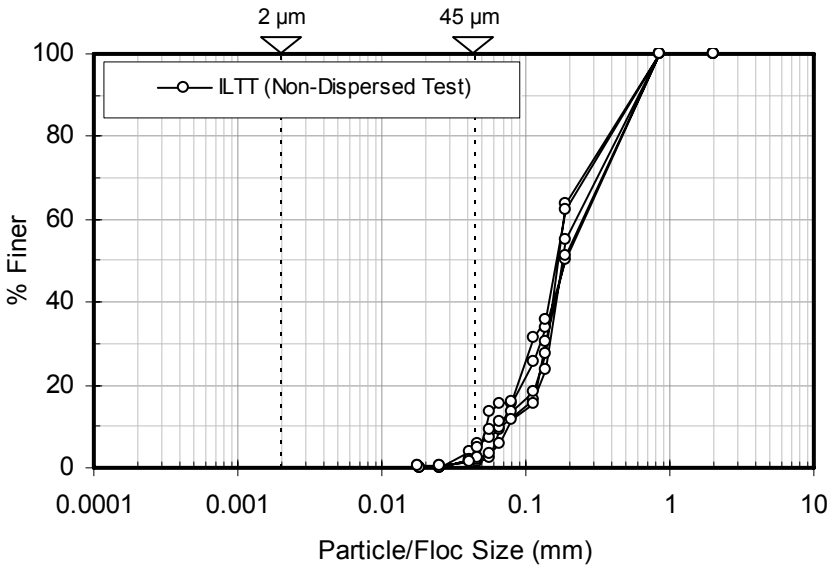

Figure 7.8 Particle size distributions of laboratory non-sheared ILTT

7.3.1.4 Laboratory sheared ILTT

It was hypothesized that shearing of ILTT during pumping, pipelining and deposition will change particle size distribution by disrupting floc structure. To quantify the particle size distribution of sheared ILTT, the freshly mixed ILTT was subjected to shearing at four shearing efforts; 300 rpm for 24 minutes, 1080 rpm for 12 minutes, 1080 rpm for 24 minutes and 2000 rpm for 24 minutes inside a mixing tank. Apparent particle size distribution of sheared ILTT was measured by a non-dispersed hydrometer test and a wet sieve test. Test results for 8 tests are shown in Figure 7.9.

The sheared ILTT apparent particle size distribution indicates that when it is subjected to shearing at 1080 rpm for 12 and 24 minutes the material has fines content of about 77% and clay size contents of about 7%. At shearing effort of 300 rpm for 24 minutes, the material has 55% fines content and 4% clay size content. At shearing effort of 2000 rpm for 24 minutes, the material appears to have similar particle size distribution as that of the sheared ILTT at 1080 rpm. For all practical purposes the intensity and length of shearing did not make much difference to the amount of floc breakage.

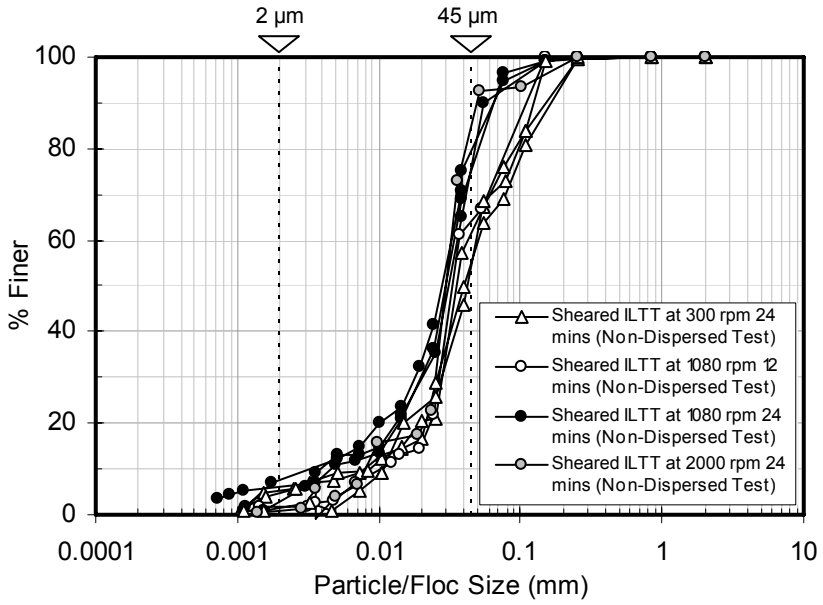

Figure 7.9 Particle size distributions of Laboratory sheared ILTT

7.3.1.5 Comparison of particle size distributions for COF and ILTT

To conclude the particle size distributions of cyclone overflow tailings and laboratory in-line thickened tailings, all particle size distributions determined for both tailings are compared in Figure 7.10.

It can be summarized that when cyclone overflow is fully dispersed it contains approximately 94% fines and 50% clay size particles but in its natural condition cyclone overflow contains approximately 94% fines and only 30% clay size particles. As the cyclone overflow is treated with the in-line thickening process, the apparent particles size distribution changes to approximately 5% fines with no detectable clay size particles. When the in-line thickened tailings is subjected to shearing at 1080 rpm for 24 minutes, the large floc structures made by the in-line thickening process are disrupted and apparent particle size distribution of the sheared in-line thickened tailings indicates fines content of about 77% and clay size contents of about 7%. At this specified rate of shearing, there remains a substantial remnant influence of the in-line thickening process in the tailings showing considerable larger particle sizes compared to that of the original cyclone overflow tailings.

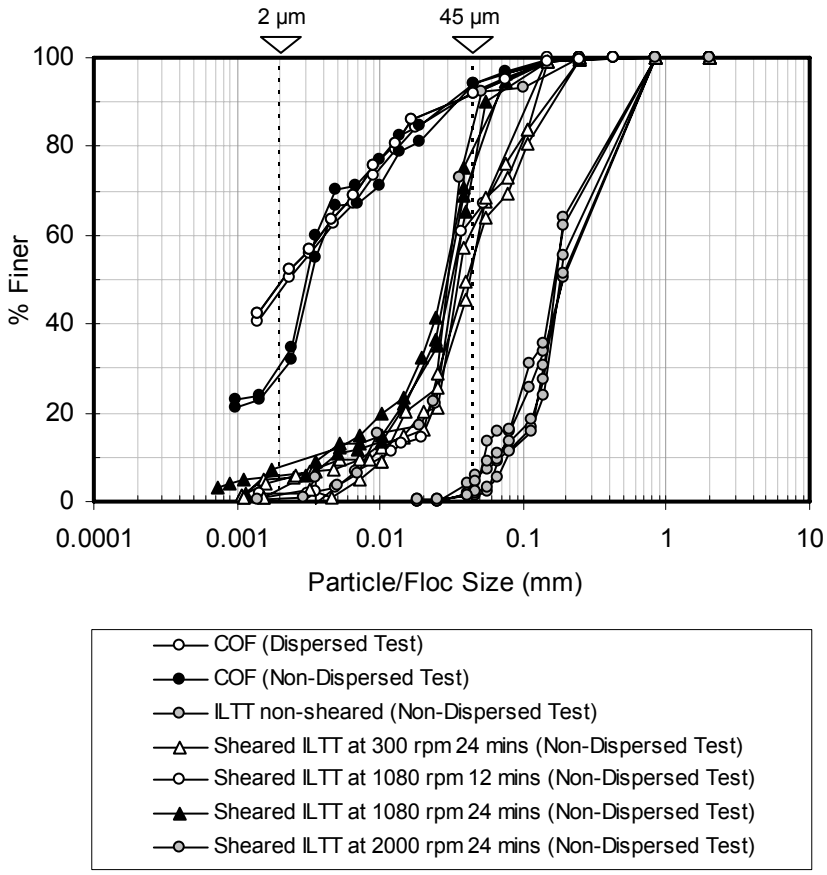

Figure 7.10 Comparison of particle size distributions

7.3.2 Specific gravity

In order to determine material specific gravity, air bubbles have to be removed from soils and there are two common methods to remove air bubbles. One is boiling and another is vacuuming. For oil sands tailings materials, if boiling is chosen, special care must be applied because existing bitumen can froth and overflow the specific gravity jar and/or soils at the bottom can dry and stick to the jar. If bitumen is extracted prior to the specific gravity test, a back calculation will be required to get the natural state specific gravity. For the boiling method, low heat and frequently rolling the jar are recommended. The boiling method becomes tedious and it is easy to introduce small air bubbles therefore for specific gravity determination of the oil sand fine tailings vacuuming is preferred.

The specific gravities of COF and ILTT were measured and the results are shown in Table 7.1. Averaged specific gravities of COF and ILTT are 2.53 and 2.48

respectively. The low specific gravity value of the COF and ILTT is the result of the bitumen attached to the fine mineral particles. The bitumen which has a specific gravity of about 1.03 is considered part of the solids as it remains with the mineral particles and results in this lower specific gravity of the material. Based on bitumen specific gravity of 1.03 and mineral specific gravity of 2.65, geotechnical bitumen contents (mass of bitumen/mass of total solids) were calculated and also shown in Table 7.1. Bitumen contents of the fines materials vary from 2.8% to 5.2% with an average bitumen content of 3.8%.

Table 7.1 Specific gravity of tested tailings

Tailings	Descriptions	G_s	f(%)	b (%)
Cyclone overflow	Bucket 4 sample received on 24th December 2005	2.53	93.9	3.0
East pond ILTT	Station 2 at 0-1m Received on 24th December 2005	2.54	87.4	2.8
West pond ILTT	Station 2 at 0-1m Received on 24th December 2005	2.45	95.3	5.2
Cyclone overflow	Received on 14th April 2008	2.52	94.0	3.3
Laboratory ILTT	Prepared from COF received on 14th April 2008	2.46	94.0	4.9

7.3.3 Atterberg limits

Figure 7.11 shows a plasticity chart containing data from the east pond ILTT, west pond ILTT, 1982 MFT (Jeeravipoolvarn et al., 2009), 2008 cyclone overflow and laboratory ILTT. The east pond ILTT has an average liquid limit of 58 and an average plasticity index of 34 and the range of values indicate that the material is clay of low to medium plasticity. For the west pond material, the ILTT has higher index value with an average liquid limit of 70 and an average plasticity index of 47 and the range of values indicate the material is clay of medium to high plasticity.

The relatively higher values of w_L and I_p of the west pond ILTT could indicate two possibilities. One is a variation in the ore type and another is the different degree of chemical additives. The east pond ILTT material is mainly estuarine ore while the west pond is mainly marine ore. The difference in the ore type can pose differences in both extraction and in-line thickening process efficiency. According to Shaw and Wang

(2005), there is no significant different in chemical dosages used in both ponds. The segregation of the material in the west pond provided tailings samples with less sand content which would result in a higher liquid limit and may also suggest a higher bitumen content. This will generally increase both w_L and I_p of the tailings. The tailings with more bitumen (usually finer tailings) tend to have a higher w_L (Scott et al., 1985). Chemical addition can also increase liquid limit as seen in Figure 7.11 where the laboratory ILTT has a much higher liquid limit than its parent COF.

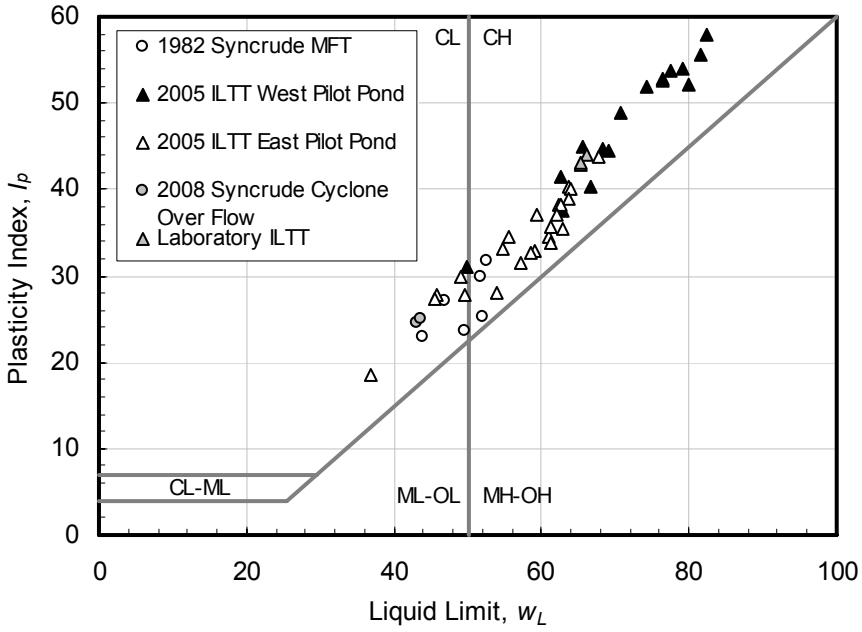

Figure 7.11 Plasticity chart

The 2008 cyclone overflow tailings show liquid limit and plasticity index of 43 and 25 respectively. These indicate that the cyclone overflow clay is of low to medium plasticity similar to the 1982 MFT. The Activity of the cyclone overflow was calculated to be 0.49 which is classified as inactive clay (Holtz and Kovacs, 1981). This confirms the dominant kaolinite clay mineral in these fine tailings materials (FTFC 1995).

For laboratory ILTT, the average liquid limit and the plasticity index are found to be 66 and 43 respectively indicating that ILTT may behave as clay of high plasticity. The Activity of ILTT is calculated to be 0.87 which is classified as normal activity (Holtz and Kovacs, 1981).

7.3.4 Mineralogy and morphology

Samples of cyclone overflow obtained on 14th April 2008 and ILTT prepared in laboratory were sent to AGAT laboratories Ltd. to determine their mineralogy compositions by X-ray diffraction (XRD) techniques. Results of the mineralogy analysis of both materials are shown in Table 7.2.

The XRD results of cyclone overflow indicate that the sample consists mainly of kaolinite (46%) [$Al_4Si_4O_{10}(OH)_8$)] and quartz (41%) [SiO_2]. Minor amounts of illite (5%) [$KAl_2(OH)_2(AlSi_3(O,OH)_{10})$], siderite (4%) [$FeCO_3$], calcite (2%) [$CaCO_3$], muscovite (2%) [$K_2Al_4[Si_6Al_2O_{20}](OH,F)_4$]), plus trace potassium feldspar (1%) [$KAlSi_3O_8$] are also found in the sample. The total clay content is 50.0%.

For ILTT, the sample consists mainly of quartz (42%) [SiO_2] and kaolinite (41%) [$Al_4Si_4O_{10}(OH)_8$)]. Minor amounts of illite (5%) [$KAl_2(OH)_2(AlSi_3(O,OH)_{10})$], chlorite (4%) [$(Mg,Fe)_5Al(AlSi_3)O_{10}(OH)_9$] siderite (4%) [$FeCO_3$], muscovite (2%) [$K_2Al_4[Si_6Al_2O_{20}](OH,F)_4$]), and calcite (2%) [$CaCO_3$]. The total clay content is 49.7%. Little difference in the mineralogy of the COF and ILTT was expected as the materials are completely dispersed in the XRD process. Both materials were tested to ensure that the ILTT was made from a representative part of the COF.

The mineralogy tests agree well with the dispersed particle size analyses of the COF (Figure 7.7) where the clay content was measured to be 50%.

Table 7.2 Mineralogy of cyclone overflow and in-line thickened tailings

Tailings	Mineral (%)								
	Rock forming minerals					Clay minerals			
	Quartz	K-Feldspar	Calcite	Muscovite	Siderite	Kaolinite	Chlorite	Illite	Smectite
COF	41	0.8	1.7	1.7	4.2	45.5	0.0	4.5	0.0
ILTT	42	0.0	1.7	2.5	4.2	40.8	3.7	5.2	0.0

Morphology of in-line thickened tailings and cyclone overflow were obtained by scanning electron microscope and a standard digital SLR with a macro lens. Macro features of cyclone overflow and inline thickened tailings are shown in Figures 7.12 and 7.13 respectively.

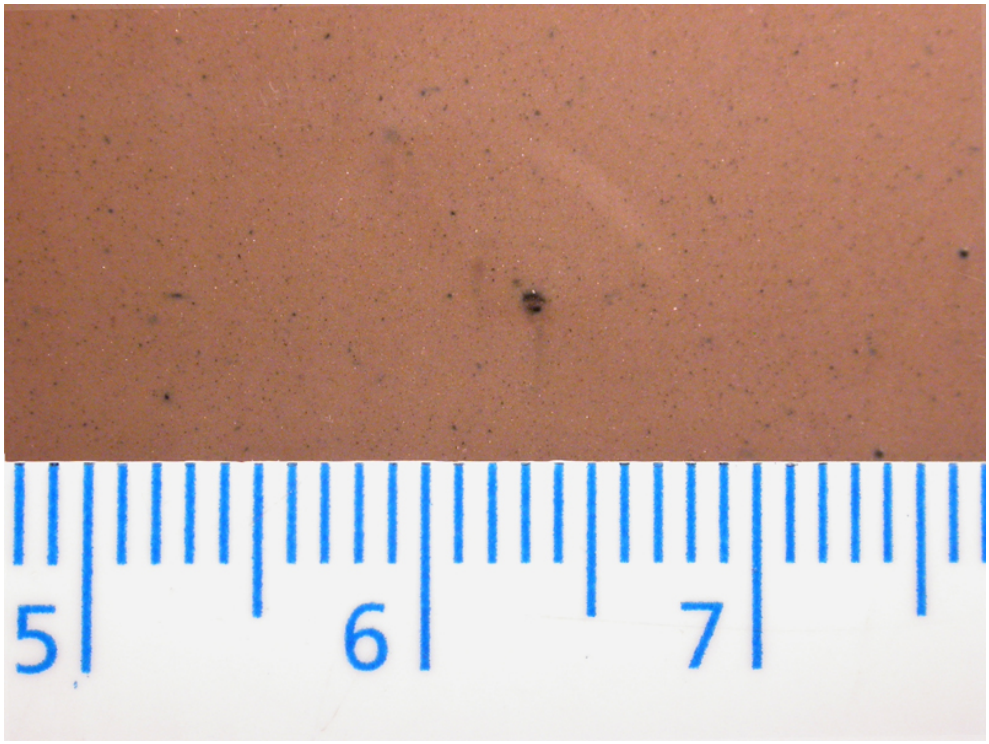

Figure 7.12 Macro photography of cyclone overflow at 27% solids content or void ratio of 6.8 (cm scale)

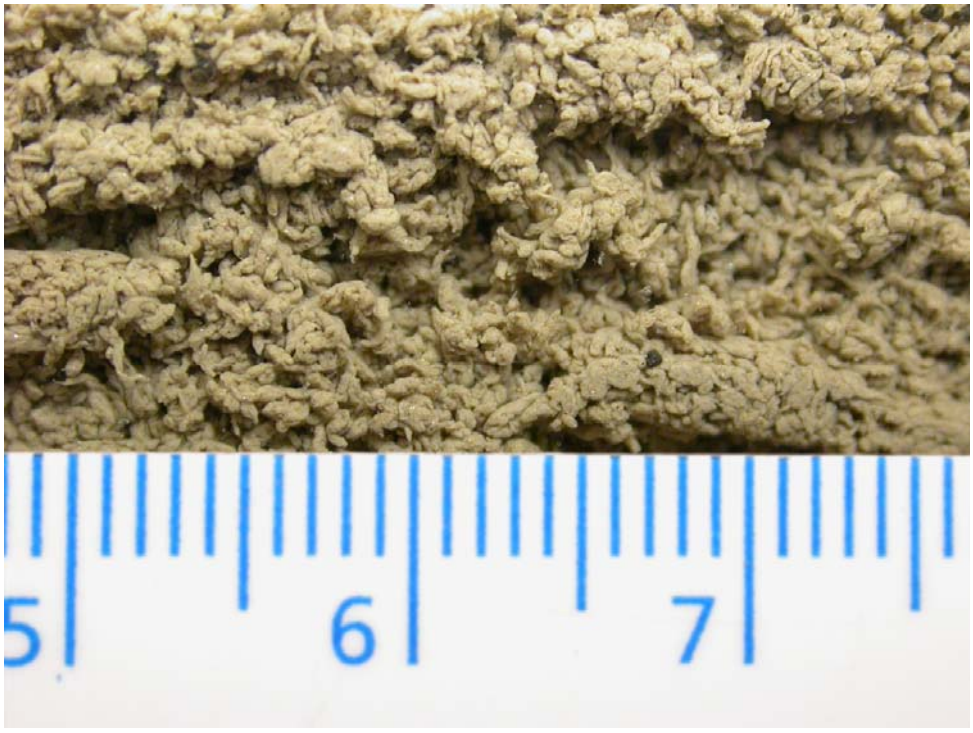

Figure 7.13 Macro photography of in-line thickened tailings at 24% solids content or void ratio of 7.8 (cm scale)

In Figure 7.12, it appears that cyclone overflow at this scale is homogeneous and shows no visible macro feature. For in-line thickened tailings, small elongate shaped flocs with approximately 0.5 mm width and 2 mm length can be observed (Figure 7.13). When these small flocs roll as they travel in a settling column, a group of flocs with sizes as large as 3 mm width and 1 cm length will form. It was observed that the group of flocs can be easily disintegrated into the small flocs when subjected to a small shearing effort such as inverting the settling column. In the field pilot ponds a group of flocs was observed to be as large as 1 cm in diameter. The large open structure of the in-line thickened tailings should provide a large hydraulic conductivity for this material.

Scanning electron microscope images of cyclone overflow and in-line thickened tailings inside a floc are compared at solids contents of about 23% and 70% in Figures 7.14 and 7.15 respectively. It is noted that all SEM images were taken by following a method given by Azam and Scott (2009).

In Figure 7.14, the comparisons of micro structure of the 23% solids content cyclone overflow (left) and the 24% solids content in-line thickened tailings (right) indicate that the in-line thickened tailings micro structure inside a floc is finer and more random. Several large booklets of clay platelets can be observed for both materials with the majority of the clay plates separated. The mode of particle association of the cyclone overflow can be classified as mild edge-to-face flocculated and dispersed. For the in-line thickened tailings, edge-to-face and edge-to-edge flocculated and aggregated patterns dominate. It can also be observed that the pore space is larger for the cyclone overflow with an average spacing of 5.5 μm while it is about 3.5 μm for the in-line thickened tailings. The smaller space between particles with similar solids contents and the different mode of particle association of the in-line thickened tailings may suggest that diffuse double layers of the clay platelets were compressed possibly due to the addition of the cationic coagulant. The compressed double layer may open up a negative double layer edge of the clay platelets which would allow more edge to face particle association pattern and allow more charge patch by anionic flocculant. The parallel structure observed in cyclone overflow tailings also suggests that both sides of the clay platelets have the same charge. The possible identical charge on both sides of the clay platelets and booklets also suggests that pH of the material is possibly above point of zero charge (PZC) as at this condition O-face and T-face on clay particles are both negatively

charged. According to Tombácz and Szekeres (2006), at pH higher than pH_{PZC} all surfaces on kaolinite clay should all be negatively charged. Therefore compressed double layers should not cause more particle association. It is noted however that Tombácz and Szekeres (2006) also showed that a compressed double layer provides a smaller stability number. Their results suggest that some type of particle association did occur at pH higher than point of zero charge.

Figure 7.15 shows scanning electron microscope images of both cyclone overflow and in-line thickened tailings at solids content of around 70% (void ratio of about 1). Both tailings samples were obtained from post large strain consolidation tests with a maximum applied stress of about 500 kPa. It appears that there is no parallel card-house structure in high solids content cyclone overflow as observed in the cyclone overflow at a lower solids content. Micro structures of both tailings appear to be quite similar which is random and packed clay structures.

Scanning electron microscope images of sheared in-line thickened tailings in a floc are shown in Figure 7.16. The micro structure of the sheared ILTT is similar to that of a non-sheared ILTT showing random structure. It is noted that round shaped clay platelets in the sheared ILTT scanning electron microscope images are not due to shearing but rather an insufficient sublimation process to remove ice on the sample's surface.

Figures 7.17 and 7.18 show the energy dispersive X-ray analyses for cyclone overflow and in-line thickened tailings. The electron beam in the scanning electron microscope covers the entire micrograph therefore the analysis is only qualitative. The traces in Figures 7.17 and 7.18 show that the mineralogy of cyclone overflow and in-line thickened tailings are similar with dominating silica and aluminum. A similar trend of the mineralogy by XRD was previously shown in Section 7.3.9.

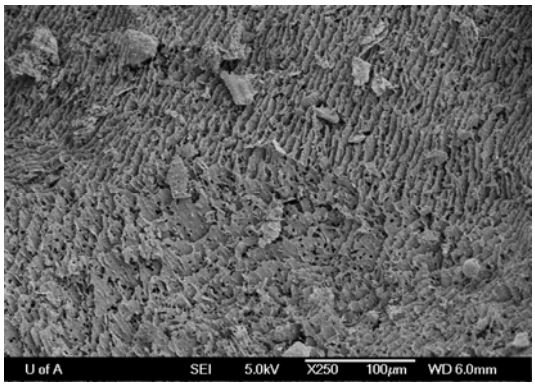

(*a*) COF ×250

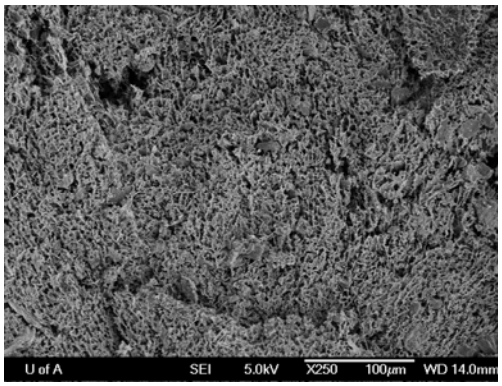

(*b*) ILTT ×250

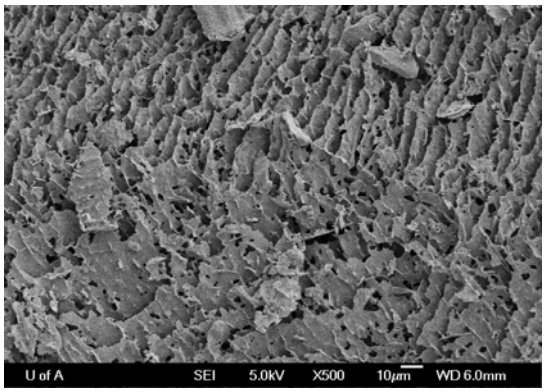

(*c*) COF ×500

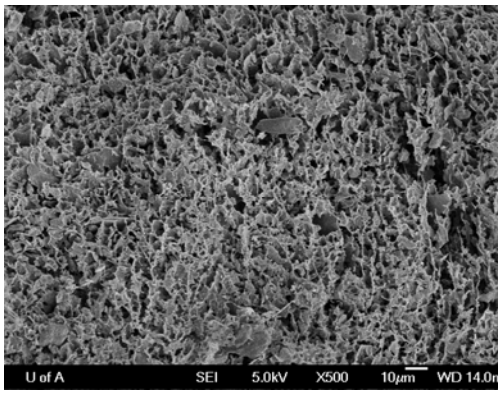

(*d*) ILTT ×500

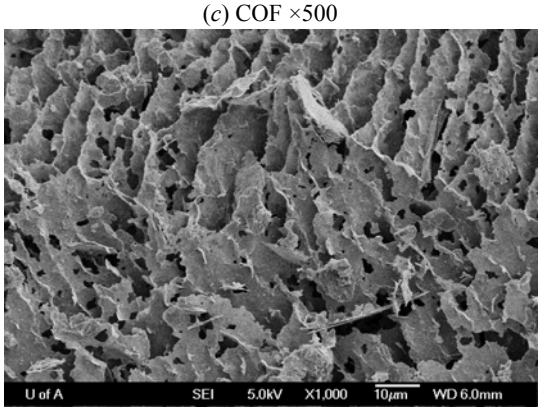

(*e*) COF ×1000

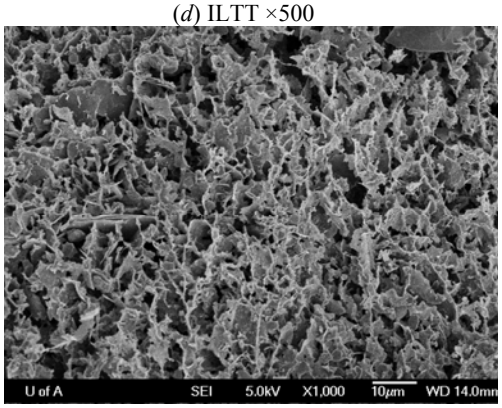

(*f*) ILTT ×1000

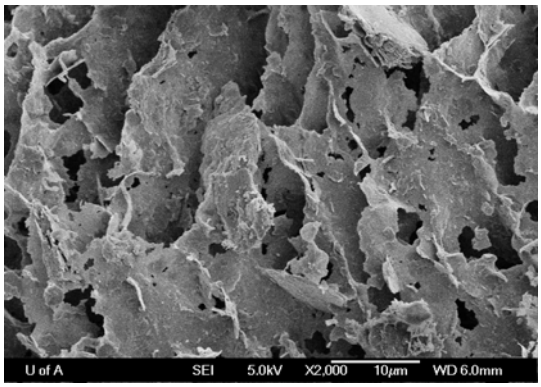

(*g*) COF ×2000

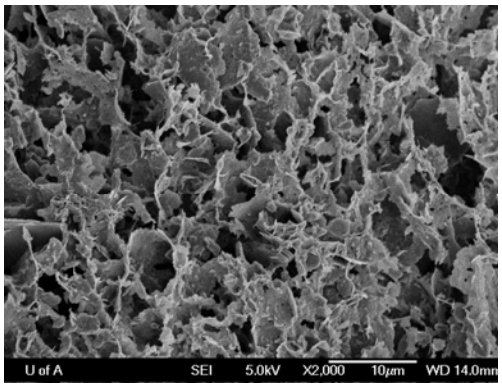

(*h*) ILTT ×2000

Figure 7.14 Scanning electron microscope images of cyclone overflow (23%S, e =8.5) and in-line thickened tailings (24%S, e =7.8)

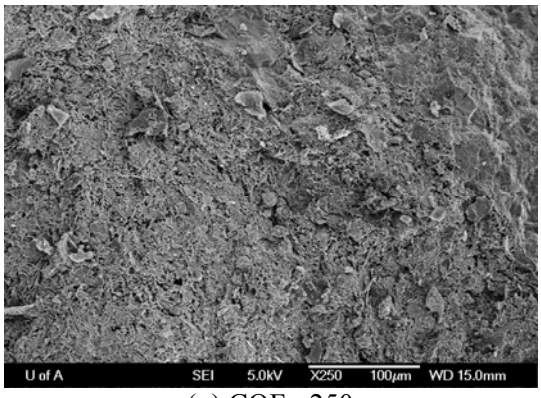

(*a*) COF ×250

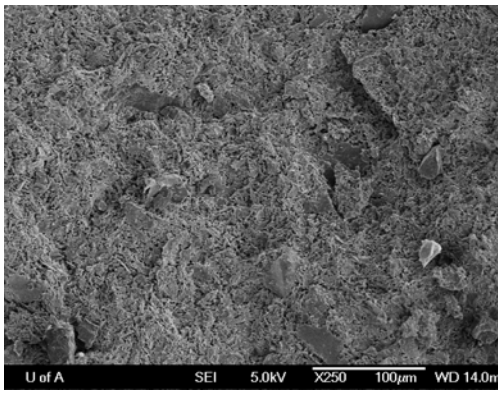

(*b*) ILTT ×250

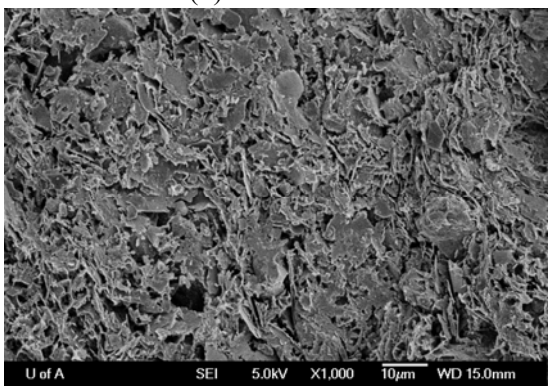

(*c*) COF ×1000

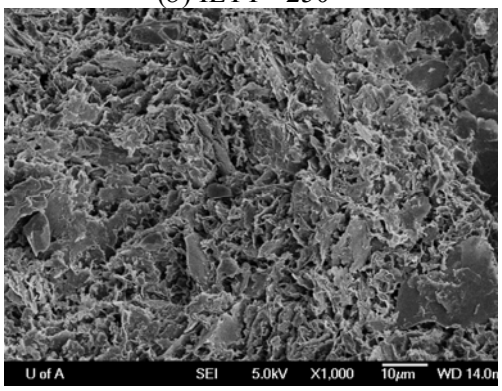

(*d*) ILTT ×1000

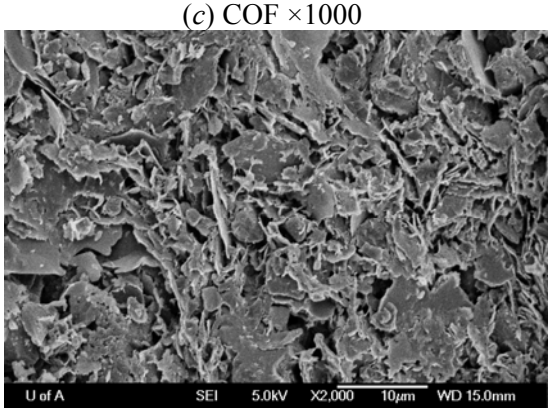

(*e*) COF ×2000

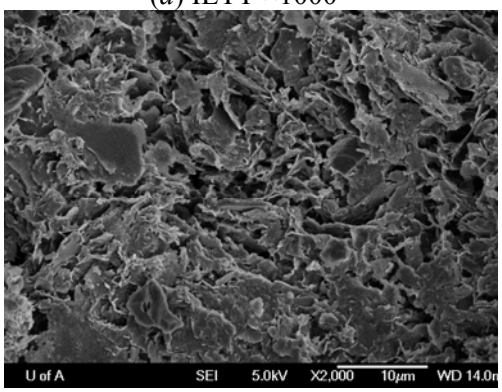

(*f*) ILTT ×2000

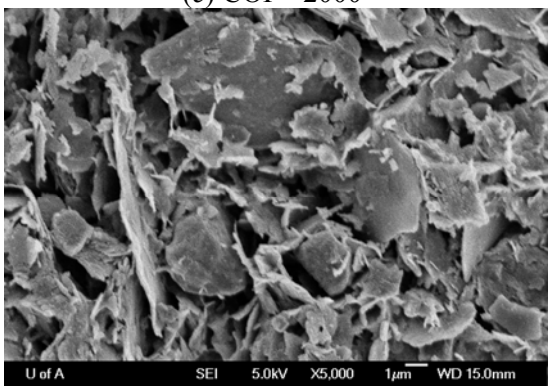

(*g*) COF ×5000

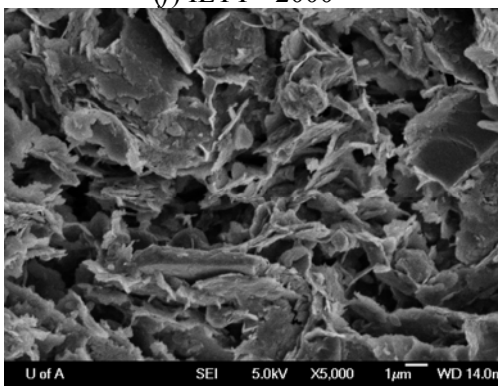

(*h*) ILTT ×5000

Figure 7.15 Scanning electron microscope images of cyclone overflow (70%S, e=1.06) and in-line thickened tailings (68%S, e=1.15)

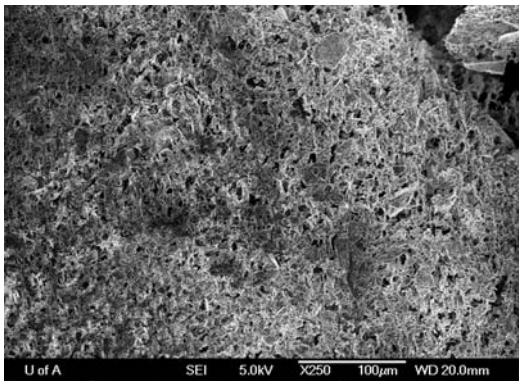

(*a*) Sheared ILTT ×250

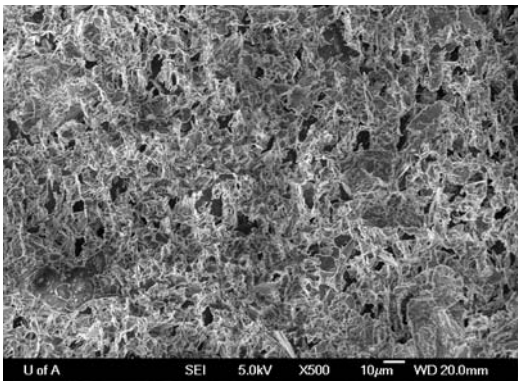

(*b*) Sheared ILTT ×500

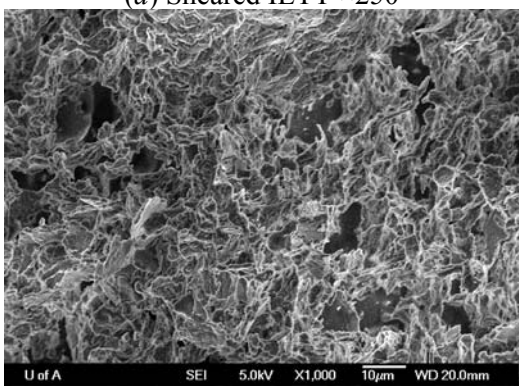

(*c*) Sheared ILTT ×1000

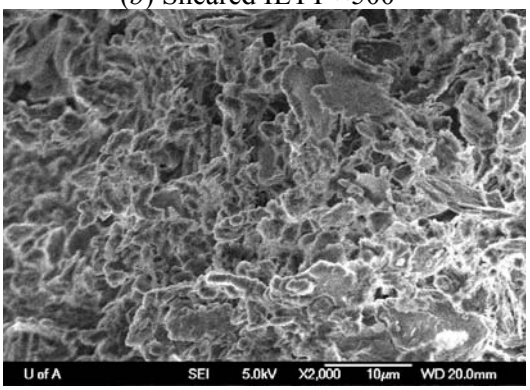

(*d*) Sheared ILTT ×2000

Figure 7.16 Scanning electron microscope images of sheared ILTT at 24% solids content and CT made from thickened tailings (55%S, 20%F)

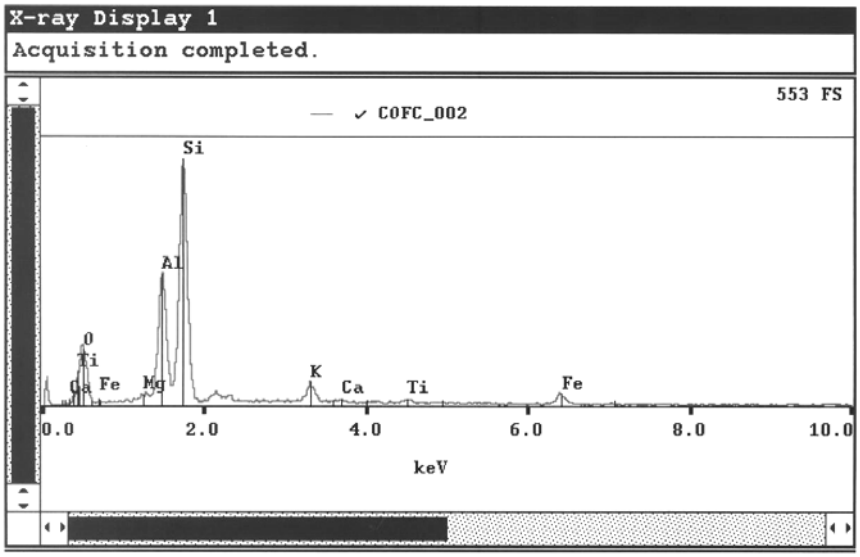

Figure 7.17 Energy dispersive X-ray analysis on cyclone overflow

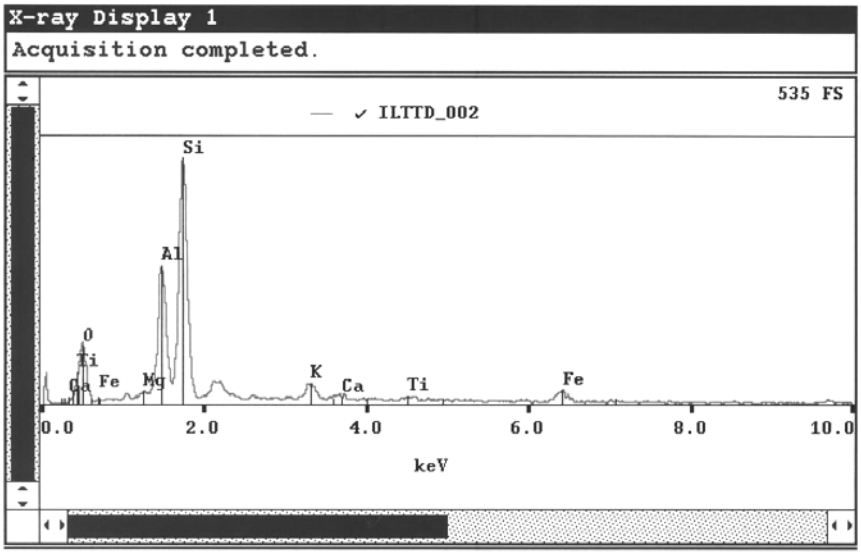

Figure 7.18 Energy dispersive X-ray analysis on in-line thickened tailings

7.4 Water chemistry

To document release water chemistry of cyclone overflow and in-line thickened tailings throughout the test program, pore fluid samples were collected by decanting supernatant fluid from various tests into 60 mL sample containers. The pore fluid samples were submitted for analytical testing to the Applied Environmental Geochemistry Research Facility at the University of Alberta. Major cations and anions in the pore fluid samples were quantified using a Dionex IC-2000 ion chromatography system. Results of water chemistry measurements for all samples are shown in Table 7.3.

In Table 7.3, cyclone overflow tailings release water in this experimental program appears to contain high Na^+ ion of about 750 mg/L. This value is relatively much larger than 258 mg/L of Na^+ ions measured in the 1982 mature fine tailings release water. Other cations such as K^+ and Ca^{2+} are also higher than that measured in the 1982 mature fine tailings. The increase of cation concentrations in this cyclone overflow tailings could possibly result in a less dispersed condition as shown in the non-dispersed particle size distribution (Figure 7.7). According to Gouy-Chapman theory, the higher electrolyte concentration in the cyclone overflow can cause a double layer to compress. The compressed double layer may allow particles to come closer and form a group of particles resulting in the smaller measured clay-size particles.

Comparison between the cyclone overflow and in-line thickened tailings water chemistry in Table 7.3 indicates that both tailings do not show significant difference in measured cations. Since the additions of the chemical flocculant and coagulant do not significantly change cation concentrations in the system, exchangeable sodium ratio (ESR) will be similar and are calculated for cyclone overflow and in-line thickened tailings to be 0.66 and 0.69 respectively. At ESR values of 0.1 or more, sodium ions will occupy adsorption sites on the clay resulting in a high potential for dispersion (Dawson et al., 1999). SAR values higher than 20 (ESR of 0.3) are likely to be in a dispersed state for oil sands fine tailings and SAR values greater than 40 (ESR of 0.6) will be in a completely dispersed state (Miller et al., 2010). In this experimental program, the calculated ESR values indicate that both materials are likely to be in a dispersed state. This statement agrees with the SEM images of the cyclone overflow tailings but not the in-line thickened tailings suggesting that the mode of particle association is more

complex and ESR can not be used to correlate to a mode of particle association for in-line thickened tailings.

Even though it is beyond the scope of this thesis, it is of interest to partially investigate if the chemical polymers used in the in-line thickening process remain in the release water. Non-dispersed particle size distribution analysis was selected for this investigation as this test can be used as a comparative indication of influence of water chemistry on tailings particle association such as shown by Miller et al. (2010). Cyclone overflow release water, freshly released in-line thickened tailings water and 180 day old released in-line thickened tailings water were used to mix with a standard kaolin powder (Acros organics kaolin code: 211740010). Dispersed particle size analysis was also performed to obtain a fully dispersed condition and all results of the particle size analysis are shown in Figure 7.19.

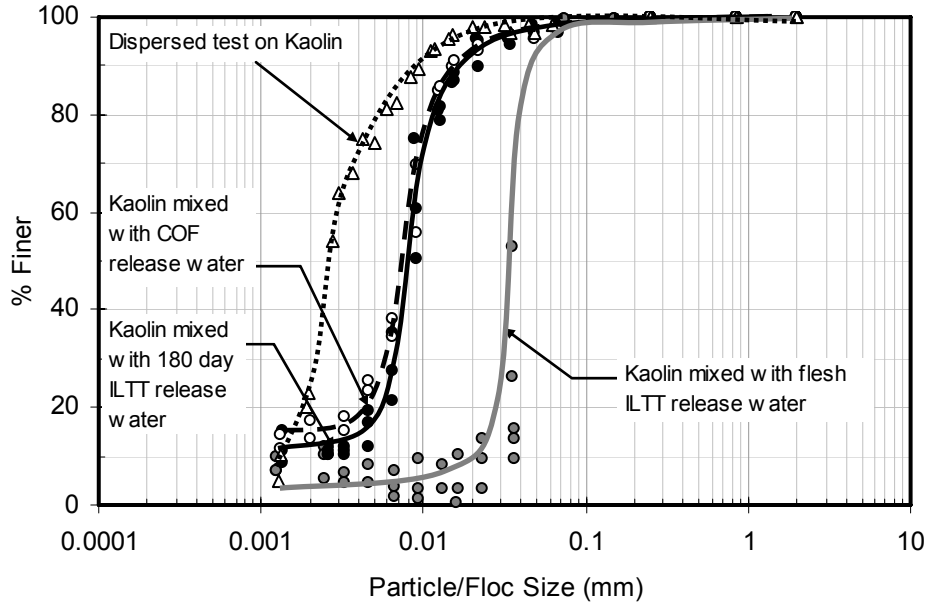

Figure 7.19 Particle size distribution of kaolinite by dispersed test and non-dispersed test with ILTT release water and COF release water

Overall it can be seen that the non-dispersed particle size distribution of the cyclone overflow and in-line thickened tailings release water with high ionic concentrations show much smaller clay size particles when compared to the dispersed test. This result is supported by the double layer theory.

Particle size distributions of cyclone overflow release water and the 180 day old in-line thickened tailings release water are similar showing percent dispersion (D_f) of 70% and 64% respectively. This suggests that residual polymers remaining in the 180 day old release water is small and does not significantly flocculate kaolinite particles in the suspension when compared to the cyclone overflow water. The fleshly released in-line thickened tailings water however shows significantly lower measured clay size particles with percent dispersion of 16%. This significantly lower percent dispersion of the kaolinite mixed with fleshly released in-line thickened tailings water suggests that there are some residual polymers existing in the release water. From this test data, it is reasonable to hypothesize that the existence and influence of the remaining chemical polymer from the in-line thickening process disappears from the release supernatant water with time.

Table 7.3 Water chemistry

Samples	pH	Conductivity (µs/cm)	Cations (mg/L)						Anions (mg/L)				
			Na^+	K^+	Mg^{2+}	Ca^{2+}	NH^{4+}	Li^+	Br^-	NO^{3-}	F^-	Cl^-	SO_4^{2-}
COF RCW	8.2	3630	760.5	13.3	7.2	8.9	0.0	0.2	0.2	29.9	2.6	626.8	472.6
COF HS, SP1, 3.2%S	8.2	3600	807.6	14.9	9.2	15.3	0.0	0.2	0.2	0.1	2.3	634.0	486.7
COF HS, SP2, 4.9%S	7.4	3600	801.4	13.8	7.8	10.1	0.0	0.2	0.0	3.3	2.7	634.8	491.5
ILTT HS 3%S	8.5	3440	768.9	13.3	6.5	8.6	5.5	0.2	0.2	28.6	2.9	617.3	468.9
ILTT HS, SP1 5%S	8.0	3140	755.4	13.5	6.6	8.8	6.5	0.2	0.2	28.2	2.9	608.6	463.0
ILTT HS 7.5%S	8.1	3340	732.0	13.3	6.1	8.4	7.1	0.2	0.2	20.3	2.9	588.3	441.4
ILTT HS 10%S	8.6	3290	755.4	14.3	7.0	10.2	7.2	0.2	0.0	33.9	2.9	607.1	461.4
ILTT HS 18.5%S	8.4	3390	759.3	13.4	6.5	9.0	5.5	0.2	0.2	23.9	2.9	608.4	462.3
ILTT-s HS, SP1 3%S (300rpm)	8.2	3410	776.9	12.9	7.1	9.7	0.0	0.2	0.2	36.0	2.7	614.9	464.6
ILTT-s HS, SP2 5%S (300rpm)	8.1	3360	753.6	12.8	6.5	8.8	0.0	0.2	0.2	31.5	2.7	600.3	449.0
ILTT-s HS, SP3 3%S (1080rpm)	8.7	3560	747.2	13.5	6.6	8.7	0.0	0.2	0.1	36.9	2.7	616.1	470.2
ILTT-s HS, SP4 5%S (1080rpm)	8.6	3370	718.7	13.1	6.2	8.2	4.1	0.2	0.2	31.6	2.8	595.9	450.0
ILTT HS, SP2 5%S	8.3	3290	712.2	12.9	6.5	8.7	5.4	0.2	0.0	33.6	2.7	604.9	453.8
ILTT HS, SP3 5%S	8.7	3130	730.2	12.3	6.8	9.9	0.0	0.2	0.1	31.9	2.6	579.6	433.0
COF LSC1	8.4	3560	-	-	-	-	-	-	-	-	-	-	-
COF LSC2	8.4	3600	-	-	-	-	-	-	-	-	-	-	-
ILTT LSC1	8.2	3340	754.0	12.9	6.5	8.5	7.6	0.2	0.2	32.5	2.6	603.1	446.8
ILTT LSC2	8.1	3410	744.2	12.6	6.3	8.1	7.5	0.2	0.2	31.5	2.5	597.5	441.1
ILTT-s LSC1	9.0	3990	776.3	17.1	7.5	10.1	6.5	0.2	0.3	8.8	3.0	648.1	463.3
ILTT-s LSC2	8.9	3980	778.3	14.0	7.9	7.7	0.0	0.2	0.2	9.3	2.7	633.5	437.0

HS- hindered sedimentation test, SP-standpipe test, LSC-Large strain consolidation test

7.5 Hindered sedimentation test

To obtain hydraulic conductivity at higher void ratios than that possible in a large strain consolidation tests, Pane and Schiffman (1997) proposed that a hindered sedimentation test can be used to obtain the material's hydraulic conductivity. The slope of the initial linear portion of the interface settlement from each hindered sedimentation test is used to calculated hydraulic conductivity corresponding to the initial void ratio via Equation 7.6 (Been, 1980; Pane and Schiffman, 1997).

$$k = v_{si}(1+e_0)\gamma_w / (\gamma_s - \gamma_w) \qquad [7.6]$$

Where v_{si} is initial settling velocity, γ_s is unit weight of solids, γ_w is unit weight of water, k is hydraulic conductivity and e_0 is an initial void ratio.

Similarly to Equation 7.6, a non linear part of the settlement curve may also be used to obtain hydraulic conductivity via Kynch theory (Tan et al., 1990). A surface void ratio is required and can be calculated from Equation 7.7.

$$e = \frac{(1+e_0)(h+v_{sp}t)}{H} - 1 \qquad [7.7]$$

Where e is a surface void ratio, e_0 is initial void ratio, h is height at an interest point, v_{sp} is a tangential velocity at an interest point and H is initial height.

With a known surface void ratio, hydraulic conductivity during a non linear part of the settlement curve can be calculated from Equation 7.8.

$$k = v_s(1+e)\gamma_w / (\gamma_s - \gamma_w) \qquad [7.8]$$

Where v_s is settling velocity

It is noted that the use of Equations 7.6 and 7.8 is widely accepted when slurry is undergoing hindered sedimentation but it is generally believed that during consolidation

this method can not be used. Pane and Schiffman (1997) stated that this equation is valid only when there is a suspension at the initial void ratio at the sediment water interface or as long as the settling velocity is constant. Toorman (1999) indicated that the initial settling rate of self-weight consolidation can also be used to estimate hydraulic conductivity where diffusive effects are negligible. Due to the fact that the influence of consolidation is not included in both equations and diffusion can not be monitored by the current laboratory set up, this technique was applied only on the early portion of the nonlinear settling curve in this study.

7.5.1 Cyclone overflow tailings

A total of five hindered sedimentation tests were performed for cyclone overflow tailings. Initial solids contents of 3.2, 4.9, 9.7, 14.7 and 23.5% (void ratios of 74.4, 47.7, 22.9, 14.3 and 8.0 respectively) were selected for the hindered sedimentation tests to cover large void ratios up to 80 (solids content of 3%) and to overlap results from the large strain consolidation tests at lower void ratios and higher effective stresses. Interface settlement measurements for the hindered sedimentation tests are shown in Figure 7.20.

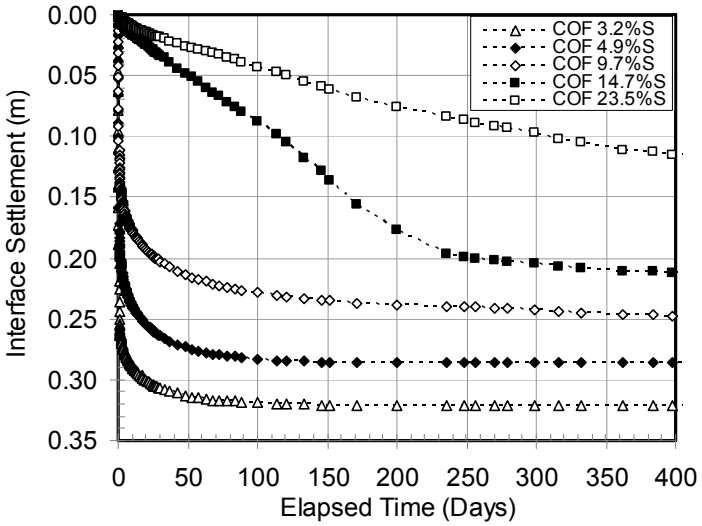

Figure 7.20 Hindered sedimentation tests for cyclone overflow

In order to obtain hydraulic conductivity data, initial settling velocities were calculated in Figure 7.21 and hydraulic conductivity was calculated from Equation 7.6. Non-linear parts of the interface settling data up to 90% total settlement were also used to obtain hydraulic conductivities via Equation 7.8 for tests at initial solids contents of 5%

and lower. Hydraulic conductivities of cyclone overflow obtained by the hindered sedimentation tests are shown in Figure 7.22.

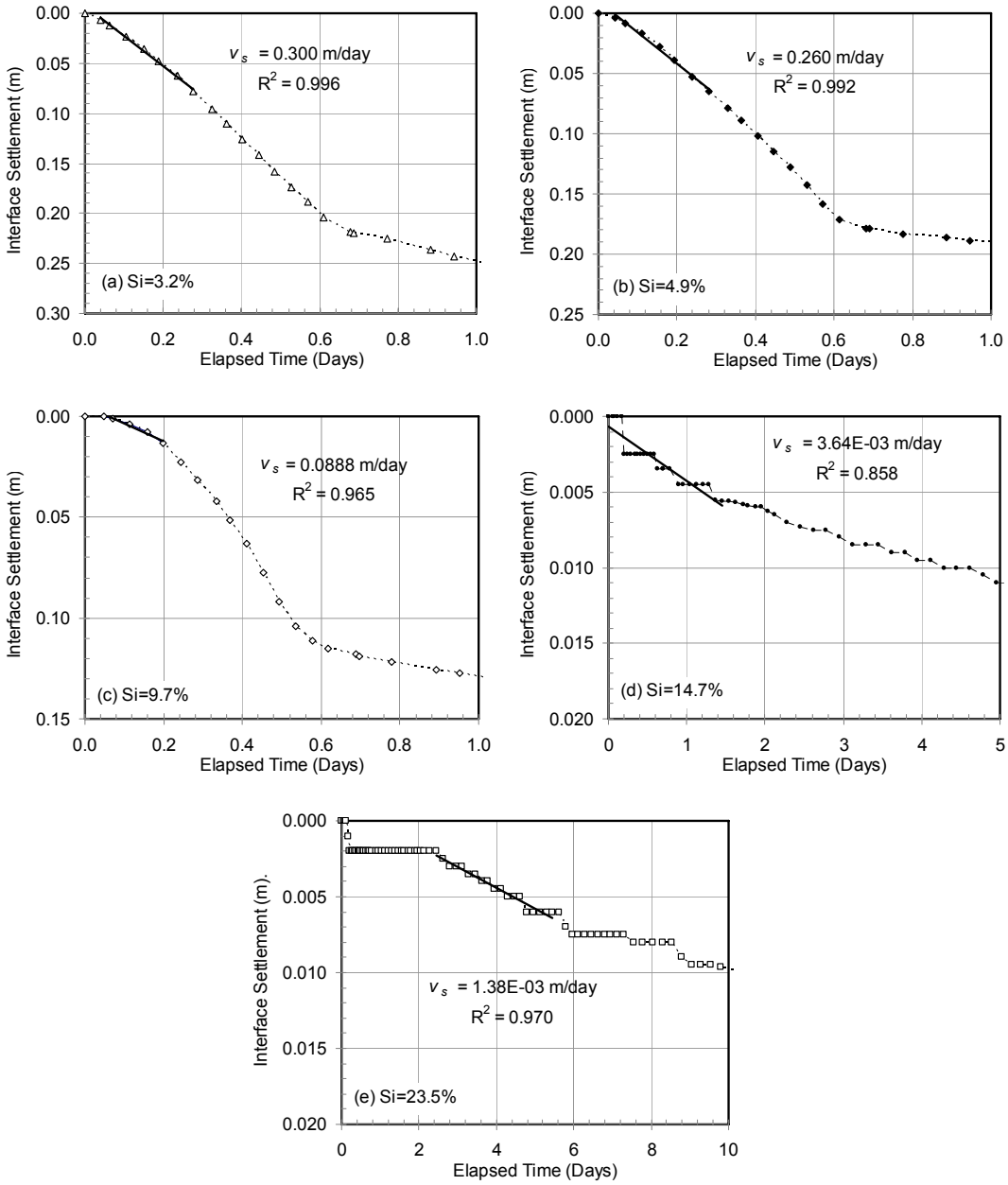

Figure 7.21 Initial settling velocities from hindered sedimentation tests on cyclone overflow tailings

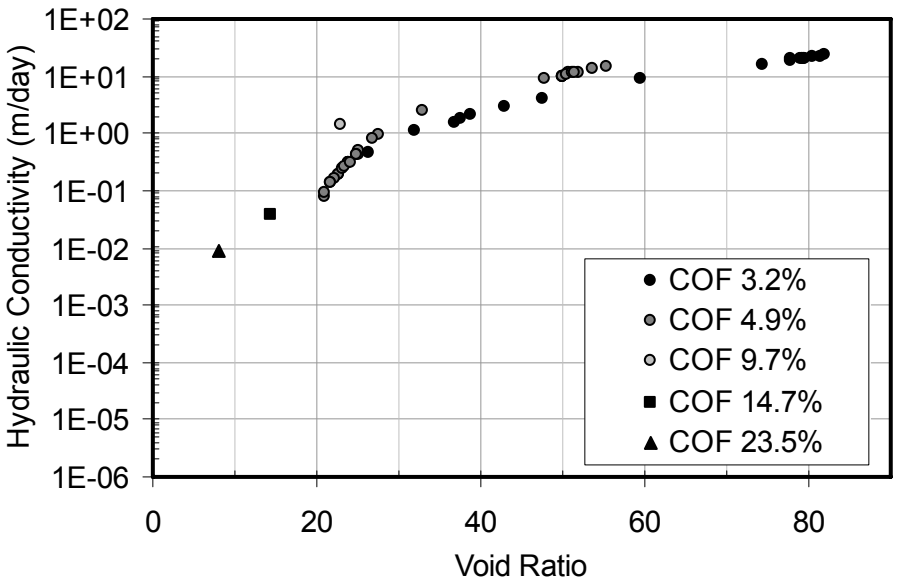

Figure 7.22 Hydraulic conductivity of cyclone overflow tailings from hindered sedimentation tests

7.5.2 Non-sheared in-line thickened tailings

A total of 14 hindered sedimentation tests were performed for ILTT at solids contents of 3, 5, 7.5, 10 and 18.5% (void ratios of 79.5, 46.7, 30.3, 22.1 and 10.8 respectively). It is noted that for higher solids contents than 5%, ILTT was prepared at 5% and was allowed to release water to the design solids content before the hindered sedimentation test was commenced.

Interface settlement results for ILTT are shown in Figure 7.23. It can be seen that the tailings settle very rapidly at all solids contents and complete most of the settlement in less than 20 minutes. Calculated interface settling rates for hydraulic conductivity calculation are shown in Figure 7.24 for all hindered sedimentation tests. Results of the hydraulic conductivity data of in-line thickened tailings obtained from the hindered sedimentation tests are shown in Figure 7.25.

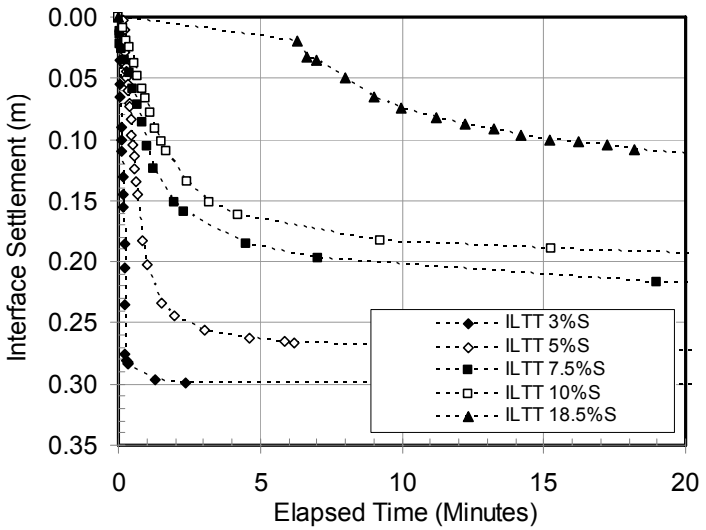

Figure 7.23 Hindered sedimentation tests for ILTT

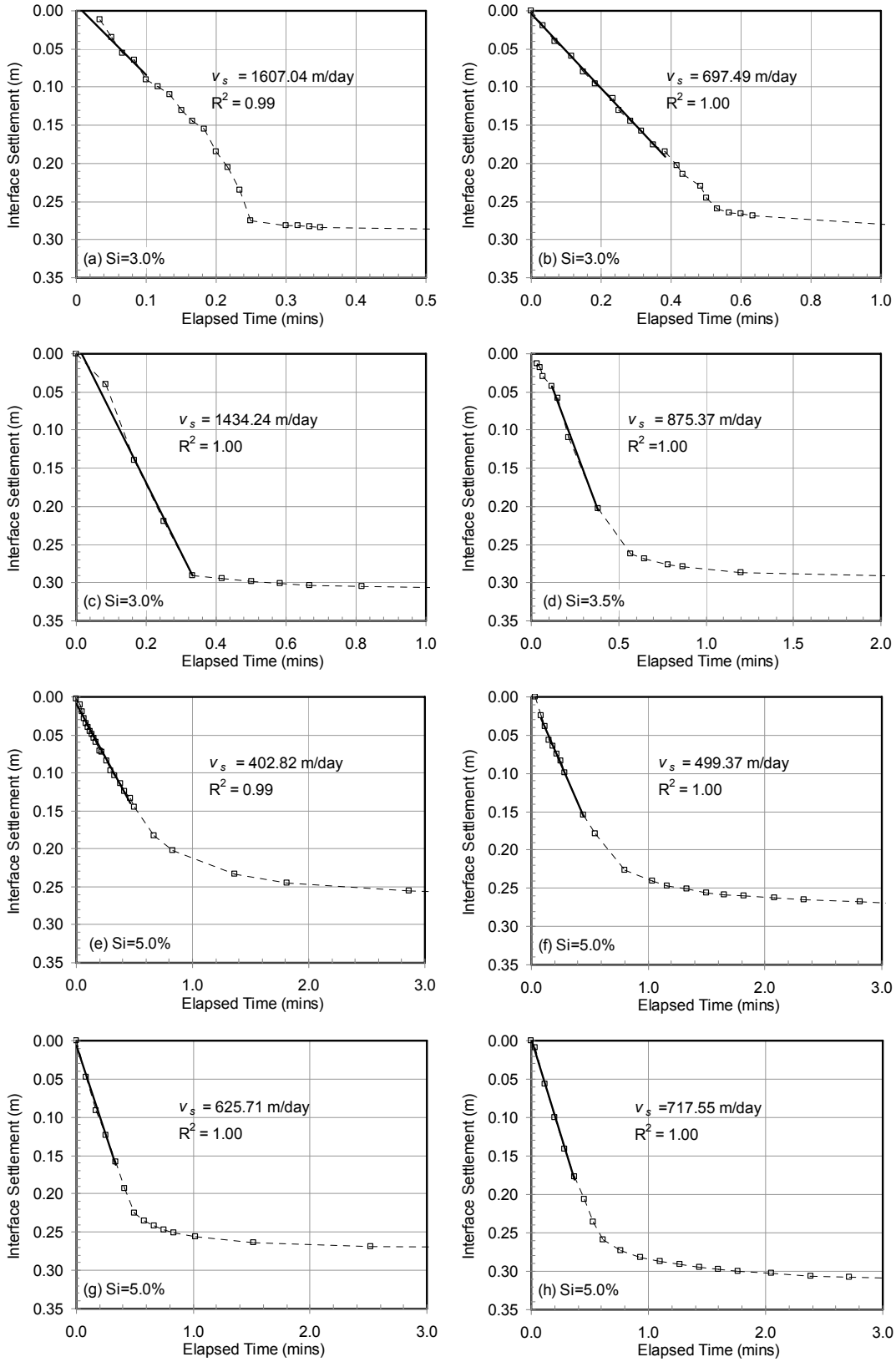

Figure 7.24 Initial settling velocities from hindered sedimentation tests on in-line thickened tailings

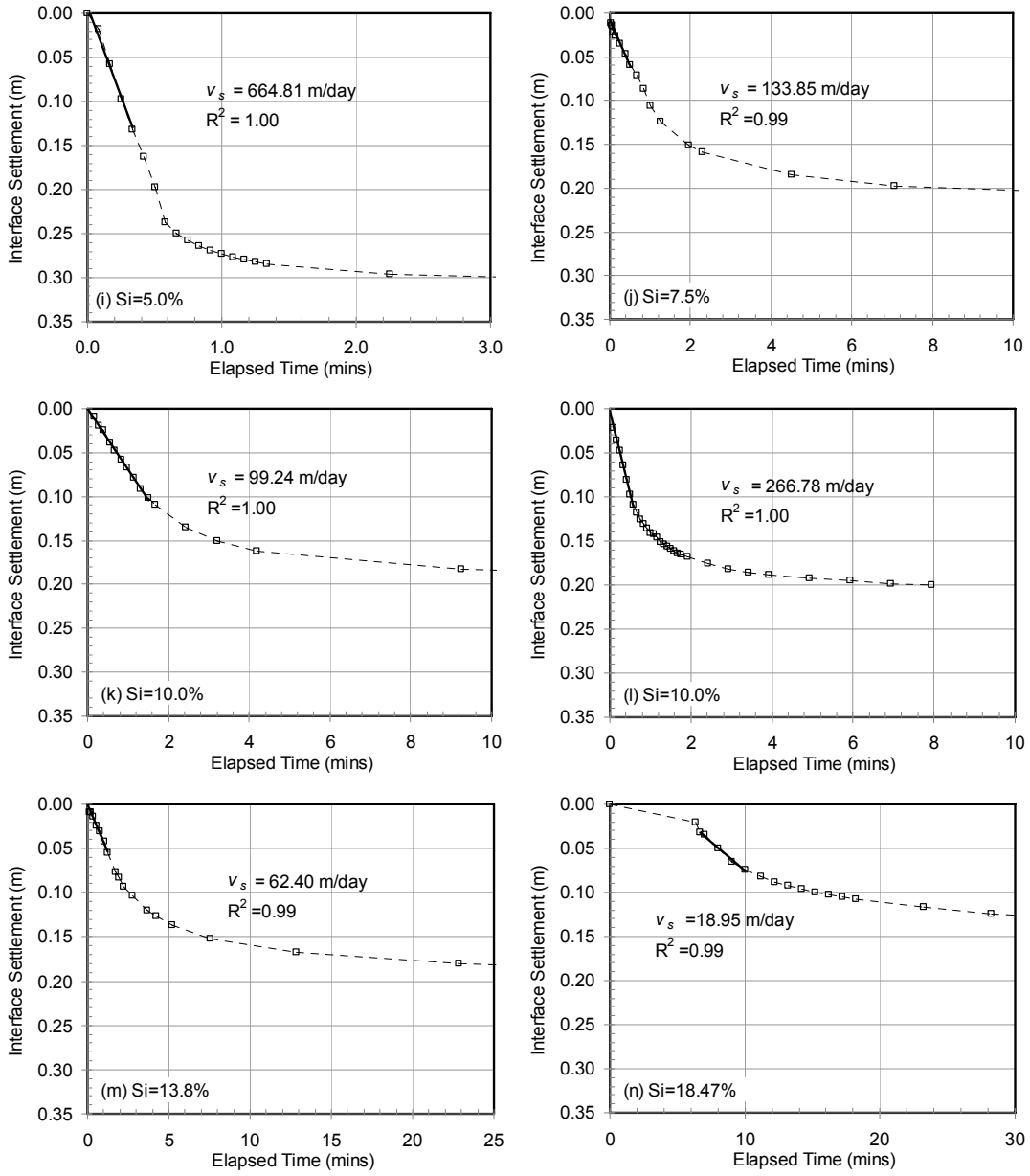

Figure 7.24 Initial settling velocities from hindered sedimentation tests on in-line thickened tailings (cont.)

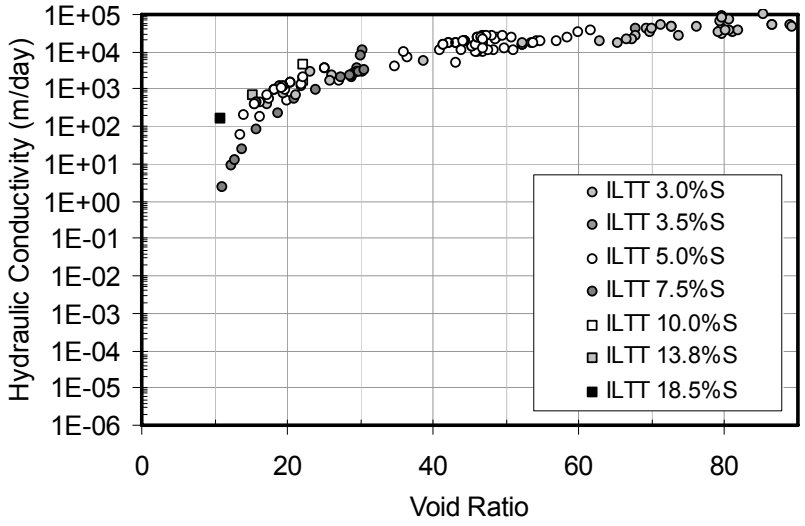

Figure 7.25 Hydraulic conductivity of in-line thickened tailings from hindered sedimentation tests

7.5.3 Sheared in-line thickened tailings

Five hindered sedimentation tests were performed for sheared in-line thickened tailings at solids contents of 3, 5 and 10% (void ratios of 79.5, 46.7 and 22.1 respectively). Three tests were performed by shearing in-line thickened tailings at 300 rpm for 24 minutes in the mixing chamber. And two tests were done at 1080 rpm for 24 minutes.

Interface settlement results for the sheared in-line thickened tailings are shown in Figure 7.26. Compared to the non-sheared in-line thickened tailings, sheared material settles significantly slower. A settling duration to complete most of the settlement is more than 200 minutes for the sheared ILTT while it takes less than 20 minutes for non-sheared material.

Calculated interface settling rates for hydraulic conductivity calculation are shown in Figure 7.27 for all five hindered sedimentation tests. Results of the hydraulic conductivity data of sheared in-line thickened tailings obtained from the hindered sedimentation tests are shown in Figure 7.28.

It can be observed in Figure 7.27 that at 300 rpm shearing, flocculation time is less compared to that of the 1080 rpm shearing. This also reflects on the hydrometer

particle size readings in Figure 7.12 showing more particles larger than 45 μm for the 1080 rpm case. Initial interface settling rates between 300 rpm and 1080 rpm shearing efforts in Figure 7.27 appear to be quite similar however hydraulic conductivities in Figure 7.28 reveal that at 1080 rpm sheared tailings is about two times less permeable than that of 300 rpm sheared tailings. The results from 1080 rpm shearing effort will be further combined with other test results also sheared at 1080 rpm to obtain sedimentation and consolidation characteristics of sheared ILTT.

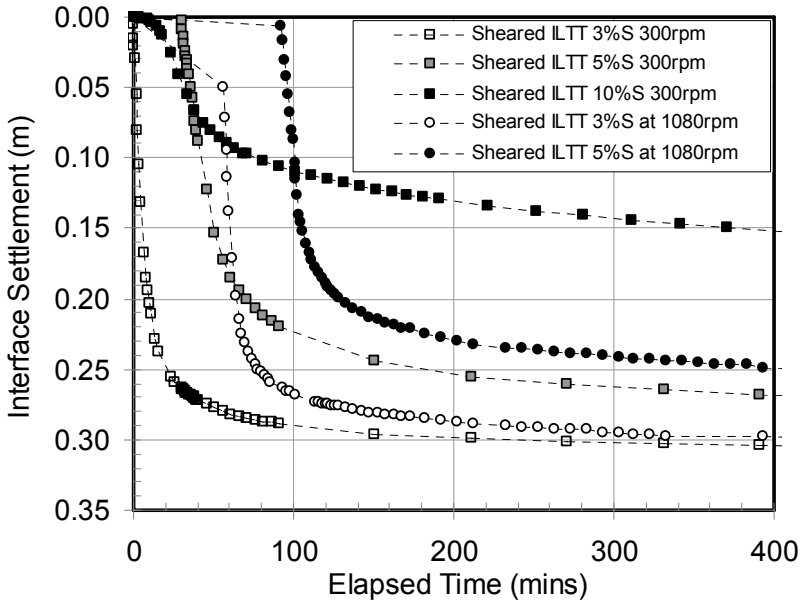

Figure 7.26 Hindered sedimentation tests for sheared in-line thickened tailings

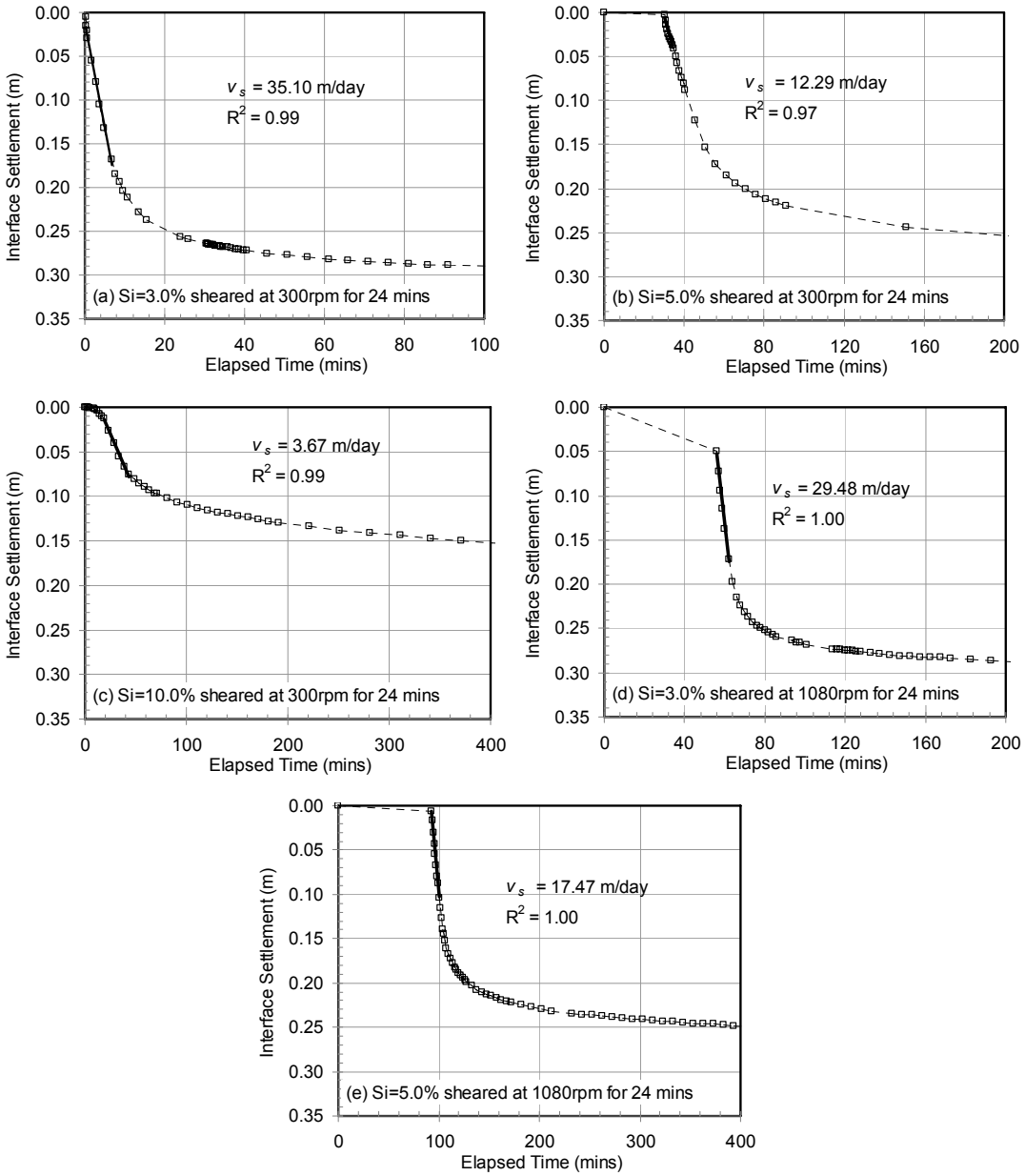

Figure 7.27 Initial settling velocities from hindered sedimentation tests on sheared in-line thickened tailings

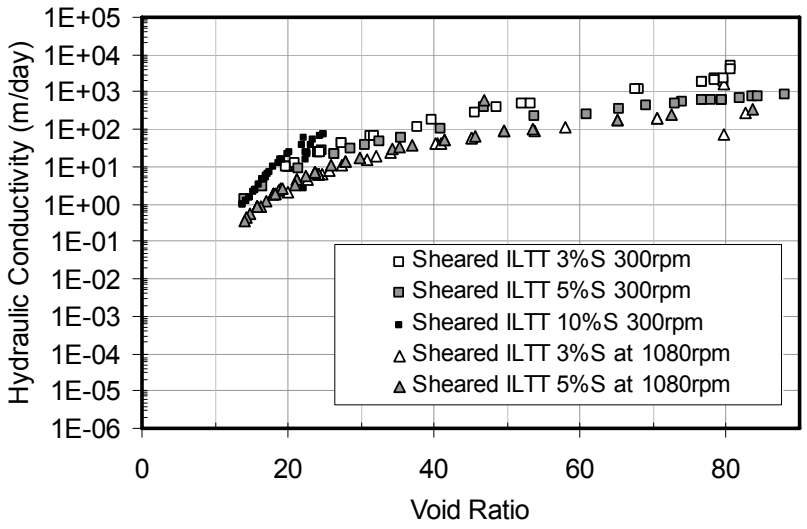

Figure 7.28 Hydraulic conductivity of sheared in-line thickened tailings from hindered sedimentation tests

7.6 Compressibility standpipe test

To determine the effective stress-void ratio relationship at very low effective stresses, a large diameter standpipe is filled with tailings, allowed to consolidate under self-weight. The consolidation process is monitored by a pore pressure transducer at the base and when consolidation is complete, the tailings is sampled in layers to determine the effective stress and void ratio with depth. The compressibility standpipe test is shown in Figure 7.29. Alternatively, compressibility at low effective stresses can also be obtained from a hindered sedimentation test with a similar procedure but instead of monitoring excess pore pressure, interface settlement is used as an indication of when the consolidation process is complete.

Figure 7.29 Compressibility standpipe tests

7.6.1 Cyclone overflow tailings

For cyclone overflow tailings, five 36 cm high and 6.5 cm diameter compressibility standpipe tests were performed after hindered sedimentation tests at initial solids contents of 3.2%, 4.9%, 9.7%, 14.7% and 23.5% (void ratio of 74.4, 47.7, 22.9, 14.3 and 8.0 respectively). One 25 cm high and 14 cm diameter compressibility standpipe test was also performed at 23.4% initial solids content (void ratio of 8.1). It is noted that in the small solids content standpipes, segregation could be of concern but the fine cyclone overflow material is a well graded material containing very little sand and therefore is not susceptible to segregation. Void ratio profiles and effective stress profiles obtained from the tests are shown in Figure 7.30. With known void ratios at corresponding effective stresses, compressibility can be obtained and the results are shown in Figure 7.31. It can be seen that with this particular experimental procedure, cyclone overflow's compressibility can be measured from void ratios of 16 to 4 which covers effective stresses from 6 to 600 Pa.

Interface settlement of the 14 cm diameter compressibility standpipe test was also monitored to obtain hydraulic conductivity through the hindered sedimentation test calculation. The interface settlement of the standpipe test is shown in Figure 7.32. Based on the initial settling velocity of 4.37×10^{-4} m/day at an initial void ratio of 8.1, hydraulic conductivity of 2.71×10^{-3} m/day was obtained.

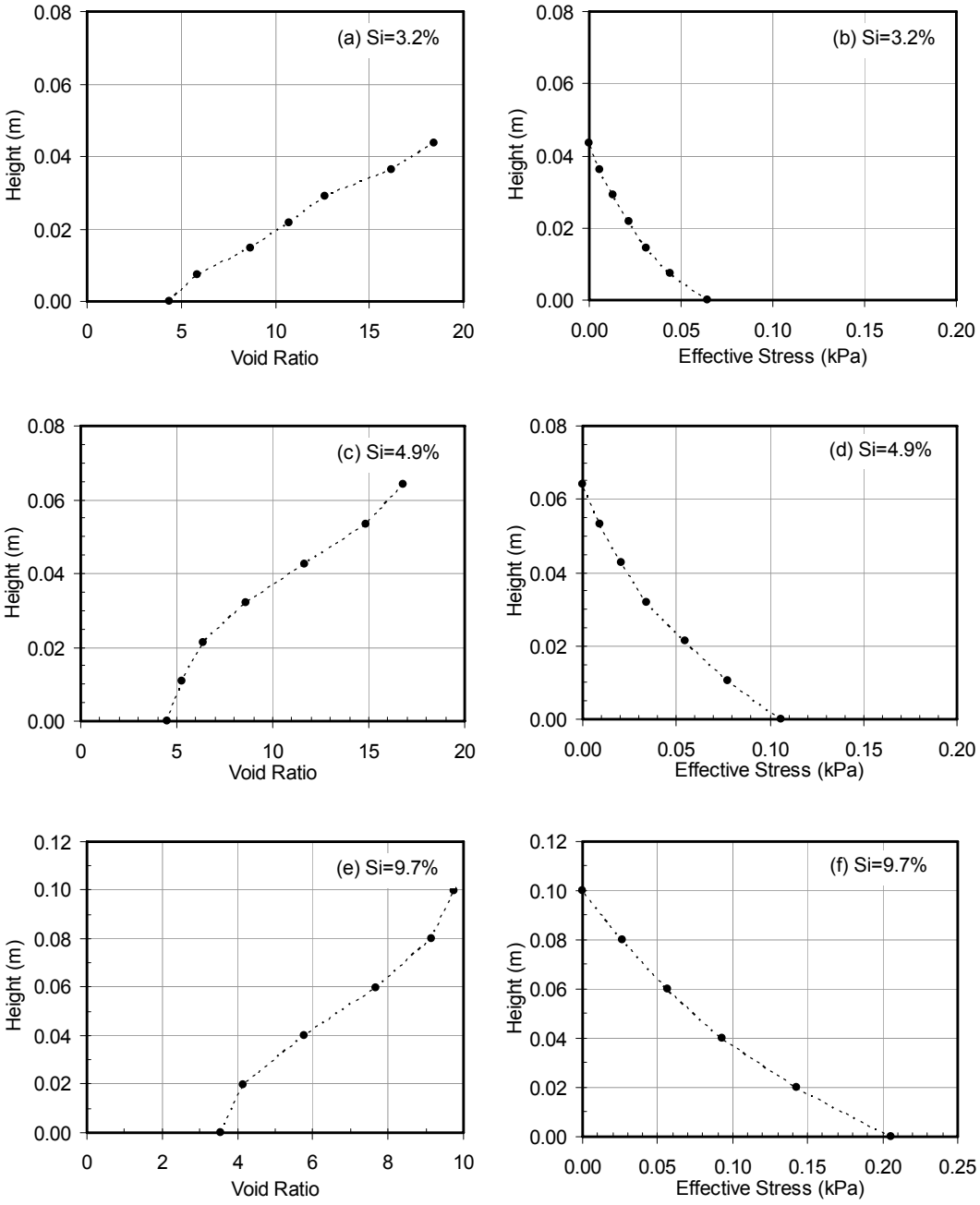

Figure 7.30 Effective stress profiles and void ratio profiles from compressibility standpipe tests on cyclone overflow tailings

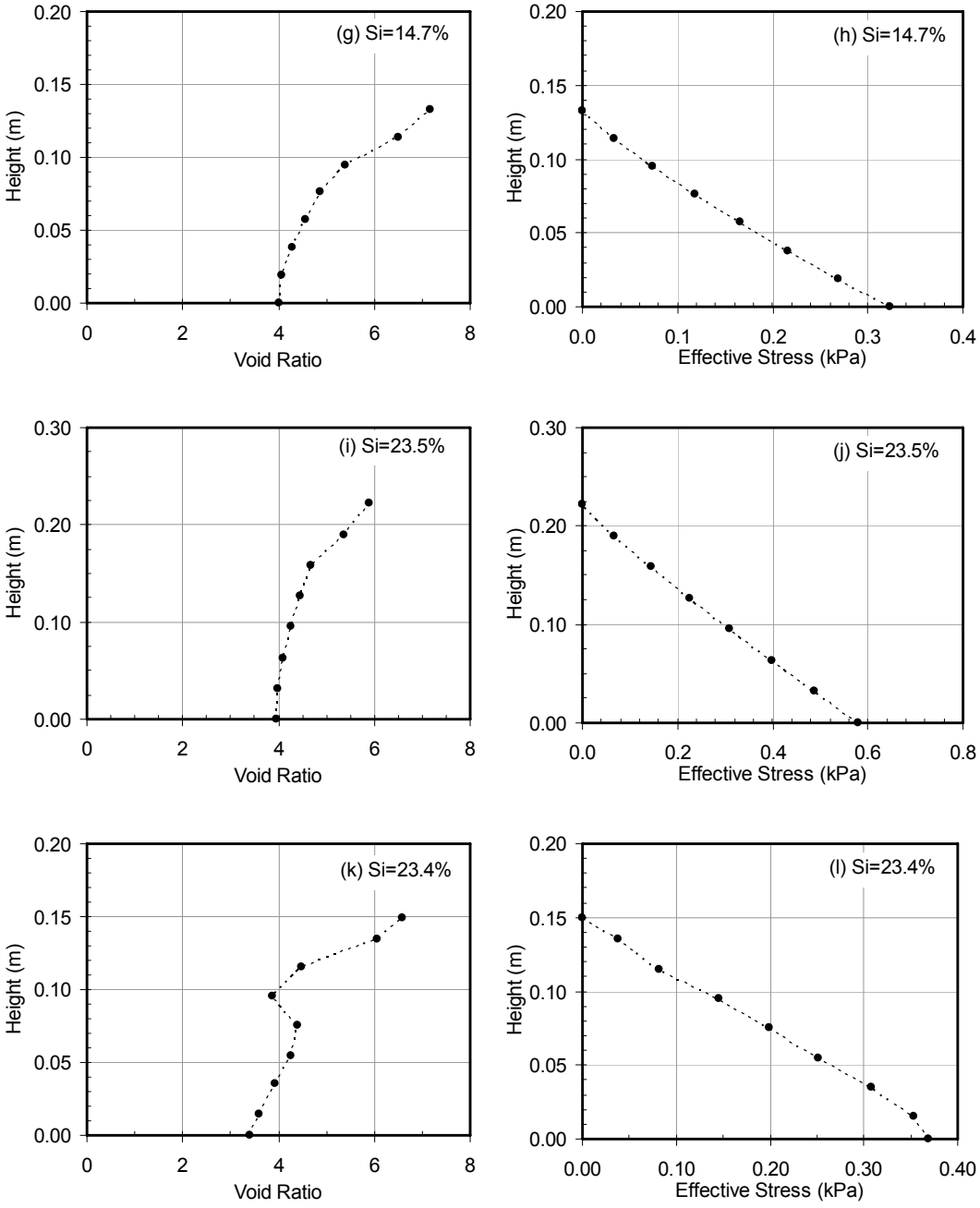

Figure 7.30 Effective stress profiles and void ratio profiles from compressibility standpipe tests on cyclone overflow tailings (Cont.)

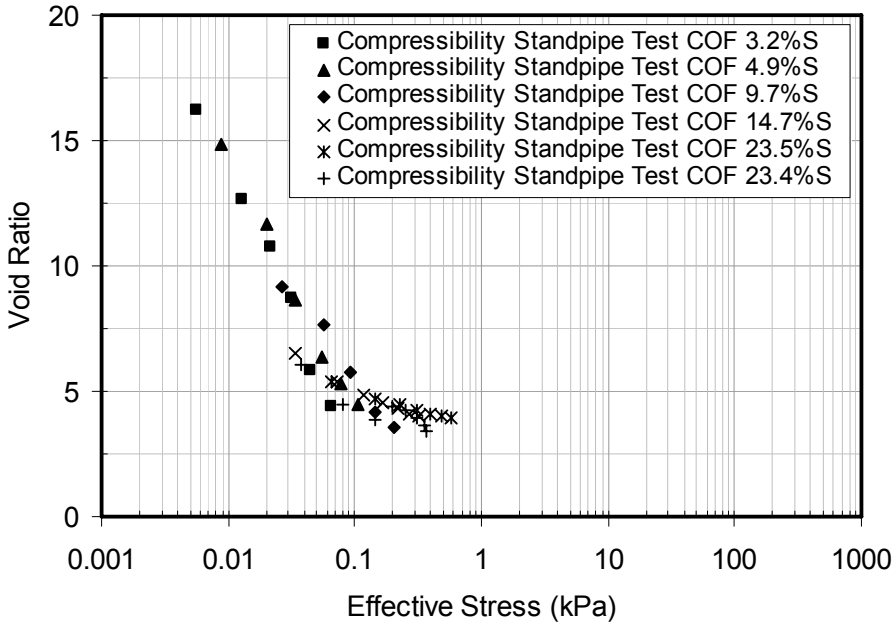

Figure 7.31 Compressibility of cyclone overflow from compressibility standpipe tests

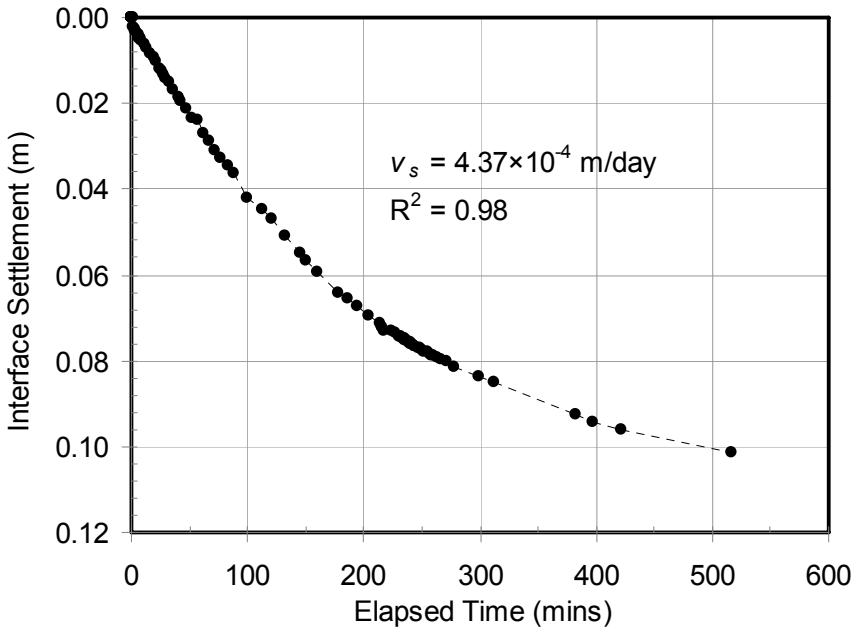

Figure 7.32 Initial settling velocity of cyclone overflow tailings in 25 cm compressibility standpipe test

7.6.2 Non-sheared in-line thickened tailings

Three compressibility standpipe tests for ILTT were performed at an initial solids content of 5% in 36 cm and 120 cm high standpipes. Data from the standpipes are shown in Figure 7.33. The 120 cm high standpipes test was performed to reach an effective stress of about 350 Pa. This height was chosen to provide an ample overlap of effective stress measurements with a large strain consolidation test which can measure effective stress as low as 100 Pa.

Compressibility of the in-line thickened tailings from the compressibility standpipe tests is shown in Figure 7.34. With this particular experimental procedure, in-line thickened tailings's compressibility can be measured from void ratios of 17 to 5 which covers effective stresses from 8 to 350 Pa.

Interface settlement of the 120 cm compressibility standpipe test was also monitored to obtain hydraulic conductivity through the hindered sedimentation test calculation. The interface settlement of the standpipe test is shown in Figure 7.35 and the hydraulic conductivity obtained from this test is shown in Figure 7.36.

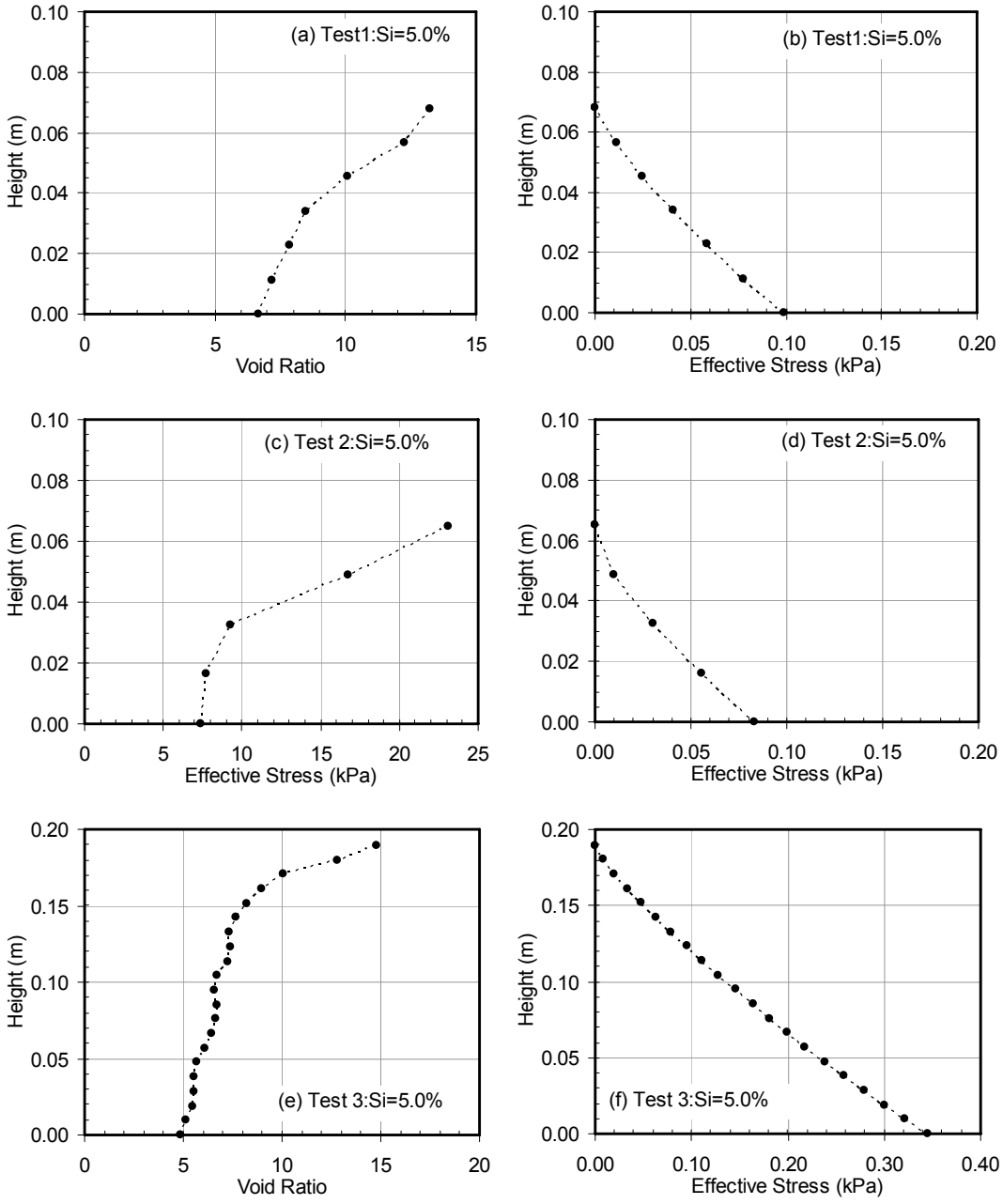

Figure 7.33 Effective stress profiles and void ratio profiles from compressibility standpipe tests on in-line thickened tailings

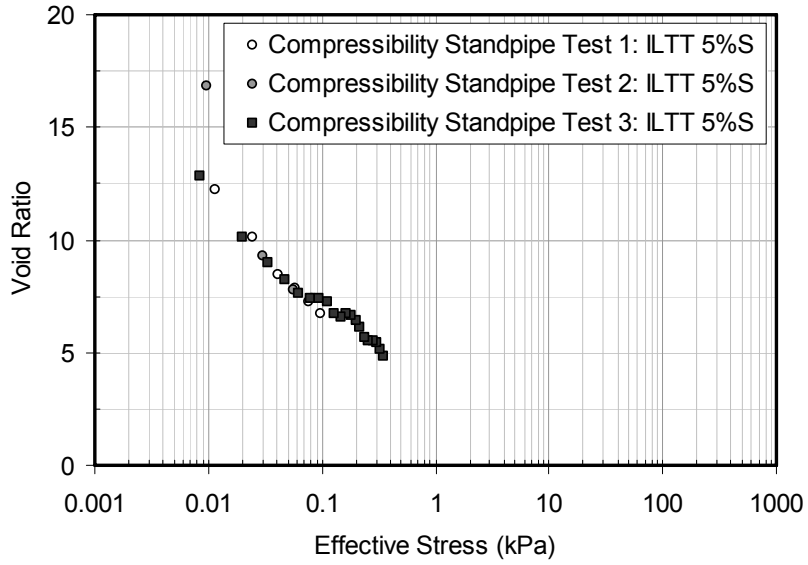

Figure 7.34 Compressibility of in-line thickened tailings from compressibility standpipe tests

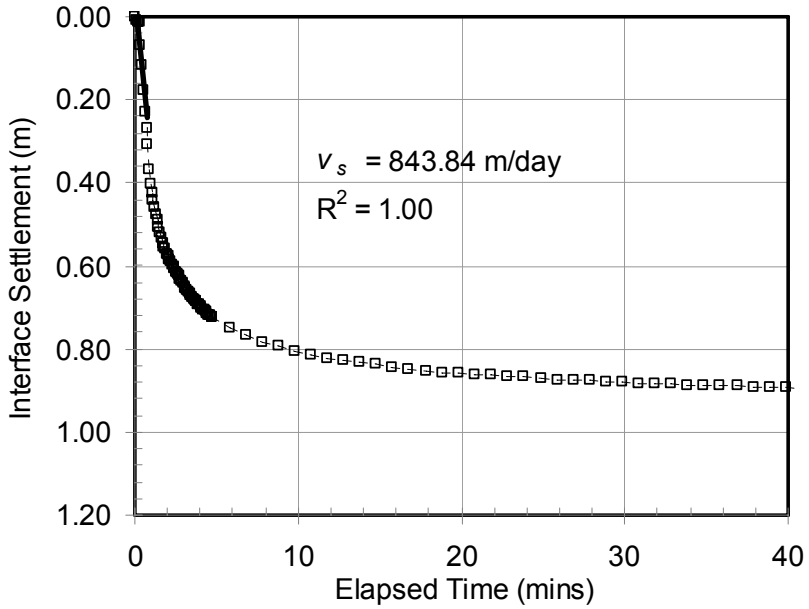

Figure 7.35 Initial settling velocity of in-line thickened tailings in 120cm compressibility standpipe test

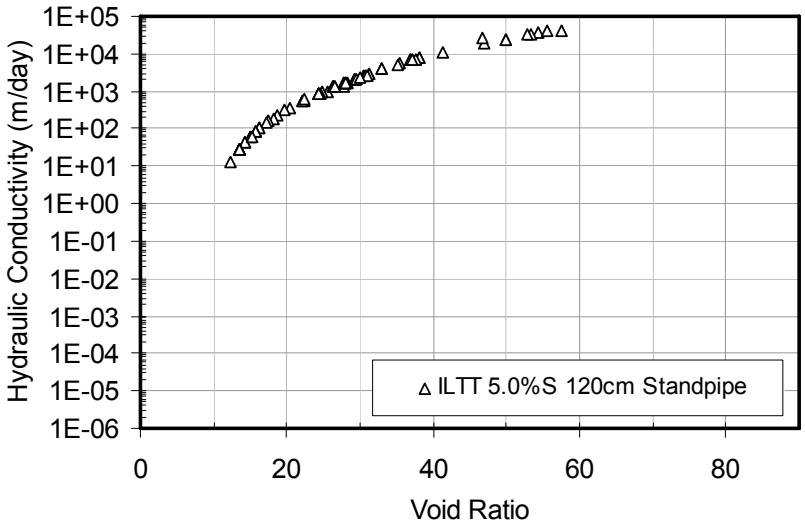

Figure 7.36 Hydraulic conductivity of in-line thickened tailings from compressibility standpipe test

7.6.3 Sheared in-line thickened tailings

Four compressibility standpipe tests for sheared in-line thickened tailings were performed at initial solids contents of 3% and 5% and shearing efforts of 300 rpm and 1080 rpm in 36 cm high standpipes. Void ratio and effective stress profiles for these tests are shown in Figure 7.37. With known effective stresses at corresponding void ratios, compressibility of sheared in-line thickened tailings from the compressibility standpipe tests are obtained in Figure 7.38.

In Figure 7.38, it can be seen that compressibility of the tailings is slightly influenced by the initial solids content; the lower initial solids content tends not to compress as much as the higher solids content at the same effective stresses. This behavior is typically found for slurry materials and is believed to be caused by different structures forming at different initial solids contents. The compressibility generally becomes unique at higher effective stresses when a distinct soil structure is formed. The test results on the 3% and 5% initial solids contents of the 1080 rpm shearing effort will be further combined with other test results.

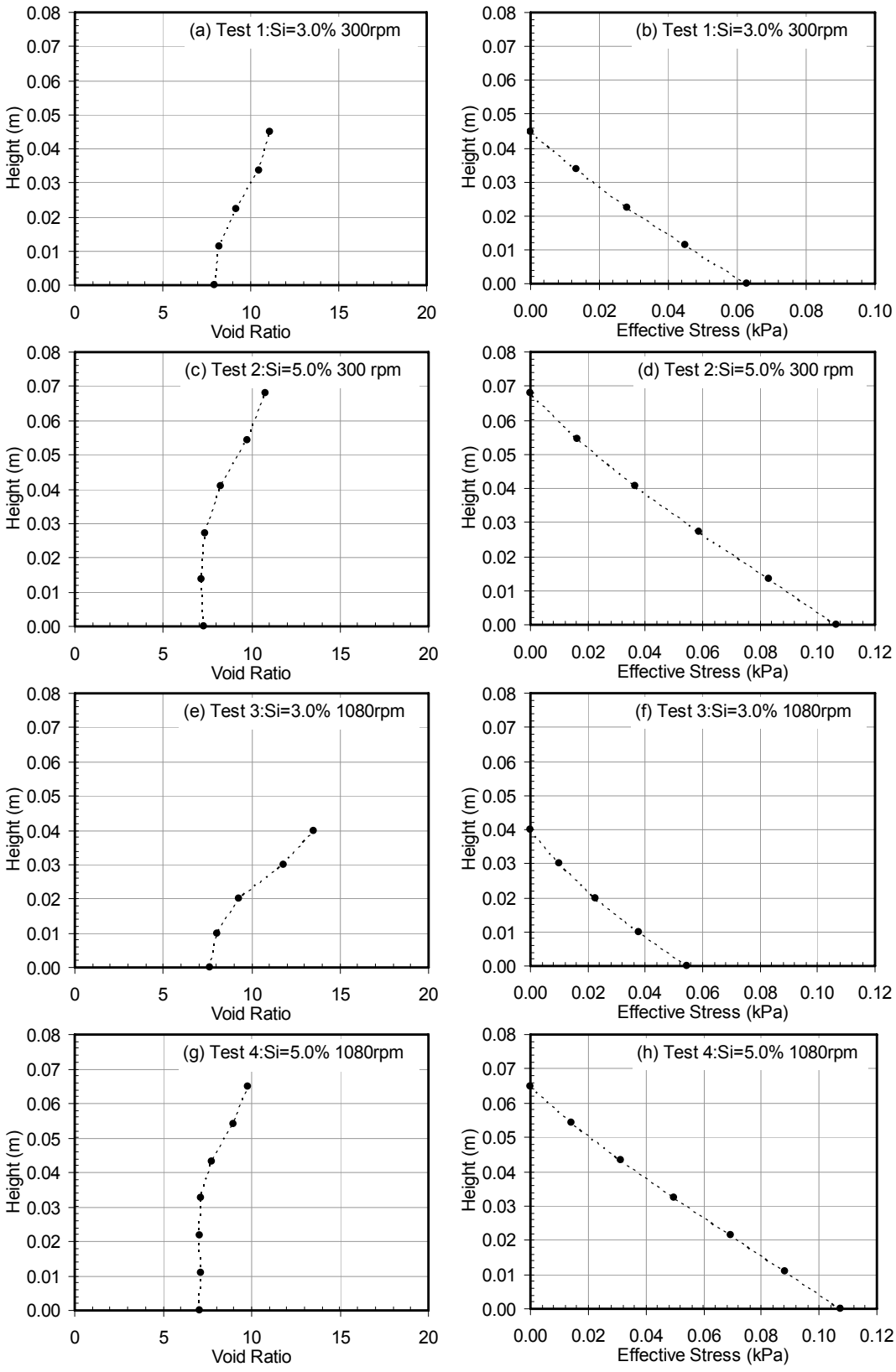

Figure 7.37 Effective stress profiles and void ratio profiles from compressibility standpipe tests on in-line thickened tailings

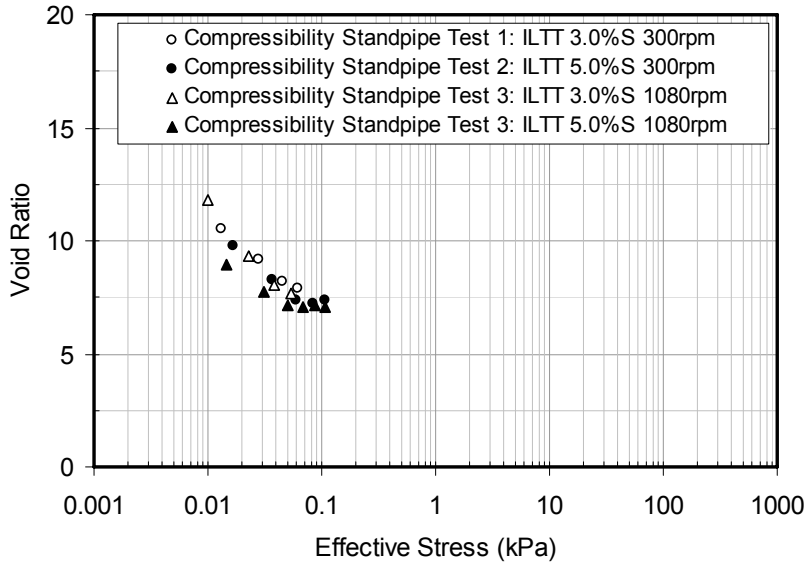

Figure 7.38 Compressibility of sheared in-line thickened tailings from compressibility standpipe tests

7.7 Large strain consolidation test with vane shear tests

A large strain consolidation test is a consolidation test that is performed on very soft soils or slurries that undergo large volume change during compression. The large reduction of void ratios during compression usually causes the material to experience large changes in material compressibility and hydraulic conductivity which are usually nonlinear. This also makes the use of the conventional Terzaghi consolidation theory to calculate hydraulic conductivity from volumetric strain-time measurements inaccurate. A conventional consolidation test is therefore inappropriate for slurry and a large strain consolidation test that can accommodate large volume changes and directly measure slurry compressibility and hydraulic conductivity is preferred.

A large strain consolidation test in this thesis refers to a multi-step loading type consolidation test (Figure 7.39). The large strain consolidation apparatus confines the test material so it can be tested at any water content. As large volume changes take place with very small stress changes at high water contents, the first applied stress, including self-weight of the slurry, is generally less than 1 kPa.

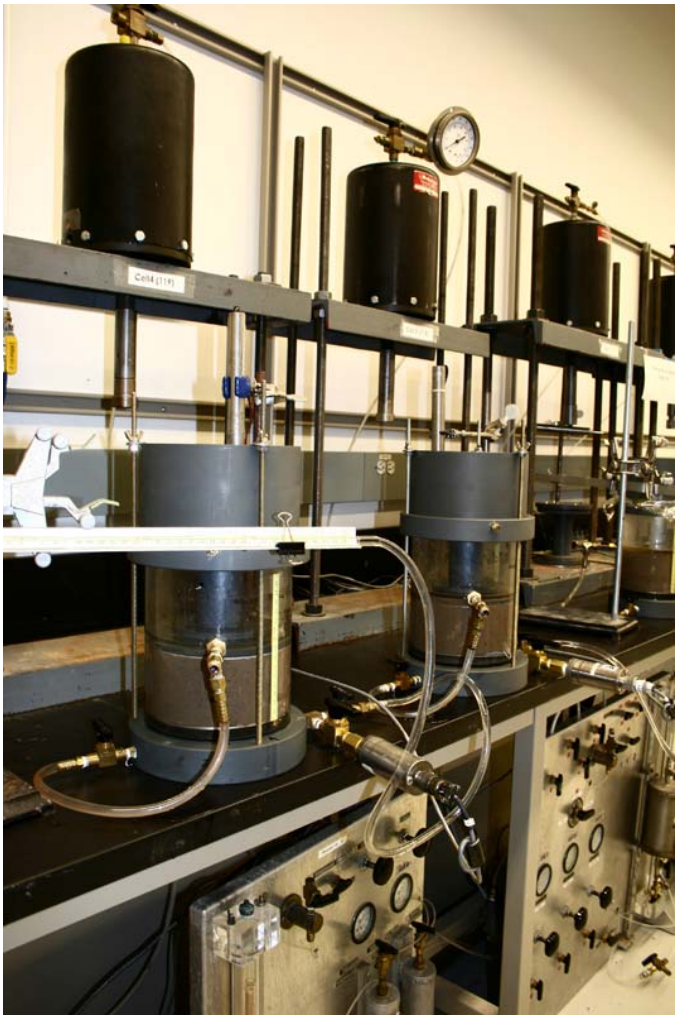

Figure 7.39 Multi-step loading large strain consolidation tests

The large strain consolidation cell has a 140 mm inside diameter and can accommodate samples up to 200 mm high. The initial height of the sample is chosen so that the diameter to height ratio is over 2:1 to minimize wall friction when vertical effective stresses become significant above 10 kPa. Hydraulic conductivity of the slurry is measured at the end of each loading step. A constant head hydraulic conductivity test with upward flow is performed with the hydraulic gradient being kept small enough so that seepage forces will not exceed the vertical stress and cause piping during the test. During the hydraulic conductivity test, the inflow is monitored until a steady state flow conditions is obtained where the hydraulic conductivity value is taken. After the hydraulic conductivity test is complete, a vane shear strength test is also performed at the end of each loading increment.

7.7.1 Cyclone overflow tailings obtained on 28th November 2005

Table 7.4 shows large strain consolidation test results on cyclone overflow tailings obtained on 28th November 2005. Initial solids content of the cyclone overflow was 30.9%. Figures 7.40, 7.41 and 7.42 show compressibility, hydraulic conductivity and undrained shear strength measurements respectively.

Table 7.4 Large strain consolidation test on COF obtained on 28 November 2005

Load	Height (mm)	ΔH (mm)	Effective stress (kPa)	Void ratio, *e*	Fines-bitumen void ratio, e_{fb}	Hydraulic Gradient, *i*	Hydraulic conductivity (m/day)	Undrained shear strength (kPa)
1	87.80	-	-	5.66	6.01	-	-	0.027
2	77.60	10.20	0.10	4.88	5.19	-	-	0.134
3	57.00	20.60	1.02	3.32	3.53	1.81	5.63E-04	0.44
4	48.00	9.00	2.49	2.64	2.80	3.27	2.39E-04	1.22
5	44.00	4.00	4.99	2.34	2.48	4.64	1.05E-04	2.41
6	39.80	4.20	9.99	2.02	2.14	7.06	6.59E-05	4.31
7	36.40	3.40	20.04	1.76	1.87	9.67	4.25E-05	8.43
8	33.00	3.40	39.35	1.50	1.60	12.42	2.47E-05	15.15
9	31.00	2.00	88.01	1.35	1.43	13.19	1.10E-05	31.90
10	29.00	2.00	187.44	1.20	1.27	16.55	7.01E-06	44.86
11	26.30	2.70	287.98	0.99	1.06	21.03	3.50E-06	-
12	26.80	-0.50	138.40	1.03	1.10	-	-	-
13	28.19	-1.39	38.22	1.14	1.21	-	-	-
14	32.26	-4.07	0.50	1.45	1.54	-	-	-

G_s = 2.53, Fines content = 93.9%

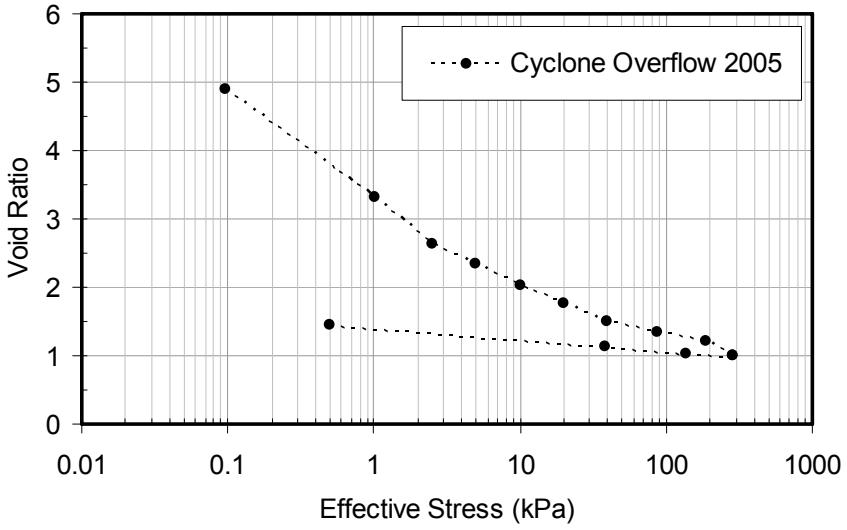

Figure 7.40 Compressibility of 2005 cyclone overflow from a large strain consolidation test

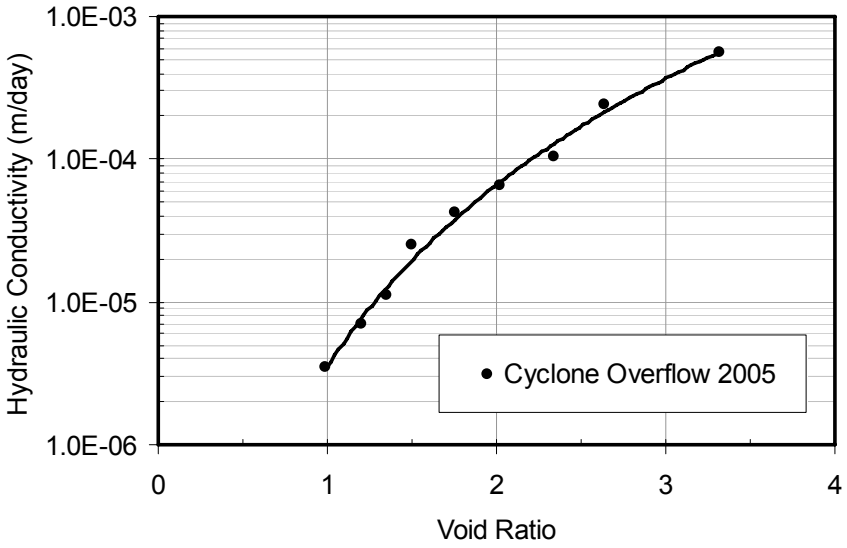

Figure 7.41 Hydraulic conductivity of 2005 cyclone overflow from a large strain consolidation test

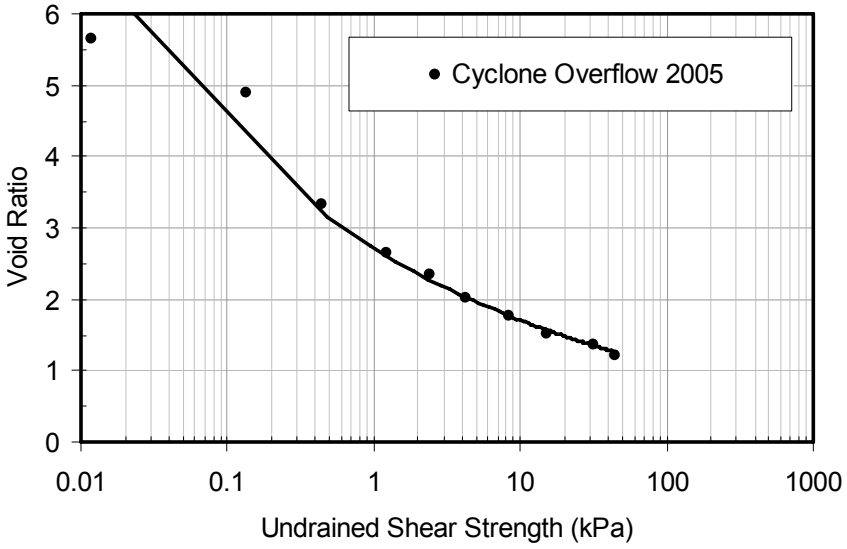

Figure 7.42 Undrained shear strength of 2005 cyclone overflow from a large strain consolidation test

7.7.2 East pond in-line thickened tailings obtained on 10th July 2006

Table 7.5 shows large strain consolidation test results on the east pilot pond in-line thickened tailings obtained on 10th July 2006. In this test, an initial solids content of the east pond ILTT was 35.5%. Figures 7.43, 7.44 and 7.45 show compressibility, hydraulic conductivity and undrained shear strength measurements of the tailings

respectively. It is noted that sample preparations required the field specimens to be mixed thoroughly therefore all the samples are remolded samples.

Table 7.5 Large strain consolidation test on east pond ILTT

Load	Height (mm)	ΔH (mm)	Effective stress (kPa)	Void ratio, *e*	Fines-bitumen void ratio, e_{fb}	Hydraulic Gradient, *i*	Hydraulic conductivity (m/day)	Undrained shear strength (kPa)
1	81.05	-	-	4.61	5.25	-	-	0.078
2	73.05	8.00	0.12	4.06	4.62	-	-	0.048
3	46.90	26.15	2.60	2.25	2.56	2.20	4.03E-04	1.28
4	42.50	4.40	5.10	1.94	2.21	3.69	1.75E-04	3.36
5	38.60	3.90	10.09	1.67	1.90	5.28	8.43E-05	3.91
6	35.36	3.24	20.09	1.45	1.65	7.95	5.48E-05	6.96
7	32.80	2.56	38.34	1.27	1.45	10.73	3.23E-05	8.11
8	30.36	2.44	89.09	1.10	1.25	13.50	2.04E-05	45.16
9	28.06	2.30	188.57	0.94	1.07	14.58	6.15E-06	48.15
10	26.66	1.40	287.08	0.85	0.96	18.00	4.87E-06	-
11	27.30	-0.64	137.90	0.89	1.01	-	-	-
12	28.80	-1.50	37.57	1.00	1.13	-	-	-
13	33.70	-4.90	0.50	1.33	1.52	-	-	-

G_s = 2.54, Fines content = 87.4%

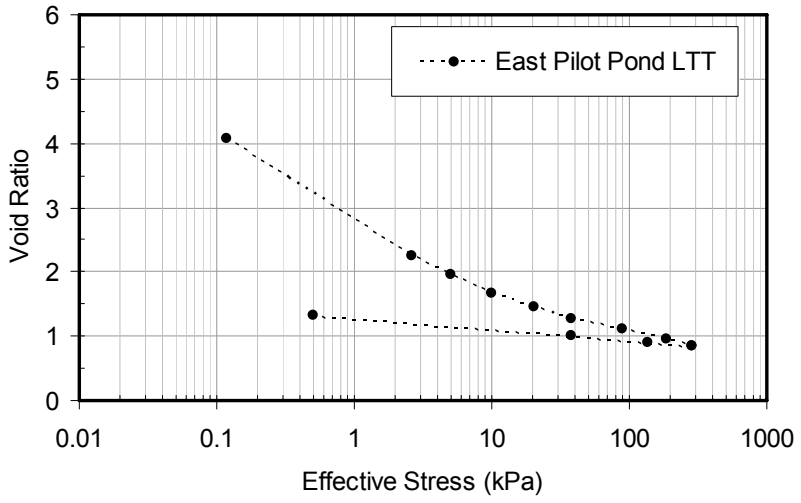

Figure 7.43 Compressibility of east pilot pond ILTT from a large strain consolidation test

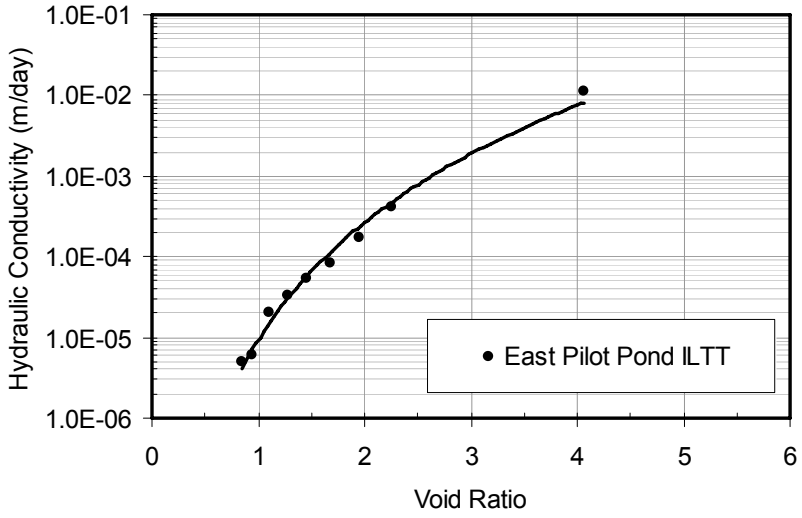

Figure 7.44 Hydraulic conductivity of east pilot pond ILTT from a large strain consolidation test

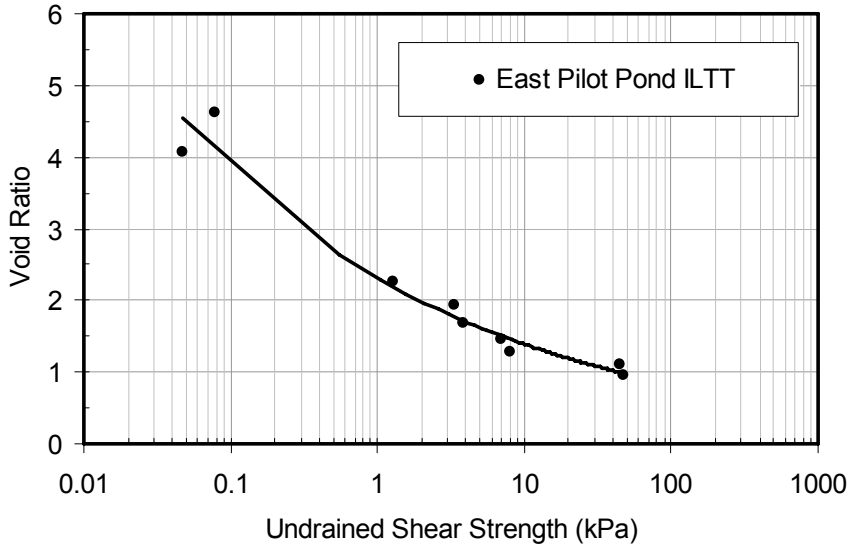

Figure 7.45 Undrained shear strength of east pilot pond ILTT from a large strain consolidation test

7.7.3 West pond in-line thickened tailings obtained on 10th July 2006

Table 7.6 shows large strain consolidation test results on the west pilot pond in-line thickened tailings obtained on 10th July 2006. In this test, an initial solids content of the west pond ILTT was 29.7%. Figures 7.46, 7.47 and 7.48 show compressibility, hydraulic conductivity and undrained shear strength measurements of the tailings

respectively. It is noted that sample preparations required the field specimens to be mixed thoroughly therefore all the samples are remolded samples.

Table 7.6 Large strain consolidation test on west pond ILTT

Load	Height (mm)	ΔH (mm)	Effective stress (kPa)	Void ratio, *e*	Fines-bitumen void ratio, e_{fb}	Hydraulic Gradient, *i*	Hydraulic conductivity (m/day)	Undrained shear strength (kPa)
1	83.00	-	-	5.80	6.06	-	-	0.079
2	72.10	10.90	0.10	4.91	5.13	-	-	0.150
3	53.20	18.90	1.02	3.36	3.51	1.7	3.99E-04	0.731
4	46.50	6.70	2.49	2.81	2.94	3.4	1.69E-04	1.79
5	42.00	4.50	5.00	2.44	2.55	5.1	8.90E-05	2.64
6	38.50	3.50	9.98	2.15	2.25	7.4	4.87E-05	4.92
7	34.90	3.60	20.02	1.86	1.94	10.1	2.91E-05	9.43
8	31.00	3.90	41.11	1.54	1.61	13.5	1.71E-05	14.41
9	28.00	3.00	89.75	1.29	1.35	15.0	6.60E-06	28.23
10	26.00	2.00	190.70	1.13	1.18	18.7	4.21E-06	52.90
11	24.10	1.90	289.04	0.97	1.02	23.6	1.70E-06	-
12	24.70	-0.60	141.17	1.02	1.07	-	-	-
13	26.22	-1.52	40.45	1.15	1.20	-	-	-
14	29.52	-3.30	0.61	1.42	1.48	-	-	-

G_s = 2.45, Fines content = 95.3%

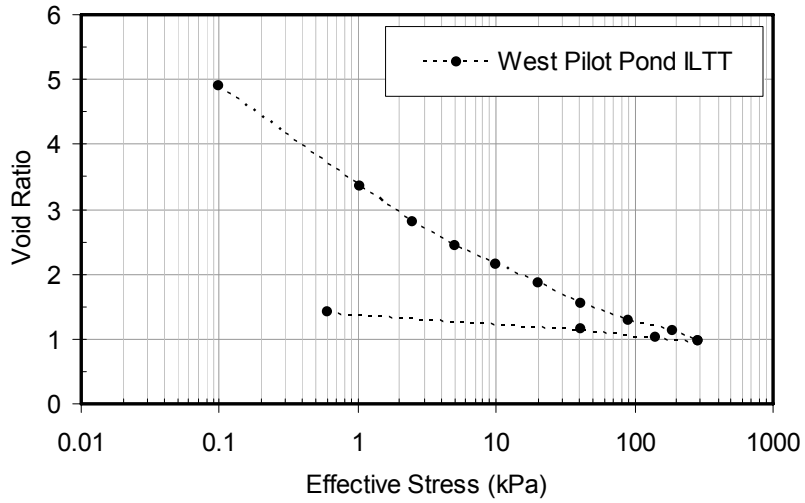

Figure 7.46 Compressibility of west pilot pond ILTT from a large strain consolidation test

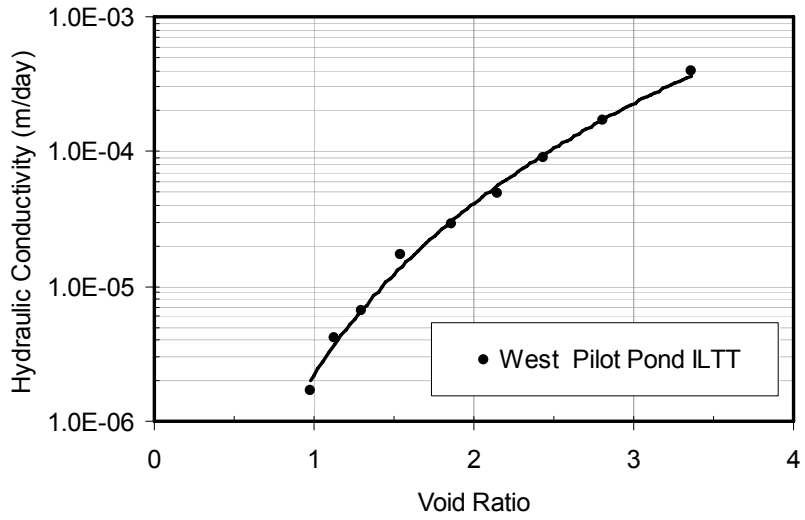

Figure 7.47 Hydraulic conductivity of west pilot pond ILTT from a large strain consolidation test

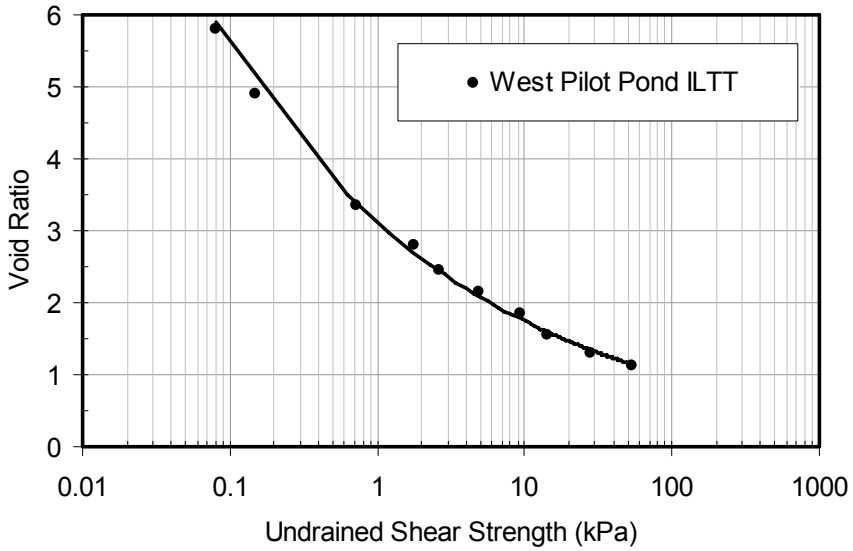

Figure 7.48 Undrained shear strength of west pilot pond ILTT from a large strain consolidation test

7.7.4 Cyclone overflow tailings obtained on 14th April 2008

Tables 7.7 and 7.8 show large strain consolidation test results with and without vane shear strength tests on the cyclone overflow tailings obtained on 14th April 2008. Two tests were performed to determine if the vane tests were influencing the subsequent compressibility and hydraulic conductivity measurements. The initial solids content of

the cyclone overflow was 29.4% in these tests. Figures 7.49, 7.50 and 7.51 show combined compressibility, hydraulic conductivity and undrained shear strength measurements of the tailings respectively.

Table 7.7 Large strain consolidation test 1 on COF obtained on 14 April 2008

Load	Height (mm)	ΔH (mm)	Effective stress (kPa)	Void ratio, *e*	Fines-bitumen void ratio, e_{fb}	Hydraulic Gradient, *i*	Hydraulic conductivity (m/day)	Undrained shear strength (kPa)
1	93.20	-	-	5.91	6.18	-	4.90E-04	-
2	81.00	12.20	0.10	5.00	5.23	-	-	0.019
3	74.90	6.10	0.86	4.55	4.76	0.34	3.74E-02	0.023
4	43.70	31.20	1.57	2.24	2.34	1.50	1.95E-04	0.51
5	39.50	4.20	2.69	1.93	2.02	2.15	1.14E-04	0.79
6	34.80	4.70	6.19	1.58	1.65	2.44	2.46E-05	1.75
7	30.75	4.05	11.21	1.28	1.34	2.76	5.79E-06	2.98
8	28.50	2.25	21.24	1.11	1.16	13.01	1.35E-05	4.83
9	24.80	3.70	50.40	0.84	0.88	14.66	6.14E-06	13.83
10	23.30	1.50	99.15	0.73	0.76	15.97	3.76E-06	22.01
11	20.80	2.50	300.72	0.54	0.57	17.89	8.90E-07	60.65
12	20.00	0.80	493.20	0.48	0.50	24.13	3.31E-07	-
13	21.00	-2.01	52.64	0.63	0.66	-	-	-
14	24.90	-5.73	0.86	1.08	1.13	-	-	-

G_s = 2.46, Fines content = 94.0%

Table 7.8 Large strain consolidation test 2 on COF obtained on 14 April 2008

Load	Height (mm)	ΔH (mm)	Effective stress (kPa)	Void ratio, *e*	Fines-bitumen void ratio, e_{fb}	Hydraulic Gradient, *i*	Hydraulic conductivity (m/day)	Undrained shear strength (kPa)
1	93.59	-	-	5.91	6.18	-	4.33E-04	-
2	80.89	12.70	0.10	4.97	5.20	-	-	-
3	74.20	6.69	0.86	4.48	4.68	0.29	7.84E-03	-
4	50.98	23.22	1.57	2.76	2.89	1.46	1.92E-05	-
5	42.49	8.49	2.69	2.14	2.23	2.37	1.18E-04	-
6	36.23	6.26	6.14	1.67	1.75	2.79	2.15E-05	-
7	32.19	4.03	11.18	1.38	1.44	6.71	1.72E-05	-
8	29.60	2.59	21.57	1.18	1.24	12.72	1.63E-05	-
9	26.23	3.38	50.47	0.94	0.98	14.35	4.13E-06	-
10	24.45	1.78	99.26	0.80	0.84	15.46	2.84E-06	-
11	21.60	2.85	301.45	0.59	0.62	17.45	4.58E-07	-
12	20.08	1.51	498.81	0.48	0.50	23.46	1.70E-07	-
13	22.12	-2.03	51.35	0.63	0.66	-	-	-
14	27.55	-5.44	0.86	1.03	1.08	-	-	-

G_s = 2.46, Fines content = 94.0%

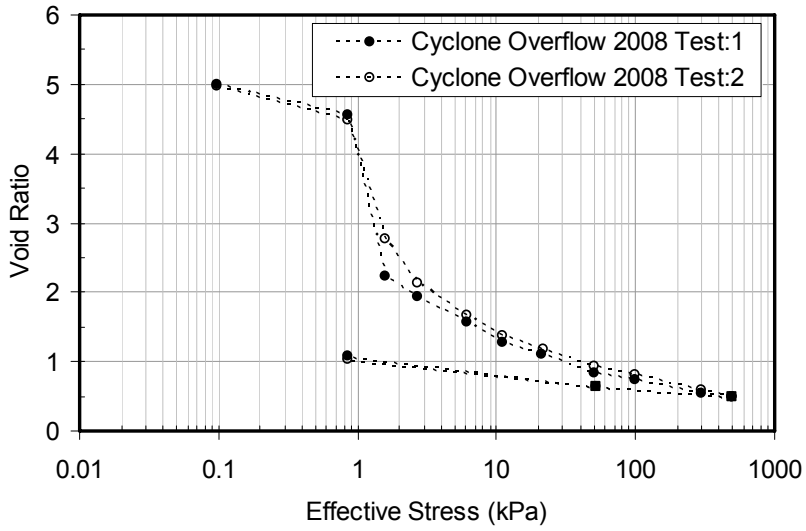

Figure 7.49 Compressibility of 2008 cyclone overflow from large strain consolidation tests

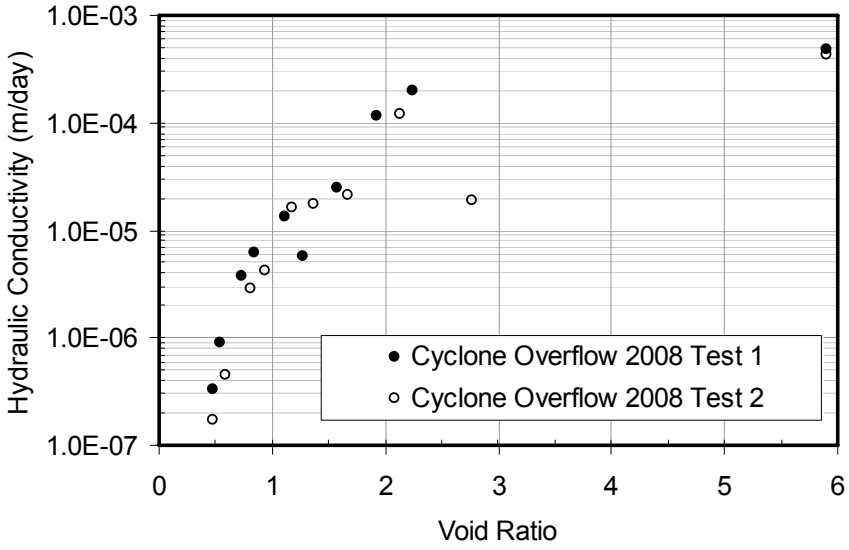

Figure 7.50 Hydraulic conductivity of 2008 cyclone overflow from large strain consolidation tests

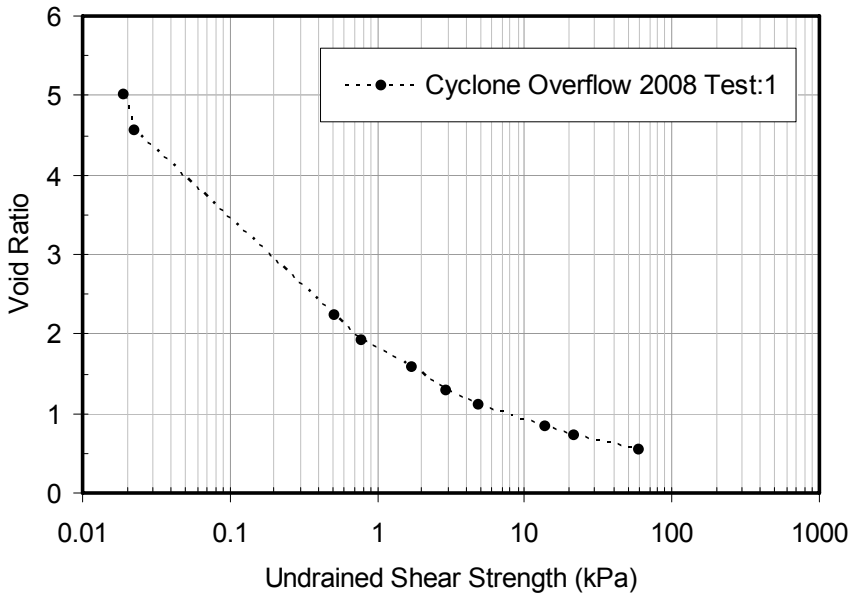

Figure 7.51 Undrained shear strength of 2008 cyclone overflow from a large strain consolidation test

7.7.5 Non-sheared laboratory in-line thickened tailings

Tables 7.9 and 7.10 show large strain consolidation test results with and without vane shear strength tests on the laboratory in-line thickened tailings made from the cyclone overflow tailings obtained on 14th April 2008. Initial solids contents were 16.9% and 16.0% for test 1 and 2 respectively. Figures 7.52, 7.53 and 7.54 shows combined compressibility, hydraulic conductivity and undrained shear strength measurements of the tailings respectively.

Table 7.9 Large strain consolidation test 1 on laboratory ILTT

Load	Height (mm)	ΔH (mm)	Effective stress (kPa)	Void ratio, *e*	Fines-bitumen void ratio, e_{fb}	Hydraulic Gradient, *i*	Hydraulic conductivity (m/day)	Undrained shear strength (kPa)
1	131.00	-	-	12.07	12.62	-	1.77E+02	-
2	78.00	53.00	0.07	6.78	7.09	-	3.59E-01	0.13
3	50.50	27.50	0.84	4.04	4.22	0.41	5.32E-03	0.84
4	42.90	7.60	1.55	3.28	3.43	0.50	8.51E-04	1.41
5	38.50	4.40	2.65	2.84	2.97	0.64	3.69E-04	1.85
6	32.54	5.96	5.43	2.25	2.35	1.60	1.43E-04	2.74
7	29.50	3.04	10.48	1.94	2.03	1.86	6.53E-05	6.10
8	25.50	4.00	30.23	1.54	1.62	5.18	3.04E-05	7.79
9	23.80	1.70	50.60	1.37	1.44	8.82	1.33E-05	13.90
10	20.20	3.60	99.28	1.02	1.06	10.40	8.18E-06	29.21
11	17.20	3.00	298.39	0.72	0.75	20.87	1.23E-06	86.07
12	16.00	1.20	498.82	0.60	0.62	23.30	3.82E-07	-
13	18.15	-2.15	50.42	0.81	0.85	-	-	-
14	21.39	-3.24	0.84	1.13	1.19	-	-	-

G_s = 2.46, Fines content = 94.0%

Table 7.10 Large strain consolidation test 2 on laboratory ILTT

Load	Height (mm)	ΔH (mm)	Effective stress (kPa)	Void ratio, *e*	Fines-bitumen void ratio, e_{fb}	Hydraulic Gradient, *i*	Hydraulic conductivity (m/day)	Undrained shear strength (kPa)
1	134.00	-	-	12.90	13.49	-	6.11E+02	-
2	79.00	55.00	0.07	7.19	7.52	-	1.23E+00	-
3	50.00	29.00	0.84	4.19	4.38	0.44	4.77E-03	-
4	42.65	7.35	1.54	3.42	3.58	0.57	7.11E-04	-
5	37.95	4.70	2.68	2.94	3.07	0.55	3.51E-04	-
6	32.52	5.44	5.46	2.37	2.48	1.60	1.26E-04	-
7	28.59	3.93	10.48	1.97	2.05	1.77	5.48E-05	-
8	24.58	4.01	28.43	1.55	1.62	5.34	8.98E-06	-
9	22.52	2.06	49.88	1.34	1.40	9.24	1.50E-05	-
10	19.92	2.60	98.96	1.07	1.12	10.40	5.64E-06	-
11	17.03	2.89	300.52	0.77	0.80	21.00	4.25E-07	-
12	15.68	1.35	499.29	0.63	0.66	23.19	3.36E-07	-
13	17.60	-1.92	50.25	0.83	0.86	-	-	-
14	20.94	-3.34	0.84	1.17	1.23	-	-	-

G_s = 2.46, Fines content = 94.0%

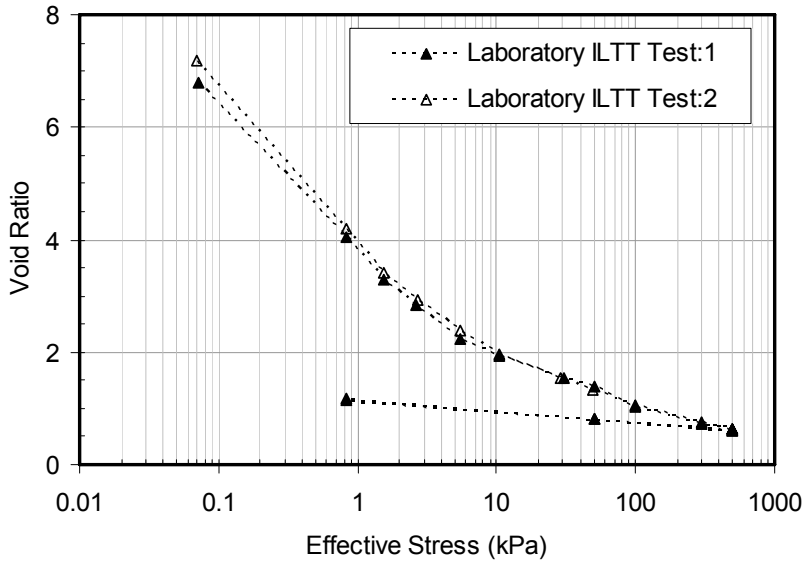

Figure 7.52 Compressibility of laboratory ILTT from large strain consolidation tests

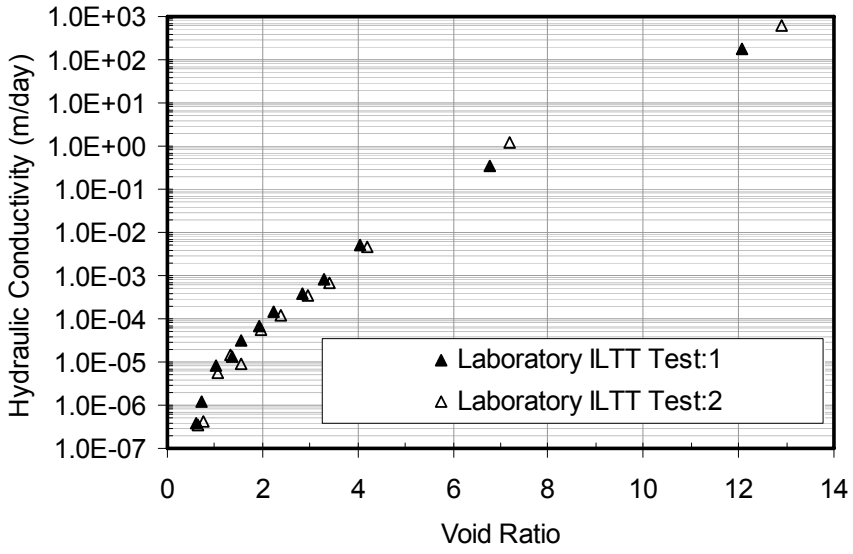

Figure 7.53 Hydraulic conductivity of laboratory ILTT from large strain consolidation tests

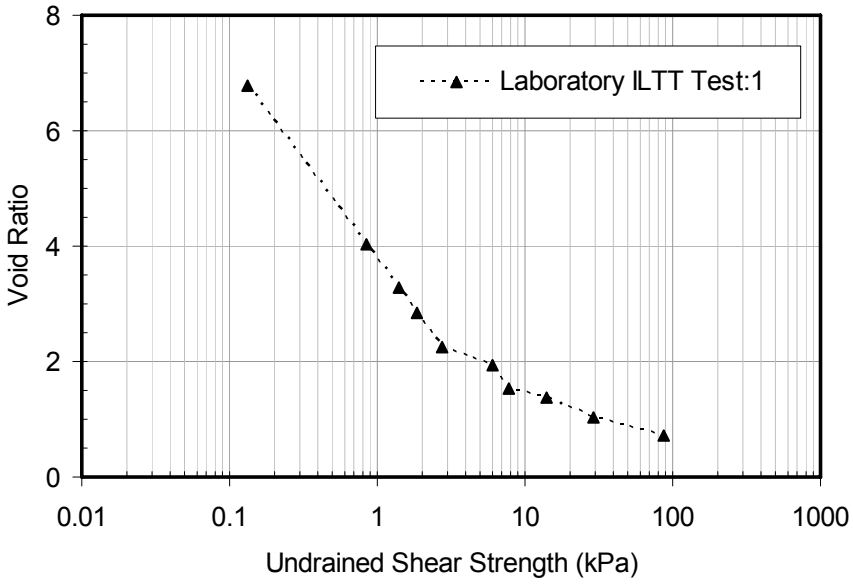

Figure 7.54 Undrained shear strength of laboratory ILTT from a large strain consolidation test

7.7.6 Sheared laboratory in-line thickened tailings

Tables 7.11 and 7.12 shows large strain consolidation test results with and without vane shear strength tests on the laboratory sheared in-line thickened tailings made from the cyclone overflow tailings obtained on 14th April 2008. The initial solids content used

for the tests was 17.1%. Figures 7.55, 7.56 and 7.57 show combined compressibility, hydraulic conductivity and undrained shear strength measurements of the tailings respectively.

Table 7.11 Large strain consolidation test 1 on laboratory sheared ILTT

Load	Height (mm)	ΔH (mm)	Effective stress (kPa)	Void ratio, *e*	Fines-bitumen void ratio, e_{fb}	Hydraulic Gradient, *i*	Hydraulic conductivity (m/day)	Undrained shear strength (kPa)
1	123.00	-	-	11.90	12.44	-	4.78E-02	-
2	74.80	48.20	0.07	6.85	7.16	-	-	0.05
3	44.50	30.30	0.83	3.67	3.83	1.52	1.10E-03	0.66
4	40.00	4.50	1.54	3.20	3.34	2.40	5.41E-04	1.13
5	33.70	6.30	2.65	2.53	2.65	2.83	2.54E-04	1.66
6	28.80	4.90	5.43	2.02	2.11	3.28	1.26E-04	3.18
7	25.50	3.30	10.47	1.67	1.75	4.24	6.80E-05	4.43
8	22.80	2.70	21.61	1.39	1.45	5.34	3.09E-05	8.85
9	19.90	2.90	49.74	1.09	1.14	9.98	1.24E-05	17.84
10	17.90	2.00	94.90	0.88	0.92	13.72	1.05E-05	34.86
11	15.80	2.10	299.64	0.66	0.69	15.68	2.38E-06	70.77
12	15.25	0.55	498.82	0.60	0.63	24.09	1.82E-06	-
13	17.12	-1.87	48.71	0.80	0.83	-	-	-
14	20.60	-3.48	0.83	1.16	1.21	-	-	-

G_s = 2.46, Fines content = 94.0%

Table 7.12 Large strain consolidation test 2 on laboratory sheared ILTT

Load	Height (mm)	ΔH (mm)	Effective stress (kPa)	Void ratio, *e*	Fines-bitumen void ratio, e_{fb}	Hydraulic Gradient, *i*	Hydraulic conductivity (m/day)	Undrained shear strength (kPa)
1	105.90	-	-	11.90	12.44	-	4.09E-02	-
2	63.80	42.10	0.06	6.77	7.08	-	-	-
3	38.80	25.00	0.83	3.73	3.90	1.45	1.00E-03	-
4	35.40	3.40	1.53	3.31	3.46	2.79	5.91E-04	-
5	29.40	6.00	2.67	2.58	2.70	3.28	2.45E-04	-
6	25.84	3.56	5.45	2.15	2.25	3.69	1.25E-04	-
7	22.87	2.97	10.47	1.79	1.87	4.83	6.90E-05	-
8	19.99	2.89	21.57	1.43	1.50	6.22	3.46E-05	-
9	17.47	2.52	50.06	1.13	1.18	11.31	1.59E-05	-
10	15.46	2.01	103.07	0.88	0.92	16.88	8.99E-06	-
11	14.10	1.36	299.04	0.72	0.75	18.62	2.36E-06	-
12	13.50	0.60	497.33	0.64	0.67	28.24	1.70E-06	-
13	14.64	-1.14	46.49	0.78	0.82	-	-	-
14	18.25	-3.61	0.83	1.22	1.28	-	-	-

G_s = 2.46, Fines content = 94.0%

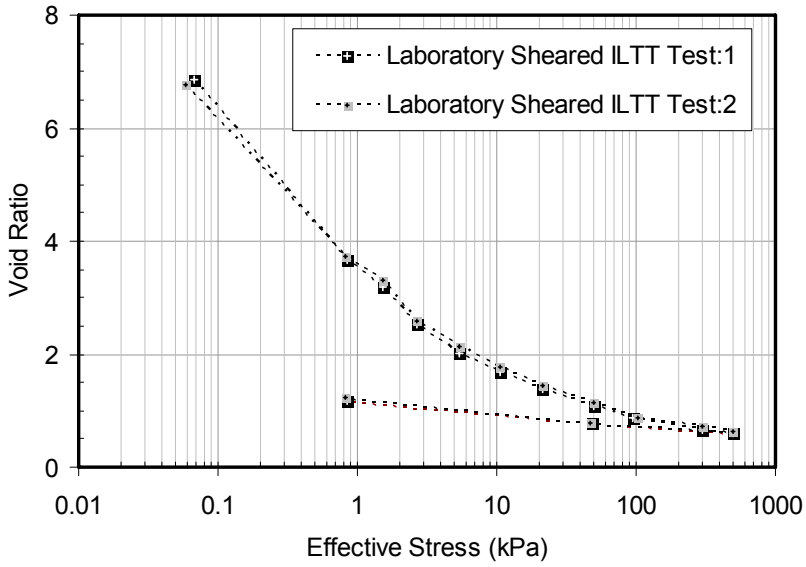

Figure 7.55 Compressibility of laboratory sheared ILTT from large strain consolidation tests

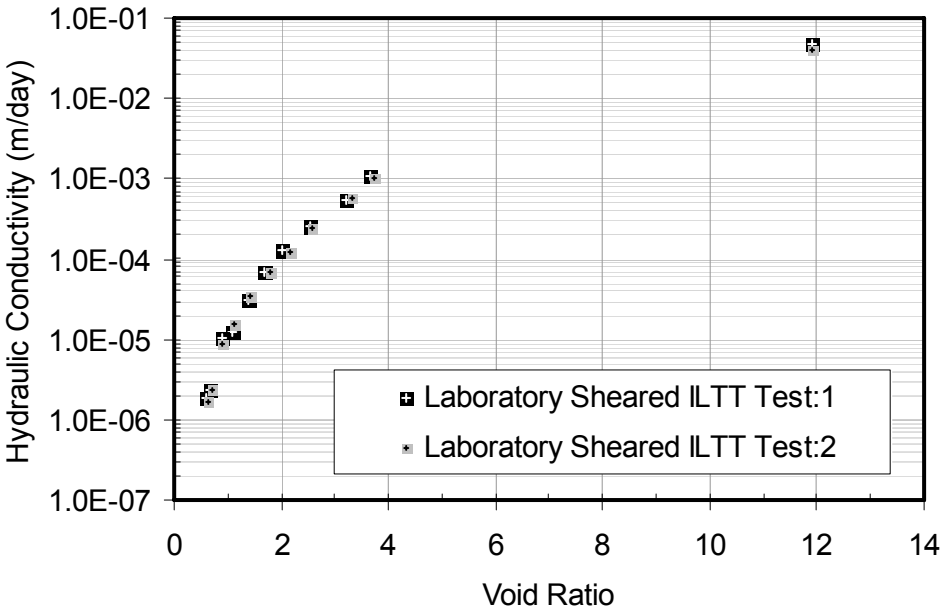

Figure 7.56 Hydraulic conductivity of laboratory sheared ILTT from large strain consolidation tests

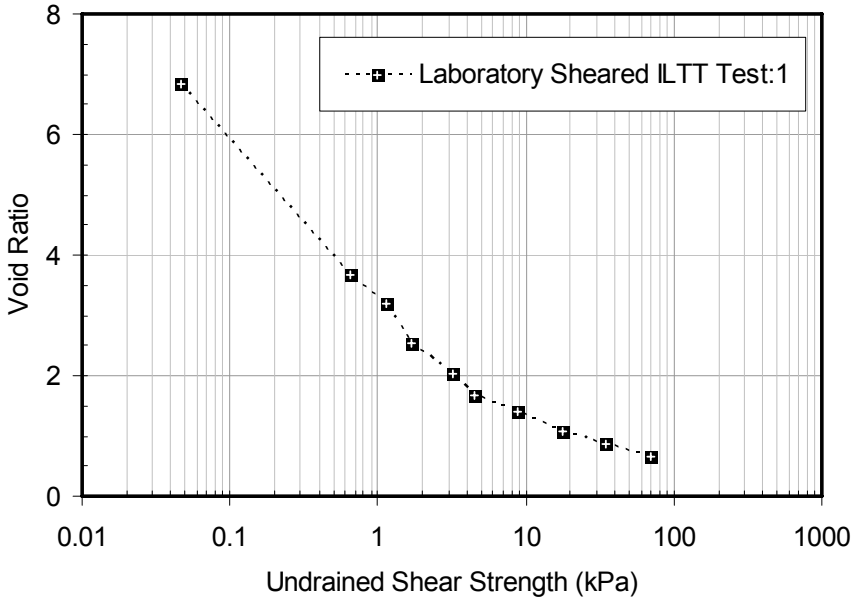

Figure 7.57 Undrained shear strength of laboratory sheared ILTT from a large strain consolidation test

7.8 Comparison of test results

Comparisons of laboratory test data are given in this section with analyses and discussions. Organization of this section is the test data for the field samples is presented and analyzed with the field data separately. Then the results of laboratory in-line thickened tailings investigation are given. Finally, the compressibility and hydraulic conductivity of the laboratory in-line thickened tailings are compared with the field history matching constitutive relationships.

7.8.1 Field samples

Figures 7.58, 7.59, 7.60 and 7.61 show comparisons of the compressibility, hydraulic conductivity and undrained shear strength of all field samples including 2005 cyclone overflow, east pilot pond ILTT and west pilot pond ILTT. From Figure 7.58, the west pond ILTT has essentially the same compressibility as the cyclone overflow. In Figure 7.59, the hydraulic conductivity of the west pond ILTT is approximately the same as that of cyclone overflow at the same void ratios while the east pond ILTT has the highest hydraulic conductivity. To eliminate the influence of coarse particles, fines-bitumen void ratio is plotted against hydraulic conductivity in Figure 7.60. Results indicate that the hydraulic conductivity of the east pond ILTT is still significantly higher

than that of the cyclone overflow. This high hydraulic conductivity behavior of the east pond ILTT possibly indicates differences in the fines micro structure, different ore type or different degree of flocculation. This difference will be further discussed when laboratory ILTT data is presented.

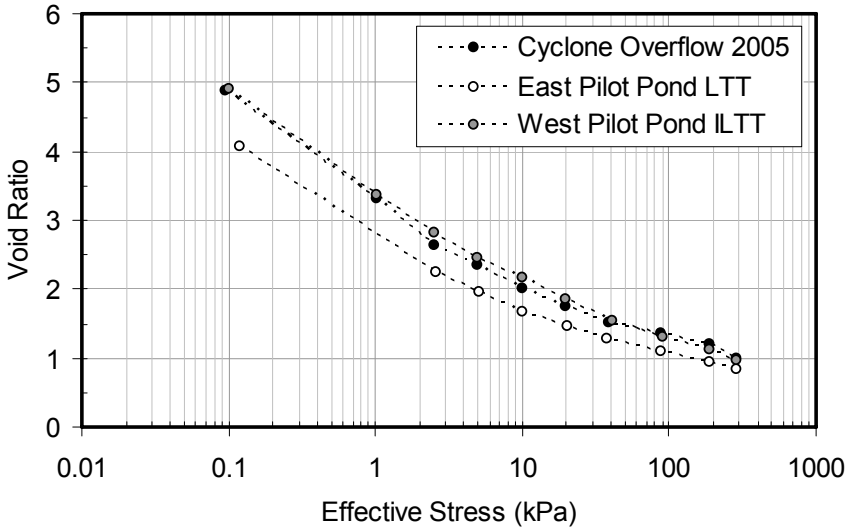

Figure 7.58 Combined compressibility of field samples

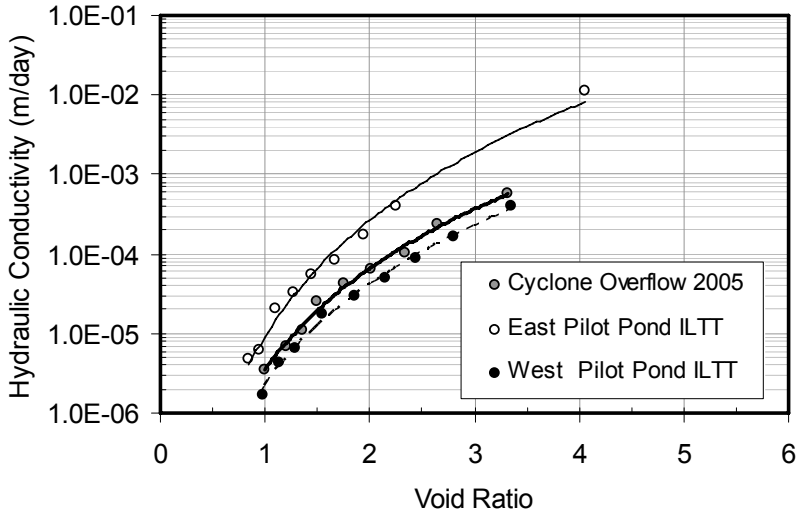

Figure 7.59 Combined hydraulic conductivity of field samples

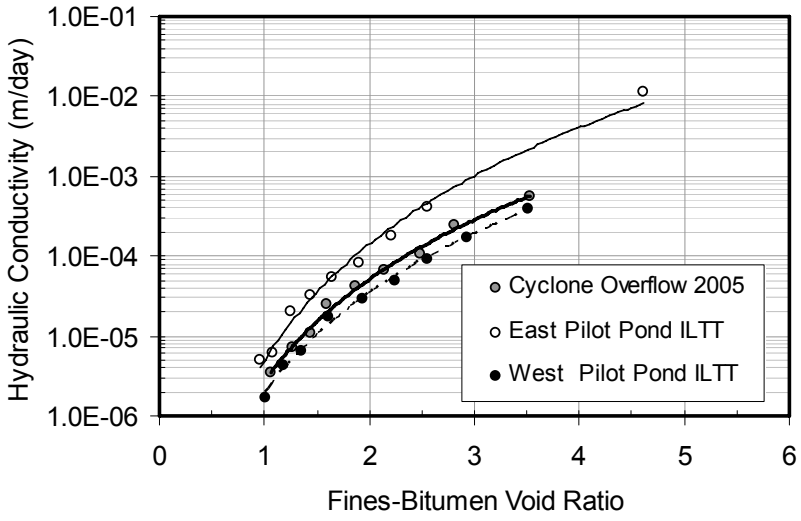

Figure 7.60 Combined hydraulic conductivity of field samples

For undrained shear strength, the west pond ILTT has higher strength compared to the cyclone overflow at effective stresses below 10 kPa (Figure 7.61). At the higher effective stresses, there appears to be no difference in the undrained shear strength between the two tailings. It is believed that the physical forces dominate the behavior of the soils at effective stresses above 10 kPa and the chemical effects are minor. As mentioned earlier, the ILTT pilot samples have gone through sample mixing and remoulding preparation processes. The structure of these samples will not be representative of the original field material.

For the east pond ILTT, the laboratory undrained shear strength is much smaller compared to the undrained strengths of cyclone overflow and west pond ILTT at effective stresses lower than 10 kPa. As the east pond ILTT has lower fines content than other two tailings, undrained shear strength data should be normalized by the fines content. The results are shown in Figure 7.62. It is found that the shear strength of the east pond material is still slightly lower than that of cyclone overflow and west pond ILTT. Undrained shear strengths of the three tailings show a possible convergent at fines void ratio below 1. In Figure 7.11, it is shown that the majority of liquid limits and plasticity indices of the east pond material are lower than the west pond material. The undrained shear strength data in Figure 7.62 also supports that the strength of the east pond material appears to be smaller. According to additional information given by Syncrude, the east

pilot pond's ore body is confirmed to be mainly estuarine ore. The estuarine ore should require less dosages for the in-line thickening process to create the floc structure, however, according to Shaw and Wang (2005) the chemical dosages in both ponds are quite similar. It is postulated, therefore, that the differences of consolidation and shear strength characteristics found in the laboratory tests for the east and west pilot pond materials are caused by the ore type.

The field history matching compressibility and hydraulic conductivity relationships for the east pilot pond are compared with the laboratory test data on the field samples in Figures 7.63 and 7.64 respectively. As discussed in Section 7.6.3, the effective stress-void ratio relationship for slurries at low effective stresses is not unique. The higher the initial solids content of the slurry, the lower is the void ratio at a specific effective stress. This behavior is shown in Figure 7.63. The laboratory consolidation test started at a solids content of 35.5% (Void ratio of 4.6) while the field compressibility material started at a solids content of about 4% (void ratio of 66). The laboratory consolidation test resulted in much lower void ratios than the field test until an effective stress of about 10 kPa was reached, after which the two relationships are identical. To determine a relevant effective stress-void ratio relationship in the laboratory at very low effective stresses, compressibility standpipe tests starting at the same initial solids content as the field deposit must be performed not large strain consolidation tests. For the hydraulic conductivity, it appears that the field hydraulic conductivity averages 2.5 times more permeable compared to the laboratory measured hydraulic conductivity. This is possibly a result of the breakdown of the floc structure in the laboratory samples as they were remolded.

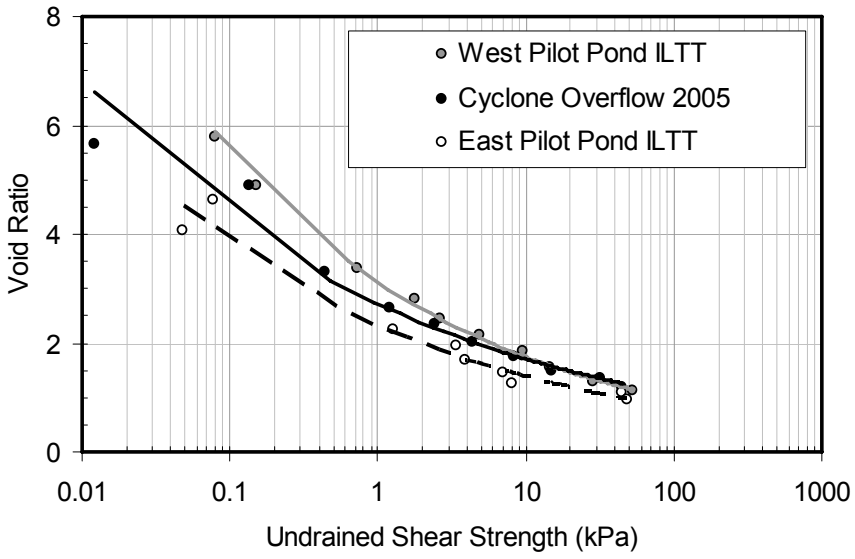

Figure 7.61 Comparison of undrained shear strength of field samples

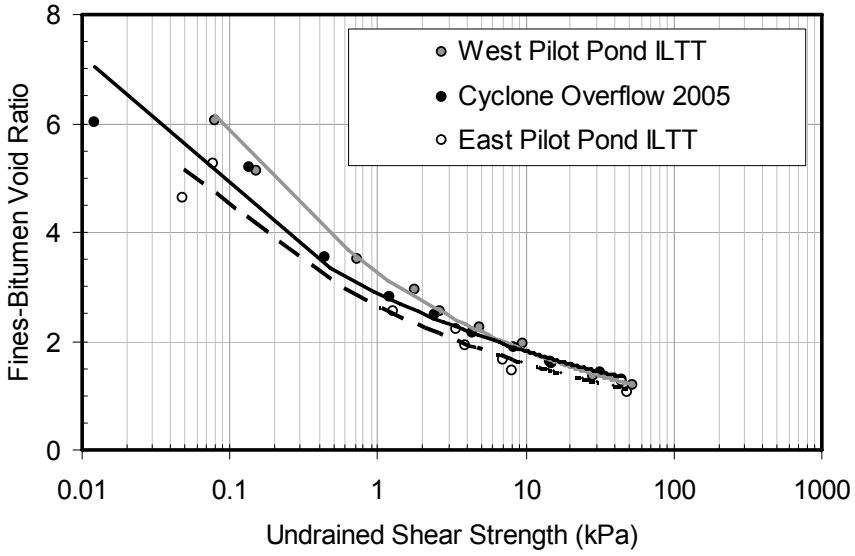

Figure 7.62 Comparison of undrained shear strength of field samples

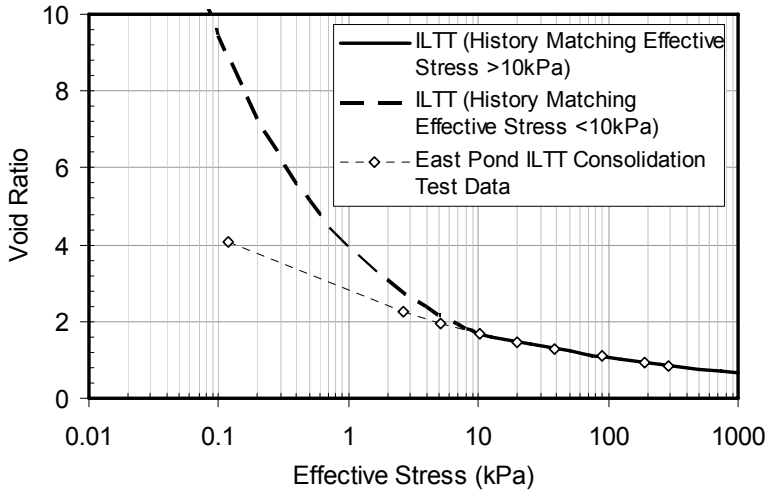

Figure 7.63 Comparison of history matching compressibility and laboratory compressibility

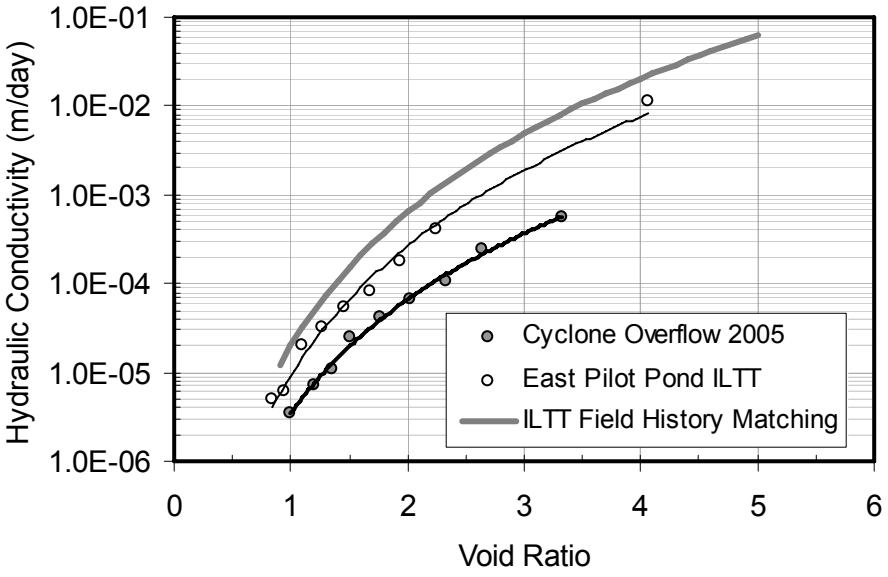

Figure 7.64 Comparison of history matching hydraulic conductivity and laboratory hydraulic conductivity

7.8.2 Laboratory data

7.8.2.1 Cyclone overflow sedimentation-consolidation characteristics

Figure 7.65 shows the combined compressibility data from large strain consolidation tests and compressibility standpipe tests on cyclone overflow tailings. With the present technique of measuring compressibility, cyclone overflow tailings' compressibility can be measured from a void ratio as high as 16 at an effective stress of 6 Pa and void ratio as low as 0.48 at an effective stress of 500 kPa.

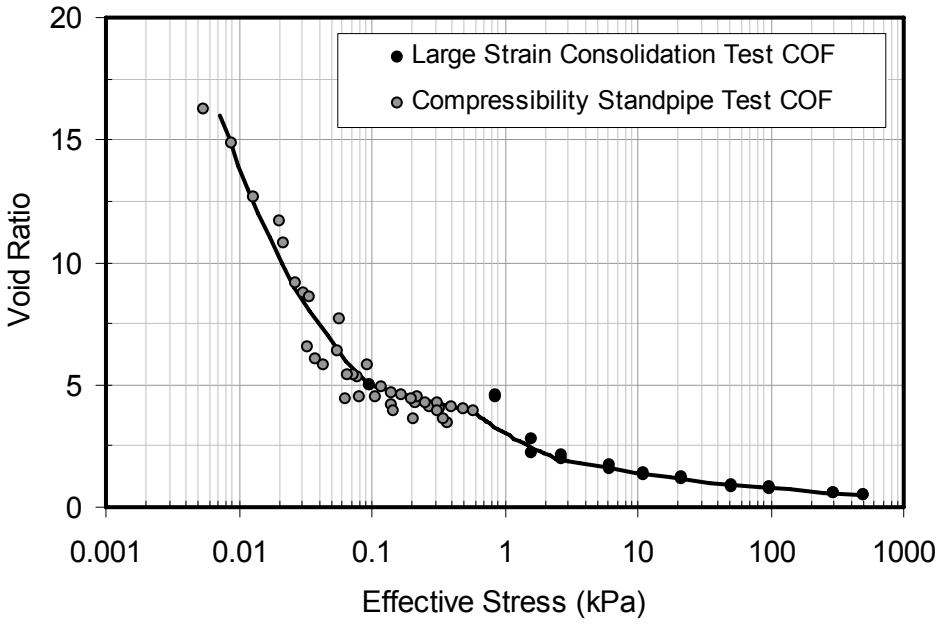

Figure 7.65 Compressibility of 2008 cyclone overflow tailings

In Figure 7.65, there appears to be significant changes of material compressibility as effective stresses increase from 0.006 kPa to 500 kPa. This compressibility behavior suggests structural changes in the material. Based on SEM images taken by a cryogenic method (Azam and Scott, 2009) for cyclone overflow tailings at a void ratio of about 5 (Figure 7.14(a)), it can be seen that a mild edge to face flocculated and dispersed structure dominates and clay plates are mostly thin and long. It is noted that the SEM images are only used in a qualitatively manner to interpret the observed behavior of the material. This structure is generally known as a card-house like structure and can be found in fine tailings at void ratios higher than 5 (Tang, 1995). It is also known from Figure 7.15 (a) that the card-house structure collapsed under high effective stresses

therefore this structure is not present at void ratios below 1. Moreover a SEM image on similar Syncrude tailings shows that the card-house structure does not exist at a void ratio of 3 (Jeeravipoolvarn, 2005). Based on the available evidence, it is postulated in Figure 7.66 for this specific cyclone overflow tailings that the large deformation that occurs between void ratios of 16 and 5 is due to the cumulative formation of the card-house structure and as a void ratio of around 5 is reached, a card-house structure possibly with true grain to grain contacts is formed. The bonding and friction between the particles requires higher effective stresses for further consolidation than during the formation stage therefore the compressibility of the material changes abruptly at a void ratio of around 5. This structure starts to collapse as the effective stress increases between void ratios of 2 and 5. The SEM images suggest that the collapse of the card-house structure occurs in a close range of void ratios between 3 and 5. The vertical effective stress required to collapse the card house structure is generally lower than 1 kPa. As a new fully collapsed card-house structure is formed a relatively constant compressibility is obtained at void ratios of about 2 and lower as with conventional soils.

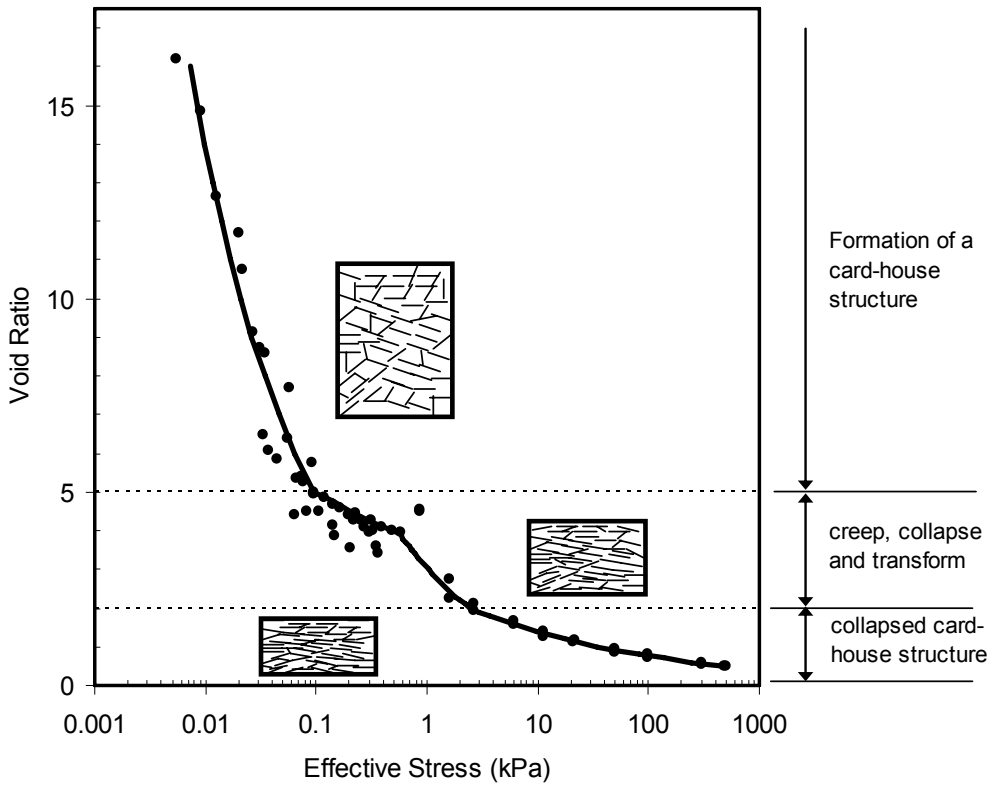

Figure 7.66 Possible structural changes in cyclone overflow tailings in one way compression

The cyclone overflow effective stress-void ratio constitutive relationship can be defined by a power law function expressed as Equation 7.9.

$$e = \begin{cases} 1.750 \times \sigma'^{-0.4500} & ;16.0 \geq e \geq 5.0 \\ 3.616 \times \sigma'^{-0.1389} & ;5.0 \geq e \geq 3.9 \\ 3.027 \times \sigma'^{-0.4649} & ;3.9 \geq e \geq 2.0 \\ 2.523 \times \sigma'^{-0.2604} & ;2.0 \geq e \geq 0.5 \end{cases} \quad [7.9]$$

Where e is void ratio and σ' is vertical effective stress in kPa.

It is noted that even though a continuous compressibility is obtained from this test program, it is known that the oil sands fine tails' compressibility at 10 kPa and lower are not unique and is dependent on initial solids content (Suthaker, 1995). The cyclone overflow tailings used in this program does not show this type of behavior due to the compressibility results from the standpipe tests with different initial solids contents being similar. They also provide a close agreement with the large strain consolidation test results (Figure 7.65). This laboratory simulation represents a continuous process of cyclone overflow compression behavior as it gets deposited and compressed from a very low solids content.

The abrupt change in cyclone overflow's compressibility found in this test program at a void ratio of about 5 (solids content of about 33%) will result in a significantly smaller settlement as consolidation proceeds. Field measurements in oil sands tailings ponds also show this behavior as fine tailings settle to about 30% solids in about two years and further consolidation is very small (Jeeravipoolvarn et al., 2009).

Figure 7.67 shows combined hydraulic conductivity data from hindered sedimentation tests and large strain consolidation tests on cyclone overflow tailings. Similar to the compressibility, combined test data provides continuous hydraulic conductivity measurements from void ratios of 80 to 0.5 (solids content of 3 to 83%). Cyclone overflow hydraulic conductivity-void ratio constitutive relationship can be defined by a power law function expressed as Equation 7.10.

$$k = 7.00 \times 10^{-6} e^{3.50} \quad [7.10]$$

Where e is void ratio and k is hydraulic conductivity in m/day.

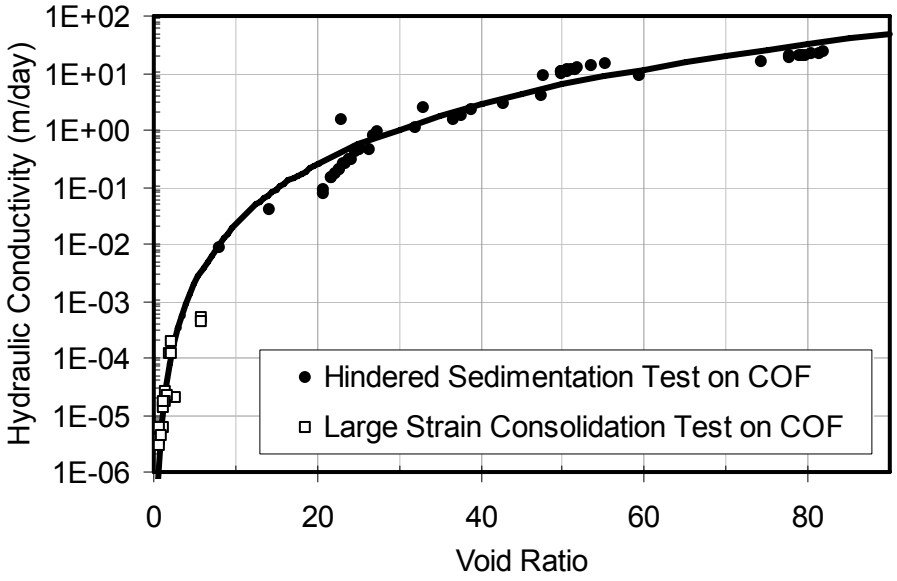

Figure 7.67 Hydraulic conductivity of 2008 cyclone overflow tailings

7.8.2.2 Laboratory ILTT sedimentation-consolidation characteristics

Combined compressibility measurements from compressibility standpipe tests and large strain consolidation tests on in-line thickened tailings are shown in Figure 7.68. Continuous compressibility is obtained and with these measuring techniques, the compressibility of the laboratory in-line thickened tailings was measured between void ratios of about 17 to 0.6 or effective stresses of about 0.009 kPa to 500 kPa.

It can be observed that there appears to be a small apparent pre-consolidation behavior of the material at an effective stress of about 0.2 kPa and void ratio of about 6.5. From macro photography in Figure 7.13, it is observed that at void ratios of about 8 and above (solids content ≤ 24%) large floc structures can be detected and at the same range of void ratio, edge-to-face and edge-to-edge micro structure can be seen from SEM images in Figure 7.14. The in-line thickened tailings micro structure appears to be random without a distinct card-house like structure as observed in the cyclone overflow

tailings. During large strain consolidation tests, it was observed that after self-weight compression was completed, a large floc structure still existed and this structure gradually disappeared as the vertical stresses greater than 0.07 kPa (self-weight stress) was applied. It is also shown in Figure 7.15 that at a void ratio of about 0.7, the random structure is compressed.

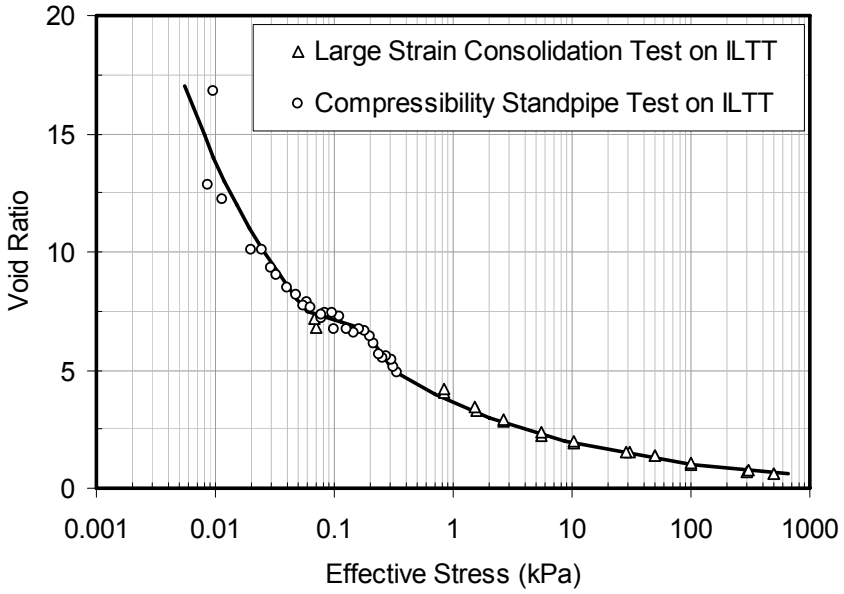

Figure 7.68 Compressibility of laboratory in-line thickened tailings

For this in-line thickened fine tailings, it is postulated in Figure 7.69 that the large deformation occurring between void ratios of 17 and 7.5 is due to the cumulative formation and compression of the large macro floc structure. When the material is compressed to a void ratio of around 7.5, the large and small floc structures start to compress together resulting in a smaller compression index than at of higher void ratios. Further compression behavior below a void ratio of 6.7 possibly relies on the yielding of the small macro flocs structures and the changing of the edge-to-face and edge-to-edge flocculated and aggregated micro structure. Over an effective stress of 0.2 kPa the random micro structure of the in-line thickened tailings continues to rearrange resulting in changes of the compression index.

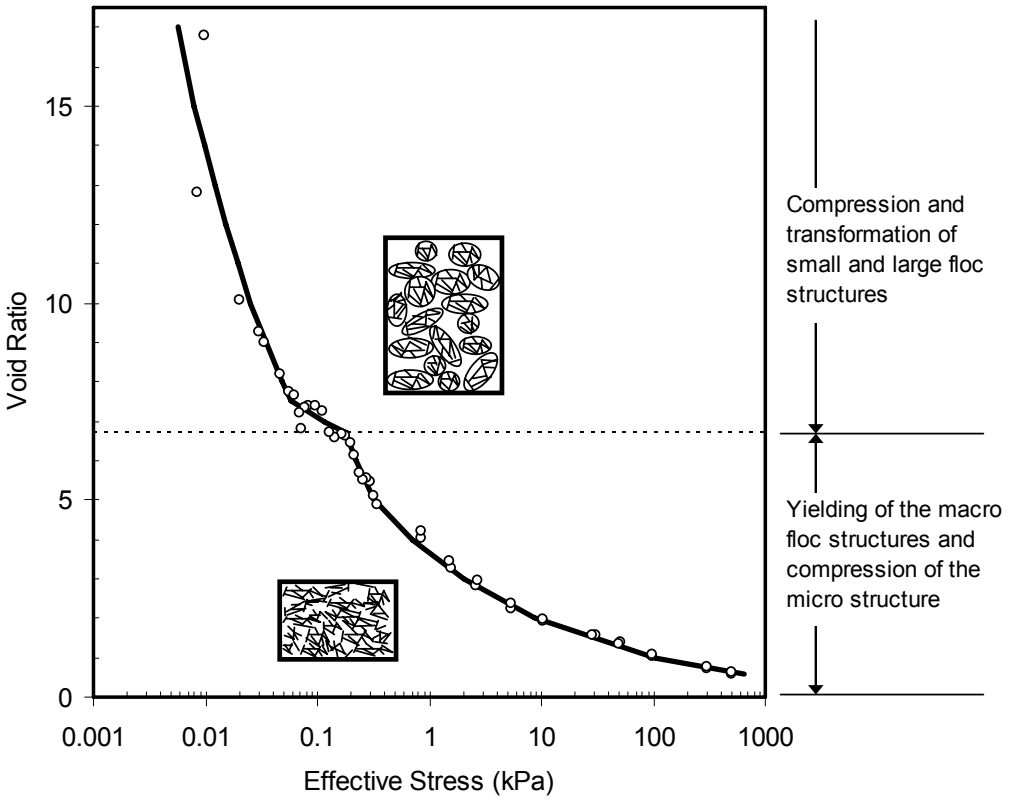

Figure 7.69 Possible structural changes in in-line thickened tailings in one way compression

In-line thickened tailings effective stress-void ratio constitutive relationship can be defined by power law functions expressed as Equation 7.11.

$$e = \begin{cases} 2.773 \times \sigma'^{-0.350} & ;17.0 \geq e \geq 7.5 \\ 5.644 \times \sigma'^{-0.100} & ;7.5 \geq e \geq 6.7 \\ 2.802 \times \sigma'^{-0.508} & ;6.7 \geq e \geq 5.0 \\ 3.641 \times \sigma'^{-0.278} & ;5.0 \geq e \geq 0.5 \end{cases} \quad [7.11]$$

Where e is void ratio and σ' is vertical effective stress in kPa.

Hydraulic conductivity measurements from hindered sedimentation and large strain consolidation tests are shown in Figure 7.70. The combination of hindered sedimentation tests and large strain consolidation tests provide a continuous hydraulic

conductivity measurement for the in-line thickened tailings from void ratios of about 80 to 0.6 and the results suggest that the hydraulic conductivity of this material starts to drop dramatically at a void ratio of about 15. It is noted that the maximum void ratio that effective stress can be measured with the present techniques is 17 which is close to this inflection point. This void ratio may be close to a maximum suspension void ratio (e_m) that corresponds to the initial development of a distinct slurry microstructure (Azam et al., 2007). As the material is compressed further this physiochemical effect is overcome at a lower void ratio of e_s or a structural void ratio where effective stress is the major control on the compressibility, that is, the physics dominates the chemistry (Azam et al., 2009; Jeeravipoolvarn et al., 2009).

In-line thickened tailings hydraulic conductivity-void ratio constitutive relationship can be defined by power law functions expressed as Equation 7.12.

$$k = \begin{cases} 6.944 \times e^{2.087} & ;80.0 \geq e \geq 40.0 \\ 8.469 \times 10^{-4} \times e^{4.530} & ;40.0 \geq e \geq 15.0 \\ 3.951 \times 10^{-8} \times e^{8.212} & ;15.0 \geq e \geq 3.0 \\ 7.000 \times 10^{-6} \times e^{3.500} & ;3.0 \geq e \geq 0.5 \end{cases} \quad [7.12]$$

Where e is void ratio and k is hydraulic conductivity in m/day.

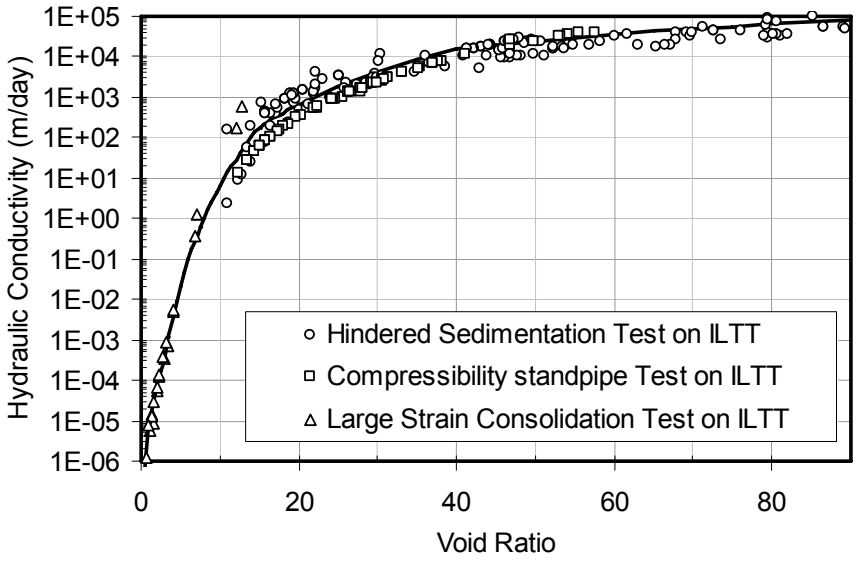

Figure 7.70 Hydraulic conductivity of laboratory in-line thickened tailings

7.8.2.3 Laboratory sheared in-line thickened tailings

Figure 7.71 show combined compressibility results for laboratory sheared in-line thickened tailings. Continuous compressibility is obtained and with these measuring techniques, the compressibility of the laboratory sheared in-line thickened tailings was measured between void ratios of about 12 to 0.6 or effective stresses of about 0.01 kPa to 500 kPa respectively. Similar apparent pre-consolidation behavior obtained in the non-sheared in-line thickened tailings can be observed in the sheared in-line thickened tailings data and a constructed compressibility curve is shown as a line in Figure 7.71. The compression index of the sheared material at void ratios of 5 and higher however is generally lower than that of the non-sheared material. The large macro floc structure was not observed in sheared material. Only a small amount of a very small floc can be observed in sheared material. This suggests that the pre-consolidation behavior in the in-line thickened tailings is possibly caused by compression of small flocs and micro structures rather than the large macro floc structure.

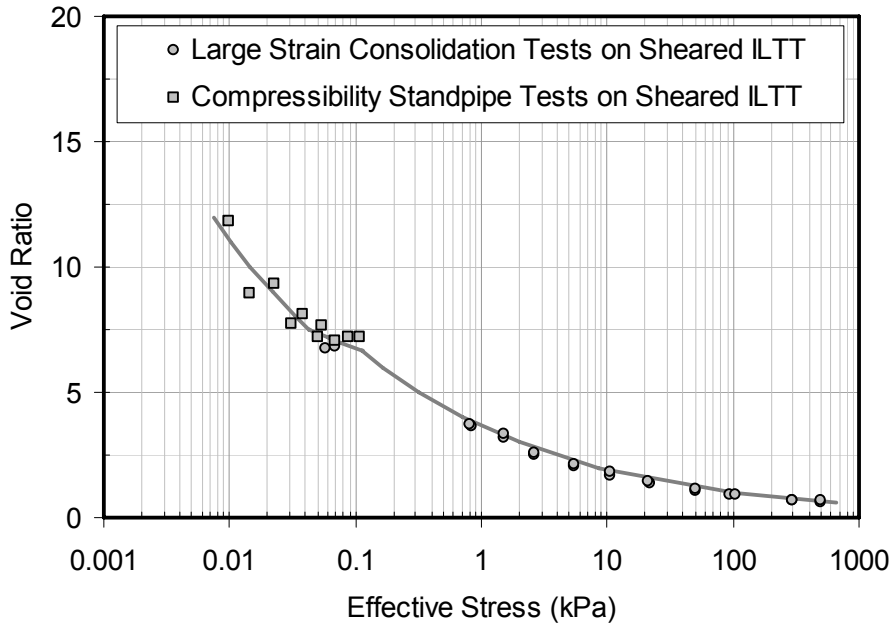

Figure 7.71 Compressibility of sheared in-line thickened tailings

In-line thickened tailings effective stress-void ratio constitutive relationship can be defined by power law functions expressed as Equation 7.13.

$$e = \begin{cases} 3.200 \times \sigma'^{-0.270} & ;12.0 \geq e \geq 7.5 \\ 5.185 \times \sigma'^{-0.117} & ;7.5 \geq e \geq 6.7 \\ 3.641 \times \sigma'^{-0.278} & ;6.7 \geq e \geq 0.5 \end{cases} \quad [7.13]$$

Where e is void ratio and σ' is vertical effective stress in kPa.

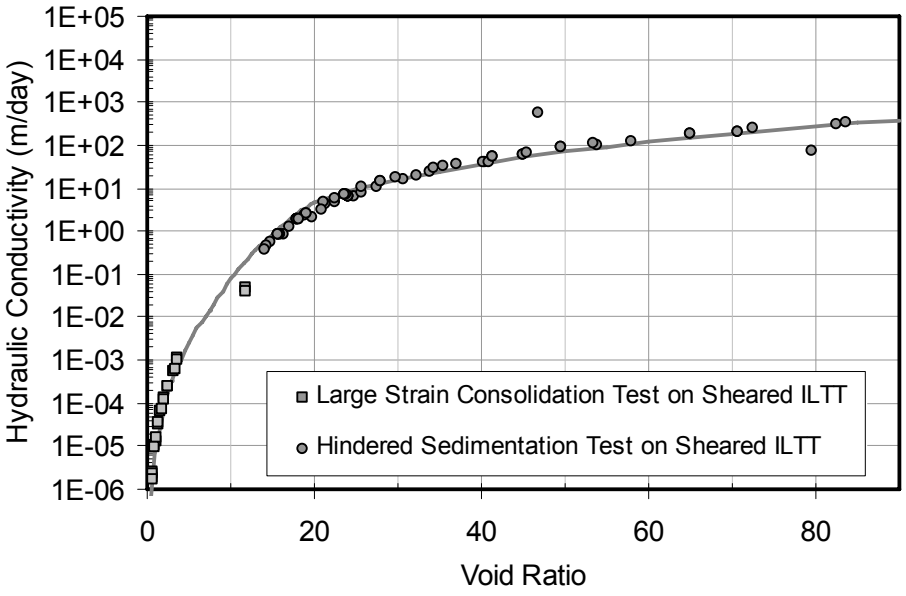

Figure 7.72 Hydraulic conductivity of sheared in-line thickened tailings

Hydraulic conductivity measurements from hindered sedimentation and large strain consolidation tests are shown in Figure 7.72. The combination of hindered sedimentation tests and large strain consolidation tests provide a continuous hydraulic conductivity measurement for the sheared in-line thickened tailings from void ratios of about 80 to 0.6.

Sheared in-line thickened tailings hydraulic conductivity-void ratio constitutive relationship can be defined by power law functions expressed as Equation 7.14.

$$k = \begin{cases} 8.280\times10^{-4}\times e^{2.900} & ;80.0 \geq e \geq 20.0 \\ 7.670\times10^{-8}\times e^{6.000} & ;20.0 \geq e \geq 7.5 \\ 3.737\times10^{-6}\times e^{4.071} & ;7.5 \geq e \geq 3.0 \\ 7.000\times10^{-6}\times e^{3.500} & ;3.0 \geq e \geq 0.5 \end{cases} \quad [7.14]$$

Where e is void ratio and k is hydraulic conductivity in m/day.

7.8.2.4 Comparison of COF, ILTT and sheared ILTT

In Figure 7.73, the compressibilities of cyclone overflow and laboratory non-sheared in-line thickened tailings are compared. The laboratory data suggests that the compressibilities of cyclone overflow and in-line thickened tailings are similar from void ratios of about 16 to 8. The compressibilities of both materials, however, follow different paths at lower void ratios. The cyclone overflow below a void ratio of about 5 becomes much less compressible (lower compression index). For in-line thickened tailings, the change in its compressibility appears to occur at a higher void ratio and is more gradual than that of cyclone overflow. In-line thickened tailings compressibility starts to change as it reaches a void ratio of around 8. The in-line thickened tailings compressibility behavior appears to withstand higher effective stresses at void ratios of 8 and below. The compressibilities of both materials converge as the effective stress gets higher.

Figure 7.74 compared non-sheared in-line thickened tailings and sheared in-line thickened tailings. A trend of the results suggests that the breakage of the floc structure at void ratios of 7.5 and higher due to shear will possibly disrupt the large and small macro floc structures. The small macro floc structure may be partly reformed and the micro structure is probably unaffected. Compression behaviors of sheared and non-sheared material are similar at void ratio below 5. It is concluded that the large and small macro floc structures shown in Figure 7.15 has an influence on material compressibility only at a void ratio of 5 and higher.

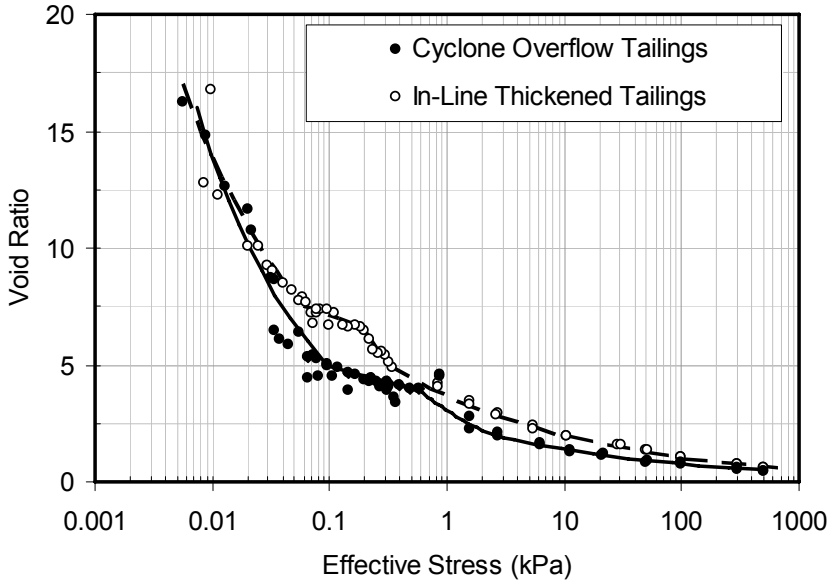

Figure 7.73 Compressibility comparison of cyclone overflow and in-line thickened tailings

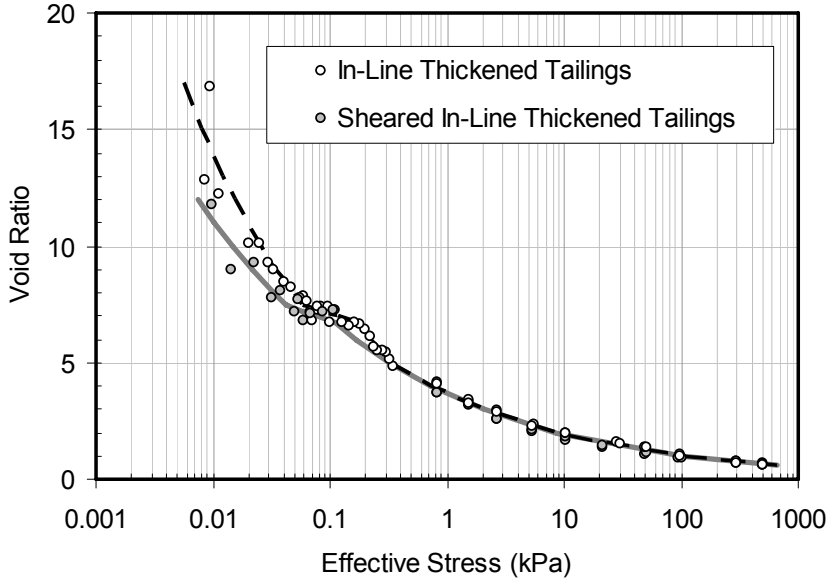

Figure 7.74 Compressibility comparison of laboratory non-sheared ILTT and sheared ILTT

The hydraulic conductivity comparison between cyclone overflow, in-line thickened tailings and sheared in-line thickened tailings is shown in Figure 7.75. ILTT

hydraulic conductivity is more than three magnitudes greater than that of the cyclone overflow tailings at a void ratio of 80. This significant increase in the hydraulic conductivity persists throughout void ratios larger than 15. The greater magnitude of hydraulic conductivity due to the in-line thickening process is decreased as the void ratio is decreased below 15 and when the void ratio is reduced to about 3 there appear to be no difference between the two materials. This result also suggests that the micro structural difference between these materials, if it exists at this void ratio, does not contribute to a significant difference in the hydraulic conductivity.

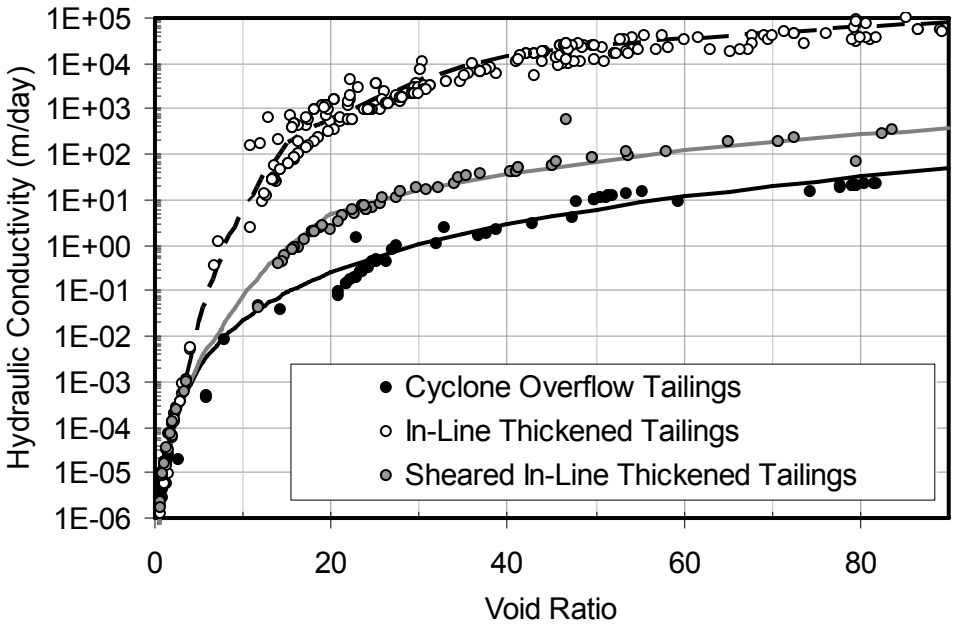

Figure 7.75 Hydraulic conductivity comparison of laboratory non-sheared ILTT, sheared ILTT and COF

The hydraulic conductivity of the sheared in-line thickened tailings is between that of cyclone overflow and non-sheared in-line thickened tailings (Figure 7.75). In order to observe the change of hydraulic conductivity behavior, void ratio and hydraulic conductivity are plotted on a log-log scale in Figure 7.76. It is found that after shearing, hydraulic conductivity of the in-line thickened tailings is reduced approximately 2 magnitudes at void ratios between 20 and 80. The remaining influence of the in-line thickening process still provides a material with a hydraulic conductivity more than 10 times larger than that of the cyclone overflow tailings. Hydraulic conductivity behavior of

all tailings start to converge at a void ratio of about 20 and the differences disappear at a void ratio of about 3.

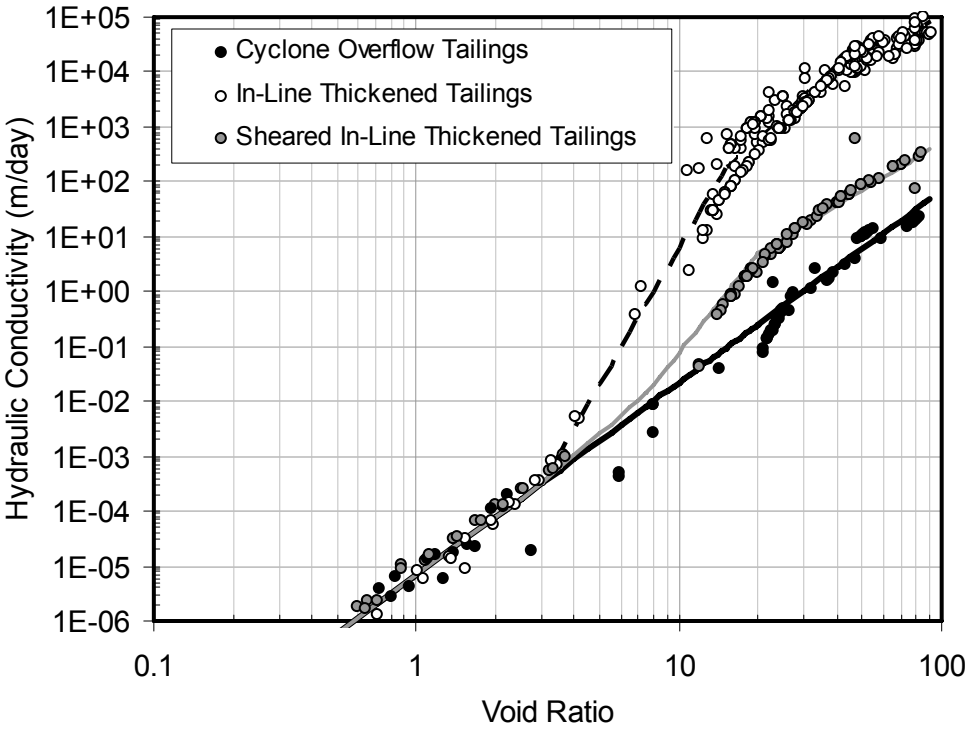

Figure 7.76 Hydraulic conductivity comparison of laboratory non-sheared ILTT, sheared ILTT and COF

Undrained shear strengths of cyclone overflow, in-line thickened tailings and sheared in-line thickened tailings are shown in Figure 7.77. The undrained shear strength of the in-line thickened tailings is the highest followed by sheared in-line thickened tailings and then cyclone overflow. It appears that the undrained shear strength of the sheared in-line thickened tailings and non-sheared in-line thickened tailings converge at lower void ratios while the shear strength of cyclone overflow tailings remains slightly lower at the lowest measured void ratio of 0.5 (solids content of 83%). The converging result of sheared and non-sheared ILTTs in the laboratory suggest that the east pilot pond field sample whose undrained shear strength is significantly lower than west pilot pond sample throughout the measured void ratios is not caused by shearing.

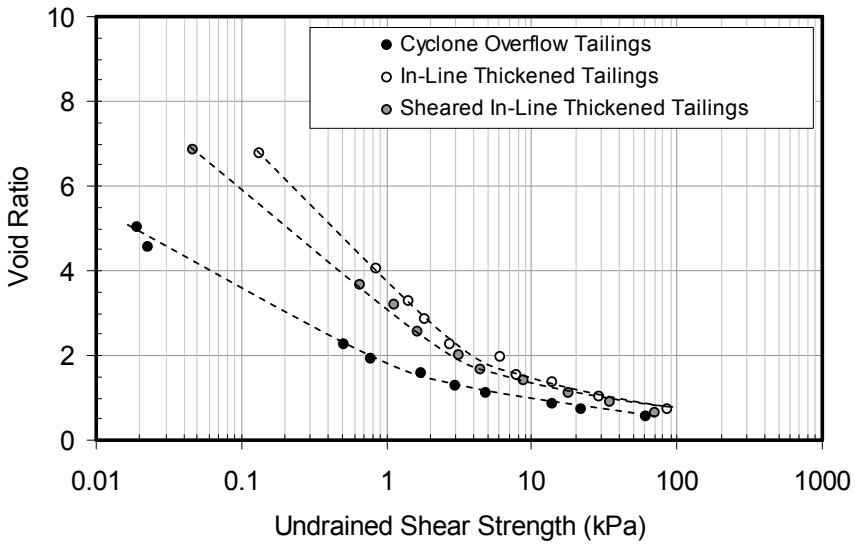

Figure 7.77 Undrained shear strength comparison of laboratory non-sheared ILTT, sheared ILTT and COF

In natural sedimentary clay deposits the undrained shear strength has been found to increase with depth and is proportional to the increase in effective stress with depth (Holtz and Kovacs, 1981). A relationship between plasticity index and a ratio between undrained shear strength and effective stress, τ_u/σ'_{vo}, for normally consolidated clays was established by Bjerrum and Simons (1960). This relationship provides a τ_u/σ'_{vo} ratio of about 0.25 for oil sands fine tailings with plasticity index of about 30. However, the large strain consolidation test results show that this ratio is not constant at all fines void ratios but increases linearly with fines void ratio (Figure 7.78). Even though the data is limited, trends of τ_u/σ'_{vo} relationship with fines-bitumen void ratios were drawn in Figure 7.78 to display undrained shear strength behavior of the tailings. The field correlation in Figure 6.16 is also shown with the laboratory data in Figure 7.78. The large values of τ_u/σ'_{vo} at high void ratios of the in-line thickened tailings in Figure 7.78 are indicative of the strong bonds in the flocs. As the flocs are compressed during consolidation the flocs break and lose strength. The sheared in-line thickened tailings' τ_u/σ'_{vo} ratio is approximately 0.73 for fines-bitumen void ratios of 8 to 3 and is considerably lower than that of the non-sheared in-line thickened tailings. The sheared and non-sheared tailings are similar at fines-bitumen void ratios of about 3 and lower. For the cyclone overflow tailings, the τ_u/σ'_{vo} ratio seems to be decreasing as the fines-bitumen void ratio is decreased. It is noted that at fines-bitumen void ratios between 4 and 6, the τ_u/σ'_{vo} ratio of cyclone

overflow is even below its hypothesized trend line. This is due to the fact that the cyclone overflow's compressibility exhibits pre-consolidation behavior at this range of void ratios. This finding may suggest that the relationship between undrained shear strength and vertical effective stress may not hold for very high water content materials.

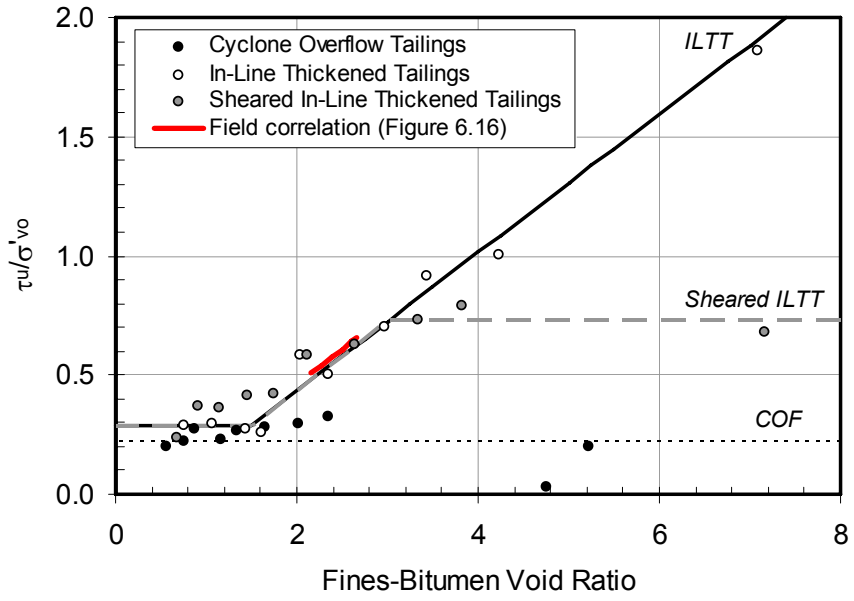

Figure 7.78 Correlation between τ_u/σ'_{vo} ratio and fines-bitumen void ratio of laboratory non-sheared ILTT, sheared ILTT and COF

Tan et al. (1994) suggests that the undrained shear strength behavior of sand-clay mixes with a sand content less than 60% may be explained with a linear mixture law. The undrained shear strengths of the tested tailings thus have been normalized by the fine-bitumen void ratio and the results are shown in Figure 7.79. Undrained shear strength and fines-bitumen void ratio relationships for cyclone overflow, sheared in-line thickened tailings and in-line thickened tailings are given in Equations 7.15, 7.16 and 7.17 respectively.

$$e_{fb} = 1.811 \times \tau_u^{-0.278} \quad [7.15]$$

$$e_{fb} = 3.014 \times \tau_u^{-0.300} \quad [7.16]$$

$$e_{fb} = 3.910 \times \tau_u^{-0.379} \quad [7.17]$$

Where e_{fb} is fines-bitumen void ratio and τ_u is undrained shear strength in kPa.

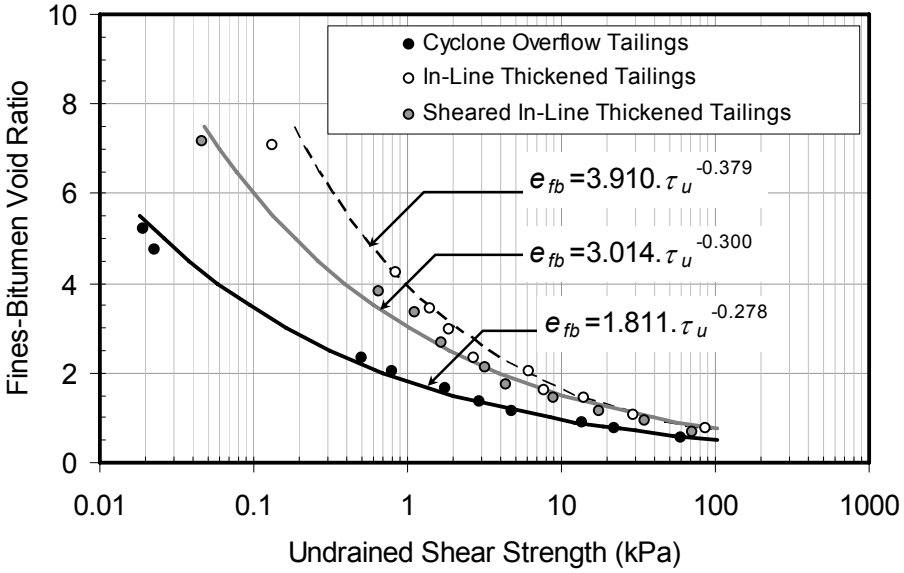

Figure 7.79 Correlation between undrained shear strength and fines-bitumen void ratio of laboratory non-sheared ILTT, sheared ILTT and COF

7.8.2.5 Comparison to the field data

ILTT pilot ponds were started in late 2005 to demonstrate the pilot scale behavior of tailings produced from the in-line thickening process (Jeeravipoolvarn et al., 2008). Geotechnical field investigations including pore pressure measurements, solids and fines content measurements and undrained shear strength measurements were performed to monitor the consolidation behavior of the deposits. Field history matching for consolidation performance was also performed by using a conventional finite strain consolidation theory to determine the field compressibility and hydraulic conductivity relationships. Both relationships are expressed as Equations 7.18 and 7.19.

$$e = \begin{cases} 4.000\sigma'^{-0.375_1} & for \quad \sigma' < 10kPa \\ 2.676\sigma'^{-0.201} & for \quad \sigma' \geq 10kPa \end{cases} \qquad [7.18]$$

$$k = 2.0 \times 10^{-5} e^{5.0} \qquad [7.19]$$

Where e is void ratio, σ' is effective stress in kPa and k is hydraulic conductivity in m/day. These two relationships are compared with the ILTT laboratory data in Figures 7.80 and 7.81 for compressibility and hydraulic conductivity respectively.

In Figure 7.80, it can be seen that the field history matching function is generally similar to the laboratory measurement. It can also be observed that the field deposit is less compressible at a void ratio of about 7 and higher. This small discrepancy appeared to be due to the fact that the history matching analysis, which uses the field interface measurements, is not sensitive in the very high compressible region.

As previously discussed in Chapter 6, from the final solids content profile and knowing the initial solids content of 3.7%, it was calculated that the pond would have an initial fill height of about 20.4 m if the pond were filled instantaneously. With this information, large strain consolidation analysis shows that the error of the history matching compressibility function will be less than 4% of the final height when compared with the laboratory results. This error is small considering that the average interface measurement from the field data used in the analysis has readings fluctuating as much as 10% within each measuring station. This small 4% difference is because only a small percentage of the material in the pond has a void ratio larger than 7. Compressibility of the material at this void ratio and higher is large therefore the error in the history matching function at this range of void ratios does not contribute to a large difference in the interface settlement calculation.

The good comparison below a void ratio of 7 in Figure 7.80 suggests that the history matching approximation of using the average interface settlement measured in the field deposit provides a good approximation of the compressibility behavior of the field in-line thickened tailings.

In Figure 7.81, a good agreement between field history matching hydraulic conductivity and laboratory measurements is obtained. It can be observed that between void ratios of 0.6 to 10 and 50 to 80, the laboratory hydraulic conductivity behavior of the ILTT models well the field history matching analysis. Between void ratios of 10 and 50 it appears that the field hydraulic conductivity is somewhat lower than the laboratory measurements. The reason for the lower hydraulic conductivity behavior in the field is postulated to be caused by pumping and pipeline shearing during the in-line thickening deposition. As floc aggregates are closer at higher solids content, the possibility of aggregates to collide and break is higher. This influence is significantly lower in a controlled laboratory environment.

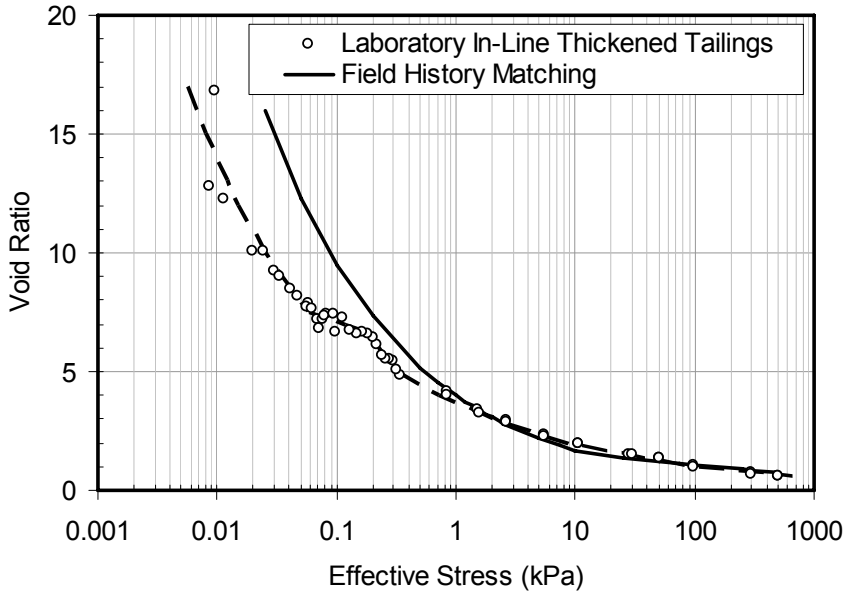

Figure 7.80 Compressibility comparison of laboratory ILTT and field history matching function

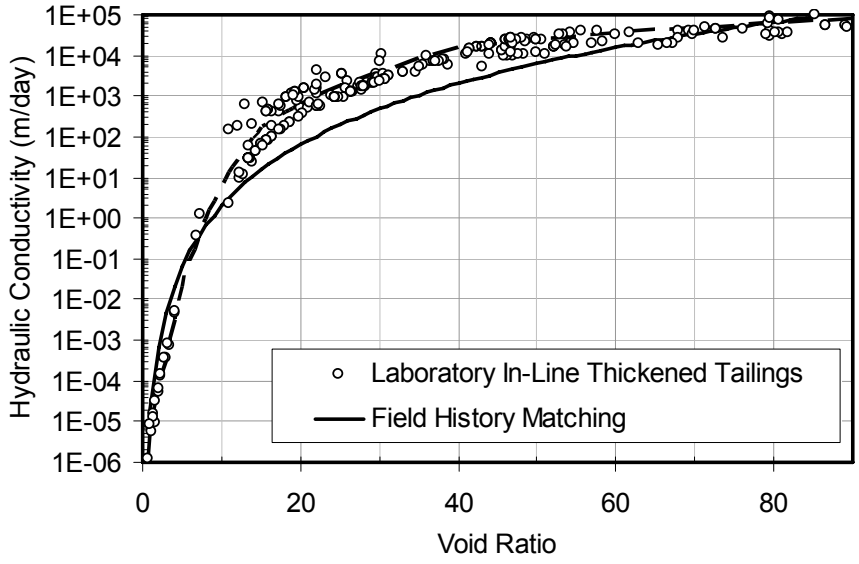

Figure 7.81 Hydraulic conductivity comparison of laboratory ILTT and field history matching function

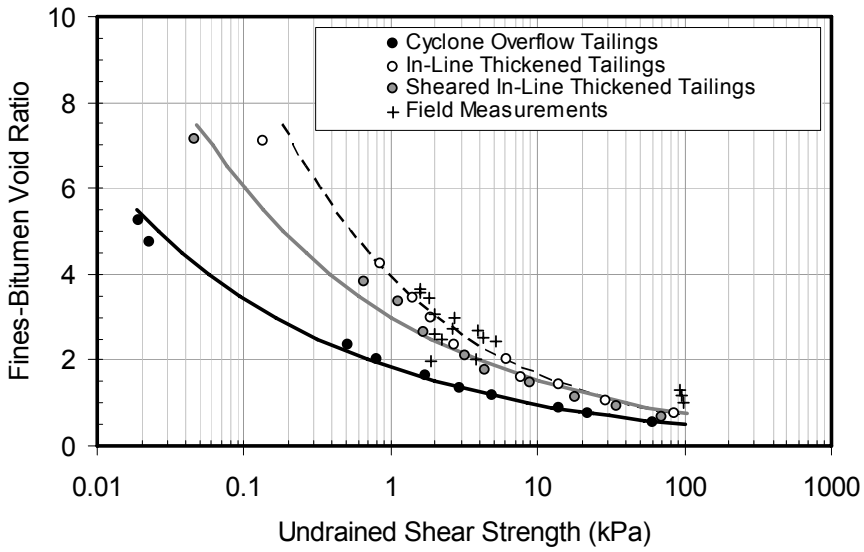

Figure 7.82 Undrained shear strength comparison of laboratory ILTT and field undrained shear strength measurement

The undrained shear strength comparison between field and laboratory results is shown in Figure 7.82 for laboratory in-line thickened tailings, laboratory sheared in-line thickened tailings, field measurements and laboratory cyclone overflow. The field undrained shear strength measurements agree well with the laboratory in-line thickened tailings samples. Cyclone overflow undrained shear strength is the lowest throughout the full range of void ratios.

7.9 Summary

A laboratory study of sedimentation and consolidation behavior of cyclone overflow, in-line thickened tailings and sheared in-line thickened tailings was conducted to investigate the changes in compressibility, hydraulic conductivity and undrained shear strength induced by the in-line thickening process. Cyclone overflow was directly obtained from Syncrude Canada Ltd. and in-line thickened tailings and sheared in-line thickened tailings were prepared by mixing the cyclone overflow tailings, recycle water, flocculant and coagulant to a design solids content under the specified mixing conditions. The in-line thickened tailings were subjected to testing after the in-line mixing was completed to represent a non-disturbed in-line thickened tailings while the sheared in-line thickened tailings were subjected to shearing after mixing to represent remolded in-line thickened tailings due to tailings transportation.

Three sub tests, a hindered sedimentation test, a compressibility standpipe test and a large strain consolidation test were combined to measure the full range of sedimentation and consolidation characteristics for cyclone overflow tailings, in-line thickened tailings and sheared in-line thickened tailings. With the given testing techniques, the void ratio-hydraulic conductivity relationship can be measured from a void ratio of 80 and lower and the effective stress-void ratio relationship can be measured from a void ratio of 16 and lower for cyclone overflow and in-line thickened tailings. Continuous data for both relationships were obtained for both tailings materials.

Comparison of 2008 cyclone overflow tailings and in-line thickened tailings shows that their compressibilities are similar at void ratios higher than 8. The compressibilities of both materials follow different paths at lower void ratios. The cyclone overflow below a void ratio of about 5 has much lower compression indices. For in-line thickened tailings, the change in its compressibility appears to occur at a higher void ratio and is more gradual than that of the cyclone overflow. In-line thickened tailings compressibility starts to change to a lower compression index as it reaches a void ratio of around 8. The in-line thickened tailings compressibility behavior appears to withstand higher effective stresses at void ratios of 8 and below. The compressibilities of both materials converge as the effective stress gets higher.

Compressibility comparisons of the non-sheared in-line thickened tailings and sheared in-line thickened tailings suggests that the breakage of the floc structure at void ratios of 7.5 and higher due to shear will possibly disrupt the large and small macro floc structures. The small macro floc structure may be partly reformed and the micro structure is probably unaffected. Compression behaviors of sheared and non-sheared material are similar at void ratios below 5. It is concluded that the large and small macro floc structures control the material compressibility only at void ratios of 5 and higher.

In-line thickened tailings hydraulic conductivity is more than three magnitudes greater than that of the cyclone overflow tailings at void ratios between 15 and 80. The increase of hydraulic conductivity due to the in-line thickening process is decreased as the void ratio is decreased below 15 and when the void ratio is reduced to about 3 there appear to be no difference between the two materials.

Shearing the in-line thickened tailings will result in reduction of its hydraulic conductivity approximately 2 fold at void ratios between 20 and 80. The remaining influence of the in-line thickening process still provides the material with hydraulic conductivity more than 10 times larger than that of the cyclone overflow tailings.

Converging hydraulic conductivity behavior of all tailings start at a void ratio of about 20. The hydraulic conductivity differences in all the tailings disappear at a void ratio of about 3.

Undrained shear strength measurements show that the in-line thickened tailings has the highest undrained shear strength followed by sheared in-line thickened tailings and then cyclone overflow tailings respectively.

The comparison of the field history matching constitutive relationships and the laboratory measured constitutive relationships resulted in a good agreement. This good agreement strengthens the validity of the geotechnical parameters obtained from this laboratory program and indicate that it is possible to model a large scale field deposit.

Field samples from the pilot scale test program were also subjected to large strain consolidation tests. Results of a comparison between the laboratory and field history matching constitutive relationships suggest that the field hydraulic conductivity behavior was higher than that of the field samples tested in the laboratory at the same void ratios possibly because of the breakdown of the floc structure in the laboratory samples as they were remolded during sampling and sample preparation procedures.

The research hypothesis of comparing in-line thickened tailings and cyclone overflow properties was that the difference in the behavior of these materials would be directly related to the effect of the flocculants and coagulant added in the in-line thickening process. The function of the additives is to bind soil particles together to form large aggregates of soil particles that will settle quickly during deposition at low solids contents. The hypothesis is that as the additives flocculate the soil particles together, the shear strength of the soil will increase as breaking the structure requires additional energy. The soil structure therefore becomes stronger. Compared to the parent cyclone

overflow, the treated tailings would not compress as much when subjected to the same applied stress. The hydraulic conductivity should also be affected by the process because the additives change the structure of the soil reducing the tortuous channels of the soil resulting in greater hydraulic conductivity. Results of the laboratory investigation have quantified the influences of the in-line thickening process on sedimentation, consolidation and shear strength characteristics of cyclone overflow tailings. Sedimentation and consolidation geotechnical parameters have been assigned for both treated and untreated tailings.

Chapter 8 Validation Standpipe Test

8.1 Introduction

In the previous chapter, it was determined that the in-line thickened tailings behavior in the pilot scale field test was similar to the compressibility and hydraulic conductivity of the material obtained in the laboratory test. This confirms that the governing physics in the field are similar to those included in the finite strain consolidation theory for this material. Small discrepancies observed between the field and the laboratory data were believed to be caused by other environmental influences in the field such as shearing, multi-dimensional flow and climate conditions. To eliminate some of the environmental factors and validate the theoretical model and experimental determined parameters, a 2 m validation standpipe test was proposed and performed to simulate a pond filling condition. The results of the test are reported in this chapter.

The standpipe test was filled in a multiple step fashion with interface settlement and pore pressure monitoring throughout an observation period of 180 days. The results from the standpipe test can serve as a comparison and validation for the laboratory compressibility and hydraulic conductivity properties of the material obtained in Chapter 7 and the finite strain consolidation model developed in Chapter 3. Comparisons between the standpipe test data and the finite strain consolidation model include interface height, excess pore pressure responses, a final void ratio profile and a final undrained shear strength profile. A quiescent standpipe test presented in Section 7.6.2 was also used as a supplement comparison at the end of this chapter. Comparative analyses of the results were performed and a summary is then given.

8.2 Standpipe test on in-line thickened tailings

The standpipe test was performed in a controlled laboratory condition to simulate filling, sedimentation and consolidation behavior of the in-line thickened tailings during pond filling. The results of the tests were used to validate the material's sedimentation and consolidation characteristics obtained in the previous chapter and the finite strain consolidation model developed in Chapter 3.

The standpipe is shown in Figure 8.1. The standpipe unit is made of polymethyl methacrylate (PMMA) with an inside diameter of 0.15 m and a height of 2.2 m. The fill level of slurry can go up to 2.0 m which will allow a maximum effective stress of over 4 kPa to be evaluated for tailings at 30% initial solids content.

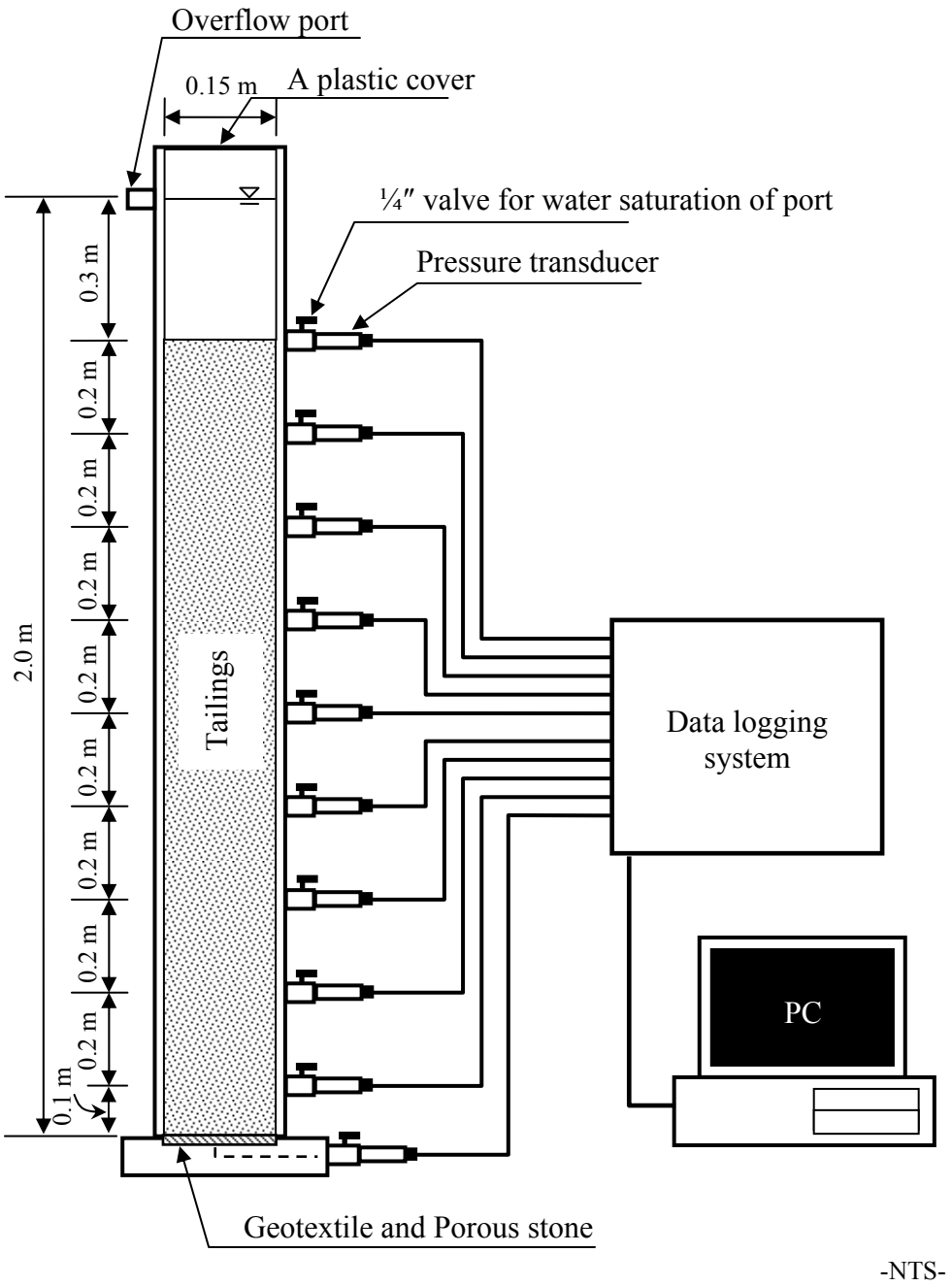

Figure 8.1 Standpipe test

Along the side of the standpipe, pressure transducers (Omegadyne PX409 series) were installed in the base, at 10 cm above the base transducer and then at 20 cm intervals. The pressure transducer's range is 103.4 kPa (15 psi) with 0.08% accuracy. A total of 10 pressure transducers were installed from elevation 0 cm (bottom of standpipe) to 170 cm. All transducers were connected to a signal conditioning unit which was connected to an Agilent 34970A data acquisition switch unit. The data was logged into a personal computer for monitoring and analysis.

8.2.1 Validation standpipe test procedures

Detailed procedures for preparation and testing of the 2 m validation standpipe test are described below. It is noted that the 120 cm supplementary standpipe test procedures are identical to the procedures for the 2 m validation standpipe.

8.2.1.1 Standpipe preparation procedures

1. Calibrate the pore pressure transducers with a precision pressure calibrator to obtain calibration factors.
2. Obtain zero readings for all transducers at atmospheric pressure then install pressure transducers along the side of the standpipe. Make sure that the ports are saturated with water without any entrapped air bubbles by running water through the ports during the installation. After all transducers are installed, close all port water saturation valves.
3. Fill the standpipe with water, insert a porous stone followed by a geotextile filter at the bottom of the standpipe and open all pressure transducer valves.
4. Based on the calibration factors and zero readings, double check measured height of water with the pressure readouts. After the proper working condition of the transducers is assured, lower the water level to the porous stone level at the bottom of the standpipe. Make sure that the pressure transducer ports are still saturated. Re-saturate the pressure transducer ports if necessary. Then close all pressure transducer valves.

8.2.1.2 Standpipe test procedure

1. Prepare in-line thickened tailings of a desired volume at an initial solids content of 5% by following the ILTT preparation procedure given in Section 7.2.4.

2. For the first layer of a multiple filling condition and a single quiescent condition, insert a funnel with a tremie discharge tube into the standpipe. Lower the bottom of the tremie discharge tube as close to the bottom of the standpipe as possible. Position a digital camera to capture interface settlement and set timing to perform elapsed time photography. Set the data logger to synchronize with the digital camera. Start the data logger and elapsed time photography at the same time. Discharge the tailings into the standpipe via the funnel and discharge tube and remove the funnel and tube as soon as all tailings are discharged. During discharging, open each transducer valve as the interface rises over the ports. For a multiple filling test, monitor the settling process for 1 day and then start the next layer. For a quiescent test, monitor until the consolidation process is complete.
3. For all layers of a multiple filling test, after one day following the deposition of the previous layer, take a final reading of interface settlement and pore pressures. Sprinkle a small amount of tailings sand near the side of the standpipe as a layer marker. Then pump the supernatant water off the top of the tailings. Turn the top handle of the layer separator (Figure 8.2) to close the bottom disc and lower the separator into the standpipe. The layer separator used in this test program is intended to minimize mixing and re-suspension of the newly deposited layer and the lower layer during a filling period. Position the bottom disc just above the top of the tailings. Lock the layer separator by a clamp at the top of the standpipe and insert a funnel with a tremie tube into the standpipe. Position a digital camera to capture interface settlement and set timing to obtain elapsed time photographs. Set the data logger to synchronize with the digital camera. Start the data logger and elapsed time photography at the same time. Discharge the tailings into the standpipe via the funnel and remove the funnel and tube as soon as all tailings are discharged. Turn the bottom disc to open position and withdrawn the layer separator carefully from the standpipe.
4. During the test, the interface settlement and the interfaces between layers and pore water pressures are monitored to evaluate the sedimentation and consolidation processes.
5. At the end of the test, supernatant water is pumped off the standpipe to expose the tailing's surface. A laboratory vane test was carried out at 10 cm intervals to the bottom of the standpipe. The vane test is performed from top down at the center of the material. After the test is complete, the vane is withdrawn and the tailings are

sampled in 2.5 cm intervals in the top 10 cm and bottom 5 cm of the standpipe. The rest of the sampling of the tailings is performed at 5 cm intervals. Sub samples are also obtained from each sample for fines content determination.

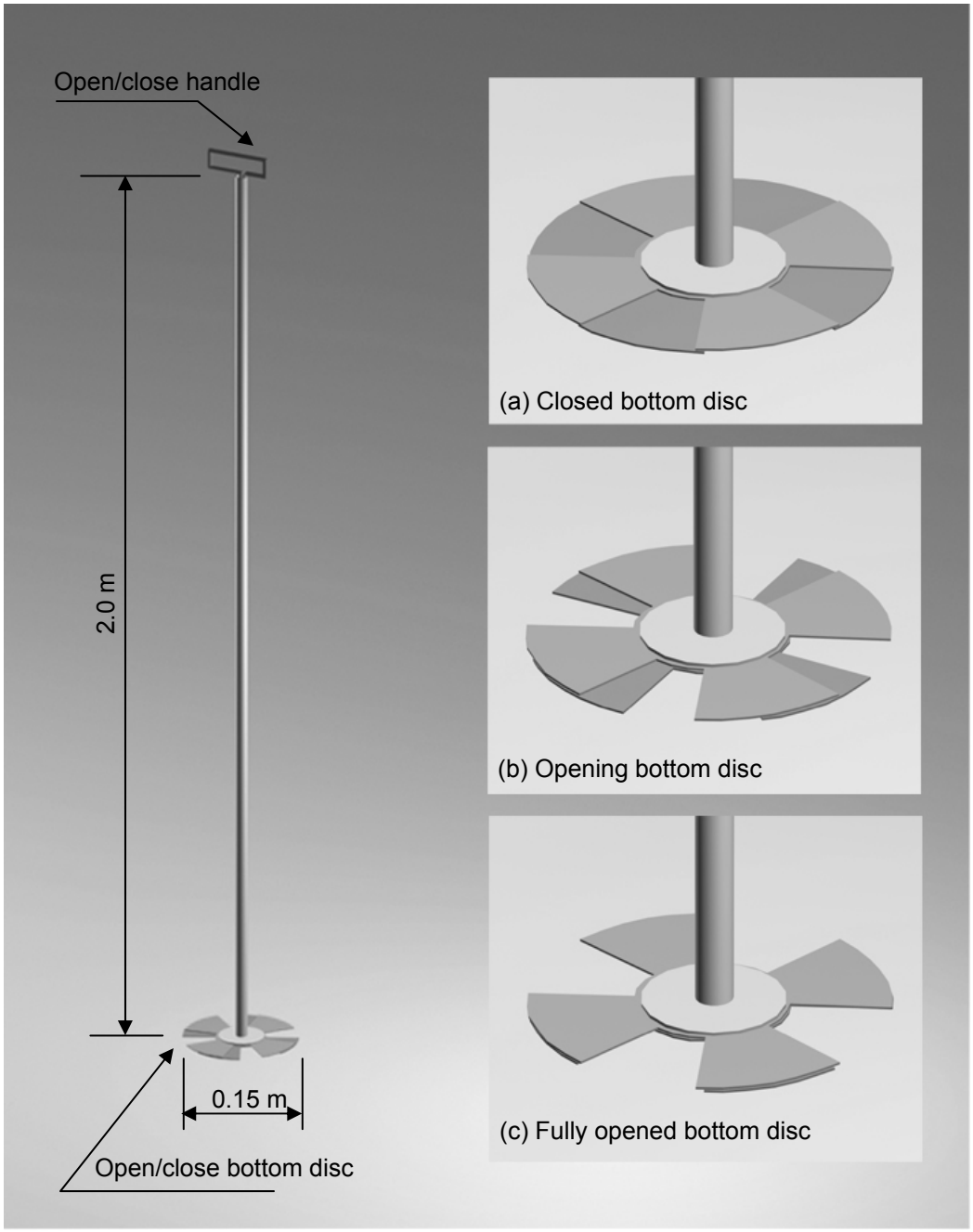

Figure 8.2 A layer separator

8.2.2 Filling episodes

An initial solids content of the in-line thickened tailings used in the validation standpipe was 5% for all lifts. A total of six filling episodes were performed for the standpipe simulation of a pond filling condition. It was designed that each layer is filled instantaneously with a fill height of 1 m. Layers 1 to 5 were designed to settle for 1 day before the next layer was filled and the final layer was allowed to settle until the excess pore water pressure was considered negligible. Filling parameters measured for the standpipe test are shown in Table 8.1. The fill volume is approximately 17.2 L or about 97.4 cm height for each layer.

Table 8.1 Filling parameters for the standpipe test

Layer	Fill volume (cm^3)	Fill duration (minutes)	Fill rate (tons/day)	Elapsed time (days)		
				Start of filling	End of filling	End of settling
1	17663	0.600	42.94	0.000	0.0004	0.999
2	17239	0.583	43.86	0.999	1.000	2.001
3	17115	0.667	38.10	2.001	2.002	3.017
4	16938	0.917	27.42	3.017	3.018	3.994
5	17141	0.583	43.65	3.994	3.995	5.005
6	17150	0.633	40.19	5.005	5.006	180.0

8.2.3 Standpipe test results

Results of the standpipe test including tailings-water interface height, interfaces between each layer, excess pore pressure profiles, a final void ratio profile and a final undrained shear strength profile are shown in this section.

8.2.3.1 Interface height measurements

Tailings-water interface measurements and interfaces between each tailings layer are shown in Figures 8.3 and 8.4 for elapsed times of 0-10 days and 0-180 days respectively. Detailed interface measurements during the rapid sedimentation period for Layers 1 to 6 are shown in Figures 8.5 to 8.10. It is noted that during filling of the tailings, the top water interface is taken as a tailings-water interface. During this period rapid increasing of the interface and turbulent flow prevent an accurate measurement and the withdrawal of the funnel and the layer separator at the end of filling smeared the interface and partially re-suspended some of the newly deposited tailings.

In Figure 8.3, six filling scenarios during a 6 day fill can be observed. The interface settlement during filling for each layer rose to a maximum height and settled very quickly. The final height at 180 days is 67.0 cm (Figure 8.4) with a remaining excess pore pressure at the bottom of less than 0.05 kPa.

Detailed interface height measurements for each layer (Figures 8.5 to 8.10) reveal that the tailings rose quickly during the filling then underwent a rapid hindered sedimentation with an initial linear interface settlement. Approximately 90% of the settlement of all the filled layers occurred within the first 10 minutes after filling. The interface settlement started to deviate from linearity as the suspension was transforming into a soil.

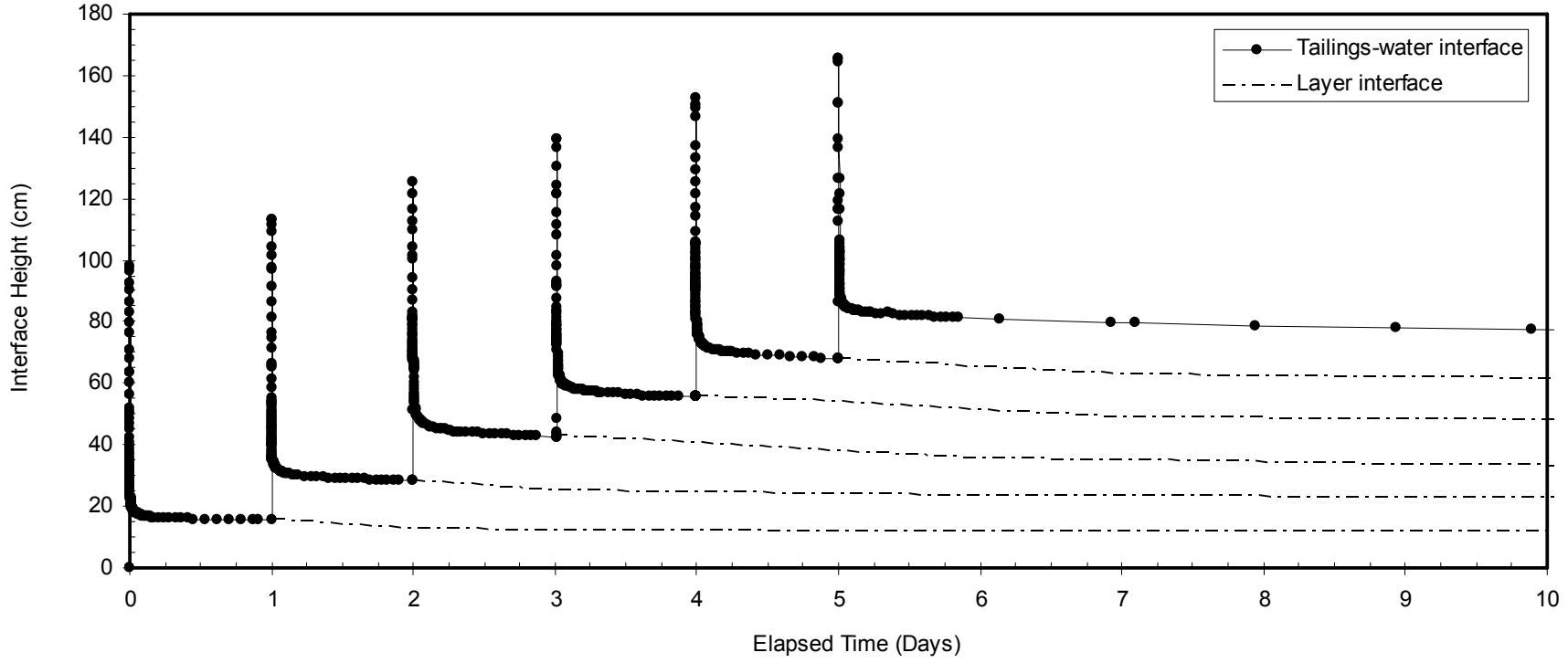

Figure 8.3 Interface height measurements of the validation standpipe between 0-10 days

322

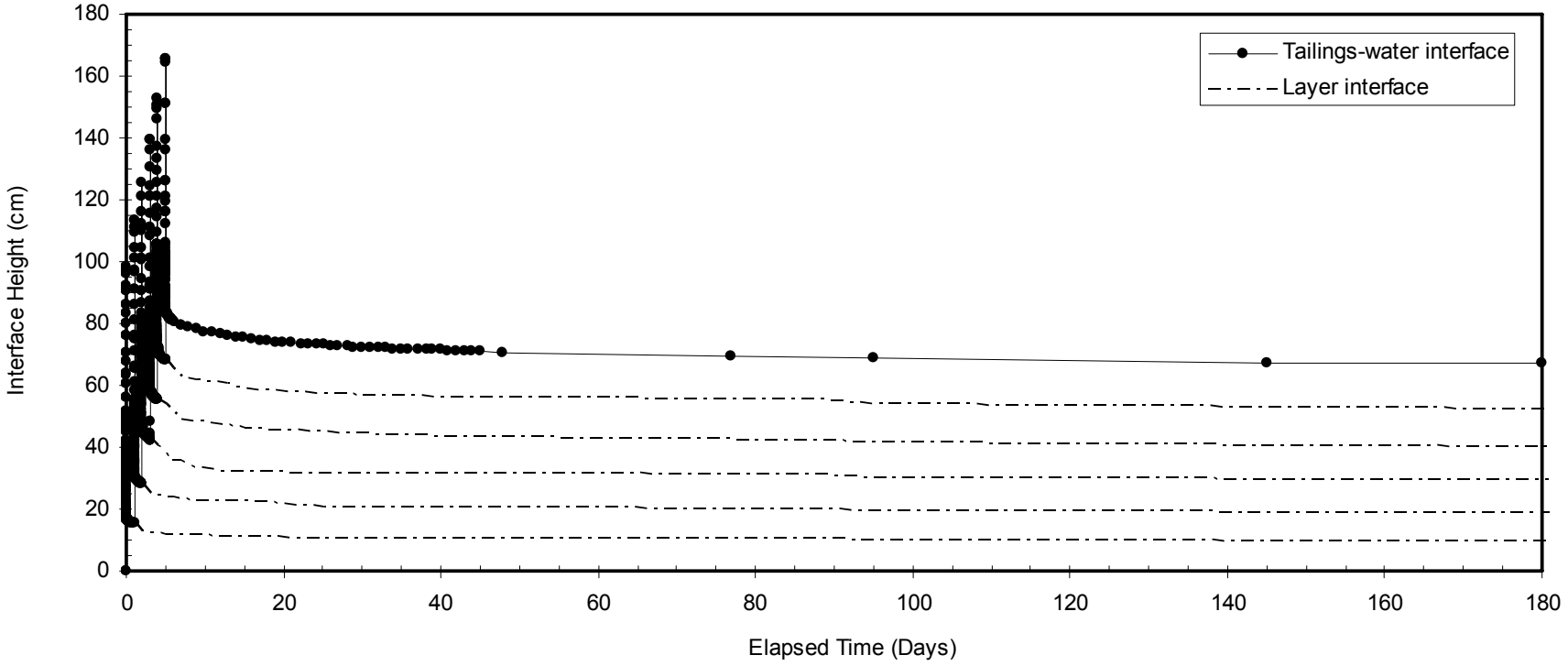

Figure 8.4 Interface height measurements of the validation standpipe between 0-180 days

323

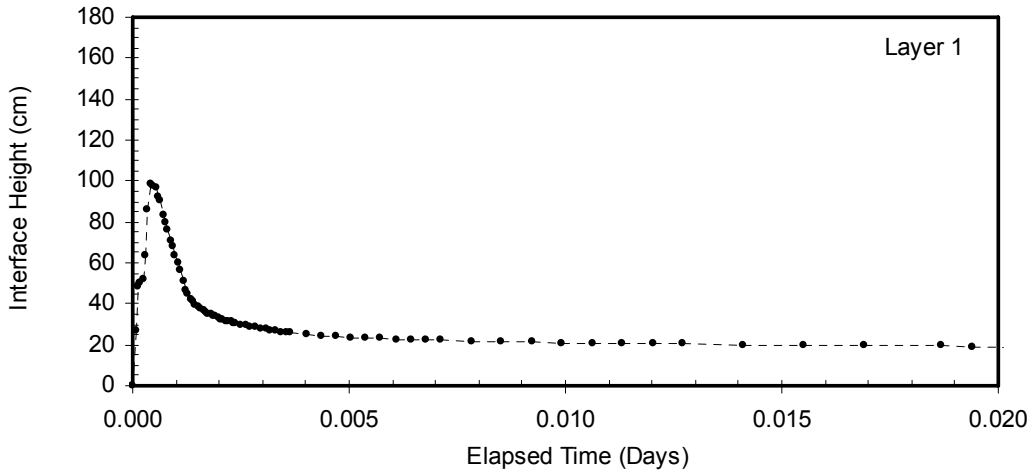

Figure 8.5 Interface height of Layer 1

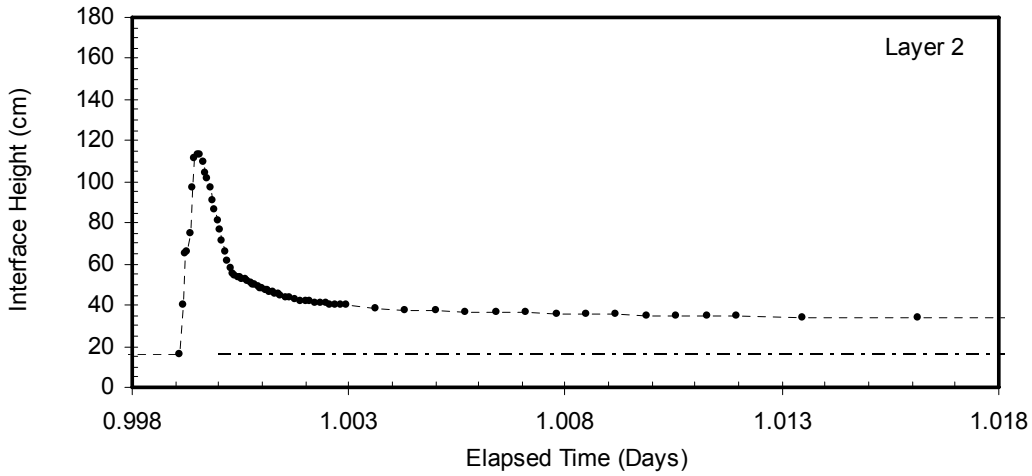

Figure 8.6 Interface height of Layer 2

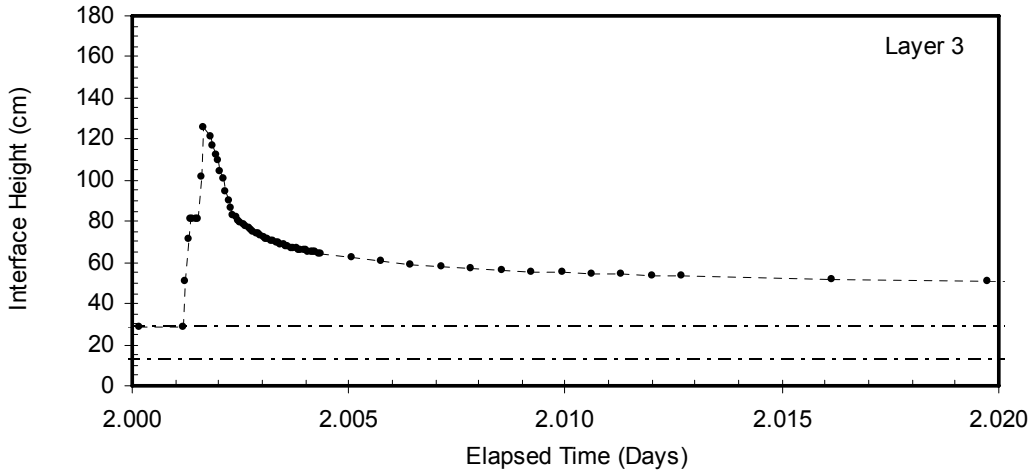

Figure 8.7 Interface height of Layer 3

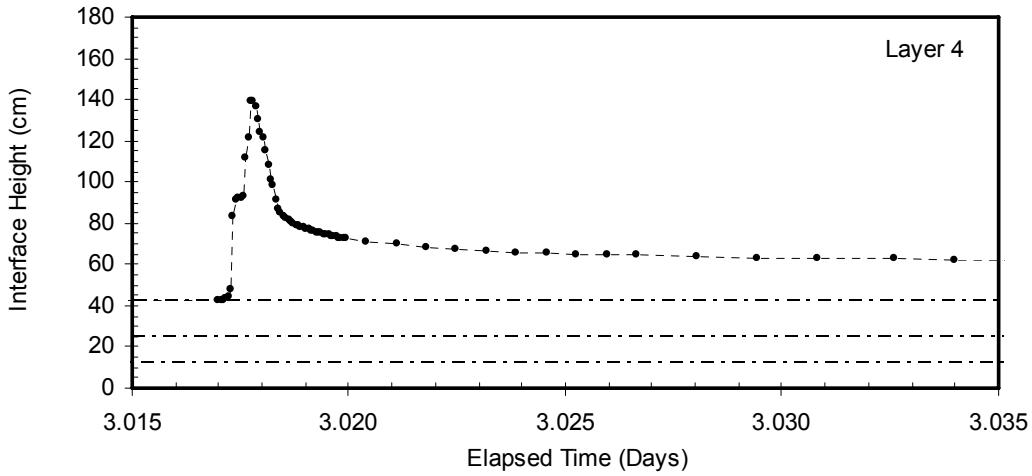

Figure 8.8 Interface height of Layer 4

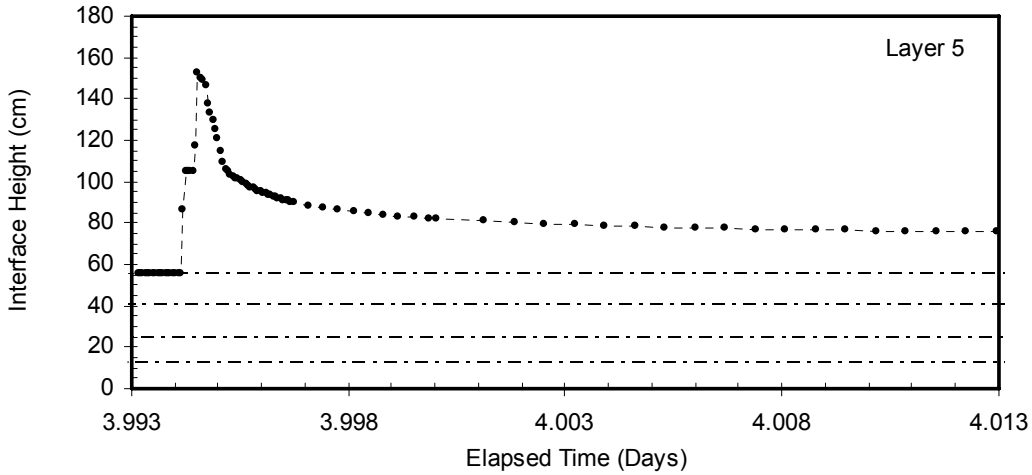

Figure 8.9 Interface height of Layer 5

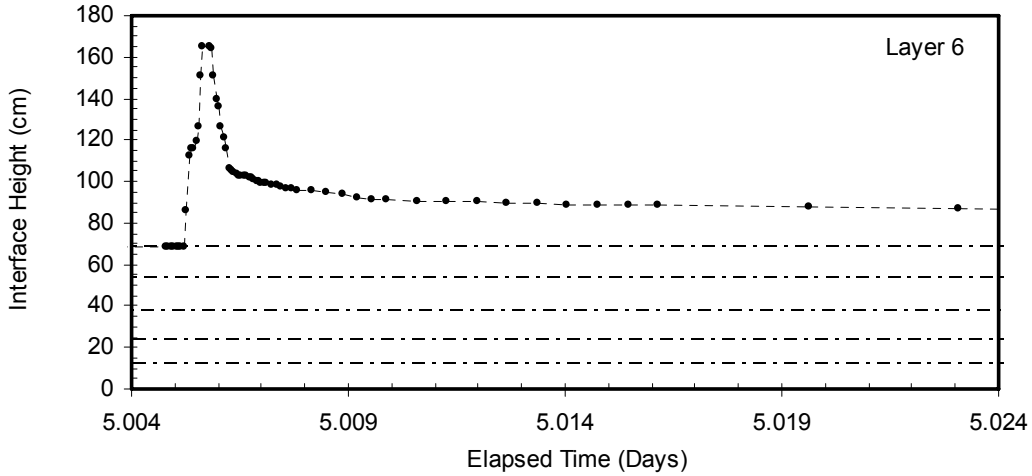

Figure 8.10 Interface height of Layer 6

8.2.3.2 Excess pore water pressure measurements

Excess pore pressure measurements after filling for Layers 1 to 6 are shown in Figures 8.11 to 8.16. The elapsed time of excess pore pressure measurements shown in the figures are 0.0005 days, 0.001 days, 0.005 days, 0.01 days, 0.05 days, 0.1 days, 0.25 days and 0.8 days after deposition. It should be noted that the initial mass of each layer can increase the excess pore pressure initially (that is at zero elapsed time) by 0.29 kPa at the bottom of the layer. This value will be used in the discussion below to evaluate the response of the soil layers to additional loads and to calculate the percent consolidation with time.

In Figure 8.11, an initial adjusted total stress (defined as the total stress minus hydrostatic pore pressure (Miller et al., 2010)) calculated from the filling of Layer 1 is shown by the grey line. The excess pore water pressure measurements mostly fall below the grey line indicating a correct magnitude of excess pore pressure response. The excess pore water pressure measurements at 0.0009 days show only a small excess pore water pressure between heights of 0.3 m and 0.7 m. Below 0.3 m, the excess pore pressure increased significantly to the bottom pressure of about 0.35 kPa, slightly higher than the theoretical initial value of 0.29 kPa. The change in the slope of the excess pore water pressure profile is an indication of the formation of a soil layer and the inflection point is a rough boundary between sedimentation and consolidation phenomena. The excess pore water pressure measurements then decreased during the 24 hour period and the bottom excess pore pressure measurement was 0.12 kPa at 0.80 days.

Figure 8.12 shows excess pore water measurements after deposition of Layer 2. It can be seen that the 1.0 day measurement (0.0005 days after deposition) has a bottom excess pore water pressure of about 0.38 kPa. By assuming that the excess pore water at the bottom just before the deposition of the layer is 0.12 kPa (last measurement from Layer 1), the maximum excess pore pressure at the bottom after the 2^{nd} layer deposition would be 0.12 + 0.29 = 0.41 kPa which agrees well with the 0.38 kPa measurement. Similar to Layer 1, Layer 2 showed an inflection point in the excess pore pressure measurements at 1 and 1.0005 days but this behavior disappeared at a later time indicating a completion of hindered sedimentation. The final bottom excess pore water measurement at 1.7995 days was 0.19 kPa.

Figure 8.13 shows excess pore water measurements after deposition of the 3rd layer. The 2.0021 day measurement (0.0005 days after deposition) showed a bottom excess pore water pressure of about 0.44 kPa. Similarly as for the previous layer it can be calculated that the maximum excess pore pressure at the bottom after deposition of Layer 3 would be 0.19 + 0.29 = 0.48 kPa which agrees well with the initial measurement of 0.44 kPa. The final bottom excess pore water measurement at 2.8016 days was 0.29 kPa .

Figure 8.14 shows excess pore water measurements after deposition of the 4th layer. The 3.0183 day measurement (0.0005 days after deposition) has a bottom excess pore water pressure of about 0.61 kPa. The maximum excess pore pressure at the bottom after the 4th layer deposition would be 0.29 + 0.29 = 0.58 kPa similar to the measured valued of 0.61 kPa. The final bottom excess pore water measurement at 3.8178 days was 0.46 kPa.

Figure 8.15 shows excess pore water measurements after deposition of the 5th layer. The 3.9950 day measurement (0.0005 days after deposition) has a bottom excess pore water pressure of about 0.76 kPa. The maximum excess pore pressure at the bottom after the deposition of Layer 5 would be 0.46 + 0.29 = 0.75 kPa similar to the measured valued at 3.9950 days. The final bottom excess pore water measurement of Layer 5 at 4.7945 days was 0.61 kPa.

Excess pore water pressure responses after the deposition of the final layer is shown in Figure 8.16. No inflection point near the top of the excess pore pressure profiles can be observed at 5.0063 days (0.0005 days after deposition). This indicates that this layer is likely settling relatively more quickly compared to other layers. Initial linear settling velocities and calculated initial hydraulic conductivity of each layer are shown in Table 8.2. The velocities and hydraulic conductivities are similar for all layers indicating a uniformity of material in the layers and subsequent analyses should not be affected by varying material properties. The final layer has a slightly higher initial settling velocity indicating a slightly higher initial hydraulic conductivity but this small difference in hydraulic conductivity should not affect subsequent analysis. It is unlikely that the lower consolidating layers would significantly contribute to a higher initial velocity of the final layer because the layer was undergoing hindered sedimentation at this stage and the settlement is very fast compared to the consolidation height change in the layers below.

In Figure 8.16, it can also be observed that at 5.0063 days or 0.0005 days after deposition, the sediment region has already reached the top interface resulting in the tailings-water interface settlement becoming nonlinear. This relatively faster settling behavior is unexpected and will be discussed in the next section.

After the deposition of Layer 6, dissipation of the excess pore pressure continued during the 180 days of monitoring and the final excess pore pressure profile at 180 days was very small with an excess pore pressure of only 0.049 kPa at the bottom of the standpipe. The percent consolidation at this time is calculated to be about 99.6%.

The percent consolidation calculated from the measured excess pore water pressure at the base of the standpipe is shown in Figures 8.17 and 8.18 for elapsed times of 0-6 days and 0-180 days respectively. During the filling period of 6 days the percent consolidation at the base of the standpipe shows a decreasing trend of the percent consolidation during the last 5 days (Figure 8.17). The decreasing trend indicates that the rate of filling is slightly faster than the rate of consolidation. One day after the last layer was deposited, the in-line thickened tailings material in the standpipe was over 50% consolidated at the base (Figure 8.17) and was at 90% consolidation at about 100 days (Figure 8.18).

As mentioned above, the filling rate was slightly faster than the consolidation rate. The trend of percent consolidation, however, is a good guide on how fast a tailings pond should be filled. A rate of deposition of one meter a day of 5% solids in-line thickened tailings is somewhat too fast to allow the tailings to increase consolidation during filling. Similar multilayer standpipe tests could be performed to determine the rate of filling, that is, the required size of a depositional pond for a tailings volume, that would result in a desired percent consolidation at the end of filling and the desired time for full consolidation. Such testing would validate large strain consolidation theoretical predictions for filling a tailings pond.

Table 8.2 Initial linear settling velocities of all six deposited layers

Layer	1	2	3	4	5	6
v_s(m/day)	730	830	750	950	850	1210
k_i (m/day)	1.0E+04	1.1E+04	1.0E+04	1.3E+04	1.2E+04	1.7E+04

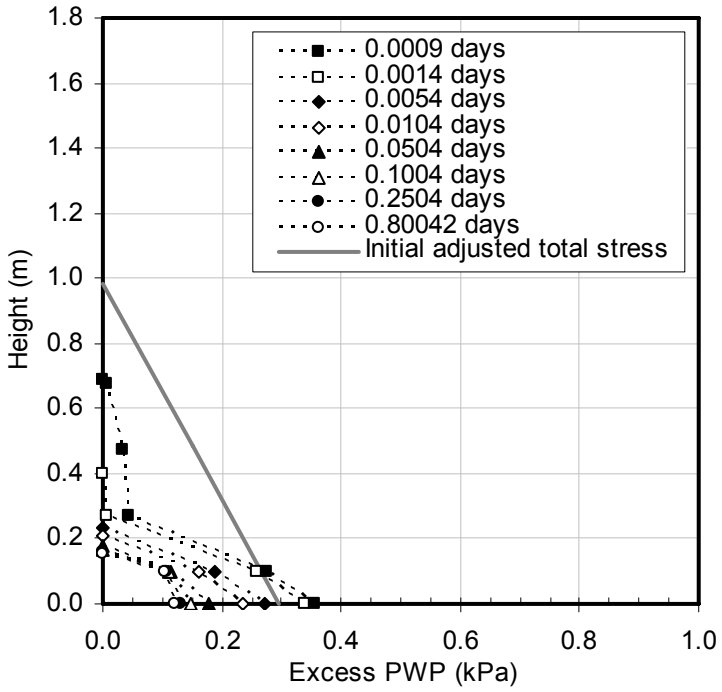

Figure 8.11 Post deposition excess pore pressure responses in Layer 1

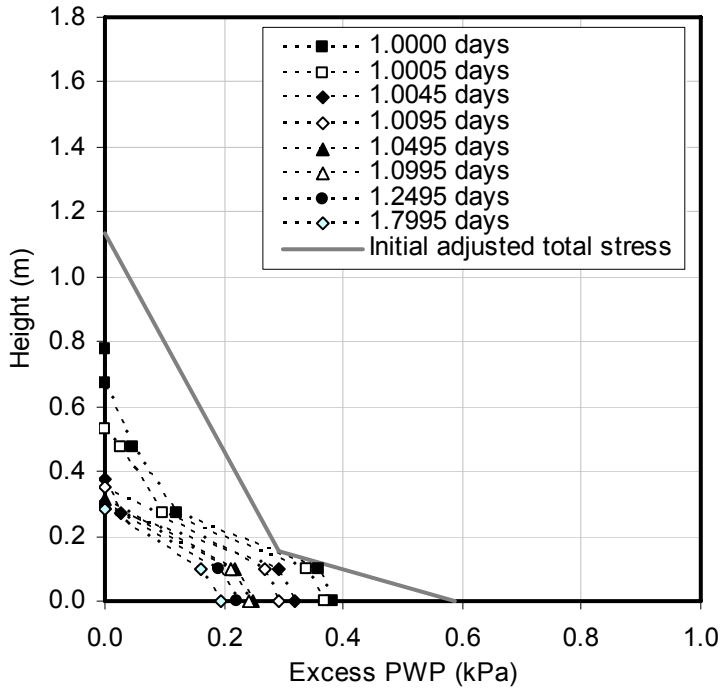

Figure 8.12 Post deposition excess pore pressure responses in Layer 2

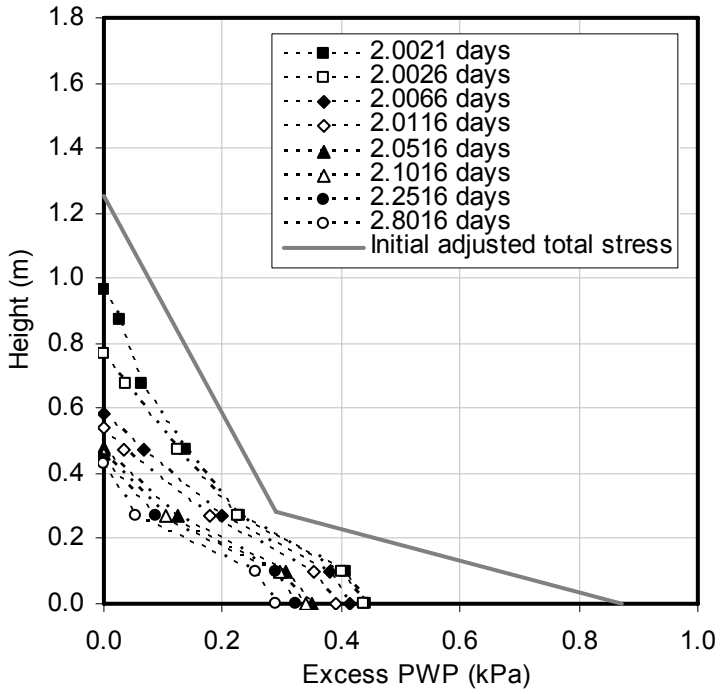

Figure 8.13 Post deposition excess pore pressure responses in Layer 3

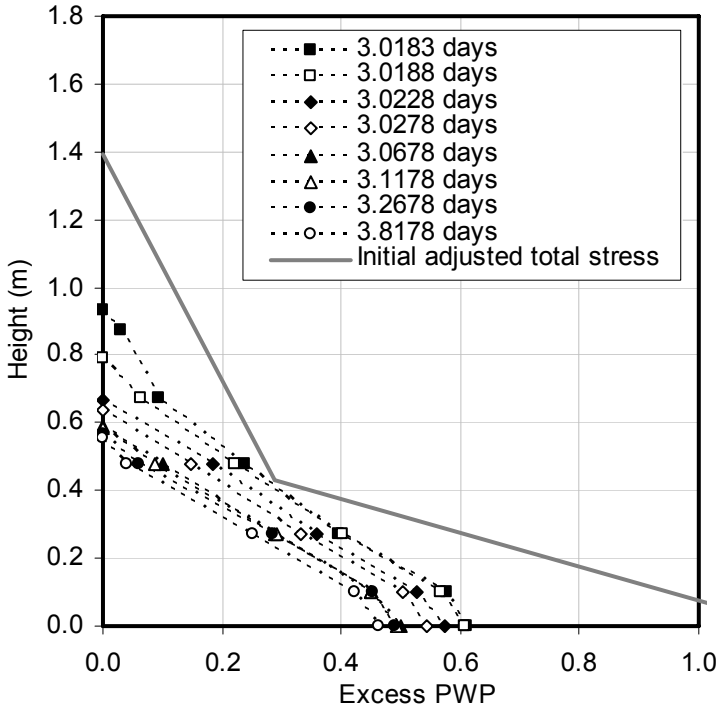

Figure 8.14 Post deposition excess pore pressure responses in Layer 4

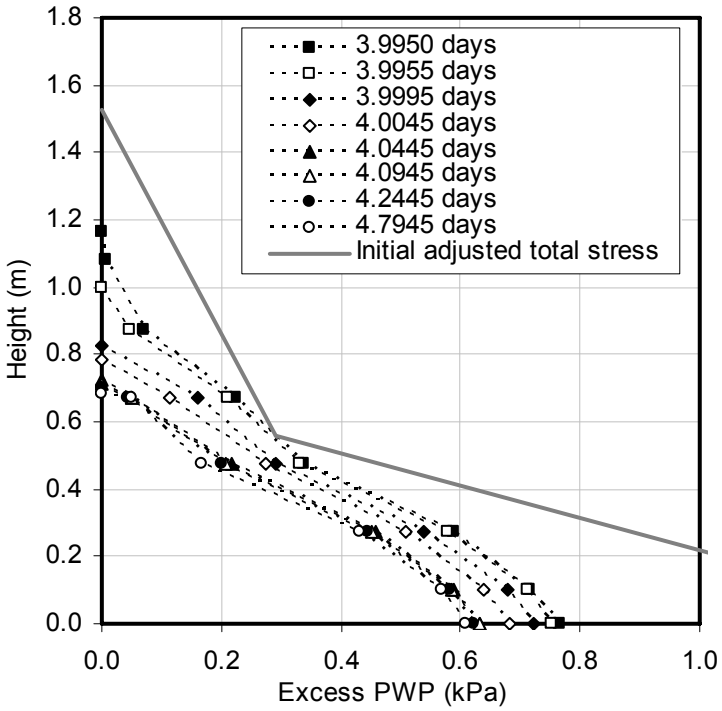

Figure 8.15 Post deposition excess pore pressure responses in Layer 5

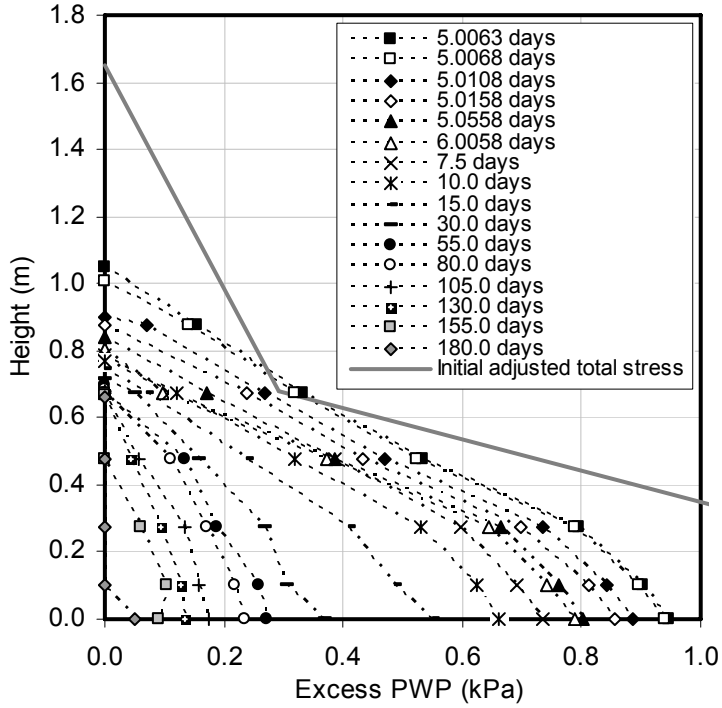

Figure 8.16 Post deposition excess pore pressure responses in Layer 6

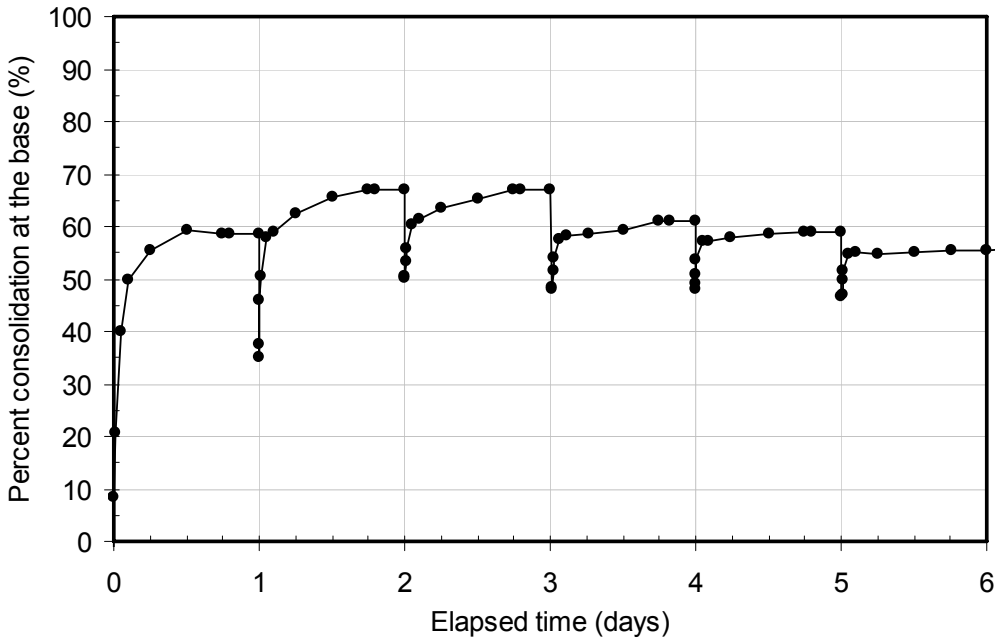

Figure 8.17 Percent consolidation at the base of the standpipe (0-6 days)

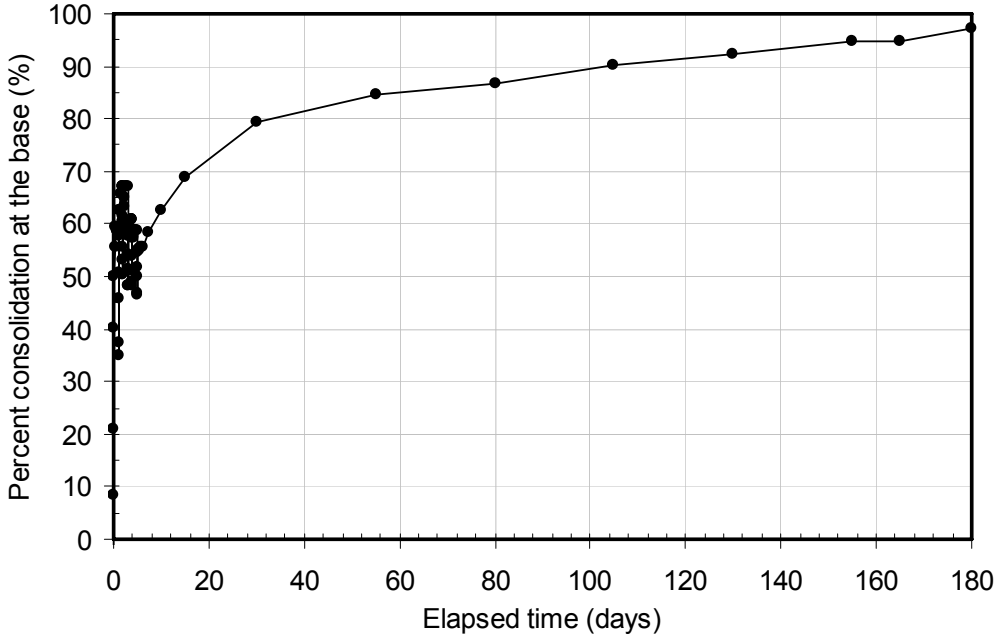

Figure 8.18 Percent consolidation at the base of the standpipe (0-180 days)

8.2.3.3 Water chemistry

To document water chemistry of the released pore water from each layer, the supernatant water from each layer was decanted and submitted to water chemistry analysis. The results of pH, conductivity and ion measurements are shown in Table 8.3. It appears that the water chemistry in the standpipe material is similar to that of in-line thickened tailings tested in Chapter 7 which did not change significantly from the pore water chemistry of the parent cyclone overflow tailings.

Table 8.3 Release water chemistry for all six deposited layers

Layer	1	2	3	4	5	6
pH	8.8	8.8	8.7	8.6	8.7	8.7
Conductivity (μs/cm)	3680	3800	3730	3720	3610	3750
Na^+	688.3	702.0	705.6	708.4	709.6	703.9
K^+	12.2	12.6	12.7	12.7	12.8	13.0
Mg^{2+}	6.1	6.0	6.0	6.0	6.1	6.0
Ca^{2+}	8.5	8.0	8.1	8.1	8.1	8.3
NH^{4+}	0.0	3.6	0.0	0.0	0.0	0.0
Li^+	0.2	0.2	0.2	0.2	0.2	0.2
Br^-	0.2	0.2	0.2	0.0	0.0	0.0
NO^{3-}	23.5	24.3	26.2	25.8	26.0	0.0
F^-	2.7	2.7	2.8	2.7	2.8	3.2
Cl^-	583.8	598.0	597.9	598.3	598.0	594.1
SO_4^{2-}	431.4	440.4	442.9	443.3	442.7	442.4

8.2.3.4 Final solids content, fines content and void ratio profiles

At the end of the standpipe test of 180 days, the in-line thickened tailings was sampled with depth by a spoon sampler from top down through the sample height of 0.67 m. The final solids content profile and fines content profile are shown in Figures 8.19 and 8.20 respectively.

The solids content profile shows that the minimum solids content is 20.8 % at the top and the maximum solids content is 39.7% at the bottom. The average solids content of the in-line thickened tailings at 180 days is 34.8%. The fines content profile generally shows that the material is quite uniform with an average fines content of about 90.6%.

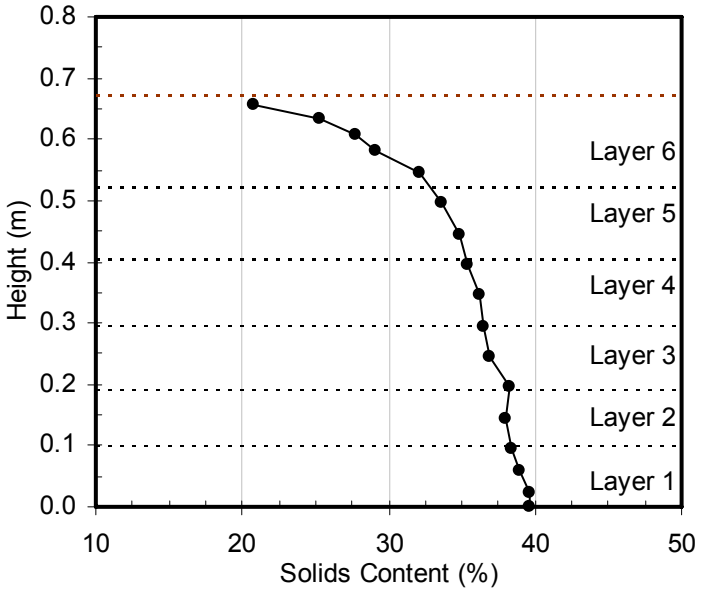

Figure 8.19 Solids content profile at the end of the test

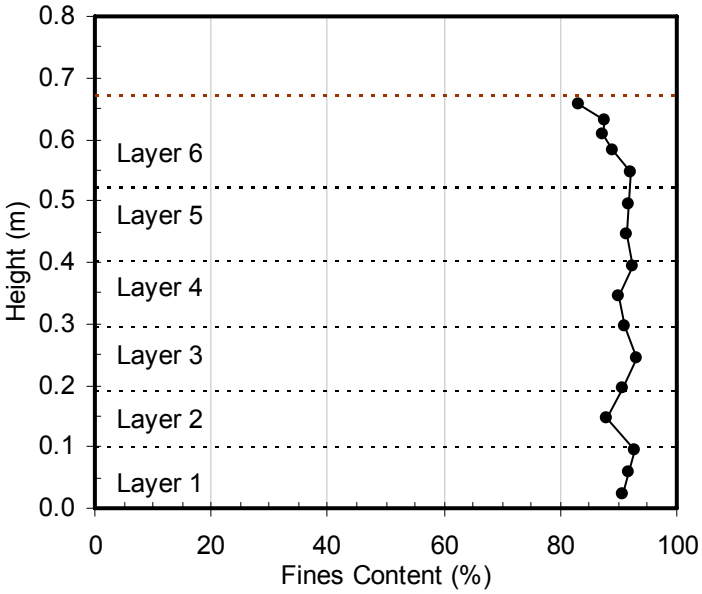

Figure 8.20 Fines content profile at the end of the test

Void ratio and calculated effective stress profiles are shown in Figures 8.21 and 8.22 respectively. The void ratios in the standpipe varied from 9.4 at the top to 3.7 at the bottom. The maximum effective stress at the bottom of the standpipe was 1.67 kPa. The maximum possible effective stress at the bottom based on the mass of the material was calculated to be about 1.75 kPa.

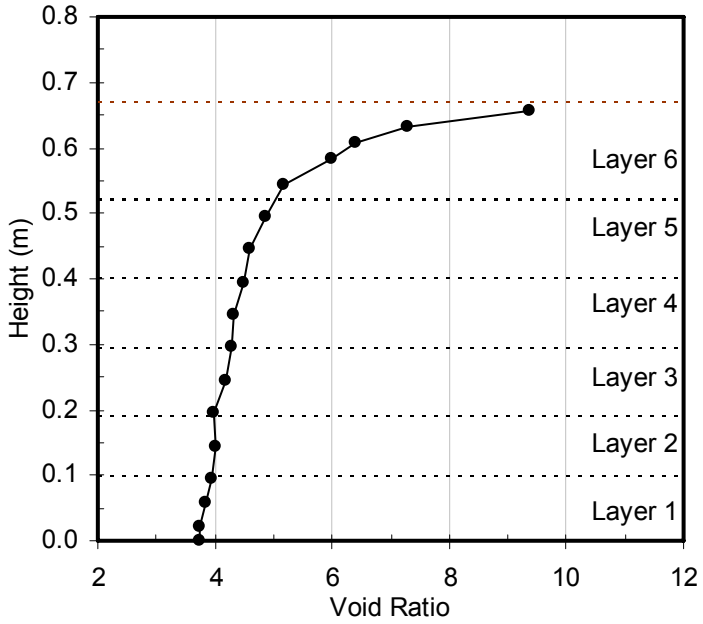

Figure 8.21 Void ratio profile at the end of the test

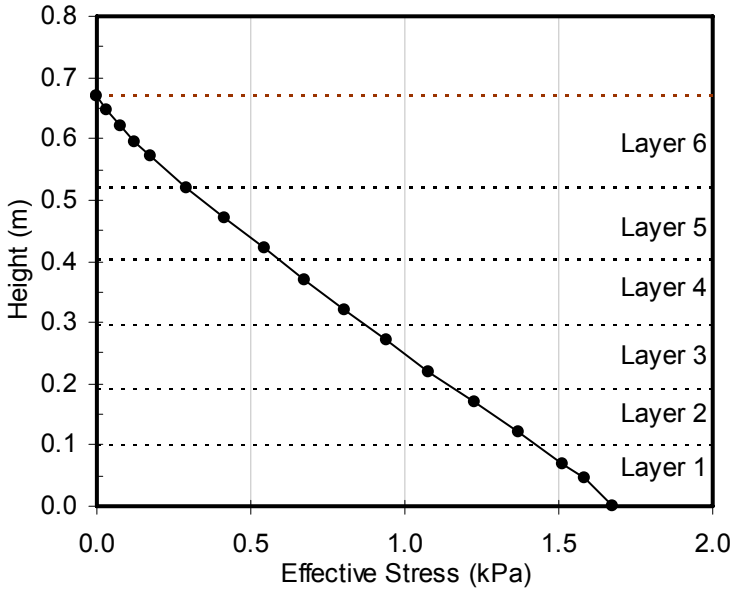

Figure 8.22 Effective stress profile at the end of the test

8.2.3.5 Final undrained shear strength profile

Undrained shear strength of the in-line thickened tailing in the validation standpipe was measured by a laboratory vane apparatus. Eight measurements were done at 10 cm intervals except at the top two locations where multiple measurements were performed. Figure 8.23 shows the vane shear strength measurements with depth.

In Figure 8.24, Equation 7.17 and the void ratio information in Figure 8.21 are used to calculate the undrained shear strength with depth and the result is compared with the undrained shear strength measurements from the standpipe. It is found that the projection of shear strength based on fines-bitumen void ratio provides a correct shape of the strength profile but it under estimates the values of the undrained shear strength existing in the standpipe with a maximum strength difference at the bottom measurement of 0.81 kPa or about 25% smaller than the measured data.

Comparison of measured undrained shear strength from the large strain consolidation tests, the standpipe test and the field results is shown in Figure 8.25. The difference is small and it appears that the standpipe data and the field data seem to form an upper boundary for all measured values. It is noted that both the standpipe data and the field data were measured similarly; they were both measured by a downhole vane measurement. The laboratory undrained shear strength measurement during the large strain consolidation tests require that a piston has to be removed during the strength measurement therefore the vertical effective stress at the vane depth is at most equal to the self-weight of the sample plus any effect of negative pore pressure. The self-weight of the sample is approximately only 0.05 kPa in most cases. Figure 8.24 also suggests that the difference between measured values from the vane during the large strain consolidation test and those from the standpipe test may be a function of depth. Three possible reasons are (i) the shear strength was partly increased by vane rod friction (ii) there is a contribution of effective stress to shear strength based on Mohr-Coulomb strength criterion and (iii) there is a thixotropic gain in strength in the material. The first reason is unlikely as the undrained shear strength was calibrated by measuring rod friction without a vane blade in the material. The measured data divided by the laboratory correlation in Equation 7.17 displays a strength ratio which is shown in Figure 8.26. The ratio is relatively high at low solids content near the top. If the slight different is caused by the effective stress, the ratio should be a function of the effective stress which is almost a straight linearly increasing line as shown in Figure 8.22. If it is because of thixotropic gain in strength, Suthaker (1995) showed that in a high water content fine tailings material, the thixotropic strength ratio is high while the ratio is lower in a lower water content material. Figure 8.26, therefore, indicates that the difference between the undrained shear strength of the ILTT in the standpipe and in the consolidation cell is

probably caused by thixotropic gain in strength as the strength ratio is high at the top where the water content is high.

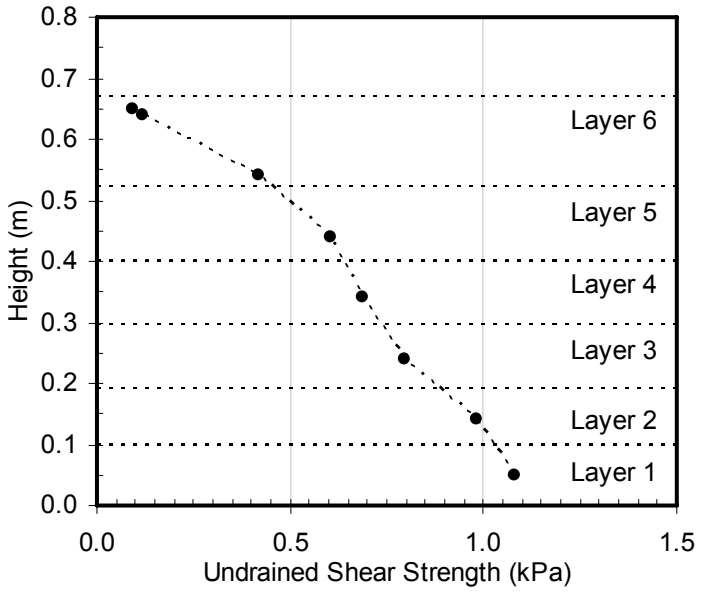

Figure 8.23 Undrained shear strength profile at the end of the test

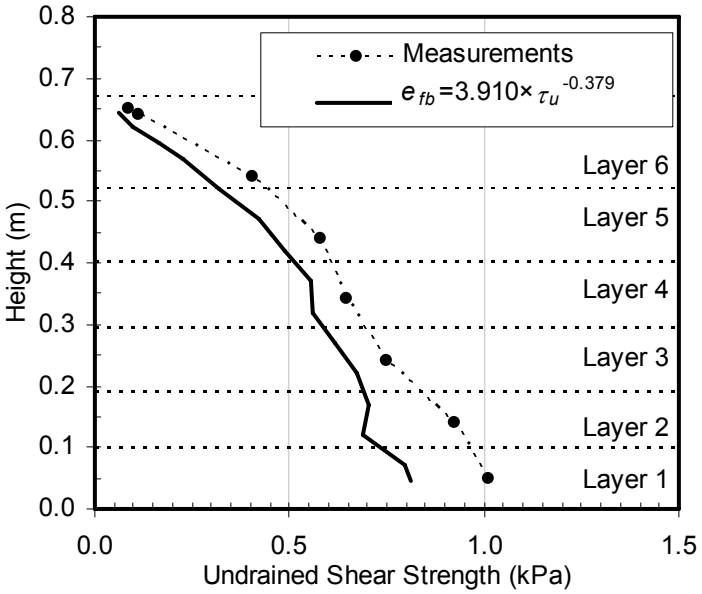

Figure 8.24 Comparison of calculated and measured undrained shear strength

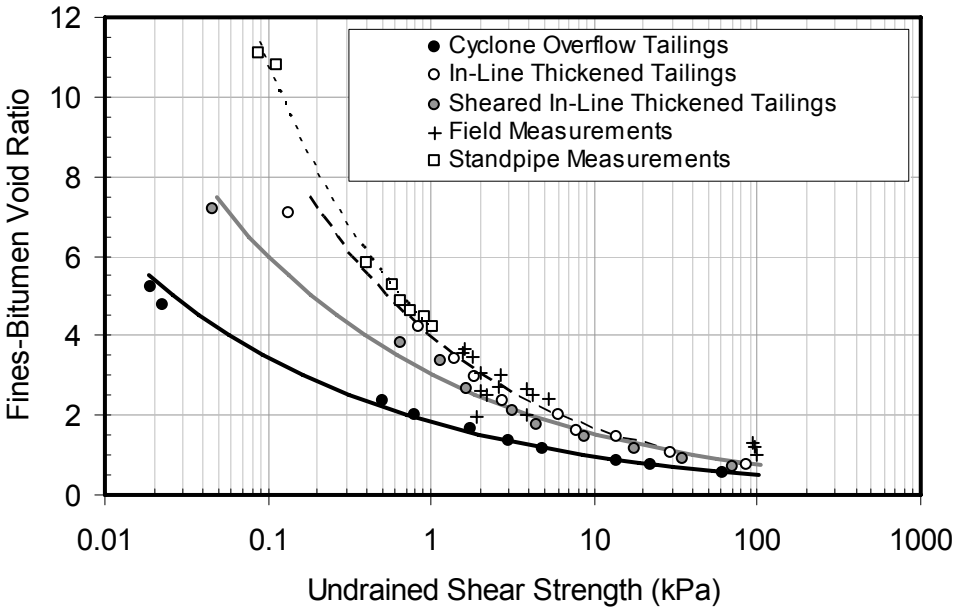

Figure 8.25 Comparison of calculated and measured undrained shear strength correlations

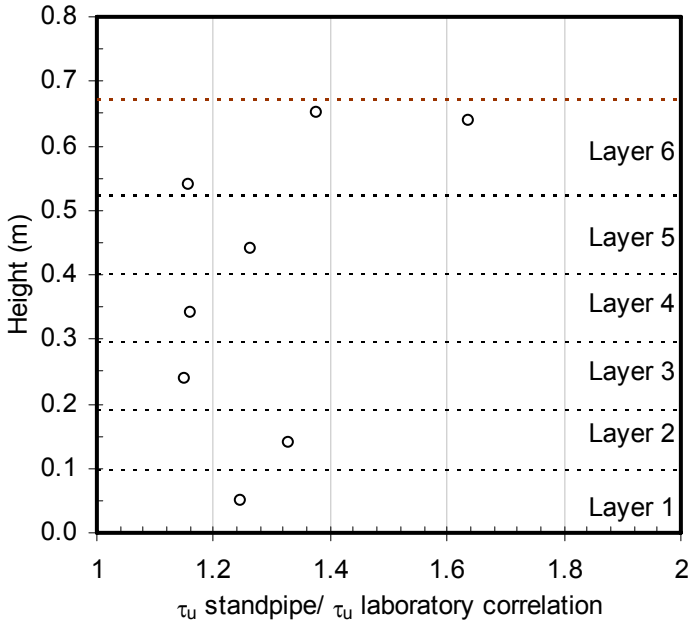

Figure 8.26 Strength ratio profile

Figure 8.27 shows a plot of undrained shear strength and effective stress ratio in the validation standpipe test on the τ_u/σ'_{vo} diagram developed earlier in Figure 7.78. It must be stressed that this diagram is only a guide due to its limitations discussed earlier in Chapter 7.

Figure 8.27 shows that the high τ_u/σ'_{vo} ratio of the in-line thickened tailings deposited in the standpipe has a similar trend as the τ_u/σ'_{vo} ratio from the consolidation tests. This high ratio of undrained shear strength to vertical effective stress is an indication of the strong bonds in the floc structure created by the in-line thickening process.

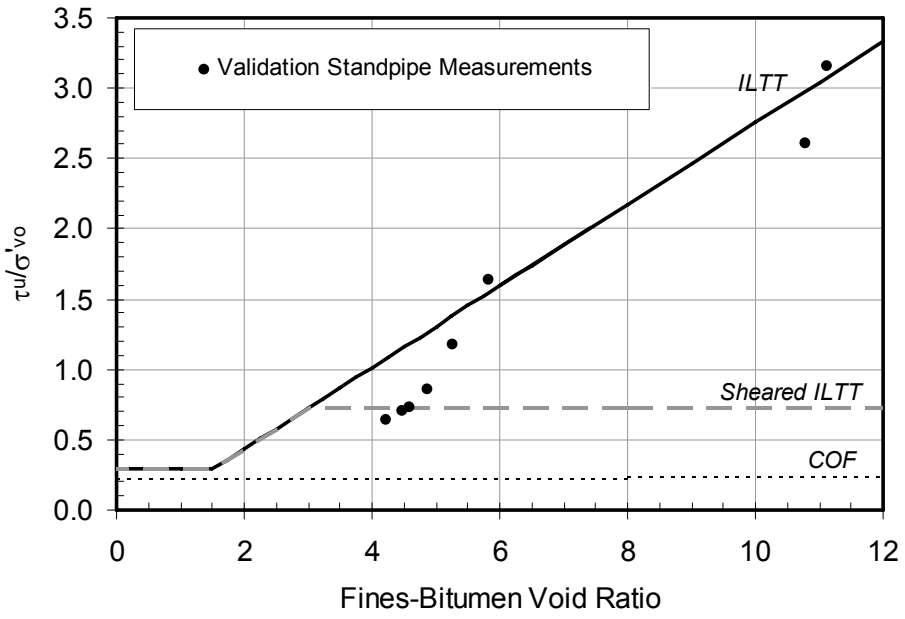

Figure 8.27 Comparison of correlations between τ_u/σ'_{vo} ratio and fines-bitumen void ratio

8.3 Validation of a theoretical model and geotechnical soil parameters on ILTT

In this section, developed finite strain consolidation models were used to model the validation standpipe. Three numerical models were used for comparison purposes. They are (i) a conventional finite strain consolidation filling model, (ii) a finite strain consolidation model without excess pore pressure dissipation during filling and (iii) a

pseudo sedimentation-consolidation model without pore water pressure dissipation during filling.

The first model, a conventional model, is a model such as presented in Section 3.2.2. The second model contains the same physics as the first model with a slight modification that during filling of a new layer, excess pore pressure dissipation is assumed to be negligible. This assumption is applied because it is realized that the deposition technique used in the validation standpipe potentially reset the timing of sedimentation and consolidation phenomena of a new layer to start after filling is complete. The last model that will be investigated is a pseudo sedimentation-consolidation model. The pseudo sedimentation model contains a compressibility function that defines a compressibility region during sedimentation to be negligible. Numerical prediction in the section will be mainly focused on the second model as it requires the least parameters and its assumption best represents the real condition of the validation standpipe test.

Model parameters for Models 1 and 2 were obtained from the experimental program in Chapter 7 and are shown in Equations 8.1 and 8.2 for compressibility and hydraulic conductivity respectively.

$$e = \begin{cases} 2.773 \times \sigma'^{-0.350} & ;17.0 \geq e \geq 7.5 \\ 5.644 \times \sigma'^{-0.100} & ;7.5 \geq e \geq 6.7 \\ 2.802 \times \sigma'^{-0.508} & ;6.7 \geq e \geq 5.0 \\ 3.641 \times \sigma'^{-0.278} & ;5.0 \geq e \geq 0.5 \end{cases} \quad [8.1]$$

$$k = \begin{cases} 6.944 \times e^{2.087} & ;80.0 \geq e \geq 40.0 \\ 8.469 \times 10^{-4} \times e^{4.530} & ;40.0 \geq e \geq 15.0 \\ 3.951 \times 10^{-8} \times e^{8.212} & ;15.0 \geq e \geq 3.0 \\ 7.000 \times 10^{-6} \times e^{3.500} & ;3.0 \geq e \geq 0.5 \end{cases} \quad [8.2]$$

Where e is void ratio, σ' is vertical effective stress in kPa and k is hydraulic conductivity in m/day.

For a pseudo sedimentation-consolidation filling model, the maximum suspension void ratio (e_m) of the tailings is arbitrary selected as 30 while the structural void ratio (e_s) is defined as 17 where the effective stress is first measurable in the compressibility plot (Figure 8.28). An interaction coefficient is then selected based on e_s and e_m as shown in Figure 8.29. It is noted that these boundary void ratios do not represent the true boundaries.

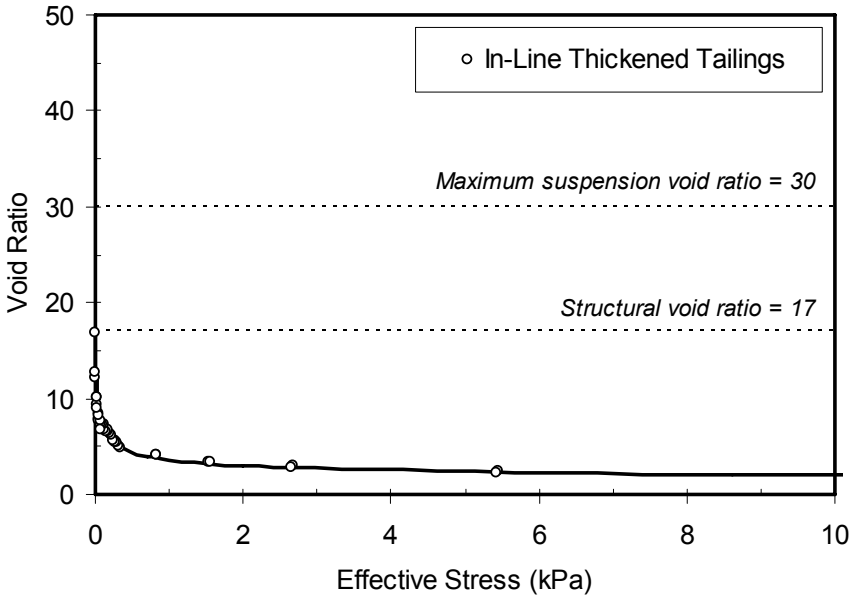

Figure 8.28 Compressibility of in-line thickened tailings and defined e_s and e_m

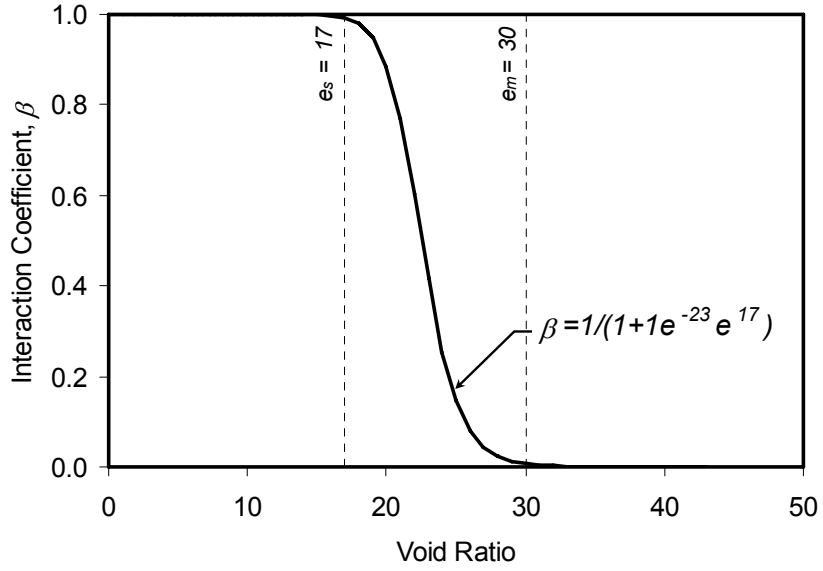

Figure 8.29 Assumed interaction coefficient for in-line thickened tailings

Using the interaction coefficient in Figure 8.29, a modified effective stress void ratio function is obtained as shown in Figure 8.30. A pseudo sedimentation-consolidation analysis may be performed by simply modifying the constitutive relationship to match the interaction coefficient modified compressibility. In order to perform this task, the interaction coefficient modified compressibility was inspected and it can be seen that the compressibility function between the extrapolated compressibility and interaction coefficient compressibility is approximately at a void ratio of 23. Therefore another power law function is assigned to the compressibility function at void ratios of 23 and above. The compressibility function used for the pseudo sedimentation-consolidation analysis then is given in Equation 8.3. The hydraulic conductivity relationship for this model remains the same as Equation 8.2.

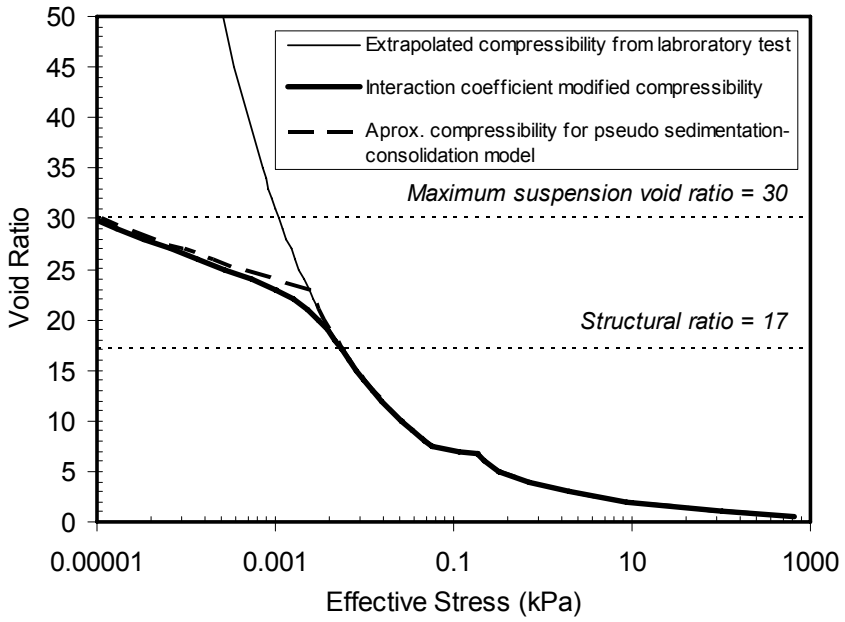

Figure 8.30 Compressibility for pseudo sedimentation-consolidation analysis

$$e = \begin{cases} 17.077 \times \sigma'^{-0.0493} ; 80.0 \geq e \geq 23.0 \\ 2.773 \times \sigma'^{-0.350} ; 23.0 \geq e \geq 7.5 \\ 5.644 \times \sigma'^{-0.100} ; 7.5 \geq e \geq 6.7 \\ 2.802 \times \sigma'^{-0.508} ; 6.7 \geq e \geq 5.0 \\ 3.641 \times \sigma'^{-0.278} ; 5.0 \geq e \geq 0.5 \end{cases} \quad [8.3]$$

Where e is void ratio and σ' is vertical effective stress in kPa.

For all models and all filled layers, the initial solids content is assigned as 5%, and the specific gravity is 2.46. Numerical parameters used for the models are $\Delta z = z/600$, Δt = 0.00001 to 0.1 for spatial and temporal resolutions for model (i) and (ii). For model (iii), $\Delta z = z/120$ and $\Delta t = 1\times10^{-7}$ to 0.1.

8.3.1 Interface settlement

Interface height comparisons between the experiment and a finite strain consolidation model without dissipation during filling are shown in Figures 8.31 and 8.32 for a period of 0-10 days and 0-180 days respectively. In Figure 8.31, Model 2 is able to well capture overall interface settlement behavior between 0-10 days. Between 0 and 180 days (Figure 8.32), the interface height prediction is slightly lower than the measurement through to the end of the settlement period.

Figures 8.33 to 8.38 show detailed interface settlement comparisons between the three models and the experimental results during the filling of all six layers. During filling of all the layers, Models 2 and 3 are able to capture the interface height better than Model 1. This is due to the fact that the during the rapid filling period, turbulent flow due to the deposition of the material and the withdrawal of the deposition instruments influenced a distinct interface settlement to be captured therefore the interface heights were taken at the top interface. As mentioned earlier, Models 2 and 3 utilized a filling condition without dissipation of excess pore pressure. This condition is more representative to the experimental condition therefore they agree better than the Model 1 during the filling. Model 1 has its excess pore pressure dissipating during filling thus it yields a smaller height after filling.

Considering the interface height predictions between Model 2 and Model 3, they are almost identical with a small difference that the pseudo sedimentation-consolidation model, Model 3, predicts slightly more settlement and slightly faster initial linear settling velocities. This is because the compressibility in Model 3 takes into account a sedimentation zone at very high void ratios. In this zone, the material is assumed to be highly compressible and cannot sustain the same effective stress as presented in the compressibility of Model 2. This also means that during the hindered sedimentation regime, consolidation has less influence in the sedimentation model. Compressibility of

in-line thickened tailings in Model 2 is known to exist at a very high void ratio and a very low effective stress (extrapolated compressibility in Figure 8.30), therefore, in Model 3 the inclusion of sedimentation which also takes place at very high void ratios does not provide a significant improvement from the prediction of a model without sedimentation. As both models are very similar and Model 3 requires parameters that are not well established, further discussion will mainly focus on the finite strain consolidation model, Model 2.

After Layer 1 filling is complete, the experiment data of interface height settling shows a slightly higher linear settling velocity compared to the models (Figure 8.33). The measured interface settlement is also lower than that of the prediction after hindered sedimentation. This may suggest a slightly higher hydraulic conductivity of the material in the validation standpipe than that used in the model.

In Layer 2 (Figure 8.34), after filling is complete, the measured linear settling velocity is significantly higher than that of the prediction. After hindered sedimentation, the interface measurements also stay lower but the difference narrows down as time progresses. This behavior implies that the compressibility in the models is similar to that of the standpipe material but there is a significant difference in hydraulic conductivity. This implication is because the short term behavior is governed by the hydraulic conductivity and the compressibility only starts to have an influence in the long term for high water content materials.

In Layer 3 (Figure 8.35), good agreement between interface measurement and prediction from Models 2 and 3 is obtained throughout the observation period.

For Layers 4 to 6 (Figure 8.36 to 8.38), the interface height measurements are located in between the predictions from Model 1 and Models 2 and 3 and the measured interface height has higher initial linear settling velocities compared to all the models. It is believed that two possibilities may be responsible for the discrepancies. One is that the deposited material in Layers 4 to 6 is slightly more permeable compared to Equation 8.2. This is plausible as in Figure 8.20 the fines contents in Layers 2, 4 and 6 are slightly on the low side. Another possible reason is that part of the newly deposited material was re-suspended while some was not. This would make tailings near the top of the newly

deposited layer having a lower solids content than the initial value. This would alter the initial settling rate of the material which is dependent on the local solids content.

It can also be observed that after hindered sedimentation in Layers 4 to 6, only in Layer 6 does the interface height stay significantly lower that the predictions. If it is assumed that the material hydraulic conductivity is identical for all layers, the lowest interface height will be the prediction of Model 1 due to the fact that consolidation occurs throughout all the elapsed times in Model 1. Therefore, the lower measured interface height of Layer 6 than that of the models after hindered sedimentation is likely caused by the slightly higher hydraulic conductivity of the lower fines content material in this layer.

Overall, the finite strain consolidation model is able to predict interface settlement of the in-line thickened tailings material. Small discrepancies between the models and the experiments are believed to be caused by small changes in the material properties and different settling conditions in the experimental standpipe.

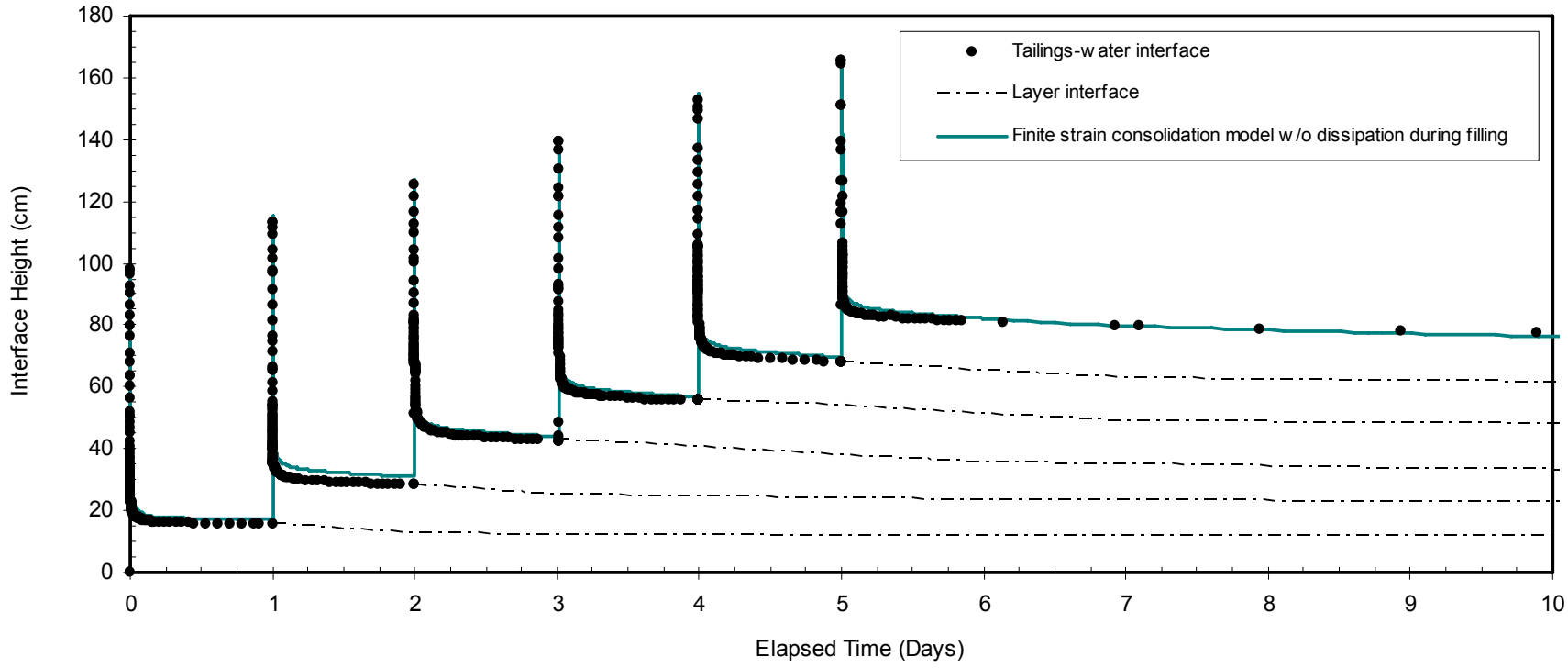

Figure 8.31 Comparison of the interface height measurements and prediction of the validation standpipe between 0-10 days

346

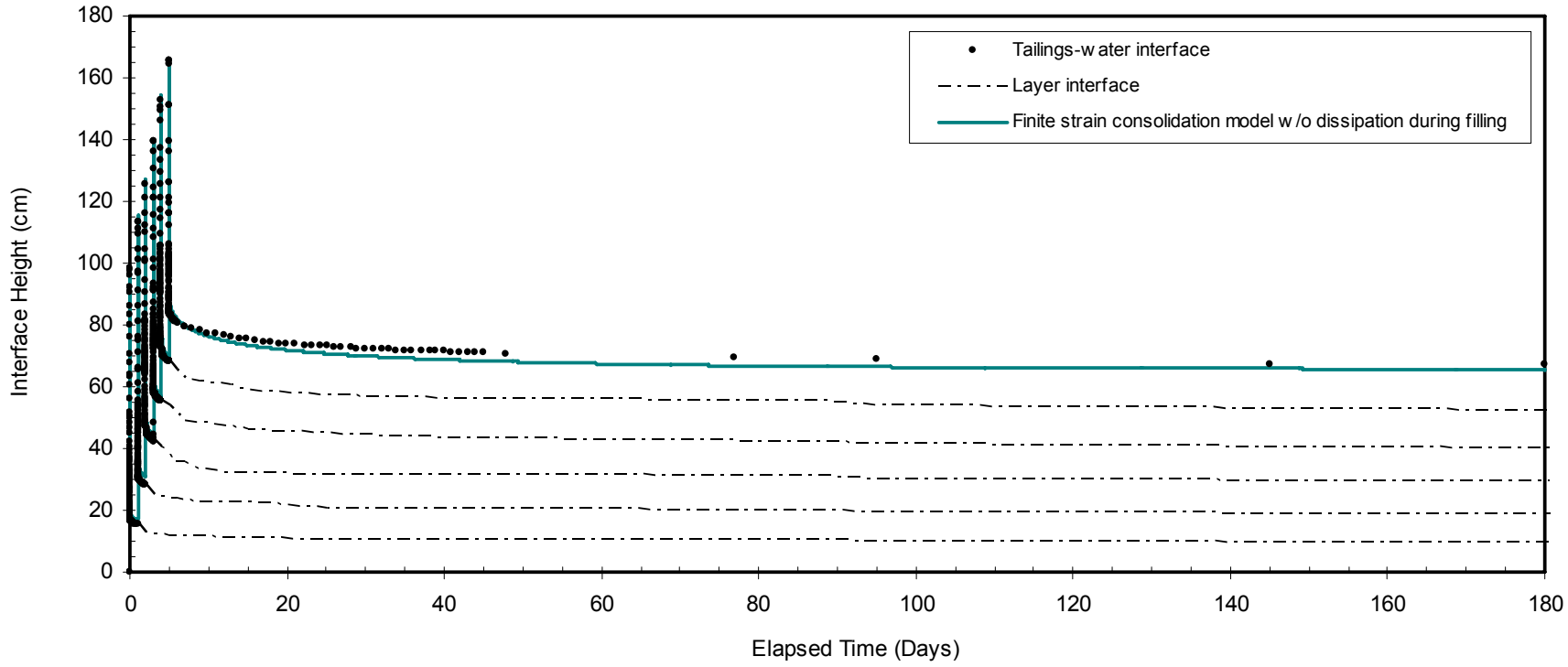

Figure 8.32 Comparison of the interface height measurements and prediction of the validation standpipe between 0-180 days

347

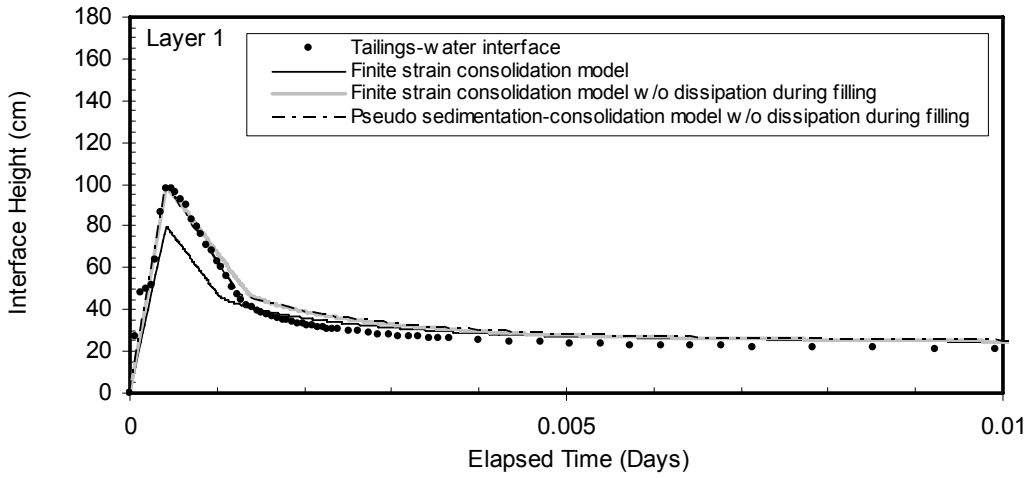

Figure 8.33 Comparison of interface settlement of Layer 1

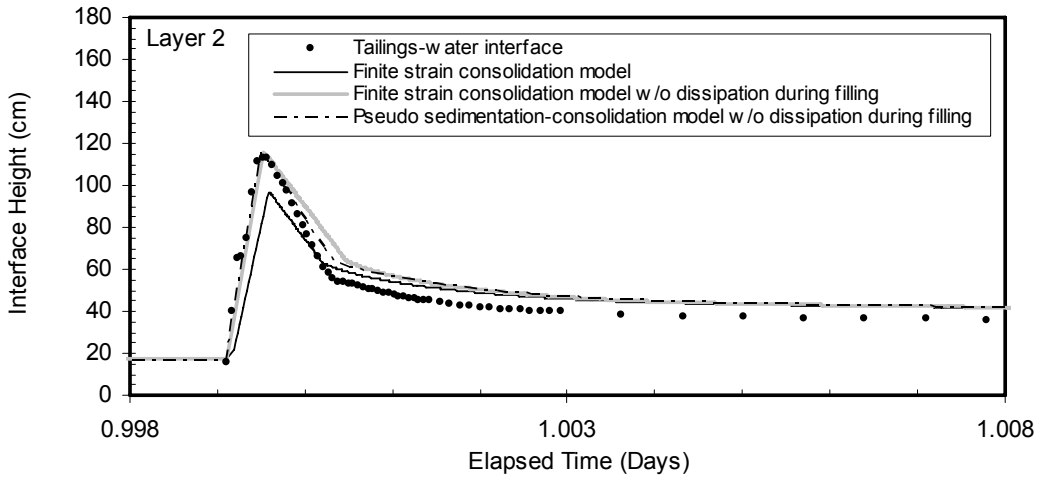

Figure 8.34 Comparison of interface settlement of Layer 2

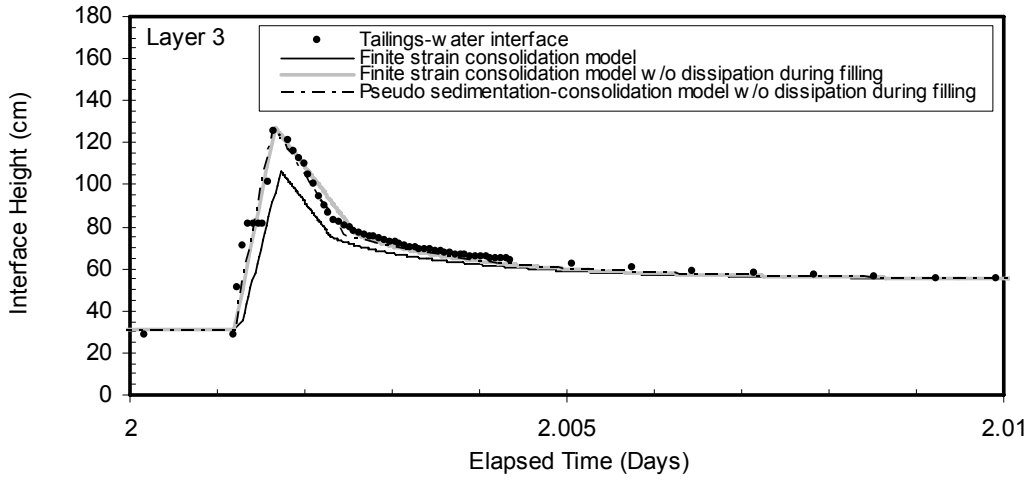

Figure 8.35 Comparison of interface settlement of Layer 3

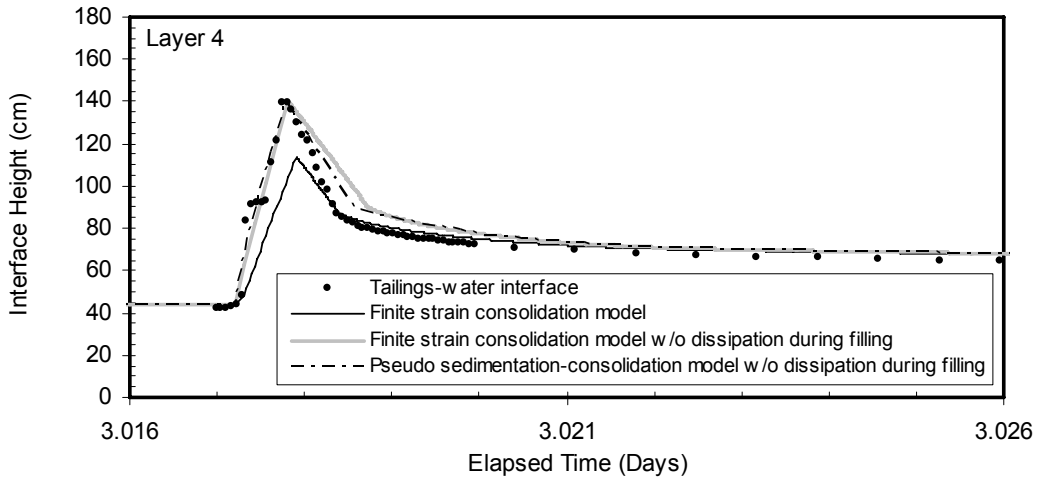

Figure 8.36 Comparison of interface settlement of Layer 4

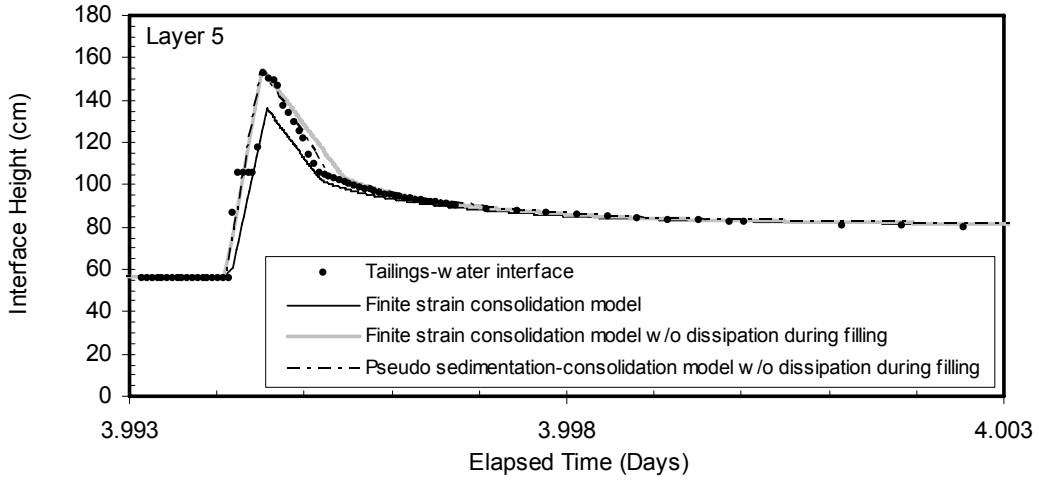

Figure 8.37 Comparison of interface settlement of Layer 5

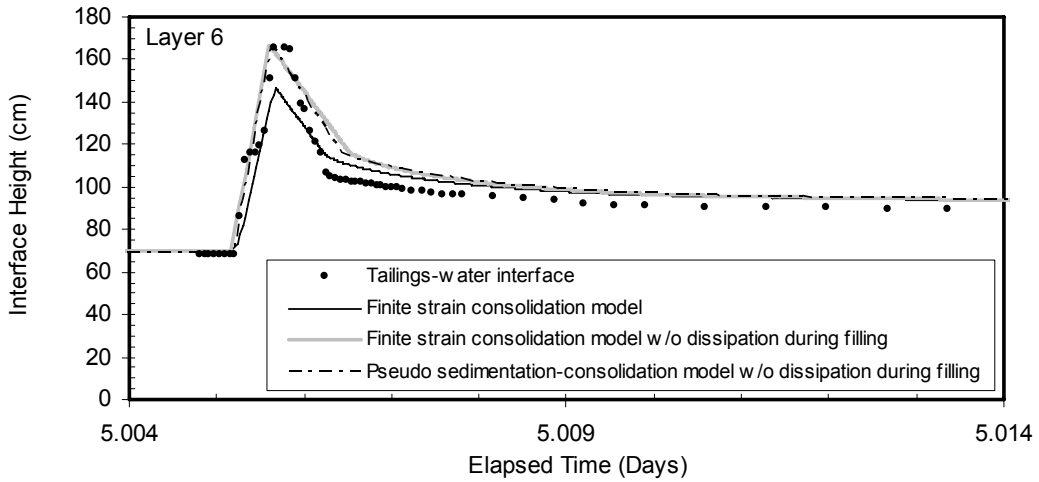

Figure 8.38 Comparison of interface settlement of Layer 6

8.3.2 Comparison of excess pore pressures profiles

Excess pore water pressure profile comparisons between a finite strain consolidation model and the validation standpipe measurements are shown in Figures 8.39 to 8.44 for Layers 1 to 6. Three profiles during quiescent conditions for of each layer, 0.0005 days, 0.005 days and 0.8 days after deposition, are used for the comparison in Layers 1 to 5. For Layer 6, six profiles at elapsed times of 5.0006 days, 5.01 days, 10 days, 15 days, 105 days and 180 days are selected.

In Figures 8.39 (a) and (b), the finite strain consolidation model with the selected constitutive relationships (Equations 8.1 and 8.2) is able to predict excess pore pressure changes adequately while at 8.39(c) shows that the finite strain consolidation model overestimates the rate of excess pore pressure dissipation.

In Figure 8.40, overall shapes and locations of the experimental results are adequately captured by the model. It can be observed that at the bottom in Figure 8.40(a), the excess pore pressure carried from Layer 1 exists in Layer 2 while the model shows almost no excess pore pressure carried over to Layer 2. Comparison of the excess pore pressure at the bottom of the standpipe in Figures 8.40 (a), (b) and (c) show a trend of faster dissipation process in the measurements than in the theory.

For Layers 3, 4 and 5, good agreement between the measurements and predictions can be seen and the same trend of faster dissipation at the bottom from the measurements is also observed (Figures 8.41, 8.42 and 8.43).

In the last layer, Layer 6, the same finding stands during the initial settling periods (Figures 8.44 (a) and (b)) while the excess pore pressure comparisons at elapsed times of 10 days and 15 days start to disagree with the experimental data; the measurements are higher near the top due to a slightly thicker profile and the measured pressures are lower near the bottom due to a faster dissipation rate (Figures 8.44 (c) and (d)). The last two comparisons at 105 days and 180 days show similar excess pore pressure responses at the bottom between experimental results and the model (Figures 8.44 (e) and (f)).

Regardless of the exclusion of a sedimentation process in the prediction, slight disagreements between the excess pore water pressure measurements from the validation standpipe and the model can come from slight differences in both the compressibility and hydraulic conductivity characteristics of the in-line thickened tailings in the standpipe and those assigned in the model. This is where a model calibration and a more detailed material determination may be required to obtain a better agreement between measured results and predictions.

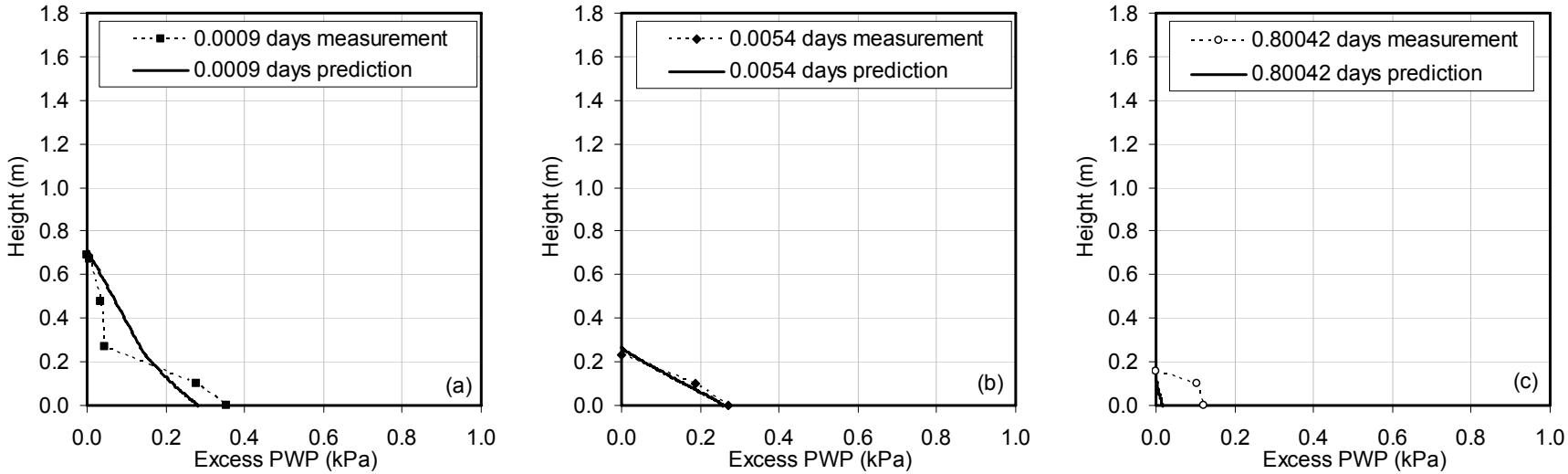

Figure 8.39 Comparison of excess pore pressure profiles between measurement and prediction for Layer 1

352

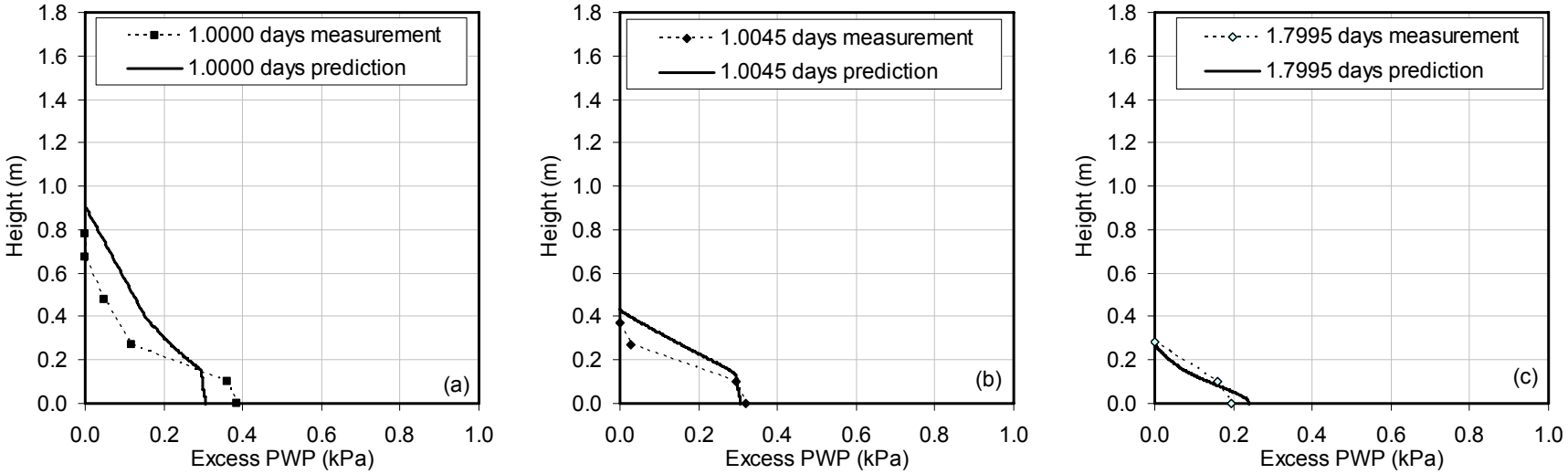

Figure 8.40 Comparison of excess pore pressure profiles between measurement and prediction for Layer 2

353

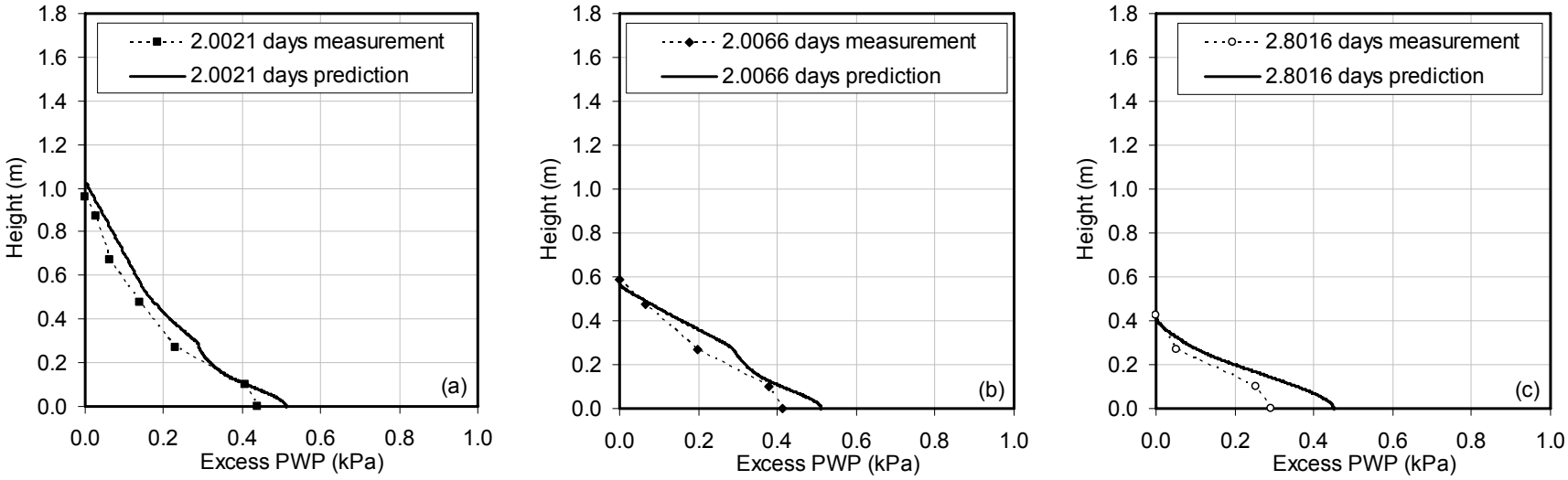

Figure 8.41 Comparison of excess pore pressure profiles between measurement and prediction for Layer 3

354

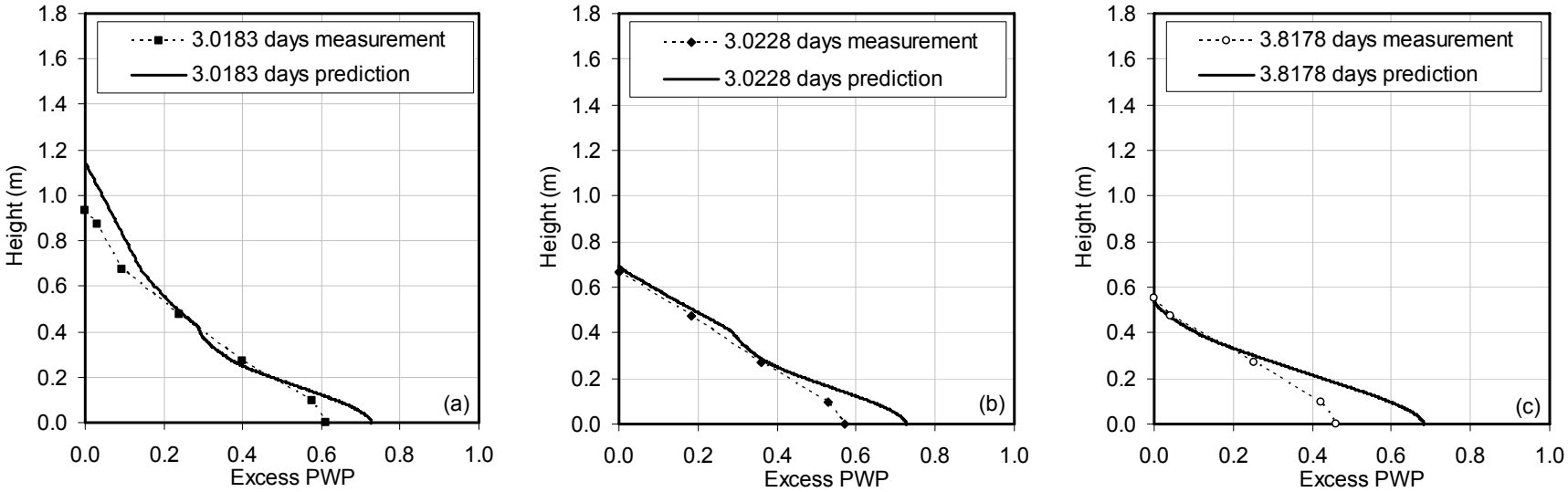

Figure 8.42 Comparison of excess pore pressure profiles between measurement and prediction for Layer 4

355

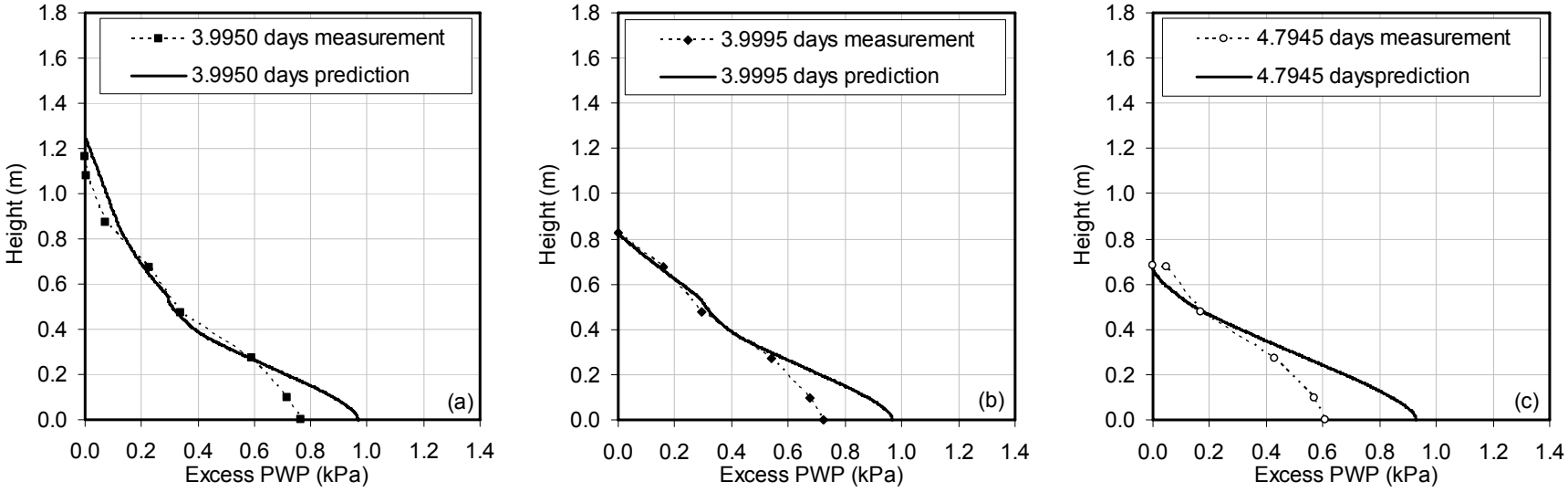

Figure 8.43 Comparison of excess pore pressure profiles between measurement and prediction for Layer 5

356

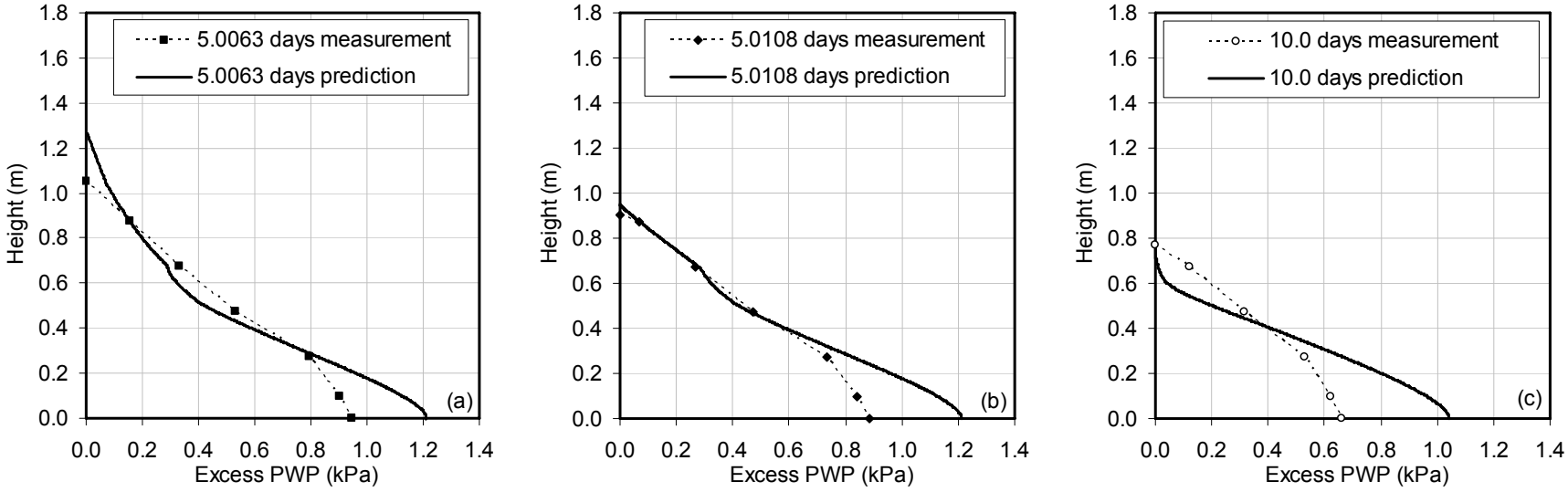

Figure 8.44 Comparison of excess pore pressure profiles between measurement and prediction for Layer 6

357

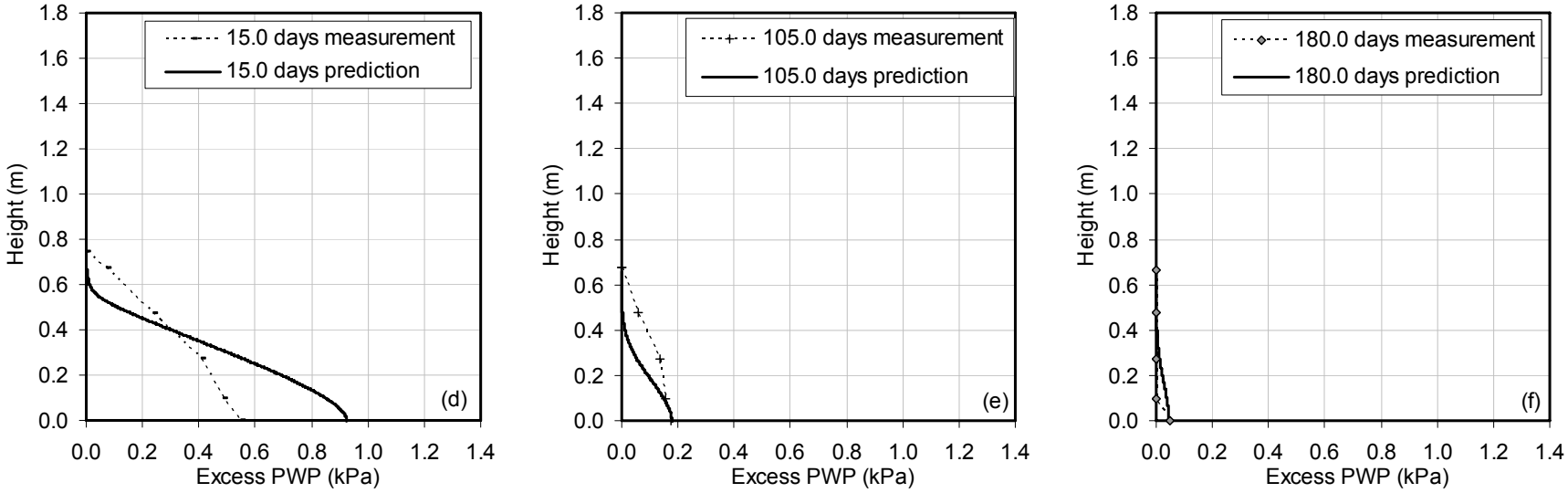

Figure 8.44 Comparison of excess pore pressure profiles between measurement and prediction for Layer 6 (Cont.)

358

8.3.3 Comparisons of final void ratio and undrained shear strength profiles

A comparison between the final measured void ratios and a prediction of the final void ratio profile is shown in Figure 8.45. Despite the similar final heights between the measurement and the prediction, the measured void ratio profile shows lower void ratios near the top Layers 5 and 6 while the measured void ratios are slightly higher than that of the prediction in Layer 4 and below.

Discrepancy in the comparison of the final void ratio profile is unexpected as the equilibrium of forces would guide the material at a certain effective stress to a specified void ratio based on material's compressibility. Explanations to the discrepancy could possibly be the influence of creep in the experimental standpipe test.

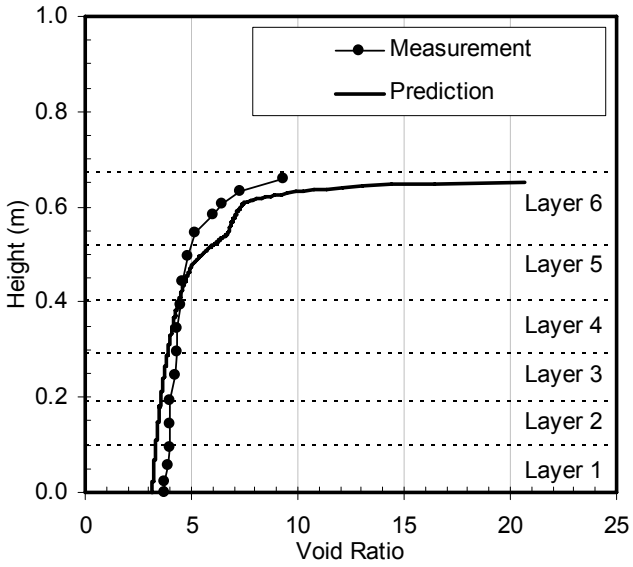

Figure 8.45 Void ratio profile comparison between measurement and prediction

A comparison of predicted and measured undrained shear strengths is shown in Figure 8.46. A similarity between the measured and the predicted undrained shear strength is not to be expected as there is a slight disagreement between the void ratio profiles. In Section 8.2.3.5, it was discussed earlier that the predicted undrained shear strength based on the established fines-bitumen void ratio - undrained shear strength correlation is lower than the measured data. The undrained shear strength comparison in Figure 8.46 therefore only illustrates that the undrained shear strength of the in-line

thickened tailings can be qualitatively captured by the application of the strength-fines-bitumen void ratio correlation with the predicted results from the numerical model.

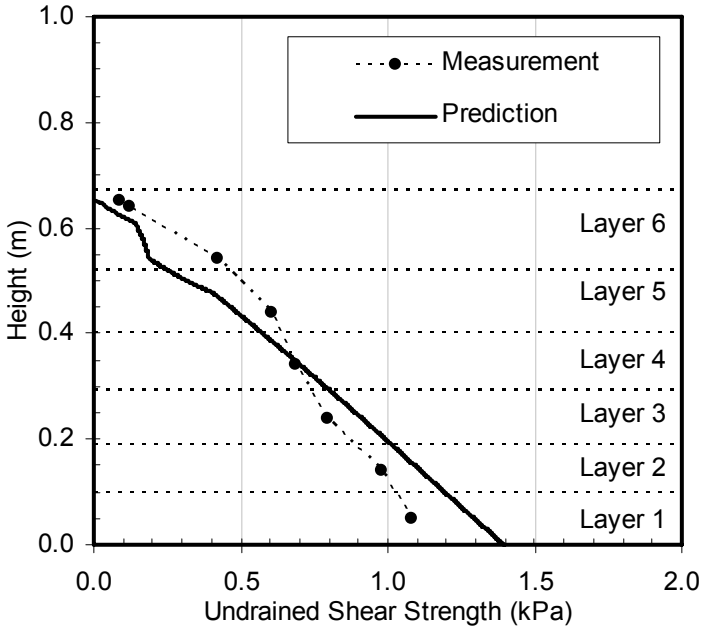

Figure 8.46 Undrained shear strength profile comparison between measurement and prediction

8.4 Supplement comparison of a 120 cm quiescent standpipe test

In the laboratory investigation of the in-line thickened tailings behavior in Chapter 7, a 120 cm compressibility standpipe test was performed by instantaneously filling a column with in-line thickened tailings at an initial solids content of 5% to obtain compressibility of the material at effective stresses up to 0.35 kPa. Parts of the material characteristics used in the validation process in this chapter are obtained from this compressibility standpipe test. Thus the standpipe test results cannot be used for a validation process. However the compressibility and hydraulic conductivity constitutive relationships for the in-line thickened tailings were derived from various tests and not mainly from this particular standpipe test. Therefore it is of interest to compare the performance of the 120 cm standpipe with the final constitutive relationships especially through the dissipation of excess pore pressures monitored during the test which was not used in the construction of the constitutive relationships.

Figures 8.47 and 8.48 show interface height comparisons at periods of 0-1.5 days and 0-0.01 days respectively. Figure 8.47 shows that the prediction closely matches the interface height at the end of the 1.5 days but overestimates the compression during the early stage of settlement. This is clearly shown in Figure 8.48 where time scale of 0-0.01 day is used. It can be observed that a slight flocculation period is observed at an elapsed time of lower than half a minute (0.0002 days) followed by rapid hindered sedimentation. The measured initial linear settling velocity is slightly higher than the prediction and the inflection point of the interface height occurred at about 0.78 m from the bottom while the model predicts this location to be about 0.53 m. It may be interpreted that the transition zone between sedimentation and consolidation which occurred in the standpipe is probably large. It also suggests that the material characteristics in this standpipe test do not strictly follow those assigned in the consolidation model. Even though a discrepancy during the transient process is observed, it can still be said that overall the interface height measurement is well captured by the model and the selected material parameters.

Figures 8.49 (a) and (b) are excess pore pressure measurements and predictions respectively. The comparison of the excess pore pressure profiles in Figure 8.49 shows excess pore pressure responses during hindered sedimentation and consolidation processes of in-line thickened tailings. The measured excess pore pressure at 0.0005 days shows a concave upward excess pore pressure profile. Theoretically if the material is homogenous while it is undergoing hindered sedimentation, the excess pore pressure profile in the hindered sedimentation region should be parallel to the initial excess pore pressure profile. This is predicted by the model but not in the measured profile. Instead the measured profile shows a much higher slope near the top indicating that the material at this location had a lower local solids content than the initial solids content of 5%. This possibility could possibly be caused by a turbulent flow after deposition or a complex water flux flowing from the bottom that may locally alter water content of the material. Following the completion of the hindered sedimentation process, a clear consolidation regime can be observed with a concave downward shape of dissipating excess pore water pressures. The shape and location of the measured excess pore water pressure profiles are similar to that predicted by the finite strain consolidation model.

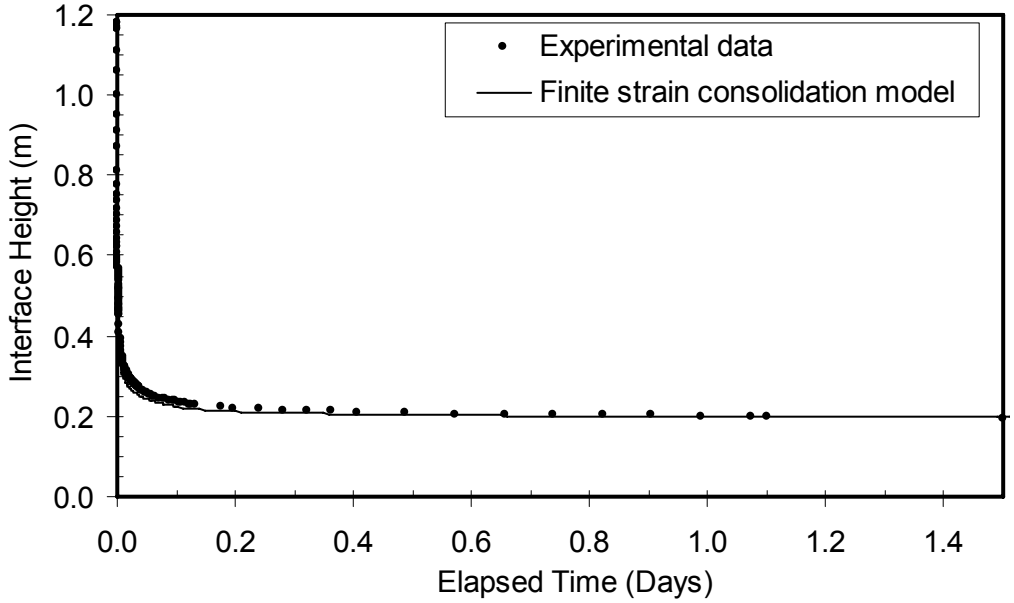

Figure 8.47 Interface height comparison between experiment and model for 120cm standpipe between 0 and 1.5 days

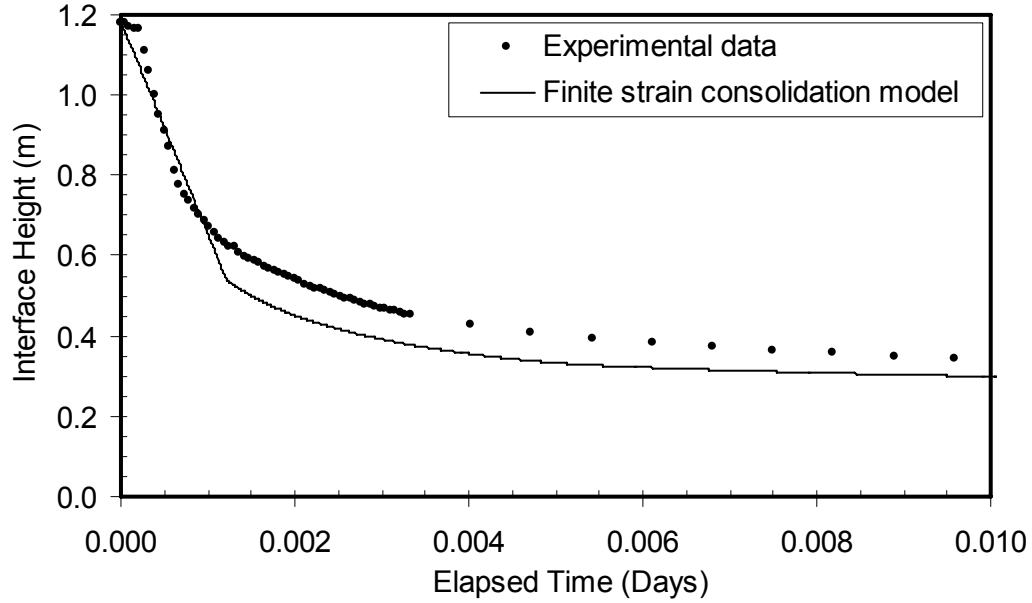

Figure 8.48 Interface height comparison between experiment and model for 120cm standpipe between 0 and 0.01 days

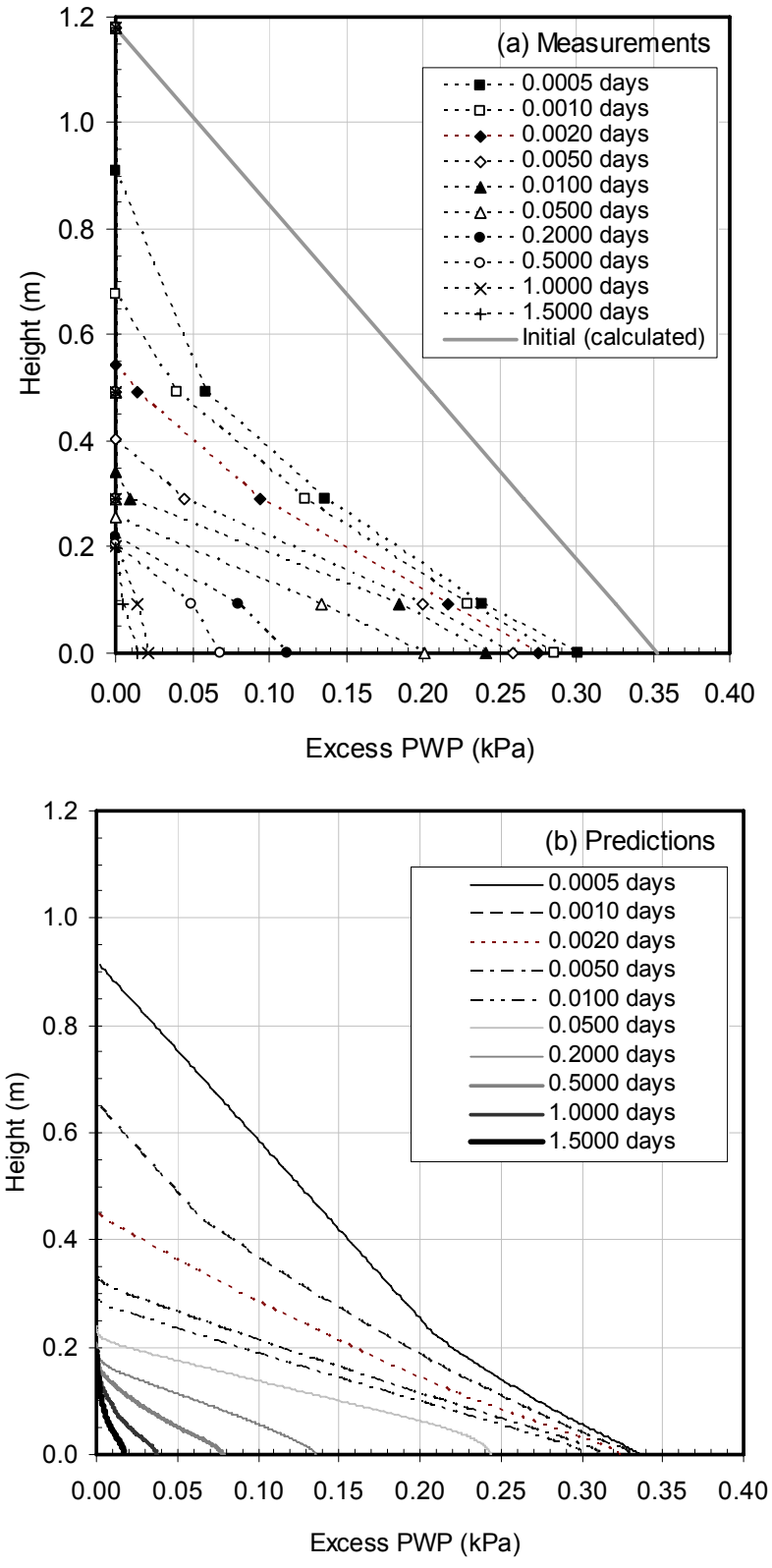

Figure 8.49 Excess pore pressure profile comparison between experiment and model for 120cm standpipe

Percent consolidation during hindered sedimentation and consolidation are calculated from excess pore water pressure measurements, measurements of interface height and excess pore water pressures predicted by a finite strain consolidation model (Figure 8.50). The calculation of the percent consolidation based on the interface settlement largely overestimates the percent consolidation calculated from the dissipation of the measured excess pore water pressures. This is due to the fact that settlement during hindered sedimentation is not caused by dissipation of excess pore water pressure and the nonlinearity of the compressibility relationship provides that the response of settlement and dissipation are not a one to one relationship. This finding was also indicated by Schiffman et al. (1984). The predicted percent consolidation by the finite strain consolidation theory closely matches those calculated from the excess pore water pressure measurements. This partly confirms that the governing physics taking place in the standpipe are those included in the theory.

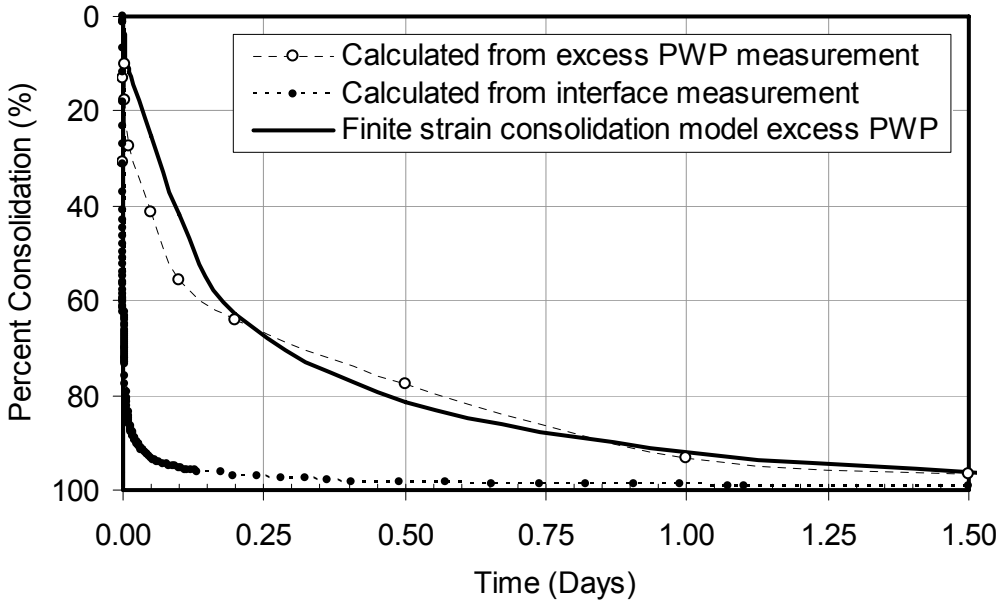

Figure 8.50 Rate of consolidation comparison between experiment and model for 120cm standpipe

Finally, a measured void ratio profile is compared with a predicted profile in Figure 8.51. Exceptionally good agreement is no surprise for the final void ratio profile as the data was used as part of the construction of the compressibility constitutive relationship utilized in the model.

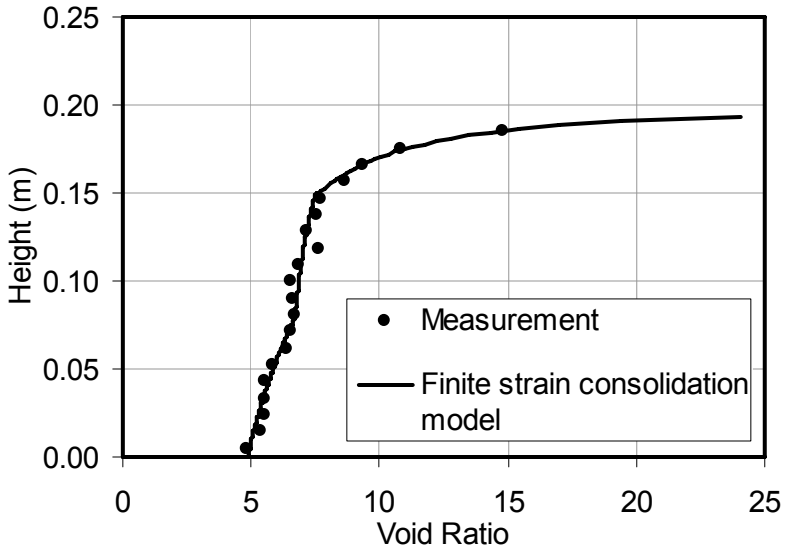

Figure 8.51 Final void ratio profile comparison between experiment and model for 120cm standpipe

8.5 Summary

A 2 m validation standpipe test was used to simulate a pond filling condition for the in-line thickened tailings in this chapter. This was performed by filling the tailings in six layers in six consecutive days and allowing the tailings to consolidate for 180 days until the consolidation was complete.

The results from the validation standpipe including interface heights, excess pore water pressures, a final void ratio profile and a final undrained shear strength profile were compared to a finite strain consolidation model with the appropriate material properties, initial conditions and boundary conditions.

The comparisons of all the geotechnical aspects between the validation standpipe and the numerical model with the properly assigned material characteristics show that a good agreement between a controlled laboratory standpipe test and a theoretical model can be obtained with an intensive material study and an understanding of depositing conditions. For the in-line thickened tailings, practically negligible deviations were found between the observed behavior and predictions of the interface height, pore pressure profiles and void ratio profiles. In the real application, complex field conditions and variations in material properties will likely complicate the application of the finite strain

consolidation analysis even further. This study highlights that the finite strain consolidation model is a suitable tool for estimating settling behavior of the in-line thickened tailings and the use of a model in practice will require a careful selection of input parameters and a good understanding of field conditions.

Chapter 9 Composite Tailings Made From the In-Line Thickened Tailings

9.1 Introduction

Composite tailings, CT, are produced by mixing and depositing a blend of cyclone underflow and MFT with a coagulant, generally gypsum ($CaSO_4$) to make the mix nonsegregating. The MFT is pumped from the existing tailings ponds where it has accumulated over the years. This procedure is consuming some of the current inventories of MFT and it releases water fairly rapidly for make-up water for the extraction plant (Matthew et al., 2002). Dewatering rates, however, are lower than expected and careful engineering of the CT process is required to prevent segregation during deposition. Another drawback is that the amount of MFT which can be added to the cyclone underflow is limited as too much fines in the CT reduces its permeability and the dewatering rate will be too slow. Generally the sand-fines ratio, SFR, of CT is only 4 or 5, that is, the fines content is from 17% to 20%.

As the oil sands tailings on average contains about 17% fines and the cyclone overflow which contains most of the fines is deposited in a tailings pond and forms more MFT, the CT process which is not continuous cannot keep up with the continuous formation of more MFT and MFT volumes continue to increase. Another problem with the present CT process is that the dosages of gypsum to prevent segregation are quite large resulting in the buildup of Ca^{2+} and SO_4^{2-} ions in the recycle water which in time will negatively affect bitumen extraction.

Figure 9.1 shows the present CT process. All mixes of MFT and cyclone underflow will lie on the straight line joining the MFT and cyclone underflow materials. The segregation boundary for untreated tailings blends is also shown. All tailings above this segregation boundary will segregate so all untreated mixes of MFT and cyclone underflow will segregate. The segregation boundary for gypsum treated tailings is also shown. All tailings below the gypsum segregation boundary will be nonsegregating so the CT mixes of MFT and cyclone underflow will become nonsegregating with the addition of a coagulant such as gypsum. Figure 9.1 also shows all possible mixes of ILTT and

cyclone underflow which lie on the line that joins these two materials. It is noted that the ILTT data is obtained from the east field pilot pond at a depth of 1 m. Possible CT mixes of ILTT and cyclone underflow lie below the untreated segregation boundary which indicates that these CT mixes would require no or little coagulant addition with a resulting increase in the quality of the recycle water for bitumen extraction.

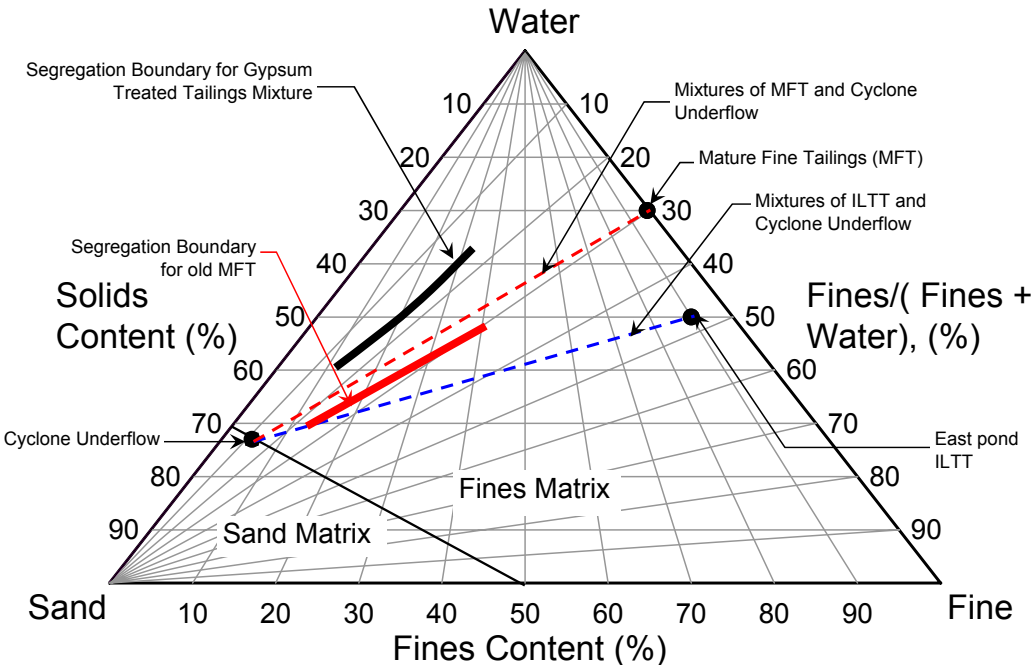

Figure 9.1 Tailings properties diagram

The greatest advantage of CT made from ILTT and cyclone underflow is the large hydraulic conductivity of the ILTT fines. As shown in Chapter 7 (Figure 7.76), at a solids content of 30% (void ratio of about 5.7) the hydraulic conductivity of ILTT is more than 20 times the hydraulic conductivity of new MFT (cyclone overflow) and even greater than that of old MFT. This means the ILTT-CT will release water and consolidate faster than MFT-CT allowing more rapid CT disposal. The greater ILTT hydraulic conductivity will also allow a larger amount of fines in the ILTT-CT than the 20% maximum in the MFT-CT. This would assist in the reduction of fine tails volume stored in tailings ponds.

In order to investigate the production of composite tailings from in-line thickened tailings, a series of static segregation tests and two large strain consolidation tests on composite tailings made from in-line thickened tailings were performed. The sand-fines

ratio used in this investigation was limited to 4:1 and no further chemical amendment was used. The hydraulic conductivity behavior of the composite tailings was also obtained from the static segregation tests and these results are combined with large strain consolidation test results for the ILTT-CT to investigate the consolidation characteristics of the ILTT-CT. Also static segregation tests on composite tailings made from cyclone overflow, COF-CT, were performed to compare with the ILTT-CT results.

This chapter begins with composite tailings preparation procedures followed by the materials index properties and water chemistry. Then a full test program including large strain consolidation tests and static segregation tests are presented and followed by results and analyses. A summary of the use of in-line thickened tailings to create composite tailings is then given.

9.2 Composite tailings preparation

In order to create composite tailings, cyclone underflow sand was shipped from Syncrude together with cyclone overflow tailings on 14th April 2008. It is noted that no additive was further processed into in-line thickened tailings and cyclone overflow tailings to create composite tailings in this investigation.

The cyclone underflow sand was characterized for its solids content, fines content, particle size distribution and specific gravity. ILTT was mixed in advance and it was allowed to settle to a solids content of around 30%. ILTT and sand were then mixed together with additional ILTT release water (if required) for 1 minute to obtain the design solids contents. Composite tailings made from the ILTT were immediately poured into different test cells for different tests to proceed. Composite tailings made from cyclone overflow were prepared similarly with an exception that for a high design solids content composite tailings, cyclone overflow tailings was allowed to settle and was consolidated to obtain a higher solids content before mixing.

9.3 Index testing

Index testing including particle size distribution, specific gravity and morphology are presented in this section to assist in the behavioral interpretation of the tailings.

9.3.1 Cyclone underflow and composite tailings

Figure 9.2 shows the particle size distribution of the cyclone underflow sand. The sand consists of about 5% fines content (< 45 μm). With a known fines content, the cyclone underflow sand was mixed with cyclone overflow to create composite tailings (COF-CT) at a SFR of 4:1. Composite tailing with in-line thickened tailings (ILTT-CT) was also prepared at the same SFR.

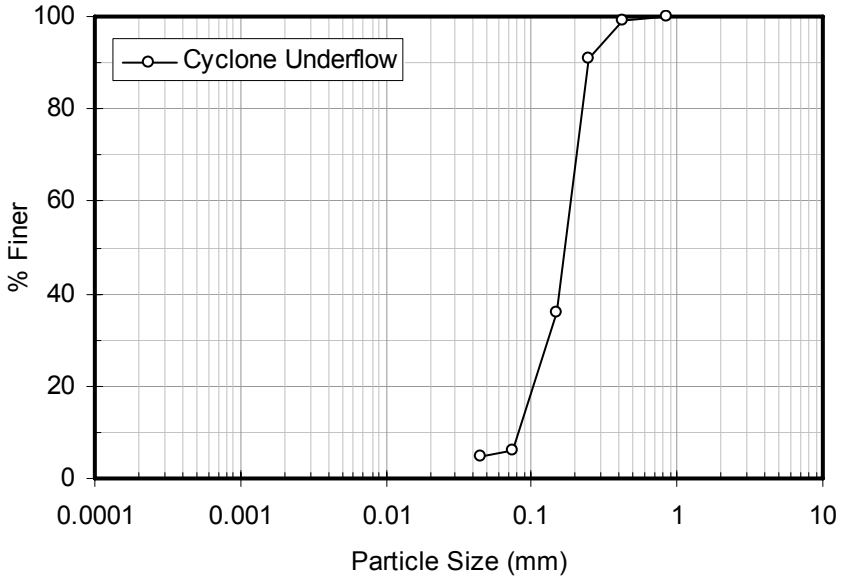

Figure 9.2 Particle size distributions of cyclone underflow sand

Non-dispersed particle size distributions of mixtures of cyclone overflow tailings with cyclone underflow sand (COF-CT) and in-line thickened tailings with cyclone underflow sand (ILTT-CT) are shown in Figure 9.3. Both particle size distributions indicate fines contents of about 20% (SFR 4:1). The COF-CT shows 4% clay size material while the ILTT-CT shows 0% clay size material. The smaller measured clay size material in the ILTT-CT is an indication of a remaining influence of the in-line thickening process.

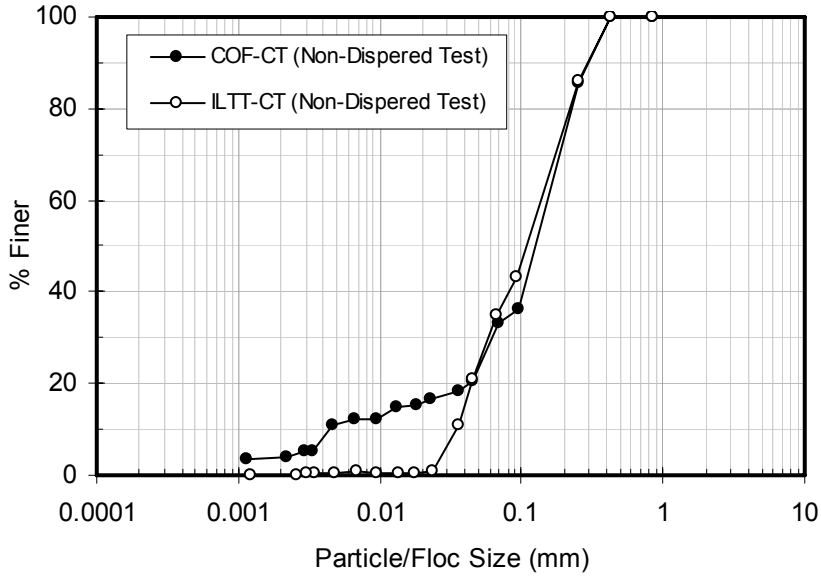

Figure 9.3 Non-dispersed particle size distributions of COF-CT and ILTT-CT

9.3.2 Specific gravity

The specific gravities of COF, ILTT, CUF and ILTT-CT were measured and the results are shown in Table 9.1. Measured specific gravity of ILTT-CT is 2.59. This specific gravity value of the ILTT-CT can also be calculated from the specific gravity values of ILTT and CUF. The bitumen content corresponding to the specific gravity of the ILTT-CT is calculated to be 1.5%.

Table 9.1 Specific gravity of tested tailings

Tailings	Descriptions	G_s	f (%)	b (%)
Cyclone overflow	Received on 14th April 2008	2.52	94.0	3.3
Laboratory ILTT	Prepared from COF received on 14th April 2008	2.46	94.0	4.9
Cyclone Underflow	Received on 14th April 2008	2.62	2.4	0.7
Composite tailings-ILTT	A mix of laboratory ILTT and cyclone underflow	2.59	20.0	1.5

9.3.3 Morphology

Scanning electron microscope images of composite tailings made from in-line thickened tailings are shown in Figure 9.4. The composite tailings were prepared at 55%

solids content and 20% fines content, this gave a fines-bitumen void ratio of about 9.7. Sand particles can be observed floating in this high void ratio clay matrix. The clay structure holding the sand can be classified as edge-to-face and edge-to-edge flocculated and aggregated pattern similar to that found in the non-sheared in-line thickened tailings in Chapter 7. It can also be seen that at some locations, the ILTT-CT clay structure exhibits a card-house like structure such as found in the cyclone overflow tailings (Figure 9.4 (*c*)).

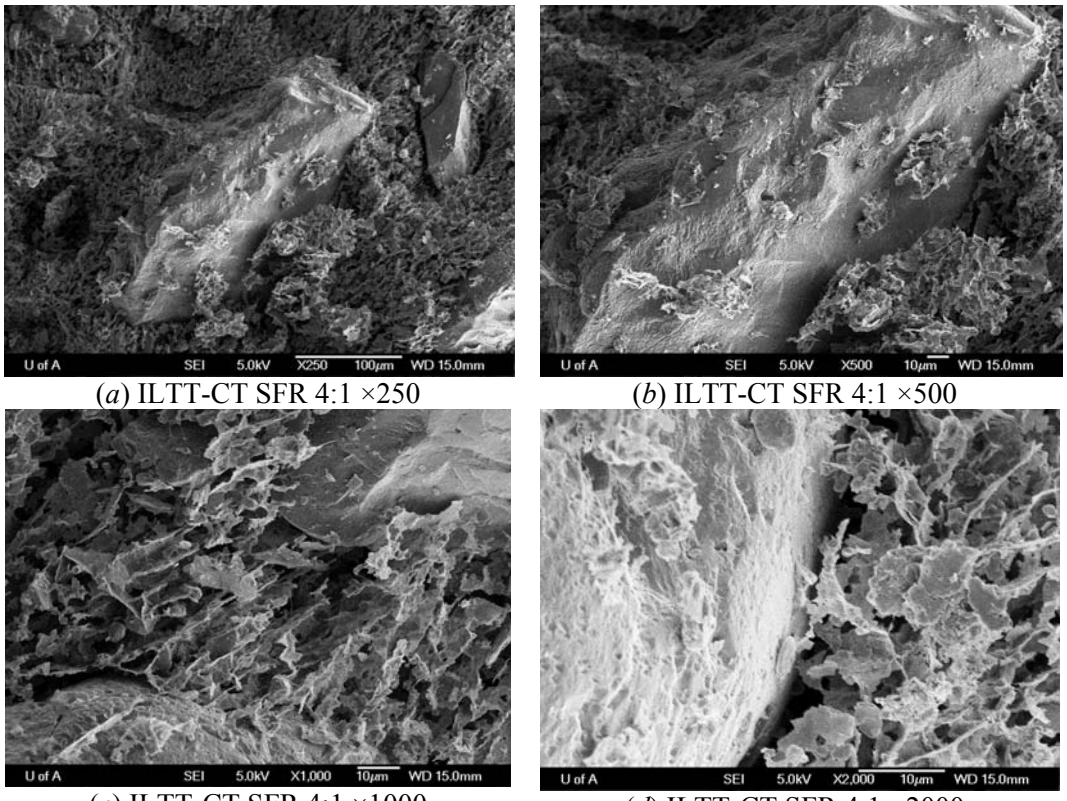

(*a*) ILTT-CT SFR 4:1 ×250 (*b*) ILTT-CT SFR 4:1 ×500

(*c*) ILTT-CT SFR 4:1 ×1000 (*d*) ILTT-CT SFR 4:1 ×2000

Figure 9.4 Scanning electron microscope images of ILTT-CT (55%S, 20%F)

9.4 Water chemistry

Release pore fluid of COF-CT and ILTT-CT were collected and tested to document pore water chemistry. Results of the pore water chemistry for both tailings are shown in Table 9.2. Similar pore water chemistry results as found in cyclone overflow tailings and in-line thickened tailings in Chapter 7 were found for the COF-CT and ILTT-CT. The results indicate that there is no significant change in the cation concentrations in the release water from both tailings.

Table 9.2 Water chemistry of composite tailings

Samples	pH	Conductivity (ms/cm)	Cations (mg/L)						Anions (mg/L)				
			Na^+	K^+	Mg^{2+}	Ca^{2+}	NH^{4+}	Li^+	Br^-	NO^{3-}	F^-	Cl^-	SO_4^{2-}
ILTT-CT LSC1	8.8	3600	-	-	-	-	-	-	-	-	-	-	-
ILTT-CT LSC2	8.5	3850	-	-	-	-	-	-	-	-	-	-	-
COF-CT HS 50.7%	8.9	4030	765.2	15.9	8.1	10.1	5.9	0.2	0.0	0.0.	3.7	635.3	588.6
COF-CT HS 56.1%	8.7	3760	733.8	15.4	8.1	11.0	7.6	0.2	0.0	0.0	3.4	606.9	558.8
COF-CT HS 60%	7.6	3830	731.3	15.6	9.6	14.2	0.0	0.2	0.2	0.0	2.6	588.5	541.0
ILTT-CT HS 50.2%	8.4	3690	690.1	14.0	7.8	10.8	0.0	0.2	0.0	16.5	3.1	577.3	480.5
ILTT-CT HS 52.5%	8.5	3850	680.5	14.3	7.2	10.3	4.9	0.2	0.2	10.6	3.3	566.4	473.2
ILTT-CT HS 61.1%	8.9	3650	686.0	14.8	8.9	12.3	0.0	0.2	0.2	13.5	2.6	562.9	502.1

HS- hindered sedimentation test, LSC-Large strain consolidation test

9.5 Large strain consolidation test on ILTT-CT

Tables 9.3 and 9.4 show large strain consolidation test results with and without vane shear strength tests on the composite tailings made from laboratory in-line thickened tailings. Initial solids contents of the composite tailings used in this test were 55.4% and 55.2% for tests 1 and 2 respectively. Figures 9.5, 9.6 and 9.7 show combined compressibility, hydraulic conductivity and undrained shear strength measurements of the tailings respectively.

Table 9.3 Large strain consolidation test 1 on ILTT-CT SFR 4:1

Load	Height (mm)	ΔH (mm)	Effective stress (kPa)	Void ratio, *e*	Fines-bitumen void ratio, e_{fb}	Hydraulic Gradient, *i*	Hydraulic conductivity (m/day)	Undrained shear strength (kPa)
1	78.93	-	-	2.09	9.47	-	3.03E-02	-
2	60.33	18.60	0.20	1.36	6.17	-	-	0.11
3	58.54	1.79	0.97	1.29	5.85	0.28	6.62E-03	0.12
4	52.34	6.19	1.67	1.05	4.75	0.33	3.04E-03	0.38
5	48.26	4.08	2.81	0.89	4.03	1.08	1.68E-03	1.12
6	46.16	2.11	5.59	0.80	3.65	1.68	1.10E-03	2.64
7	44.93	1.23	10.61	0.76	3.44	2.59	8.61E-04	3.77
8	43.03	1.90	20.82	0.68	3.10	2.01	5.95E-04	5.46
9	41.93	1.10	48.75	0.64	2.90	2.08	5.18E-04	7.14
10	40.93	1.00	98.30	0.60	2.73	3.00	4.23E-04	11.82
11	39.83	1.10	299.44	0.56	2.53	3.17	2.96E-04	38.78
12	39.13	0.70	498.35	0.53	2.41	4.25	2.59E-04	-
13	39.56	-0.43	48.33	0.55	2.48	-	-	-
14	40.19	-0.63	0.97	0.57	2.59	-	-	-

Gs = 2.59, Fines content = 20.2%

Table 9.4 Large strain consolidation test 2 on ILTT-CT SFR 4:1

Load	Height (mm)	ΔH (mm)	Effective stress (kPa)	Void ratio, *e*	Fines-bitumen void ratio, e_{fb}	Hydraulic Gradient, *i*	Hydraulic conductivity (m/day)	Undrained shear strength (kPa)
1	78.03	-	-	2.10	9.32	-	1.97E-02	-
2	59.03	19.00	0.20	1.35	5.97	-	-	-
3	56.58	2.45	0.96	1.25	5.54	1.11	9.88E-03	-
4	50.11	6.46	1.67	0.99	4.40	1.25	2.33E-03	-
5	48.02	2.09	2.81	0.91	4.03	1.25	1.87E-03	-
6	45.65	2.37	5.59	0.82	3.61	1.85	1.25E-03	-
7	44.46	1.19	10.61	0.77	3.40	2.61	9.50E-04	-
8	42.71	1.76	19.84	0.70	3.10	1.89	6.84E-04	-
9	41.43	1.28	49.99	0.65	2.87	1.93	5.53E-04	-
10	40.33	1.10	98.74	0.60	2.68	3.16	4.96E-04	-
11	38.84	1.49	299.97	0.55	2.41	3.28	3.35E-04	-
12	38.13	0.71	498.99	0.52	2.29	4.64	2.99E-04	-
13	38.78	-0.65	50.05	0.54	2.40	-	-	-
14	39.36	-0.58	0.96	0.57	2.51	-	-	-

Gs = 2.59, Fines content = 20.8%

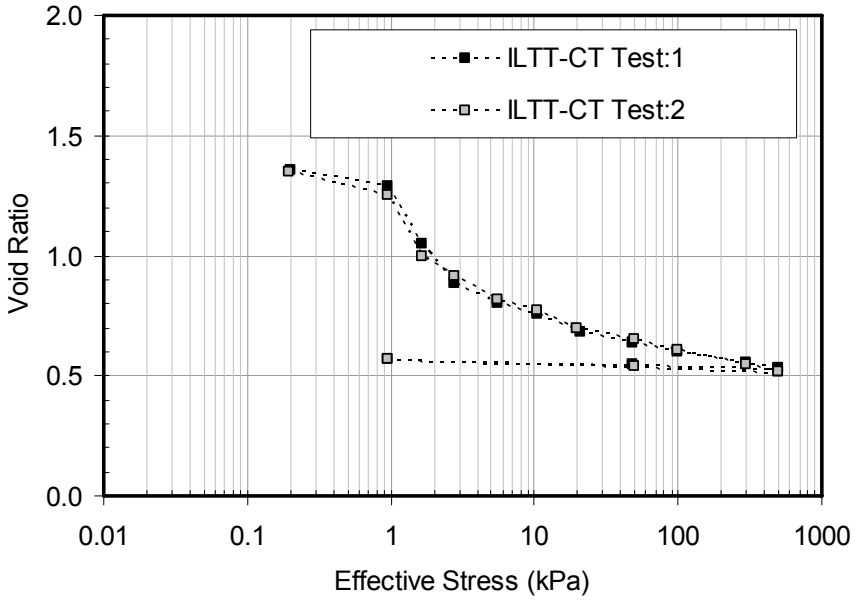

Figure 9.5 Compressibility of ILTT-CT SFR 4:1 from a large strain consolidation test

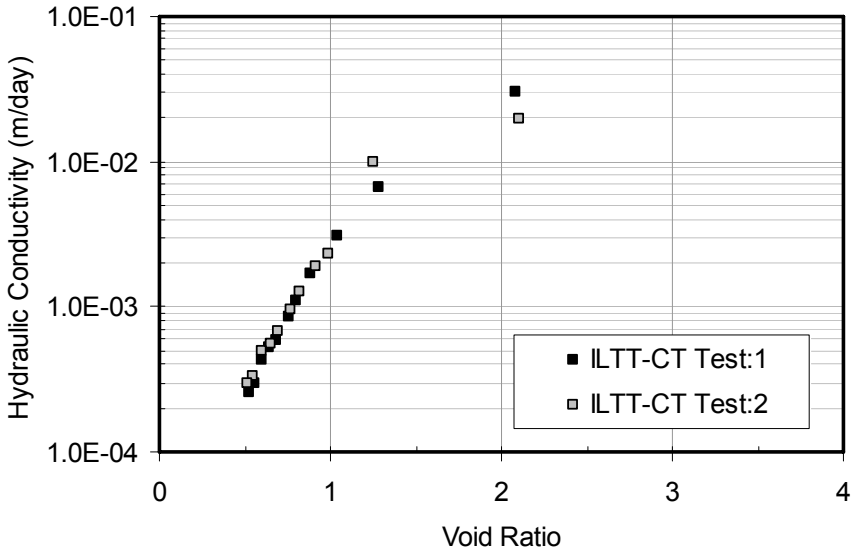

Figure 9.6 Hydraulic conductivity of ILTT-CT SFR 4:1from a large strain consolidation test

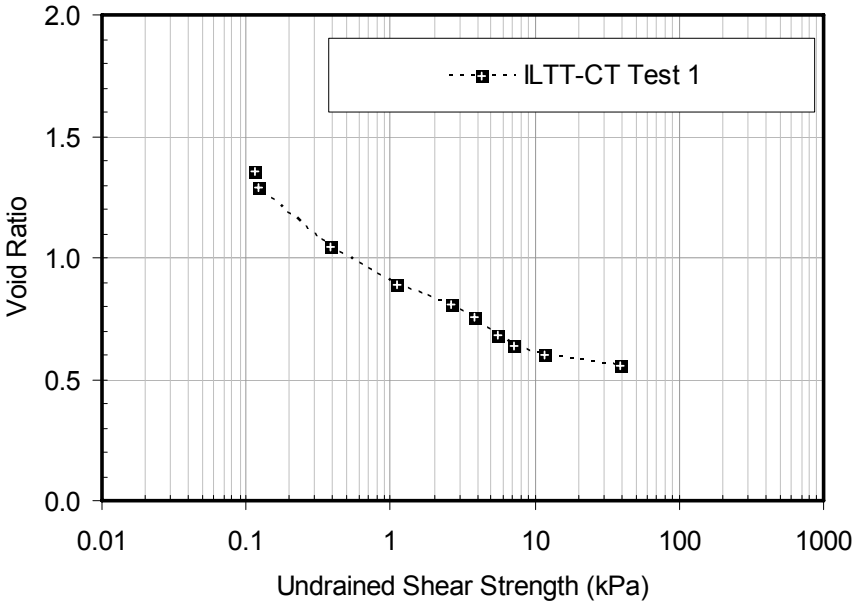

Figure 9.7 Undrained shear strength of ILTT-CT SFR 4:1 from a large strain consolidation test 1

9.6 Segregation boundaries of composite tailings

A series of static segregation tests on COF-CT and ILTT-CT were performed in this section at SFR of 4:1 with no further chemical amendment for either tailings. Segregation criterion used to find a segregation boundary in this investigation was 95% fines capture. The results are as follows.

9.6.1 Static segregation tests on composite tailings made from COF

Table 9.5 shows four static segregation tests on composite tailings made from cyclone overflow. Four solids contents (50.7%, 56.1%, 59.5% and 65.2%) were used with designed fines content of 20% or SFR of 4:1. Figure 9.8 shows interface settlements of all four tests. The initial settling velocities and hydraulic conductivity corresponding to the initial void ratios were calculated and shown in Table 9.5.

Table 9.5 Static segregation tests on COF-CT

Test	Initial solids content (%)	Designed fines content (%)	Void ratio	v_s (m/day)	Hydraulic conductivity (m/day)	Fines capture (%)	Fines-bitumen void ratio
1	50.7	20.0	2.52	3.55E-03	-	49.3	11.57
2	56.1	20.0	2.03	2.01E-03	-	92.2	9.31
3	59.5	20.0	1.76	1.52E-03	2.64E-03	95.6	8.10
4	65.2	20.0	1.38	1.16E-03	1.74E-03	-	6.35

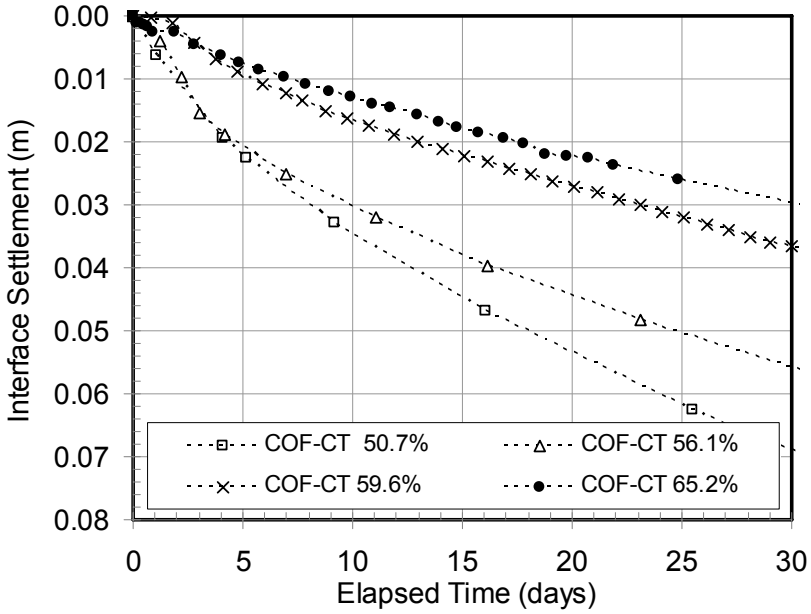

Figure 9.8 Interface settlement of COF-CT

In Figure 9.9, solids content and fines profiles are shown side by side for COF-CT with solids content of 50.7%, 56.1% and 59.5%. Calculated fines captures in Table 9.5 show that at initial solids contents of 50.7% and 56.1%, COF-CT segregated and an interpolated static segregation boundary for COF-CT at 95% fines capture is 58.9% solids content (e_{fb} = 8.3, FWR = 22.3%). According to Equation 7.15, this solids content corresponds to an undrained shear strength of the fines of about 4.2 Pa before any sedimentation or consolidation takes place.

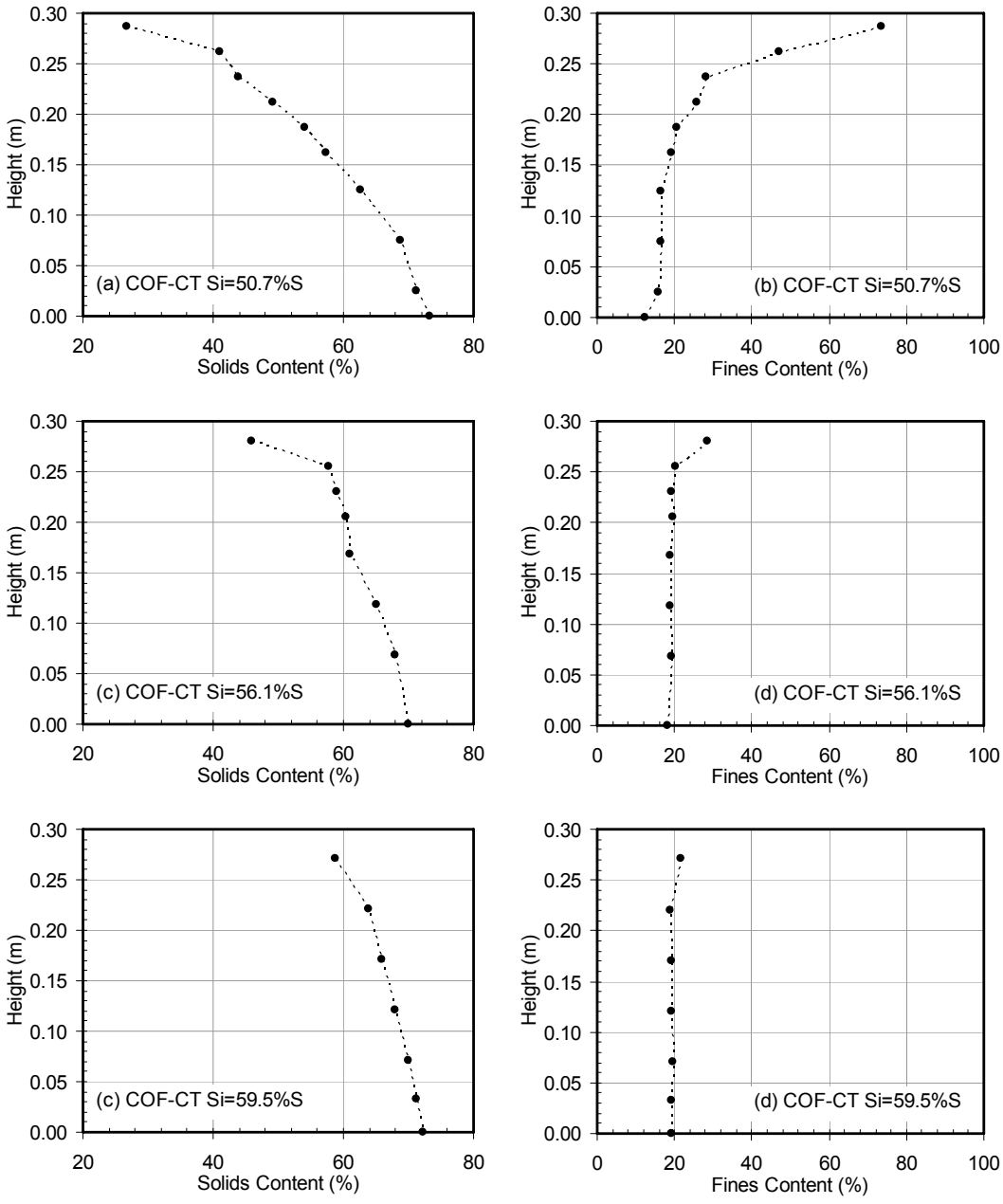

Figure 9.9 Solids and fines content profiles of COF-CT SFR 4:1

9.6.2 Static segregation tests on composite tailings made from ILTT

Table 9.6 shows four static segregation tests on composite tailings made from in-line thickened tailings. Four solids contents (50.2%, 52.8%, 61.1% and 65.6%) were used with designed fines content of 20% or SFR of 4:1. Figure 9.10 shows interface settlement of all four tests. The initial settling velocities were measured and used to obtain hydraulic conductivities corresponding to the initial void ratios. The results are shown in Table 9.6.

Table 9.6 Static segregation tests on ILTT-CT

Test	Initial solids content (%)	Designed fines content (%)	Void ratio	v_s (m/day)	Hydraulic conductivity (m/day)	Fines capture (%)	Fines-bitumen void ratio
1	50.2	20.0	2.57	9.27E-01	-	64.8*	11.81
2	52.8	20.0	2.32	1.42E-01	2.97E-01	97.0	10.64
3	61.1	20.0	1.65	2.00E-02	3.33E-02	96.5	7.58
4	65.6	20.0	1.36	1.57E-02	2.34E-02	-	6.24

* calculated from solids content profile

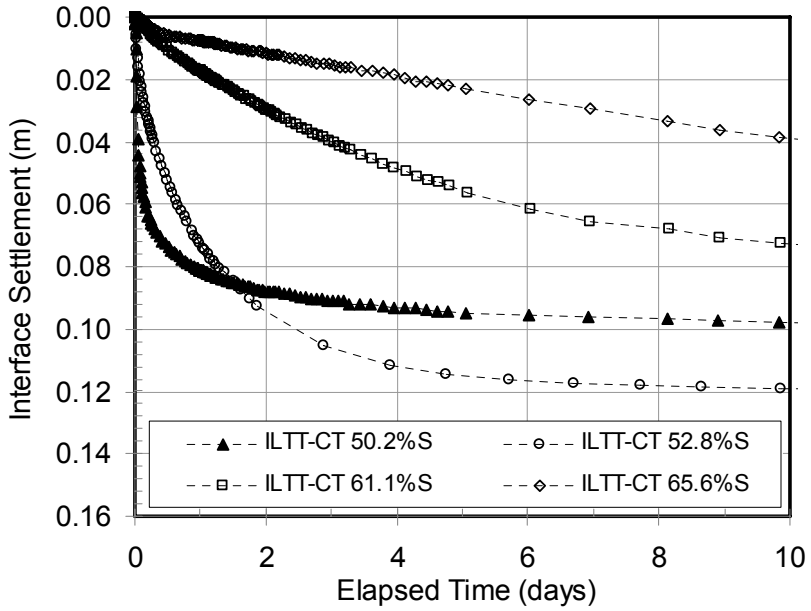

Figure 9.10 Interface settlement of ILTT-CT

Figure 9.11 shows solids content and fines content profiles of ILTT-CT with solids content of 50.2%, 52.8% and 61.1%. It can be seen that the ILTT-CT segregated at 50.2% initial solids content. Fines captures for each test are shown in Table 9.6 which gives a static segregation boundary of ILTT-CT at 52.6% solids content (e_{fb} = 10.7, FWR = 18%). From undrained shear strength correlation for sheared in-line thickened tailings in Equation 7.16, this solids content corresponds to an undrained shear strength of 14.5 Pa. It is noted that these undrained shear strength values are extrapolated. Even though it

does not appear that the undrained shear strength of the fines correlates well with the segregation behavior because COF-CT and ILTT-CT segregate at different undrained shear strengths (4.2 Pa and 14.5 Pa respectively), a trend of higher undrained shear strength material and lower solids content at a segregation boundary is achieved. It is noted that the influence of the ions in the cyclone underflow sand was not taken into account in this experiment therefore the correlation between undrained shear strength and fines-bitumen void ratio used in the undrained shear strength extrapolation may not hold for the composite tailings.

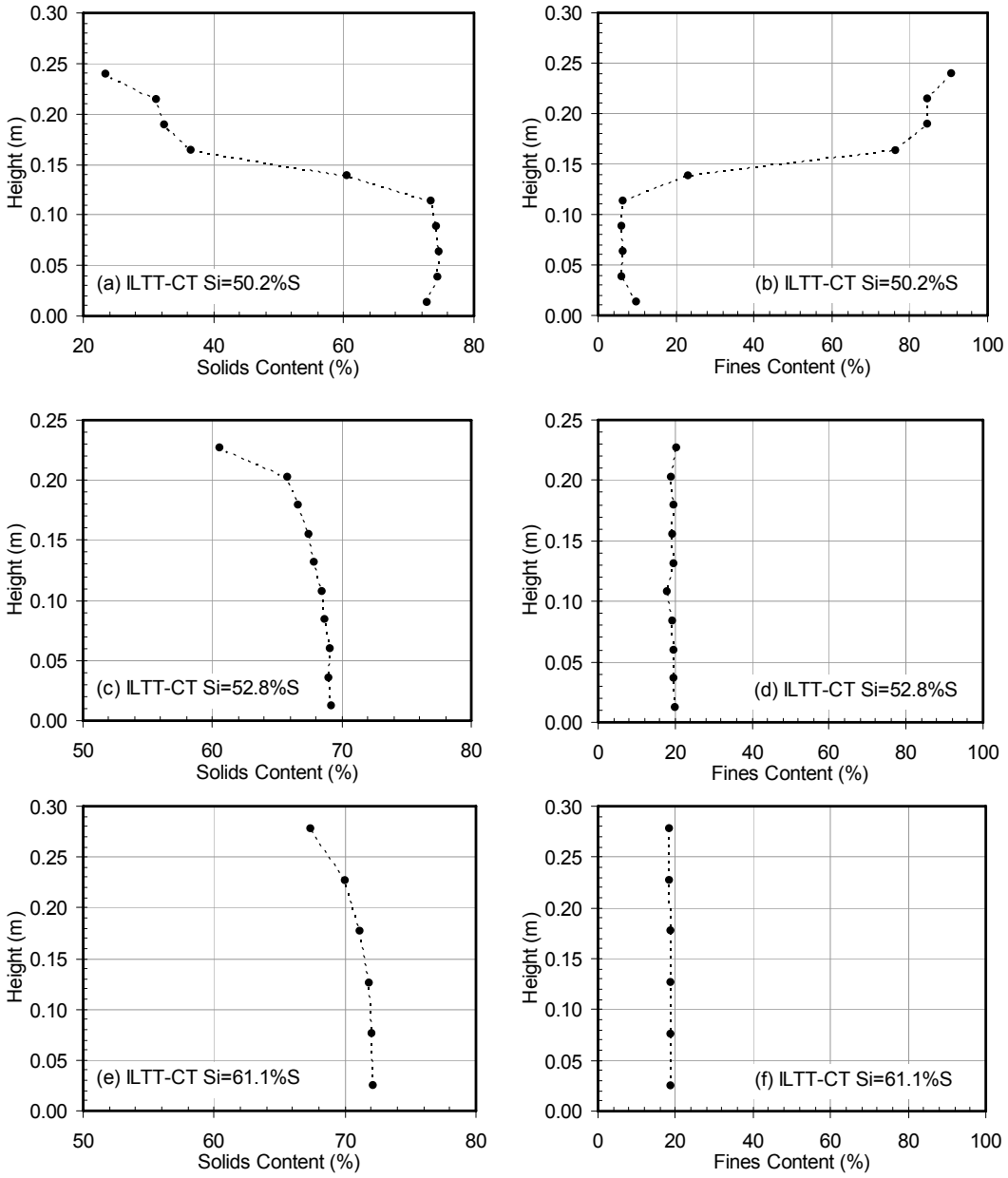

Figure 9.11 Solids and fines content profiles of ILTT-CT SFR 4:1

Hydraulic conductivity of COF-CT and ILTT-CT are plotted against fines-bitumen void ratio with hydraulic conductivity constitutive relationships of in-line thickened tailings, sheared in-line thickened tailings and cyclone overflow in Figure 9.12.

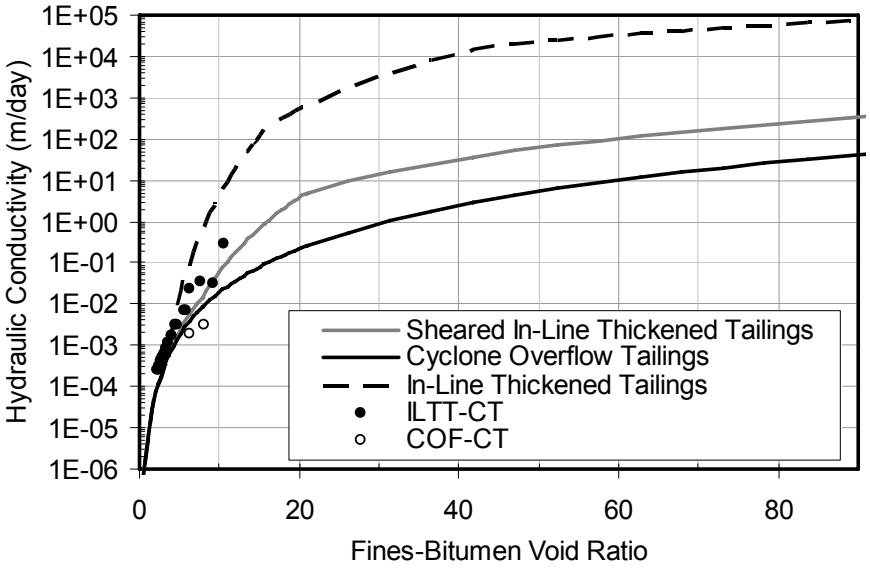

Figure 9.12 Hydraulic conductivity of ILTT-CT and COF-CT

Hydraulic conductivity measurements of the ILTT-CT locate in between the hydraulic conductivities of non-sheared and sheared in-line thickened tailings. The COF-CT's hydraulic conductivity is slightly lower than the fitted hydraulic conductivity function for the cyclone overflow tailings. The trends of the results suggest that the hydraulic conductivities of both composite tailings are controlled by the fines used to create the composite tailings. It can also be seen that at a solids content of about 60% where nonsegregating mixes can be obtained from both tailings, ILTT-CT hydraulic conductivity is about 10 times more permeable compared to that of the COF-CT (Tables 9.5 and 9.6). Hydraulic conductivity of the ILTT-CT can be expressed as Equation 9.1.

$$k = 0.0035 \times e^{4.0} \qquad [9.1]$$

Where e is void ratio and k is hydraulic conductivity in m/day.

Compressibility of the ILTT-CT is shown in Figure 9.13. An apparent pre-consolidation stress is shown. The pre-consolidation behavior occurs at a void ratio of

about 1.3 or fines-bitumen void ratio of about 5.8 and effective stress of about 1 kPa. Compressibility of the ILTT-CT can be expressed as Equation 9.2.

$$e = \begin{cases} 1.250 \times \sigma'^{-0.0478} & ;1.35 \geq e \geq 1.25 \\ 1.250 \times \sigma'^{-0.308} & ;1.25 \geq e \geq 0.85 \\ 0.962 \times \sigma'^{-0.099} & ;0.85 \geq e \geq 0.5 \end{cases} \quad [9.2]$$

Where e is void ratio and σ' is vertical effective stress in kPa.

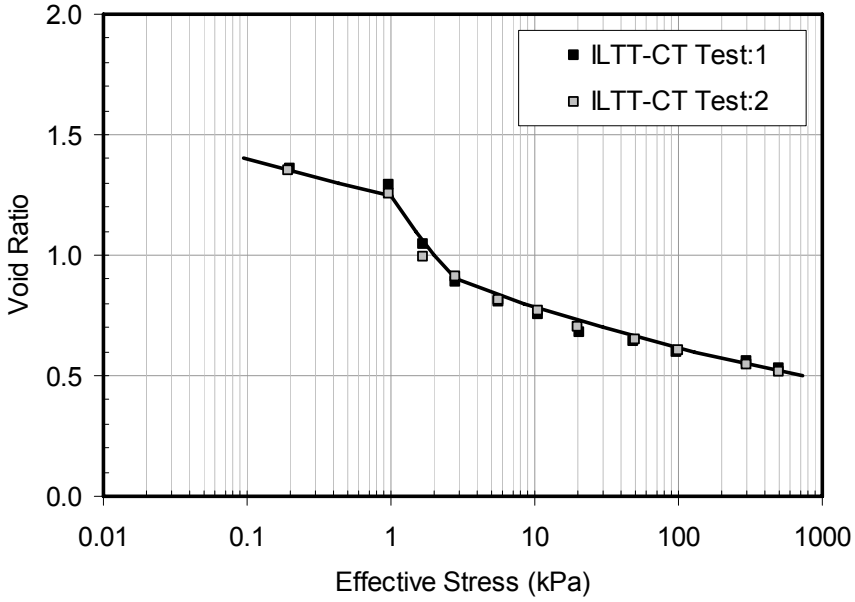

Figure 9.13 Compressibility of ILTT-CT SFR 4:1 from a large strain consolidation test

Undrained shear strength with fines-bitumen void ratio of the ILTT-CT is shown in Figure 9.14. The undrained shear strength measurements on ILTT-CT are similar to the sheared in-line thickened tailings at a fines-bitumen void ratio of about 6. At the lower fines-bitumen void ratios, the undrained shear strength of the ILTT-CT diverges from that of sheared in-line thickened tailings and is considerably larger. The higher measured undrained shear strength of the ILTT-CT at lower void ratios is likely caused by the coarse sand particles starting to touch one another. It is noted that the sand matrix is in a loose sand state at a void ratio of about 0.65 or a fines-bitumen void ratio of about 3.0 (for 20% fines content) as indicated by the sand-fines matrix boundary in Figure 9.15.

The measurements show that the undrained shear strength of the ILTT-CT becomes significantly larger than that of ILTT fines starting at a void ratio of about 4.5 possibly indicating a significant contribution of the coarse particles in this range of void ratios. The interactions of the coarse particles likely occur at a fines-bitumen void ratio higher than 3 possibly due to bridging of various particles' shapes and sizes in a soil. Previous testing of MFT-CT, however, did not show such a high shear strength in this range of void ratios. It is postulated that the mix of the large flocs of ILTT with sand has a synergistic effect on shear strength.

A correlation between undrained shear strength and void ratio for the ILTT-CT can be expressed as Equation 9.3.

$$e = 0.920 \times \tau_u^{-0.159} \qquad [9.3]$$

Where e is void ratio and τ_u is undrained shear strength in kPa.

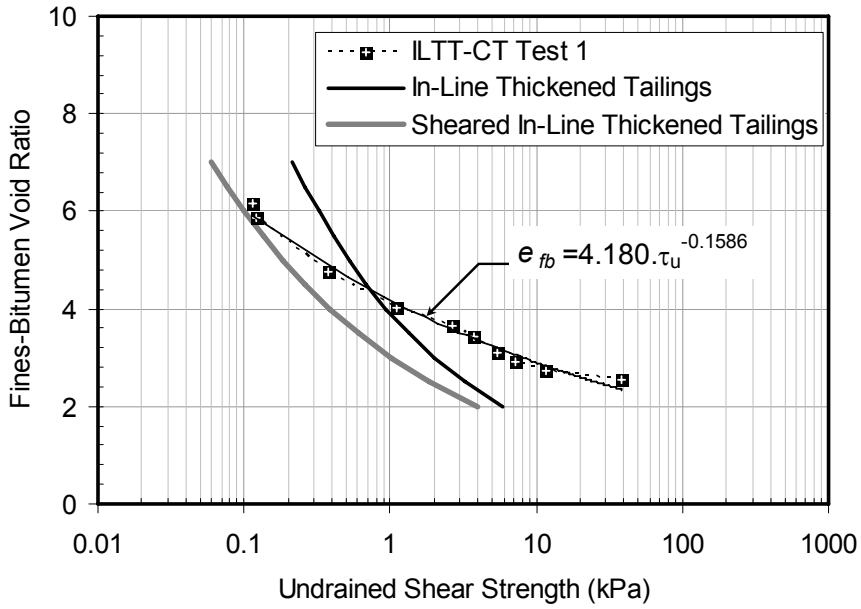

Figure 9.14 Undrained shear strength of ILTT-CT SFR 4:1

Static segregation points of both COF-CT and ILTT-CT at a SFR of 4:1 are shown in Figure 9.15. In Figure 9.15, the MFT-CT segregation boundary at a SFR of 4:1

is at a solids content of 65% which is significantly higher than the 59% solids content for the COF-CT found in this experimental program. Considering the pore water chemistry of the cyclone overflow in Table 9.2, most cation concentrations in this 2008 cyclone overflow have increased significantly compared that of old MFT. A divalent cation such as calcium is more than double the concentration of the old MFT indicating the possibility of a double layer compression which may potentially lead to particle coagulation. This behavior can also be observed in the non-dispersed particle size distribution of the cyclone overflow showing less clay size particles as discussed previously in Section 7.3.1.

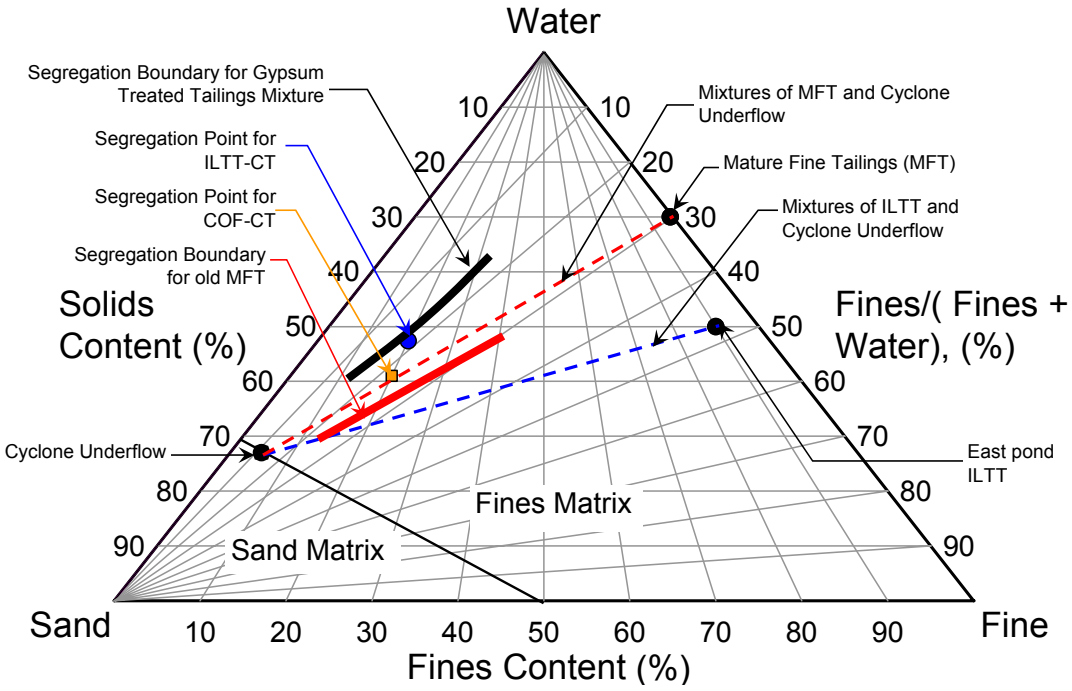

Figure 9.15 Segregation boundaries of COF-CT and ILTT-CT at SFR 4:1

The results in this composite tailings investigation confirm that composite tailings made from in-line thickened tailings will have a high hydraulic conductivity behavior inherited from the flocculated fines. The shearing of the ILTT during mixing with the sand did not disrupt the floc structure significantly and only reduced the ILTT hydraulic conductivity by a small amount. Composite tailings made with in-line thickened tailings can be deposited at a similar solids content as that of gypsum treated MFT-CT as their static segregation boundaries are essentially comparable at a SFR of 4:1.

9.7 Summary

An investigation of the use of in-line thickened tailings to create a composite tailings at a SFR of 4:1 without any further coagulant chemical amendment was presented in this chapter. At this SFR, it was found that the composite tailings made with in-line thickened tailings (ILTT-CT) had a static segregation point of 52.6% solids content and the composite tailings made with cyclone overflow tailings (COF-CT) had a static segregation point of 58.9% solids content. The segregation boundary of the ILTT-CT is comparable to that of the gypsum treated CT and is much higher than the segregation boundary of the old mature fine tailings. Therefore under a static condition, nonsegregating behavior of ILTT-CT can be achieved by mixing in-line thickened tailings with cyclone underflow sand at a FWR higher than 18%.

Compressibility, hydraulic conductivity and undrained shear strength of the ILTT-CT were measured. Undrained shear strength measurements indicate that the ILTT-CT has undrained shear strength similar to that of the sheared in-line thickened tailings at fines-bitumen void ratio of about 6. At lower fines-bitumen void ratios, the undrained shear strength of the ILTT-CT diverges from that of sheared in-line thickened tailings and is significantly larger. The higher measured undrained shear strength of the ILTT-CT at lower fines-bitumen void ratios is believed to be caused by the synergistic contribution of the large flocs of ILTT and the sand particles. This greater shear strength of ILTT-CT is very important as it allows the CT to reach a shear strength of 5 kPa at a void ratio above 3 to meet the ERCB definition of a solid deposit.

It was found that hydraulic conductivity measurements of the ILTT-CT at large void ratios locate in between the hydraulic conductivities of non-sheared and sheared in-line thickened tailings. While the COF-CT's hydraulic conductivity is slightly lower than that of the cyclone overflow tailings. The trends of the results suggest that the hydraulic conductivities of both composite tailings are controlled by the fines used to create the tailings. The ILTT-CT thus will have a high hydraulic conductivity property inherited from the ILTT fines. Composite tailings at a solids content of about 60% therefore can be made from in-line thickened tailings with an advantage of having a hydraulic conductivity about 10 times greater than that of the composite tailings made from cyclone overflow. Therefore ILTT-CT will consolidate about 10 times faster than the COF-CT.

The combination of faster consolidation and higher shear strength means that the ILTT-CT will be able to be reclaimed much earlier than MFT-CT. Judicial deposition techniques may result in it being reclaimed as it is being deposited.

Chapter 10 Summary, Conclusions and Recommendations

10.1 Summary

This thesis investigated the influence of the in-line thickening process on oil sands fine tailings sedimentation, consolidation and shear strength characteristics. In order to accomplish the understanding of this material, laboratory studies, numerical studies and field studies were executed and the results were combined to evaluate the overall behavior of the tailings. Three main types of tailings namely cyclone overflow tailings, in-line thickened tailings and sheared in-line thickened tailings were investigated in this study.

It was found that after cyclone overflow tailings went through the in-line thickening process, the apparent particle size changed dramatically as well as the plasticity of the material. A detailed laboratory investigation revealed that the in-line thickened tailings is over three magnitudes more permeable compared to the cyclone overflow during sedimentation. This significant improvement of the hydraulic conductivity becomes less as effective stress starts to develop and disappears when a void ratio of about 3 is obtained. Measured compressibility of the in-line thickened tailings generally indicated that the material required a higher effective stress to compress compared to the cyclone overflow. Undrained shear strength measurements showed that the in-line thickened tailings has a higher undrained shear strength throughout the measured void ratios. The significant shifts in hydraulic conductivity and compressibility were explained by the macro and micro structural change as the materials evolve from a slurry to a soil.

Experiments on the sheared in-line thickened tailings were intended to simulate the influence of tailings transportation on the in-line thickened tailings sedimentation and consolidation behavior. Shearing of the in-line thickened tailings results in a hydraulic conductivity reduction approximately 2 magnitudes during sedimentation. The remaining influence of the in-line thickening process still provided the material with hydraulic

conductivity more than 10 times larger than that of the cyclone overflow tailings. Compressibilities of the non-sheared and sheared materials are similar at void ratios of 5 and below. The non-sheared material exhibits a higher compression index at higher void ratios which is postulated to be due to the compression of the large and small macro floc structures.

With the utilization of a one dimensional finite strain consolidation theory, field constitutive behavior was extracted from the field measurements. The comparison between the laboratory compressibility and hydraulic conductivity relationships and those from the large scale field experiment shows good agreement. Similarly, a comparison between the results of the validation standpipe test, performed to simulate a pond filling condition, and the theoretical model using the experimentally determined material properties revealed a good agreement. It is concluded that the small scale laboratory determined parameters and a finite strain consolidation theory can be used to predict the large scale field behavior for the fast settling in-line thickened tailings.

The use of the in-line thickened tailings to create composite tailings was also investigated and it was found that a static segregation boundary of this material is similar to that of the gypsum treated composite tailings. Composite tailings therefore can be made from in-line thickened tailings with an advantage of having a hydraulic conductivity about 10 times greater than that of the composite tailings made from the cyclone overflow tailings.

10.2 Observations and Conclusions

Detailed observations and conclusions by Chapter are

Chapter 3: One dimensional finite strain consolidation modeling

- For a pond filling numerical experiment, when the same amount of tailings is placed and the same amount of time is allowed for tailings to consolidate, the same amount of settlement can be expected regardless of the filling schedule.
- For a one dimensional single pond filling condition, a quiescent finite strain consolidation model can be used to estimate the interface settlement prediction

both in filling and quiescent periods but the quiescent model cannot be utilized for a multiple filling step.

- For a pond with a cross-section area changing with height, the filling interface curve can become nonlinear therefore this curve can not be estimated by a quiescent model.
- Full implementation of a continuous interaction function technique has shown that the sedimentation and consolidation phenomena can be modeled with the large strain consolidation theory using an interaction coefficient. From the presented numerical simulations, good predictions can be obtained. The numerical method used for the model is uncomplicated and gives satisfying results. The sedimentation-consolidation model was also compared to experimental results in the literature. The results show that the model gives good approximations. When compared to fluid dynamic models, the presented model gives qualitatively similar predictions.
- The pre-consolidation behavior modeled by a Weibull compressibility function is a better form of compressibility for mature fine tailings compared to the conventional power law. Results from this approach give a slight improvement of interface settlement prediction. Void ratio, effective stress and excess pore pressure profile predictions however show a negligible advantage of this method.
- For creep analyses, both creep type 1 and type 2 increase deformations with time due to a viscous effect. As a result, the interface prediction with creep further overestimates the measured interface settlement data. As the compressibility investigations showed small success, it is recommended that possible mechanisms that affect micro and macro structures and therefore hydraulic conductivity of the slurry should be further investigated to extend the current stage of understanding.

Chapter 4: Thickener modeling by a finite strain consolidation theory

- A finite strain consolidation theory was utilized for modeling of slurry settling behavior in a continuously operating thickener. This modeling was performed by multi-node addition and elimination. The developed thickener model was compared with a fluid dynamic model from the literature and a quantitatively good agreement was obtained.

- A total of two thickener models were developed; one with an initial filling period and another with instantaneously filling. A comparison of both models confirmed that an initial filling rate does not have any influence on the steady state void ratio profile during a continuously operating thickener. This is because the steady state operation is not dependent on the initial rate of filling but the rate of filling/withdrawing during continuous operation.
- A parametric study of the model was also performed to investigate the influence of solids volume flow rate and initial material height on steady state void ratio profiles. It was found that a slower solids volume flow rate generally provides a higher solids thickener underflow. This is due to a longer residence time. It was also shown that overflowing of a thickener or ineffective use of a thickener can occur when the solids volume flow rate is too fast.
- The concept of a high compression thickener by increasing the initial material thickness was investigated and it was found that an increase of the bed thickness can increase the underflow solids content. Results also suggest that there is a possibility of an optimum height where a minimum void ratio can be achieved under a specified solids volume flow rate. Increase in height is not only increasing the self-weight stress but also increasing the residence time and the length of the drainage path.

Chapter 5: Multi dimensional finite strain consolidation modeling

- A quasi-multi-dimensional finite strain consolidation theory was derived in terms of excess pore water pressure. The major assumptions used in the theory are that the pore fluid is permitted to flow in any direction but that deformation is strictly vertical. Mixing, flowing, sliding and shearing are neglected. The equations were coded in a FlexPDE finite element program which was implemented for modeling of 2*D* and 3*D* consolidation problems.
- Based on the derived theory, a comparative study was performed to investigate the consolidation model's behavior of slurry for ponds with various shapes and boundary conditions for the quiescent condition. Only one driving mechanism, a vertical self-weight stress, was examined in all simulations and horizontal and vertical hydraulic conductivity were assumed identical.
- The 2*D* consolidation model studies show that there is no shape effect for a rectangular shaped containment pond and is not different than 1*D* consolidation

behavior. For V-shaped cross sectional ponds, the steeper the dyke slope, the better the rate of consolidation. For trapezoidal shaped ponds, the dyke slope does not show a significant effect at the center of the pond. However at the toe of the dyke, it can be observed that the steeper the dyke the better the rate of consolidation. The surface slope of the pond is found to give a small increase in the rate of consolidation due to a shorter horizontal drainage path. The larger the angle of the surface slope of the pond, the faster the initial rate of consolidation.

- Drainage from all boundaries is the ideal case for slurry dewatering. Drainage through the foundation has a pronounced influence on the initial rate of consolidation while drainage through a dyke has negligible effect at the center of a pond. In the area between the dyke and the center of a pond, the dyke drainage, however, helps to increase the rate of consolidation. The smaller the base width the more the effect of the drainage through dykes. It is noted that blinding of the foundation drainage could occur in a longer term and was not studied here.
- The shape of a cylinder-cone containment vessel provides an increase in the initial rate of reduction in void ratio. The increased rate is faster than the 2*D* V-shaped pond with the same slope. This is due to the three-dimensional flow.

Chapter 6 Field investigation of the in-line thickened tailings

- Field pilot programs were conducted and were successfully complete.
- Two ILTT pilot ponds were filled. The major difference between the ponds was the discharge method. The west pond had a half-pipe chute discharge while the east pond had a sub-TT discharge (tremie technique). The latter discharging method was a lower energy deposition technique which minimized aggregate rupture in the ILTT material.
- In the east pilot pond, it was found that the tailings compressed from an initial solids content of 3.7% to 31.2% (void ratios of 65.6 and 5.5 respectively) in about 7.4 days after the filling period was over and to about 50% solids content (void ratio of 2.5) at a depth of 1 m in 4 months. The fines content profiles were consistent with depth and have an average value of 89%. The pore pressure measurements in this pond showed some consolidation at the bottom at all stations as the pond had a pervious foundation. It appeared that a layer of tailings consolidated at the bottom and sealed it preventing further significant downward drainage

- Evident segregation was found in the west pilot pond. A hypothesis on the cause of segregation was that the high discharging energy in this pond broke floc structure allowing the sand to settle out.
- The east pilot pond was history matched by utilizing a finite strain consolidation theory and by searching compressibility and hydraulic conductivity functions based on power law relationships.
- Comparison of the field history matching constitutive relationships indicated that the field ILTT was more difficult to compress than typical MFT because of the fairly strong large flocs in the ILTT.
- The field ILTT was more permeable than typical MFT. At 30% solids content the field hydraulic conductivity was about 20 times more permeable than that of MFT. This great difference in hydraulic conductivity was caused by the difference in structure of the flocculated ILTT vs. the dispersed MFT.

Chapter 7: Laboratory investigation of the in-line thickened tailings

- A laboratory study of sedimentation and consolidation behavior of cyclone overflow, in-line thickened tailings and sheared in-line thickened tailings was conducted to investigate the changes in compressibility, hydraulic conductivity and undrained shear strength induced by the in-line thickening process.
- Cyclone overflow was directly obtained from Syncrude Canada Ltd. and in-line thickened tailings and sheared in-line thickened tailings were prepared by mixing the cyclone overflow tailings, recycle water, flocculant and coagulant to a design solids content under the specified mixing conditions. The in-line thickened tailings were subjected to testing after the in-line mixing was completed to represent a non-disturbed in-line thickened tailings while the sheared in-line thickened tailings were subjected to shearing after mixing to represent remolded in-line thickened tailings due to tailings transportation.
- Three sub tests, a hindered sedimentation test, a compressibility standpipe test and a large strain consolidation test were combined to measure the full range of sedimentation and consolidation characteristics for cyclone overflow tailings, in-line thickened tailings and sheared in-line thickened tailings. With the given testing techniques, the void ratio-hydraulic conductivity relationship can be measured from a void ratio of 80 and lower and the effective stress-void ratio relationship can be measured from a void ratio of 16 and lower for cyclone

overflow and in-line thickened tailings. Continuous data for both relationships were obtained for both tailings materials.

- Comparison of 2008 cyclone overflow tailings and in-line thickened tailings shows that their compressibilities are similar at void ratios higher than 8. The compressibilities of both materials follow different paths at lower void ratios. The cyclone overflow below a void ratio of about 5 has much lower compression indices. For in-line thickened tailings, the change in its compressibility appears to occur at a higher void ratio and is more gradual than that of the cyclone overflow. In-line thickened tailings compressibility starts to change to a lower compression index as it reaches a void ratio of around 8. The in-line thickened tailings compressibility behavior appears to withstand higher effective stresses at void ratios of 8 and below. The compressibilities of both materials converge as the effective stress gets higher.
- Compressibility comparisons of the non-sheared in-line thickened tailings and sheared in-line thickened tailings suggests that the breakage of the floc structure at void ratios of 7.5 and higher due to shear will possibly disrupt the large and small macro floc structures. The small macro floc structure may be partly reformed and the micro structure is probably unaffected. Compression behaviors of sheared and non-sheared material are similar at void ratios below 5. It is concluded that the large and small macro floc structures control the material compressibility only at void ratios of 5 and higher.
- In-line thickened tailings hydraulic conductivity is more than three magnitudes greater than that of the cyclone overflow tailings at void ratios between 15 and 80. The increase of hydraulic conductivity due to the in-line thickening process is decreased as the void ratio is decreased below 15 and when the void ratio is reduced to about 3 there appear to be no difference between the two materials.
- Shearing the in-line thickened tailings will result in reduction of its hydraulic conductivity approximately 2 magnitudes at void ratios between 20 and 80. The remaining influence of the in-line thickening process still provides the material with hydraulic conductivity more than 10 times larger than that of the cyclone overflow tailings.
- Converging hydraulic conductivity behavior of all tailings start at a void ratio of about 20. The hydraulic conductivity differences in all the tailings disappear at a void ratio of about 3.

- Undrained shear strength measurements show that the in-line thickened tailings has the highest undrained shear strength followed by sheared in-line thickened tailings and then cyclone overflow tailings respectively.
- The comparison of the field history matching constitutive relationships and the laboratory measured constitutive relationships resulted in a good agreement. This good agreement strengthens the validity of the geotechnical parameters obtained from this laboratory program and indicate that it is possible to model a large scale field deposit.
- Field samples from the pilot scale test program were also subjected to large strain consolidation tests. Results of a comparison between the laboratory and field history matching constitutive relationships determined that the field hydraulic conductivity behavior was higher than that of the field samples tested in the laboratory at the same void ratios. This difference in hydraulic conductivity was probably caused by the breakdown of the floc structure in the field samples as they were remolded during sampling and sample preparation procedures in the laboratory.
- The research hypothesis of comparing in-line thickened tailings and cyclone overflow properties was that the difference in the behavior of these materials would be directly related to the effect of the flocculants and coagulant added in the in-line thickening process. The function of the additives is to bind soil particles together to form large aggregates of soil particles that will settle quickly during deposition at low solids contents. The hypothesis is that as the additives flocculate the soil particles together, the shear strength of the soil will increase as breaking the structure requires additional energy. The soil structure therefore becomes stronger. Compared to the parent cyclone overflow, the treated tailings would not compress as much when subjected to the same applied stress. The hydraulic conductivity should also be affected by the process because the additives change the structure of the soil reducing the tortuous channels of the soil resulting in greater hydraulic conductivity. Results of the laboratory investigation have quantified the influences of the in-line thickening process on sedimentation, consolidation and shear strength characteristics of cyclone overflow tailings. Sedimentation and consolidation geotechnical parameters have been assigned for both treated and untreated tailings.

Chapter 8: Validation of in-line thickened tailings

- A 2 m validation standpipe test was used to simulate a pond filling condition for the in-line thickened tailings in this chapter. This was performed by filling the tailings in six layers in six consecutive days and allowing the tailings to consolidate for 180 days until the consolidation was complete.
- The results from the validation standpipe including interface heights, excess pore water pressures, a final void ratio profile and a final undrained shear strength profile were compared to a finite strain consolidation model with the appropriate material properties, initial conditions and boundary conditions.
- The comparisons of all the geotechnical aspects between the validation standpipe and the numerical model with the properly assigned material characteristics show that a good agreement between a controlled laboratory standpipe test and a theoretical model can be obtained with an intensive material study and an understanding of depositing conditions. For the in-line thickened tailings, practically negligible deviations were found between the observed behavior and predictions of the interface height, pore pressure profiles and void ratio profiles. In the real field application, complex field conditions and variations in material properties will likely complicate the application of the finite strain consolidation analysis. This study highlights that the finite strain consolidation model is a suitable tool for estimating settling behavior of the in-line thickened tailings and the use of a model in practice will require a careful selection of input parameters and a good understanding of field depositional processes.

Chapter 9 Composite tailings made from the in-line thickened tailings

- At a SFR of 4:1 without any further coagulant chemical amendment, it was found that the composite tailings made with in-line thickened tailings (ILTT-CT) had a static segregation point of 52.6% solids content and the composite tailings made with cyclone overflow tailings (COF-CT) had a static segregation point of 58.9% solids content. The segregation boundary of the ILTT-CT is comparable to that of the gypsum treated CT and is much higher than the segregation boundary of the old mature fine tailings CT. Therefore under a static condition, nonsegregating behavior of ILTT-CT can be achieved by mixing in-line thickened tailings with cyclone underflow sand at a FWR higher than 18%.

- Undrained shear strength measurements indicate that the ILTT-CT has an undrained shear strength similar to that of the sheared in-line thickened tailings at a fines-bitumen void ratio of about 6. At lower fines-bitumen void ratios, the undrained shear strength of the ILTT-CT diverges from that of the sheared in-line thickened tailings and is significantly larger. The higher measured undrained shear strength of the ILTT-CT at lower fines-bitumen void ratios is believed to be caused by the synergistic contribution of the large flocs of ILTT and the sand particles. This greater shear strength of ILTT-CT is very important as it allows the CT to reach a shear strength of 5 kPa at a void ratio above 3 to meet the ERCB definition of a solid deposit.
- Hydraulic conductivity measurements of the ILTT-CT at large void ratios locate in between the hydraulic conductivities of non-sheared and sheared in-line thickened tailings. The COF-CT's hydraulic conductivity is slightly lower than that of the cyclone overflow tailings. The trends of the results suggest that the hydraulic conductivities of both composite tailings are controlled by the fines used to create the tailings. The ILTT-CT thus will have a high hydraulic conductivity property inherited from the ILTT fines.
- Composite tailings at a solids content of about 60% therefore can be made from in-line thickened tailings with an advantage of having a hydraulic conductivity about 10 times greater than that of the composite tailings made from cyclone overflow. Therefore ILTT-CT will consolidate about 10 times faster than the COF-CT.
- The combination of faster consolidation and higher shear strength means that the ILTT-CT will be able to be reclaimed much earlier than MFT-CT. Judicial deposition techniques may result in it being reclaimed as it is being deposited.

10.3 Recommendations for future study

It is recommended that future research on the application of flocculated oil sands tailings should be focused on how to link all processes occurring in the tailings during its life time into one complete analysis. A combined analysis of flocculation, sedimentation, consolidation, segregation, deposition, freeze-thaw and desiccation is very important to assess the overall tailings behavior. If a 5 kPa undrained shear strength is established to be a goal for a successful reclamation, it will never be achieved this by only considering

chemical additives or sedimentation alone. Essentially, a combined recognition of several processes that can be quantified using existing measurements and theories is necessary.

For constitutive relationships used in the one dimensional finite strain consolidation analysis, it is recommended that possible mechanisms that affect micro and macro structures and therefore hydraulic conductivity of the slurry should be further investigated to extend the current stage of understanding. Examples of possible mechanisms include channeling, thixotropy effect on hydraulic conductivity, segregation of bitumen and ultra fines. For multi-dimensional modeling, future extensions should be aimed to include three dimensional self-weight stress analysis, horizontal deformation and flowing and sliding mechanisms.

The author also recommends that laboratory and theoretical studies to extend a fundamental understanding of tailings sedimentation and consolidation should be focused on a micro scale. Since a considerable amount of data already is available for macro scale studies, it would be of great interest to study the relationship between micro scale measurements and macro scale behavior.

Bibliography

Abu-Hejleh, A.N., and Znidarčić, D. 1995. Desiccation Theory for Soft Cohesive Soils. Journal of Geotechnical Engineering, **121**(6): 493-502.

Achari, G., Joshi, R.C., Bentley, L.R., and Chatterji, S. 1999. Prediction of the hydraulic conductivity of clays using the electric double layer theory. Canadian Geotechnical Journal, **36**: 783-792.

Alexis, A., Le bras, G., and Thomas, P. 2004. Experimental Bench for Study of Settling-Consolidation Soil Formation. Geotechnical Testing Journal, **27**(6): 1-11.

AGRA. 1997. Progress on MFT Modeling. Report to Syncrude Canada Ltd, Engineering report, AGRA Earth & Environmental limited, Edmonton, Alberta.

Apex Engineering Inc. and Applied Environmental Geochemistry Research Facility (AEGRF), Dept. Civil and Environmental Eng, University of Alberta, 2005. Pumping and pipelining shear effect on NST of 5:1 and 6:1 Using Albian Sands January, 2004 tailings (second report on second extension project), submitted to Albian Sands Energy Inc. and Canadian Natural Resources Ltd., July 2005, p.18.

Apex Engineering Inc. and Applied Environmental Geochemistry Research Facility (AEGRF), Dept. Civil and Environmental Eng, University of Alberta, 2005. NST production at SFR of 5:1 and 6:1 (report on first extension project), submitted to Albian Sands Energy Inc. and Canadian Natural Resources Ltd., April 2005, p.43.

ASTM Standard D4186-06, 2006. Standard Test Method for One-Dimensional Consolidation Properties of Saturated Cohesive Soils Using Controlled-Strain Loading, ASTM International, West Conshohocken, PA, DOI: 10.1520/D4186-06, www.astm.org.

ASTM Standard C837-99, 1999. Standard Test Method for Methylene Blue Index of Clay, ASTM International, West Conshohocken, PA, DOI: 10.1520/C0837-99, www.astm.org.

ASTM Standard D2487-06e1, 2006e1. Standard Practice for Classification of Soils for Engineering Purposes, ASTM International, West Conshohocken, PA, DOI: 10.1520/D2487-06E01 , www.astm.org.

ASTM Standard D4221-99, 1999 (2005). Standard Test Method for Dispersive Characteristics of Clay Soil by Double Hydrometer, ASTM International, West Conshohocken, PA, DOI: 10.1520/D4221-99R05, www.astm.org.

ASTM Standard D422-63, 1963 (2007). Standard Test Method for Particle-Size Analysis of Soils, ASTM International, West Conshohocken, PA, DOI: 10.1520/D0422-63R07, www.astm.org.

Auzerais, F. M., Jackson, R., and Russel, W.B. 1988. The Resolution of Shocks and the Effects of Compressible Sediments in Transient Settling. Journal of Fluid Mechanics, **195**:437-462.

Azam, S. and Scott, J.D. 2009. Influence of microstructure on self-weight settling of laterite ore slurries. Proceeding of the Thirteenth International Conference on Tailings and Mine Waste, 1-4 November 2009, Banff, Alberta, Canada: 149-158.

Azam, S. and Scott, J.D. 2005. Revisiting the ternary diagram for tailings characterization and management. Geotechnical News, **23**(4): 43-46.

Azam, S., Jeeravipoolvarn, S., and Scott, J.D. 2009. Numerical modeling of tailings thickening for improved mine waste management. Journal of Environmental Informatics, **13**(2):111-118.

Azam, S., Scott, J.D., and Jeeravipoolvarn, S. 2007. When does a slurry become a soil? Geotechnical News. BiTech, BC, **25**(3):44-46.

Banas, L. 1991. Thixotropic behaviour of oil sands tailings sludge. M.S.c. thesis, Department of Civil and Environmental Engineering, University of Alberta, Edmonton, AB.

Bartholomeeusen G., Sills, G.C., Znidarčić, D., Van Kesteren, W., Merckelbach, L.M., Pyke, R., Carrier III, W.D., Lin, H., Penumadu, D., Winterwerp, H., Masala, S. and Chan, D. 2002. Sidere: numerical prediction of large-strain consolidation. Géotechnique, **52**(9): 639-648.

Bartholomeeusen G. 2003. Compound shock waves and creep behavior in sediment beds. Ph.D. thesis, Oxford University, UK.

Been, K. 1980. Stress strain behaviour of cohesive soil deposited under water. Ph.D. thesis, Oxford University, UK.

Been, K. and Sills, G.C. 1981. Self-weight consolidation of soft soils. Géotechnique, **31**(4):519-535.

Boratenec, D. 2003. Fundamentals of Rapid Dewatering of Composite Tailings, M.S.c. thesis, Department of Civil and Environmental Engineering, University of Alberta, Edmonton, AB.

Bjerrum, L. and Simons, N.E. 1960. Comparison of Shear Strength Characteristics of Normally Consolidated Clays, 1st PSC, ASCE, 711-726.

Bjerrum, L. 1967. Seventh Rankine Lecture, Engineering geology of Norwegian normally consolidated marine clay as related to the settlements of buildings. Géotechnique, **17**(2): 81-118.

Bowder, J.J., and Danial, D.E., 1987. Hydraulic conductivity of compacted clay to dilute organic chemicals. Journal of Geotechnical Engineering, **113**(12): 1432-1448.

Bromwell, L.G. 1984. Consolidation of mining wastes. Sedimentation consolidation models: predictions and validation: *In* proceedings of a symposium, R.N. Yong and F.C. Townsend Eds, ASCE, Newyork: 275-295.

Bromwell L.G., and Oxford T.P. 1977. Waste clay dewatering and disposal. *In* Proceedings of the Conference on Geotechnical Practice for Disposal of Solid Waste Materials, June 13-15, 1977, the University of Michigan, Ann Arbor, Michigan : 541-558.

Bürger, R. and Karlsen, K.H. 2001. On some upwind difference schemes for the phenomenological sedimentation-consolidation model. Journal of Engineering Mathematics, **41**:145–166.

Bürger, R., Damasceno, J.J.R. and Karlsen, K.H. 2004. A mathematical model for batch and continuous thickening of flocculated suspensions in vessels with varying cross-section. International Journal of Mineral Processing, **73**: 183-208.

Bürger, R.,and Narváez, A. 2007. Steady-state, control, and capacity calculations for flocculated suspensions in clarifier-thickeners. International Journal of Mineral Processing, **84**: 274-298.

Burgos, R., and Concha, F. 2005. Furthur development of software for the design and simulation of industrial thickeners. Chemical Engineering Journal, 111: 135-144.

Bustos, M.C., Concha, F., Burger, R. and Tory, E.M. 1999. Sedimentation and Thickening: Phenomenological Foundation and Mathematical Theory. Kluwer Academic publishers.

Bustos, M.C. and Concha F. 1988. Simulation of Batch Sedimentation with Compression. AIChE Journal, **34**(5):859-861.

Cargill, K.W. 1982. Consolidation of Soft Layers by Finite Strain Analysis. U.S. Army Engineer Waterways Experimentation Station. Vicksburg, Mississippi, Miscellaneous Paper GL-82-3.

Cargill, K.W. 1984. Prediction of Consolidation of Very Soft Soil. Journal of Geotechnical Engineering, **110**(6): 775-795.

Caríssimi, E., and Rubio, J. 2005. The flocs generator reactor – FGR: a new basis for flocculation and solid-liquid separation. International Journal of Mineral Processing, **75**:237-247.

Carrier, W.D., III, Bromwell, L.G., and Somogyi, F. 1983. Design Capacity of Slurried Mineral Waste Ponds. Journal of Geotechnical Engineering, **109**(5): 699-716.

Caughill, D.L. 1992. Geotechnics of non-segregating oil sand tailings, M.S.c. thesis, Department of Civil and Environmental Engineering, University of Alberta, Edmonton, AB.

Chalaturnyk, R.J., Scott, J.D. and Ozum, B. 2004. Environmentally Acceptable Deposition of Oil Sands Tailings, SWEMP 2004, 8 International Symposium on Environmental Issues and Waste Management in Energy and Mineral Production May 17-20, 2004 Antalya, Turkey, 6p.

Chiappone, A., Marello, S., Scavia, C. and Setti, M. 2004. Clay mineral characterization through the methylene blue test: comparison with other experimental techniques and applications of the method. Canadian Geotechnical Journal, **41**:1168-1178.

Christian, J.B. 1994. Improve clarifier and thickener design and operation. Chemical Engineering Progress 90(7): 50-56.

Coe, H.S., and Clevenger, G.H. 1916. Methods for determining the capacities of slime settling tanks. Trans. AIME 55: 356–385.

Crowder J.J. and Grabinsky, M.W. 2005. Assessment of the modified slump test as a measure of the yield stress of high density thickened tailings [Discussion]. Canadian Geotechnical Journal, **43**: 316-318.

Dawson, R. F., Sego, D.C., and Pollock, G.W. 1999. Freeze Thaw Dewatering of Oil Sands Fine Tails. Canadian Geotechnical Journal, **36**:587–598.

Dixon, D.C., 1979. Momentum balance aspects of free settling theory, part II: Continuous steady state thickening, Sep. Science, 12:192-201.

Donahue, R., Sego, D., Burke, B., Krahn, A., Kung, J. and Islam, N. 2008. Impact of ion exchange properties on the sedimentation properties oil sands mature fine tailings and synthetic clay slurries. First international Oil Sands Tailings Conference. Edmonton, AB, December 7-10, 55-63.

Eckert, W.F., Masliyah, J.H., Gray, M.R. and Fedorak, P.M. 1996. Prediction of Sedimentation and Consolidation of Fine Tails. AIChE Journal, **42**(4): 960 - 972.

Edil, T. B. and Fox, P.J. 2000. Geotechnics of High Water Content Materials, ASTM international Publisher.

Elder, D.M. 1985, Stress strain and strength behvaiour of very soft soil sediment, D.Phil. Thesis, Oxford University, UK.

Elnaggar, H.A., Krizek, R.J. and Karadi, G.M. 1973. Effect of non-Darcian flow on time rate of consolidation. Journal of the Franklin Institute **296**:323-337.

ERCB. 2009. Alberta's Energy Reserves and Supply/Demand Outlook 2009-2018 (ST98-2009). The Energy Resources Conservation Board of Alberta (ERCB), Calgary, Alberta: 220 p.

ERCB. 2009. Directive 074 Tailings Performance Criteria and Requirements for Oil Sands Mining Schemes. The Energy Resources Conservation Board of Alberta (ERCB), Calgary, Alberta: 5-10.

EUB. (Alberta Energy and Utilities Board) Statistical Series (ST) 2004-98, 2004, "Alberta's Reserves 2003 and Supply/Demand Outlook 2004-2013), http://www.ercb.ca.

EUB (Alberta Energy and Utilities Board) Statistical Series (ST) 2006-98, 2004, "Alberta's Energy Reserves 2005 and Supply/Demand Outlook 2006-2015), http://www.ercb.ca.

Farrow, J.B., Johnston, R.R.M., Simic, K., and Swift, J.D. 2000. Consolidation and aggregate densification during gravity thickening. Chemical Engineering Journal, 80: 141-148.

Fedorak, P.M., Coy, D.L., Salloum, M.J. and Dudas, M.J. 2002. Methanogenic potential of tailings samples from oil sands extraction plants, Canadian Journal of Microbiology. **48**: 21-33.

Fox, P.J. and Baxter, C.D.P. 1997. Consolidation properties of soil slurries from hydraulic consolidation test. Journal of Geotechnical and Geoenvironmental Engineering, **123**(8): 770-776.

FTFC. 1995. Advance in oil sands tailings research. Fine Tailings Fundamental Consortium (FTFC), Oil Sands and Research Division, Alberta Department of Energy, Edmonton, Alberta.

Garrido, P., Burgos, R., Concha, F., Bürger, R. 2003. Software for the design and simulation of gravity thickeners. Mineral Engineering, 16: 85-92.

Garrido, P., Burgos, R., Concha, F., Bürger, R., 2004. Settling velocities of particulate systems:13. A Simulator for batch and continuous sedimentation of flocculated suspensions. International Journal of Mineral Processing, 73:131–144.

Gawu, S.K.Y., and Fourie, A.B. 2004. Assesment of the modified slump test as a measure of the yield stress of high-density thickened tailings. Canadian Geotechnical Journal, **41**(1): 39-47.

Gibson, R.E., England, G.L. and Hussey M.J.L. 1967. The Theory of One-dimensional Consolidation of Saturated Clays. I. Finite Non-linear Consolidation of Thin Homogeneous Layers. Géotechnique, **17**(3): 261–273.

Gibson, R.E., Schiffman, R.L., and Cargill, K.W. 1981. The theory of one-dimensional consolidation of saturated clays. II. Finite nonlinear consolidation of thick homogeneous layers. Canadian Geotechnical Journal, **18**: 280-293.

Gjerapic, G., Johnson, J., Coffin, J. and Znidarcic, D. 2008. Determination of Tailings Impoundment Capacity via Finite-Strain Consolidation Models. GeoCongress 2008: Characterization, Monitoring and Modeling of Geosystems, 795-805.

Green, D. 1995. High compression thickeners are gaining wider acceptance in mineral processing. Filtration & Separation: Thickeners in Mineral Processing, 32(10): 947.

Guo, C. 2009. Rapid Densification of the Oil Sands Mature Fine Tailings (MFT) by Microbial Activity. Ph.D. Thesis, University of Alberta, Edmonton, Canada.

Hawlader, B.C., Muhunthan, B. and Imai, G. 2008. State-dependent constitutive model and numerical of self-weight consolidation. Géotechnique, **58**(2): 133-141.

Hogg, R. 1987. Agglomerate structure in flocculated suspensions and its effect on sedimentation and dewatering. Minerals & Metallurgical Processing, **4**(2):108-114.

Hogg, R. 2000. Flocculation and dewatering. International Journal of Mineral Processing, **58**:223-236.

Hogg, R., Bunnaul, P., and Suharyono, H. 1993. Chemical and physical variables in polymer-induced flocculation. Minerals and Metallurgical Processing, **10**(2): 81-85.

Huerta, A. and Rodriguez, A. 1992. Numerical analysis of non-linear large-strain consolidation and filling. Computer and Structures, **44**(1/2): 357-365.

Hamdi, P. 1973. Performance of very soft mud and the very light loads and consolidation of a muddy bottom under a wide sand fill. Proceedings of 8th ICSMFE, **22**:159-163.

Holowenko, F. M., MacKinnon, M.D., and Fedorak, P.M. 2000. Methanogens and sulfate-reducing bacteria in oil sands fine tailings wastes. Canadian Journal of Microbiol, **46**: 927–937.

Holtz, R.D. and Kovacs, W.D. 1981. An Introduction to Geotechnical Engineering. Prentice-Hall, Englewood Cliffs, NJ, 733 p.

Holdich, R.G. and Butt, G. 1997. Solid/liquid separation by sedimentation. Proceedings of the Institution of Mechanical Engineers, Part E, Journal of Process Mechanical Engineering, **211**(1): 43-52.

Islam, N. 2008. The role of cation exchange on the sedimentation behaviour of oil sands tailings. M.Eng. report, Department of Civil and Environmental Engineering, University of Alberta, Edmonton, AB.

Imai, G. 1979. Development of a New Consolidation Test Procedure Using Seepage Force. Soils and Foundations, **19**(3): 45–60.

Imai, G. 1981. Experimental Studies on Sedimentation Mechanism and Sediment Formation of Clay Materials. Soils and Foundations, **21**(1): 7–20.

Imai, G., Yano, K., and Aoki, S. 1984. Applicability of Hydraulic Consolidation Test for Very Soft Clayey Soils. Soils and Foundations, **24**(2): 29–42.

Imai, G. 1981. Experimental studies on sedimentation mechanism and sediment formation of clay materials. Soils and Foundations, **21**(1): 7-20.

Imai, G. and Hawlader, B.C. 1997. An elastio-viscoplastic analysis of self weight consolidation. Computer Methods and Advances in Geomechanics, 1065-1070.

Imai, G., and Tang, Y. X. 1992. A constitutive equation of one-dimensional consolidation derived from inter-connected tests. Soils and Foundation, **32**(2): 83-96.

Inoue, T., Tan, T.S., and Lee, S. 1990. An investigation of shear strength of slurry clay. Soils and Foundations, **30**(4): 1-10.

Ito, T. and Matsui, T. 1975. Plastic flow mechanism of clays. *In* Proceedings of JSCE, **236**: 109-123.

Jeeravipoolvarn, S. 2005. Compression Behaviour of Thixotropic Oil Sands Tailings. M.S.c. thesis, Department of Civil and Environmental Engineering, University of Alberta, Edmonton, AB.

Jeeravipoolvarn, S., Scott, J.D., and Chalaturnyk, R.J. 2009. 10 m standpipe tests on oil sands tailings: long term experimental results and prediction. Canadian Geotechnical Journal, **46**:875-888.

Jeeravipoolvarn, S., Chalaturnyk, R.J., and Scott, J.D. 2009. Sedimentation-consolidation modeling with an interaction coefficient. Computer and Geotechnics, **36**(5):751-761.

Jeeravipoolvarn, S., Chalaturnyk, R.J. and Scott, J.D. 2008. Consolidation Modeling of Oil Sands Fine Tailings: History Matching, *In* Proceedings of 61st Canadian Geotechnical Conference, Edmonton, AB, September 22-24:190-197.

Jeeravipoolvarn, S., Scott, J.D., Donahue, R., and Ozum, B. 2008. Characterization of Oil Sands Thickened Tailings. *In* Proceedings of International Oil Sands Tailings Conference, December 7-10, Edmonton, AB:132-142.

Jeeravipoolvarn, S., Scott, J.D., and Chalaturnyk, R.J. 2007. Large strain consolidation tests on Syncrude mature fine tailings: Effect of shearing on consolidation characteristics. Submitted to Syncrude Canada Ltd, 39 p.

Kim, Y.T. and Leroueil, S. 2001. Modeling the viscoplastic behaviour of clay during consolidation: application to Berthierville clay in both laboratory and field conditions. Canadian Geotechnical Journal, **38**:484-497.

Koppula, S.D. 1970. The consolidation of soil in two dimensions and with moving boundaries, Ph.D. thesis, Department of Civil and Environmental Engineering, University of Alberta, Edmonton, AB.

Krizek, R.J. and Somogyi, F. 1984. Perspectives on modellingconsolidation of dredged materials. Sedimentation consolidation models: predictions and validation: *In* proceedings of a symposium, R.N. Yong and F.C. Townsend Eds, ASCE, Newyork: 296–332.

Kynch, G.J. 1952. A theory of Sedimentation. Transactions of Faraday Society, **48**: 166-176.

Lee, K. 1979. An analytical and experimental study of large strain soil consolidation. DPhil, University of Oxford.

Lee, S.L., Karunaratene, G.P., Yong, K.Y. and Geneshan, V. 1987. Layered Clay-Sands Scheme of Land Reclamation. Journal of Geotechnical Engineering, ASCE, **113**(9): 984-995.

Leroueil, S., Kabbaj, M., Tavenas, F. and Bouchard, R. 1985. Stress-strain-strain rate relation for the compressibility of sensitive natural clays. Géotechnique, **35**(2): 159-180.

Li, Y. and Metha, A.J. 1998. Assessment of Hindered Settling of Fluid Mudlike Suspensions. ASCE Journal of hydraulic Engineering, **124**: 176-178.

Lin, T.W., and Lohnes, R.A. 1984. Sedimentation and self weight consolidation of dredge spoil. Sedimentation consolidation models: predictions and validation: *In* proceedings of a symposium, R.N. Yong and F.C. Townsend Eds, ASCE, Newyork: 464-480.

Martin, R.T., Bromwell, L.G., and Sholine, J.H. 1977. Field tests of phosphatic clay dewatering. *In* Proceedings of the Conference on Geotechnical Practice for Disposal of Solid Waste Materials, June 13-15, 1977, the University of Michigan, Ann Arbor, Michigan : 559-598.

Masala, S. 1998. Numerical Solution of sedimentation and consolidation of fine tailings, M.S.c. thesis, Department of Civil and Environmental Engineering, University of Alberta, Edmonton, AB.

Matsui, T. and Ito, T. 1977. Flow mechanism of clay-layer system and microscopic meaning on shear parameters of soils. 9th ICSMFE, Special Session 9: 143-152.

Matthews, J.G., Shaw, W.H., MacKinnon, M.D. and Cuddy, R.G. 2002. Development of composite tailings technology at Syncrude. International Journal of Surface Mining, Reclamation, and Environment, **16**(1): 24-39.

McNabb, A. 1960. A Mathematical treatment of one-dimensional soil consolidation. Quarterly of Applied Mathematics, **17**(4): 337-347.

Merckelbach, L. M., and Kranenburg, C. 2004. Equation for effective stress and permeability of soft mud-sand mixtures. Géotechnique, **54**(4): 235–243.

Merckelbach, L. M. and Kraneburg, C. 2004. Determining effective stress and permeability equations for soft mud from simple laboratory experiments. Géotechnique, **54**(9): 581–591.

Mesri, G. 1975. New design procedure for stability of soft clays, Discussion. Journal of Geotechnical Engineering, **101**(GT4): 1090-1093.

Mihiretu, Y., Chalaturnyk, R.J. and Scott J.D. 2006. Settling of sand through a clay slurry. *In* Proceedings of 59th Canadian Geotechnical Conference, Vancouver, BC, October 1-4 2006: 319-326.

Mihiretu, Y., Chalaturnyk, R.J. and Scott J.D. 2008. Tailings segregation fundamentals from flow behaviour perspective. *In* First international Oil Sands Tailings Conference. Edmonton, AB, December 7-10: 112-120.

Miller, W. Scott, J.D. and Sego, D.C., 2010. Influence of the extraction process on the characteristics of oil sands fine tailings, Submitted to CIM Journal.

Miller, W. Scott, J.D. and Sego, D.C., 2010. Effect of extraction water chemistry on the self-weight consolidation of oil sands fine tailings, Submitted to CIM Journal.

Miller, W. Scott, J.D. and Sego, D.C., 2010. Effect of extraction water chemistry on the consolidation of oil sands fine tailings, Submitted to CIM Journal.

Miller, W. Scott, J.D. and Sego, D.C., 2010. Influence of extraction process and coagulant addition on thixotropic strength of oil sands fine tailings, Submitted to CIM Journal.

Mishler, R.T. 1912 Settling slimes at the Tigre Mill. Engineering and Mining Journal, 94:643-646.

Mitchell, J.K. 1960. Fundamental aspects of thixotropy in soils. Journal of soil Mechanics Foundation Divisions American Society of Civil Engineers, **83**(3): 19-52.

Mitchell, J. K. 1993. Fundamentals of soil behavior. New York, John Wiley and Sons Inc.

Monte, J.L. and Krizek, R.J 1976. One-dimensional mathematical model for large strain consolidation. Géotechnique, **26**(3): 495-510.

Morin, W., Shafer, T. and Gangopadhyay, K. 1984. Dredge slurry stabilization for Seagirt Marine Terminal. Sedimentation consolidation models: predictions and validation: *In* proceedings of a symposium, R.N. Yong and F.C. Townsend Eds, ASCE, Newyork: 501-521.

Morin, M. 2008. AST Methylene Blue Procedure: Sludge & Slurries. *Natural Resources Canada*, Canada Energy Technology Centre, Advanced Separation Technologies, Tailings & Emulsions.

Myint, W.B., Wong, K.S., Victor, C., and Teh, C.I. 2003. Compression Tests of Ultra-Soft Soil Using an Hydraulic Consolidation Cell. Geotechnical Testing Journal, **26**(3): 310-319

Nageswaran, S. 1983. Effect of gas bubbles on the sea-bed behaviour. Ph.D. thesis, Oxford University, UK.

Nasser, M.S., and James, A.E. 2007. Numerical simulation of the continuous thickening of flocculated kaolinite suspensions. International of Mineral Processing, 84: 144-156.

Olsen, H.W. 1996. Darcy's law in saturated kaolinite, water Resources Research, **2**(6): 287-295.

Olsen, H.W., Nichols, R.W. and Rice, T.L. 1985. Low gradient permeability measurements in a triaxial system. Géotechnique, **35**(2): 145-157.

Olsen, R.E. and Daniel, D.E. 1981. Measurement of hydraulic conductivity of fine grained soils, In permeability and ground water contaminant transport, Edited by T.F. Zimmie and C.O. Riggs. American Society for Testing and Materials, Special Technical Publication 746: 18-64.

Olson, R.E. and Ladd, C.C. 1979. One-dimensional consolidation problems. Journal of Geotechnical Engineering, **105**(1): 11–30.

Osipov, V.I., Nikolaeva, S. K. and Sokolov, V.N. 1984. Microstructural changes associated with thixotropic phenomena in clay soils. Géotechnique, **34**: 293-303.

Pane, V. and Schiffman, R.L. 1985. A note on sedimentation and consolidation. Géotechnique, **35**(1):69-72.

Pane, V. and Schiffman, R.L. 1997. Permeability of clay suspensions. Géotechnique, **47**: 273-288.

Philip, J.R. and Smiles, D.E. 1982. Macroscopic analysis of the behavior of colloidal suspensions, Adv. Colloid Interface Sci., **17**: 83-103.

Pollock, G. 1988. Large Strain Consolidation of Oil Sand Tailings Sludge, M.S.c. thesis, Department of Civil and Environmental Engineering, University of Alberta, Edmonton, AB.

Pollock, G. 2004. Consolidation Modeling of Oilsand Tailings. CONRAD Tailings Seminar. Alberta Research Council, November 8, Edmonton, AB.

Qui, Y. 2000. Optimum Deposition for Sub-Aerial Tailings Disposal. Ph.D. thesis, Department of Civil and Environmental Engineering, University of Alberta, Edmonton, AB.

Qui, Y. and Sego, D.C. 2007. Optimum deposition for sub-aerial tailings disposal model applications. International Journal of Mining, Reclamation and Environment, **21**(1): 65-74.

Rattanakawin, C. and Hogg, R. 2001. Aggregate size distributions in flocculation. Colloids and Surfaces, A : Physicochemical and Engineering Aspects, **177**:87-98.

Renko, E.K. 1998. Modeling hindered batch settling Part II: A model for modeling solids profile of calcium carbonate slurry. Water SA, **24**(4): 331-336.

Rudman, M., Simic, K., Paterson, D.A., Strode, P., Brent, A. and Sutalo, I.D. 2008. Raking in gravity thickeners. International Journal of Mineral Processing, **86**: 114-130.

Salem, A.M. and Krizek, R.J. 1973. Consolidation Characteristics of Dredging Slurries. Journal of the Waterways, Harbors and Coastal Engineering Division, **99**(4): 439-457

Schiffman, R.L., Pane, V., and Gibson, R.E. 1984. The theory of One-Dimensional Consolidation of Saturated Clays IV: An overview of Nonlinear Finite Strain Sedimentation and Consolidation. Sedimentation/Consolidation Models, Edited by R.N. Yong and F.C. Townsend, ASCE: 1-29.

Schiffman, R.L. 2001. Theories of Consolidation. University of Colorado Press, Colorado, Boulder, USA.

Seed, H.B., Woodward, R.J., Jr. and Lundgren, R. 1964. Clay Mineralogical Aspects of the Atterberg Limits. Journal of the soil Mechanics and Foundation Division, ASCE, 90(SM4): 107-131.

Seed, H.B., Woodward, R.J., Jr. and Lundgren, R. 1964. Fundamental Aspects of the Atterberg Limits. Journal of the soil Mechanics and Foundation Division, ASCE, 90(SM6): 107-131.

Shodja. H.M. and Feldkamp, J.R. 1993. Numerical analysis of sedimentation and consolidation by the moving finite element method. International Journal of Numerical Methods in Geomechanics, 17:753-769.

Scott, J. D. and Dusseault, M.B. 1982. Behaviour of Oil Sands Tailings. 33rd Annual Technical Meeting of the Petroleum Society of the Canadian Institute of Mining and Metallurgy, Calgary, Alberta, June, Paper no. 82-33-85, 19 p.

Scott, J. D., Dusseault, M.B. and Carrier III, W.D. 1985, Behaviour of the clay/bitumen/water sludge system from oil sands extraction plants, Journal of Applied Clay Science, **1**: 207-218.

Scott, J.D., Chalaturnyk, R.J. and Jeeravipoolvarn, S. 2004. Settlement of Tailings Slurries by Creep Compression. *In* Proceedings of CIM Edmonton 2004 Conference, Edmonton, A.B., 9-12 May 2004, Canadian Institute of Mining, Metallurgy and Petroleum, 8 p.

Scott, J.D., Jeeravipoolvarn, S. and Chalaturnyk, R.J. 2008. Tests for Wide Range of Compressibility and Hydraulic Conductivity of Flocculated Tailings. *In* Proceedings of the 61st Canadian Geotechnical Conference, September 22-24, Edmonton, AB: 738-745.

Scully, R.W., Schiffman, R.L., Olsen, H.W. and Ko, H.Y. 1984. Validation of consolidation properties of phosphatic clay at very high void ratios. Sedimentation consolidation models: predictions and validation: *In* proceedings of a symposium, R.N. Yong and F.C. Townsend Eds, ASCE, Newyork: 158-181.

Seed, H. B., Woodward, R.J., Jr. and Lundgren, R., 1964a, On Mineralogical Aspects of the Atterberg Limits, Journal of the Mechanics and Foundation Division, ASCE, **90**(SM6): 75-106.

Seed, H. B., Woodward, R.J., Jr. and Lundgren, R., 1964b, Fundamental Aspects of the Atterberg Limits, Journal of the Mechanics and Foundation Division, ASCE, **90**(SM4): 107-131.

Seneviratne, N.H., Fahey, M., Newson, T.A. and Fujiyasu, Y. 1996. Numerical modelling of consolidation and evaporation of slurried mine tailings. International Journal for Numerical and Analytical Methods in Geomechanics, 20:647-671.

Sethi, A. 1995. Methylene Blue Test for Clay Activity Determination in Fine Tails. MRRT Procedures.

Shaw, W. and Wang, N. 2005. In-Line Thickened Tailings Pilot Program. Preliminary pilot results for a promising new method for thickening of high fines tailings streams. 6p.

Shaw, W. and Wang, N. 2006. In-Line Thickened Tailings Pilot Program. CIM Fort McMurray, Oil Sands Discovery Center Auditorium, Fort McMurray, Alberta, February 21, 2006.

Shodja H.M. and Feldkamp JR. 1993. Numerical analysis of sedimentation and consolidation by the moving finite element method. International Journal for Numerical Methods in Geomechanics, **17**: 753-769.

Sills, G. C. 1995 Time dependent processes in soil consolidation. *In* Proc. Int. Symp. Compression and Consolidation of Clayey Soils, Hiroshima, Japan (ed. H. Yoshikuni & O. Kusakabe), pp. 875-890. Rotterdam: Balkema.

Sills, G. 1998. Development of structure in sedimenting soils, Philosophical Transactions of the Royal Society A. **356**:2515-2534.

Skempton, A. W. 1994. Notes on the compressibility of clays. Quarterly Journal of the Geological Society, London. **100**(2): 119-135.

Smith. R. E. and Wahls. H. E. 1969. Consolidationunder constant rates of strain. Journal of Soil Mechanics. Foundation Division. ASCE, **95**(SM2): 519-539.

Somogyi, F. and Gray, D.H. 1977. Engineering Properties Affecting Disposal of Red Muds. Proceedings ASCE Specialty Conference on Geotechnical Practice for Disposal of Solids Waste Minerals, Ann Arbor, Mich, pp. 1-22.

Somogyi, F. 1980. Large Strain Consolidation of Fine Grained Slurries. Presented at the Canadian Society for Civil Engineering, Winnipeg, Manitoba, May 29-30.

Somogyi, F., Carrier III, W.D., Lawver, J.E. and Beckman, J.F. 1984. Waste phosphatoc clay disposal in mine cuts. Sedimentation consolidation models: predictions and validation: *In* proceedings of a symposium, R.N. Yong and F.C. Townsend Eds, ASCE, Newyork: 545-580.

SOSG (Suncor Oil Sand Group Limited) 1996. Suncor Steepbank Mine Application Second Request for Supplemental Information. Report to Alberta Environmental Utility Board.

Seneviratne, N.H., Fahey, M, Newson, T.A. and Fujiyasu, Y. 1996. Numerical modelling of consolidation and evaporation of slurried mine tailings. International Journal for Numerical and Analytical Methods in Geomechanics, **20**:647–671

Sheeran, D. E. and Krizek, R. J. 1971. Preparation of homogeneous soil samples by slurry consolidation.Journal of Materials. JMLSA, 6(2): 356-373.

Spott, J. and Townsend, R.C. 1977. Dewatering Dredge Material with Wicks. *In* Proceedings of the Conference on Geotechnical Practice for Disposal of Solid Waste Materials, June 13-15, 1977, the University of Michigan, Ann Arbor, Michigan: 599-614.

Sridharan, A., and Venkatappa Rao, G. 1973. Mechanisms controlling volume change of saturated clays and the role of the effective stress concept. Géotechnique **23**(2): 359-382.

Sridharan, A., and Venkatappa Rao, G. 1979. Shear strength behavior of saturated clays and the role of the effective stress concept. Géotechnique **29**(2): 177-193.

Sridharan, A., and Prakash, K. 2001. A consolidation and permeability behavior of segregated and homogeneous sediments. Geotechnical Testing Journal, **24**(1): 109-120.

Sridharan, A., and Prakash, K. 1999. Simplified Seepage Consolidation Test for Soft Sediments. Geotechnical Testing Journal, **22**(3): 235-244.

Strueby, B. 2004. CT Experience to Date at Syncrude. CONRAD Tailings Seminar. Alberta Research Council, November 8, Edmonton, AB.

Suharyono, H. and Hogg, R., 1996. Flocculation in flow through pipes and in-line mixers. Minerals and Metallurgical Processing **13**:501–505

Suthaker, N.N. and Scott, J.D. 1994. Large Strain Consolidation of Oil Sand Fine Tails in a Wet Landscape. 47th Canadian Geotechnical Conference, Halifax, Nova Scotia, 514-523.

Suthaker, N. N. 1995. Geotechnics of Oil Sand Fine Tailings, Ph.D. thesis, Department of Civil and Environmental Engineering, University of Alberta, Edmonton, AB.

Suthaker, N.N. and Scott, J.D. 1997. Thixotropic strength measurement of oil sand fine tailings. Canadian Geotechnical Journal, **34**: 974-984.

Suthaker, N.N. and Scott, J.D. 1996. Measurement of Hydraulic Conductivity in Oil Sand Tailings Slurries. Canadian Geotechnical Journal, **33**(4): 642-653.

Sworska, A., Laskowski, J.S. and Cymerman, G. 2000. Flocculation of the Syncrude fine tailings: Part I. Effect of pH, polymer dosage and Mg^{2+} and Ca^{2+} cations. International Journal of Mineral Processing, **60**: 143-152.

Sworska, A., Laskowski, J.S. and Cymerman, G. 2000. Flocculation of the Syncrude fine tailings: Part II. Effect of hydrodynamic conditions. International Journal of Mineral Processing, **60**: 153-161.

Tang, J. 1997. Fundamental Behaviour of Composite Tailings. M.S.c. thesis, Department of Civil and Environmental Engineering, University of Alberta, Edmonton, AB.

Tang, J., Biggar, K.W., Scott, J.D. and Sego, D.C. 1997. Examination of mature fine tailings using a scanning electron microscope, Canadian Geotechnical Conference, Ottawa, Ontario, 746-754.

Tan, T.S., Yong, K.Y., Leong, E.C. and Lee, S.L., 1990. Sedimentation of clayey slurry. Journal of Geotechnical Engineering, **116**(6): 885-898.

Tan, T.S., Goh, T., Karunaratne, G.P., Inoue, T. and Lee, S. 1991. Yield stress measurement by a penetration method. Canadian Geotechnical Journal, **28**: 517-522.

Tan, T.S., Goh, T., Karunaratne, G.P. and Lee, S. 1994. Shear strength of very soft clay-sand mixtures. Geotechnical Testing Journal, GTJODJ, **17**(1):27-34.

Tan, T.S. 1995. Sedimentation to consolidation: A geotechnical perspective. In Proceedings of Compression and Consolidation of Clayey Soils, Yoshikuni & Kusakabe (eds). Hiroshima, Japan: 937-948.

Terzaghi, K., Peck, R.B. and Mesri, G. 1996. Soil Mechanics in Engineering Practice, Third Edition, John Wiley & Sons, Inc., 549 p.

Terzaghi, K. 1943. Theoretical Soil Mechanics, John Wiley and Sons, Inc., New York, New York, 510 p.

Tombácz, E. and Szekeres, M. 2006. Surface charge heterogeneity of kaolinite in aqueous suspension in comparison with montmorillonite. Applied Clay Science: **34**:105-124.

Touhidi-Baghini, A. 1998. Absolute Permeability of McMurray Formation Oil Sands at Low Confining Stresses, Ph.D. thesis, Department of Civil and Environmental Engineering, University of Alberta, Edmonton, AB.

Toorman, E.A. 1999. Sedimentation and self-weight consolidation: constitutive equations and numerical modeling. Géotechnique, **49**(6):709–726

Wang, Y.-H. and Siu W.-K. 2006. Structure characteristics and mechanical properties of kaolinite soils. I. Surface charges and structural characterizations. Canadian Geotechnical Journal, **43**: 587-600.

Watari, Y. 1984, Reclamation with clayey soils and methods of earth spreading on the surface, JSSMFE/NUS/AIT Seminar on Soil Improvement and Construction Technique in Soft Ground, Singapore: 103-119.

Weiland, R.H., Bunnaul, P. and Hogg, R. 1994. Centrifugal dewatering of flocculated clays. Minerals & Metallurgical Processing, **13**(3):93-97.

Wheeler, S.J. 1988. A concept model of soils containing large gas bubbles. Géotechnique, **38**: 389-397.

Wheeler, S.J., Sham, W.K. and Thomas, S.D. 1990. Gas pressure in unsaturated offshore soils. Canadian Geotechnical Journal, **27**: 79-89.

Wheeler, S.J. 1990. Movement of large gas bubbles in unsaturated fine-grained sediments. Marine Geotechnology, **9**:113-129.

Wichman, B.G.H.M. 2000. A finite strain theory for gassy sludge. Géotechnique, **50**(1): 35-41.

Wong, R.C.K., Mills, B.N. and Liu, Y.B. 2008. Mechanistic Model for One-Dimensional Consolidation Behavior of Nonsegregating Oil Sands Tailings. Journal of Geotechnical and Geoenvironmental Engineering, **34**(2): 195-202.

Xu, Y. and Cymerman, G. 1999. Flocculation of fine oil sand tails. Polymers in Mineral Processing, Canadian Institute of Mining, Metallurgy and Petroleum, Edmonton, Alberta, Canada: 591–604.

Yan, J. and James, A.E. 1997. The yield surface of viscoelastic and plastic fluids in a vane viscometer. Journal of Non-Newtonian Fluid Mechanics, **70**: 237–253.

Yang, J. and Chalaturnyk, R.J. 2004. Computational Fluid Dynamics Simulation of Thickener. *In* Proceedings of CIM Edmonton 2004 Conference, Edmonton, A.B., 9-12 May 2004, Canadian Institute of Mining, Metallurgy and Petroleum, 8 p.

Yong, R. N., Siu, S. K. H. and Sheeran, D. E. 1983. On the stability and settling of suspended solids in settling ponds. Part I. Piece-wise linear consolidation analysis of sediment layer. Canadian Geotechnical Journal, **20**(4): 817–826.

Yong, R. N. and Elmonayeri, D. 1984. On the stability and settling of suspended solids in settling ponds. Part II. Diffusion analysis of initial settling of suspended solids. Canadian Geotechnical Journal, **21**: 644-656.

Yuan, S. and Shaw, W. 2007. Novel Processes for Treatment of Syncrude Fine Transition and Marine Ore Tailings. Canadian Metallurgical Quarterly, **46**(3): 265-272.

van Olphen. H. 1977. An Introduction to Clay Colloid Chernistry. John Wiley & Sons,New York, N.Y.

Znidarčić, D., Schiffman, R.L., Pane, V., Croce, P., Ko, H.-Y. and Olsen, H.W. 1986. Theory of one-dimensional consolidation of saturated clays: Part V constant rate of deformation testing and analysis. Géotechnique, **36**(2): 227-237.